

University of Alberta
Department of Civil &
Environmental Engineering



Structural Engineering Report No. 259

**SEISMIC REHABILITATION OF
REINFORCED CONCRETE COLUMNS
THROUGH CONFINEMENT
BY STEEL COLLARS**

by
Munawar A. Hussain
and
Robert G. Driver

May 2005

**Seismic Rehabilitation of Reinforced Concrete Columns
Through Confinement By Steel Collars**

Part 1

by

Munawar A. Hussain

and

Robert G. Driver

Structural Engineering Report No. 259

**Department of Civil and Environmental Engineering
University of Alberta
Edmonton, Alberta, Canada**

May 2005

ABSTRACT

The research presented in this report is a part of a larger research program on the seismic rehabilitation of reinforced concrete frames using steel plate shear walls. Steel plate shear walls are highly ductile, but seismically deficient reinforced concrete frames tend to be incompatible due to their lack of ductility. Therefore, this rehabilitation scheme requires the improvement in ductility of the concrete frames. The research presented herein is a comprehensive experimental and analytical investigation into the improvement of behaviour of seismically deficient reinforced concrete columns through confinement by steel collars. The experimental research was divided into two phases.

In the phase 1 experimental program, the axial behaviour of collared columns was investigated and it was demonstrated that a significant enhancement in both strength and ductility can be achieved. In the phase 2 experimental program, the behaviour of collared columns under axial load and lateral cyclic loading was investigated. The results showed that the confinement arising from the presence of the collars leads to excellent cyclic behaviour, indicating that this scheme shows promise of being an effective means of rehabilitating seismically deficient reinforced concrete columns.

Existing concrete confinement models are unable to predict the behaviour of collared columns because of the lack of an explicit flexural stiffness parameter. Therefore, a new confinement model has been developed that takes into account the significant flexural stiffness of the confining elements. This model requires as input the behavioural curves of collars in terms of the confining pressure versus lateral strain relationships. These curves are obtained through finite element analyses. Non-dimensional models were also developed for the confining behaviour of HSS collars and solid steel collars with rigid corner connections.

Using the confined concrete material curves obtained by the proposed model, good predictions of the behaviour of the axially loaded columns tested in phase 1 were obtained. Moreover, envelopes to the moment versus drift hysteresees were determined using the model that showed very good agreement with the experimental results up to a lateral drift of about 10% for columns tested with a long shear span and 5% for columns tested with short shear span in the phase 2 experimental program.

ACKNOWLEDGEMENTS

The research presented in this report was funded primarily by the Natural Sciences and Engineering Research Council of Canada. The authors are also thankful to the University of Alberta for providing an F.S. Chia Ph.D. scholarship and to Prof. G.L. Kulak for providing additional financial support to the first author.

Various researchers contributed to this project. Contributions and ideas at the formative stages by Profs. G.L. Kulak, G.Y. Grondin, and D.J.L. Kennedy are gratefully acknowledged. Occasional discussions during the course of the project with these researchers and with Prof. A.E. Elwi, on aspects related to concrete material modelling, also added significantly to the quality of the work. The research also benefited from the valuable suggestions of the committee members for the Ph.D. examination of the first author: Profs. B. Massicotte (Ecole Polytechnique de Montréal), B. Jar, H. Soleymani, G.Y. Grondin, and A.E. Elwi.

The technical assistance of the staff of the I.F. Morrison Structural Engineering Laboratory, L. Burden and R. Helfrich, during the experimental part of this research was invaluable. The authors are also thankful to the numerous graduate students who provided assistance during the casting of the test specimens, to L. Callele for providing assistance in conducting tension coupon and stub-column tests, and to M. Kuzik for welding many of the collars used in the test program.

Donations to the project by Reliable Tubes Ltd., Unicon Concrete Ltd., and Master Builders are gratefully acknowledged and a special thanks is given to the Centre for Engineering Research (C-FER Technologies Ltd.), Edmonton, Canada, who provided the test facility for two of the columns in the research program.

TABLE OF CONTENTS

1. INTRODUCTION.....	1
1.1 Foreword.....	1
1.2 Seismic Rehabilitation.....	1
1.3 Unstiffened Thin Steel Plate Shear Walls.....	3
1.3.1 Evolution of Unstiffened Thin Steel Plate Shear Walls.....	3
1.3.2 Characteristics of Steel Plate Shear Walls.....	6
1.3.3 Steel Building with Steel Plate Shear Walls.....	7
1.3.4 Seismic Rehabilitation of Reinforced Concrete Buildings.....	8
1.3.1.1 VA Medical Center in Charleston, South Carolina (Baldelli, 1983).....	8
1.3.1.2 Oregon State Library Building in Salem, Oregon (Robinson and Ames, 2000).....	9
1.4 Proposed Rehabilitation Scheme.....	10
1.4.1 Challenges Arising and Proposed Solutions.....	11
1.4.2 Steel Collar Configurations.....	12
1.5 Scope and Objectives.....	13
1.5.1 Phase 1.....	14
1.5.2 Phase 2.....	14
1.6 Report Format and Organization.....	15
1.7 References.....	22
2. LITERATURE REVIEW.....	25
2.1 Introduction.....	25
2.2 Confinement of Concrete.....	26
2.2.1 Comparison Between Hydraulic and Rebar Confinement.....	27

2.2.2	Enhancement in Strength and Ductility due to Confinement.....	28
2.2.3	Effect of Gage Length.....	29
2.2.4	Effect of Strain Rate.....	29
2.2.5	Effect of Strength of Concrete.....	30
2.2.6	Effect of Type of Aggregate.....	30
2.2.7	Effect of Yield Stress of Confining Steel.....	31
2.2.8	Effect of Spacing of Confining Steel.....	32
2.2.9	Effect of Amount of Confining Steel.....	32
2.2.10	Effect of Strain Gradient.....	33
2.2.11	Effect of Distribution of Confining Steel and Resulting Tie Configuration.....	34
2.3	Confinement Models.....	34
2.3.1	Chan (1955).....	34
2.3.2	Roy and Sozen (1964).....	35
2.3.3	Soliman and Yu (1967).....	35
2.3.4	Sargin (1971).....	36
2.3.5	Kent and Park (1971).....	36
2.3.6	Vallenas <i>et al.</i> (1977).....	37
2.3.7	Sheikh and Uzumeri (1982).....	38
2.3.8	Manader <i>et al.</i> (1988b).....	38
2.3.9	Saatcioglu and Razvi (1992).....	39
2.3.10	Chung <i>et al.</i> (2002).....	40
2.3.11	Légeron and Paultre (2003).....	40
2.3.12	Fam and Rizkalla (2001).....	41
2.4	Deficiencies in the Existing Confinement Models.....	42
2.4.1	Flexural Stiffness of Confining Elements.....	42
2.4.2	Variation of Confining Pressure with Axial Load History.....	44
2.5	Code Requirments for Concrete Confinement.....	45
2.5.1	Current Code Requirements (ACI 318-02 and CSA A23.3-94).....	45

2.5.2	Evolution of Requirement in ACI 318.....	47
2.6	Rehabilitation of Reinforced Concrete Columns by Jacketing.....	49
2.6.1	Valluvan <i>et al.</i> (1993).....	50
2.6.2	Chai <i>et al.</i> (1990).....	50
2.6.3	Marsh (1992).....	51
2.6.4	Aboutaha <i>et al.</i> (1996).....	51
2.6.5	Xiao and Wu (2003).....	52
2.6.6	Ghobarah <i>et al.</i> (1997).....	52
2.7	Summary.....	53
2.8	References.....	63
3.	EXPERIMENTAL BEHAVIOUR OF COLLARED COLUMNS UNDER CONCENTRIC LOADING.....	67
3.1	Introduction.....	67
3.2	Research Significance.....	68
3.3	Description of Test Specimens.....	68
3.3.1	Specimen Preparation.....	68
3.3.2	Internal Reinforcement Details.....	69
3.3.3	HSS Collar Confinement.....	70
3.4	Material Properties.....	71
3.5	Test Set-Up.....	73
3.6	Instrumentation.....	73
3.7	Loading Protocol.....	74
3.8	Test Results.....	75
3.8.1	Load versus Dispalcement Response.....	75
3.8.2	Load versus Strain curves.....	75
3.8.3	Confined Concrete Material Curves.....	76
3.8.4	Peak Loads and Strains at Peak Loads.....	76
3.8.5	Failure Criterion.....	77

3.8.6	Depth of Concrete Spalling.....	77
3.8.7	Theoretical Capacities of Columns.....	78
3.8.8	Strength Enhancement of Concrete.....	78
3.8.9	Moduli of Toughness of Columns.....	79
3.8.10	Column Load vs. Bolt Force.....	79
3.8.11	Collar Confinement and Tie Bars Strain Data.....	79
3.9	Discussion.....	80
3.9.1	Ductility Enhancement and Modes of Failure.....	80
3.9.2	Strength Enhancement Criteria.....	82
3.9.3	Bolted vs. Welded Collars.....	83
3.9.4	Collar Spacing.....	83
3.9.5	Collar Stiffness.....	85
3.9.6	Active Confining Pressure.....	86
3.9.7	Measured Strains of Transverse Steel.....	87
3.10	Summary and Conclusions.....	89
3.11	References.....	168
4.	PERFORMANCE OF COLLARED COLUMNS UNDER CYCLIC LOADING.....	169
4.1	Introduction.....	169
4.2	Experimental Program.....	170
4.2.1	Test Specimens.....	170
4.2.2	Material Properties.....	172
4.2.3	Test Set-up.....	173
4.2.4	Instrumentation.....	173
4.2.5	Testing Procedure.....	174
4.3	Test Results.....	178
4.3.1	Test Observations.....	178
4.3.1.1	Specimen CL0.....	178

4.3.1.2	Specimen CL1.....	179
4.3.1.3	Specimen CL2.....	180
4.3.1.4	Specimen CL3.....	181
4.3.1.5	Specimen CL4.....	181
4.3.1.6	Specimen CL5.....	182
4.3.1.7	Specimen CL6.....	182
4.3.1.8	Specimen CL7.....	183
4.3.1.9	Specimen CL8.....	183
4.3.2	Hysteresis Curves.....	184
4.3.3	Revised Yield Displacements.....	185
4.3.3.1	Method 1 (alternative 1).....	185
4.3.3.2	Method 1 (alternative 2).....	185
4.3.3.3	Method 1 (alternative 3).....	186
4.3.3.4	Method 1 (alternative 4).....	186
4.3.3.5	Method 1 (alternative 5).....	186
4.3.3.6	Method 2.....	186
4.3.4	Revised Hysteresis Curves.....	187
4.3.5	Comparison of Envelope Curves.....	187
4.3.5.1	Secant Stiffness at 0.25% Drift.....	188
4.3.5.2	Average Peak Moments.....	192
4.3.5.3	Modulus of Toughness.....	193
4.3.5.4	Normalized Modulus of Toughness.....	193
4.3.6	Stiffness Retention.....	193
4.3.7	Energy Dissipation Characteristics.....	194
4.3.7.1	Energy Dissipation Per Cycle.....	194
4.3.7.2	Cumulative Energy Dissipated versus Cycle Number.....	195
4.3.7.3	Normalized Cumulative Energy Dissipated versus Cycle Number.....	197

4.3.8	Equivalent Viscous Damping Ratio.....	199
4.3.9	Curvature Distributions in the Test Regions.....	201
4.3.10	Other Ductility Parameters.....	202
4.4	Effect of Various Parameters on Column Behaviour.....	205
4.4.1	Effect of Axial Load.....	205
4.4.1.1	Comparison of Columns CL1 and CL3.....	206
4.4.1.2	Comparison of Columns CL5 and CL7.....	209
4.4.1.3	Discussion on the Effect of Axial Loads.....	212
4.4.2	Effect of Collar Spacing.....	213
4.4.2.1	Comparison of Columns CL2 and CL3.....	213
4.4.2.2	Comparison of Columns CL6 and CL7.....	215
4.4.2.3	Discussion on the Effect of Collar Spacing.....	217
4.4.3	Effect of Size of Collar.....	218
4.4.3.1	Comparison of Columns CL3 and CL4.....	218
4.4.3.2	Comparison of Columns CL7 and CL8.....	220
4.4.3.3	Discussion on the Effect of Size of Collars.....	221
4.4.4	Effect of Shear-Span.....	223
4.4.4.1	Comparison of columns CL1 and CL5.....	223
4.4.4.2	Comparison of Columns CL2 and CL6.....	224
4.4.4.3	Comparison of Columns CL3 and CL7.....	227
4.4.4.4	Comparison of Columns CL4 and CL8.....	228
4.4.4.5	Discussion on the Effect of Shear-Span.....	230
4.5	Prediction of Envelope to Hysteresis Curves.....	230
4.5.1	Flexural Deformations.....	231
4.5.1.1	Plastic Hinge Length.....	232
4.5.1.2	Analytical Moment-Versus-Curvature Relationship.....	233
4.5.2	Rotations at Column Base Due to Anchorage Slip.....	234

4.5.3	Predicted Envelope Curves.....	236
4.6	Summary.....	238
4.7	Conclusions.....	238
4.7.1	Conclusions Based on Experimental Results.....	238
4.7.1.1	Effect of Axial load.....	240
4.7.1.2	Effect of Collar Spacing.....	240
4.7.1.3	Effect of Collar Size.....	241
4.7.1.4	Effect of Shear-Span.....	242
4.7.2	Conclusions Based on Analytical Results.....	242
4.8	References.....	377
5.	MODEL FOR CONCRETE CONFINED EXTERNALLY BY STEEL COLLARS.....	380
5.1	Introduction.....	380
5.2	Predictions by Existing Confinemnt Models.....	381
5.3	Finite Element Analysis.....	382
5.3.1	Geometric Modelling.....	382
5.3.2	Boundary Conditions and Loading.....	383
5.3.3	Solution Strategy.....	384
5.3.4	Material Properties.....	384
5.3.4.1	Concrete.....	384
5.3.4.2	Reinforcing Bars, Steel HSS, and Threaded rods.....	385
5.3.5	Preliminary Finite Element Results and New Direction.....	385
5.3.6	Confining Pressure versus Lateral Strain Relationships.....	386
5.4	Proposed Model for Confinement of Concrete.....	389
5.4.1	Lateral Displacement Compatibility.....	390
5.4.2	Effect of Unconfined Concrete in the Core.....	393
5.4.3	Behaviour of Confined Concrete in Core.....	394

5.4.4	Behaviour of Unconfined Concrete in Core.....	399
5.4.5	The Descending Branch.....	400
5.4.6	Application of the Proposed Model.....	407
5.5	Summary and Conclusions.....	410
5.6	References.....	446

6. NON-DIMENSIONAL MODEL FOR COLUMN CONFINING BEHAVIOUR OF HSS AND SOLID COLLARS WITH RIGID CORNER CONNECTIONS.....450

6.1	Introduction.....	450
6.2	Confining Stress vs. Lateral Strain Relationship.....	451
6.3	Finite Element Model.....	452
6.3.1	Concrete Material Curve.....	453
6.3.2	Steel Material Curve.....	453
6.3.3	Generation of Steel Material Curves for Parametric Study.....	454
6.4	Contact of Collars with the Concrete Column.....	456
6.5	Model for HSS Collars for Square Concrete Columns.....	456
6.5.1	Non-Dimensional Parameters.....	456
6.5.2	Ranges of Parameters and Reference Model.....	460
6.5.3	Scale Effect.....	462
6.5.4	Parametric Study and Prediction Equation.....	463
6.5.4.1	Overview of Regression Analysis.....	464
6.5.4.2	Effect of Parameter β_1 on the Confining Behaviour of HSS Collar.....	465
6.5.4.2	Effect of Parameter β_2 on the Confining Behaviour of HSS Collars.....	467
6.5.4.3	Effect of Parameter β_3 on the Confining Behaviour of HSS Collars.....	468
6.5.4.4	Effect of Parameter β_4 on the Confining Behaviour of	

	HSS Collars.....	469
6.5.4.5	Effect of Parameter β_5 on the Confining Behaviour of HSS Collars.....	470
6.5.4.6	Effect of Parameter β'_5 on the Confining Behaviour of HSS Collars.....	473
6.5.4.7	Effect of Parameter β_6 on the Confining Behaviour of HSS Collars.....	474
6.5.4.8	Effect of Collar Smearing on the Confining Behaviour of HSS Collars.....	475
6.5.4.9	Expressions for $(\beta_8)_{\max}$ and γ_o for HSS Collars.....	477
6.5.4.10	Verification of the Proposed Model for HSS Collars.....	477
6.5.4.11	Application of the Proposed Model to Real Cases.....	480
6.5.4.12.1	Column C06.....	480
6.5.4.12.2	Column C09.....	482
6.6	Model for Solid Collars.....	485
6.6.1	Non-Dimensional Parameters for Solid Collars.....	485
6.6.2	Ranges of Parameters and Reference Model for Solid Collars.....	487
6.6.3	Scale Effect for Solid Collars.....	488
6.6.4	Parametric Study and Prediction Equation for Solid Collars.....	488
6.6.4.1	Effect of Parameter β_1 on the Confining Behaviour of Solid Collars.....	489
6.6.4.2	Effect of Parameter β_2 on the Confining Behaviour of Solid Collars.....	490
6.6.4.3	Effect of Parameter β_3 on the Confining Behaviour of Solid Collars.....	492
6.6.4.4	Effect of Parameter β_5 on the Confining Behaviour of Solid Collars.....	493
6.6.4.5	Effect of Parameter β'_5 on the Confining Behaviour	

	of Solid Collars.....	494
6.6.4.6	Effect of Parameter β_6 on the Confining Behaviour of Solid Collars.....	495
6.6.4.7	Effect of Collar Smearing on the Confining Behaviour of Solid Collars.....	496
6.6.4.8	Expressions for $(\beta_8)_{\max}$ and γ_o for Solid Collars.....	497
6.6.4.8	Verification of the Proposed Model for Solid Collars.....	499
6.7	Comparison of Equations for HSS and Solid Collars.....	500
6.8	Summary and Conclusions.....	502
6.9	References.....	577
7.	SUMMARY, CONCLUSIONS, AND RECOMMENDATIONS.....	578
7.1	Introduction.....	578
7.2	Summary.....	579
7.3	Conclusions.....	581
7.3.1	Concentrically Loaded Columns.....	581
7.3.2	Columns Under Cyclic Loading.....	582
7.3.2.1	Effect of Axial Loads.....	584
7.3.2.2	Effect of Collar Spacing.....	585
7.3.2.3	Effect of Collar Size.....	586
7.3.2.4	Effect of Shear-Span.....	587
7.3.2.5	Conclusions Based on Analytical Results.....	587
7.4	Recommendations for Future Research.....	588
7.5	References.....	592

APPENDICES

A. DERIVATION OF EQUATIONS FOR CONFINING STEEL.....	593
A.1 Introduction.....	593
A.2 Derivation of Equation 2.8.....	593
A.3 Derivation of Equation 2.10.....	595
A.4 Appendix A Notation.....	597
A.5 References.....	599
B. PROGRAM MCP.....	600
B.1 Objective.....	600
B.2 Fortran Source Code.....	600
B.3 Operation.....	605
C. YIELDING OF LONGITUDINAL BARS AT YIELD DISPLACEMENT.....	607
C.1 References.....	611
D. Moment Versus Reinforcing Bar Strain Relationships.....	612
D.1 Specimen CL0.....	612
D.2 Specimen CL1 and CL5.....	613
D.3 Specimens CL2, CL3, CL4, CL6, CL7, and CL8.....	615
E. Average Envelopes to Moment versus Drift Hystereses.....	628
F. Determination of Yield Displacement.....	633
G. Energy Dissipation.....	657
H. Distribution of Energy Dissipation in Columns.....	666
H.1 Column CL1.....	666
H.2 Column CL2.....	667
H.3 Column CL3.....	668
H.4 Column CL4.....	669
H.5 Column CL5.....	670

H.6	Column CL6.....	671
H.7	Column CL7.....	672
H.8	Column CL8.....	673
I.	Moment versus Curvature Hysteresis.....	686
J.	Ductility Parameters.....	691
K.	PROGRAM MCR.....	700
K.1	Objective.....	700
K.2	Fortran Source Code.....	700
K.3	A Sample Input File.....	706
L.	PROGRAM C4P.....	709
L.1	Objective.....	709
L.2	Fortran Source Code.....	709
L.3	A Sample Input File.....	713

LIST OF TABLES

Table 3.1	Description of column specimens.....	92
Table 3.2	Properties of concrete.....	93
Table 3.3	Properties of rebars and HSS.....	94
Table 3.4	Strain rate data and moduli of toughness of columns.....	95
Table 3.5	Column axial strain and spalling data.....	96
Table 3.6	Load data and strength enhancement factors.....	97
Table 4.1	Detail of test specimens.....	244
Table 4.2	Cylinder strengths of concrete.....	245
Table 4.3	Properties of steel rebars and steel HSS.....	246
Table 4.4	Lengths of test regions and types of instrumentations.....	247
Table 4.5	Analytical and experimental moment capacities of Columns.....	248
Table 4.6	Summary of yield displacements determined by different methods.....	249
Table 4.7	Detail of number of complete cycles at different ductility levels and total number of cycles sustained by the specimens.....	250
Table 4.8	Values of moments and drifts from the envelope curves at 0.25% drift, at peak moment, and at failure.....	251
Table 4.9	Stress in concrete and steel longitudinal bars before the application of horizontal loads.....	252
Table 4.10	Cracking moments of columns.....	253
Table 4.11	Moduli of toughness and normalized moduli of toughness for the test specimens.....	254
Table 4.12	Equivalent plastic hinge lengths and most damage region of the test specimens.....	255
Table 4.13	Curvature ductility factors for column CL0 to CL8.....	256
Table 4.14	Axial load indices for column CL0 through CL8.....	257
Table 4.15	Ratios of shear-span a to effective depth d	258

Table 5.1	Measured and assumed properties of confined concrete columns for developing models for strain at peak stress and slope of descending branch.....	412
Table 5.2	Relevant data and computed values of ε_{cc} and ε_{cc85} for phase 1 columns.....	413
Table 5.3	Relevant data and computed values of ε_{cc} and ε_{cc85} for phase 2 columns.....	414
Table 6.1	Detail of finite element models to study the effect of scale on the confining behaviour of HSS collars.....	503
Table 6.2	Detail of finite element models to study the effect of variation of β_1 on the confining behaviour of HSS collars.....	504
Table 6.3	Detail of finite element models to study the effect of variation of β_2 on the confining behaviour of HSS collars.....	505
Table 6.4	Relationship between: (a) γ_2 and β_2 ; and (b) λ_2 and β_2 for HSS collars.....	506
Table 6.5	Detail of finite element models to study the effect of variation of β_3 on the confining behaviour of HSS collars.....	507
Table 6.6	Relationship between: (a) λ_3 and β_3 ; and (b) γ_3 and β_3 for solid collars.....	508
Table 6.7	Detail of finite element models to study the effect of variation of β_4 on the confining behaviour of HSS collars.....	509
Table 6.8	Relationship between: (a) γ_4 and β_4 ; and (b) λ_4 and β_4 for HSS collars.....	510
Table 6.9	Detail of finite element models to study the effect of variation of f_y and E_s keeping β_5 constant on the confining behaviour of HSS collars.....	511
Table 6.10	Detail of finite element models to study the effect of variation of f_y , keeping E_s and n constant on the confining behaviour of HSS collars.....	512
Table 6.11	Relationship between: (a) γ_5 and β_5 ; and (b) λ_5 and β_5 for HSS collars.....	513

Table 6.12	Detail of finite element models to study the effect of variation of E_s , keeping f_y and n constant on the confining behaviour of HSS collars.....	514
Table 6.13	Relationship between: (a) γ'_5 and β'_5 ; and (b) λ'_5 and β'_5 for HSS collars.....	515
Table 6.14	Detail of finite element models to study the effect of variation of β_6 on the confining behaviour of HSS collars.....	516
Table 6.15	Relationship between: (a) γ_6 and β_6 ; and (b) λ_6 and β_6 for HSS collars.....	517
Table 6.16	Detail of finite element models to study the effect of smearing on the confining behaviour of HSS collars.....	518
Table 6.17	Relationship between: (a) γ_s and β_3 ; and (b) λ_s and β_3 for HSS collars.....	519
Table 6.18	Detail of finite element models to check the proposed equations.....	520
Table 6.19	Detail of equivalent models obtained after collar smearing in order to apply proposed equations for the confining of HSS collars.....	521
Table 6.20	Coefficients of multiple determinations R^2 up to various level of lateral strains for columns confined by HSS collars.....	522
Table 6.21	Detail of finite element models to study the effect of scale on the confining behaviour of solid collars.....	523
Table 6.22	Detail of finite element models to study the effect of variation of β_1 on the confining behaviour of solid collars.....	524
Table 6.23	Detail of finite element models to study the effect of variation of β_2 on the confining behaviour of solid collars.....	525
Table 6.24	Relationship between: (a) γ_2 and β_2 ; and (b) λ_2 and β_2 for solid collars.....	524
Table 6.25	Detail of finite element models to study the effect of variation of β_3 on the confining behaviour of solid collars.....	527
Table 6.26	Relationship between: (a) γ_3 and β_3 ; and (b) λ_3 and β_3 for solid collars.....	528

Table 6.27	Detail of finite element models to study the effect of variation of f_y keeping E_s and n constant on the confining behaviour of solid collars.....	529
Table 6.28	Relationship between: (a) γ_5 and β_5 ; and (b) λ_5 and β_5 for solid collars.....	530
Table 6.29	Detail of finite element models to study the effect of variation of E_s keeping f_y and n constant on the confining behaviour of solid collars.....	531
Table 6.30	Relationship between: (a) γ'_5 and β'_5 ; and (b) λ'_5 and β'_5 for solid collars.....	532
Table 6.31	Detail of finite element models to study the effect of variation of n on the confining behaviour of solid collars.....	533
Table 6.32	Relationship between: (a) γ_6 and β_6 ; and (b) λ_6 and β_6 for solid collars.....	534
Table 6.33	Detail of finite element models to study the effect of collar smearing on the confining behaviour of solid collars.....	535
Table 6.34	Relationship between: (a) γ_s and β_3 ; and (b) λ_s and β_3 for solid collars.....	536
Table 6.35	Detail of finite element models to test the proposed equations for the confining behaviour of solid collars.....	537
Table 6.36	Coefficients of multiple determinations R^2 up to various level of lateral strains for column confined by solid collars.....	538
Table G.1	Energy dissipated by specimen CL0 based on overall system.....	657
Table G.2	Energy dissipated by specimen CL1 based on overall system.....	658
Table G.3	Energy dissipated by specimen CL2 based on overall system.....	659
Table G.4	Energy dissipated by specimen CL3 based on overall system.....	660
Table G.5	Energy dissipated by specimen CL4 based on overall system.....	661
Table G.6	Energy dissipated by specimen CL5 based on overall system.....	662
Table G.7	Energy dissipated by specimen CL6 based on overall system.....	663
Table G.8	Energy dissipated by specimen CL7 based on overall system.....	664

Table G.9	Energy dissipated by specimen CL8 based on overall system.....	665
Table H.1	Energy dissipated up to different heights of the test region for column CL1.....	674
Table H.2	Energy dissipated up to different heights of the test region for column CL2.....	675
Table H.3	Energy dissipated up to different heights of the test region for column CL3.....	676
Table H.4	Energy dissipated up to different heights of the test region for column CL4.....	677
Table H.5	Energy dissipated up to different heights of the test region for column CL5.....	678
Table H.6	Energy dissipated up to different heights of the test region for column CL6.....	679
Table H.7	Energy dissipated up to different heights of the test region for column CL7.....	680
Table H.8	Energy dissipated up to different heights of the test region for column CL8.....	681
Table J.1	Ductility ratios and energy damage indicator for column CL0.....	691
Table J.2	Ductility ratios and energy damage indicator for column CL1.....	692
Table J.3	Ductility ratios and energy damage indicator for column CL2.....	693
Table J.4	Ductility ratios and energy damage indicator for column CL3.....	694
Table J.5	Ductility ratios and energy damage indicator for column CL4.....	695
Table J.6	Ductility ratios and energy damage indicator for column CL5.....	696
Table J.7	Ductility ratios and energy damage indicator for column CL6.....	697
Table J.8	Ductility ratios and energy damage indicator for column CL7.....	698
Table J.9	Ductility ratios and energy damage indicator for column CL8.....	699

LIST OF FIGURES

<u>Figure</u>	<u>Title</u>	<u>Page</u>
Figure 1-1	Resemblance of steel plate shear wall to a cantilever plate girder	16
Figure 1-2	Schematic diagram of the proposed rehabilitation system; (b) conventional rebar hoop reinforcement; (c) HSS collar with welded collar connections; (d) HSS collars with bolted collar connections (assembled view); and (e) HSS collar with bolted collar connections (exploded view)	17
Figure 1-3	Modelling of SPSW panel using strip model	18
Figure 1-4	Deformed configuration of steel plate shear wall modelled by diagonal strips (deformations amplified 100 times)	18
Figure 1-5	Typical elevation of a reinforced concrete structure rehabilitated by steel plate shear walls	19
Figure 1-6	Schematic of different types of collars: (a) HSS collar with bolted corner connections; (b) HSS collar with welded corner connections; and (c) collar cut from steel plates	19
Figure 1-7	Views of typical column specimens in set-up with: (a) bolted; and (b) welded collars in the test region	20
Figure 1-8	Three of the nine phase 2 columns at different stage of collar installation	21
Figure 1-9	A typical phase 2 column in the test set-up	21
Figure 2-1	Deformed configuration of steel plate shear wall modeled by diagonal strips	55
Figure 2-2	Relationship between coefficient k_1 and lateral confining pressure f_l	55
Figure 2-3	Model for the stress versus strain curve of confined and unconfined concrete proposed by Chan (1955)	56
Figure 2-4	Model for the stress versus strain curve of confined concrete proposed by Roy and Sozen (1964)	56
Figure 2-5	Model for the stress versus strain curve of confined concrete proposed by Soliman and Yu (1967)	57
Figure 2-6	Model for the stress versus strain curve of confined concrete proposed by Sargin (1971)	57
Figure 2-7	Model for the stress versus strain curve of confined and unconfined concrete proposed by Kent and Park (1971)	58

Figure 2-8	Modified Kent and Park model for the stress versus strain behaviour of confined concrete by Park et al. (1982)	58
Figure 2-9	Model for the stress versus strain curve of confined concrete proposed by Vallenias et al. (1977)	59
Figure 2-10	Model for the stress versus strain curve of confined concrete proposed by Sheikh and Uzumeri (1982)	59
Figure 2-11	Model for the stress versus strain curve of confined concrete proposed by Mander <i>et al.</i> (1988b)	60
Figure 2-12	Model for the stress versus strain curve of confined concrete proposed by saatcioglu and Razvi (1992)	60
Figure 2-13	Model for the stress versus strain curve of confined Concrete proposed by Chung et al. (2002)	61
Figure 2-14	Model for the stress versus strain curve of confined concrete proposed by Légeron and Paultre (2003)	61
Figure 2-15	Model for the stress versus strain curve of confined concrete proposed by Fam and Rizkalla (2001)	62
Figure 2-16	Maximum unsupported length, L_u , for steel ties according to ACI 318-02	62
Figure 3-1	Column reinforcement details	98
Figure 3-2	Typical collars: (a) pre-test: (i) bolted collar; (ii) and welded welded collar (b) post-test: (i) deformed bolted collar; and weld fracture at corner of welded collar	99
Figure 3-3	Schematic of set-up for a typical column specimen	100
Figure 3-4	Views of typical column specimens in set-up with bolted; and welded collars in the test region	101
Figure 3-5	Stress versus strain curves for rebars	102
Figure 3-6	Stress versus strain curves for HSS and epoxy grout	102
Figure 3-7	Load versus displacement for column C00A	103
Figure 3-8	Load versus displacement for column C00B	103
Figure 3-9	Load versus displacement for column C01	104
Figure 3-10	Load versus displacement for column C02	104
Figure 3-11	Load versus displacement for column C03	105

Figure 3-12	Load versus displacement for column C04	105
Figure 3-13	Load versus displacement for column C05	106
Figure 3-14	Load versus displacement for column C06	106
Figure 3-15	Load versus displacement for column C07	107
Figure 3-16	Load versus displacement for column C08	107
Figure 3-17	Load versus displacement for column C09	108
Figure 3-18	Load versus displacement for all columns	108
Figure 3-19	Load versus average axial strain curves for column C00A	109
Figure 3-20	Load versus average axial strain curves for column C00B	109
Figure 3-21	Load versus average axial strain curves for column C01	110
Figure 3-22	Load versus average axial strain curves for column C02	110
Figure 3-23	Load versus average axial strain curves for column C03	111
Figure 3-24	Load versus average axial strain curves for column C04	111
Figure 3-25	Load versus average axial strain curves for column C05	112
Figure 3-26	Load versus average axial strain curves for column C06	112
Figure 3-27	Load versus average axial strain curves for column C08	113
Figure 3-28	Load versus average axial strain curves for column C09	113
Figure 3-29	Total load, concrete load, and steel load versus strain curves for column C00A	114
Figure 3-30	Total load, concrete load, and steel load versus strain curves for column C00B	114
Figure 3-31	Total load, concrete load, and steel load versus strain curves for column C01	115
Figure 3-32	Total load, concrete load, and steel load versus strain curves for column C02	115
Figure 3-33	Total load, concrete load, and steel load versus strain curves for column C03	116
Figure 3-34	Total load, concrete load, and steel load versus strain curves for column C04	116
Figure 3-35	Total load, concrete load, and steel load versus strain curves for column C05	117

Figure 3-36	Total load, concrete load, and steel load versus strain curves for column C06	117
Figure 3-37	Total load, concrete load, and steel load versus strain curves for column C07	118
Figure 3-38	Total load, concrete load, and steel load versus strain curves for column C08	118
Figure 3-39	Total load, concrete load, and steel load versus strain curves for column C09	119
Figure 3-40	Normalized concrete material curves	119
Figure 3-41	Appearance of columns at the end of tests	120
Figure 3-42	Column load versus tension in the collar bolts	121
Figure 3-43	Column load versus tension in the collar bolt for column C05	121
Figure 3-44	Column load versus strain of tie bars in the test region of column C00A	122
Figure 3-45	Column load versus strain of tie bars in the test region of column C00B	123
Figure 3-46a	Column load versus strain of collars (SG5 and SG6) for column C01	124
Figure 3-46b	Column load versus strain of collars (SG7 and SG8) for column C01	125
Figure 3-46c	Column load versus strain of collars (SG9 and SG10) for column C01	126
Figure 3-46d	Column load versus strain of collars (SG27 and SG28) for column C01	127
Figure 3-46e	Column load versus strain of collars (SG33 and SG34) for column C01	128
Figure 3-46f	Column load versus strain of collars (SG35 and SG36) for column C01	129
Figure 3-46g	Column load versus strain of bolts (SG17 and SG18) for column C01	130
Figure 3-46h	Column load versus strain of bolts (SG19 and SG20) for column C01	131
Figure 3-46i	Column load versus strain of bolts (SG29 and SG30) for column C01	132

Figure 3-46j	Column load versus strain of bolts (SG31 and SG32) for column C01	133
Figure 3-47a	Column load versus strain of collar (SG5 and SG6) for column C02	134
Figure 3-47b	Column load versus strain of collar (SG7 and SG8) for column C02	135
Figure 3-47c	Column load versus strain of collar (SG13 and SG14) for column C02	136
Figure 3-47d	Column load versus strain of collar (SG21 and SG22) for column C02	137
Figure 3-47e	Column load versus strain of collar (SG33 and SG34) for column C02	138
Figure 3-47f	Column load versus strain of collar (SG35 and SG36) for column C02	139
Figure 3-47g	Column load versus strain of bolt (SG17) for column C02	140
Figure 3-47h	Column load versus strain of bolts (SG19 and SG20) for column C02	141
Figure 3-47i	column load versus strain of bolt (SG29) for column C02	142
Figure 3-47j	Column load versus strain of bolts (SG31 and SG32) for column C02	143
Figure 3-48a	Column load versus strain of collar (SG7 and SG8) for column C04	144
Figure 3-48b	Column load versus strain of collar (SG15 and SG16) for column C04	145
Figure 3-48c	Column load versus strain of collar (SG27 and SG28) for column C04	146
Figure 3-48d	Column load versus strain of collar (SG33 and SG34) for column C04	147
Figure 3-48e	Column load versus strain of bolts (SG17 and SG18) for column C04	148
Figure 3-48f	Column load versus strain of bolts (SG19 and SG20) for column C04	149
Figure 3-48g	Column load versus strain of bolts (SG29 and SG30) for column C04	150

Figure 3-48h	Column load versus strain of bolts (SG31 and SG32) for column C04	151
Figure 3-49a	Column load versus strain of collar (SG6) for column C05	152
Figure 3-49b	Column load versus strain of collar (SG7) for column C05	153
Figure 3-49c	Column load versus strain of collar (SG8) for column C05	154
Figure 3-49d	Column load versus strain of collar (SG9) for column C05	155
Figure 3-49e	Column load versus strain of collar (SG10) for column C05	156
Figure 3-49f	Column load versus strain of collar (SG21) for column C05	157
Figure 3-49g	Column load versus strain of collar (SG22) for column C05	158
Figure 3-49h	Column load versus strain of bolt (SG17) for column C05	159
Figure 3-50a	Column load versus strain of collar (SG34 and SG35) for column C06	160
Figure 3-50b	Column load versus strain of collar (SG42 and SG43) for column C06	161
Figure 3-51a	Column load versus strain of collar (SG34) for column C07 (first loading)	162
Figure 3-51b	Column load versus strain of collar (SG35) for column C07 (first loading)	163
Figure 3-51c	Column load versus strain of collar (SG42) for column C07 (first loading)	164
Figure 3-51d	Column load versus strain of collar (SG43) for column C07 (first loading)	165
Figure 3-52	Column load versus strain of collar (SG36 and SG37) for column C09	166
Figure 4-1	Reinforcement details of columns CL0 to CL8	259
Figure 4-2	Photograph showing the detail of set-up for prestressing and Release of prestressing in the threaded rods	259

Figure 4-3	Photograph showing the reinforcement of a typical collared column with no splicing in the longitudinal bars of the column	260
Figure 4-4	Photograph showing three columns ready for pouring	260
Figure 4-5	Construction sealant applied at potential location of leakages	261
Figure 4-6	Loading scheme: (a) with long shear span; (b) with short shear span	261
Figure 4-7	A typical HSS collar with welded corner connections	262
Figure 4-8	Installation of HSS collars on the concrete columns	263
Figure 4-9	Stress versus strain curves for rebars, HSS, and epoxy grout	264
Figure 4-10	A typical stub column in the loading set-up	264
Figure 4-11	Deformed configuration of stub columns	265
Figure 4-12	Photograph of a typical column in test set-up	265
Figure 4-13	Photograph for showing assembly for horizontal loading	266
Figure 4-14(a)	Photograph showing the attachment of horizontal loading assembly to the column specimen	267
Figure 4-14(b)	Photograph showing the knife edge support and flat load cell for measuring vertical loads	267
Figure 4-15	Photograph showing cable transducers and LVDTs for measuring the rotation of collars	268
Figure 4-16	Photograph showing rotation meter for measuring the rotation of collars	268
Figure 4-17	Sequence of imposed horizontal displacements (adapted from Ghee <i>et al.</i> (1989))	269
Figure 4-18	Appearances of test region of specimen CL0 at different stages of test	270
Figure 4-19	Appearances of test region of specimen CL1 at different stages of the test	272
Figure 4-20	Appearances of test region of specimen CL2 at different stages of test	274
Figure 4-21	Appearances of test region of specimen CL3 at different stages of test	275

Figure 4-22	Appearances of test region of specimen CL4 at different stages of test	276
Figure 4-23	Appearances of test region of specimen CL5 at the test end of the test	377
Figure 4-24	Appearances of test region of specimen CL6 at different stages of test	278
Figure 4-25	A close-up of ruptured longitudinal bars of specimen CL6 at the end of test	279
Figure 4-26	Appearance of test region of specimen CL7 at different stages of test	280
Figure 4-27	Appearances of test region of specimen CL8 at different stages of test	281
Figure 4-28	Moment at column base versus lateral drift hysteresis for specimen CL0	282
Figure 4-29	Moment at column base versus lateral drift hysteresis for specimen CL1	282
Figure 4-30	Moment at column base versus lateral drift hysteresis for specimen CL2	283
Figure 4-31	Moment at column base versus lateral drift hysteresis for specimen CL3	283
Figure 4-32	Moment at column base versus lateral drift hysteresis for specimen CL4	284
Figure 4-33	Moment at column base versus lateral drift hysteresis for specimen CL5	284
Figure 4-34	Moment at column base versus lateral drift hysteresis for specimen CL6	285
Figure 4-35	Moment at column base versus lateral drift hysteresis for specimen CL7	285
Figure 4-36	Moment at column base versus lateral drift hysteresis for column CL8	286
Figure 4-37	Revised moment versus lateral drift hysteresis for column CL0	286
Figure 4-38	Revised moment versus lateral drift hysteresis for column CL1	287
Figure 4-39	Revised moment versus lateral drift hysteresis for column CL2	287

Figure 4-40	Revised moment versus lateral drift hysteresis for column CL3	288
Figure 4-41	Revised moment versus lateral drift hysteresis for column CL4	288
Figure 4-42	Revised moment versus lateral drift hysteresis for column CL5	289
Figure 4-43	Revised moment versus lateral drift hysteresis for column CL6	289
Figure 4-44	Revised moment versus lateral drift hysteresis for column CL7	290
Figure 4-45	Revised moment versus lateral drift hysteresis for column CL8	290
Figure 4-46	Envelope curves for specimen CL0 and CL1 (assumed projected part for CL1)	291
Figure 4-47	Envelope curves for specimen CL0 and CL2	291
Figure 4-48	Envelope curves for specimen CL0 and CL3	292
Figure 4-49	Envelope curves for specimen CL0 and CL4 (assumed projected part for CL4)	292
Figure 4-50	Envelope curves for specimen CL0 and CL5	293
Figure 4-51	Envelope curves for specimen CL0 and CL6	293
Figure 4-52	Envelope curves for specimen CL0 and CL7	294
Figure 4-53	Envelope curves for specimen CL0 and CL8	294
Figure 4-54	Peak moments of the columns from the average envelope curves	295
Figure 4-55	Normalized peak moments of the columns from the average envelope curves	295
Figure 4-56	Modulus of toughness for all the columns	296
Figure 4-57	Normalized modulus of toughness for all the specimens	296
Figure 4-58	Normalized secant stiffness versus lateral drift for specimens CL0 and CL1	297
Figure 4-59	Normalized secant stiffness versus lateral drift for specimens CL0 and CL2	297
Figure 4-60	Normalized secant stiffness versus lateral drift for specimens CL0 and CL3	298

Figure 4-61	Normalized secant stiffness versus lateral drift for specimens CL0 and CL4	298
Figure 4-62	Normalized secant stiffness versus lateral drift for specimens CL0 and CL5	299
Figure 4-63	Normalized secant stiffness versus lateral drift for specimens CL0 and CL6	299
Figure 4-64	Normalized secant stiffness versus lateral drift for specimens CL0 and CL7	300
Figure 4-65	Normalized secant stiffness versus lateral drift for specimens CL0 and CL8	300
Figure 4-66	Energy absorbed by specimen CL0 per cycle based on overall system	301
Figure 4-67	Energy absorbed by specimen CL1 per cycle based on overall system	301
Figure 4-68	Energy absorbed by specimen CL2 per cycle based on overall system	302
Figure 4-69	Energy absorbed by specimen CL3 per cycle based on overall system	302
Figure 4-70	Energy absorbed by specimen CL4 per cycle based on overall system	303
Figure 4-71	Energy absorbed by specimen CL5 per cycle based on overall system	303
Figure 4-72	Energy absorbed by specimen CL6 per cycle based on overall system	304
Figure 4-73	Energy absorbed by specimen CL7 per cycle based on overall system	304
Figure 4-74	Energy absorbed by specimen CL8 per cycle based on overall system	305
Figure 4-75(a)	Cumulative energy dissipated versus cycle number for specimens CL1 and CL0 based on overall system	306
Figure 4-75(b)	Normalized cumulative energy dissipated versus cycle number for specimens CL1 and CL0 based on overall system	306
Figure 4-76(a)	Cumulative energy dissipated versus cycle number for specimens CL2 and CL0 based on overall system	307

Figure 4-76(b)	Normalized cumulative energy dissipated versus cycle number for specimens CL2 and CL0 based on overall system	307
Figure 4-77(a)	Cumulative energy dissipated versus cycle number for specimens CL3 and CL0 based on overall system	308
Figure 4-77(b)	Normalized cumulative energy dissipated versus cycle number for specimens CL3 and CL0 based on overall system	308
Figure 4-78(a)	Cumulative energy dissipated versus cycle number for specimens CL4 and CL0 based on overall system	309
Figure 4-78(b)	Normalized cumulative energy dissipated versus cycle number for specimens CL4 and CL0 based on overall system	309
Figure 4-79(a)	Cumulative energy dissipated versus cycle number for specimens CL5 and CL0 based on overall system	310
Figure 4-79(b)	Normalized cumulative energy dissipated versus cycle number for specimens CL5 and CL0 based on overall system	310
Figure 4-80(a)	Cumulative energy dissipated versus cycle number for specimens CL6 and CL0 based on overall system	311
Figure 4-80(b)	Normalized cumulative energy dissipated versus cycle number for specimens CL6 and CL0 based on overall system	311
Figure 4-81(a)	Cumulative energy dissipated versus cycle number for specimens CL0 and CL7 based on overall system	312
Figure 4-81(b)	Normalized cumulative energy dissipated versus cycle number for specimens CL7 and CL0 based on overall system	312
Figure 4-82(a)	Cumulative energy dissipated versus cycle number for specimens CL8 and CL0 based on overall system	313
Figure 4-82(b)	Normalized cumulative energy dissipated versus cycle number for specimens CL8 and CL0 based on overall system	313
Figure 4-83	Hysteretic damping ratio versus lateral drift for specimens CL1 and CL0	314
Figure 4-84	Hysteretic damping ratio versus lateral drift for specimens CL2 and CL0	314
Figure 4-85	Hysteretic damping ratio versus lateral drift for specimens CL3 and CL0	315
Figure 4-86	Hysteretic damping ratio versus lateral drift for specimens CL4 and CL0	315
Figure 4-87	Hysteretic damping ratio versus lateral drift for specimens CL5 and CL0	316
Figure 4-88	Hysteretic damping ratio versus lateral drift for specimens CL6 and CL0	316

Figure 4-89	Hysteretic damping ratio versus lateral drift for specimens CL7 and CL0	317
Figure 4-90	Hysteretic damping ratio versus lateral drift for specimens CL8 and CL0	317
Figure 4-91	Curvature distribution in the test region of column CL1 at different levels of displacement ductility	318
Figure 4-92	Curvature distribution in the test region of column CL2 at different levels of displacement ductility	318
Figure 4-93	Curvature distribution in the test region of column CL3 at different levels of displacement ductility	319
Figure 4-94	Curvature distribution in the test region of column CL4 at different levels of displacement ductility	319
Figure 4-95	Curvature distribution in the test region of column CL5 at different levels of displacement ductility	320
Figure 4-96	Curvature distribution in the test region of column CL6 at different levels of displacement ductility	320
Figure 4-97	Curvature distribution in the test region of column CL7 at different levels of displacement ductility	321
Figure 4-98	Curvature distribution in the test region of column CL8 at different levels of displacement ductility	321
Figure 4-99	Definition of various terms in ductility parameters (adapted from Sheikh and Houry (1993))	322
Figure 4-100	Curvature ductility, μ_{φ} , for column CL0	322
Figure 4-101	Curvature ductility, μ_{φ} , for column CL1	323
Figure 4-102	Curvature ductility, μ_{φ} , for column CL2	323
Figure 4-103	Curvature ductility, μ_{φ} , for column CL3	324
Figure 4-104	Curvature ductility, μ_{φ} , for column CL4	324
Figure 4-105	Curvature ductility, μ_{φ} , for column CL5	325
Figure 4-106	Curvature ductility, μ_{φ} , for column CL6	325

Figure 4-107	Curvature ductility, μ_{φ} , for column CL7	326
Figure 4-108	Curvature ductility, μ_{φ} , for column CL8	326
Figure 4-109	Cumulative ductility ratio for column CL0 and CL1	327
Figure 4-110	Cumulative ductility ratio for column CL0 and CL2	327
Figure 4-111	Cumulative ductility ratio for column CL0 and CL3	328
Figure 4-112	Cumulative ductility ratio for column CL0 and CL4	328
Figure 4-113	Cumulative ductility ratio for column CL0 and CL5	329
Figure 4-114	Cumulative ductility ratio for column CL0 and CL6	329
Figure 4-115	Cumulative ductility ratio for column CL0 and CL7	330
Figure 4-116	Cumulative ductility ratio for column CL0 and CL8	330
Figure 4-117	Cumulative energy damage indicator for CL0 and CL1	331
Figure 4-118	Cumulative energy damage indicator for CL0 and CL2	331
Figure 4-119	Cumulative energy damage indicator for CL0 and CL3	332
Figure 4-120	Cumulative energy damage indicator for CL0 and CL4	332
Figure 4-121	Cumulative energy damage indicator for CL0 and CL5	333
Figure 4-122	Cumulative energy damage indicator for CL0 and CL6	333
Figure 4-123	Cumulative energy damage indicator for CL0 and CL7	334
Figure 4-124	Cumulative energy damage indicator for CL0 and CL8	334
Figure 4-125	Moment at column base versus lateral drift (%) envelope curves for column CL1 and CL3	335
Figure 4-126	Relationship between normalized secant stiffness and lateral drift (%) for column CL1 and CL3	335
Figure 4-127	Cumulative energy dissipated based on overall system versus cycle number for columns CL1 and CL3	336
Figure 4-128	Cumulative normalized dissipated energy based on overall system versus cycle number for columns CL1 and CL3	336

Figure 4-129	Hysteretic damping versus lateral drift (%) for columns CL1 and CL3	337
Figure 4-130	Cumulative ductility ratio versus cycle number for columns CL1 and CL3	337
Figure 4-131	Cumulative energy damage indicator versus cycle number for columns CL1 and CL3	338
Figure 4-132	Moment at column base versus lateral drift (%) envelope curves for column CL5 and CL7	338
Figure 4-133	Relationship between normalized secant stiffness and lateral drift (%) for column CL5 and CL7	339
Figure 4-134	Cumulative energy dissipated based on overall system versus cycle number for columns CL5 and CL7	339
Figure 4-135	Cumulative normalized dissipated energy based on overall system versus cycle number for columns CL5 and CL7	340
Figure 4-136	Hysteretic damping versus lateral drift (%) for columns CL5 and CL7	340
Figure 4-137	Cumulative ductility ratio versus cycle number for columns CL5 and CL7	341
Figure 4-138	Cumulative energy damage indicator versus cycle number for columns CL5 and CL7	341
Figure 4-139	Moment at column base versus lateral drift (%) envelope curves for column CL2 and CL3	342
Figure 4-140	Relationship between normalized secant stiffness and lateral drift (%) for column CL2 and CL3	342
Figure 4-141	Cumulative energy dissipated based on overall system versus cycle number for columns CL2 and CL3	343
Figure 4-142	Cumulative normalized dissipated energy based on overall system versus cycle number for columns CL2 and CL3	343
Figure 4-143	Hysteretic damping versus lateral drift (%) for columns CL2 and CL3	344
Figure 4-144	Cumulative ductility ratio versus cycle number for columns CL2 and CL3	344
Figure 4-145	Cumulative energy damage indicator versus cycle number for columns CL2 and CL3	345

Figure 4-146	Moment at column base versus lateral drift (%) envelope curves for column CL6 and CL7	345
Figure 4-147	Relationship between normalized secant stiffness and lateral drift (%) for column CL6 and CL7	346
Figure 4-148	Cumulative energy dissipated based on overall system versus cycle number for columns CL6 and CL7	346
Figure 4-149	Cumulative normalized dissipated energy based on overall system versus cycle number for columns CL6 and CL7	347
Figure 4-150	Hysteretic damping versus lateral drift (%) for columns CL6 and CL7	347
Figure 4-151	Cumulative ductility ratio versus cycle number for columns CL6 and CL7	348
Figure 4-152	Cumulative energy damage indicator versus cycle number for columns CL6 and CL7	348
Figure 4-153	Moment at column base versus lateral drift (%) envelope curves for column CL3 and CL4	349
Figure 4-154	Relationship between normalized secant stiffness and lateral drift (%) for column CL3 and CL4	349
Figure 4-155	Cumulative energy dissipated based on overall system versus cycle number for columns CL3 and CL4	350
Figure 4-156	Cumulative normalized dissipated energy based on overall system versus cycle number for columns CL3 and CL4	350
Figure 4-157	Hysteretic damping versus lateral drift (%) for columns CL3 and CL4	351
Figure 4-158	Cumulative ductility ratio versus cycle number for columns CL3 and CL4	351
Figure 4-159	Cumulative energy damage indicator versus cycle number for columns CL3 and CL4	352
Figure 4-160	Moment at column base versus lateral drift (%) envelope curves for column CL7 and CL8	352
Figure 4-161	Relationship between normalized secant stiffness and lateral drift (%) for column CL7 and CL8	353
Figure 4-162	Cumulative energy dissipated based on overall system versus cycle number for columns CL7 and CL8	353

Figure 4-163	Cumulative normalized dissipated energy based on overall system versus cycle number for columns CL7 and CL8	354
Figure 4-164	Hysteretic damping versus lateral drift (%) for columns CL7 and CL8	354
Figure 4-165	Cumulative ductility ratio versus cycle number for columns CL7 and CL8	355
Figure 4-166	Cumulative energy damage indicator versus cycle number for columns CL7 and CL8	355
Figure 4-167	Moment at column base versus lateral drift (%) envelope curves for column CL1 and CL5	356
Figure 4-168	Relationship between normalized secant stiffness and lateral drift (%) for column CL1 and CL5	356
Figure 4-169	Cumulative energy dissipated based on overall system versus cycle number for columns CL1 and CL5	357
Figure 4-170	Cumulative normalized dissipated energy based on overall system versus cycle number for columns CL1 and CL5	357
Figure 4-171	Hysteretic damping versus lateral drift (%) for columns CL1 and CL5	358
Figure 4-172	Cumulative ductility ratio versus cycle number for columns CL1 and CL5	358
Figure 4-173	Cumulative energy damage indicator versus cycle number for columns CL1 and CL5	359
Figure 4-174	Moment at column base versus lateral drift (%) envelope curves for column CL2 and CL6	359
Figure 4-175	Relationship between normalized secant stiffness and lateral drift (%) for column CL2 and CL6	360
Figure 4-176	Cumulative energy dissipated based on overall system versus cycle number for columns CL2 and CL6	360
Figure 4-177	Cumulative normalized dissipated energy based on overall system versus cycle number for columns CL2 and CL6	361
Figure 4-178	Hysteretic damping versus lateral drift (%) for columns CL2 and CL6	361
Figure 4-179	Cumulative ductility ratio versus cycle number for columns CL2 and CL6	362

Figure 4-180	Cumulative energy damage indicator versus cycle number for columns CL2 and CL6	362
Figure 4-181	Moment at column base versus lateral drift (%) envelope curves for column CL3 and CL7	363
Figure 4-182	Relationship between normalized secant stiffness and lateral drift (%) for column CL3 and CL7	363
Figure 4-183	Cumulative energy dissipated based on overall system versus cycle number for columns CL3 and CL7	364
Figure 4-184	Cumulative normalized dissipated energy based on overall system versus cycle number for columns CL3 and CL7	364
Figure 4-185	Hysteretic damping versus lateral drift (%) for columns CL3 and CL7	365
Figure 4-186	Cumulative ductility ratio versus cycle number for columns CL3 and CL7	365
Figure 4-187	Cumulative energy damage indicator versus cycle number for columns CL3 and CL7	366
Figure 4-188	Moment at column base versus lateral drift (%) envelope curves for column CL4 and CL8	366
Figure 4-189	Relationship between normalized secant stiffness and lateral drift (%) for column CL4 and CL8	367
Figure 4-190	Cumulative energy dissipated based on overall system versus cycle number for columns CL4 and CL8	367
Figure 4-191	Cumulative normalized dissipated energy based on overall system versus cycle number for columns CL4 and CL8	368
Figure 4-192	Hysteretic damping versus lateral drift (%) for columns CL4 and CL8	368
Figure 4-193	Cumulative ductility ratio versus cycle number for columns CL4 and CL8	369
Figure 4-194	Cumulative energy damage indicator versus cycle number for columns CL4 and CL8	369
Figure 4-195	A model column along with a typical curvature distribution diagram	370
Figure 4-196	Confined concrete material curve for column CL0 obtained by model proposed by Mander <i>et al</i> (1988b)	370
Figure 4-197	Confined concrete material curve for collared columns (CL1 to CL8)	371

Figure 4-198	Analytical moment versus curvature relationship for column CL1	371
Figure 4-199	Predicted and experimental average envelope curves for column CL0	372
Figure 4-200	Predicted and experimental average envelope curves for column CL0 (enlarge view)	372
Figure 4-201	Predicted and experimental average envelope curves for column CL1	373
Figure 4-202	Predicted and experimental average envelope curves for column CL2	373
Figure 4-203	Predicted and experimental average envelope curves for column CL3	374
Figure 4-204	Predicted and experimental average envelope curves for column CL4	374
Figure 4-205	Predicted and experimental average envelope curves for column CL5	375
Figure 4-206	Predicted and experimental average envelope curves for column CL6	375
Figure 4-207	Predicted and experimental average envelope curves for column CL7	376
Figure 4-208	Predicted and experimental average envelope curves for column CL8	376
Figure 5-1	Prediction of confined concrete material curve for column C06 by existing confinement model	415
Figure 5-2	Plan and elevation of a typical finite element model for an externally confined column	416
Figure 5-3	Concrete material curves with modified descending branches	416
Figure 5-4	Effect of concrete material curves on the confining pressure versus lateral strain curve of collars of column C01	417
Figure 5-5	Effect of concrete material curve on the confining pressure versus lateral strain curve of collars of column C06	417
Figure 5-6	Confined concrete material curves for column C06	418
Figure 5-7	Column load versus axial strain for column C06	418

Figure 5-8	A typical behavioural curve of steel collars	419
Figure 5-9	Proposed material curve for concrete confined externally by steel collars	419
Figure 5-10	Discrete and smeared collars on a concrete prism under different stresses	420
Figure 5-11	A typical confining pressure versus lateral strain curve	420
Figure 5-12	Unconfined concrete: (a) between tie levels; (b) at tie level; (c) between HSS collars; and (d) HSS collar level (fully confined)	421
Figure 5-13	A typical relationship between confining pressure versus lateral strain with confining pressure consisting of active and passive components	421
Figure 5-14	Behaviour of spalling concrete in column C01	422
Figure 5-15	Slope of descending branch of column C01	422
Figure 5-16	Slope of descending branch of column C02	423
Figure 5-17	Slope of descending branch of column C03	423
Figure 5-18	Slope of descending branch of column C04	424
Figure 5-19	Idealized stress versus strain curve for column C01	424
Figure 5-20	Idealized stress versus strain curve for column C02	425
Figure 5-21	Idealized stress versus strain curve for column C03	425
Figure 5-22	Idealized stress versus strain curve for column C04	426
Figure 5-23	Relationship between α and ω	426
Figure 5-24	Relationship between β and ω	427
Figure 5-25	Confining pressure versus lateral strain curves for collars with bolted corner connections (phase 1)	427
Figure 5-26	Confining pressure versus lateral strain curves for collars with welded corner connections (phase 1)	428
Figure 5-27	Confining pressure versus lateral strain curves for column CL1 to CL8 (phase 2)	428
Figure 5-28	Confining pressure versus axial strain for column C01	429
Figure 5-29	Confining pressure versus axial strain for column C02	429

Figure 5-30	Confining pressure versus axial strain for column C03	430
Figure 5-31	Confining pressure versus axial strain for column C04	430
Figure 5-32	Confining pressure versus axial strain for column C05	431
Figure 5-33	Confining pressure versus axial strain for column C06	431
Figure 5-34	Confining pressure versus axial strain for column C07	432
Figure 5-35	Confining pressure versus axial strain for column C08	432
Figure 5-36	Confining pressure versus axial strain for column C09	433
Figure 5-37	Confined concrete material curve for reduced cores in the phase 1 columns with bolted collars	433
Figure 5-38	Confined concrete material curve for reduced cores in the phase 1 columns with welded collars	434
Figure 5-39	Confined concrete material curves for reduced cores in the phase 2 columns CL1 and CL8	434
Figure 5-40	Confined concrete material curves of columns C01 to C09	435
Figure 5-41	Confined concrete material curves of columns CL1 and CL8	435
Figure 5-42	Stress versus strain for 20 mm diameter vertical bars of phase 1 columns	436
Figure 5-43	Stress versus strain curves of 25 mm diameter vertical bars of phase 2 columns	436
Figure 5-44	Load versus strain curves for column C01	437
Figure 5-45	Load versus strain curves for column C02	437
Figure 5-46	Load versus strain curves for column C03	438
Figure 5-47	Load versus strain curves for column C04	438
Figure 5-48	Load versus strain curves for column C05	439
Figure 5-49	Load versus strain curves for column C06	439
Figure 5-50	Load versus strain curves for column C07	440
Figure 5-51	Load versus strain curves for column C08	440

Figure 5-52	Load versus strain curves for column C09	441
Figure 5-53	Load versus strain curves for column CL1	441
Figure 5-54	Load versus strain curves for column CL2	442
Figure 5-55	Load versus strain curves for column CL3	442
Figure 5-56	Load versus strain curves for column CL4	443
Figure 5-57	Load versus strain curves for column CL5	443
Figure 5-58	Load versus strain curves for column CL6	444
Figure 5-59	Load versus strain curves for column CL7	444
Figure 5-60	Load versus strain curves for column CL8	445
5		
Figure 6-1	Confinement mechanism	539
Figure 6-2	(a) Typical confining stress versus lateral strain curves; (b) Relationship between β_7 and β_8	539
Figure 6-3	Unconfined concrete: (a) between tie levels; (b) at tie levels; (c) between HSS collars; and (d) at HSS collar level (fully confined)	540
Figure 6-4	Plan and elevation of a typical finite element model for a column confined externally by steel collars	540
Figure 6-5	Concrete material curves with modified descending branch	541
Figure 6-6	(a) Calibration of Ramberg-Osgood model; (b) Variation of n keeping f_y and E_s constant; and (c) variation of f_y and E_s such that their ratio remains constant at constant value of n	541
Figure 6-7	HSS steel material curves: (a) having different values of f_y and E_s and n constant; and (b) having different values of E_s keeping f_y and n constant	542
Figure 6-8	(a) Average confining pressure on elements versus average lateral strain; (b) distribution of confining stress along the width of the column	543
Figure 6-9	The dimensionless parameters independent of scale effect	544

Figure 6-10	Effect of β_1 on the confining behaviour	544
Figure 6-11	Relationship between: (a) λ_1 and β_1 ; and (b) γ_1 and β_1	545
Figure 6-12	Effect of variation of β_2 on the confining behaviour	545
Figure 6-13	Relationship between: (a) λ_2 and β_2 ; and (b) γ_2 and β_2	546
Figure 6-14	Effect of variation of β_3 on the confining behaviour	546
Figure 6-15	Relationship between: (a) λ_3 and β_3 ; and (b) γ_3 and β_3	547
Figure 6-16	Effect of variation of β_4 on the confining behaviour	547
Figure 6-17	Relationship between λ_4 and β_4	548
Figure 6-18	Effect of variation of f_y and E_s such that β_5 remains constant	548
Figure 6-19	Effect of variation of f_y keeping E_s constant on the confining behaviour	549
Figure 6-20	Relationship between λ_5 and β_5	549
Figure 6-21	Effect of change of modulus of elasticity E_s on the confining behaviour keeping f_y constant	550
Figure 6-22	Relationship between λ'_5 and β'_5	550
Figure 6-23	Effect of β_6 on the confining behaviour of HSS collars	551
Figure 6-24	Relationship between β_6 and λ_6 for HSS collars	551
Figure 6-25	Effect of collar smearing on the confining behaviour of collars	552
Figure 6-26	Relationship between λ_s and β_3	552
Figure 6-27	Confinement stress versus lateral strain curves for case 1 (Table 6-20)	553
Figure 6-28	Confinement stress versus lateral strain curves for case 2 (Table 6-20)	553

Figure 6-29	Confinement stress versus lateral strain curves for case 3 (Table 6-20)	554
Figure 6-30	Confinement stress versus lateral strain curves for case 4 (Table 6-20)	554
Figure 6-31	Confinement stress versus lateral strain curves for case 5 (Table 6-20)	555
Figure 6-32	Confinement stress versus lateral strain curves for case 6 (Table 6-20)	555
Figure 6-33	Confinement stress versus lateral strain curves for case 7 (Table 6-20)	556
Figure 6-34	Confinement stress versus lateral strain curves for case 8 (Table 6-20)	556
Figure 6-35	Confinement stress versus lateral strain curves for case 9 (Table 6-20)	557
Figure 6-36	Confinement stress versus lateral strain curves for case 10 (Table 6-20)	557
Figure 6-37	Confinement stress versus lateral strain curves for case 11 (Table 6-20)	558
Figure 6-38	Confinement stress versus lateral strain curves for case 12 (Table 6-20)	558
Figure 6-39	Confinement stress versus lateral strain curves for case 13 (Table 6-20)	559
Figure 6-40	Confinement stress versus lateral strain curves for case 14 (Table 6-20)	559
Figure 6-41	Stress versus strain curve for HSS 51 x 51 x 6.35 mm	560
Figure 6-42	Confinement stress versus lateral strain curves for column C06	560
Figure 6-43	Load versus strain curves for column C06	561
Figure 6-44	Stress versus strain curve for HSS 76x51x6.35 mm	561
Figure 6-45	Confinement stress versus lateral strain curves for column C09	562
Figure 6-46	Load versus strain curves of column C09	562
Figure 6-47	Effect of scale on the confining behaviour of solid collars	563
Figure 6-48	Effect of variation of β_1 on the confining behaviour of solid collars	563

Figure 6-49	Relationship between λ_1 and β_1 for β_1 ranges: (a) $\beta_1 = 0.004$ to 0.024 ; and (b) $\beta_1 = 0.024$ to 0.056	564
Figure 6-50	Relationship between γ_1 and β_1 for β_1 ranges: (a) $\beta_1 = 0.004$ to 0.024 ; and (b) $\beta_1 = 0.024$ to 0.056	564
Figure 6-51	Effect of variation of β_2 on the confining behaviour of solid collars	565
Figure 6-52	Relationship between λ_2 and β_2 for β_2 ranges: (a) $\beta_2 = 0.000096$ to 0.00288 ; and (b) 0.00288 to 0.0192	565
Figure 6-53	Relationship between γ_2 and β_2 for β_2 ranges: (a) $\beta_2 = 0.000096$ to 0.00288 ; and (b) $\beta_1 = 0.00288$ to 0.0192	566
Figure 6-54	Effect of variation of β_3 on the confining behaviour of solid collars	566
Figure 6-55	Relationship between: (a) λ_3 and β_3 and (b) γ_3 and β_3 for solid collars	567
Figure 6-56	Effect of variation of β_5 on the confining behaviour of solid collars	567
Figure 6-57	Relationship between λ_5 and β_5 for solid collars	568
Figure 6-58	Effect of variation of β'_5 on the confining behaviour of solid collars	568
Figure 6-59	Relationship between γ'_5 and β'_5 for solid collars	569
Figure 6-60	Effect of variation of β_6 on the confining behaviour of solid collars	569
Figure 6-61	Relationship between λ_6 and β_6 for solid collars	570
Figure 6-62	Effect of smearing on the confining behaviour of solid collars	570
Figure 6-63	Relationship between λ_s and β_3 for solid collars	571
Figure 6-64	Confinement stress versus lateral strain curve for case 1 (Table 6.35)	571
Figure 6-65	Confinement stress versus lateral strain curve for case 2 (Table 6.35)	572
Figure 6-66	Confinement stress versus lateral strain curve for case 3 (Table 6.35)	572
Figure 6-67	Confinement stress versus lateral strain curve for case 4 (Table 6.35)	573

Figure 6-68	Confinement stress versus lateral strain curve for case 5 (Table 6.35)	573
Figure 6-69	Confinement stress versus lateral strain curve for case 6 (Table 6.35)	574
Figure 6-70	Confinement stress versus lateral strain curve for case 7 (Table 6.35)	574
Figure 6-71	Confinement stress versus lateral strain curve for case 8 (Table 6.35)	575
Figure 6-72	Confinement stress versus lateral strain curve for case 9 (Table 6.35)	575
Figure 6-73	Confinement stress versus lateral strain curve for case 10 (Table 6.35)	576
Figure 7-1	Plan and elevation of new solid steel collars having two diagonally opposite corners with bolted connection and the remaining two corners with continuous connection	591
Figure 7-2	Elevation of test frame	592
Figure A-1	Confining pressure for circular columns	598
Figure A-2	Confining pressure for rectangular columns	598
Figure C-1	Effect of strength of concrete on M_{nuc} and M_{yuc} of a singly reinforced section	610
Figure C-2	Effect of strength of concrete on the ratio of M_{yuc} to M_{nuc} of a singly reinforced concrete section	610
Figure D-1	Location of strain gages on the longitudinal bars of columns (collars not shown for clarity)	617
Figure D-2	Moment at column base versus longitudinal bar strains for column CL0	618
Figure D-3	Moment at column base versus strains of tie bars for column CL0	619
Figure D-4	Moment at column base versus longitudinal bar strains for column CL1	620
Figure D-5	Moment at column base versus longitudinal bar strains for column CL2	621
Figure D-6	Moment at column base versus longitudinal bar strains for column CL3	622
Figure D-7	Moment at column base versus longitudinal bar strains for column CL4	623

Figure D-8	Moment at column base versus longitudinal bar strains for column CL5	624
Figure D-9	Moment at column base versus longitudinal bar strains for column CL6	625
Figure D-10	Moment at column base versus longitudinal bar strains for column CL7	626
Figure D-11	Moment at column base versus longitudinal bar strains for column CL8	627
Figure E-1	Envelopes to moment versus lateral drift hysteresis for column CL0	628
Figure E-2	Envelopes to moment versus lateral drift hysteresis for specimen CL1	628
Figure E-3	Envelopes to moment versus lateral drift hysteresis for specimen CL2	629
Figure E-4	Envelopes to moment versus lateral drift hysteresis for specimen CL3	629
Figure E-5	Envelopes to moment versus lateral drift hysteresis for specimen CL4	630
Figure E-6	Envelopes to moment versus lateral drift hysteresis for specimen CL5	630
Figure E-7	Envelopes to moment versus lateral drift hysteresis for specimen CL6	631
Figure E-8	Envelopes to moment versus lateral drift hysteresis for specimen CL7	631
Figure E-9	Envelopes to moment versus lateral drift hysteresis for specimen CL8	632
Figure F-1	Determination of yield displacement for column CL0 using the first cycle (method 1 (alternative 2))	633
Figure F-2	Determination of yield displacement for column CL1 using the first cycle (method 1 (alternative 2))	633
Figure F-3	Determination of yield displacement for column CL2 using the first cycle (method 1 (alternative 2))	634
Figure F-4	Determination of yield displacement for column CL3 using the first cycle (method 1 (alternative 2))	634

Figure F-5	Determination of yield displacement for column CL4 using the first cycle (method 1 (alternative 2))	635
Figure F-6	Determination of yield displacement for column CL5 using the first cycle (method 1 (alternative 2))	635
Figure F-7	Determination of yield displacement for column CL6 using the first cycle (method 1 (alternative 2))	636
Figure F-8	Determination of yield displacement for column CL7 using the first cycle (method 1 (alternative 2))	636
Figure F-9	Determination of yield displacement for column CL8 using the first cycle (method 1 (alternative 2))	637
Figure F-10	Determination of yield displacement for column CL0 using average envelope (method 1 (alternative 3))	637
Figure F-11	Determination of yield displacement for column CL1 using average envelope (method 1 (alternative 3))	638
Figure F-12	Determination of yield displacement for column CL2 using average envelope (method 1 (alternative 3))	638
Figure F-13	Determination of yield displacement for column CL3 using average envelope (method 1 (alternative 3))	639
Figure F-14	Determination of yield displacement for column CL4 using average envelope (method 1 (alternative 3))	639
Figure F-15	Determination of yield displacement for column CL5 using average envelope (method 1 (alternative 3))	640
Figure F-16	Determination of yield displacement for column CL6 using average envelope (method 1 (alternative 3))	640
Figure F-17	Determination of yield displacement for column CL7 using average envelope (method 1 (alternative 3))	641
Figure F-18	Determination of yield displacement for column CL8 using average envelope (method 1 (alternative 3))	641
Figure F-19	Determination of yield displacement for column CL0 using average envelope (method 1 (alternative 4))	642
Figure F-20	Determination of yield displacement for column CL1 using average envelope (method 1 (alternative 4))	642
Figure F-21	Determination of yield displacement for column CL2 using average envelope (method 1 (alternative 4))	643

Figure F-22	Determination of yield displacement for column CL3 using average envelope (method 1 (alternative 4))	643
Figure F-23	Determination of yield displacement for column CL4 using average envelope (method 1 (alternative 4))	644
Figure F-24	Determination of yield displacement for column CL5 using average envelope (method 1 (alternative 4))	644
Figure F-25	Determination of yield displacement for column CL6 using average envelope (method 1 (alternative 4))	645
Figure F-26	Determination of yield displacement for column CL7 using average envelope (method 1 (alternative 4))	645
Figure F-27	Determination of yield displacement for column CL8 using average envelope (method 1 (alternative 4))	646
Figure F-28	Determination of yield displacement for column CL0 using average envelope (method 1 (alternative 5))	646
Figure F-29	Determination of yield displacement for column CL1 using average envelope (method 1 (alternative 5))	647
Figure F-30	Determination of yield displacement for column CL2 using average envelope (method 1 (alternative 5))	647
Figure F-31	Determination of yield displacement for column CL3 using average envelope (method 1 (alternative 5))	648
Figure F-32	Determination of yield displacement for column CL4 using average envelope (method 1 (alternative 5))	648
Figure F-33	Determination of yield displacement for column CL5 using average envelope (method 1 (alternative 5))	649
Figure F-34	Determination of yield displacement for column CL6 using average envelope (method 1 (alternative 5))	649
Figure F-35	Determination of yield displacement for column CL7 using average envelope (method 1 (alternative 5))	650
Figure F-36	Determination of yield displacement for column CL8 using average envelope (method 1 (alternative 5))	650
Figure F-37	Determination of yield displacement for column CL0 using using area equalization method (case 1)	651
Figure F-38	Determination of yield displacement for column CL0 using using area equalization method (case 2)	651

Figure F-39	Determination of yield displacement for column CL0 using using area equalization method (case 3)	652
Figure F-40	Determination of yield displacement for column CL1 using using area equalization method	652
Figure F-41	Determination of yield displacement for column CL2 using using area equalization method	653
Figure F-42	Determination of yield displacement for column CL3 using using area equalization method	653
Figure F-43	Determination of yield displacement for column CL4 using using area equalization method	654
Figure F-44	Determination of yield displacement for column CL5 using using area equalization method	654
Figure F-45	Determination of yield displacement for column CL6 using using area equalization method	655
Figure F-46	Determination of yield displacement for column CL7 using using area equalization method	655
Figure F-47	Determination of yield displacement for column CL8 using using area equalization method	656
Figure H-1	Distribution of energy absorption mechanism in specimen CL1	682
Figure H-2	Distribution of energy absorption mechanism in specimen CL2	682
Figure H-3	Distribution of energy absorption mechanism in specimen CL3	683
Figure H-4	Distribution of energy absorption mechanism in specimen CL4	683
Figure H-5	Distribution of energy absorption mechanism in specimen CL5	684
Figure H-6	Distribution of energy absorption mechanism in specimen CL6	684
Figure H-7	Distribution of energy absorption mechanism in specimen CL7	685
Figure H-8	Distribution of energy absorption mechanism in specimen CL8	685
Figure I-1	Moment versus curvature hysteresis for column CL0	686
Figure I-2	Moment versus curvature hysteresis for column CL1	686
Figure I-3	Moment versus curvature hysteresis for column CL2	687
Figure I-4	Moment versus curvature hysteresis for column CL3	687

Figure I-5	Moment versus curvature hysteresis for column CL4	688
Figure I-6	Moment versus curvature hysteresis for column CL5	688
Figure I-7	Moment versus curvature hysteresis for column CL6	689
Figure I-8	Moment versus curvature hysteresis for column CL7	689
Figure I-9	Moment versus curvature hysteresis for column CL8	690

NOTATION

a	=	shear-span;
a	=	a coefficient in Ramberg-Osgood model;
a_s	=	a factor to account for collar smearing;
A_1 to A_m	=	variables of a physical problem;
A_c	=	$A_c = A_g - A_{st}$; area of the concrete in the gross column cross-section;
A_{ch}	=	cross-sectional area measured out-to-out of the transverse reinforcement;
A_{co}	=	area of core bounded by centreline of perimeter ties for conventional columns;
	=	gross area of the column for collared columns;
A_{collar}	=	area of cross section of a side of collar;
A_g	=	gross area of the section;
A_{rcc}	=	area of the reduced concrete core due to spalling of concrete cover and parabolic spalling between ties;
A_{sh}	=	total cross-sectional area of transverse reinforcement (including crossties) within spacing S and perpendicular to dimension h_c ($= 2 \times A_{tie}$);
A_{sp}	=	cross-sectional area of the spiral;
A_{spc}	=	cross-sectional area of the spalling concrete in column core;
A_{st}	=	cross-sectional area of longitudinal bars of column;
A_{tie}	=	cross-sectional area of one leg of the hoop reinforcement;
c	=	distance from extreme compression fiber to the neutral axis of section;

- d = distance from the centroid of the tensile steel to the extreme compression face of the column;
- d' = distance from the compression face of concrete to the reinforcing bars in compression;
- d_b = diameter of longitudinal bars of columns;
- d_c = diameter of concrete core measured out-to-out of spiral;
- d_s = diameter of spiral steel;
- d_e = distance between the centroid of tensile and compressive longitudinal bars of a columns;
- e_i = area of i th moment versus curvature loop;
- E_e = maximum elastic strain energy;
- E_i = energy dissipated in i th loop of column under lateral cyclic loading;
- E_N = cumulative normalized energy dissipated under lateral cyclic loading;
- E_c = secant modulus of elasticity of unconfined concrete;
- $(E_{ct})_i$ = the slope of an i th secant line to average confining pressure versus lateral strain curve of equivalent confining tube;
- E_{ct} = the slope of a general secant line to average confining pressure versus lateral strain curve of equivalent confining tube;

- $(E_c)_i$ = slope of an *ith* secant line corresponding to a general point *i* on the confined concrete material curve; $(E_c)_i = \frac{(f_{cc})_i}{(\varepsilon_{cc})_i}$;
- E_{co} = initial tangent modulus of elasticity of unconfined concrete;
- E_d = cumulative energy damage indicator;
- E_s = modulus of elasticity of steel;
- E_{sref} = reference value of modulus of elasticity of steel;
- f_c = stress of unconfined concrete in the spalling concrete;
- f'_c = compressive strength of concrete based on standard cylinders;
- f_{ca} = stress in concrete due to axial for columns under lateral cyclic loading;
- f_{cc} = applied stress on confined concrete in column; $f_{cc} = \frac{P_{conc}}{A_c}$;
- $(f_{cc})_i$ = stress of confined concrete corresponding to a general point *i* on the confined concrete material curve;
- f'_{cc} = strength of the confined concrete of the columns, (max. of f_{cc});
- f_l = lateral confining pressure;
- f'_{co} = unconfined concrete strength of the column; $f'_{co} = 0.85f'_c$;

f_{ccr}	=	stress of confined concrete in the reduced core;
f_s	=	stress in steel longitudinal bars of the column;
f_{sa}	=	stress in longitudinal steel bars due to axial for columns under lateral cyclic loading;
f_{true}	=	stress in steel collars at true strain, ε_{true} ,
f_y	=	yield strength of steel;
f_{yh}	=	specified yield strength of the spiral or hoop reinforcement;
f_{yref}	=	reference value of yield stress of steel;
h	=	depth of the column cross section;
h_c	=	cross-sectional dimension of the column core, mm; measured center-to-center of confining reinforcement, ($\approx l_h$);
h_x	=	maximum horizontal spacing of hoop or crosstie legs on all faces of the column,
h_{column}	=	width of column (inside length of a collar);
h_{collar}	=	depth of the collar perpendicular to column axis;
h_f	=	length of most damaged region of columns under cyclic loading;
I_{collar}	=	moment of inertia of collar;
K_s	=	strength enhancement factor;
H_1	=	height of concrete column measured from the top of footing;
H_2	=	distance of the point of application of lateral from the base of the column;

- H_3 = distance of the point of application of vertical load from the column base;
- H_{\max} = maximum horizontal loads in columns under lateral cyclic loading;
- k_1 = ratio of enhancement in concrete strength to the lateral confining pressure;
- K_{op} = modulus of toughness up to peak load;
- K_{of} = modulus of toughness up to failure;
- K_{occp} = modulus of toughness for column concrete up to peak load;
- K_{occf} = modulus of toughness for column concrete up to failure;
- K_s = strength enhancement factor;
- L = length of column from base to the point of application of horizontal load;
- L_p = plastic hinge length;
- L_u = maximum unsupported length of steel ties in columns;
- L_1 = location of strain gage No. 1 on the longitudinal bars of the column;
- L_2 = location of strain gage No. 2 on the longitudinal bars of the column;
- L_3 = location of strain gage No. 3 on the longitudinal bars of the column;
- L_4 = location of strain gage No. 4 on the longitudinal bars of the column;
- L_5 = location of strain gage No. 5 on the longitudinal bars of the column;
- L_6 = location of strain gage No. 6 on the longitudinal bars of the column;
- L_7 = location of strain gage No. 7 on the longitudinal bars of the column;

- L_8 = location of strain gage No. 8 on the longitudinal bars of the column;
- L_9 = location of strain gage No. 9 on the longitudinal bars of the column;
- L_{10} = location of strain gage No. 10 on the longitudinal bars of the column;
- L_{11} = location of strain gage No. 11 on the longitudinal bars of the column;
- L_{12} = location of strain gage No. 12 on the longitudinal bars of the column;
- L_p = plastic hinge length;
- M = applied moment on a column;
- M_y = yield moment;
- M_{if} = ideal flexural strength;
- M_{max} = maximum moments in columns under lateral cyclic loading;
- M_{ncc} = nominal flexural strength based on confined concrete;
- M_{nuc} = nominal flexural strength based on unconfined concrete;
- $(M_{peak})_i$ = peak moment in a cycle;
- M_{ycc} = flexural strength at the first yield of tensile longitudinal steel based on confined concrete;
- M_{yuc} = flexural strength at the first yield of tensile longitudinal steel based on unconfined concrete;
- N_ϕ = cumulative curvature ductility ratio;
- n = strength enhancement ratio;
- n = a coefficient in Ramberg-Osgood model;

- P = axial load on column;
- $P_{c\max}$ = maximum load carried by the concrete of the column, (max. of P_{conc});
- P_{\max} = maximum load carrying capacity of the column as obtained from test;
- P_o = theoretical capacity of the column; $P_o = 0.85f'_c(A_g - A_{st}) + A_{st}f_y$;
- P_{oc} = theoretical capacity of the column concrete; $P_{oc} = 0.85f'_c(A_g - A_{st})$;
- P_{occ} = theoretical capacity of the concrete core of the column; $P_{occ} = 0.85f'_c(A_{co} - A_{st})$;
- P_{orcc} = theoretical capacity of the concrete core reduced by spalling; $P_{orcc} = 0.85f'_c(A_{rcc} - A_{st})$;
- P_{ta} = total axial load on columns under lateral cyclic loading;
- P_{ca} = axial load load shared by concrete of columns under lateral cyclic loading;
- P_{sa} = axial load shared by steel longitudinal bars of columns under lateral cyclic loading;
- s = center-to-center spacing of ties or collars;
- s' = clear spacing between collars or ties;
- s'_r = clear collar spacing ratio;
- S_i = slope corresponding to the peaks of *ith* moment versus curvature loop;
- S_1 = slope of initial line of the moment versus curvature envelope;
- t = the thickness of collar parallel to column axis;

T_f	=	flange thickness;
T_w	=	Web thickness;
u_{hco}	=	outward displacement of concrete prism;
u_{hci}	=	the inward displacement of concrete prism;
u_{ht}	=	the lateral displacement of the equivalent confining tube;
V_m	=	Variance using mean values;
V_p	=	Variance using predicted values;
R^2	=	Coefficient of multiple determination;
α	=	ratio of ε_{cc} to ε_{co} ;
β	=	ratio of ε_{cc85} to ε_{co85} ;
β_1	=	a coefficient to calculate the depth of Whitney stress block
β_1 to β_8	=	non-dimensional behavioural parameters of the equivalent confining tube;
$(\beta_7)_{\max}$		maximum value of β_7 ;
$(\beta_8)_{\max}$		maximum value of β_8 ;
β_{eq}	=	equivalent viscous damping;

- β_i = inherent viscous damping;
- β_o = hysteretic damping ratio;
- ε_{cc20} = strain in post-peak region at 20% of the confined concrete strength;
- ε_{50h} = enhancement in concrete strain due to confinement at 50% of unconfined concrete strength;
- $(\varepsilon_{cc})_i$ = axial strain of confined concrete corresponding to a general point i on the confined concrete material curve;
- ε_c = strain of confined or unconfined concrete at any stress;
- ε_{cc} = strain at peak stress of the confined concrete or the strain corresponding to $P_{c\max}$;
- ε_{co85} = the strain 85% of peak stress of unconfined column concrete in the post-peak region;
- ε_{cc85} = strain in post-peak region at 85% of the confined concrete strength;
- ε_{cc50} = strain in post-peak region at 50% of the confined concrete strength;
- ε_{cc30} = strain in post-peak region at 30% of the confined concrete strength;
- ε_{cf} = strain in post-peak region at 80% of the confined concrete strength;
- ε_{ce} = strain at the start of peak strength plateau of confined concrete;
- ε_{cs} = strain at the end of peak strength plateau of confined concrete;
- ε_{co} = strain at peak stress of unconfined concrete;
- ε_f = strain at column failure;
- $\dot{\varepsilon}_f$ = strain rate up to the failure of column;

- ε_l = average lateral strain;
- ε_o = average longitudinal strain of concrete cylinders at peak stress;
- $\dot{\varepsilon}_p$ = strain rate up to peak load of column;
- $\varepsilon_{p \max}$ = average longitudinal strain corresponding to P_{\max} ;
- ε_{sh} = strain at the start of strain hardening;
- ε_s = strain at which spalling of concrete starts;
- ε_s = strain in steel longitudinal bars of the column;
- ε_{true} = A general value of strain in material under consideration;
- ε_y = yield strain of steel longitudinal bars of the column;
- ε_s = strain at which spalling of concrete starts during axial load history;
- λ_1 to λ_6 = fuctions in terms of non-dimensional parameters β_1 to β_6 , respectively;
- γ_1 to γ_6 = fuctions in terms of non-dimensional parameters β_1 to β_6 , respectively;
- λ_s and γ_s = fuctions to account for collar smearing;
- φ = curvature of the column section;
- φ_{\max} = maximum curvature of the column cross section;
- φ_y = yield curvature;

- φ_1 = curvature corresponding to the point of intersection of the initial tangent line to the horizontal line drawn at peak of the moment versus curvature envelope curve;
- φ_2 = curvature corresponding to failure on the moment versus curvature envelope curve;
- φ_i = maximum curvature corresponding to cycle i ;
- φ_ϵ = curvature at the location of strain gages on the longitudinal bars;
- ρ = reinforcement ratio;
- ρ_b = reinforcement ratio at balanced condition;
- ρ_g = ratio of total longitudinal reinforcement area to the gross cross-sectional area of the column;
- ρ_s = volumetric ratio of spiral steel to core concrete;
- ρ_t = ratio of the volume of the confining steel to the volume of the concrete core, %;
- Δ_y = yield displacement;
- σ_{ct} = average confining pressure of the confining tube;
- σ_h = average confining pressure which takes into account the response of concrete;
- σ_{h01} = the magnitude of confining pressure at an axial strain of 0.10;
- μ = displacement ductility;
- μ_φ = curvature ductility (μ_φ^* indicates the lower bound value);

- ν_c = secant Poisson's ratio of concrete at a given level of axial strain;
- ν_{co} = initial secant Poisson's ratio of concrete;
- θ_{slip} = Rotation at column base due to anchorage slip;
- Δ_a = displacement at the point of application of horizontal load due to rotation caused by anchorage slip;
- Δ_{sl} = displacement at the point of application of horizontal load due to sliding of columns at bases;
- Δ_{sh} = displacement at the point of application of horizontal load due to shear deformation;
- Δ_p = displacement at the point of application of horizontal load due to plastic rotation at plastic hinge;
- Δ_{total} = total displacement at the point of application of horizontal load;
- $\Delta\varepsilon$ = difference of strain of longitudinal bars on the push and pull sides of column;

1. INTRODUCTION

1.1 Foreword

With the rapid development of the science of earthquake engineering, many associated changes have been made over the past three decades to design codes and standards. As a result of these changes, many existing buildings have been deemed seismically deficient. Older codes generally relied on the provision of strength to resist seismic loads without giving due consideration to proper detailing to enhance ductility and energy dissipation at potential locations of plastic hinges. New codes are based on the design philosophy of reducing seismic forces by producing ductile, energy-dissipating structural systems that undergo inelastic structural response during an earthquake. Buildings can also become seismically deficient simply due to the rezoning of seismic activity in the area, which is related to developments in the geo-sciences. A change of function of the building or a change of occupancy can also make the building seismically deficient. For example, a building satisfying the Life Safety performance level for a design earthquake may need to be upgraded to satisfy the Immediate Occupancy performance level (ATC, 1976) if its function changes during its design life.

The collapse and damage of reinforced concrete buildings in recent earthquakes around the globe have confirmed the existence of a large number of seismically deficient reinforced concrete buildings. These buildings need to be seismically upgraded. The seismic performance of a structure during an earthquake depends on its mass, stiffness, strength, deformability (ductility), robustness, damping (energy-dissipating capability), and the characteristics of the ground motion itself. The rehabilitation objectives can be achieved by modifying one or more of these characteristics.

1.2 Seismic Rehabilitation

After the 1971 San Fernando, California earthquake, in which many reinforced concrete buildings collapsed and/or became severely damaged, revolutionary changes were made in codes for the design and detailing provisions for earthquake-resistant concrete structures and these codes have continually been upgraded since then. At the same time, attention was given to the rehabilitation of existing seismically deficient reinforced concrete structures. Various rehabilitation schemes have been developed. Some schemes work primarily through the enhancement of strength and stiffness, while others work predominantly through the enhancement of

deformability (ductility) and damping, resulting in the reduction of earthquake demand on the structures.

Theoretically, it is possible to achieve certain rehabilitation objectives by increasing strength or stiffness only. Generally, however, it is not possible to increase strength or stiffness alone. For example, the addition of concrete shear walls, steel braced frames, steel moment resisting frames, steel bracings, or buttresses would all increase both the strength and stiffness of the structure.

The rehabilitation objectives may also require increasing the overall deformability of the structure by increasing the deformability and energy dissipation capabilities of its critical components. This can be achieved, for example, through jacketing. Different types of jacketing have been used in the past for the rehabilitation of reinforced concrete frame elements such as: (1) concrete jacketing; (2) steel plate jacketing; and (3) jacketing by composite materials. The enhanced ductility of the structural members arising principally through confinement may not be utilized fully due to the presence of non-ductile joints elsewhere in the seismically deficient structure and due to drift limitations according to certain performance objectives.

Rehabilitation objectives can also be achieved by reducing the earthquake demand on the structure by installing base isolation devices and/or energy dissipating units. In order to install the energy dissipating units, a steel frame may also need to be installed on which energy dissipating units are mounted. Due to installation of this frame, the stiffness of the structure also increases. Energy dissipation capability of the structure can also be improved by providing concrete confinement.

The focus of the larger research program, of which this report is a part, is to investigate the performance of seismically deficient reinforced concrete frames rehabilitated by thin, unstiffened steel plate shear walls. These walls resist the lateral load through the development of a tension field after out-of-plane buckling of the plates occurs. There exists no evidence in the literature of a case where such a steel plate shear wall has been used as a means of rehabilitation for the seismic upgrade of a reinforced concrete building. However, stiffened steel plate shear walls have been used in the past for the upgrade of seismically deficient reinforced concrete buildings in two known cases (Baldelli, 1983; and Robinson and Ames, 2000). The rehabilitation objectives were achieved through the enhancement of strength and stiffness only. Ductility and energy dissipating capabilities of the steel plate shear walls could not be mobilized because of the presence of a non-ductile reinforced concrete frame bordering the steel plate shear wall.

Steel plate shear walls have also been used as a primary lateral load resisting system in a number of new high-rise buildings, primarily in Japan and North America, to resist wind and earthquake loads (Thorburn *et al.*, 1983; Driver *et al.*, 1996; Fujitani *et al.*, 1996; Celebi, 1997; and Astaneh-Asl, 2001). In earlier research, buckling of the steel plate shear wall was considered to be the end of its useful behaviour. Hence, in several existing buildings with steel plate shear walls as a lateral load resisting system, the out-of-plane buckling of the plate was prevented either by providing stiffeners or by using thick steel plates. In Japan, heavily stiffened steel plate shear walls are used that develop their full plastic strength prior to out-of-plane buckling. These walls not only resist the large earthquake-induced lateral loads but also dissipate earthquake-induced energy (Takahashi *et al.*, 1973). In the United States, thick steel panels were provided in early steel plate shear wall buildings to prevent out-of-plane buckling of the steel panels under shear loading.

Later, work at the University of Alberta proposed the use of thin, unstiffened steel plate shear walls. These provide an excellent lateral load resisting system for wind and earthquake loading, especially in zones of high seismic activity. The system can be idealized as a vertical plate girder cantilevered from its base, as shown in Figure 1-1. The boundary columns are analogous to the flanges of the plate girder and the beams serve as the stiffeners. The boundary beams and columns can be connected to each other either with shear connections or moment-resisting connections. By providing moment-resisting beam-to-column connections, the redundancy of the system is greatly improved.

1.3 Unstiffened Thin Steel Plate Shear Walls

The purpose of steel plate shear walls is to resist bending moment and shear force due to the lateral load resulting from wind or earthquake. The shear force is resisted by the development of a diagonal tension field in the steel infill panel. The bending moment is resisted primarily by the development of axial loads in the columns. In plate girders, the bending stiffness of the flange is low and is generally unable to provide anchorage to the diagonal tension field, resulting in a partial diagonal tension field developing to resist the shear force. This limitation is overcome in steel plate shear walls by providing flexurally stiff boundary columns that provide anchorage to the diagonal tension field.

1.3.1 Evolution of Unstiffened Thin Steel Plate Shear Walls

Steel plate shear walls have been used as a lateral load resisting system in a number of buildings, primarily in Japan and North America. It was Wagner (1931) who first demonstrated

through the behaviour of aluminium panels under shear used in aircrafts that the useful behaviour of the panels does not end with their out-of-plane buckling. He demonstrated that if the panels under shear loading are provided with stiff boundary members, the load-resisting mechanism of the panels changes from pure shear to a diagonal tension field. He assumed that the shear capacity of the aluminium panels with stiff boundary members depends purely on the tension field action, usually called pure diagonal tension field theory. For relatively thicker panels for which the buckling strength is not negligible, Kuhn *et al.* (1952) and Kuhn (1956) developed an incomplete tension field theory based on the assumption that panel shear capacity depends on both the diagonal tension field and the pure shear. Later, Basler (1961) extended the incomplete diagonal tension field theory to the design of plate girders for shear.

Stiffened steel plate shear walls have been widely used in Japan to resist seismic lateral load. Takahashi *et al.* (1973) tested 12 single panels (stiffened and unstiffened) and two single bay, two-storey, full-scale stiffened steel plate shear walls with and without reinforced openings, under lateral cyclic loading. The stiffened single panels and steel plate shear walls (in which out-of-plane buckling was prevented) showed excellent hysteretic behaviour under cyclic loading. The hystereses were stable and exhibited little pinching, indicating that a significant amount of energy was absorbed. Conversely, the unstiffened panels showed pinched hysteretic behaviour. Based on this work, Takahashi *et al.* (1973) recommended that the elastic out-of-plane buckling of the steel plate should be prevented. Only inelastic buckling of the individual panels between the stiffeners was permitted. Although the energy absorption capability of the steel plate shear walls increases significantly due to stiffening, the cost involved in stiffening the panels may become prohibitive.

Later, the post-buckling strength of the steel plate shear wall was recognized in Japan by Mimura and Akiyama (1977). They proposed a model to predict the behaviour of unstiffened steel plate shear walls (with steel plates that buckle before reaching their shear yield loads) under monotonic and cyclic loading.

In the early 1980s in North America, it was recognized that the post-buckling strength of steel plate shear walls should be considered in their design and both analytical (Thorburn *et al.*, 1983) and experimental research (Timler and Kulak, 1983) was initiated to substantiate this idea. Later, Tromposch and Kulak (1987) tested another steel plate shear wall specimen similar to the one tested by Timler and Kulak (1983), but with some important differences. The major differences between the work of Timler and Kulak (1983) and Tromposch and Kulak (1987) are: 1) In the Timler and Kulak specimen, pin connections were provided between the beams and columns, while in the Tromposch and Kulak specimen conventional shear connections were provided; 2) In

the Timler and Kulak specimen, no axial load was applied to the columns, while in the Tromposch and Kulak specimen axial load was applied to the columns except in the last cycle where the specimen was pushed monotonically to its ultimate capacity; 3) The Timler and Kulak specimen was subjected to three cycles of loading up to the service load deflection and then it was loaded monotonically to failure in one direction, whereas the Tromposch and Kulak specimen was subjected to 28 fully reversed cycles with increasing load magnitude up to 67% of the ultimate load capacity. Then the specimen was pushed in one direction up to its ultimate load; and 4) In the Tromposch and Kulak specimen, relatively stiff boundary beams were used to provide better anchorage to the thin infill panel.

Driver *et al.* (1996, 1998a, 1998b) reported the test results of a half-scale, four-storey unstiffened steel plate shear wall under lateral cyclic loading and constant gravity load. This was the first large-scale multi-storey test and was conducted to verify existing theories and design formulae. The specimen was fixed at the base and lateral loads were applied horizontally at the four floor levels and service gravity loads were applied to the columns. Moment-resisting beam-to-column connections were provided to maximize the ability of the wall to dissipate energy under seismic loading. This test provided further evidence supporting the suitability of unstiffened steel plate shear walls for seismic applications. A nonlinear finite element model was also developed to predict the behaviour of the large-scale steel plate shear wall. The strip model, developed by Thorburn *et al.* (1983) was also substantiated by applying it to the large-scale steel plate shear wall.

Lubell *et al.* (2000) reported quasi-static tests on two single- and one four-storey unstiffened steel shear wall specimens. Each specimen was of one-fourth scale. The results showed significant energy dissipation and good displacement ductilities exhibited by these walls. The strip model developed by Thorburn *et al.* (1983) was used to predict the behaviour of these wall panels. It was found that the strip model gives good prediction of the post-yield strengths (ultimate capacities) of the steel plate shear wall specimens. However, the predictions of the elastic stiffness of the specimens by the strip model were not satisfactory.

Rezai (1999) reported the seismic behaviour of an unstiffened steel plate shear wall under shake-table tests. The specimen consisted of a single bay, four-story shear wall specimen of one-fourth scale similar to the one tested by Lubell *et al.* (2000) under quasi-static loading. Due to the limited capacity of the shake-table, the specimen could not be failed (the steel plate did not yield). The effect of the first mode was found to be dominant. It was reported that the frequency of the first mode of vibration decreased (, *i.e.*, the time period of the fundamental mode of vibration increased) with an increase in the amplitude of vibration of the shake-table due to a

reduction in the stiffness of the SPSW specimen at these large amplitudes of vibration. It was concluded from the results of shake-table tests, that the design of steel plate shear walls would often be controlled by the limit on lateral drift and not by strength. Based on this fact, the need for the development of a sophisticated analytical tool for the accurate prediction of the stiffness of steel plate shear wall was emphasized.

Behbahanifard (2003) reported the test results of a single bay three-story shear wall specimen under seismic loading. The specimen consisted of the top three storeys of the four-storey specimen tested by Driver *et al.* (1998a). For the accurate predictions of the behaviour of steel plate shear walls, finite element models based on nonlinear dynamic explicit formulations were developed.

Recently, the concept of the unstiffened steel plate shear wall has also gained popularity among the researchers of other countries such as the United States (Cacesse *et al.*, 1993; Elgaaly *et al.* 1993; Xue and Lu, 1994; Elgaaly and Liu, 1997; and Astaneh-Asl, 2001) and the United Kingdom (Roberts and Sabouri-Ghomi, 1991; and Sabouri-Ghomi and Roberts, 1992).

1.3.2 Characteristics of Steel Plate Shear Walls

Based on the observations and test results of previous research, it is known that properly designed steel plate shear walls possess superior ductility, robust resistance to degradation under severe cyclic loading (stable hysteretic behaviour), high capacity for plastic energy absorption, strength and high initial stiffness, high redundancy when moment-resisting beam-to-column connections are provided, and less weight on the foundations as compared to concrete shear walls, which further reduces the seismic loads on the building. Conventionally, in steel frame buildings in Canada, concrete shear walls have been used as the lateral load resisting system. After a significant amount of research on steel plate shear walls, it has become evident that steel plate shear walls provide a competitive, and potentially superior, lateral load resisting system with respect to economy and performance. In addition to the attributes listed above, steel plate shear walls occupy less usable space as compared to concrete walls. Moreover, the speed of construction of steel plate walls is higher than that of reinforced concrete shear walls. Caccese *et al.* (1993) reported that cost savings of as much as 50% were achieved in structures employing steel plate shear walls as compared to comparable moment resisting frames. Similarly, it has been shown by Troy and Richard (1979) and Timler *et al.* (1998) that the steel plate shear walls are more cost-effective than moment resisting frames and reinforced concrete shear walls. Disadvantages of steel plate shear walls are that they require some form of

fire protection and may be susceptible to vibration when used as a shear core surrounding elevators.

1.3.3 Steel Buildings with Steel Plate Shear Walls

Thorburn *et al.* (1983) reported that the Shin Nittetsu Building is the first steel building in Japan, completed in 1970, in which steel plate shear walls were used as the lateral load resisting system. This is an office building constructed for the Nippon Steel Company of Tokyo. The building consists of 20 floors and was provided with five H-shaped stiffened steel plate walls to resist the lateral loads. The 2.75 mx3.7 m steel panels of thicknesses varying from 4.5 mm in upper storeys to 12 mm in lower storeys were stiffened orthogonally. The fire protection was provided by encasing the steel plates in 50 mm thick dry wall.

Roberts (1995) reported that the second steel building in Japan in which stiffened steel plate shear walls were used as the lateral load resisting system is the 53-storey Shinjuku Nomura Office Tower. Stiffened steel plates of 3 mx5 m of thickness varying from 6 to 12 mm were bolted to the frame members to form eight T-shaped shear walls. Sprayed fire protection of 50 mm thick was applied to the steel plate shear walls.

The Olive View Medical Center building located in the northeast San Fernando valley, California is the first building in the United States in which stiffened steel plate shear walls were used as a primary lateral load resisting system. The reconstruction of this building was commenced in 1976 after the original building was badly damaged in the 1971 San Fernando earthquake and was razed. As a reaction, this new building was kept highly stiff. In this six-storey building, reinforced concrete shear walls were used in the lower two storeys and stiffened steel plate shear walls were used in the four upper storeys. The thickness of the steel plates varied from 16 mm to 19 mm. This building sustained the January 17, 1994 Northridge earthquake safely with minor structural damage but considerable non-structural damage and is located 16 km from the epicenter of this earthquake.

In the 16-storey Moffit Hospital building in California, both concrete and steel plate shear walls were used as lateral load resisting systems. The steel plate thickness varies from 10 mm to 32 mm. The reinforced concrete shear walls were placed around the elevator core to avoid the problem of vibration due to the elevator movements. To provide more rigidity and fire resistance, additional reinforced concrete walls of 250 mm thickness were constructed and connected on both sides of the steel plate shear walls by reinforcing ties.

The lateral load resisting system of the 30-storey Hyatt Regency Hotel in Dallas, Texas consists of steel braced frames in the long direction of the building plan and stiffened steel plate shear walls in the short direction. The thickness of steel plates varies from 13 mm to 39 mm. The construction of this building was completed in 1978.

1.3.4 Seismic Rehabilitation of Reinforced Concrete Buildings

Two known seismically deficient reinforced concrete buildings have been upgraded using stiffened steel plate shear walls: (1) the VA Medical Center in Charleston, South Carolina and (2) the Oregon State Library. A description of these buildings is given in the following. However, no evidence was found of the use of unstiffened steel plate shear walls, which resist lateral load by the development of a diagonal tension field, for the rehabilitation of seismically deficient reinforced concrete frames.

1.3.4.1 VA Medical Center in Charleston, South Carolina (Baldelli, 1983)

During the San Fernando earthquake in 1971, two Veterans Administration hospitals collapsed and as a result, all VA hospitals in the areas of earthquake activity were evaluated structurally. The VA Medical Center in Charleston, South Carolina was found to be seismically deficient and it was decided to strengthen the hospital complex consisting of several buildings. The three main buildings each consisted of flat slabs with columns at 6.1 meters on center in the two major directions and were originally designed to resist lateral loads caused by wind only. The resulting design base shear was about 3% of the total dead load and was carried by isolated stair walls and by frame action. According to the new VA earthquake code at the time of the upgrade, the structure should be able to resist a base shear equal to 15% of the total dead load. It was found by analysis that the columns of the buildings were severely over-stressed under this base shear. And, therefore, it became necessary to strengthen the complex.

It was decided to strengthen the buildings by adding shear walls in both the transverse and longitudinal directions of the buildings. They provide additional load-resisting elements and reduce the span of the roof and floor diaphragms. Previously, only concrete shear walls were used in strengthening VA buildings but for the Charleston VA hospital, many of the new shear walls were constructed of steel.

The analysis results showed that the central wing of the building in the transverse direction could only be rehabilitated by adding shear walls at four locations approximately 30.5 meter apart. Thus, in the five story building, a total of 60 shear walls (4 frames x 3 walls per floor x 5 floors)

were required. The walls could be either concrete or steel. The VA required that during the strengthening operation, disruption of service in the building should be a minimum. Moreover, the use of hospital floor space should be kept to a minimum and the new shear walls needed to be able to accommodate future penetrations for piping or ducts.

In order to meet the above demands, shear walls made of steel were used for the interior locations and concrete shear walls were used for the exterior locations between the columns. The steel shear wall panels incorporated vertical and horizontal stiffeners and were prefabricated and connected in place to minimize the disruption. A subpanel can be removed easily to create an opening for ducts and the surrounding stiffeners can be strengthened. The connections of the panel were designed in such way that welding can be done from one side only. Buckling of the web plate was not permitted in the design of the steel plate shear wall panels. This design feature was controlled by the thickness of the web plate and the area of the web plate enclosed by stiffeners. Edge plates were provided at the end of the panel to make the connection with the concrete frame with anchor bolts. The rehabilitation of the building was done by increasing strength and stiffness without making use of the ductility of the steel plate shear walls.

1.3.4.2 Oregon State Library in Salem, Oregon (Robinson and Ames, 2000)

This building was constructed in 1937 as a cast-in-place reinforced concrete frame with pan joist floors framing into rectangular girders and columns. After about 60 years of service, it was found that the building required seismic strengthening. It was required that the library building remain open and functional during the rehabilitation operation and that the renovation and strengthening design preserve the historic finishes of the building. To meet these objectives, the seismic upgrade of the building was completed using stiffened steel plate shear walls. The construction of steel plate shear walls was less disruptive to building's occupants as compared to the construction of reinforced concrete shear walls. Furthermore, the moisture created during the concrete pouring operation could damage the historic books in the building.

The steel plates were designed such that they could be carried by two workers and installed manually without using cranes or large equipment. The connection of the steel plates to each other was made with the help of structural Tees, which also acted as stiffeners for the plates. Bolted connections were used instead of welded connections to avoid the risk of fire in the library. The existing building had no well-defined lateral load resisting system so it was assumed that the existing building was unable to resist any lateral load. Therefore, the steel plate shear walls were designed to resist the full design lateral load. The connection of the steel plate shear walls to the existing reinforced concrete building was made with both drilled-in expansion type

and adhesive type anchors. The seismic rehabilitation of the building was accomplished by increasing the lateral stiffness and strength of the building, without making use of the ductility of the steel plate shear walls.

1.4 Proposed Rehabilitation Scheme

As discussed in the foregoing, thin, unstiffened steel plate shear walls possess many technical and economical attributes that make the system desirable as a lateral load resisting system, particularly in high seismic zones. Therefore, a rehabilitation scheme for the upgrade of seismically deficient reinforced concrete buildings is proposed that makes use of steel plate shear walls. In addition to the attributes of the shear wall panels themselves, it was required that the proposed scheme have following features:

- 1) Unlike the rehabilitation of concrete buildings by stiffened steel plate shear walls through enhancement in strength and stiffness only (Baldelli, 1983; and Robinson and Ames, 2000), it is desired that the proposed rehabilitation scheme exploit the significant ductility and energy dissipation capability of the steel plate shear walls, in addition to providing increased strength and stiffness. Perhaps the main reason for not using the ductility of the steel plate shear walls in the rehabilitation of these buildings was the problem of ductility incompatibility between the steel plate shear walls and the reinforced concrete frames. The existing seismically deficient reinforced concrete frames are non-ductile due to poor detailing and construction practice at the time of their construction. In these buildings, no effort was made to improve the ductility and robustness of these frames.
- 2) In the rehabilitation of concrete buildings using stiffened steel plate shear walls (Baldelli, 1983; and Robinson and Ames, 2000), the connection of the shear walls to the reinforced concrete frame was made by mechanical and adhesive type anchor bolts, for which chipping, drilling, and grouting were required. These procedures can be highly disruptive in an occupied building. Therefore, in the proposed rehabilitation scheme, it was required that chipping and drilling be minimized or eliminated.

The above requirements led to a system for rehabilitating deficient reinforced concrete frames that is illustrated schematically in Figure 1-2. The connection of the steel plate shear walls to the columns of the reinforced concrete frame is made using external steel collars and the connection of the plate to the beam is made with through bolts (Figure 1—2(a)) or steel collars passing through the slab (not shown), for which some drilling and chipping would be required. Besides providing connection points for the shear wall, the steel collars enhance both the strength and

ductility of the concrete columns through confinement and address the problem of ductility incompatibility between the steel plate shear wall and the surrounding reinforced concrete frame. The collars enhance the axial, flexural, and shear strength of the columns. Other methods of connecting the steel plate shear walls to the reinforced concrete frame have been proposed (see Driver *et al.*, 2001) but are beyond the scope of this report. It is to be noted that although it is not the main focus of this report, steel collars alone can be used for strength and ductility enhancement of columns under static gravity load effects.

1.4.1 Challenges Arising and Proposed Solutions

In order to obtain better insight into the proposed rehabilitation scheme, a pushover analysis was performed on a single storey, single bay reinforced concrete frame with steel infill panel. The steel plate was modelled by the strip model originally proposed by Thorburn *et al.* (1983) for infill panels within a steel frame (Figure 1-3). The diagonal strips were oriented at an angle from the vertical, α , of 45 degrees. The deformed configuration of the panel (amplified 100 times) is shown in Figure 1-4. It is clear from this figure that the tension field of the steel plate shear wall induces high curvature ductility demand on the surrounding columns. In addition, the columns are subjected to high shear forces. Reinforced concrete frames that are in need of seismic rehabilitation generally are non-ductile, lack in shear reinforcement, and possess poor reinforcement details in the joints and short lap splices at the locations of plastic hinges. Therefore, it is highly improbable that the existing columns can resist these seismic demands. This is the reason why the existing reinforced concrete buildings described previously (Baldelli, 1983; and Robinson and Ames, 2000) were rehabilitated by stiffening and strengthening, without making use of the ductility of the steel plate shear wall.

In order to make use of the benefit of the ductility and energy dissipation capability of the steel plate shear walls, the ductility and the shear resistance of the surrounding columns need to be enhanced by some means. The curvature ductility, shear resistance, and energy dissipation capabilities of the concrete columns can all be enhanced by confinement of the column concrete using the proposed steel collars. In addition, the demand on the columns can be reduced by the following methods:

- 1) minimizing the steel infill panel thickness;
- 2) use of a low yield point steel such as those available currently in Japan (Yamaguchi *et al.*, 1998) that also possess high ductility, enhanced hysteresis characteristics, lower

strain rate dependency, longer low-cycle fatigue life, and improved weldability over conventional structural steels;

- 3) use of plate penetrations such as the machined slits described by Hitaka and Matsui (2003) who reported, based on tests of 42 one-third scale specimens, behaviour that is ductile and stable, and strength and stiffness that can be adjusted independently by changing the slit configuration.

An elevation of a typical seismically deficient reinforced concrete frame that has been rehabilitated using the proposed scheme is shown in Figure 1-5. For the columns to which the steel plate shear wall is connected, a high degree of confinement is required because of the high ductility demand imposed. In Figures 1-2 and 1-5, collars are shown at a closer spacing near the joint and at a wider spacing near mid-height. The length of the region of closely spaced collars depends on the nature of the demand imposed and may be a significant portion of the column length, as for the case shown in Figure 1-3 which shows high curvature ductility demand away from the joints. For columns away from the steel plate shear walls, it is anticipated that the confinement requirement will be relatively low as compared to columns to which steel plate shear walls are connected, and that the collars can be installed near the frame joints only. The curvature ductility requirements at these locations depend on how much ductility is available from the composite system. Structures designed for gravity loads only may possess a significant inherent lateral strength capacity that may be adequate to resist minor to moderate earthquakes (Bracci *et al.*, 1995). Whether the joint requires strengthening to improve the overall ductility of the system is case dependent, but methods are available to do so.

A significant amount of research has been conducted on methods to improve the behaviour of columns with short lap splices. Valluvan *et al.* (1993) studied the performance of short lap splices in columns rehabilitated by different methods, but among them, confinement by grouted-angles-and-straps was the best rehabilitation method. An angle-and-strap system consists of four angles placed at the four corners of a column that are then connected to each other by welding steel straps on to them. The stiffness of the proposed collars is much higher than these angle-and-straps, so it is anticipated that short lap splices will behave at least as well under collar confinement.

1.4.2 Steel Collar Configurations

Steel collars can be fabricated in various ways. For example, they can be made from steel hollow structural sections (HSS), steel wide flange sections or channels, or cut from thick steel plates.

The corner connections can be welded or bolted. Figure 1-6 shows examples of collars made from steel HSS with bolted and welded corner connections, and solid steel collars cut from steel plates with two continuous corners and two bolted corners. The bolted collars can simply be clamped to the column at the required spacing. In order to install collars with welded corner connections (Figure 1-6(b)), on-site welding is required which may not be economically feasible. It is anticipated that the solid collars made by cutting thick steel plates may be most economical as compared to other collar configurations. However, in the experimental program of this research project, only the collars made from HSS were used due to their low weight-to-stiffness ratio. However, numerical work on both hollow and solid collars having rigid corner connections has been carried out (Chapter 6).

The development of economical collar configurations is ongoing at the University of Alberta. The present focus is collars made by cutting steel plates with two rigid and two bolted corners (Figure 1-6(c)). However, no matter what type of collar is used, for this purpose it must have sufficient flexural stiffness to anchor the tension field of the steel plate shear walls without significant deformation and without a significant reduction in the confining pressure on the concrete column. The confining pressure of these collars is contributed by both axial and flexural stiffness of the sides of the collars. The effect of axial and flexural stiffness of collars in confining the concrete was segregated numerically by Hussain and Driver (2001).

1.5 Scope and Objectives

The proposed rehabilitation scheme results in a structural system that consists of steel plate shear wall panels bounded by a reinforced concrete frame confined by steel collars, as shown in Figures 1-2 and 1-5. The overall objective of the ongoing research program is to study the behaviour of this composite system and to optimize it in terms of both performance and economics. Before testing such a rehabilitated frame under simulated seismic loading, it was considered important to conduct a comprehensive investigation of the fundamental behaviour of the collared columns themselves since they play a pivotal role in the seismic performance of this composite system (because the seismically deficient concrete frame is vulnerable as compared to the steel plate shear wall). This study of the collared column behaviour forms the scope of the report. Although the confined behaviour of locations of lapped longitudinal bars is important, this has been left for future research. For organizational purposes, the scope of the report is divided into two main phases: in phase 1, the behaviour of collared columns under concentric axial loading was investigated, and in phase 2, the behaviour of collared columns under simulated seismic loading was studied.

1.5 1 Phase 1

In this phase, the behaviour of reinforced concrete columns confined externally by steel HSS collars with bolted or welded corner connections under concentric axial loading was studied both experimentally and numerically. In the experimental part of this phase, a total of 11 columns were tested; five columns were confined by collars with bolted corner connections, four were confined by collars with welded corner connections, and two columns (control columns) were provided with conventional tie reinforcement in the test region for comparison. The major parameters included in this study were: type of collars (bolted or welded); size of collars (axial and flexural stiffness); and spacing of collars. Figure 1-2 shows a typical conventional hoop reinforcement cage, an HSS collar with welded corner connections, and assembled and exploded views of an HSS collar with bolted corner connections. Figure 1-7 shows a typical column with bolted collars and a typical column with welded collars in the test setup.

Finite element models were developed to determine the behaviour of these collars in terms of confining pressure vs. lateral strain. An existing empirical model, developed originally for FRP confinement, was modified to provide a tool for determining the confined concrete material curves based on the confining pressure vs. lateral strain response. In addition, non-dimensional parameters for square solid and HSS collars were identified to eliminate the scale effect. Models were then developed for predicting the behaviour of the collars in terms of these non-dimensional parameters by performing nonlinear multiple regressions on the data generated by a parametric study conducted through finite element analyses.

1.5.2 Phase 2

In phase 2, a total of nine columns were tested under simulated seismic loading. In one column (control column), the confinement was provided by conventional tie reinforcement in the test region. In the remaining eight columns, the confinement in the test region was provided by steel HSS collars with welded corner connections. The major parameters included in this study were: size of collars; spacing of collars; shear span; and axial load index. Figure 1-8 shows some of the phase 2 columns at different stages of collar installation using epoxy grout. Figure 1-9 shows a typical phase 2 column in the test set-up.

In addition to the experimental work, a plastic hinge analysis was performed to predict the envelope curves to the hysteresses of the collared columns.

1.6 Report Format and Organization

Each chapter of this report has its own bibliography placed at the end of the chapter. The notation is consistent throughout the report and is listed in the prefatory pages.

For organizational purposes, the report has been divided into seven chapters. Chapter 2 presents a literature review of subjects directly related to this report: the most common seismic deficiencies in existing reinforced concrete frame buildings due to poor reinforcement details; experimental and analytical studies on confinement; a historical account of ACI code developments related to column confinement; and experimental studies on jacketed columns which have certain behavioural characteristics that are similar to collared columns. Chapter 3 presents the experimental program, experimental results, and related discussion on the columns tested under concentric monotonic loading. Chapter 4 presents the experimental program, test results, discussion, and prediction of envelope curves to the hysteresses of the columns tested under simulated seismic loading. Chapter 5 presents a model for determining the confined concrete material curves of the collared columns, which is then verified by comparing the predicted results with experimental results given in Chapter 3. In Chapter 6, the confining behaviour of collars in terms of confining pressure vs. lateral strain is presented. Non-dimensional parameters are identified both for HSS and solid collars with rigid corner connections. The results of parametric studies are presented and then empirical models are developed by performing multiple nonlinear regressions on the data generated through finite element analyses. Each of the developed models is then validated by comparison with a number of typical cases. In Chapter 7, a summary, conclusions, and recommendations for future research are presented.

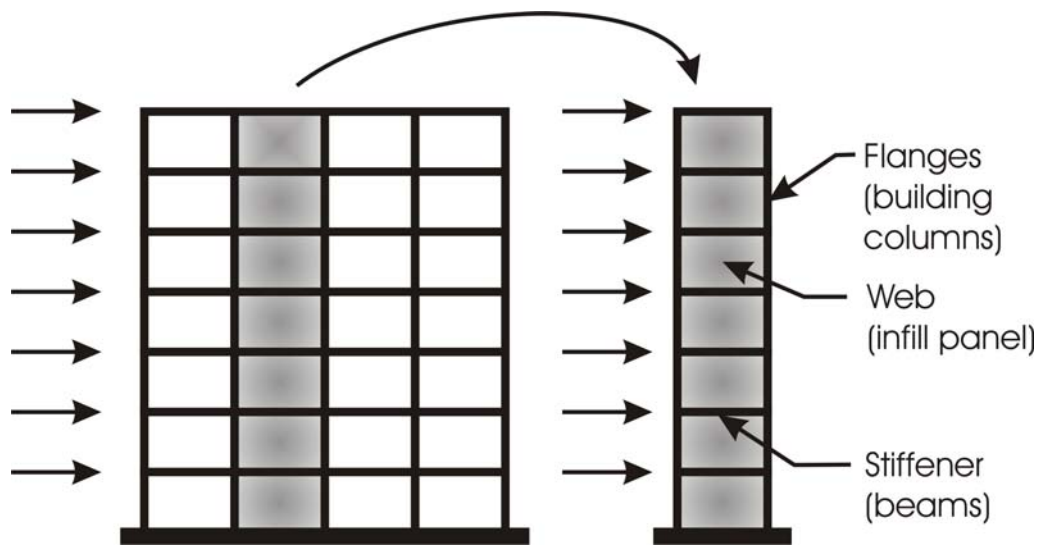
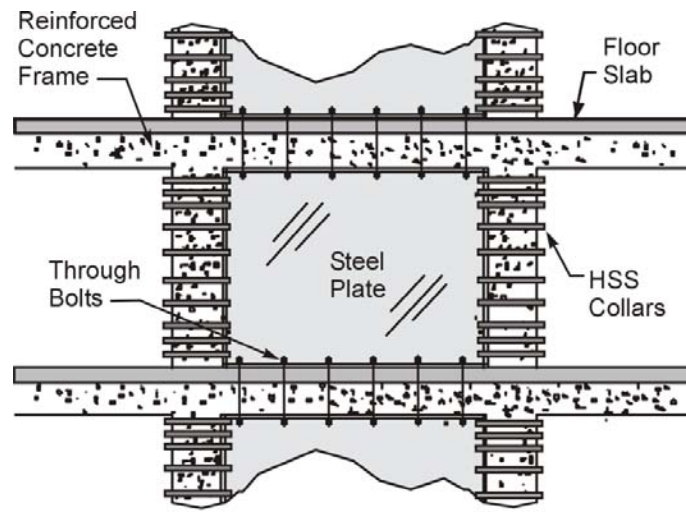


Figure 1-1: Resemblance of steel plate shear wall to a cantilever plate girder.



(a)



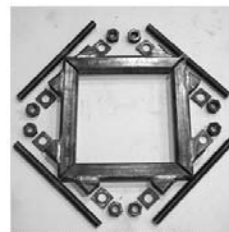
(b)



(c)



(d)



(e)

Figure 1-2: (a) Schematic diagram of the proposed rehabilitation system; (b) conventional rebar hoop reinforcement; (c) HSS collar with welded collar connections; (d) HSS collar with bolted collar connections (assembled view); and (e) HSS collar with bolted collar connections (exploded view).

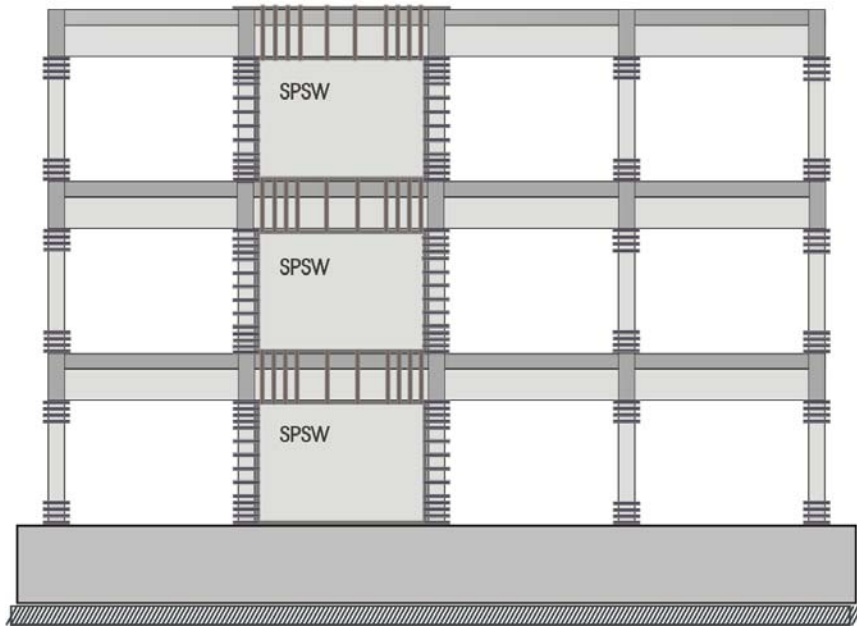


Figure 1-5: Typical elevation of a reinforced concrete structure rehabilitated by steel plate shear walls

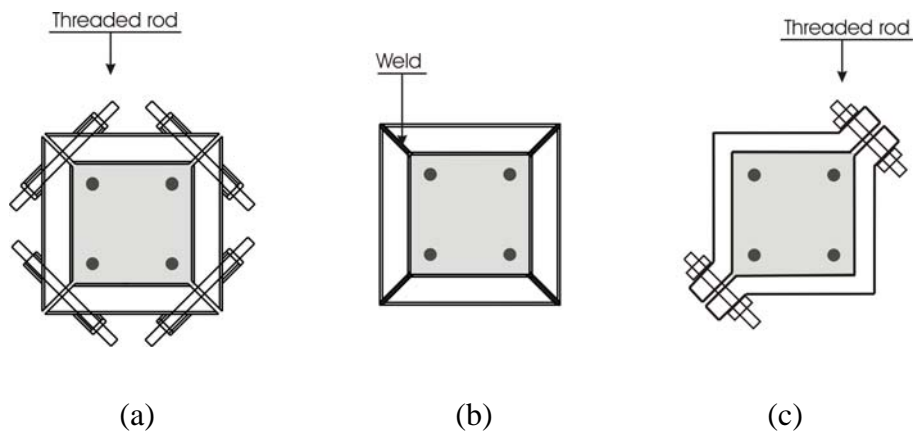
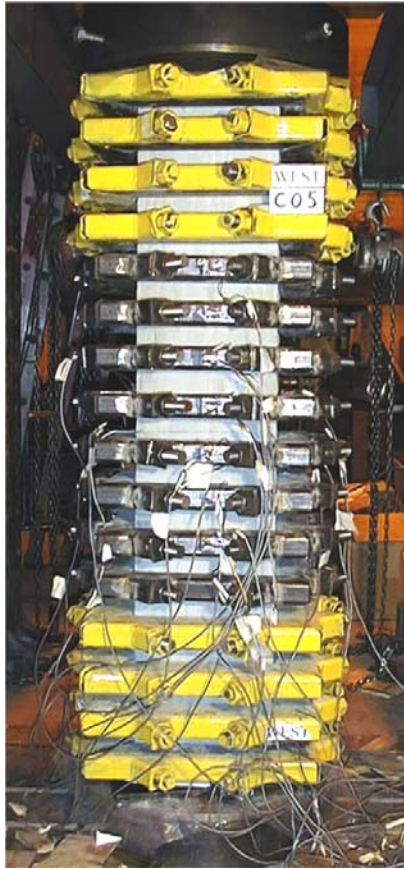


Figure 1-6: Schematic of different types of collars: (a) HSS collar with bolted corner connections; (b) HSS collar with welded corner connections; and (c) collar cut from steel plates



(a) Column C05



(b) Column C06

Figure 1-7: Views of typical column specimens in set-up with: (a) bolted; and (b) welded collars in the test region



Figure 1-8: Three of the nine phase 2 columns at different stages of collar installation



Figure 1-9: A typical phase 2 column in the test set-up.

1.7 References

- Applied Technology Council (ATC). 1996. Seismic evaluation and retrofit of concrete buildings. Safety Commission, State of California, Report No. SSC 96-01 (ATC-40), Vol. 1 and 2, November.
- Astaneh-Asl, A., 2001. Seismic behaviour and design of steel shear walls. Steel TIPs Report, Structural Steel Educational Council, July, Moraga, CA.
- Baldelli, J. A. 1983. Steel shear walls for existing buildings. Engineering Journal, AISC, Second Quarter, pp. 70-77.
- Basler, K., 1961. Strength of plate girders in shear. Journal of Structural Division. Proceedings of the American Society of Civil Engineers. Vol. 87, No. ST7, October, pp. 151-180.
- Behbahanifard, M.R. 2003. Cyclic behaviour of unstiffened steel plate shear walls. PhD Dissertation, Department of Civil and Environmental Engineering, University of Alberta, Edmonton, AB, Canada.
- Bracci, J.M., Reinhorn, A.M., and Mander, J.B. 1995. Seismic retrofit of reinforced concrete buildings designed for gravity loads: Performance of Structural Model. ACI Structural Journal, Vol. 92, No. 6, pp. 711-723.
- Caccese, V., Elgaaly, M., and Chen, R. 1993. Experimental study of thin steel-plate shear walls under cyclic load. Journal of Structural Engineering, ASCE, Vol. 119, No. 2, pp. 573-587.
- Celebi, M., 1997. Response of Olive View Hospital to Northridge and Whittier Earthquakes. Journal of Structural Engineering, ASCE, Vol. 123, No. 4, April, pp. 389-396.
- Driver, R.G., Grondin, G.Y., Behbahanifard, M.R., and Hussain, M.A. 2001. Recent developments and future directions in steel plate shear wall research. North American Steel Construction Conference, Ft. Lauderdale, FL, May 9-12.
- Driver, R.G., Kulak, G.L., Elwi, A.E., Kennedy, D.J.L. 1998b. FE and simplified models of steel plate shear wall. Journal of Structural Engineering, Vol. 124, No. 2, pp. 121-130.
- Driver, R.G., Kulak, G.L., Kennedy, D.J.L., and Elwi, A.E. 1996. Seismic behaviour of steel plate shear walls, Structural Engineering Report 215, Department of Civil Engineering, University of Alberta, Canada.
- Driver, R.G., Kulak, G.L., Kennedy, D.J.L., Elwi, A.E., 1998a. Cyclic test of four-story steel plate shear wall. Journal of Structural Engineering, ASCE, Vol. 124, No. 2, pp. 121-130.
- Elgaaly, M., Caccese, V., and Du, C. 1993. Postbuckling behavior of steel-plate shear walls under cyclic loads. Journal of Structural Engineering, ASCE, Vol. 119, No. 2, pp. 588-605.
- Elgaaly, M. and Liu, Y. 1997. Analysis of thin-steel-plate shear walls. Journal of Structural Engineering, Vol. 123, No. 11, pp. 1487-1496.
- Fujitani, H., Yamanouchi, H., Okawa, I., Sawai, N., Uchida, N., and Matsutani, T., 1996. Damage and performance of tall buildings in 1995 Hyogoken Nanbu Earthquake. Proceedings,

- The 67th Regional Conference, Council on Tall Building and Urban Habitat, Chicago, pp. 103-105.
- Hitaka, T., and Matsui, C. 2003. Experimental study on steel plate shear wall with slits. *Journal of Structural Engineering*, ASCE, Vol. 129, No. 5. pp.586-595.
- Hussain, M.A. and Driver, R.G. 2001. Finite element study on the strength and the ductility of externally confined rectangular and square concrete columns," *Proc., Canadian Society for Civil Engineering, Annual Conference, Victoria, BC, Canada, May 30-June 2.*
- Kuhn, P., Peterson, J.B. and Levin, L.R., 1952. A summary of diagonal tension: Part II – Experimental evidence. Technical Memorandum No. 2662, National Advisory Committee for Aeronautics, Washington, D.C.
- Kuhn, P., 1956. *Stresses in aircrafts and shell structures.* McGraw-Hill Book Co., New York, N.Y.
- Lubell, A.S., Prion, H.G.L., Ventura, C. E., Rezai, M. 2000. Unstiffened steel plate shear wall performance under cyclic loading. *Journal of Structural Engineering.* Vol. 126, No. 4, pp. 453-460.
- Mimura, H. and Akiyama, H. 1977. Load-deflection relationship of earthquake resistant steel shear walls with a diagonal tension field. *Transactions, Architectural Institute of Japan*, 260, October, pp. 109-114 (in japanese).
- Rezai, M., 1999. Seismic behaviour of steel plate shear walls by shake table testing. PhD Dissertation, Department of Civil Engineering, University of British Columbia, Vancouver, Canada.
- Roberts, T.M. 1995. Seismic resistance of steel plate shear walls. *Engineering Structures*, Vol. 17, No. 5, pp. 344-351.
- Roberts, T.M. and Sabouri-Ghomi, S.S. 1991. Hysteretic characteristics of unstiffened plate shear panels. *Thin-Walled Structures*, Vol. 12, pp.145-162.
- Robinson, K. and Ames, D. 2000. Steel Plate shear Walls (Library Seismic Upgrade). *Modern Steel Construction*, pp. 56-60.
- Sabouri-Ghomi, S. and Roberts, T.M. 1992. Nonlinear dynamic analyses of steel plate shear walls including shear and bending deformations. *Engineering Structures*, Vol. 14, No. 5, pp. 309-317.
- Takahashi, Y., Takemoto, Y., Takeda, T., and Takagi, M., 1973. Experimental study on thin steel shear walls and particular bracings under alternative horizontal load. Preliminary Report, IABSE Symposium on Resistance and Ultimate Deformability of Structures Acted on by Well-defined Repeated Loads, Lisbon, Portugal, pp. 185-191.
- Timler, P.A., 1998. Design procedure development, analytical verification, and cost evaluation of steel plate shear wall structures. *Earthquake Engineering Research Facility, Technical Report No. 98-01*, Department of Civil Engineering, University of British Columbia. Vancouver, BC.
- Timler, P.A. and Kulak, G.L. 1983. Experimental study of steel plate shear walls. *Structural Engineering Report No. 114*, Department of Civil Engineering, University of Alberta, Edmonton, Alberta, Canada.

- Thorburn, L.J., Kulak, G.L., and Montgomery, C.J., 1983. Analysis of steel plate shear walls. Structural Engineering Report No. 107, Department of Civil Engineering, University of Alberta, Edmonton, Canada.
- Tromposch, E.W. and Kulak, G.L. 1987. Cyclic behaviour of thin panel steel plate shear walls. Structural Engineering Report No. 145, Department of Civil Engineering, University of Alberta, Edmonton, Alberta, Canada.
- Troy, R.G. and Richard, R.M., 1979. Steel plate shear wall resist lateral load, cut costs. Civil Engineering, ASCE, Vol.49, February, pp. 53-55.
- Valluvan, R., Kreger, M. E., and Jirsa, J. O. 1993. Strengthening of column splices for seismic retrofit of nonductile reinforced concrete frames. ACI Structural Journal, Vol. 90, No. 4, pp. 432-440.
- Wagner, H., 1931. Flat sheet metal girders with very thin webs, Part I-General theories and assumptions. Technical Memorandum. No.604, National Advisory Committee for Aeronautics, Washington, DC.
- Xue, M. and Lu, L.-W. 1994. Interaction of infilled steel shear wall panels with surrounding frame members. Proceedings Structural Stability Research Council, Annual Technical Session, Bethlehem, PA. pp. 339-354.
- Yamaguchi, T., Nakata, Y., Takeuchi, T., Ikebe, T., and Nagao, T., 1998. Seismic control devices using low yield point steel. Nippon steel Co., Technical Report No. 368, Japan.

2. LITERATURE REVIEW

2.1 Introduction

The behaviour of columns plays a key role in the performance of reinforced concrete frames during earthquakes. The failures of columns are generally more catastrophic than those of beams. In past earthquakes such as the 1971 San Fernando (Fung *et al.*, 1971), 1989 Loma Prieta (NIST, 1990), 1994 Northridge (EERI, 1994), 1995 Kobe (EERI, 1995), and 1999 Kocaeli (Sezen *et al.*, 2003), non-ductile reinforced concrete frames were severely damaged and collapsed. The most common deficiency in non-ductile reinforced concrete frames is inadequate flexural strengths due to short and lightly confined lap splices located in the potential plastic hinge regions. The brittle mode of failure that often occurs due to this deficiency can be mitigated by providing external confinement by, for example, steel jackets in the plastic hinge region (Aboutaha *et al.*, 1996; Chai *et al.* 1990; and Valluvan *et al.*, 1993). In spite of using the strong column–weak beam concept in design, according to the recommendations of various codes, the formation of plastic hinges in the columns above the bases (at the foundation) cannot be avoided. In order to prevent the formation of plastic hinges in the columns of upper stories, Paulay (1986) demonstrated that the ratio of nominal flexural strength of the columns to that of the beams meeting at a joint should be in the range of 2.0 to 2.5. Satisfying the code requirements of the strong column–weak beam concept, therefore, does not guarantee that the plastic hinges will not form in the columns during strong earthquakes. Similarly, Mitchell and Paultre (1994) also reported that the formation of plastic hinges in columns is still possible despite the application of strong column–weak beam concept.

In the case of conventional concrete frames, plastic hinges generally form in the columns or beams close to the joints. However, in the case of concrete frames with steel infill panels (steel plate shear walls), the columns are subjected to high curvature ductility demands that extend well beyond the joint region due to the demand from the tension field that develops in the plate, as shown in the finite element model in Figure 2-1. In contrast, the beams are not affected as much by the tension field because in multi-storey structures there is little difference in the magnitude of oppositely acting tension field forces in the adjacent storeys. The present research focus is on the improvement of curvature ductility of concrete columns with poor reinforcement details through confinement using steel collars at locations away from the lap splices. The system can be used for rehabilitation of concrete frames either with or without steel plate shear walls. The behaviour of plastic hinges at the location of lap splices under steel collar confinement will be addressed in future research. In addition to poor reinforcement details, buildings can also be seismically

deficient due to configurational deficiencies such as: incomplete load path; vertical irregularities; horizontal irregularities; and inappropriate beam/column relative strengths (ATC-40, 1996). The discussion of these particular deficiencies is beyond the scope of this report.

This chapter provides an overview of the literature in key areas related to the present research. As such, the nature of concrete confinement is reviewed and several of the most prominent confinement models are discussed. In addition, the present requirements of ACI 318 pertaining to confinement are described as well as the historical progression of their development. Due to certain similarities with the behaviour of concrete confined by steel collars, some research into confinement using steel jackets is also summarized.

2.2 Confinement of Concrete

Confined concrete is defined as concrete that is restrained in the directions normal to the applied stress. There are two types of confinement: active confinement and passive confinement. When the transverse stress is externally applied, the confinement is called active confinement; for example, an axially loaded cylinder subjected to lateral fluid pressure is actively confined. The tests conducted by Richart *et al.* (1928) on test specimens confined by lateral fluid pressure showed that both the strength and ductility of the concrete were greatly increased.

The confinement of concrete by closely spaced spirals or hoops, or other non-prestressed means, is passive in nature. At low levels of axial concrete stress, the transverse reinforcement is virtually unstressed and thus the concrete behaves as if unconfined. The benefits of confinement are seen when the axial stresses approach the uniaxial capacity. At this point, the concrete increases in volume due to progressive internal fracturing and it bears against the transverse reinforcement, which in turn applies a confining reaction to the concrete. This confining action increased both the strength and the ductility of the concrete.

Numerous experimental studies have been performed on concrete confinement since the start of research in late 1920s. Some studies were performed on small-scale specimens (Richart *et al.*, 1928, 1929; Iyengar, 1970; Ahmad and Shah, 1982, 1985) and some were performed on large-scale specimens (Vallenas *et al.*, 1977; Sheikh and Uzumeri, 1980; Scott *et al.*, 1982; Mander *et al.*, 1988a). These studies show that the behaviour of confined concrete is affected by various factors summarized in the following.

2.2.1 Comparison Between Hydraulic and Rebar Confinements

Richart *et al.* (1928) tested concrete cylinders under constant hydraulic confining pressures. However, from specimen to specimen, the confining pressure was varied. Enhancement in both the strength and ductility of the concrete was achieved. The strength of concrete confined by an active hydrostatic fluid pressure can be represented by the following relationships:

$$[2.1] \quad f'_{cc} = f'_{co} + k_1 f_l$$

and the strain at peak stress of the confined concrete, ε_{cc} , is given by the following equation:

$$[2.2] \quad \varepsilon_{cc} = \varepsilon_{co} \left(1 + k_2 \frac{f_l}{f'_{co}} \right)$$

where:

- f'_{cc} = strength of confined concrete;
- ε_{cc} = strain at peak stress of the confined concrete;
- f_l = lateral confining pressure by fluid;
- ε_{co} = strain at peak stress of unconfined concrete; and
- f'_{co} = strength of unconfined concrete;

The values of the coefficients k_1 and k_2 depend on the concrete mix design and the lateral confining pressure and are related to each other by the equation (Richart *et al.*, 1928): $k_2 = 5k_1$. The coefficient k_1 assumes high values at low confining pressure and low values at high confining pressure. Saatcioglu and Razvi (1992) developed the following equation (also plotted in Figure 2-2) between the coefficient k_1 and the lateral confining pressure, f_l , by performing a regression analysis on the test results of Richart *et al.* (1928):

$$[2.3] \quad k_1 = 6.7(f_l)^{-0.17}$$

A similar trend was observed by Balmer (1949) in his tests, where k_1 varied from 4.5 to 7.0, with an average value of 5.6.

Richart *et al.* (1929) also conducted tests on spirally reinforced concrete cylinders. It was found that Equation 2.1 gives a good prediction of the confined strength of spirally reinforced cylinders for an average value of $k_1 = 4.1$, *i.e.*, the enhancement in strength of concrete with passive confining pressure resulting from closely spaced circular steel spirals was approximately the same as that for concrete with active confining pressure from hydraulic fluid. It was also reported by Iyengar *et al.* (1970) that confinement by hydraulic confining pressure and by circular spirals produce almost identical enhancement in concrete strength. Furthermore, the expression for strain at peak stress of confined concrete (Equation 2.2) based on the test results of concrete under hydraulic confining pressure is used in the confinement model proposed by Mander *et al.* (1988b). The confinement model proposed by Saatcioglu and Razvi (1992) makes use of both Equations 2.1 and 2.2 based on the test results of hydraulically confined concrete. Both of these models give a good prediction of the behaviour of concrete confined by steel rebars, confirming the similarity between the hydraulic confinement and rebar confinement.

2.2.2 Enhancement in Strength and Ductility due to Confinement

It has been shown experimentally that square hoops do not confine the concrete as effectively as circular spirals. This is because the confining reaction can only be applied in the corner regions of the hoops since the bending resistance (flexural stiffness) of the transverse steel between the corners is insufficient to restrain the expansion of the concrete along the whole length of bar. Therefore, the concrete is only effectively confined in the corner and central regions of the cross-section and disruption of a considerable portion of the core area occurs.

Iyengar *et al.* (1970) reported the test results of a large number of small-scale cylinders and prisms confined by circular spirals, square spirals, and hoops. A term “confinement index” was defined to quantify the level of confinement. It was found that for the same level of confinement index, the cylinders confined by circular spirals showed a greater enhancement in concrete strength as compared to those confined by square spirals and hoops. However, confinement by square spirals was found to be more effective than that of the square hoops. It was also found that for the same value of confinement index, the strain at peak stress of confined concrete was higher for concrete cylinders confined by circular spirals than that of those confined by square spirals and hoops. Also, the strain at peak stress of concrete prisms confined by square spirals was higher than that of prisms confined by square hoops.

Mander *et al.* (1988a) tested a large number of full-size columns with circular, square or rectangular cross-sections. Based on the test results, it was found that circular columns confined by spiral reinforcement performed better than square and rectangular columns with respect to both enhancement in concrete strength and strain at peak stress of confined concrete. Based on the test results of full-scale concrete columns confined externally by steel HSS (hollow structural sections) collars, Hussain and Driver (2004) also reported that both the strength and ductility of concrete increases through confinement.

2.2.3 Effect of Gage Length

Ahmad and Shah (1985) studied the effect of gage length on the stress vs. strain curves of unconfined and steel spiral confined concrete, through the test results of small-scale specimens. For the unconfined concrete, the following observations were made: (1) stress vs. strain curves for smaller gage lengths (102 mm) were stiffer than those obtained for larger gage lengths (311 mm). However, only a very small difference was observed in the secant modulus of elasticity, E_c , based on strain gages and large gage lengths (311 mm); (2) The strain at peak stress for a small gage length is smaller than that for a large gage length; and (3) The curves for small gage lengths were more ductile as compared to those for large gage lengths in the descending part beyond the peak.

For the confined concrete specimens, the following observations were made on the stress vs. strain curves: (1) For specimens with gage lengths less than or equal to the spiral spacing, a flatter descending branch of the stress-strain curve was obtained when the spiral spacing was close to the gage length; (2) In the specimens with gage lengths greater than the spiral spacing, a less steep (flatter) descending branch of the stress-strain curve was obtained when the gage length was close to the spiral spacing.

2.2.4 Effect of Strain Rate

Ahmad and Shah (1985) studied the effect of the longitudinal strain rate on the behaviour of confined and unconfined small-scale cylindrical concrete specimens. Spiral steel was used for confining the confined concrete. Two strain rates—a static strain rate (32×10^{-6} /sec) and a dynamic strain rate (30000×10^{-6} /sec)—were used. The secant modulus of elasticity and the peak strength of the plain concrete were increased due to the increase in strain rate. The post-peak behaviour of the plain concrete specimens under high strain rates could not be obtained due to

the explosive nature of the failure at maximum stress. It was also observed that the strain rate had no effect on the initial tangent modulus of elasticity of plain concrete. It was also found that the effect of strain rate on the secant moduli of elasticity of confined and unconfined concrete were about the same. By increasing the strain rate, both the peak stress and the strain at peak stress for confined concrete were increased. The descending branch of the stress-strain curve of the confined concrete became steeper due to the increase in the strain rate.

Scott *et al.* (1982) also studied the effect of strain rate on the behaviour of large-scale confined and unconfined concrete specimens. Two strain rates (3.3×10^{-6} /sec and 0.0167/sec) were used. (The strain rate 0.0167/sec is equivalent to that expected during earthquakes). For unconfined concrete specimens, both the secant modulus of elasticity and peak stress increase by increasing the strain rate. However, the strain at peak stress for plain concrete specimens appears to decrease by increasing the strain rate. For confined concrete specimens, it was observed that by increasing the strain rate, the peak stress, the strain at peak stress, and the slope of descending branch all increase.

2.2.5 Effect of Strength of Concrete

Based on their test results, Ahmad and Shah (1982) reported that the effectiveness of confinement decreases with the increase in concrete strength. This is because the higher strength concrete shows less lateral strain at peak stress as compared to that of low strength concrete. Models proposed by Razvi and Saatcioglu (1999), Cusson and Paultre (1995), Légeron and Paultre (2003) for predicting the behaviour of high-strength concrete also appreciate this phenomenon. According to these models, the strain at peak stress of confined concrete decreases with the increase of strength of unconfined concrete and the slope of the descending branch increases with the increase of strength of unconfined concrete.

2.2.6 Effect of Type of Aggregate

It was also observed by Ahmad and Shah (1982) in their tests that confinement reinforcement was less effective for light-weight concrete as compared to normal-weight concrete. The light-weight aggregate concrete shows characteristics similar to those of high strength concrete; the lateral expansion of light-weight concrete at peak stress is less than that of normal-weight concrete. In addition, similar to high strength concrete, the lightweight aggregate concrete exhibits low toughness, low ductility, and rapid of loss resistance after reaching the peak stress (Wang *et al.*, 1978; and Zhang and Gjrv, 1991).

2.2.7 Effect of Yield Stress of Confining Steel

Ahmad and Shah (1982) studied the effect of yield stress of the confining steel on the confining behaviour. For this purpose, the results of specimens with steel spiral wires with yield stresses of 276 MPa, 1116 MPa, and 1433 MPa were used. This effect was studied on two concrete strengths: 34 MPa and 45 MPa. In the case of 34 MPa concrete, the stress in the confining steels at the peak strength of the confined concrete was found to be approximately 276 MPa for all cases, meaning that one of the steels just reached its yield stress and the others did not yield. In the case of 45 MPa concrete, the stress in the confining steels at the peak strength of the confined concrete was equal to about 173 MPa in each case, indicating that none of the steels had yielded at this point.

In cases where yielding of the confining steel takes place after reaching the peak stress of the confined concrete, clearly the yield stress of the confining steel will not affect the peak stress of the confined concrete.

However, the slope of the descending branch is affected by the yield strength of the confining steel. Ahmad and Shah (1982) also predicted that the descending branch of the high-strength concrete could be made flat by using confining steel of very high yield strength. It is to be noted that the stress in the confining steel at peak stress of the confined concrete is less for 45 MPa concrete as compared to that of 34 MPa. This is because the lateral expansion of concrete at its peak stress reduces with the increase in the strength of the concrete.

Sheikh and Uzumeri (1980) observed in their testing program that by reducing the yield stress of the confining steel, the strength enhancement of the confined concrete decreases. This is not contrary to the Ahmad and Shah (1982) findings where yielding of the confining steel takes place either at the peak stress or after the peak stress of the confined concrete. In the case of the Sheikh and Uzumeri (1980) experimental program, a reduction in yield stress of the confining steel due to heat treatment led to yielding before reaching the peak stress of the confined concrete and, as a result, a reduction in the peak stress of the confined concrete took place.

Chung *et al.* (2002) reported based on their test results on 65 concrete columns of 200 x 200 mm cross-section that yielding of confining steel after the maximum load results in improved ductility. Yielding of the confining steel before and close to the peak load deteriorates the ductility of the confined concrete columns.

2.2.8 Effect of Spacing of Confining Steel

The behaviour of confined concrete is highly dependent on the spacing of the confining steel. Scott *et al.* (1982) reported, based on their test results, that with the increase of spacing of transverse reinforcement, keeping other parameters constant, the efficiency of confinement decreases.

If the spacing of transverse steel is too large, it becomes ineffective no matter how high the volumetric ratio of transverse steel is. Iyengar *et al.* (1970) reported, based on their test results, that the confinement is only effective if the spacing of the confining steel is less than the least lateral dimension of the column. For spacing of the confining steel equal to the least lateral dimension, virtually no enhancement in strength and ductility was observed. Similarly, Ahmad and Shah (1982), based on their test results, reported that the effect of confinement became negligible in specimens for spiral spacings equal to 1.25 times the diameter of the confined concrete core.

2.2.9 Effect of Amount of Confining Steel

The amount of confining steel in the columns has a significant effect on the behaviour of the column. Scott *et al.* (1982) reported that an increase in the amount of transverse reinforcement in the columns enhances the peak stress and longitudinal strain at first hoop fracture, and it decreases the slope of the declining branch of the confined concrete. In this research program, enhancements in concrete strength due to confinement equal to 22% and 24% were obtained for columns with volumetric ratios of tie steel equal to 0.0174 and 0.0182 (both at 72 mm on centres), respectively, tested under concentric monotonic axial loading at a slow strain rate (3.3×10^{-6} /sec).

In addition, enhancements in concrete strength equal to 41% and 79% were obtained for columns with volumetric ratios of tie steel equal to 0.0140 (at 98 mm on centres) and 0.0309 (at 64 mm on centres), respectively, tested under concentric monotonic axial loading at a high strain rate (0.0167/sec). The difference in the enhancement of concrete strength is the combined effect of change of spacing and change of volumetric ratio of transverse steel.

Sheikh and Uzumeri (1980) also reported that the amount of transverse reinforcement has a significant effect on the behaviour of confined concrete. It was observed that by increasing the

amount of transverse steel reinforcement, both the strength and ductility of concrete increases. In this research program, a total of 24 concrete columns of 305x305 mm in cross-section and 1955 mm overall height were tested under concentric monotonic axial loading at the same strain rates with different types of tie configurations and spacings. Enhancements in concrete strength equal to 18% and 70% were obtained for columns with volumetric ratios of tie steel equal to 0.008 (at 57 mm on centres) and 0.0227 (at 38 mm on centres), respectively, tested under concentric monotonic axial loading. The difference in the enhancement of concrete strength is the combined effect of change of spacing and change of volumetric ratio of transverse steel.

Mander *et al* (1988a) also reported, based on their tests on 500 mm diameter and 1500 mm long circular columns, that the most significant parameter affecting the behaviour of confined concrete is the quantity of the transverse reinforcement. In this research program, enhancements in concrete strength equal to 24% and 76% were obtained for columns with volumetric ratios of tie steel equal to 0.008 (with 119 mm spiral pitch) and 0.0182 (with 41 mm spiral pitch), respectively, tested under concentric monotonic axial loading. The difference in the enhancements of concrete strength is from the combined effect of the change of spacing and the change of volumetric ratio of transverse steel.

2.2.10 Effect of Strain Gradient

Scott *et al.* (1982) tested a total of 27 columns of size 450x450x1200 mm under concentric and eccentric axial loading at low and high strain rates. They observed that the presence of a strain gradient across the section that is steep enough to position the neutral axis within the limits of the cross-section increased the extreme longitudinal compressive strain at which first fracture of a hoop took place by 2.0 to 3.3 times as compared to the average compressive strain of a similar concentrically loaded column. It is to be noted that the average compressive strain of the concentrically and eccentrically loaded specimens were more or less the same at the fracture of the first hoop, however. In addition, the reduction in load after the peak was reached was smaller in the eccentrically loaded columns. Therefore, it was concluded that it is conservative to calculate the moment vs. curvature relationships of concrete members with the neutral axis within the section based on the stress vs. strain curve of concrete obtained from concentric load tests. The strain gradient of members in which the neutral axis lies outside of the section is similar to that of columns under concentric loading. Therefore, for such members, using the stress vs. strain curves of concrete obtained from concentric load tests results in a low level of conservatism.

2.2.11 Effect of Distribution of Longitudinal Steel and Resulting Tie Configuration

Sheikh and Uzumeri (1980) showed that the distribution of longitudinal steel and the resulting tie configuration has an effect on the confining behaviour of a column. Four patterns for the distribution of longitudinal steel around the core and the resulting tie configurations were investigated. It was found that the columns with well-distributed longitudinal bars around the column core showed a greater enhancement in strength and ductility. Scott *et al* (1982) also reported that by increasing the numbers of longitudinal bars around the column core, while keeping the longitudinal reinforcement ratio constant, the effectiveness of confinement was improved.

2.3 Confinement Models

Creating a model to predict the stress vs. strain behaviour of confined concrete has always been a challenge to researchers. Since the start of research in this field, numerous models have been proposed for this purpose such as those developed by Chan (1955); Roy and Sozen (1964); Soliman and Yu (1967); Sargin (1971); Kent and Park (1971); Vallenias *et al.* (1977); Sheikh and Uzumeri (1982); Mander *et al.* (1988b); Saatcioglu and Razvi (1992); Fam and Rizkalla (2001); Chung *et al.* (2002); and Légeron and Paultre (2003). All of these models are for the confinement of concrete by steel reinforcing bars except the model proposed by Fam and Rizkalla (2001), which is for the confinement of concrete by circular fiber-reinforced polymer tubes. A brief description of these models is given in the following.

2.3.1 Chan (1955)

Chan (1955) proposed a model for the stress vs. strain curve of unconfined and confined concrete shown in Figure 2-3, based on the test results of small-scale specimens (152 x 152 x 292 mm and 152 x 92 x 1321 mm) tested under axial load with small eccentricity. It was assumed that the strength enhancement factor, K_s , due to confinement, and the strain at peak stress of confined concrete, ε_{cc} , depend on the volumetric ratio of the confining steel to the core concrete. Equations for the strength enhancement factor, K_s , and strain at peak stress of confined concrete, ε_{cc} , were proposed.

While modelling the behaviour of unconfined concrete by this trilinear curve (OABC), the slope of line BC is always negative. In case of confined concrete, the slope of line BC depends on the level of confinement and for higher levels of confinement, it can be positive as shown in Figure 2-3.

2.3.2 Roy and Sozen (1964)

Based on the test results of small-scale prisms (127 x 127 x 635 mm) confined by steel rectilinear ties, Roy and Sozen (1964) concluded that confinement improves ductility without enhancing the strength of concrete. Based on these observations, a stress vs. strain model for confined concrete was proposed which is shown in Figure 2-4. The model curve consists of two linear segments; OA and AB. The slope of the descending branch depends on the level of confinement. In order to define the descending branch, an equation for ε_{cc50} was proposed, where, ε_{cc50} is the strain in the post-peak region at which the confined concrete stress becomes equal to 50% of the strength of the confined concrete. The variables considered for the ductility of the concrete were the volumetric ratio of confining steel to core concrete and the ratio of the shorter column dimension to the center-to-center spacing of tie steel.

2.3.3 Soliman and Yu (1967)

Soliman and Yu (1967) proposed a model to predict the stress vs. strain behaviour of concrete confined by steel reinforcement (Figure 2-5) based on eccentric compression tests on small-scale concrete specimens with cross-sections 76 x 152 mm, 102 x 152 mm, and 127 x 152 mm, having a simple tie arrangement (each tie consisted of only a single hoop). The overall height of the specimens was 1321 mm and they were divided into two end zones and a middle prismatic zone. The length of the end zone (including the tapered portion) was 406 mm and the length of the test region was 508 mm.

It was assumed that the confined concrete material curve depends on the area of the steel tie bar, the tie spacing, and the section geometry. The proposed curve (OABC) consists of three segments. The segment OA is a parabola that starts from the origin and ascends to its apex at point A ($\varepsilon_{ce}, f'_{cc}$). Segment AB is a horizontal line at the maximum confined concrete stress, f'_{cc} , up to a strain, ε_{cs} . Segment BC represents a linear descending branch of the material curve, the slope of which is determined using the strain quantity ε_{cf} (the strain in the

post-peak region that corresponds to a confined concrete stress of $0.8f'_{cc}$). In order to define the confined concrete material curves by this model, the values of f'_{cc} , ϵ_{ce} , ϵ_{cs} , and ϵ_{cf} are required, for which they proposed equations.

2.3.4 Sargin (1971)

The model for the stress vs. strain curve of concrete confined by rectilinear steel ties proposed by Sargin (1971) is shown Figure 2-6. The model is based on the results of small-scale concrete specimens (127 x 127 x 635 mm) tested under concentric and eccentric loading. No considerable difference in concrete strength for concentrically and eccentrically loaded specimens was obtained. A single continuous equation was proposed for the complete stress vs. strain response of confined concrete depicted in Figure 2-6. In the equation, shown in the figure, the variable A controls the slope of the ascending branch and D controls the path of the descending branch. In order to define the confined material curves by this model, the values of f'_{cc} and ϵ_{cc} are required. Based on his test results, Sargin (1971) proposed equations for the strength enhancement factor, K_s , and the strain at peak stress of confined concrete, ϵ_{cc} , both of which depend on the following variables: volumetric ratio of lateral steel reinforcement to concrete core; ratio of tie spacing to the width of concrete core; yield strength of steel; and unconfined concrete strength. Knowing the strength enhancement factor, the strength of confined concrete, f'_{cc} , can be calculated as follows: $f'_{cc} = K_s f'_{co}$.

2.3.5 Kent and Park (1971)

Kent and Park (1971) proposed a model to predict the stress vs. strain curve of concrete in rectangular or square columns confined by transverse steel hoops. The model curve ABCD (Figure 2-7) consists of three parts: (1) ascending branch AB, represented by a parabola which starts from the origin and terminates at point B ($0.002 f'_{co}$); (2) descending branch, represented by a straight line that extends to a stress equal to $0.2 f'_{co}$; and (3) the residual stress, for confined concrete only, represented by a horizontal straight line. The model is based on the results of previously existing experimental studies on small-scale column specimens with four corner bars and square ties as reported by Roy and Sozen (1965), Bertero and Felippa (1965), and Soliman and Yu (1967), in which no significant enhancement in concrete strength was observed. Hence, to be on the conservative side, this model assumes no enhancement in

concrete strength and no enhancement in strain at peak stress due to confinement. The presence of confinement steel only affects the slope of the descending branch. The slope of the descending branch becomes less steep by increasing the amount of confining steel and vice versa. The slope of the descending branch depends on the concrete strength, the volumetric ratio of confining steel to core concrete, and the ratio of tie spacing to the minimum core dimension.

Later, tests were performed on more realistic nearly full-size reinforced concrete columns as reported by Scott *et al.* (1982) and Park *et al.* (1982). Enhancement in both the concrete strength and ductility were observed in these tests due to confinement. As a consequence, the Kent and Park model was modified (Park *et al.* 1982) to take into account the enhancement in both concrete strength and strain at peak stress strain due to confinement, as shown in Figure 2-8, in addition to the effect of confinement on the slope of descending branch (which was in the original model). The model assumes that the factor for the enhancement of strength and strain at peak stress of the confined concrete is the same and depends on the following variables: (1) concrete strength; (2) yield strength of confining steel; and (3) volumetric ratio of confining steel.

2.3.6 Vallenias *et al.* (1977)

Vallenias *et al.* (1977) proposed a model (Figure 2-9) to predict the stress vs. strain curve for rectangular or square concrete columns confined by steel hoops. The model is based on the test results of large-scale square column specimens (254 x 254 x 762 mm) in which enhancement in both strength and ductility was observed. In As a consequence, the proposed model takes into account both the enhancement in concrete strength and strain at peak stress due to confinement. However, the basic structure of this model is similar to the one proposed by Kent and Park (1971), *i.e.*, the model curve (ABCD) consists of three parts: (1) the ascending branch (AB), represented by a parabola; (2) the descending branch (BC), represented by a straight line; and (3) the residual stress equal to 30% of the confined concrete strength, represented by a horizontal straight line (CD).

The model assumes that the behaviour of the confined concrete depends on the following variables: (1) strength of concrete; (2) ratio of the volume of the confining steel to the volume of confined concrete core; (3) ratio of tie spacing to the minimum core dimension; (4) ratio of the cross-sectional area of longitudinal bars to the cross-sectional area of the column, which takes into account the effect of longitudinal bars in confining the column concrete; (5) ratio of nominal diameter of hoop reinforcement to the nominal diameter of the longitudinal steel bars; (6) yield stress of the confining steel.

2.3.7 Sheikh and Uzumeri (1982)

Sheikh and Uzumeri (1982) proposed a model (Figure 2-10) for predicting the stress vs. strain curve of concrete in square concrete columns confined by transverse steel reinforcement. The proposed model curve consists of four segments: (1) ascending branch (AB), represented by a parabola starting from the origin and ascending to a point A (ϵ_{s1} , f'_{cc}); (2) sustaining branch (AB), represented by a horizontal straight line at the maximum confined concrete stress, f'_{cc} , to point B (ϵ_{s2} , f'_{cc}); (3) descending branch (BD), represented by a sloping straight line extending up to the residual stress level; and (4) the residual stress equal to $0.3f'_{cc}$, represented by a horizontal straight line. The proposed model curve depends on the following variables: (1) strength of concrete; (2) center-to-center spacing of transverse reinforcement; (3) center-to-center distance of perimeter hoop (core dimension); (4) distribution of longitudinal steel; (5) volumetric ratio of confining steel; and (6) stress in the confining steel at peak stress of the confined concrete. The model takes into account the effect of ineffectively confined regions in the column core on the strength enhancement factor. The effectiveness of confinement decreases with the increase of ineffectively confined regions in the core. The amount of ineffectively confined regions in the core depends on the spacing and configuration of ties and the distribution of longitudinal bars.

The major difference between this model and the model proposed by Vallenias *et al.* (1977) is in how the effect of longitudinal bars in confining the concrete is taken into account. Vallenias *et al.* (1977) takes this factor into account by assessing the ratio of cross-sectional area of longitudinal bars to the cross-sectional area of the column, whereas Sheikh and Uzumeri (1982) consider the distribution of longitudinal bars around the core perimeter.

2.3.8 Mander *et al.* (1988b)

Mander *et al.* (1988b) proposed a model (Figure 2-11) for predicting the stress vs. strain curve of concrete confined by circular hoops, or rectangular hoops with or without supplementary cross-ties. The model also takes into account the effect of strain rate and allows for cyclic loading (but only the quasi-static part of the model is discussed herein). The model can also account for unequal confining stresses along each of the longitudinal faces of the column core. Similar to that by Sargin (1971), the model makes use of a single equation proposed by Popovics (1973) (originally developed for predicting the behaviour of unconfined concrete) for tracing the

complete stress vs. strain curve of confined concrete. Similar to Sheikh and Uzumeri (1982), the effect of ineffectively confined regions in the core was also considered. A confinement effectiveness coefficient was defined in terms of these ineffectively confined regions in the core. In order to plot the confined concrete material curve using this equation, the compressive strength of confined concrete, f'_{cc} , and the strain at peak stress, ϵ_{cc} , are required. The confined compressive strength, f'_{cc} , is determined using a constitutive model for multiaxial compressive stresses, and the strain at peak stress, ϵ_{cc} , is determined using Equation 2.2. The failure criterion is defined using an energy balance approach. The longitudinal compressive strain in the concrete at which fracture of the first hoop takes place is considered to be the failure strain. The failure strain of concrete is determined by equating the strain energy capacity of the transverse reinforcement to the strain energy stored in the concrete as a result of confinement. The model assumes that the confining behaviour of concrete depends on the amount of confining steel expressed in terms of the sectional reinforcement ratio, the yield stress of confining steel, the distribution of longitudinal steel around the core perimeter, the center-to-center spacing of confining steel, and the strength of unconfined concrete.

2.3.9 Saatcioglu and Razvi (1992)

Saatcioglu and Razvi (1992) proposed an analytical model (Figure 2-12) for the stress vs. strain behaviour of concrete confined by circular and rectilinear steel reinforcement. The model takes into account the effect of the distribution of longitudinal reinforcement around the core perimeter. It gives good predictions for circular, square, and rectangular sections confined with steel spirals, rectilinear hoops, cross-ties, welded wire fabric, and combinations of different types of lateral reinforcement. The model recognizes the potential differences in confinement pressures in the two orthogonal directions and allows for the superposition of confinement effects of different types and arrangements of reinforcement. The model can handle concentric and eccentric loading, and slow and fast strain rates. The model curve (Figure 2-12) consists of three segments. Segment AB is a parabola that starts from the origin and goes to point B (ϵ_{cc} , f'_{cc}). The descending branch BC is represented by a sloping straight line, the slope of which depends on the level of confinement and is determined based on the strain ϵ_{cc85} , which is the strain of the confined concrete in the post-peak region at a stress equal to $0.85f'_{cc}$. The descending branch is followed by a horizontal straight line at the residual stress level equal to $0.20f'_{cc}$. The model provides equations for calculating the values of the confined concrete strength, f'_{cc} , strain at peak stress of confined concrete, ϵ_{cc} , and strain at 85% of the confined concrete strength in the

post-peak region, ε_{cc85} . The model assumes that the behaviour of confined concrete depends on the amount of confining steel expressed in terms of the sectional reinforcement ratio, the yield stress of the confining steel, the centre-to-centre spacing of ties, the distribution of longitudinal bars, and the strength of unconfined concrete.

2.3.10 Chung *et. al* (2002)

Chung *et al.* (2002) proposed a model (Figure 2-13) for the stress vs. strain curve of concrete confined laterally by rectilinear tie reinforcement in square concrete columns, based on the test results of 65 columns of 200x200 mm cross-section and 600 mm height of unconfined concrete strengths varying from 20 to 54 MPa. The model assumes that the confining behaviour of concrete depends on the volumetric ratio of confining steel to the core concrete, the tie configuration, the yield strength of the tie steel, the diameter of the ties, the centre-to-centre spacing of ties, the distribution of longitudinal bars, and the unconfined concrete strength. The model accounts for transverse reinforcement of low and high yield strength. The model is not based on the assumption of yielding of the tie steel at the peak stress of confined concrete, as was assumed in the previously existing confinement models, but it provides an equation for determining the stress in the tie steel at that point. It is assumed that the stress in the tie steel at the peak stress of confined concrete is a function of the modulus of elasticity of the tie steel, the configuration of the ties, the volumetric ratio of the tie steel, and the strength of concrete.

The model curve (OACD) consists of three segments. The Popovics (1973) equation was used to model the first segment from point O to point A (ε_{cc} , f'_{cc}). The descending branch is represented by a sloping straight line AC, the slope of which can be determined with the help of ε_{cc85} , which is the strain of confined concrete at $0.85f'_{cc}$ in the post-peak region. The descending branch is followed by a horizontal line at the residual stress of $0.30f'_{cc}$. The model gives equations for the strength enhancement factor, K_s , which is used to calculate the strength of confined concrete as $f'_{cc} = K_s f'_{co}$, the strain at peak stress of confined concrete, ε_{cc} , and the strain at $0.85f'_{cc}$ in the post-peak region, ε_{cc85} .

2.3.11 Légeron and Paultre (2003)

A more general model (Figure 2-14) for the confinement of concrete was proposed by Légeron and Paultre (2003) that can accommodate circular, square, and rectangular columns. It assumes

that discrete confinement elements can be replaced by an equivalent continuous confinement tube. The model is valid for normal- and high-strength concrete and can handle transverse reinforcement of low and high yield strength. The model curve (OAC) consists of two parts: the ascending branch OA, represented by an equation proposed by Popovics (1973) and the descending branch AC, represented by an expression obtained by modifying an equation proposed by Fafitis and Shah (1985). The model assumes that the confining behaviour of concrete depends on the sectional reinforcement ratio of transverse steel, the centre-to-centre spacing of ties, the tie configuration, the yield strength of the tie steel, the diameter of the ties, the distribution of longitudinal bars, and the unconfined concrete strength. Similar to Chung *et al* (2002), the model does not assume that the tie steel yields at the peak stress of the confined concrete. Rather, it provides an equation for calculating the stress in the tie steel at that point. The tie steel stress can be equal to or lower than the yield stress at the peak stress of confined concrete. Légeron and Paultre (2003) proposed the following equation in terms of the effective sectional transverse steel ratio, ρ_{sex} or ρ_{sey} , and the unconfined concrete strength, f'_c , to determine the yielding of the confining steel at peak stress of confined concrete:

$$[2.4] \quad \rho_{sex} \text{ or } \rho_{sey} = \frac{(f'_c)^{0.6}}{1000}$$

When the effective sectional steel ratio provided in a column, ρ_{sex} or ρ_{sey} , is larger than the value given by the right-hand side of the Equation 2.4, the confinement steel yields at the peak load regardless of its yield strength due to the higher strain at peak stress. (This relationship is likely to break down for very high values of the steel ratio due to the assumption in the model of a continuous reinforcing tube.) Conversely, if the amount of confining steel in a column is less than this amount, then it will not yield at the peak stress of the confined concrete. The effective sectional steel ratios take into account the effect of ineffectively confined regions in the core by the procedures defined by Sheikh and Uzumeri (1982) or Mander *et al.* (1988b).

2.3.12 Fam and Rizkalla (2001)

An analytical model has been proposed to predict the behaviour of axially loaded short concrete columns confined by fiber-reinforced polymer (FRP) circular tubes (Figure 2-15). The model is applicable to totally filled and partially filled tubes; that is, the concrete core can be with or without a central hole. The model is capable of predicting the behaviour of a confined column when the load is applied to the concrete core only, as well as when the load is applied to the concrete core and the tube simultaneously. The biaxial strength criterion for the FRP is used to

account for the biaxial state of stress. The model is based on equilibrium and radial displacement compatibility.

The stress vs. strain behaviour of FRP is linear. Therefore, the confining pressure induced by the FRP tube is variable. Consequently, a step-by-step strain incremental technique, utilizing the equations proposed by Mander *et al.* (1988b) for constant confining pressure, is used to develop the confined stress-strain curve. The secant Poisson's ratio of confined concrete depends on the confining pressure. Small increments of axial strain are taken so that during each increment, the confining pressure and the secant Poisson's ratio of confined concrete can be assumed constant. In an increment, several unknowns are encountered. Hence, an iterative procedure is used to get convergence on the values of the unknown variables within an increment. After convergence, the next increment on axial strain is taken and the process is repeated until convergence is achieved. In this way, the complete stress-strain curve for FRP confined concrete is traced until the fracture of the FRP (Figure 2-15). In Chapter 5, a model is proposed for predicting the behaviour of columns confined externally by steel collars having significant axial and flexural stiffness that makes use of relationships for the dilation of confined concrete proposed by Fam and Rizkalla (2001).

2.4 Deficiencies in the Existing Confinement Models

The existing confinement models are unable to predict the behaviour of concrete confined by steel collars with significant axial and flexural stiffness principally because of the following two reasons: (1) the existing models lack an explicit flexural stiffness parameter for the confining element; and (2) the confining pressure imposed by steel collars varies through the axial load history because of their high stiffness. The first reason applies to all models cited, while the second is addressed to some degree in some of the more recent models. These two deficiencies in the existing confinement models are elaborated in the following.

2.4.1 Flexural Stiffness of Confining Elements

Both the axial and flexural stiffnesses of the confining elements contribute to concrete confinement. In the existing models for the confinement of concrete by rebars, the most important parameter for concrete confinement is the amount of confining steel, expressed as either a volumetric ratio of the confining steel to core concrete or in terms of the sectional ratio of confinement reinforcement. These transverse steel ratios are directly related to the cross-sectional area of the confining elements. However, they do not give direct information

about the diameter of the tie bars, which is also related to their flexural stiffness. Conventionally, in concrete columns, the confinement is provided by small diameter ties having significant axial stiffness but negligible flexural stiffness. Therefore, no explicit parameter for flexural stiffness was introduced in the existing confinement models. Most of the confinement models are based on regression analyses performed on the test results of columns. Therefore, any effect of the small flexural stiffness of the transverse ties is implicitly incorporated in the other parameters of the models. Researchers like Kent and Park (1971), Iyengar (1970), and Saatcioglu and Razvi (1992) recognized the effects of the flexural stiffness of the confining elements in addition to their axial stiffness in confining the concrete, but no explicit flexural stiffness parameter was included in their models. This aspect of the existing confinement models makes them unsuitable for modelling concrete columns confined by steel collars with significant flexural stiffness.

ACI 318-02 requires that the diameter of the tie steel not be less than #3 (10 mm). The code also requires that the distance between two neighbouring corners of ties, cross-ties, or both (which is also referred to as the unsupported length, L_u) on any side of the exterior boundaries of confined core of concrete columns shall not exceed 14 in. (355 mm), as depicted in Figure 2-16. Moreover, the clear distance between an unsupported longitudinal bar and an adjacent supported bar on the same face of the column may not be more than 6 in. (152 mm). (Supported longitudinal bars are those that are supported by a cross-tie or placed in the corner of a hoop with an included angle not more than 135 degrees.) It is to be noted that the unsupported length, L_u , is not a function of the diameter of the tie bar. By providing these restrictions on the reinforcement of columns, the intent of the code is, in part, to provide sufficient lateral restraint (due to flexural stiffness of ties) to the unsupported longitudinal bars of the columns (between two supported bars) to prevent them from buckling. These restrictions specified by the code on the detailing of column steel may help to confine the concrete.

Hussain and Driver (2001) demonstrated through finite element study that the flexural stiffness of confining elements has a significant effect on the behaviour of confined concrete. The effect of flexural and axial stiffness of the confining elements on the behaviour of confined concrete was segregated numerically. Khaloo and Bozorgzadeh (2001) also demonstrated the contribution of flexural stiffness of confining elements to the behaviour of confined concrete based on the results of two experimental studies (Khaloo *et al.*, 1999; Khaloo and Bozorgzadeh 2001).

Khaloo and Bozorgzadeh (2001) tested eight elliptical-shaped high-strength light weight aggregate concrete columns of 152 x 229 mm cross-section and 762 mm height under axial loading. The confinement was provided with steel wires of 4.52 mm diameter with a yield strength of 621 MPa. Four longitudinal bars of the same wire were placed longitudinally in the

column to hold the lateral reinforcement in the desired configuration. The results of this study were compared with those of similar columns confined by steel reinforcement of larger diameter (Khaloo *et al.*, 1999). Comparing the results of the two studies, the effect of flexural stiffness of confining steel on the behaviour of high-strength light weight concrete columns was evaluated. It was concluded that columns confined by hoops of small diameter wires showed considerably lower strength and ductility than those confined by a larger diameter hoop for the same unsupported length, amount and spacing of confining steel, and concrete strength. It was also observed that the effect of flexural stiffness became more prominent in high-strength concrete.

2.4.2 Variation of Confining Pressure with Axial Load History

The confining pressure can be constant or variable through the axial load history of the columns. When the confining material behaves plastically, constant confining pressure can be assumed, as is often done in confinement models for traditional tied columns. The existing models by Sargin (1971), modified Kent and Park (Park *et al.*, 1982), Vallenias *et al.* (1977), Sheikh and Uzumeri (1982), Mander *et al.* (1988b), and Saatcioglu and Razvi (1992) for predicting the behaviour of confined concrete are based on the assumption that the confining pressure remains constant throughout the axial load history. The confinement models proposed by Mander *et al.* (1988b) and Saatcioglu and Razvi (1992) directly use equations proposed by Richart *et al.* (1928) that were developed based on the test results of concrete cylinders under constant hydraulic confining pressure. The assumption of constant confining pressure remains valid if the confining steel yields at or before the peak stress of the confined concrete because the greatest influence of confinement on the compressive behaviour of the concrete occurs near and beyond the peak stress. Therefore, these existing models assume that yielding of the tie steel occurs at the peak stress.

Sheikh and Uzumeri (1982) assumed, in the derivation of their confinement model, that the stress in the tie steel at the peak stress of confined concrete could be less than the yield strength of the tie steel. However, no equation was proposed for the calculation of this stress and hence, while applying this model to predict the behaviour of confined columns, yielding of the tie steel at the peak stress of confined concrete was assumed. The most recent models for concrete confined by rebars or high-strength wires, such as those proposed by Chung *et al.* (2002) and Légéron and Paultre (2003), do not assume that yielding of the confining steel necessarily occurs at the peak stress of the confined concrete and they provide equations to calculate this stress. In situations where the stress in the confining steel is less than the yield strength, the confining pressure on the columns cannot be assumed constant through the axial load history.

Variable confining pressure is generated through the use of confining elements that remain elastic through the axial load history of the confined columns and have considerable stiffness. For example, the confining pressure generated by FRP confinement varies because the material remains elastic through the axial load history (Fam and Rizkalla, 2001). The confining pressure in columns confined by steel collars (HSS collars or solid steel collars) also varies through the axial load history of the columns because of their high stiffness, as demonstrated by Hussain and Driver (2003).

2.5 Code Requirements for Concrete Confinement

2.5.1 Current Requirements (ACI 318–02 and CSA–A23.3–94)

The confinement requirements for square and rectangular columns are derived from those for circular columns with spiral reinforcement. Because the hoops in rectangular and square collars are less efficient than spirals in providing confinement, an allowance is included to give the hoops (and cross-ties) a greater total cross-sectional area than the requirements for spirals. The hoops are assumed to yield at the peak axial column stress. According to ACI 318-02, the confinement requirements for square and rectangular columns at the location of plastic hinges are controlled by the one of the following equations that gives the higher greater value of A_{sh} :

$$[2.5] \quad A_{sh} = 0.3sh_c \left[\frac{f'_c}{f_{yh}} \right] \left[\frac{A_g}{A_{ch}} - 1 \right]$$

$$[2.6] \quad A_{sh} = 0.09sh_c \left[\frac{f'_c}{f_{yh}} \right]$$

where:

A_{ch} = area of rectangular core of column measured out-to-out of hoop;

A_g = gross area of the section;

A_{sh} = total cross-sectional area of transverse reinforcement (including cross-ties) within spacing s and perpendicular to dimension h_c ($= 2 \times A_{tie}$);

- A_{tie} = cross-sectional area of one leg of the hoop reinforcement;
- f'_c = specified compressive strength of concrete as measured from standard cylinders;
- f_{yh} = specified yield strength of transverse reinforcement but not more than 60 000 psi (414 MPa);
- h_c = cross-sectional dimension of the column core measured centre-to-centre of confining reinforcement;
- s = centre-to-centre spacing of transverse reinforcement in the longitudinal direction of the column;
- ρ_s = volumetric ratio of spiral steel

Equation 2.6 provides a minimum transverse reinforcement area to account for large columns for which Equation 2.5 does not result in a sufficient level of confinement.

In order to provide a certain efficiency of the confinement mechanism and to prevent buckling of the longitudinal bars, the code also requires that the centre-to-centre spacing of the transverse reinforcement shall not exceed (a) one-quarter of the minimum member dimension, (b) six times the diameter of the longitudinal reinforcement, and (c) s , as defined by the following equation (both s and h_x are in inches):

$$[2.7] \quad s = 4 + \left(\frac{14 - h_x}{3} \right)$$

where:

- h_x = maximum unsupported length of rectangular hoops measured between perpendicular legs of the hoop or supplementary cross-ties;

2.5.2 Evolution of Requirements in ACI 318

Prior to the publication of ACI 318-71, the confinement requirements for circular columns with spiral reinforcement were controlled by the following equation:

$$[2.8] \quad \rho_s = 0.45 \left[\frac{f'_c}{f_{yh}} \right] \left[\frac{A_g}{A_c} - 1 \right]$$

where:

A_c = area of the concrete measured to outside diameter of spiral;

This equation is derived on the basis that the loss in load carrying capacity of the column due to the spalling of concrete cover is compensated by the enhancement of concrete strength in the core due to confinement. The spiral reinforcement is assumed to yield. The derivation of this equation is given in Appendix A.

Equation 2.8 does not provide sufficient confinement for large circular columns. Therefore, in ACI 318-71, a lower limit to the volumetric ratio of the spiral steel was introduced:

$$[2.9] \quad \rho_s = 0.12 \left[\frac{f'_c}{f_{yh}} \right]$$

Prior to ACI 318-71, there were no codified equations available for the confinement of square and rectangular columns. In ACI 318-71, the following equation was introduced to calculate the area of one leg of the hoop reinforcement in these columns (the derivation of this equation is also given in Appendix A):

$$[2.10] \quad A_{tie} = \frac{L_u \rho_s s}{2}$$

where L_u is the unsupported length of rectangular hoops measured between perpendicular legs of the hoop or supplementary cross-ties, as shown in Figure 2-16.

The derivation of Equation 2.10 is given in the commentary of ACI 318-71 and is also reproduced in Appendix A. This equation was derived based on the assumption that rectangular hoops are 50% less effective in confining the concrete than spirals. Substituting the values of ρ_s from Equations 2.8 and 2.9 into Equation 2.10, the following equations are obtained:

$$[2.11] \quad A_{tie} = 0.225sL_u \left[\frac{f'_c}{f_{yh}} \right] \left[\frac{A_g}{A_c} - 1 \right]$$

$$[2.12] \quad A_{tie} = 0.06sL_u \left[\frac{f'_c}{f_{yh}} \right]$$

Writing Equations 2.11 and 2.12 in terms of A_{sh} , as defined by ACI 318-83 and later versions, and assuming that the section is square and contains only a perimeter hoop (and replacing L_u by h_c and A_c by A_{ch}), the following equations are obtained:

$$[2.13] \quad A_{sh} = 2 \times A_{tie} = 0.45sh_c \left[\frac{f'_c}{f_{yh}} \right] \left[\frac{A_g}{A_{ch}} - 1 \right]$$

$$[2.14] \quad A_{sh} = 2 \times A_{tie} = 0.12sh_c \left[\frac{f'_c}{f_{yh}} \right]$$

It should be noted that L_u and h_c are the same for a square column with only a perimeter hoop. Although Equation 2.10 (ACI 318-71) is based on the assumption that the confinement efficiency of the hoop reinforcement is 50% of that of spirals, in ACI 318-83, this estimate was increased to 75%, resulting in the following revised requirement:

$$[2.15] \quad A_{tie} = \frac{L_u \rho_s s}{3}$$

In terms of A_{sh} , Equation 2.15 becomes:

$$[2.16] \quad A_{sh} = 2 \times A_{tie} = 2 \left[\frac{l_h \rho_s s}{3} \right]$$

Substituting the value of ρ_s from Equation 2.8 into Equation 2.16 (and replacing L_u by h_c and A_c by A_{ch}), the following equation is obtained:

$$[2.17] \quad A_{sh} = 0.3sh_c \left[\frac{f'_c}{f_{yh}} \right] \left[\frac{A_g}{A_{ch}} - 1 \right]$$

For large-sized columns, Equation 2.14 was adopted in ACI 318-83, without modification, and is repeated here:

$$[2.18] \quad A_{sh} = 0.12sh_c \left[\frac{f'_c}{f_{yh}} \right]$$

In all subsequent editions of the code, the confinement reinforcement was controlled by the same equations as those contained in ACI 318-02 (Equations 2.5 and 2.6).

2.6 Rehabilitation of Reinforced Concrete Columns by Jacketing

Widely spaced ties and short lap splices of longitudinal bars located in the plastic hinge regions of reinforced concrete columns are the most common problems that render the columns seismically deficient due to their resulting lack of ductility and energy dissipation capabilities. A number of jacketing techniques have been developed to overcome these deficiencies such as steel jacketing, active confinement by wire prestressing, concrete jacketing, and jacketing by composite materials. For example, the California Department of Transportation (CALTRANS) has adopted the use of steel jackets for the seismic upgrade of bridge columns. Numerous experimental studies have been conducted to study the performance of seismically deficient reinforced concrete columns rehabilitated by jacketing. Among them, some studies appreciate the effect of the flexural stiffness of the jackets in confining the concrete. In the following, the details of a few experimental studies on rehabilitated reinforced columns are presented.

2.6.1 Valluvan *et. al* (1993)

This paper presents techniques for strengthening tensile lap splices of the longitudinal reinforcement in the columns of seismically deficient reinforced concrete structures. Twelve, two-third scale specimens (one without rehabilitation and 11 rehabilitated) with lap splices in the longitudinal bars were tested under alternating axial tensile and compressive loads. The specimens were 305 x 305 mm in cross-section and 1829 mm in length. High strength rods of 38 mm (1.5 in.) diameter were embedded at the top and bottom ends to apply a tensile load to the specimens. The compressive load was applied with plates with holes (to permit tension rods pass through it), grouted on the top and bottom of the specimens. Several techniques were used for rehabilitation of the short lap splices in these specimens: welding of lapped bars; welding of lapped bars with an additional tie to overcome the outward thrust due to the eccentricity in the splice; ungrouted steel angles and straps; grouted steel angles and straps; ungrouted external ties; grouted external ties; partially grouted external ties; and additional internal ties. Based on the test results, the following conclusions were drawn.

With respect to performance, the grouted angle and straps scheme is the preferred scheme for the rehabilitation of column splices. However, difficulty of construction makes the scheme less attractive as compared to rehabilitation by providing external ties. The external tie scheme is easier to construct and is cost effective provided there is no limitation on the rehabilitated column dimensions. Adding internal ties is not a suitable rehabilitation scheme for column splices because the concrete core is affected during chipping.

Welded splices would be a suitable rehabilitation scheme when there are limitations on the column dimensions. In older structures, the carbon content of the steel is relatively lower than that of the steel used in current practice; hence, the older steel is more weldable. Strict quality control is required for proper welding of spliced bars such as chemical analysis and proper welding procedures and inspection.

2.6.2 Chai *et al.* (1990)

Chai *et al* (1990) reported on an experimental program for studying the effectiveness of steel jackets in enhancing the seismic performance of circular and rectangular concrete columns with inadequate lap splices and insufficient transverse reinforcement. The experimental program consisted of a total of 24 columns of circular and rectangular cross-sections with long and short shear spans. Circular flexural columns were rehabilitated with cylindrical steel jackets and the

gap between the concrete and steel jacket was about 6.35 mm (1/4in.) and was filled with cement-based grout. Rectangular flexural columns were rehabilitated with three types of steel jackets: elliptical steel jackets (the gaps between the steel jacket and the column were filled with concrete, rectangular steel jackets with grids of horizontal and vertical steel stiffeners (the gaps between steel and concrete were filled with cement-based grout), and jacketing consisting of side by side vertical channels enclosed by horizontal channels with bolted corner connections (the gaps between the column and the steel channels were filled with cement-based grout). The latter two schemes of jacketing rectangular columns make use of the out-of-plane flexural stiffness of the confining elements. Circular shear columns were rehabilitated with cylindrical steel jackets and rectangular shear columns were rehabilitated with elliptical steel jackets only.

The result showed that ductility, strength, energy dissipation capability, and shear strength of seismically deficient reinforced concrete columns were greatly improved by steel jacketing. However, comparison of the various jacketing schemes for rectangular concrete columns showed that the elliptical steel jackets proved to be the best rehabilitation scheme in terms of performance.

2.6.3 Marsh (1992)

Marsh (1992) reported the test results of 18 in. diameter circular reinforced concrete columns with inadequate lap splices rehabilitated by pretensioned steel hoops in the splice region. The rehabilitated columns showed significant enhancement in lateral load resistance, flexural strength, and ductility.

2.6.4 Aboutaha *et al.* (1996)

Aboutaha *et al.* (1996) studied the effectiveness of different types of steel jackets for improving the strength and ductility of reinforced concrete columns with widely spaced ties and inadequate lap splices in the longitudinal reinforcement at the location of plastic hinges. The experimental program consisted of a total of 11 large-scale columns with different widths tested under lateral cyclic loading without axial load (having no axial load was considered more critical for splices). Four columns were tested without strengthening and acted as reference columns. Seven columns were tested after strengthening. Six of these columns were strengthened with grouted steel jackets with and without anchor bolts (the function of anchor bolts is to stiffen the steel jackets to improve confinement) and the remaining was strengthened with closely spaced collars made from steel channels (C100x11) with bolted corner connections. A total of three collars were used in the plastic hinge region. These collars were not clamped onto the columns but instead a

gap was kept between the collars and the columns that was filled later with a non-shrink grout. On one side of the column, an anchor bolt was also used that passed through the channel and into the column, presumably to assess the benefits of additional anchorage.

The test results showed that a thin rectangular steel jacket combined with adhesive anchor bolts is highly effective in improving the seismic performance of reinforced concrete columns with inadequate lap splices. The columns rehabilitated with channel collars experienced an early splice failure, although the collars were relatively widely spaced, they were flexible for the column size (910x460 mm), and were not prestressed to the column.

2.6.5 Xiao and Wu (2003)

An improved jacketing method is presented in this paper to rehabilitate square and rectangular reinforced concrete columns that have inadequate longitudinal bar splices located in the plastic hinge regions enclosed by widely spaced ties. Jackets made by welding together thin steel plates were grouted onto the columns and then stiffened by providing flexurally stiff confining elements at the locations of plastic hinges. Thin jackets provide an enhancement in shear strength and the stiffeners tend to enhance the strength, ductility, and energy-dissipation through confinement. In this experimental program, three types of stiffeners were used in the plastic hinge regions: stiffeners made from thick steel plates, stiffeners made from steel angles, and stiffeners made from square steel hollow structural sections (HSS). In all the cases, the corner connections of the stiffeners were welded and the stiffeners were welded onto the thin steel plate jackets. Five 254x254 mm columns, rehabilitated by this scheme, were tested in double-curvature with the inflection point at midheight of the column, under constant axial load and lateral cyclic loading. Test results showed improved behaviour of the rehabilitated columns with respect to the enhancement in the shear strength and ductility. An ultimate drift ratio of more than 8% was obtained for these columns showing the efficiency of this rehabilitation scheme and the benefits of providing flexurally stiff elements. The authors also proposed a procedure for the design of these jackets.

2.6.6 Ghobarah *et al.* (1997)

Rectangular steel jackets are unable to confine rectangular concrete columns effectively because of their low flexural stiffness. Ghobarah *et al.* (1997) developed a steel jacket made from corrugated steel to effectively confine beam-to-column joints. The experimental program consisted of four large-scale beam-to-column joint specimens. One specimen satisfied the code requirements of reinforcement detailing and the remaining three had insufficient transverse

reinforcement. Two of the specimens—the one with sufficient reinforcement and the other without—were tested without external jacketing. The other two specimens without sufficient internal tie reinforcement were tested after rehabilitation by corrugated steel jacketing. In one such specimen, corrugated steel jacketing was provided on the beam, column, and joint region and in the other specimen jacketing was provided on the column and joint only. The results show that confinement with corrugated steel jacketing improves the performance of the beam-to-column joints through enhancement in shear strength and ductility. Corrugated steel jackets confine the concrete effectively through their out-of-plane flexural stiffness.

2.7 Summary

The focus of the present research is to improve the seismic performance of reinforced concrete frames through providing external confinement by HSS collars at the location of plastic hinges or through a combination of HSS collars and steel plate shear walls. In either case, the collar confinement plays a pivotal role in the seismic performance of the rehabilitated frames. Therefore, the nature of confinement is reviewed in this chapter. Research on the confinement of concrete started in 1920s. Summaries of several experimental research studies conducted since then, on small- and large-scale specimens, are reported. A comparison between hydraulic and rebar confinement is presented. It has been reported extensively in the literature based on experimental studies that confinement improves both the strength and ductility of concrete. Through the results of existing experimental research, effects of various parameters, such as: gauge length, strain rate, strength of concrete, type of aggregate, yield stress of confining steel, spacing of confining steel, amount of confining steel, strain gradient, and distribution of longitudinal bars around the core and the resulting tie configurations, on the behaviour of confined concrete are reported.

Important characteristics of collar confinement are: (1) collars provide confinement through their axial and flexural stiffnesses (the flexural stiffness of collars is significantly higher than that of conventional rebar ties and, therefore, it cannot be ignored); and (2) the confining pressure under the collars varies through the axial load history of the collared columns.

Brief summaries of the existing confinement models of Chan (1955), Roy and Sozen (1964), Soliman and Yu (1967), Sargin (1971), Kent and Park (1971), Vallenás *et al.* (1977), Sheikh and Uzumeri (1982), Mander *et al.* (1988b), Saatcioglu and Razvi (1992), Fam and Rizkalla (2001), Chung *et al.* (2002), and Légeron and Paultre (2003) have been presented. All of these models are for the confinement of concrete by steel reinforcing bars except the model proposed by Fam and Rizkalla (2001), which is for the confinement of concrete by circular fiber-reinforced polymer

tubes. It is highlighted in the chapter that these models may be unable to predict the behaviour of concrete confined by HSS collars because of the lack of an explicit flexural stiffness parameter and/or because these models cannot account for variations in confining pressure through the axial load history of the columns.

Due to certain similarities with the behaviour of concrete confined by steel collars, some research into confinement using steel jackets is also summarized, including the work of Chai *et al.* (1990), Marsh (1992), Aboutaha *et al.* (1996), Xiao and Wu (2003), and Ghobarah *et al.* (1997). Although the rehabilitation of short lap splices is not the main focus of the present research, a summary of experimental research conducted by Valluvan *et al.* (1993) for the improvement of the performance of short lap splices under cyclic loading is also presented in this chapter because they commonly exist in seismically deficient reinforced concrete buildings. In addition, the evolution of the ACI 318 code with respect to steel confinement requirements of rectangular/square reinforced concrete columns is also presented in this chapter.

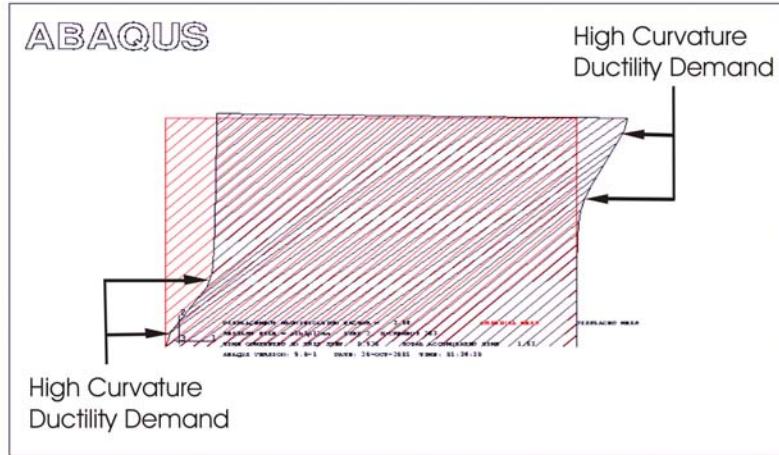


Figure 2-1: Deformed configuration of steel plate shear wall modelled by diagonal strips

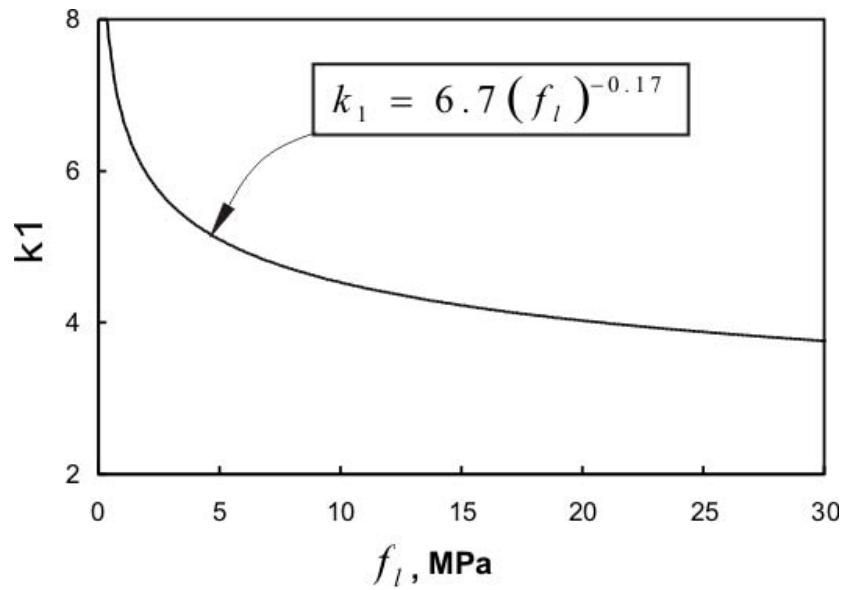


Figure 2-2: Relationship between coefficient k_1 and lateral confining pressure f_l

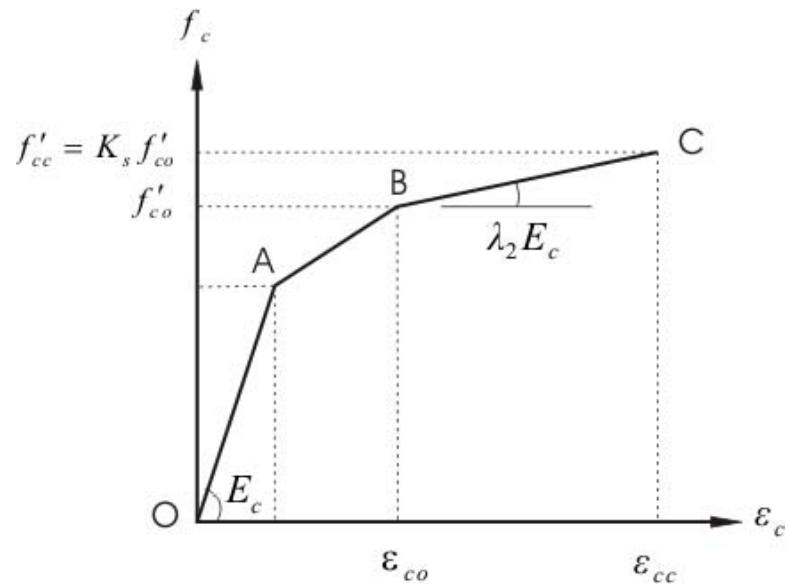


Figure 2-3: Model for the stress vs. strain curve of confined and unconfined concrete proposed by Chan (1955)

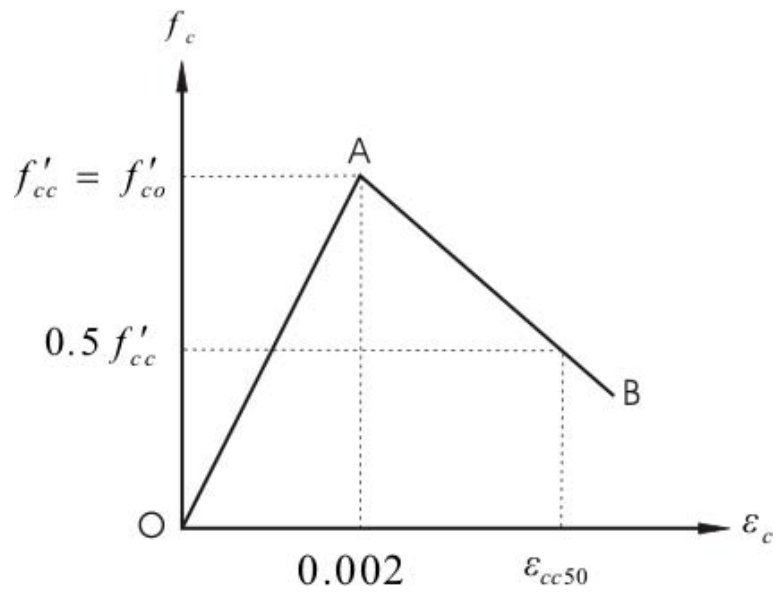


Figure 2-4: Model for the stress-strain curve of confined concrete proposed by Roy and Sozan (1964)

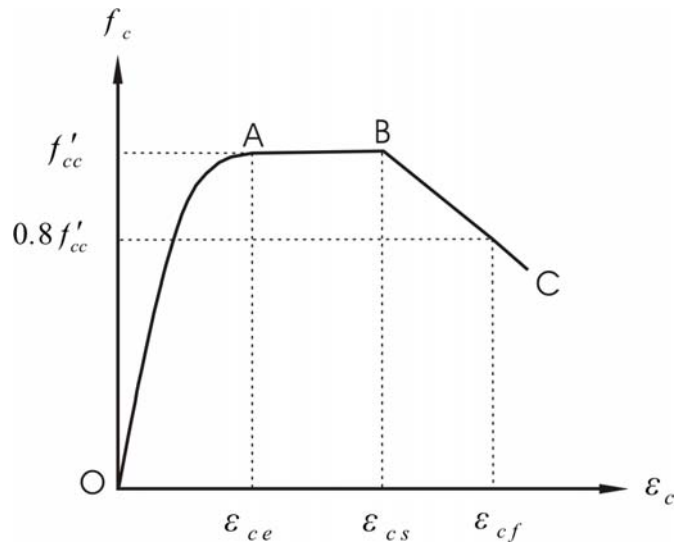


Figure 2-5: Model for the stress vs. strain curve of confined concrete proposed by Soliman and Yu (1967)

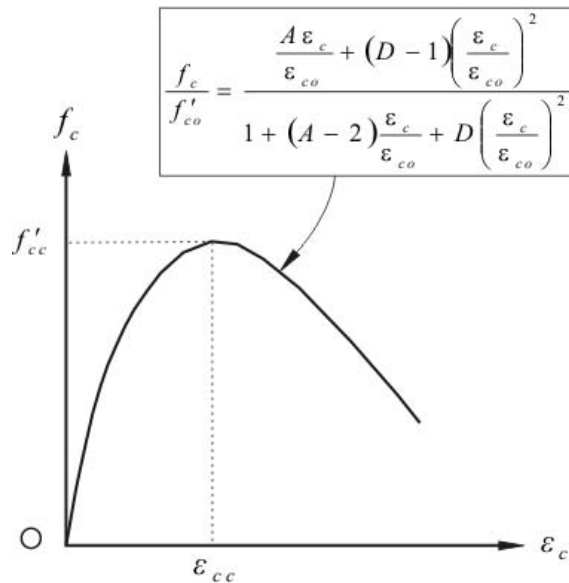


Figure 2-6: Model for the stress vs. strain curve of confined concrete proposed by Sargin (1971)

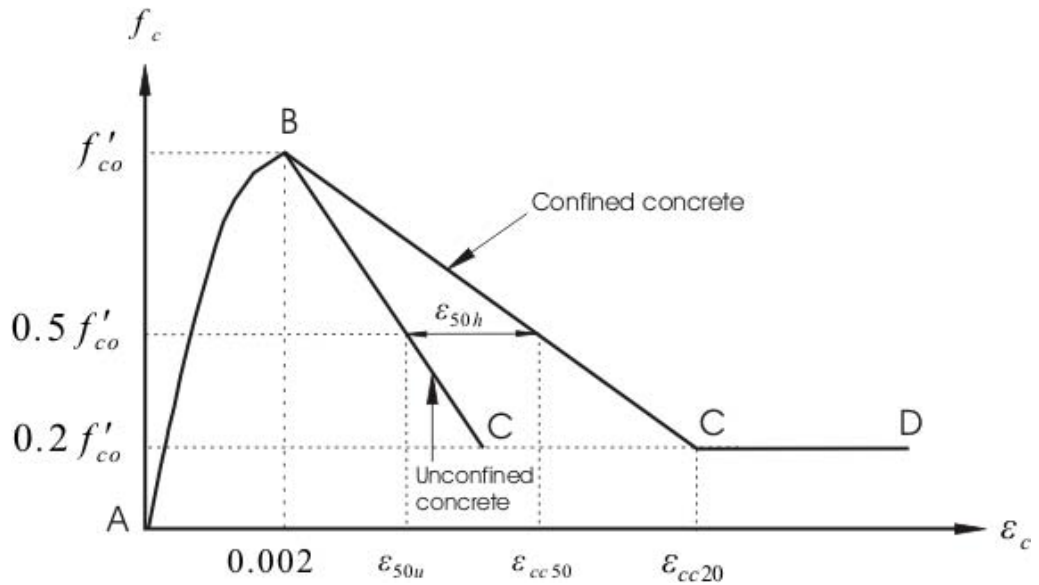


Figure 2-7: Model for the stress vs. strain curve of confined and unconfined concrete proposed by Kent and Park (1971)

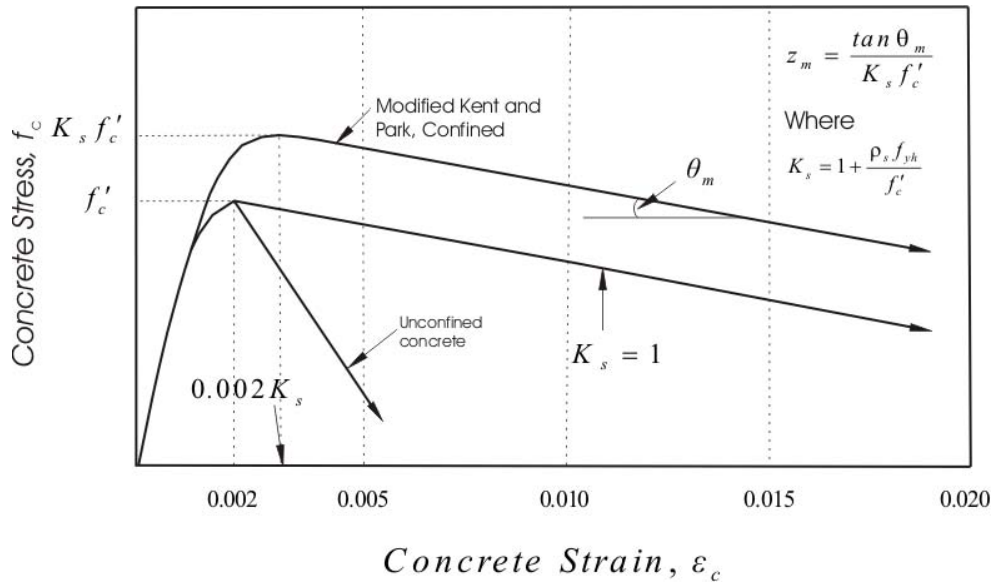


Figure 2-8: Modified Kent and Park model for the stress vs. strain behaviour of confined concrete by Park *et al.* (1982)

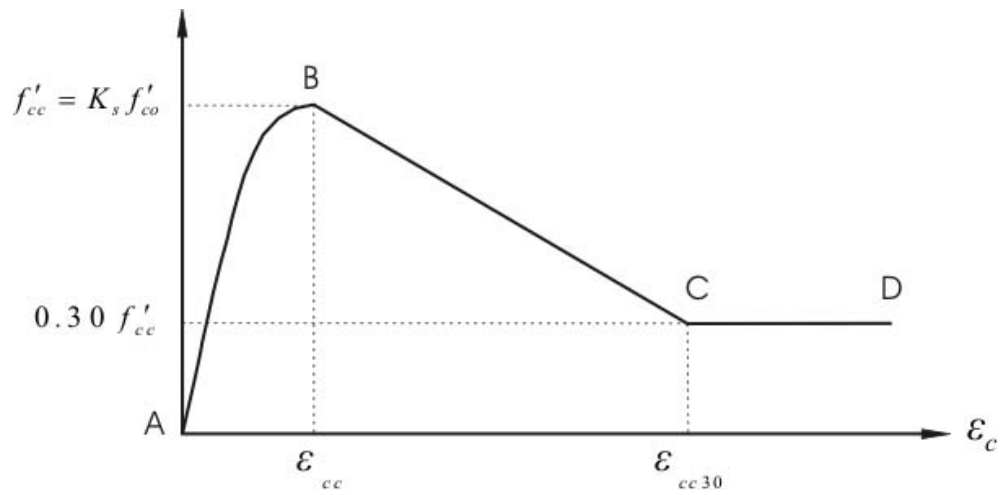


Figure 2-9: Model for the stress vs. strain curve of confined concrete proposed by Vallenias *et al.* (1977)

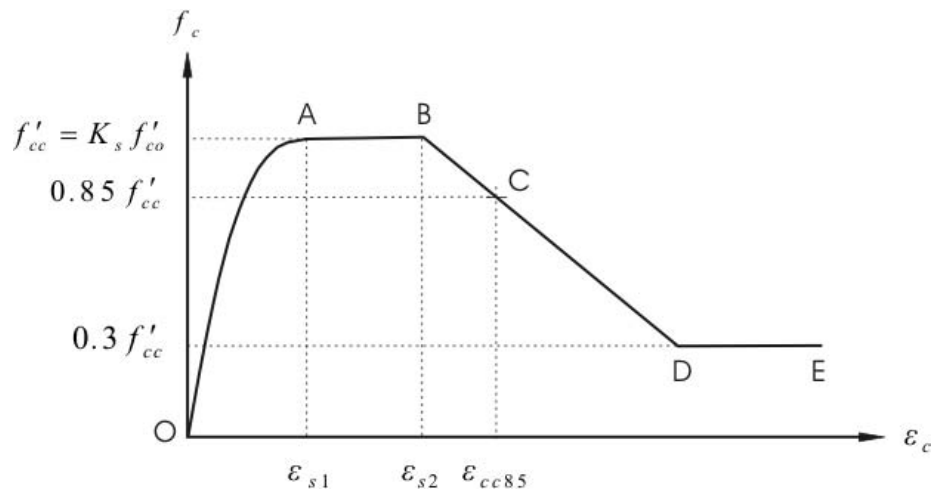


Figure 2-10: Model for the stress vs. strain curve of confined concrete proposed by Sheikh and Uzumeri (1982)

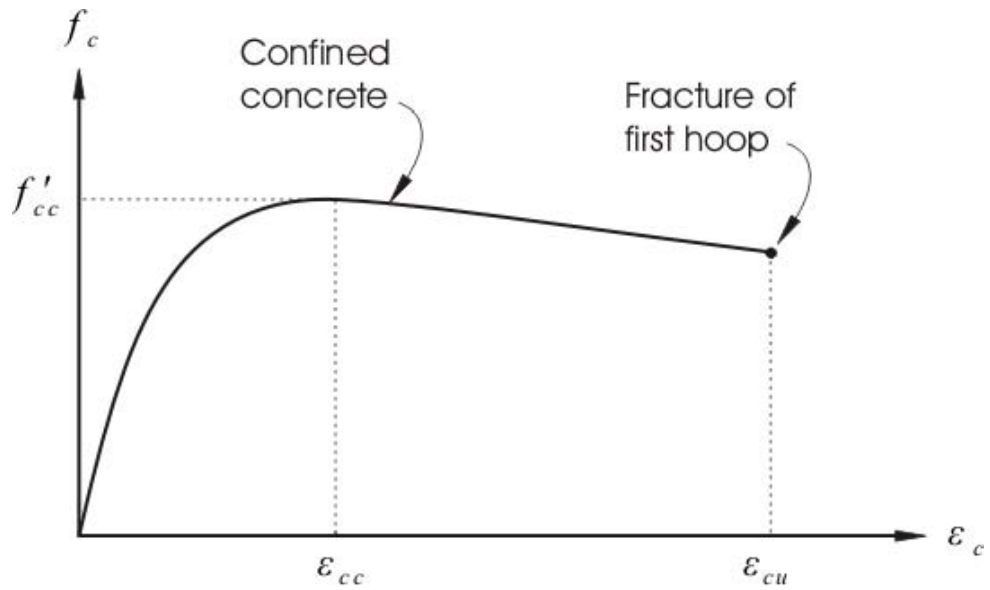


Figure 2-11: Model for the stress vs. strain curve of confined concrete proposed by Mander *et al.* (1988b)

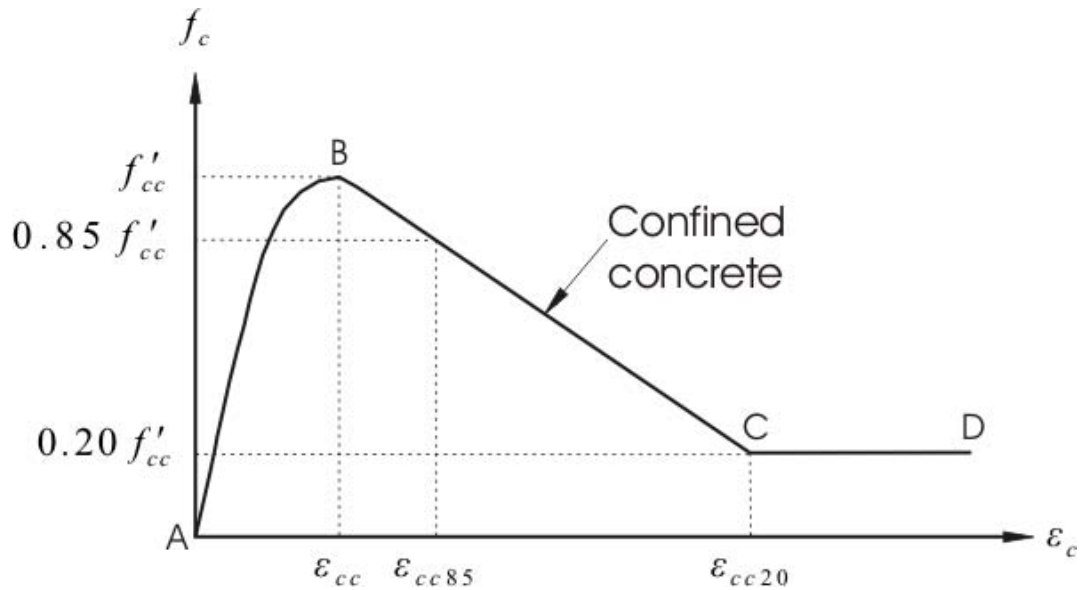


Figure 2-12: Model for the stress vs. strain curve of confined concrete proposed by Saatcioglu and Razvi (1992)

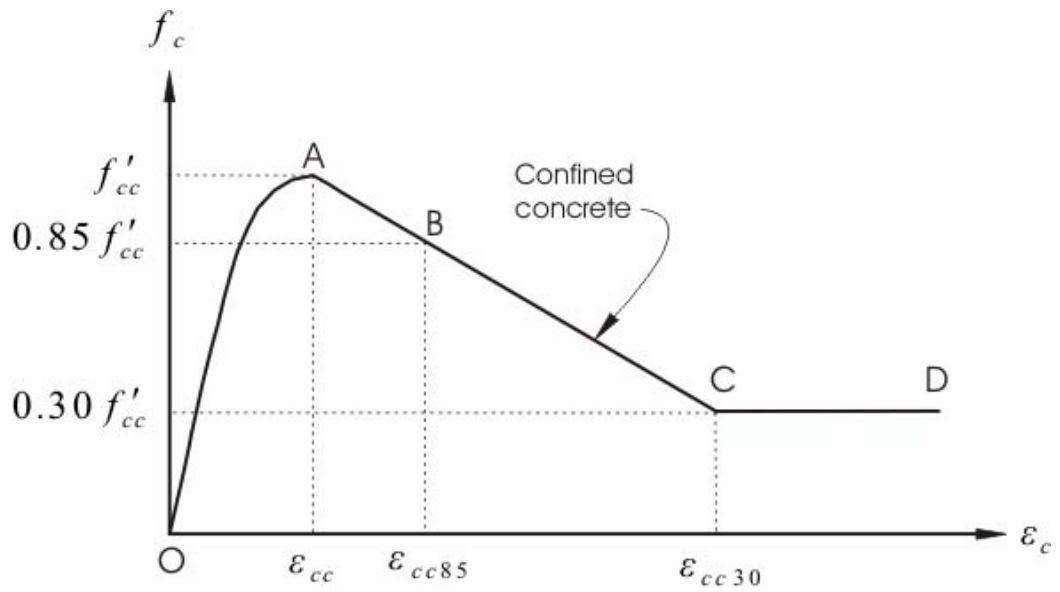


Figure 2-13: Model for the stress vs. strain curve of confined concrete proposed by Chung *et al.* (2002)

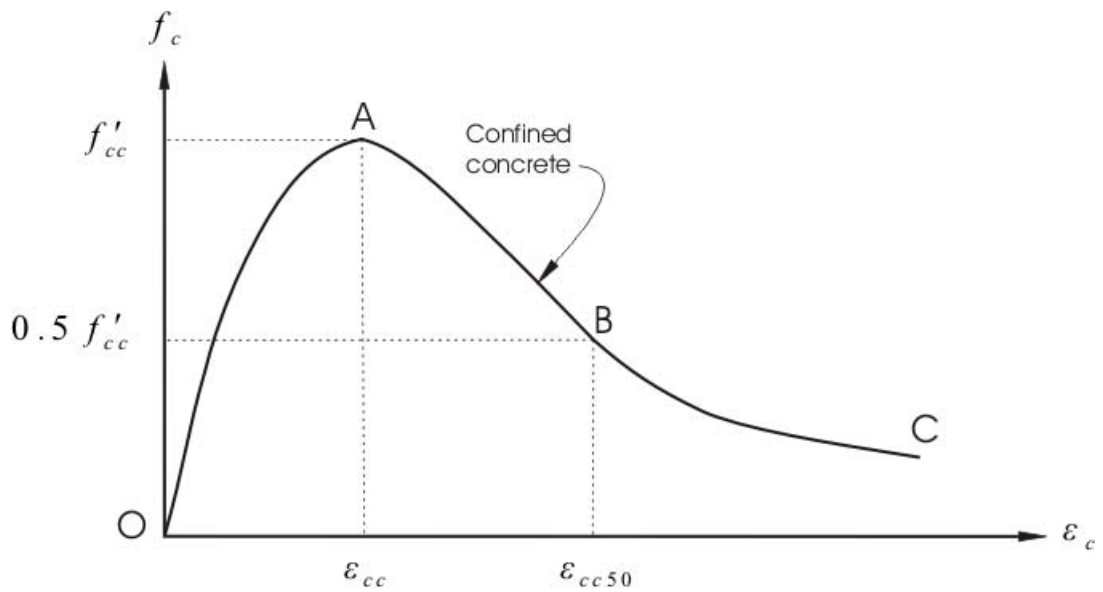


Figure 2-14: Model for the stress vs. strain curve of confined concrete proposed by Légéron and Paultre (2003)

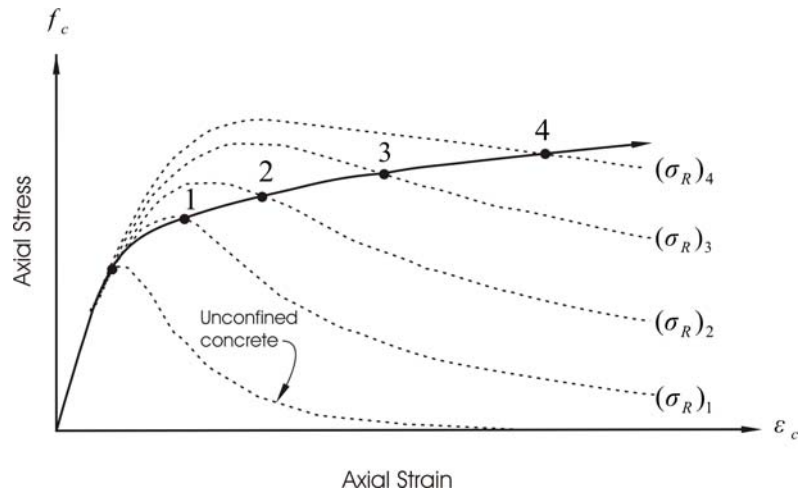
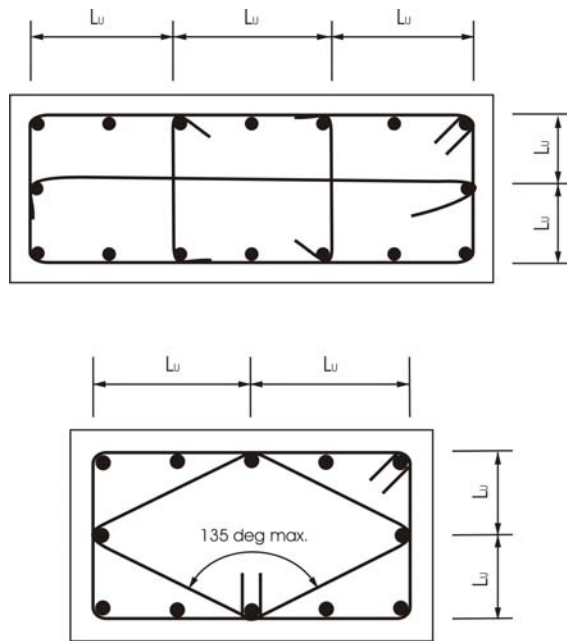


Figure 2-15: Model for the stress vs. strain curve of confined concrete proposed by Fam and Rizkalla (2001).



$$L_u < 14 \text{ in. (355 mm)}$$

Figure 2-16: Maximum unsupported length, L_u , for steel ties according to ACI 318-02

2.8 References

- Aboutaha, R.S, Engelhardt, M.D., Jirsa, J.O., and Kreger, M.E. 1996. Retrofit of concrete columns with inadequate lap splices by the use of rectangular steel jackets. *Earthquake Spectra*, Vol. 12, No. 4, November, pp. 693-714.
- ACI Committee 318. 2002. Building code requirements for structural concrete (318-02) and commentary (318R-02). American Concrete Institute, Detroit, 391 pp.
- Ahmad, S.H. and Shah, S.P. 1982. Stress-strain curves of concrete confined by spiral reinforcement. *ACI Journal*, November-December, pp. 484-490.
- Ahmad, S.H. and Shah, S.P. 1985. Behavior of hoop confined concrete under high strain rates. *ACI Journal*, September-October, pp. 634-647.
- Applied Technology Council (ATC).1996. Seismic evaluation and retrofit of concrete buildings. seismic, safety commission, State of California, Report No. SSC 96-01(ATC-40), Vol. 1 and 2, November.
- Balmer, G.G. 1949. Shearing strength of concrete under high triaxial stress—computation of Mohr's envelope as a curve. SP-23, Structural Research Laboratory, U.S. Bureau of Reclamation.
- Bertero, V.V., and Felippa, C. 1965. Discussion of "Ductility of concrete," by Roy, H.E.H. and Sozen, M.A. *Flexural Mechanics of Reinforced Concrete*, SP-12, ACI-ASCE, Detroit, November, pp. 227-234.
- Chai, Y.H., Priestley, M.J.N., Seible, F. 1990. Retrofit of bridge columns for enhanced seismic performance. *Proceedings of U.S.-Japan Workshop on Seismic Retrofit of Bridges*, Tsukuba, Japan, December, pp. 321-339.
- Chan, W.W.L. 1955. The ultimate strength and deformation of plastic hinges in reinforced concrete frameworks. *Magazine of Concrete Research*, Vol. 7, No. 21, November, pp.121-132.
- Chung., H., Yang, K., Lee, Y., and Eun, H. 2002. Stress-strain curve of laterally confined concrete. *Engineering Structures*. Vol. 24, pp. 1153-1163.
- Earthquake Engineering Research Institute. 1994. Northridge Earthquake January 17, 1994, Preliminary Reconnaissance Report. Technical Editor John F. Hall, No. 94-01, Oakland, California, 104pp.
- Earthquake Engineering Research Institute. 1995. The Hyogo-Ken Nanbu Earthquake January 17, 1995, Preliminary Reconnaissance Report. Technical Editors Craig D. Comartin, Marjorie Greene and Susan K. Tubbesing, No. 95-04, Oakland, California, February 1995, 116pp.
- Fafitis, A., and Shah, S.P. 1985. Lateral reinforcement for high-strength concrete. *ACI Special Publication*, SP 87-12, pp. 213-232.
- Fam, A. and Rizkalla, S.H. 2001. Confinement model for axially loaded concrete confined by circular fiber-reinforced polymer tubes. *ACI Structural Journal*, Vol. 98, No. 4, pp. 451-461.

- Fung, G.G.; Lebeau, R.J.; Klein, E.D.; Belvedere, J. and Goldschmidt, A.F. 1971. Field investigation of bridge damage in the San Fernando Earthquake. Technical Report, Bridge Department, Division of Highways, California Department of Transportation, Sacramento, 209 pp.
- Ghobarah, A., Aziz, T.A., and Biddah, A. 1997. Rehabilitation of reinforced concrete frame connections using corrugated steel jacketing. *ACI Structural Journal*, Vol. 94, No. 3, pp. 283-293, May-June.
- Hussain, M.A., and Driver, R.G. 2001. Finite element study on the strength and ductility of externally confined rectangular and square concrete columns. 29th Annual Conference of the Canadian Society for Civil Engineering, Victoria, B. C., Canada, May 30-June 2, 2001.
- Hussain, M.A., and Driver, R.G., 2003. Finite element analysis of reinforced concrete columns seismically upgraded by external collar confinement, 1st Conference on Response of Structures to Extreme Loading, Elsevier, Toronto, August 3-6, 2003.
- Hussain, M.A., and Driver, R.G. 2004. Experimental study on the seismic performance of externally confined reinforced concrete columns," *Proceedings, 13th World Conference on Earthquake Engineering*, Paper 578, Vancouver, Canada, August 1-6.
- Iyengar, K.T.S.R., Desayi, P., and Reddy, K.N. 1970. Stress-strain characteristics of concrete confined in steel binders. *Magazine of Concrete Research*, Vol. 22, No. 22, pp. 173-184.
- Kent, D.C., and Park, R. 1971. Flexural members with confined concrete. *Journal of the Structural Division, ASCE*, Vol. 97, No. ST7, pp. 1969-1990.
- Khaloo, A.R. and Bozorgzadeh, A. 2001. Influence of confining hoop flexural stiffness on the behavior of high-strength lightweight concrete columns. *ACI Structural Journal*, Vol. 98, No. 5, September-October, pp.657-664.
- Khaloo, A.T., El-Dash, K.M., and Ahmad, S.H. 1999. Model for light weight concrete columns confined by either single hoops or interlocking double spirals. *ACI Structural Journal*, Vol. 96, No. 6, November-December, pp.883-890.
- Légeron, F. and Paultre, P. 2003. Uniaxial confinement model for normal- and high-strength concrete columns. *Journal of Structural Engineering*, Vol. 129, No. 2, pp. 241-252.
- Mander, J.B., Priestley, M.J.N., and Park, R. 1988a. Observed Stress-Strain Behaviour of Confined Concrete. *Journal of Structural Engineering*, Vol. 114, No. 8, pp. 1827-1849.
- Mander, J.B., Priestley, M.J.N., and Park, R. 1988b. Theoretical stress-strain model for confined concrete. *Journal of Structural Engineering*, Vol. 114, No. 8, pp. 1804-1826.
- Marsh, L. 1992. Seismic retrofit for R/C column bar splices. *Proceedings of the 1992 Structures Congress, ASCE*, San Antonio, Texas, April 13-15.
- Mitchell, D. and Paultre, P. 1994. Ductility and overstrength in seismic design of reinforced concrete structures. *Canadian Journal of Civil Engineering*, Vol.21, pp. 1049-1060.
- National Institute of Standards and Technology. 1990. Performance of structures during the Loma Prieta Earthquake of October 17, 1989. NIST Publication 778, January.
- Park, R., Priestley, M.J.N., and Gill, W.D. 1982. Ductility of squared-confined concrete columns. *Journal of the Structural Division, ASCE*, Vol. 108, No. ST4, pp. 929-950.

- Paulay, T. 1986. A critique of the special provisions for seismic design of the building code requirements for reinforced concrete (ACI 318-83). *ACI Journal*, March-April, pp. 274-283.
- Popovics, S. 1973. A Numerical approach to the complete stress-strain curve of concrete. *Cement and Concrete Research*, Vol. 3, pp. 583-599.
- Razvi, S., and Saatcioglu, M. 1999. Confinement model for high-strength concrete. *Journal of Structural Engineering*, Vol. 125, No. 3, pp. 281-289.
- Richart, F.E., Brandtzaeg, A., and Brown, R.L. 1928. A study of the failure of concrete under combined compressive stresses. University of Illinois Engineering Experimental Station, Bulletin No. 185, 104pp.
- Richart, F.E., Brandtzaeg, A., and Brown, R.L. 1929. The failure of plain and spirally reinforced concrete in compression. University of Illinois Engineering Experimental Station, Bulletin No. 190, 74pp.
- Roy, H.E.H. and Sozen, M.A. 1964. Ductility of concrete. Proceedings of the International Symposium on Flexural Mechanics of Reinforced Concrete, ASCE-ACI, Miami, November, 1964, pp. 213-224.
- Saatcioglu, M. and Razvi, S.R. 1992. Strength and ductility of confined concrete. *Journal of Structural Engineering*, Vol. 118, No. 6, pp. 1590-1607.
- Sargin, M. 1971. Stress-strain relationships for concrete and the analysis of structural concrete sections. Study No. 4, Solid Mechanics Division, University of Waterloo, 167pp.
- Scott, B.D., R. Park, and Priestley, M.J.N. 1982. Stress-strain behavior of concrete confined by overlapping hoops at low and high strain rates. *ACI Journal*, January-February, pp. 13-27.
- Sezen, H., Whittaker, A.S., Elwood, K.J., and Mosalam, K.M. 2003. Performance of reinforced concrete buildings during the August 17, 1999 Kocaeli, Turkey Earthquake, and seismic design and construction practice in Turkey. *Engineering Structures*, Vol. 25, pp. 103-114.
- Sheikh, S.A. and Uzumeri, S.M. 1980. Strength and ductility of tied concrete columns. *Journal of the Structural Division, ASCE*, Vol. 106, No. ST5, pp. 1079-1102.
- Sheikh, S.A. and Uzumeri, S.M. 1982. Analytical model for concrete confinement in tied columns. *Journal of the Structural Division, ASCE*, Vol. 108, No. ST12, pp. 2703-2722.
- Soliman, M.T.M, and Yu, C.W. 1967. The flexural stress strain relationship of concrete confined by rectangular transverse reinforcement. *Magazine of Concrete Research*, Vol. 19, No. 61, December, pp. 223-238.
- Vallenas, J., Bertero, V.V., and Popov, E.P. 1977. Concrete confined by rectangular hoops subjected to axial loads," Report 77/13. Earthquake Engineering Research Centre, University of California, Berkeley, CA.
- Valluvan, R., Kreger, M. E., and Jirsa, J.O. 1993. Strengthening of column splices for seismic retrofit of nonductile reinforced concrete frames. *ACI Structural Journal*, Vol. 90, No. 4, pp. 432-440.

- Wang, P.T., Shah, S.P., and Naaman, A.E. 1978. Stress-strain curves of normal and lightweight concrete in compression. *ACI journal*, November, pp. 603-611.
- Xiao, Y., and Wu, H. 2003. Retrofit of reinforced concrete columns using partially stiffened steel jackets. *ASCE, Journal of Structural Engineering*, Vol. 129, No. 6, pp. 725-732.
- Zhang, M. and Gjrv, O.E. 1991. Mechanical properties of high-strength lightweight concrete. *ACI Material Journal*, Vol. 88, No. 3, May-June, pp. 240-247.

3. EXPERIMENTAL BEHAVIOUR OF COLLARED COLUMNS UNDER CONCENTRIC LOADING¹

3.1 Introduction

Reinforced concrete structures designed and constructed before and during the 1970s in various parts of the world are often seismically deficient because of the lack of stringent design and detailing provisions in the codes and standards available at that time. Some structures have also been deemed seismically deficient because of the rezoning of seismic activity in the area. It is well-known that the response of a structure during an earthquake is a function of its stiffness, strength, and ductility, as well as the ductility demand arising from the seismic input. Hence, seismically vulnerable reinforced concrete structures can be upgraded by making enhancements in stiffness, strength, and/or ductility. The strength and stiffness of a structure can be increased by adding structural walls (Baldelli, 1983) or steel bracing (Abou-Elfath and Ghobarah, 2000), for example, and the ductility at the location of plastic hinges can be improved by methods such as jacketing (Ghobarah *et al.*, 1997; Xiao and Wu, 2003; and Priestley *et al.*, 1992). The choice of a particular rehabilitation scheme is highly case dependent. Rehabilitation of structures such that they remain elastic during a major earthquake is most often an uneconomical solution. Therefore, seismic rehabilitation schemes that make use of ductility enhancement at the location of plastic hinges have become increasingly popular in recent years.

Failures of columns are generally more catastrophic than those of beams during strong motion and, therefore, enhancement in strength and ductility at the location of plastic hinges in the columns has been the focus of various research studies (Sakai and Sheikh, 1989). The rehabilitation of circular reinforced concrete columns by wrapping and bonding with composite materials such as carbon and glass fibres has been the subject of several recent investigations (Neale and Demers, 1999; and Sheikh and Yau, 2002) because of their high strength-to-weight ratios and resistance to corrosion. Because of their negligible flexural stiffness, these materials develop confining pressure onto the columns through in-plane membrane stresses only and, hence, are most effective for circular columns. Therefore, the move towards the use of flexurally stiff confining elements for the seismic upgrade of square and rectangular reinforced concrete columns was natural. Flexurally stiff corrugated steel jackets have been used for the seismic rehabilitation of reinforced concrete structures with rectangular cross-sections in which confining pressure is developed by passive restraint (Gobarah *et al.*, 1997). Existing confinement models have been developed primarily to describe the behaviour of columns with relatively small

¹ A version of this chapter has been published. Hussain and Driver 2005. *ACI Structural Journal*, Vol. 102, No. 2, March-April, pp. 242-251.

diameter conventional ties having significant axial but low flexural stiffness. Although these models may recognize the effect of aspects other than axial stiffness on confinement (e.g., the longitudinal bar spacing) and may include the effect of the inherent low flexural stiffness of the ties implicitly through empirical calibrations, they do not explicitly include the flexural stiffness of the ties in the formulation. Therefore, several models are available that give good agreement with the test results of conventionally reinforced columns, but they are unable to provide good predictions for columns with confining elements that are both axially and flexurally stiff. Recently, effort has been made both numerically (Hussain and Driver, 2001) and experimentally (Khaloo and Bozorgzadeh, 2001) to segregate the effect of the flexural stiffness of the confining elements by keeping their cross-sectional areas constant.

As a means of strengthening existing reinforced concrete columns, a relatively simple scheme is proposed herein that confines the concrete externally with hollow structural section (HSS) collars that possess a combination of significant flexural and axial stiffness. These collars not only provide the benefits of efficient confinement, but they also inhibit spalling of the outer concrete shell and provide additional shear reinforcement. Although the primary application of this system is likely to be for seismic rehabilitation, in order to provide a fundamental understanding of the confining behaviour in these strengthened columns an experimental investigation was carried out on columns under concentric axial load. This chapter describes the experimental program, the test results, and the conclusions drawn therefrom.

3.2 Research Significance

Rehabilitation of circular reinforced concrete columns can be achieved effectively by wrapping them with composite materials. Because the confining pressure is developed through membrane action, this method is considerably less effective for the commonly occurring cases of square and rectangular columns. However, square and rectangular reinforced concrete columns can be efficiently seismically upgraded by using confining elements that possess significant flexural stiffness, such as HSS collars. The experimental program described herein confirms the effectiveness of the confinement mechanism and provides insight into the influence of the important parameters.

3.3 Description of Test Specimens

3.3.1 Specimen Preparation

Fabrication and testing was conducted in the I. F. Morrison Structural Engineering Laboratory at the University of Alberta. A total of 11 columns of 300x300 mm cross-section and 1500 mm in

height, as depicted in Figure 3-1, were cast. Two columns (C00A and C00B) were control columns with conventional tie reinforcement and the remainder (C01 through C09) had external collar confinement.

The casting of the columns was done vertically and an internal vibrator was used to consolidate the concrete. Four cylinders of 150x300 mm and four cylinders of 100x200 mm were cast as per the requirements of ASTM standard C192 for each test column for defining the material properties. The curing conditions for the cylinders and the columns themselves were identical: moist-cured for the first seven days and then under ambient laboratory conditions up to the time of testing.

3.3.2 Internal Reinforcement Details

Each column had four nominally 20 mm diameter longitudinal bars, making the longitudinal reinforcement ratio equal to 1.33%. In placing the transverse reinforcement, the columns were divided into three parts: top and bottom end zones (each 350 mm long), and the test region (800 mm long). The reinforcement details for each of these columns are shown in Figure 3-1. Columns C01 through C09 had external confinement by HSS collars and, in order to study the effect of external confinement separately, no tie reinforcement was provided in the test region. The tie reinforcement in the test region of column C00A satisfied the gravity load design criteria of ACI 318-02 and CSA Standard A23.3-94. According to these codes, the maximum center-to-center spacing of ties required for this column is 300 mm. However, due to the geometric constraint of the test region length, a spacing of 267 mm was used. Column C00B satisfied the seismic plastic hinge requirements of these codes. Both codes require that the total area of rectilinear transverse reinforcement be not less than that given by either of the following equations:

$$[3.1] \quad A_{sh} = 0.3s h_c f'_c / f_{yh} (A_g / A_{ch} - 1)$$

$$[3.2] \quad A_{sh} = 0.09s h_c f'_c / f_{yh}$$

This resulted in the selection of a spacing of 70 mm on centers between adjacent ties for column C00B. Both control columns had ties with 135 degree hooks that extended at least six bar diameters into the core, meeting the seismic requirements of the two codes. In the end zones of all columns, closely spaced ties (as well as external collars, as described below) were provided to prevent failure from occurring near the reaction points.

3.3.3 HSS Collar Confinement

Typical collars made from HSS sections with bolted or welded corner connections are shown in Figure 3-2a. The former case was intended to provide a corner connection that allows relative rotation of the adjacent collar sides, while the latter was intended to approach a fixed corner condition. These two types of connections permit an assessment of the performance of collars that bound the likely corner conditions, but are not intended to represent the only means of assembling the collars for column rehabilitation applications. Indeed, collars welded only on two opposite corners in the shop and then bolted to the column at the other two corners are likely to be most practical and economical. Furthermore, other types of bolted connections could be selected by the designer for reasons of economics that provide a higher degree of rotational restraint than those selected for the experimental program. Three sizes of HSS were used in the fabrication of the collars used in this study: HSS102x51x6.35, HSS76x51x6.35, and HSS51x51x6.35. The HSS collar segments were oriented so that the largest moment of inertia ($1.95 \times 10^6 \text{ mm}^4$, $0.919 \times 10^6 \text{ mm}^4$, $0.319 \times 10^6 \text{ mm}^4$, respectively) was available to resist lateral expansion of the concrete in the column and were bevelled at 45° at the corners.

In the case of collars with bolted corner connections, 25.4 mm diameter high strength threaded rods were used to make a diagonal connection between the HSS sides, as shown in Figure 3-2a(i). To provide proper seating for the nuts and plate washers of the threaded rods, bevelled attachments of HSS51x51x6.35 were welded to the sides of the collar. In order to transfer to the concrete columns all of the clamping force applied by the tightening of the nuts, the sides of the collars were cut slightly short to avoid contact of the adjacent sides during the tightening operation. The collars on column C01 were tightened to be just snug with the column, minimizing the active confinement pressure, and the pretensioning force in the bolts is considered to be negligible. In the cases of columns C02, C03, C04, and C05, a significant initial pretensioning force was applied to the bolts (65.1 kN, 145.9 kN, 68.9 kN, and 90.2 kN, respectively), as measured with an annular load cell placed around the bolt shank. The bolts for column C03 had a significantly higher preload in order to study the potential benefits of active confining pressure.

In the case of collars with welded corner connections, a partial penetration single-V groove weld was deposited all around the corner joints using the shielded metal arc welding process. The simplest means of fabricating these collars was to weld all four corners in a custom jig and then thread the completed collar over the test column, a method that obviously could not be used for rehabilitation in the field. To facilitate this procedure, the inner dimensions of the collars were

kept 10 to 12 mm larger than those of the column cross-section. The collars were positioned so that the gap between the collar and the column was equal on all sides. The gap was sealed from the bottom with a construction sealant and was then filled with a low viscosity epoxy grout. The confining pressure on the columns provided by the welded collars is passive.

In the test regions, either four, six, or eight collars at equal spacings were used. The details of each specimen are presented in Table 3.1. (The distinction between columns C02 and C03 lies only in the degree of initial active confining pressure.) Figure 3-3 shows the schematic of a typical test specimen in the set-up with welded collars in the test region. In order to prevent failure of the column in the end zones, closely spaced, flexurally stiff collars were provided at these locations to supplement the internal ties. Figure 3-4 shows photographs of columns C05 and C06 (with bolted and welded collars, respectively, in the test region) in the test set-up.

The volumetric ratios of transverse confining steel, ρ_t , for all of the test columns are given in Table 3.1. The volume of the confining steel for the welded collars was calculated by multiplying the cross-sectional area of the HSS by the perimeter of the collar measured at the centroid of the HSS cross-section. For the bolted collars, since the contribution of the HSS to confinement is limited by the behaviour of the bolts, the volume of the confining steel was taken as the net cross-sectional area of the bolts running at the centerline of the collars. In both cases, since the collars are placed externally and prevent most of the spalling, the volume of the concrete was calculated based on the gross area of the column and the center-to-center vertical spacing of the collars. Hence, the core of the collared columns was considered equal to the cross-sectional dimensions of the columns. For columns C00A and C00B, the volume of the tie steel was calculated in the usual way, and the volume of the concrete was based on the core of the column within the reinforcing cage. The core dimensions for columns C00A and C00B were 215x215 mm and 220x220 mm, respectively, based on the centerline of the ties.

3.4 Material Properties

To produce a quantity of concrete sufficient for a single column and the cylinders required (0.19 m³) for the associated material tests, the mix consisted of 137.8 kg of coarse aggregate varying in size from 5 mm to 14 mm, 173.2 kg of fine aggregate, and 60.0 kg of Portland cement. Water was added to the mix based on laboratory experience to achieve a target cylinder strength of 35 MPa, however since the moisture contents of the aggregates were not measured, the w/c ratio is not precisely known. The mechanical properties of the concrete for each column were determined by testing standard cylinders according to the procedures outlined in ASTM standard C469 and are given in Table 3.2. The testing of each set of cylinders was carried out just prior to

testing the associated column. The ultimate strengths, f'_c , and the corresponding standard deviations are based on at least four cylinder tests. (The strengths of the concrete in columns C07 and C08 are significantly higher than the target value due to an error in the quantity of water added to the mix.) The stress vs. strain curve for each cylinder was plotted, from which the secant modulus of elasticity, E_c , and the strain at peak stress, ϵ_o , were determined. Poisson's ratio was determined using 100x200 mm cylinders and was found to have an overall mean value of 0.15.

Reinforcing bars conformed to CSA standard G30.18 and the threaded rods were of grade B7 as per ASTM standard A193/A. Testing of both was conducted according to ASTM standard A370. Three tension coupons were tested for each type of bar. Figure 3-5 shows the mean stress vs. strain curves for the reinforcing bars and threaded rods. The mean yield stress, modulus of elasticity, ultimate stress, and strain at ultimate stress are presented in Table 3.3. Only the 15 mm and 20 mm diameter bars exhibited a well-defined yield plateau. For other cases, the yield stress was determined by the 0.2% offset method. The strain hardening modulus was found to be 3863 MPa and 9837 MPa for the 15 mm and 20 mm bars, respectively, and the strain at the onset of strain hardening was 0.015 and 0.0062, respectively, for these bars.

The HSS conformed to CSA Standard G40.21-98 350W. Stub-column tests were performed to find the material properties of the HSS. For each size of HSS (nominal depths of 102, 76, and 51 mm), one stub-column was tested. The heights of these stub-columns were 300 mm, 250 mm, and 200 mm, respectively, conforming to the recommendations of the Structural Stability Research Council (Technical Memorandum No. 3: stub-column test procedure). The measured cross-sectional areas were 1734 mm², 1375 mm², and 1085 mm², respectively. The end faces of the stub-columns were machined at 90 degrees to the longitudinal axis. Six strain gages were installed at mid-height of each stub-column for alignment and determining the stress vs. strain relationships. In addition, two linear variable differential transformers (LVDTs) were also installed on opposite faces of each stub-column over a gage length of 100 mm. The loading of these stub-columns was done in a universal testing machine using displacement control. An electronic data acquisition system was used to record the data. The strains measured by the strain gages were close to the average strain based on the LVDTs in the initial parts of the curves. The strain gages ceased to function at approximately 0.02 strain and, hence, the remaining part of the curve was obtained using the LVDTs only. The average stress vs. strain curves for the stub-columns based on the LVDT measurements and the measured cross-sectional areas of the stub columns are shown in Figure 3-6. Since the entire cross-section was tested and the lengths of the stub-columns were sufficiently long, these stress vs. strain curves

include the effects of residual stresses. Key material properties of the HSS are also listed in Table 3.3.

A low viscosity epoxy was used to make the grout used under the welded collars. The epoxy itself consists of two parts: resin and hardener. The grout was a high strength, high modulus mortar with a mixture of fine sand, resin, and hardener in a ratio of 4:2:1. The compound was initially highly flowable. After pouring the grout into the gap between the column and the collar, a steel strip was vibrated into the grout to ensure that there were no air pockets remaining. In order to determine the material properties of the epoxy grout, three 51x51x51 mm cubes made from the same mix that was used for grouting the collars were tested in compression. A strain rate of 9.45×10^{-5} per second was maintained during the testing of these cubes. The mean stress vs. strain curve of the epoxy grout is also depicted in Figure 3-6. The mean modulus of elasticity, peak stress, and strain at peak stress were found to be 3.42 GPa, 84.0 MPa, and 0.0325, respectively.

3.5 Test Set-up

All of the columns were tested in a universal testing machine with a compressive capacity of 6.5 MN with the exception of column C08, which was tested in a 15 MN machine due to its high strength. In the case of column C07, the specimen was loaded initially in the lower capacity machine, but needed to be transferred to the high capacity machine in order to fail the specimen completely. The columns were tested vertically under concentric loading. Each specimen was carefully plumbed and then grouted with plaster at the top and bottom to ensure uniform bearing. The head of the machine was locked for rotations, so the columns were tested under fixed end conditions.

3.6 Instrumentation

Applied loads were measured by load cells integral to the testing machines. Deformations were recorded by DC-operated LVDTs. One LVDT was provided at each of the four corners of the column to record the deformation over the gage length (the 800 mm test region), as shown in Figure 3-3. Electrical resistance strain gages were mounted on the longitudinal rebars at mid-height of all the columns. Strain gages were also mounted on the HSS of the bolted and welded collars installed on some columns. In some bolted collars, the threaded rods were also instrumented with strain gages. The locations of the strain gages on the collars and bolts is discussed with the presentation of strain gage data. In addition, for the columns with bolted

collars (except C01), an annular-shaped load cell was mounted on the threaded rods of the collars to measure the bolt tension, which is directly related to the confining pressure.

3.7 Loading Protocol

Initially, a load of about 200 kN was applied to each column to check the instrumentation and data acquisition system and then removed. The testing of columns C00A, C00B, C01, C02, C03, C04, C05, C06, C08, and C09 was carried out after 98, 103, 82, 93, 207, 80, 88, 200, 648, and 118 days, respectively, after casting the columns. The loading of column C07 was done in two phases, as discussed previously. The first occurred after 199 days and the second after 650 days from the date the specimen was cast. Most columns were loaded monotonically to failure, however one column with bolted collars and one with welded collars were subjected to multiple cycles (15 for C05 and 18 for C07) of load from zero to near their respective compressive capacities and back, in order to examine the robustness of the system. In particular, the cycles successfully verified that the collars would not decrease in their effectiveness of confining the concrete in the columns due to deterioration or slip as the confining pressure was repeatedly applied and released. All the columns were tested under stroke control.

The strain rate in the test region was controlled indirectly by controlling the speed of the machine head. Most of the tests were started with a slow head displacement rate which was then increased in the latter stages of the tests, although in some cases the head displacement rate was kept constant throughout the test. The strain in the test region for each of the specimens was plotted with respect to time, revealing a similar trend for all the specimens. The rate of strain in the test region was relatively low initially and became higher near the end of the tests. This change in the strain rate in the test region was partly due to the change in the head displacement rate and partly due to the softening of the test region at higher strains. The average strain rates up to the peak load and up to the end of tests are given in Table 3.4. The strains at which the depths of spalling of concrete were measured (Table 3.5) are the strains that correspond to the end of tests. For columns that failed suddenly, the average strain rates at the peak load and at failure are equal. Column C05 could not be failed; therefore, only the strain rate up to the end of the test has been reported.

The strain rates for testing the cylinders to determine f'_c varied from 1.5×10^{-5} /sec to 3.5×10^{-5} /sec (average of 2.5×10^{-5} /sec). Therefore, the strain rates of the columns up to the peak loads are generally in the range of 3% to 24% of the average strain rate of the cylinders. According to Mander *et al.* (1988), the effect of strain rate on the behaviour of the test specimens can be

ignored if the strain rate is no greater than 1×10^{-6} /sec and they proposed a model to account for the effect of strain rate on the behaviour of the test specimens if the strain rates exceed this value. For some columns in the current research, the strain rates up to the peak are slightly higher than this value and for the remaining they are lower. The model was applied to all the columns and it was found that the effect of strain rate on the behaviour of the columns was negligible. The effect of strain rate on the cylinder strength of concrete was also calculated based on the average strain rate of 2.5×10^{-5} /sec. It was found that the reported cylinder strengths should be reduced by about 1% to bring them to their corresponding quasi-static values and it was considered reasonable to ignore this minor effect. In addition, the conclusions based on the comparisons of columns with each other are not significantly affected because this effect is about the same in all the columns.

3.8 Test Results

3.8.1 Load Versus. Displacement Response

The load vs. average displacement (based on the four LVDTs) curves for all of the columns are shown in Figures 3-7 through 3-17. Figure 3-13 shows the load vs. average displacement curve for column C05. It is clear from this figure that after reaching the capacity of the testing machine (6.5 MN), the load was cycled as described previously, but the specimen could not be failed. (This column was not moved to the higher capacity machine for reasons that are described subsequently.) Similarly, the capacity of column C07 also exceeded the capacity of the machine (6.5 MN) and the load was cycled but the specimen could not be failed. The specimen was then moved to a higher capacity machine (15 MN) and was loaded monotonically to failure. Figure 3-15 shows the combined load vs. average displacement curve for column C07 as well as the envelope curve that is used in the subsequent studies. Figure 3-18 shows the load vs. average displacement curves of all the columns for comparison purposes. (The multiple load cycles applied to columns C05 and C07, as described previously, are not shown in the figure for clarity of the other curves.)

3.8.2 Load vs. Strain Curves

Figures 3-19 through 3-28 show the load vs. average axial strain curves for all the columns except for column C07 (the wires for the strain gages on the longitudinal bars of this column were damaged during collar installation and hence no strain data are available for the longitudinal bars of this column) based on both the LVDTs and the strains gages on the longitudinal rebars. The

curves based on strain gages and LVDTs show reasonably good agreement up to the yielding of the longitudinal bars. However, in the cases of columns C00B, C03, C04, C06, and C09, the curves based on the strain gages show slightly stiffer behaviour. This effect is somewhat more pronounced in column C00A (Figure 3-19), and would be apparent even if the curves for this column were plotted to the same scale as those of other columns. The reasons for this discrepancy are not known. It is also apparent from these figures that the load vs. strain curves based on strain gages show a jump in the strain at the onset of yielding of the longitudinal bars of the columns. After this jump, the load vs. strain curves based on the strain gages tend to follow those based on the LVDTs. For the section analysis of the columns, the jump in the strain of the longitudinal bars has been neglected and it has been assumed that the rebars remained fully composite with the concrete throughout the majority of the test. (This relationship is unlikely to hold right up to failure due to the localized concrete crushing and rebar bending due to the concrete expansion in the lateral direction.)

3.8.3 Confined Concrete Material Curves

Based on full composite action between the longitudinal rebars and the concrete, the load carried by the concrete, P_{conc} , can be obtained by subtracting the load carried by the longitudinal rebars (derived from the strain data) from the total column load. This was done using a FORTRAN based program MCP developed for this purpose, the listing of which is given in Appendix B. The procedure was applied to all the columns and the resulting curves of total load, concrete load, and steel (rebar) load vs. strain are shown in Figures 3-29 through 3-39. The concrete load vs. strain curves for all the columns are then converted to confined concrete stress, f_{cc} , vs. strain curves by dividing their ordinate by A_c (where, $A_c = A_g - A_{st}$). These curves are commonly referred to as confined concrete material curves. In order to compare directly the effect of confinement on the behaviour of the concrete in the columns, it is necessary to normalize the concrete material curves of the columns with respect to their unconfined concrete strengths, f'_{co} , taken as $0.85f'_c$ which is commonly used to relate *in situ* strengths to standard cylinder strengths. These normalized curves are shown in Figure 3-40. It should be noted that the descending branches of these curves may not be accurate because of the localization of axial strains and lateral bending of the longitudinal bars in the test regions.

3.8.4 Peak Loads and Strains at Peak Loads

Two of the most important parameters that characterize the performance of the column specimens are the maximum load attained during the test (*i.e.*, the peak load) and the strain achieved at this point. The former indicates the capacity of the column and the latter is a measure of the ductility. A summary of experimental and computed results for these and other related quantities is shown in Tables 3.5 and 3.6. The maximum column load attained in the test is denoted by P_{\max} and the maximum load carried by the concrete of the column by $P_{c\max}$. The average column strain at which P_{\max} occurs is denoted by $\varepsilon_{p\max}$ and the average column strain at which $P_{c\max}$ occurs by ε_{cc} . It can be observed from Table 3.5 that these strains are similar.

3.8.5 Failure Criterion

In order to provide a means of direct comparison of ductilities in this study, a column is considered to have failed when its load drops to 85% of its maximum capacity, a value often used to define failure of plain concrete. For column C00B, although the capacity decreases to less than 85% following the first peak, this is not considered failure because there is no reliance on the contribution of the unconfined concrete cover to the column capacity. The strain corresponding to this load is called the failure strain, ε_f . Figure 3-41 shows the appearance of typical columns at the end of the tests. It should be noted that many of the columns were loaded well beyond the failure strain as defined here.

3.8.6 Depth of Concrete Spalling

Table 3.5 also lists the average depth of spalling into the core at the end of each test, measured to sound concrete midway between collars or ties in the test region. This value is taken as the overall mean depth from several measurements on each of the four sides of the column. The strains at which cover spalling was first visually observed and the strains at which the depths of cover spalling were measured are reported in Table 3.5. In the cases of columns C01, C02, and C03, some portions of the columns were completely damaged due to localization of strains, so the average depth of cover spalling was based on the remaining portion of the test region. For columns C04 and C09, the spalling was sudden and was not well-distributed over the test region. The strain at which spalling of the unconfined concrete of column C00A initiated was not observed precisely but it occurred at a relatively low strain. In this case, at the end of the test deterioration was so extensive that no meaningful spalling value could be measured. For

column C00B, the spalling was well-distributed over the test region but the strains at which measurements were taken were well beyond the peak load. Conversely, for columns C05, C06, C07, and C08, the spalling was well-distributed over the test region and the strains at which the cover spalling measurements were taken are close to the peak load. Based on these four columns, for which the spalling measurements appear to be most representative of the peak load condition, the average depth of spalling into the core can be approximated by $0.29s'$, where s' is the clear spacing between collars.

3.8.7 Theoretical Capacities of Columns

In addition to the experimental column capacities, the theoretical capacities of various components of the columns, based on unconfined concrete strengths, are presented in Table 3.6. P_o is the theoretical capacity of the column including the contribution of the longitudinal reinforcing steel, P_{oc} is the theoretical capacity of the column without the contribution of the steel, and P_{occ} is the theoretical capacity of the column based on the core of the column without the contribution of the steel. For conventional columns, the region of the column enclosed by the centerline of the ties is considered to be the core, whereas for collared columns, the gross column area is considered to be the core. For the latter, therefore, P_{oc} is equal to P_{occ} . P_{orcc} is the capacity of the column based on the reduced core (taking into account the approximately parabolic concrete spalling between confining elements), without the contribution of the reinforcing steel. The depth of spalling into the core between the collars or ties was taken equal to $0.29s'$, as observed in the tests, in the calculation of P_{orcc} . For example, in the case of tied column C00B, the total cover spalling for the calculation of P_{orcc} is $(40 + 0.29s')$ mm, with s' taken in millimetres, since the effective cover to the centerline of the ties is 40 mm.

3.8.8 Strength Enhancement of Concrete

The ratios P_{\max} / P_o , $P_{c\max} / P_{oc}$, $P_{c\max} / P_{occ}$, and $P_{c\max} / P_{orcc}$, corresponding to the peak loads, are also presented in Table 3.6. There are two distinct peaks in the load vs. axial displacement curve of column C00B (see Figure 3-30). At the first peak, the concrete cover is carrying a portion of the vertical load and the concrete is behaving as unconfined. The subsequent drop in load is due to cover spalling, after which the strength of the core concrete

begins to increase due to the development of confinement up to the second peak. To reflect this spalling behaviour, the load ratios P_{\max} / P_o and $P_{c\max} / P_{oc}$ given in Table 3.6 for column C00B correspond to the first peak and $P_{c\max} / P_{occ}$, and $P_{c\max} / P_{orcc}$ correspond to the second. The fact that the second peak is higher than the first for P_{\max} but lower for $P_{c\max}$ can be explained by observing that at the second peak, significant strain hardening of the longitudinal bars has developed, as supported by strain measurements.

On column C04 and C09, the collar spacing was relatively large and spalling occurred suddenly near the peak load. Therefore, the maximum load obtained has some contribution from the surface concrete between the collars. Since this is not considered to represent a reduced core, a value of $P_{c\max} / P_{orcc}$ is not presented in Table 3.6 for these columns.

3.8.9 Moduli of Toughness of Columns

The modulus of toughness is defined as the energy absorbed by the test region of a column per unit volume of the test region of the column. This can be calculated as the area under the load vs. displacement curve of the column up to the desired level of displacement divided by the volume of the column in the test region (taken here as the original volume, 0.30x0.3x0.8 m). The moduli of toughness of the columns up to the peak load (K_{op}) and up to the failure load (K_{of}) are given in Table 3.4. Moduli of toughness based on the contribution of the concrete alone up to the peak column load (K_{occp}) and up to the failure load of columns (K_{occf}) are also reported in Table 3.4. The difference between the total value and the one for the concrete alone represents the absorption of energy by the longitudinal bars of the columns.

3.8.10 Column Load vs. Bolt Force

As mentioned previously, an annular-shaped load cell was mounted on the threaded rods of the collars in the test region of columns C02, C03, C04, and C05 to measure the tension in the bolts during the tests. Figure 3-42 shows the column load vs. bolt tension for these columns. The curve for column C05 is shown up to a point just before cycling the load for clarity of other curves. Figure 3-43 shows the complete column load vs. bolt tension curve for column C05. There was very little reduction in the collar bolt force upon the removal of column load, which verifies the robustness of the collar confinement.

3.8.11 Collar Confinement and Tie Bars Strain Data

The control columns, C00A and C00B, had tie reinforcement in the test region. One of the ties in the test regions of each column was instrumented with two strain gages as shown in Figures 3-44 and 3-45, respectively. These figures also show the load vs. tie strain curves for columns C00A and C00B, respectively.

All the collars of columns C01, C02, C04, and C05 (with bolted collars) were instrumented with strain gages. Only the middle two collars of columns C06, C07, and C09 (with welded collars) were instrumented with strain gages. The strain gages on the collars of column C07 were only functional in the first of the two loading sequences. No strain gages were installed on the collars of the columns C03 and C08.

In both bolted and welded collars, the strain gages were installed in pairs—with one on the side of the collar and the other on the top—and oriented parallel to the axis of the HSS member. This configuration gave sufficient distance between the gages to provide accurate data regarding flexural behaviour of the collars. In all cases, the gage pairs were mounted on the HSS midway between the column corners. The bolts in some of the bolted collars in the test regions of some columns were also instrumented with strain gages. Only one strain gage was installed on a bolt. The results obtained from this strain gage may not represent the true tension in the bolt due to the probable bending of the bolt at high column loads. Figures 3-46 through 3-52 show the load vs. strain curves of the collars as well as some bolts in bolted collars in the test regions.

3.9 Discussion

3.9.1 Ductility Enhancement and Modes of Failure

As expected, column C00A showed brittle failure because of the relatively wide spacing of the ties. The degree of confinement was very low and the column behaviour was typical for unconfined concrete. The peak load was reached at a strain of 0.0035, as shown in Table 3.5. Column C00B showed ductile failure because of the closely spaced hoops in the test region. The peak load (second peak) was reached at an average strain in the test region of 0.0305, which is about nine times the analogous strain for column C00A. The modulus of toughness up to the peak load, K_{op} , of column C00B is 11.5 times that of column C00A, as determined from the values in Table 3.4. Moreover, the capacity decline was relatively gradual and the failure strain,

ε_f , was 0.0556. For both of the tied columns, it was observed after the tests that the hoops did not open, confirming that they were adequately anchored into the column core.

Columns C01, C02, C03 and C04, with bolted collars, showed ductile failure, although the ductility of column C04 was somewhat lower due to the relatively large collar spacing. The ductility up to failure of column C05, also with bolted collars, could not be determined because the strength of this column exceeded the capacity of the 6.5 MN testing machine and therefore could not be failed. The experimental capacities (Table 3.6) of this column are reported just before cycling the load. Because the collars had to be removed from this column for installation on another, thus releasing the confining pressure, it was felt that reinstalling the collars and reloading with the higher capacity machine would not give results consistent with the other columns where the collars were installed prior to any load being applied. For this reason, the curves shown in Figures 3-18, 3-35 and 3-40 for column C05 are terminated prematurely and the failure strain is not known.

Columns C06, C07, C08, and C09, with welded collars, exhibited brittle failure that was triggered by the fracture of a corner weld in one or more of the collars. Since the volumetric transverse steel ratios, ρ_t , for these columns are very high, as shown in Table 3.1, and the collars have a high flexural stiffness which also has an effect on the confining pressure, it is anticipated that if the ductility of the collar joints were improved, these columns would exhibit significantly higher ductility. It has been demonstrated by Caner and Bažant (2002) that the high transverse steel ratios provided by the welded collars should be sufficient to suppress the concrete softening indefinitely. However, the models used in their analyses assumed a "smeared" confining element that provides continuous confinement, rather than discrete collars where softening can occur between the collars. Nevertheless, improved column ductility would certainly have been exhibited had the collar welds not failed.

A typical deformed bolted collar and fractured welded collar at the end of the tests are shown in Figure 3-2b. The plastic flexural deformations are evident in the bolted collar. The appearance of three columns (C02, C04, and C05) at the end of the tests (with collars removed) that had different collar spacings but were otherwise identical are shown in Figure 3-41. (It must be kept in mind that columns C02 and C04 were each loaded to a strain well beyond the strain occurring at the peak load.) The localized damage seen in column C04 is a result of the relatively large collar spacing that resulted in less efficient confinement. Lateral displacements can be observed in columns C02 and C04 due to the formation of an inclined shear failure plane at high axial strains. Similar observations were made by Cusson and Paultre (1994) in the testing of high-strength concrete columns. Since column C05 was not failed completely, the photograph of this column is

representative of the typical condition of columns near their peak capacity, with local shallow spalling between collars but otherwise good integrity. By the end of the tests, the condition of the concrete between collars tended to decline significantly, but generally no deterioration of the concrete occurred directly under the collars. Figure 3-41 also shows the two tied columns (C00A and C00B) and a representative welded column (C07) after the tests for comparison. In particular, for column C00B one can see that the effective core area is much smaller for an internally tied column than a collared column.

3.9.2 Strength Enhancement Criteria

The enhancement in the strength of the columns can be seen by studying the ratios P_{\max} / P_o , $P_{c\max} / P_{oc}$, $P_{c\max} / P_{occ}$, and $P_{c\max} / P_{orcc}$. The ratios P_{\max} / P_o of the confined columns are all greater than 1.0, which means that the actual capacity of the columns is higher than the theoretical unconfined capacity. This is because of the strength enhancement through confinement. For the same reason, the ratio $P_{c\max} / P_{oc}$ shows that the capacity of the confined concrete in the columns is higher than that of the theoretical unconfined concrete capacity. Table 3.6 also shows that the ratios P_{\max} / P_o and $P_{c\max} / P_{oc}$ for the unconfined column C00A are somewhat greater than 1.0. This is attributed to the variation in the properties of the materials and the variability of the factor (0.85) used to convert f'_c to f'_{co} . The ratio $P_{c\max} / P_{occ}$ differs from $P_{c\max} / P_{oc}$ only for the tied columns, where it accounts for the cover spalling that takes place outside the ties and uses $P_{c\max}$ taken at the second peak (for column C00B), as discussed previously, giving a meaningful account of the effects of the material confinement. The ratio $P_{c\max} / P_{orcc}$ is higher than the other three ratios, as it accounts also for the spalling that penetrates into the core between the confining elements. This ratio is considered to represent the actual strength enhancement factor of the concrete, although the ratio $P_{c\max} / P_{occ}$ can also be considered of practical relevance. It can be seen from Tables 3.1 and 3.6 that an increase in the level of confinement, as represented by ρ_l , results in a concomitant increase in the strength enhancement factor. In this study, the maximum observed strength enhancement factors due to confinement (column C07) are 2.31 and 3.12, based on the ratios $P_{c\max} / P_{occ}$ and $P_{c\max} / P_{orcc}$, respectively. For comparison, the strength enhancement factors for column C00B, with closely spaced internal ties, are 1.96 and 2.70, based on the ratios $P_{c\max} / P_{occ}$ and $P_{c\max} / P_{orcc}$, respectively.

In the following discussions, a distinction is made between the strength enhancement factor, described above, and the actual degree of strength enhancement which is taken as the strength enhancement factor minus 1.0. The latter, which can be expressed as strength enhancement as a percent of the unconfined strength simply by multiplying by 100, permits a meaningful comparison of the strength enhancement factors presented in Table 3.6.

3.9.3 Bolted Versus Welded Collars

It was observed that no failure occurred in the collars with bolted collar connections. These collars deformed gradually during the loading of the column but no sudden drop in column load took place. However, the failure of the columns with welded collars was brittle due to fracture of the welds in the collar corners. Inspection of the failure surfaces revealed that the welds were of about half penetration. Nevertheless, in each case the axial strains achieved in the columns prior to failure of the collars were large.

The welded collars provide a higher level of confinement than bolted collars for two reasons. The volumetric ratio of the confining steel, ρ_t , of the welded collars is higher than that of the bolted collars because the behaviour of the bolted collars is largely dependent on the deformations of the bolts rather than the HSS members themselves. Moreover, the fixed corner connections result in a significantly higher flexural stiffness. To study the effect of the corner connection of the collars (bolted vs. welded) on the behaviour of the confined columns, the results of columns C01, C02, and C04 can be compared with those of columns C06, C07, and C09, respectively, as given in Table 3.6. Each of the three pairs of columns is identical except for the collar corner connection. The mean strength enhancement of the concrete in the columns with welded collars is about 2.41 and 1.95 times that of the columns with bolted collars based on the ratios $P_{c\max} / P_{occ}$ and $P_{c\max} / P_{orcc}$, respectively.

The strains at peak stress, ε_{cc} , of the concrete confined by welded and by bolted collars (Table 3.5) are comparable. The moduli of toughness up to the peak load, K_{op} , for columns with welded collars is higher than those for columns with bolted collars due to the high degree of confinement of welded collars as compared to analogous bolted collars. However, the failure strain, ε_f , of the columns with welded collars was generally lower than that of those with bolted collars due to premature fracture of the collar welds. Had the corner welds in the welded collars not failed, both the strain at peak stress of concrete, ε_{cc} , and the failure strain, ε_f , of the columns

with welded collars would likely have been higher than those of the columns with analogous bolted collars.

3.9.4 Collar Spacing

The collar spacing has a major effect on the behaviour of the columns because as the spacing increases, the efficiency of the confinement mechanism decreases due to both the increased unconfined length itself and a decrease in the parameter ρ_t . With an increase in collar spacing, the strength enhancement factor and the ductility of the column both decrease. This can be observed for bolted collars by comparing the results of columns C02, C04, and C05 and for welded collars by comparing columns C07 and C09. The ratio $P_{c\max} / P_{orcc}$ is not available for columns C04 and C09, as discussed previously. Therefore, the effect of spacing has been studied based on the ratio $P_{c\max} / P_{occ}$. The clear spacing between the collars, s' , for columns C02 and C04 was 1.61 and 2.70, respectively, times that of column C05. The enhancement in concrete strength of these columns was 0.49 and 0.23, respectively, times that of column C05. The clear spacing of collars for column C04 was 1.67 that of C02 and its strength enhancement was 0.48 times that of column C02. It is observed for these cases that the strength enhancement is cut in half by increasing the clear collar spacing by approximately 60%. If we define s'_r as the ratio of the larger clear spacing to the smaller clear spacing and n as the associated ratio of strength enhancements (less than 1.0) and note that when s'_r equals 1.0 then n must also be 1.0, an excellent approximation of the strength enhancement ratio, n , can be obtained for the specimens tested from:

$$[3.3] \quad n = \frac{1}{(s'_r)^{1.5}}$$

Equation 3.3 gives values of 0.49, 0.46, and 0.23 for s'_r equal to 1.61, 1.67, and 2.70, respectively, as compared to the experimentally obtained values of 0.49, 0.48, and 0.23.

The strain at $P_{c\max}$, ϵ_{cc} , is used to evaluate the effect of spacing on ductility. The monotonic loading of column C05 was terminated at a strain of 0.030. However, due to the cycling of the load, the strain of the column was increased ϵ to 0.043. The ductilities (taken as ϵ_{cc}) of columns C02 and C04 are 0.81 and 0.13, respectively, times that of column C05. The ductility of column C04 is 0.16 times that of column C02. Hence, the ductility is more sensitive to the change

in clear spacing between the collars at higher spacings where the degree of confinement is less. The ductility of column C09 is 0.95 times that of column C07. The level of confinement is higher in the case of these columns as compared to columns C02 and C04 due to the rigid collar corner connections and therefore the ductility is less sensitive to the clear spacing between the collars.

3.9.5 Collar Stiffness

The flexural and axial stiffnesses of the collars (size of the collars) also have an effect on the behaviour of the columns. Increasing the size of a collar also affects the parameter ρ_t (Table 3.1). An increase in the stiffness of the collars increases both the strength and the ductility of the column. This can be observed for bolted collars by comparing the results of columns C01 and C02 and for welded collars by comparing columns C06, C07, and C08. The strength enhancement of the concrete of column C02 is 1.14 times that of column C01 based on the ratio $P_{c\max} / P_{orcc}$. The strain ϵ_{cc} for column C02 is 1.4 times that of column C01. (It must be recognized that these differences may be due not only to the difference in the stiffnesses of the collars, but the small change in the quantity ρ_t and the difference in the initial active confining pressure may also contribute.) The axial and flexural stiffnesses of the collars of column C02 were 1.31 and 2.88, respectively, times those of column C01. Although it is clear that the provision of flexurally stiff confining elements has a significant beneficial effect on the degree of confinement, the large difference in the stiffness of the collars in these columns seems to have a comparatively small effect on strength. This is likely because the degree of confinement in these columns is highly dependent on the fact that the collar bolts used are relatively flexible components as compared to the HSS themselves. The change in collar stiffness seems to have a somewhat more pronounced effect on ductility than strength.

The strength enhancement of columns C07 and C08 are 1.09 and 1.07, respectively, times that of column C06 and the strength enhancement of column C08 is 0.98 times that of column C07. The axial stiffnesses of the collars for columns C07 and C08 are 1.31 and 1.62, respectively, times that of column C06 and their flexural stiffnesses are 2.88 and 6.11, respectively, times that of column C06. The axial and flexural stiffnesses of the collars of column C08 are 1.24 and 2.12, respectively, times those of column C07. These significant differences in the stiffness of the collars of columns C06, C07 and C08 seem to have a marginal effect on the behaviour of the columns. Although the higher concrete material strengths of columns C07 and C08 may have reduced somewhat their potential strength enhancement due to reduced lateral expansion, this phenomenon is attributed primarily to the high level of confinement provided by the rigid corner connections in the welded collars. This is consistent with the findings of Hussain and Driver

(2001) in a previous numerical study, where it was found that at higher levels of confinement, the strength enhancement of concrete becomes less sensitive to the variation in the confining pressure. Many existing confinement models appreciate this phenomenon and it was first observed by Richart *et al.* (1928). It is noted that the strength enhancement of column C07 is very slightly higher than that of column C08, despite the fact that the collars are of lower stiffness. This discrepancy is attributed to the variability of the concrete strength and the modification factor 0.85. It is concluded that although the provision of flexural stiffness in the confining elements has significant benefits, there is clearly a threshold beyond which the rate of increasing benefit diminishes rapidly.

3.9.6 Active Confining Pressure

Figure 3-42 shows the column load vs. bolt force (in the middle of the test region) for columns C02, C03, C04, and C05. The initial parts of the curves are almost vertical, which means that the expansion of the concrete was negligible in this region. When the column strain in the test region reaches the strain of the unconfined concrete at the peak stress, the expansion of the concrete becomes rapid and, hence, the force in the bolt increases. In the rehabilitation of buildings, the collars would be installed on the columns under service load conditions. Practically no expansion of the columns takes place under service loads and therefore the confining pressure for the enhancement in ductility and strength of the columns will still be developed.

The complete curve of column load vs. bolt force, including the load cycles, for column C05 is shown in Figure 3-43. When the column load is returned to zero, there is a slight reduction in the bolt force due to elastic recovery in the concrete lateral strain. The peak bolt force is again obtained by increasing the column load back to near to the column capacity. The column did not lose capacity under positive loading cycles, confirming the robustness of the system.

Columns C02 and C03 are identical except that column C03 had an initial active confining pressure 2.24 times that of C02. The strength enhancement of column C03 was 1.39 times that of C02. Column C03 exhibited more rapid softening in the descending branch than did column C02, as seen in Figure 3-18, however, the strains at the peak loads were similar. The column load vs. bolt force curves for columns C02 and C03 (Figure 3-42) are not similar. There is a rapid reduction in the bolt force of column C03 after the peak load, combined with a rapid reduction of the column load. This may be attributed to the rapid spalling of concrete observed between the collars because of the high tensile stresses in this region due to the higher confining pressure and/or to the sudden elongation of some of the bolts from yielding due to the higher preload. The performance of column C03 is better than that of column C02 up to the peak load

and it is anticipated that the performance of column C03 would have been better up to failure if no reduction in the confining pressure had taken place. This is consistent with observations of Krstulovic-Opara and Thiedeman (2000) who, based on the test results of concrete columns confined by self-stressing composites, concluded that active confinement is more effective than passive confinement in restraining cracking and improving crack stability.

3.9.7 Measured Strains of Transverse Steel

The transverse steel consists of either conventional tie reinforcement or external collars. The ties yielded in both columns C00A and C00B as is clear from Figures 3-44 and 3-45, respectively. One of the two strain gages on the tie reinforcement of each column revealed strains that greatly exceed the yield strain. It is also clear from these figures that the strain in the tie reinforcement becomes evident at the initial stage of column load.

Figures 3-46a through 3-46j show the relationships between the column load and collar and bolt strains for column C01. The location of the various strain gages are also shown in these figures. The collar strains are zero at zero column load because no significant initial active confining pressure was present in the collars of this column. Figures 3-46a through 3-46f show the load vs. strain response of the HSS collars at the gage locations. The initial parts of these curves are vertical, indicating that virtually no strain takes place in the collars in the initial parts of the tests. The gradient of strain in the cross-section of the collars is evident from the figures. At a certain column load, the strains at the outer face of the collars become much higher than those recorded using strain gages installed relatively closer to the concrete column due to yielding. An examination of these figures shows that both the inner and outer strain gages show tensile strain after the initial vertical parts of the curves; however, the outer tensile strain is much higher than the inner tensile strain, indicating that the section is subjected to tension as well as bending moment (with the tensile stress being higher than the maximum bending stress). Subsequently, the inner strain gages start showing compressive strains, indicating that flexural behaviour has begun to dominate. Since the outer gages are farther from the neutral axis than the inner ones, the strains have much larger magnitudes at high column loads. Figures 3-46g through 3-46j show the relationship between the column loads and bolt strains. The bolts are relatively flexible components in the collars and hence they attract some strain in the initial stages of the tests, as seen in Figures 3-46g through 3-46j. Moreover, the figures show that the bolts yield extensively as the column loads become large.

Figures 3-47a through 3-47j show the relationships between the column load and collar and bolt strains for column C02. The strains for this case are not zero at zero column load because of the

presence of initial active confining pressure due to the pre-tensioning of the bolts. Figures 3-47a through 3-47f show the load vs. strain response of the collars at the gage locations. With the exception of the non-zero initial strains, the behaviour is similar to that described for column C01. Figures 3-47g through 3-47j show the relationship between the column loads and bolt strains. These curves are almost vertical initially, indicating that very little strain took place in the bolts of this column in the initial stage of the test.

A comparison of the strain data from the HSS collars shows that the strains are much higher for column C01 than for column C02. This was expected because the collars of column C02 are stiffer than those of column C01. The strains of the collar bolts of columns C01 and C02 are comparable.

Figures 3-48a through 3-48h show the column load vs. strain curves of the collars and bolts for column C04. Initial active confining pressure was present in this column due to the pre-tensioning of the bolts. Therefore, the collar strains are not zero at zero column load. Figures 3-48a through 3-48d show the relationship between the column load and the strains of the HSS collars for column C04. The initial parts of these curves are vertical. The magnitudes of the strains of the collars of column C04 are less than those of the strains of the collars of column C01 and are comparable to those of column C02. The lower strains in the collars of column C04 as compared to those of columns C01 are due to the fact that the test was ended at a lower level of axial strain. The outer strains are much higher than the inner strains. The strain gradient indicates the presence of bending stresses in the sides of the collars. Figures 3-48e through 3-48h show the relationships between the column load and the strains in the collar bolts. The initial part of these curves are almost vertical indicating that no lateral strain of the column took place in the initial stage of the test. The strains in the bolts of this column (C04) are less than those of columns C01 and C02 because the test had to be stopped at a relatively low level of axial strain due to the more rapid drop in the column load.

Figures 3-49a through 3-49h show the relationship between the column load and collar and bolt strains of column C05. Initial active confining pressure was applied to this column due to the pre-tensioning of the bolts which induces tensile as well as bending stresses on the HSS collars. The strains measured by the inner and outer gages are initially compressive and tensile, respectively. By increasing the column load, the outer strains increase up to the end of the test. The inner strains behave differently. With the initial increase in column load, the inner compressive strains tend to decrease in magnitude initially and may even go slightly into tension, indicating the dominance of tensile behaviour in the collars. However, in the later stages of the test, these strains tend to become increasingly compressive, indicating the existence of high

bending stresses in later stages of the test. An examination of the strain data shows that the strains in the collars of column C05 are generally somewhat lower at the same level of axial load than those of columns C02 and C04 that have the same collar size. This is because of the presence of higher confining pressure in column C05 as compared to columns C02 and C04 due to the closer spacing of collars and higher initial pretension force that tends to reduce the effective Poisson's ratio of the concrete. These curves show that cycling the axial load does not jeopardize the efficiency of the collar confinement. The lower bolt and collar strains in column C05 at the end of the test as compared to those of columns C01 and C02 are due to the fact that the test of column C05 was ended prematurely at low level of axial strain.

It should be noted that the relationships between the column axial load and the bolt strains described above are considered of general use only, but have been presented for completeness. Because of the presence of bending in the bolts, the specific values of strain obtained inevitably include both axial and flexural components. Moreover, some bolts were reused after straightening. For these reasons, the load variations in the bolts should be obtained from the annular load cell data rather than the strains presented here.

Figures 3-50a through 3-52 show the relationships between the column load and collar strains for columns C06, C07, and C09 (columns with welded collars). There is no active confining pressure in these column. Therefore, the collar strains are zero at zero column load. Initially, both the inner and outer strains of the collars of columns C06 and C09 are tensile, but as the column load increases the outer strains continue to increase, while the inner strains tend to become compressive in the later stages of the tests due to bending of the collars. The inner and outer stains in the collars of column C07 remain tensile throughout the test, although the outer strain is larger in magnitude than the inner due to bending of the collars.

3.10 Summary and Conclusions

A total of 11 full-scale reinforced concrete columns that were confined externally by HSS collars were tested under quasi-static concentric loading, with multiple cycles being applied in two of the cases that verified the robustness of the confinement mechanism. The overall objective of the research program is to investigate the effectiveness of this relatively simple external confinement system for the rehabilitation of seismically deficient reinforced concrete buildings. The tests reported herein represent the first phase of this investigation. The effect of parameters such as type of collar corner connection, spacing of collars, stiffness of collars, and the effect of active confining pressure on the confined material curve have been studied. Based on the test results, the following main conclusions have been drawn:

1. External confinement by HSS collars has excellent potential for rehabilitation of seismically deficient reinforced concrete structures through enhancement in both strength and ductility. The collared columns exhibited a maximum strength enhancement factor of 3.12 (column C07; strain at peak stress equal to 0.026), calculated based on the reduced core of the column, and a maximum observed strain at peak stress of 0.043 (column C05; strength enhancement factor equal to 2.57). By comparison, a conventionally confined column satisfying the plastic hinge requirements of ACI 318 and CSA Standard A23.3 (column C00B) exhibited a strength enhancement factor of 2.70 and a strain at peak stress of 0.030. Clearly, the comparative overall benefit in strength for the collared columns is much greater when considering that the size of the core itself is considerably larger, as discussed in item 2;
2. External confinement by HSS collars prevents the spalling of concrete cover under the collars and inhibits spalling between the collars. The effective core area of externally confined columns is therefore significantly larger than that of conventional columns;
3. On average, columns confined by collars having welded corner connections show an enhancement in strength, based on the reduced core area, of 1.95 times that of equivalent columns with bolted collars. The strain at peak stress of the concrete confined by the two types of collars are comparable and generally are close to ten times that which would be expected for unconfined concrete. The lower failure strain exhibited by columns with welded collars is attributed to the lack of ductility of the welds in the collars themselves and it may be increased significantly with deeper weld penetration;
4. The spacing of the collars has a profound effect on the confined material curve. It was observed that by increasing the clear spacing by about 60%, the enhancement in concrete strength was cut in half. The effect of a change in collar spacing on the strain at peak stress of the confined concrete was more prominent at higher spacings (lower levels of confinement) and it became less influential at smaller spacings (higher levels of confinement). These observations are not expected to hold at very large spacings, where the degree of confinement is very low;
5. The mere presence of HSS collars has a large effect on column strength due, in part, to their high stiffness. By increasing the HSS stiffness, an enhancement in both strength and ductility was observed, although the benefits in strength were relatively small as compared to the increase in collar stiffness. For bolted collars, this is attributed to the fact that the behaviour is

influenced by the deformations of the bolts, which are relatively flexible components of the system. For welded collars, it is attributed to the high level of confinement achieved by the presence of the rigid corner connections, which in turn reduces the impact of the moment of inertia of the HSS member itself. Therefore, when increasing the collar stiffness, there is a threshold beyond which the rate of increasing benefit diminishes rapidly; and

6. The column with relatively high initial active confining pressure showed improved behaviour up to the peak load, but exhibited rapid softening in the post-peak part of the curve, likely due to some combination of rapid spalling of the concrete between the collars and yielding of the bolts. An enhancement in concrete strength was observed that was 1.39 times that of the otherwise similar column by increasing the initial confining pressure by 2.24 times.

Table 3.1: Description of column specimens

Specimen	Transverse Steel					
	Type	Size (mm)	Spacing on Centers (mm)	Type of Corner Connection	Cross- sectional Area (mm ²)	Volumetric Ratio, ρ_t (%)
C00A	Conventional rebars	$\phi 10$	267	—	100	0.70
C00B		$\phi 15$	70	—	200	5.19
C01	Collars made from hollow structural sections (HSS)	HSS 51x51x6.35	122	bolted	375*	4.81*
C02		HSS 76x51x6.35	122	bolted	375*	5.15*
C03		HSS 76x51x6.35	122	bolted	375*	5.15*
C04		HSS 76x51x6.35	170	bolted	375*	3.68*
C05		HSS 76x51x6.35	95	bolted	375*	6.63*
C06		HSS 51x51x6.35	122	welded	1085	13.92
C07		HSS 76x51x6.35	122	welded	1375	18.90
C08		HSS 102x51x6.35	122	welded	1734	25.48
C09		HSS 76x51x6.35	170	welded	1375	13.50

* Based on bolts

Table 3.2: Properties of concrete

Specimen	Cylinder Strength, f'_c		Modulus of Elasticity, E_c (MPa)	Strain at Peak Stress, ϵ_o
	Mean (MPa)	St. Dev. (MPa)		
C00A	34.4	3.21	22 860	0.0026
C00B	35.0	4.23	23 210	0.0026
C01	37.9	1.20	20 670	0.0031
C02	38.7	2.11	19 840	0.0032
C03	37.8	1.90	25 330	0.0025
C04	37.8	1.73	22 020	0.0029
C05	36.4	1.05	20 050	0.0033
C06	34.8	2.83	23 340	0.0025
C07	47.0	1.41	24 750	0.0032
C08	52.8	1.55	26 890	0.0033
C09	36.3	3.25	24 390	0.0025

Table 3.3: Properties of rebars and HSS

Description of Specimen	Size (mm)	f_y (MPa)	E_s (MPa)	Ultimate Stress (MPa)	Strain at Ultimate Stress
Rebars	φ10	450	202 800	717	0.1000
	φ15*	453	202 250	617	0.1350
	φ20*	431	205 100	668	0.1150
Threaded rods	φ25	811	202 100	950	0.0610
Steel hollow structural sections	HSS 51x51x6.35	497	203 400	642	0.0887
	HSS 76x51x6.35	445	202 700	506	0.0234
	HSS 102x51x6.35	410	201 350	489	0.0166

*Steel with well-defined yield plateau

Table 3.4: Strain rate data and moduli of toughness of columns

Specimen	$\dot{\epsilon}_p$ (1/sec)	$\dot{\epsilon}_f$ (1/sec)	K_{op} (kN·m/m ³)	K_{of} (kN·m/m ³)	K_{occp} (kN·m/m ³)	K_{occf} (kN·m/m ³)
C00A	0.69x10 ⁻⁶	0.69x10 ⁻⁶	89.88	110.76	75.99	93.54
C00B	4.75x10 ⁻⁶	8.63x10 ⁻⁶	1033.92	1937.66	842.48	1547.46
C01	2.98x10 ⁻⁶	5.32x10 ⁻⁶	1458.53	2718.80	1276.87	2360.88
C02	2.70x10 ⁻⁶	3.90x10 ⁻⁶	1848.43	2937.07	1593.70	2554.60
C03	2.78x10 ⁻⁶	4.33x10 ⁻⁶	2044.73	2725.76	1808.31	2375.32
C04	0.80x10 ⁻⁶	2.43x10 ⁻⁶	224.33	699.00	194.63	608.80
C05	2.24x10 ⁻⁶	2.24x10 ⁻⁶	2918.64	N.A.	2620.80	N.A.
C06	2.83x10 ⁻⁶	2.83x10 ⁻⁶	2095.07	2358.17	1890.19	2075.18
C07	3.02x10 ⁻⁶	3.02x10 ⁻⁶	2813.36	3296.32	2627.74	3076.79
C08	5.97x10 ⁻⁶	5.97x10 ⁻⁶	3004.82	3181.98	2841.03	3011.38
C09	2.28x10 ⁻⁶	2.44x10 ⁻⁶	1317.01	1800.70	1152.69	1562.93

Table 3.5: Column axial strain and spalling data

Specimen	$\varepsilon_{p\max}$	ε_{cc}	ε_f	Average depth of core spalling (mm)	Strain at the start of spalling	Strain at which spalling measured
C00A	0.0035	0.0035	0.0041	—	—	—
C00B	0.0034/ 0.0305*	0.0033/ 0.0300*	0.0556	18	0.0070	0.0830
C01	0.0300	0.0250	0.0547	21	0.0040	0.0864
C02	0.0356	0.0350	0.0551	20	0.0037	0.0839
C03	0.0350	0.0320	0.0455	22	0.0049	0.0707
C04	0.0064	0.0057	0.0173	34	0.0033	0.0500
C05	0.0430§	0.0430§	—	15	0.0045	0.0430
C06	0.0359	0.0350	0.0394	19	0.0025	0.0406
C07	0.0283	0.0264	0.0323	19	0.0037	0.0328
C08	0.0318	0.0300	0.0334	20	0.0045	0.0335
C09	0.0267	0.0250	0.0349	38	0.0041	0.0365

* Presented for the two distinct load peaks observed (see Fig. 3.30)

§ Lower bound values

Table 3.6: Load data and strength enhancement factors

Specimen	Experimental Capacities		Computed Capacities				$\frac{P_{\max}}{P_o}$	$\frac{P_{c \max}}{P_{oc}}$	$\frac{P_{c \max}}{P_{occ}}$	$\frac{P_{c \max}}{P_{orcc}}$
	P_{\max} (kN)	$P_{c \max}$ (kN)	P_o (kN)	P_{oc} (kN)	P_{occ} (kN)	P_{orcc} (kN)				
C00A	3475	2939	3114	2597	—	—	1.12	1.13	—	—
C00B	3342/ 3419*	2850/ 2747*	3159	2642	1404	1016	1.06	1.08	1.96	2.70
C01	4874	4185	3378	2861	2861	2119	1.44	1.46	1.46	1.97
C02	5283	4568	3438	2921	2921	2164	1.54	1.56	1.56	2.11
C03	6093	5379	3370	2853	2853	2114	1.81	1.89	1.89	2.54
C04	4135	3611	3370	2853	2853	1676	1.23	1.27	1.27	—
C05	6600§	5906§	3265	2748	2748	2294	2.02	2.15	2.15	2.57
C06	6409	5730	3144	2627	2627	1947	2.04	2.18	2.18	2.94
C07	8882	8193	4065	3548	3548	2628	2.19	2.31	2.31	3.12
C08	9802	9087	4503	3985	3985	2953	2.18	2.28	2.28	3.08
C09	5123	4474	3257	2740	2740	1609	1.57	1.63	1.63	—

* Presented for the two distinct load peaks observed (see Fig. 3.30)

§ Lower bound values

All dimensions are in millimeters
 All columns have 4- ϕ 20 vertical bars

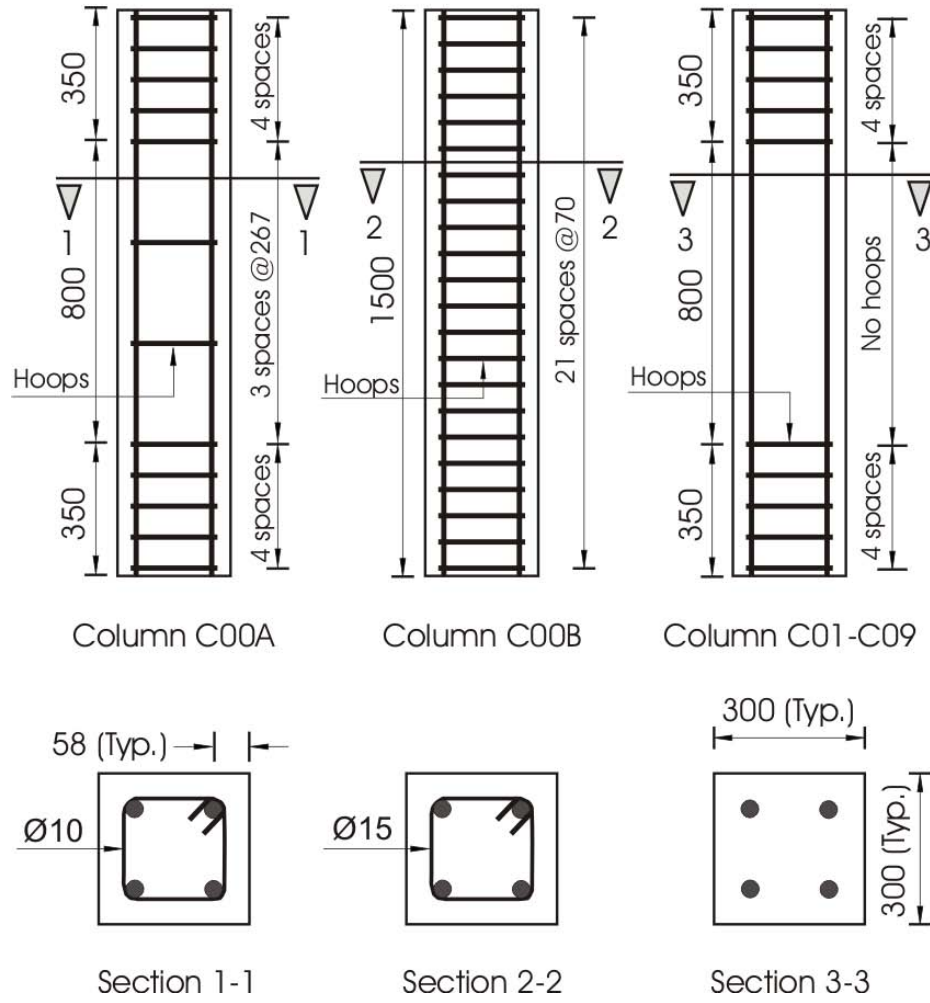
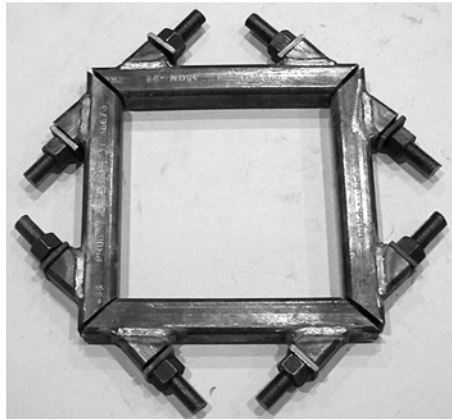
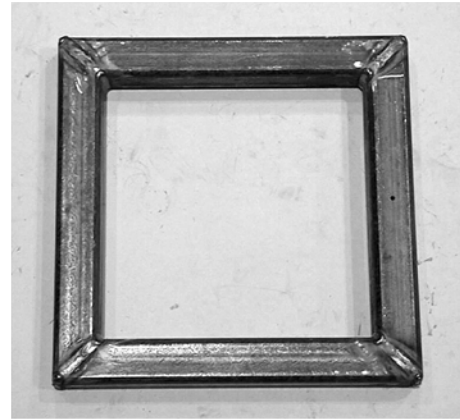


Figure 3-1: Column reinforcement details

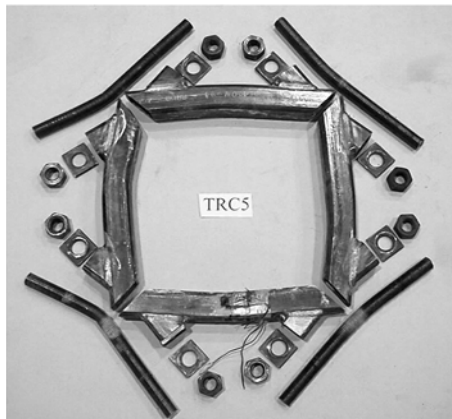


(i)



(ii)

Figure 3.2a



(i)



(ii)

Figure 3.2b

Figure 3-2: Typical collars: (a) pre-test: (i) bolted collar; and (ii) welded collar
(b) post-test: (i) deformed bolted collar; and (ii) weld fracture at corner of welded collar

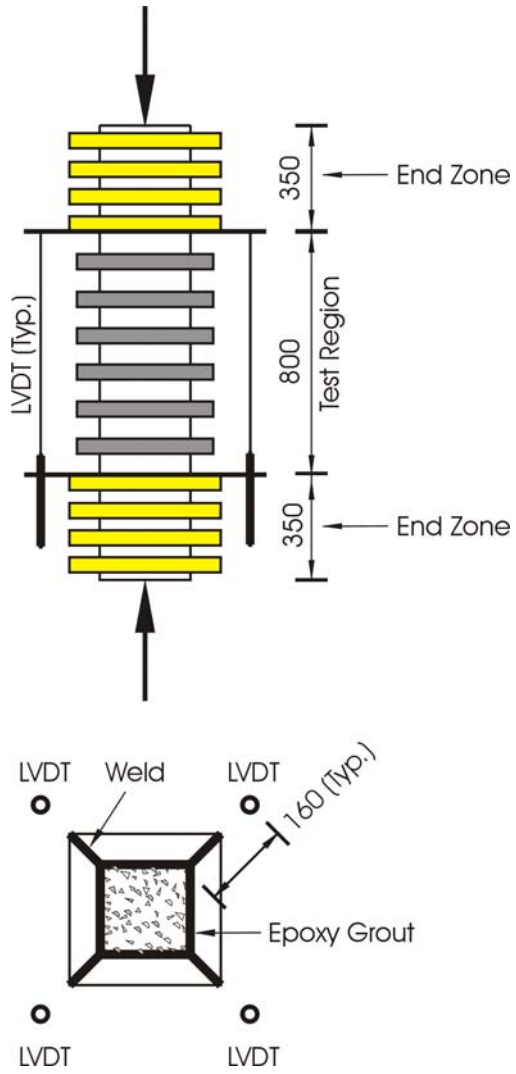
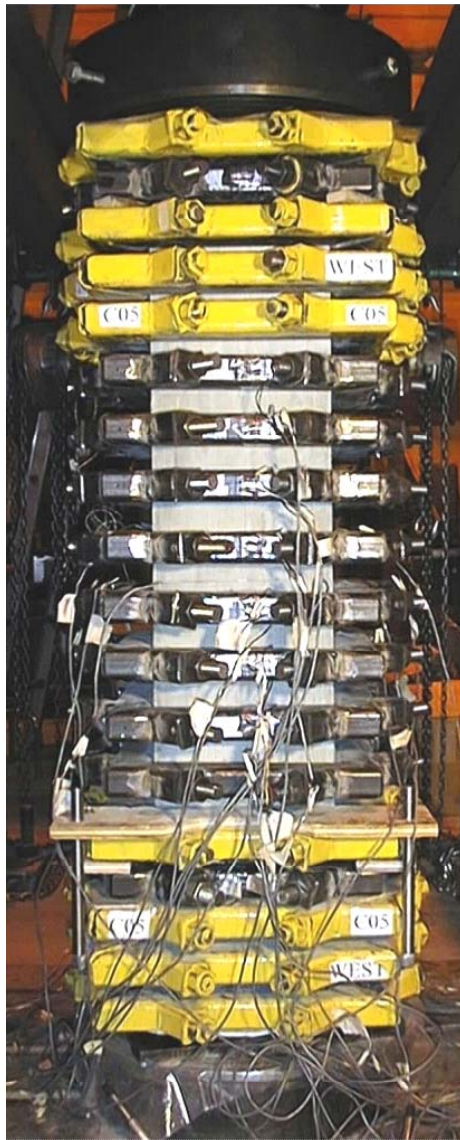
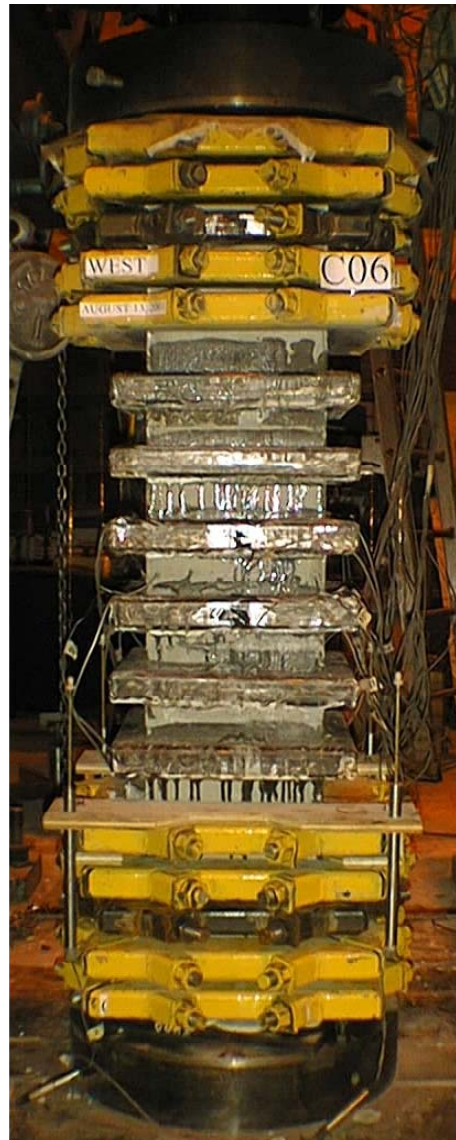


Figure 3-3: Schematic of set-up for a typical column specimen



(a) Column C05



(b) Column C06

Figure 3-4: Typical column specimens in set-up with: (a) bolted; and (b) welded collars in the test region

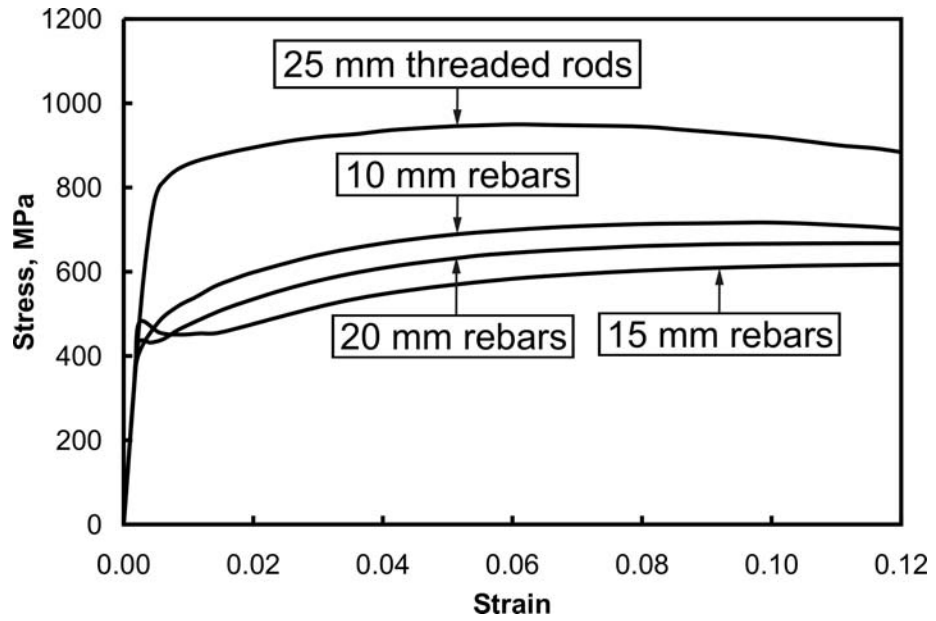


Figure 3-5: Stress vs. strain curves for rebar

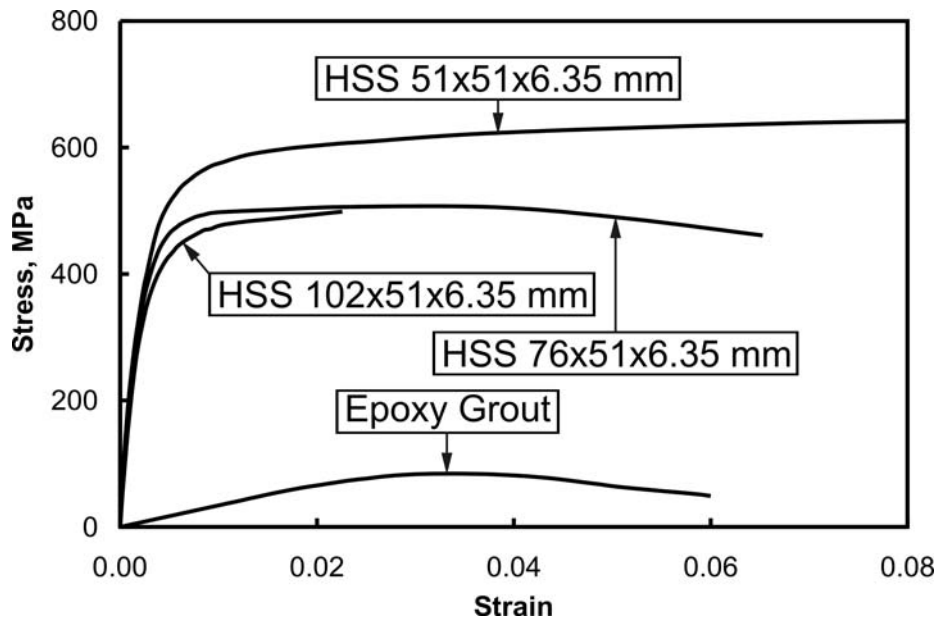


Figure 3-6: Stress vs. strain curves for HSS and epoxy grout

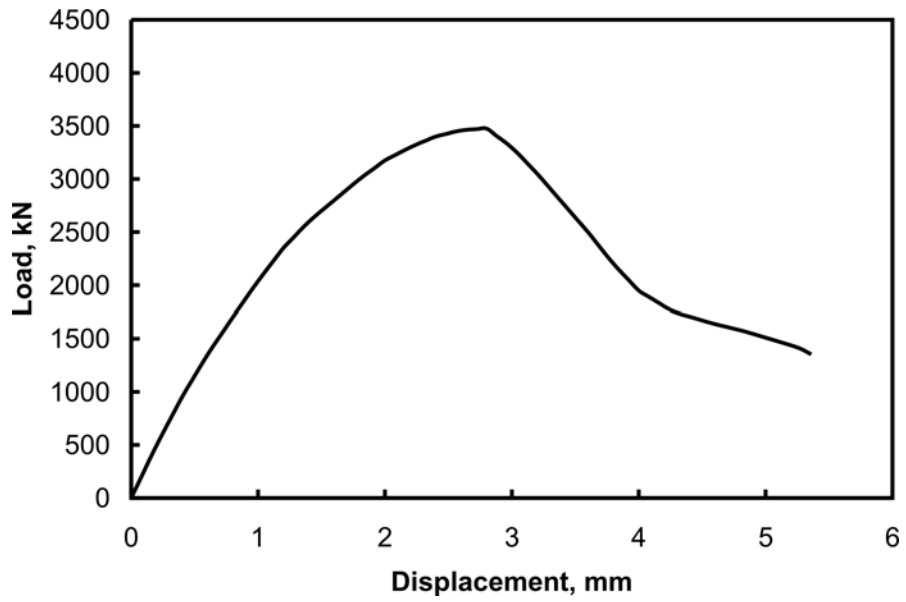


Figure 3-7: Load vs. axial displacement for column C00A

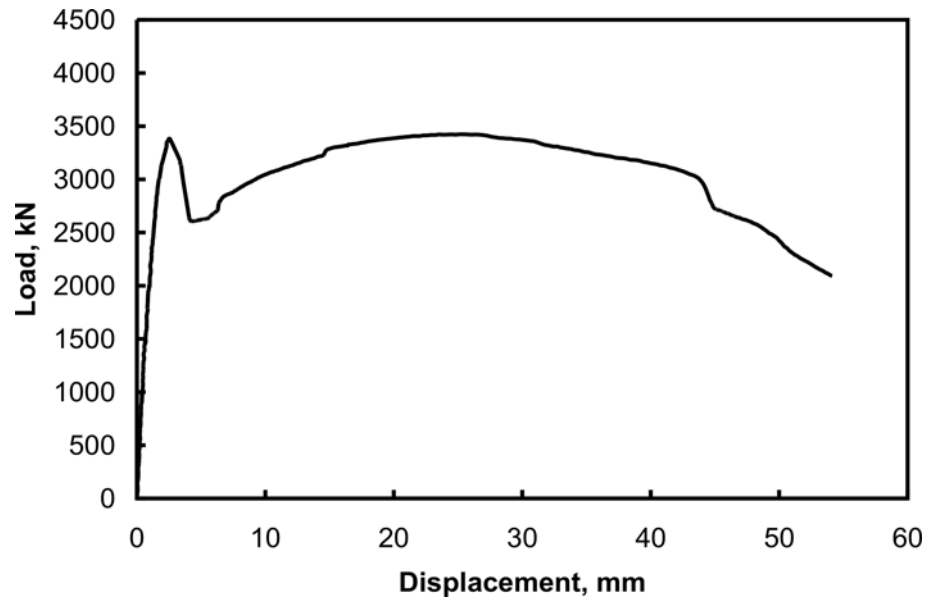


Figure 3-8: Load vs. axial displacement for column C00B

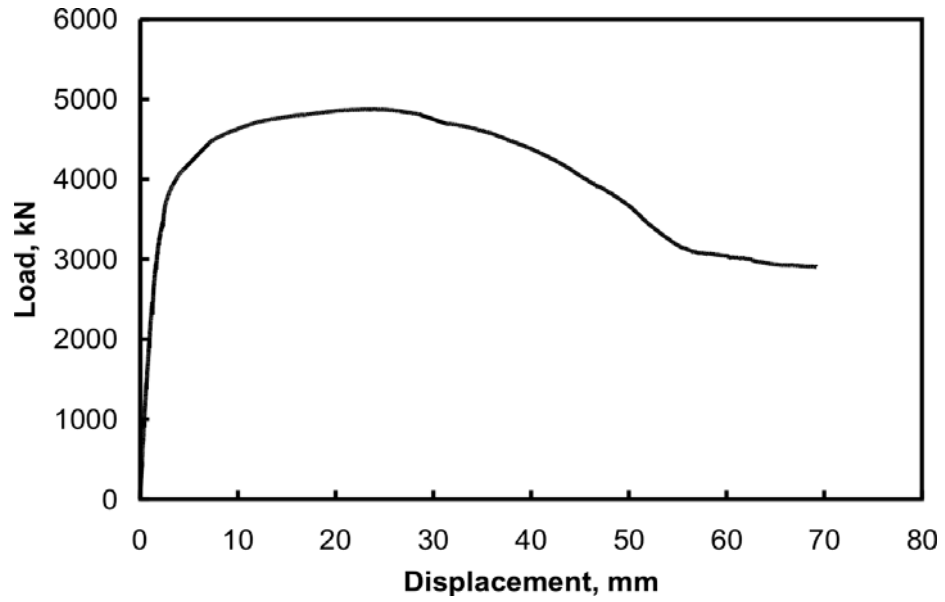


Figure 3-9: Load vs. axial displacement for column C01

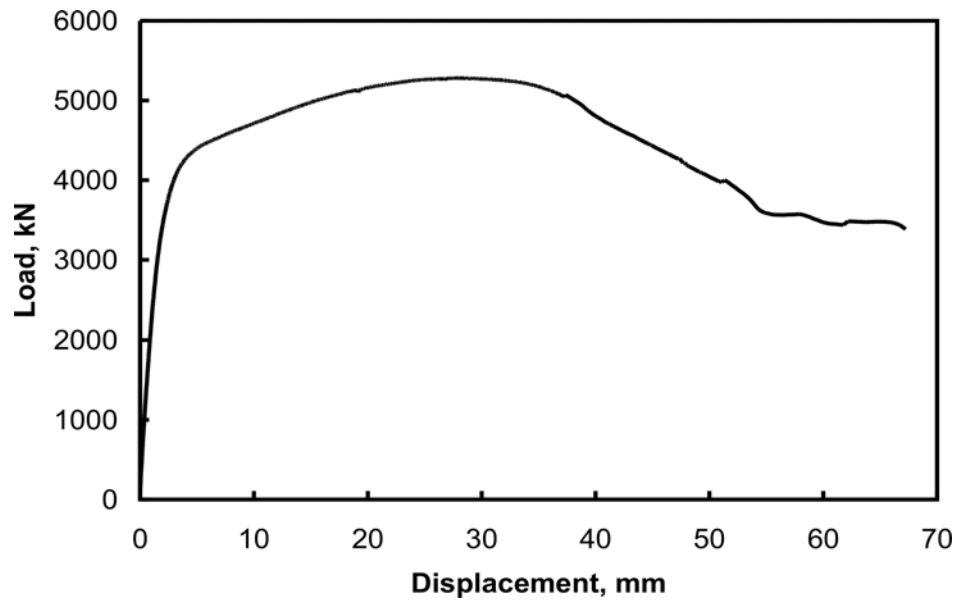


Figure 3-10: Load vs. axial displacement for column C02

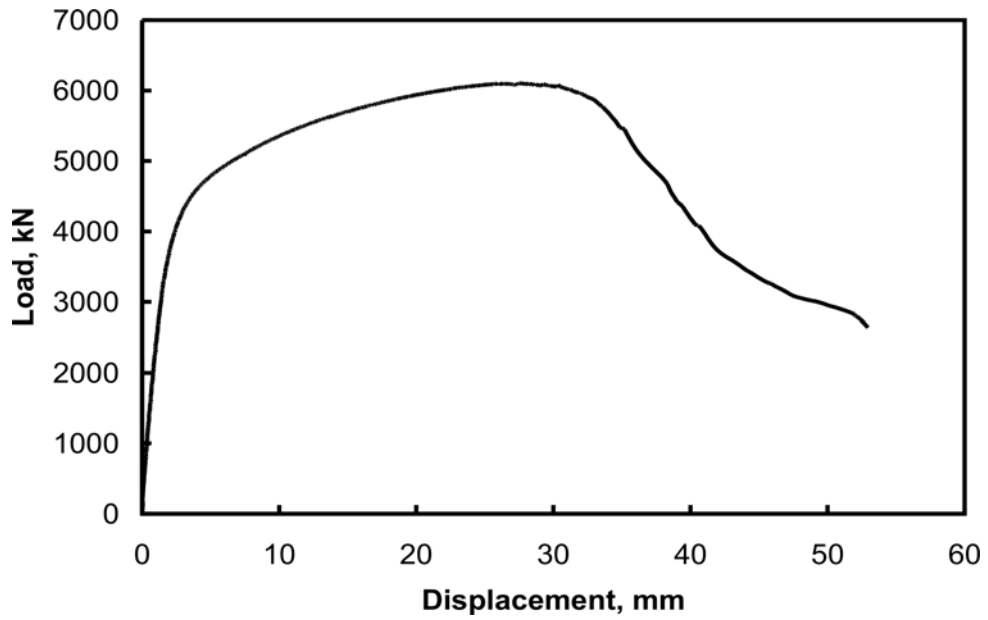


Figure 3-11: Load vs. axial displacement for columns C03

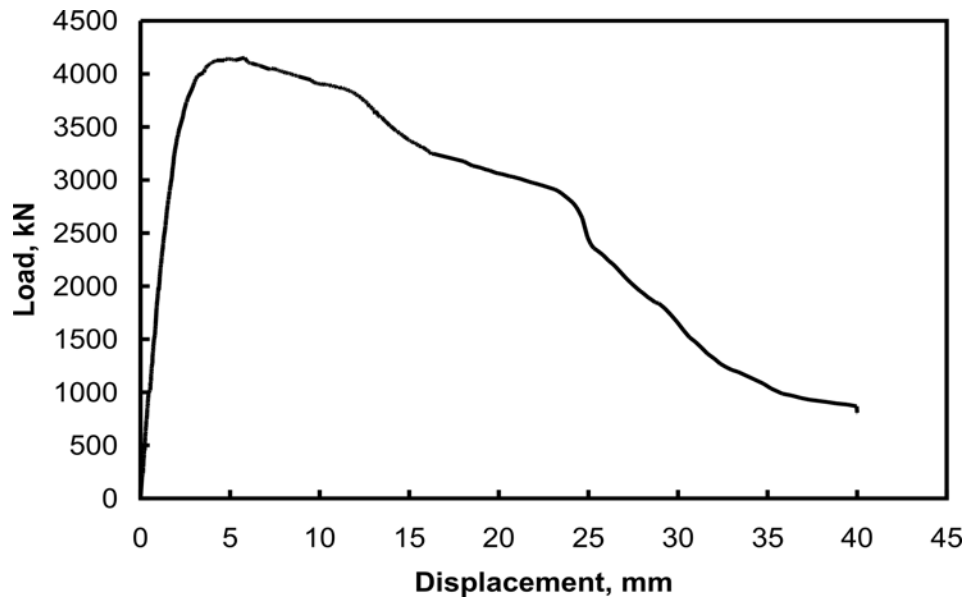


Figure 3-12: Load vs. axial displacement for columns C04

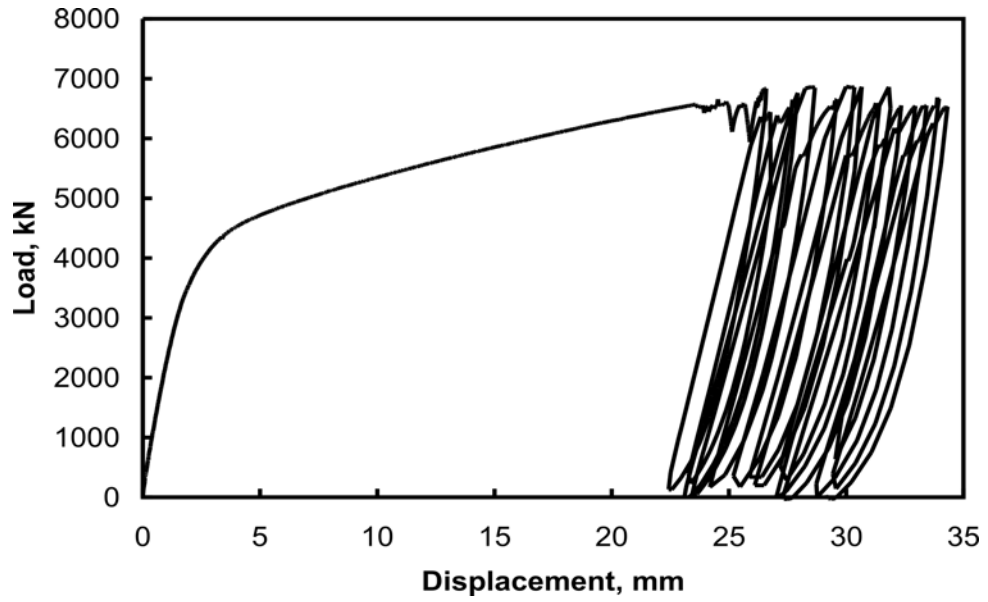


Figure 3-13: Load vs. axial displacement for columns C05

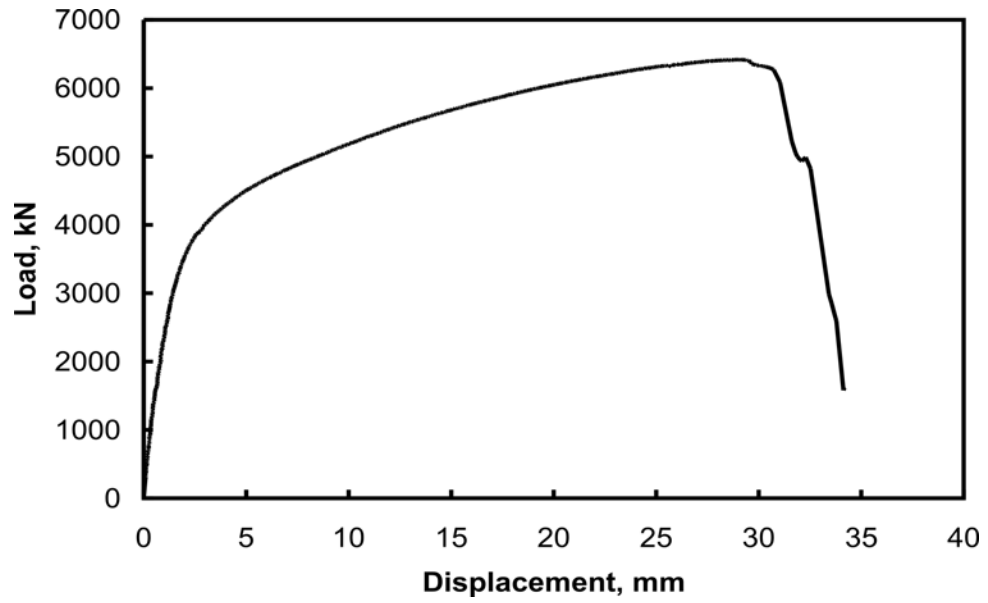


Figure 3-14: Load vs. axial displacement for columns C06

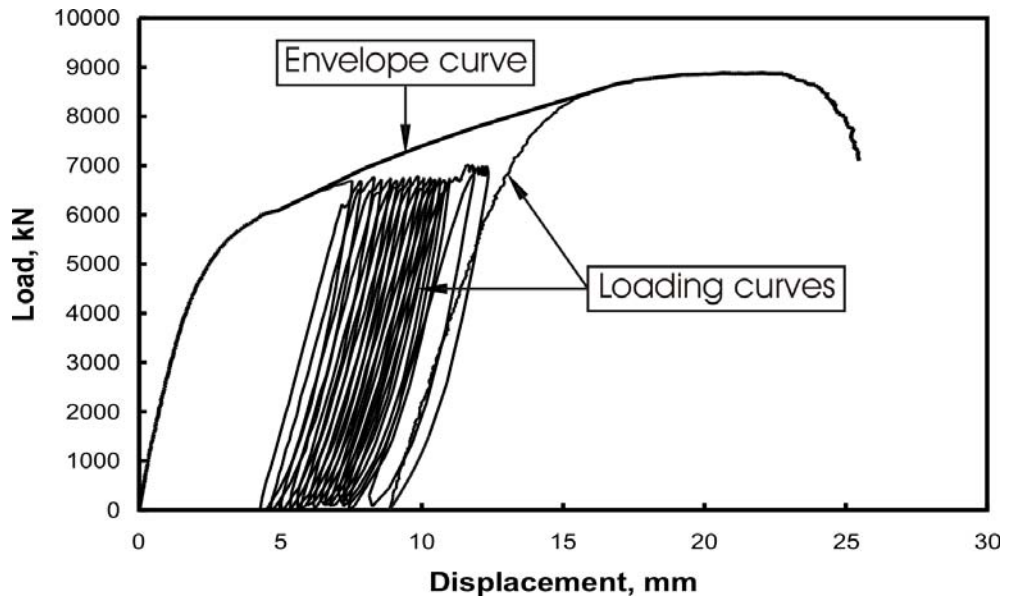


Figure 3-15: Load vs. axial displacement for column C07

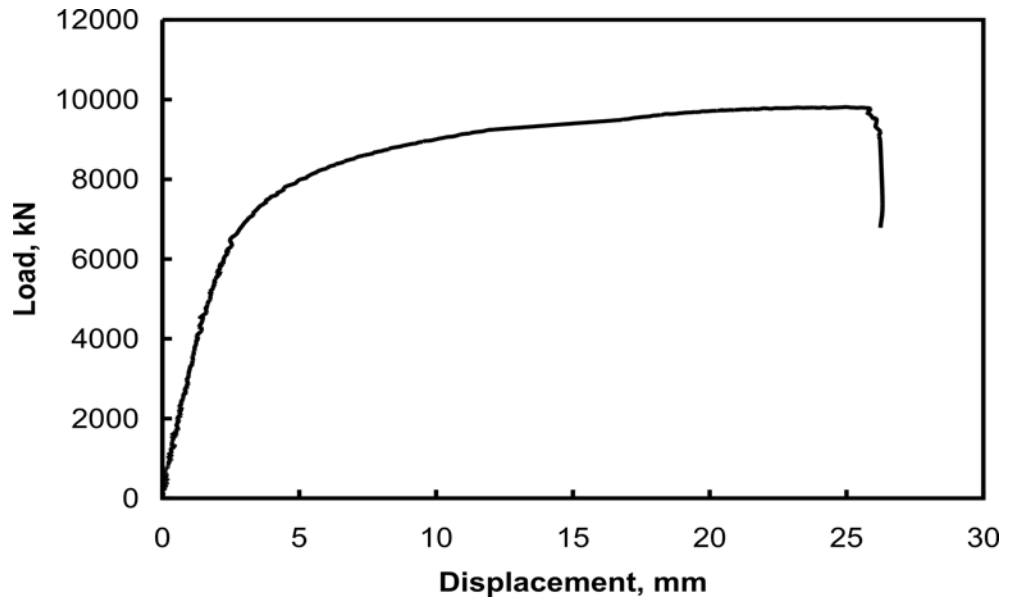


Figure 3-16: Load vs. axial displacement for column C08

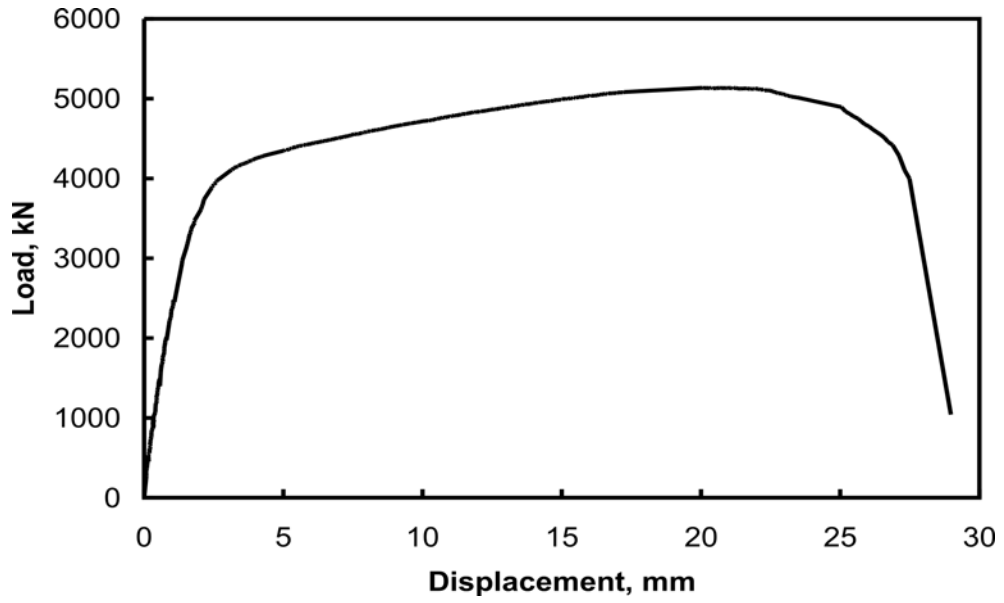


Figure 3-17: Load vs. axial displacement of column C09

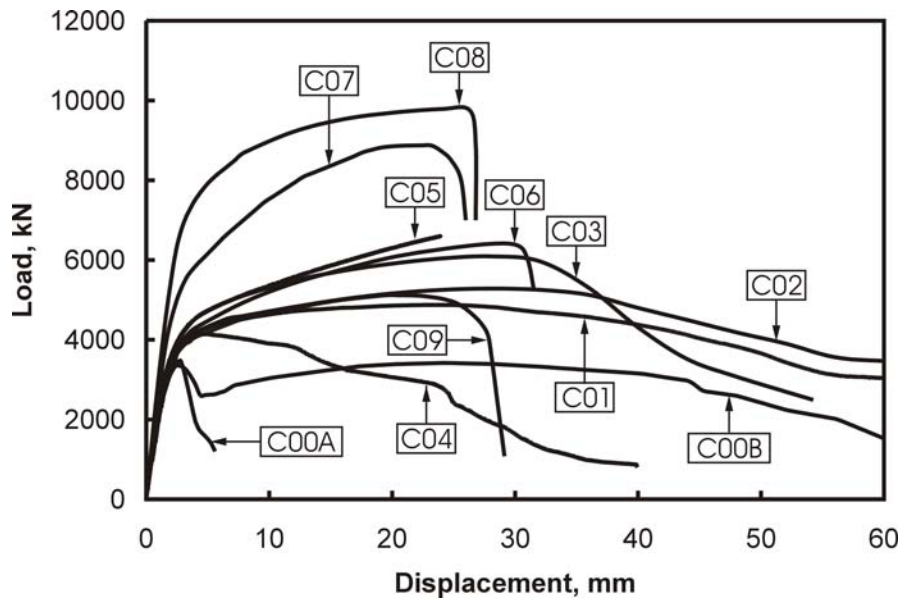


Figure 3-18: Load vs. axial displacement curves

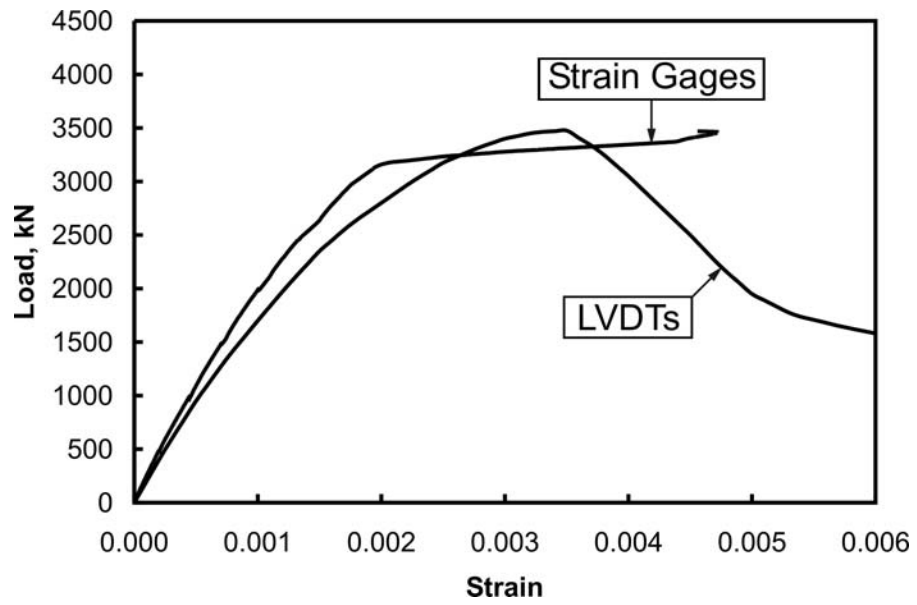


Figure 3-19: Load vs. average axial strain curves for column C00A

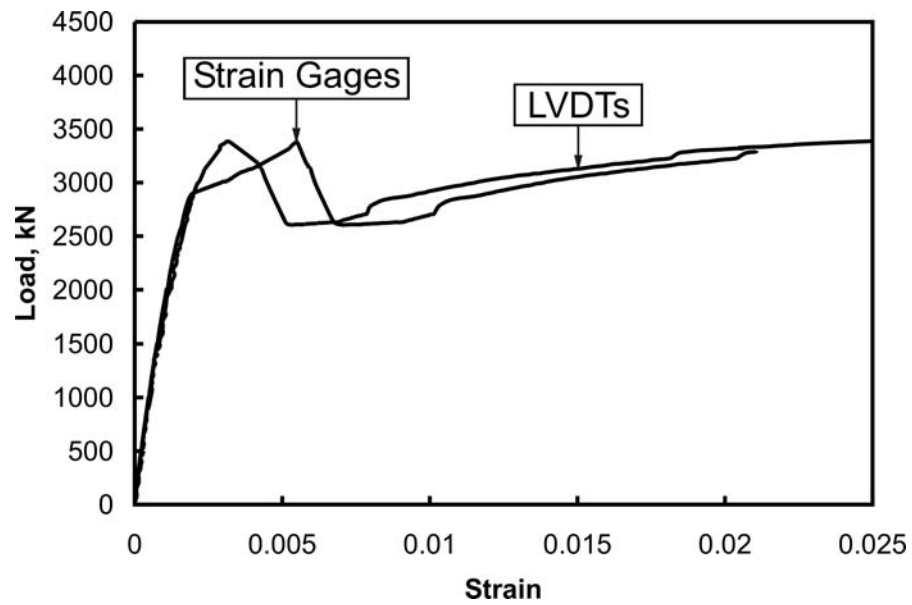


Figure 3-20: Load vs. average axial strain curves for column C00B

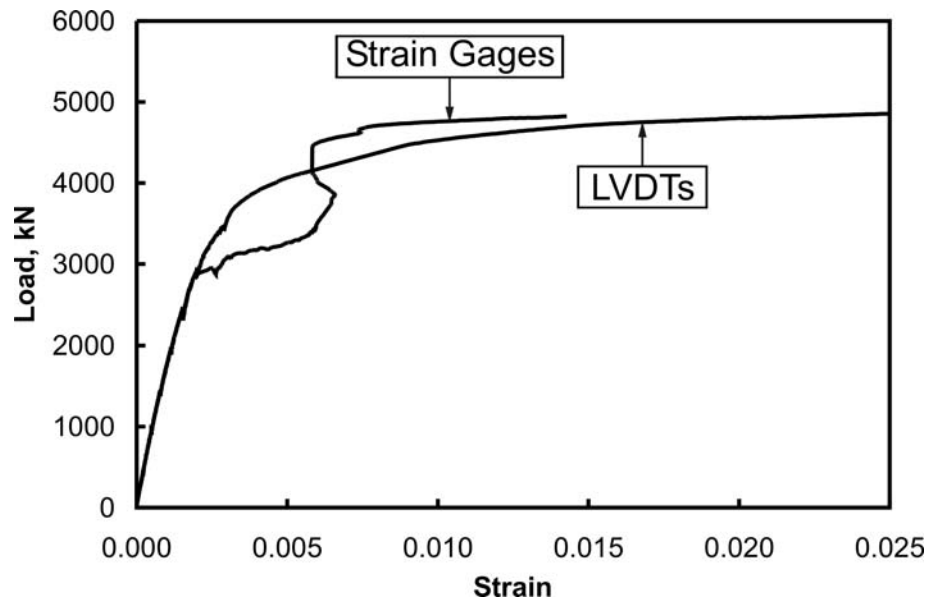


Figure 3-21: Load vs. average axial strain curves for column C01

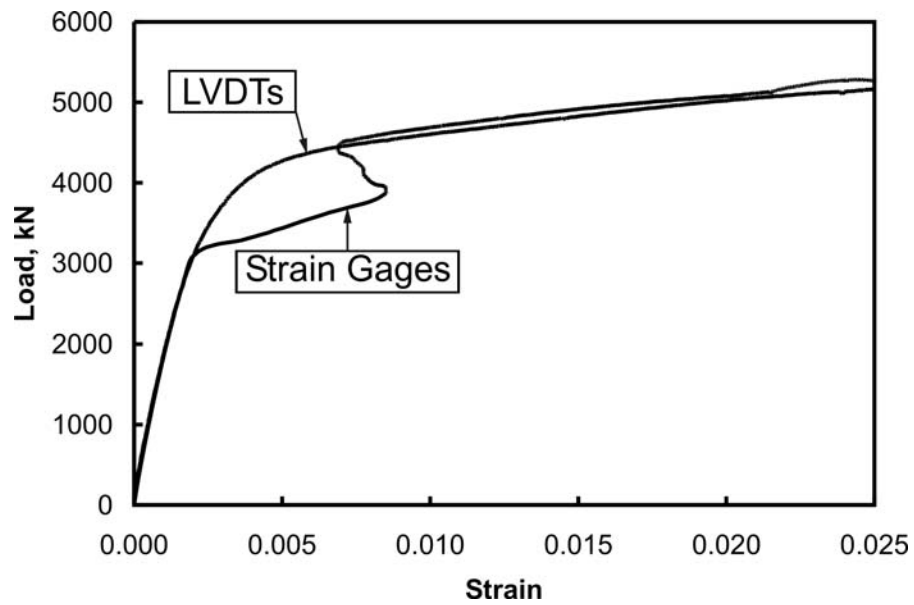


Figure 3-22: Load vs. average axial strain curves for column C02

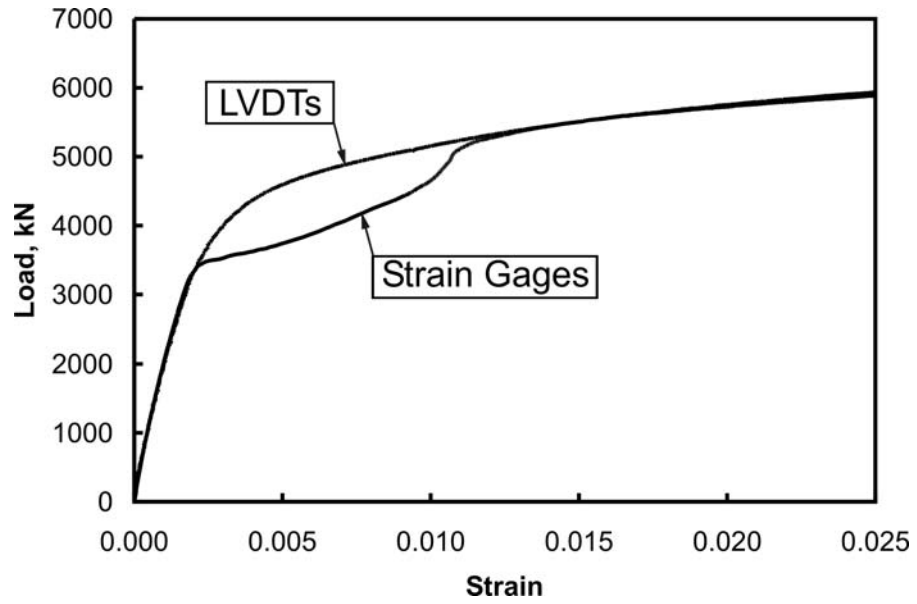


Figure 3-23: Load vs. average axial strain curves for column C03

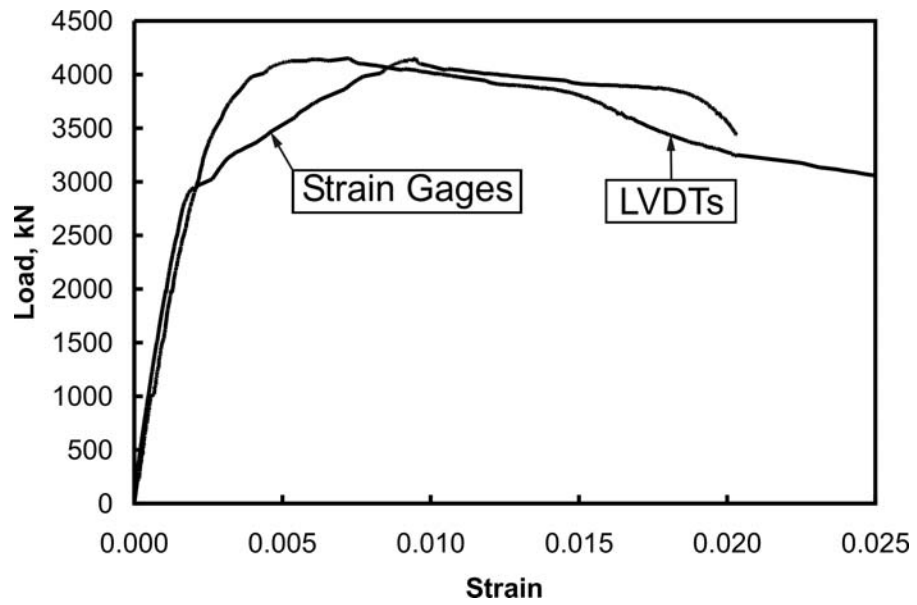


Figure 3-24: Load vs. average axial strain curves for column C04

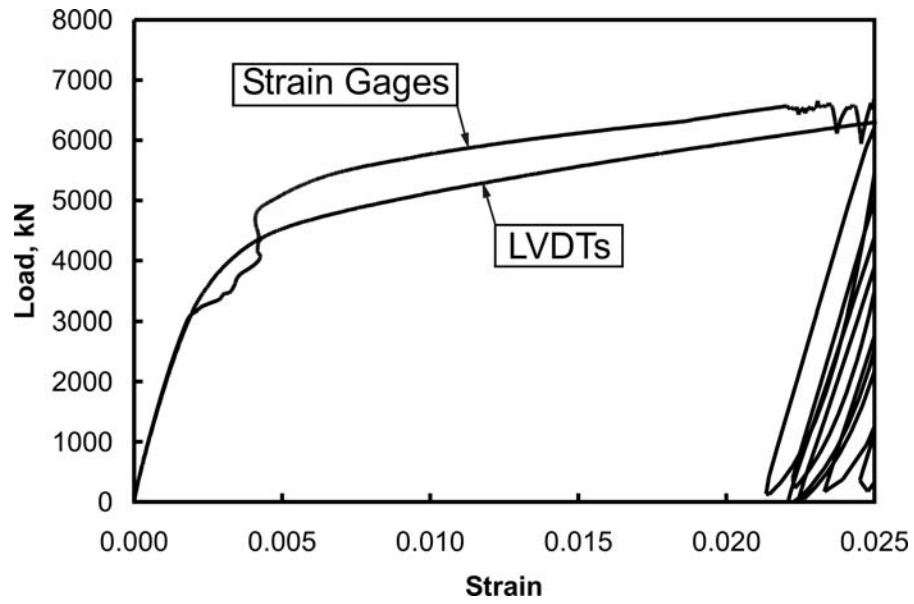


Figure 3-25: Load vs. average axial strain curves for column C05

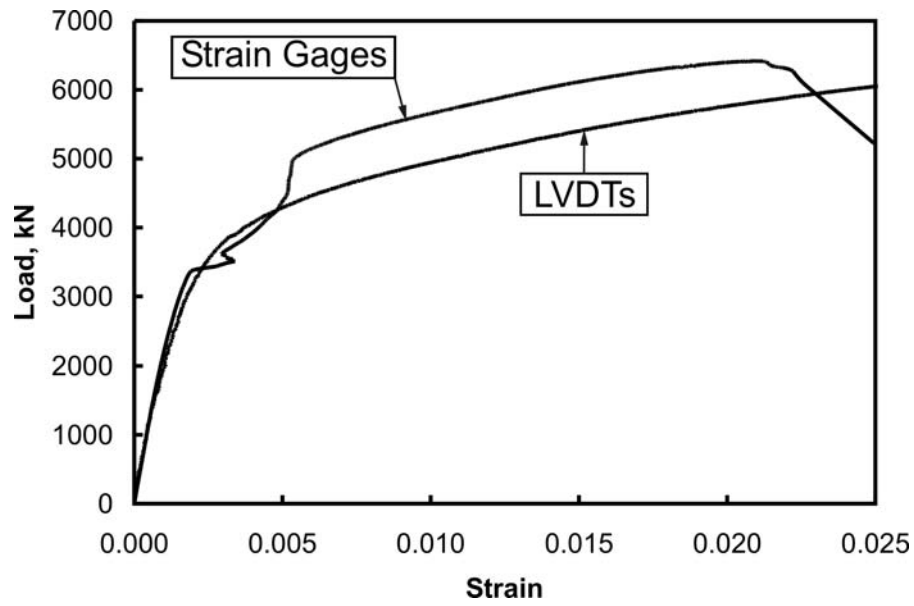


Figure 3-26: Load vs. average axial strain curves for column C06

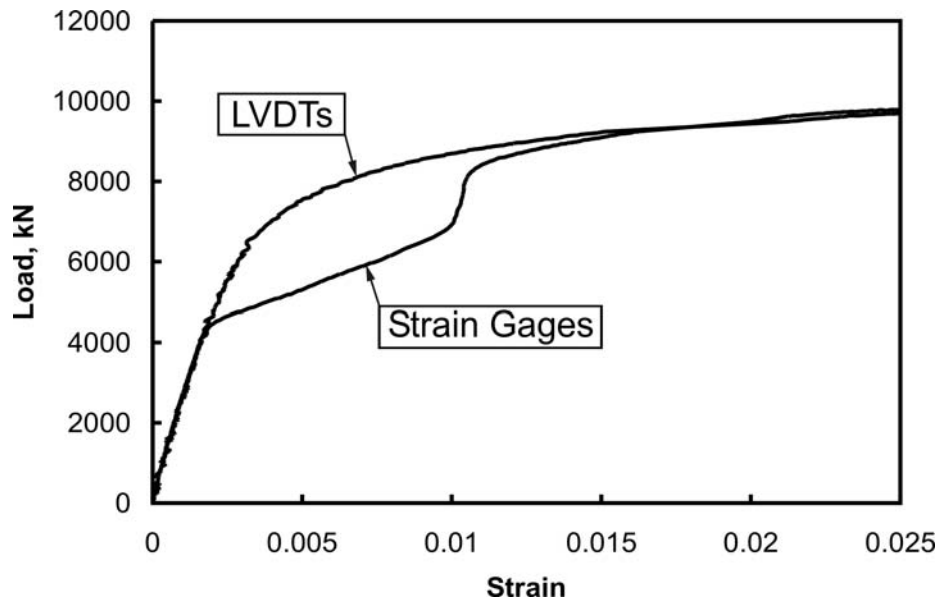


Figure 3-27: Load vs. average axial strain curves for column C08

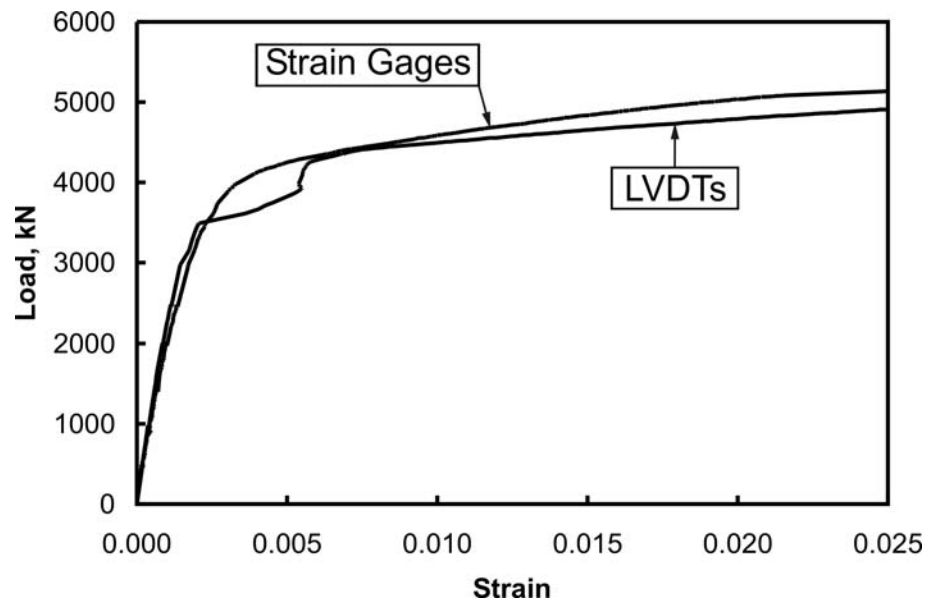


Figure 3-28: Load vs. average axial strain curves for column C09

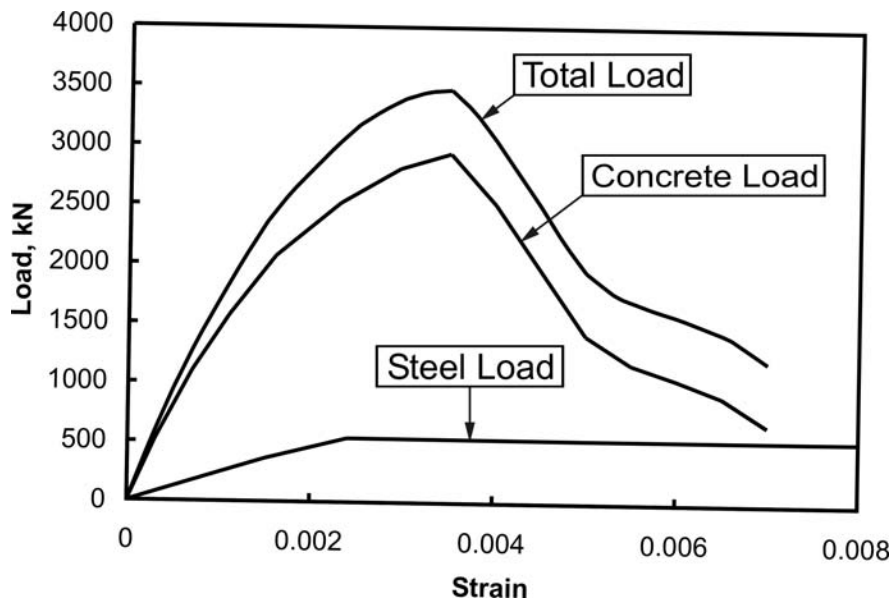


Figure 3-29: Total load, concrete load, and steel load vs. strain curves for C00A

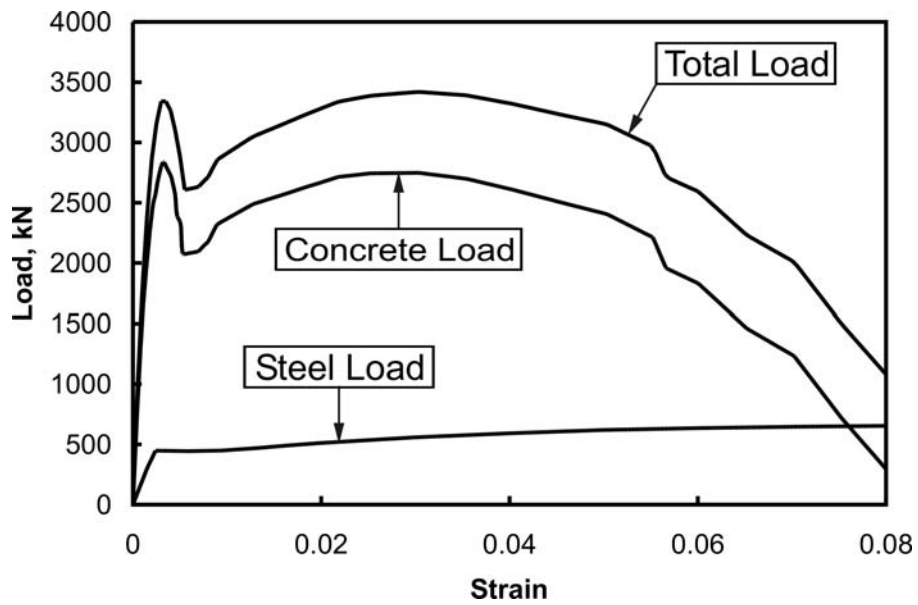


Figure 3-30: Total load, concrete load, and steel load vs. strain curves for C00B

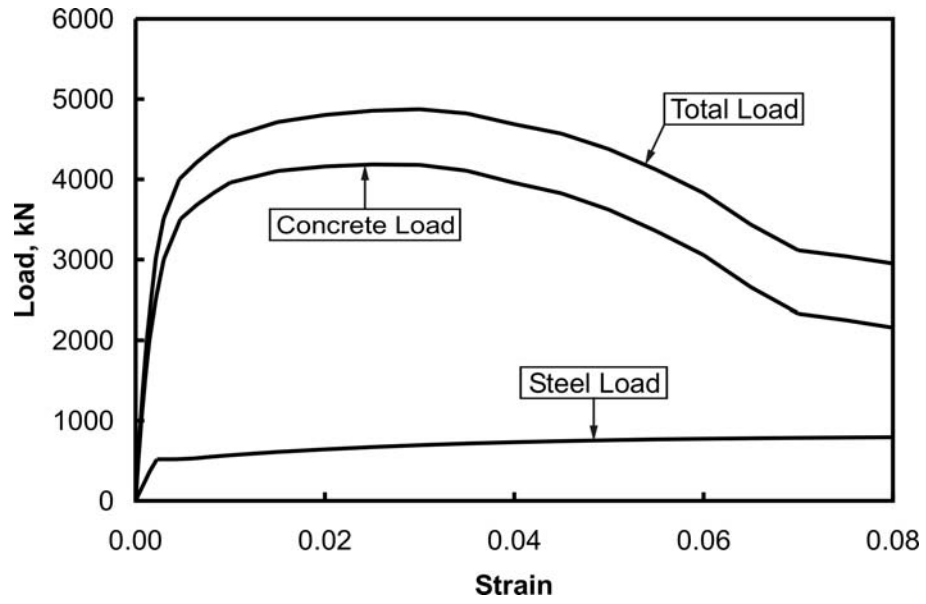


Figure 3-31: Total load, concrete load, and steel load vs. strain curves for C01

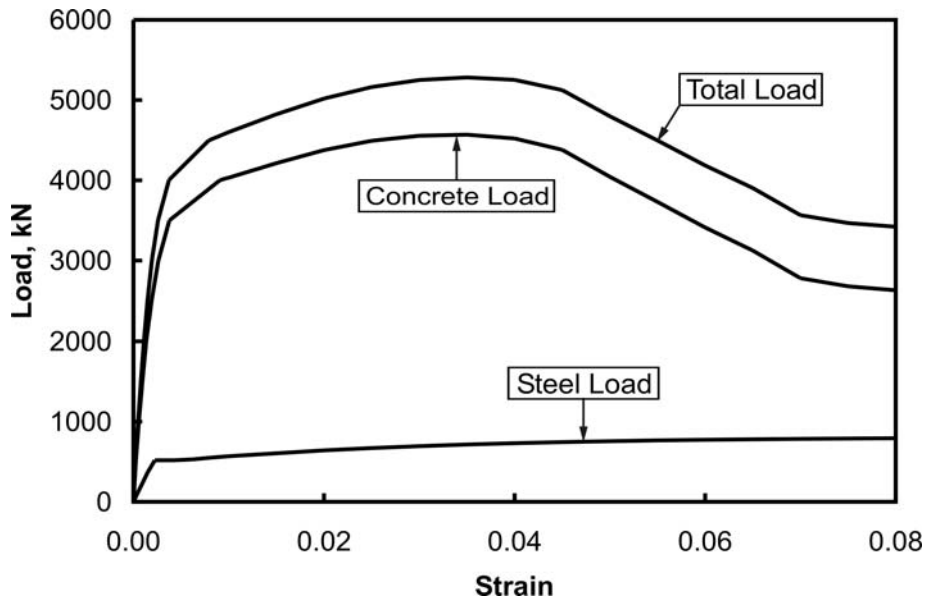


Figure 3-32: Total load, concrete load, and steel load vs. strain curves for C02

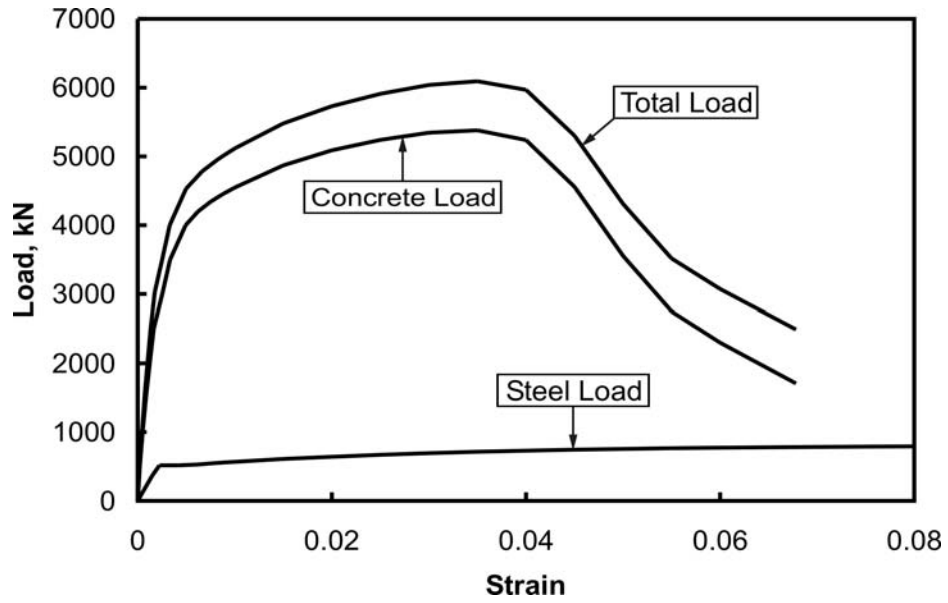


Figure 3-33: Total load, concrete load, and steel load vs. strain curves for C03

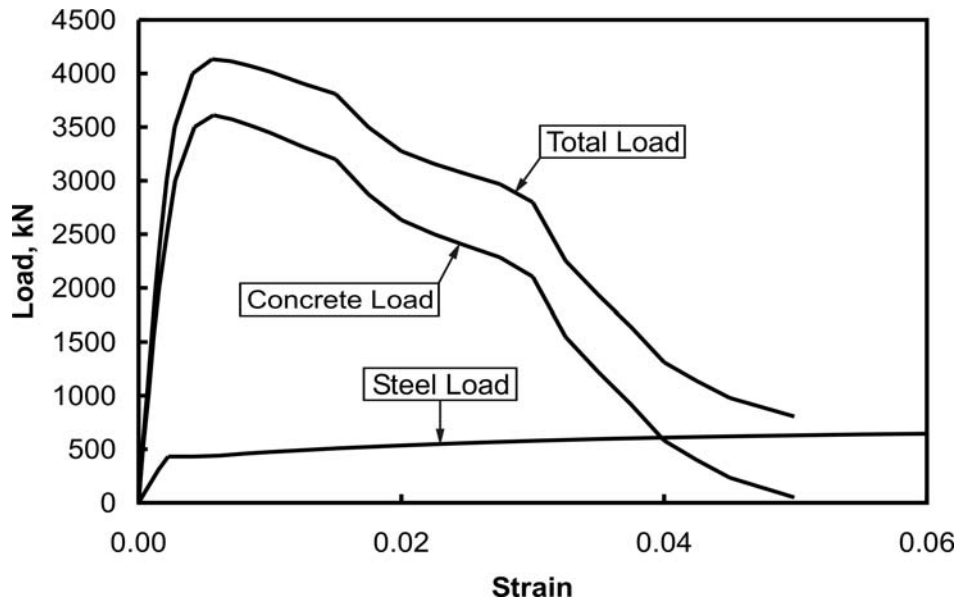


Figure 3-34: Total load, concrete load, and steel load vs. strain curves for C04

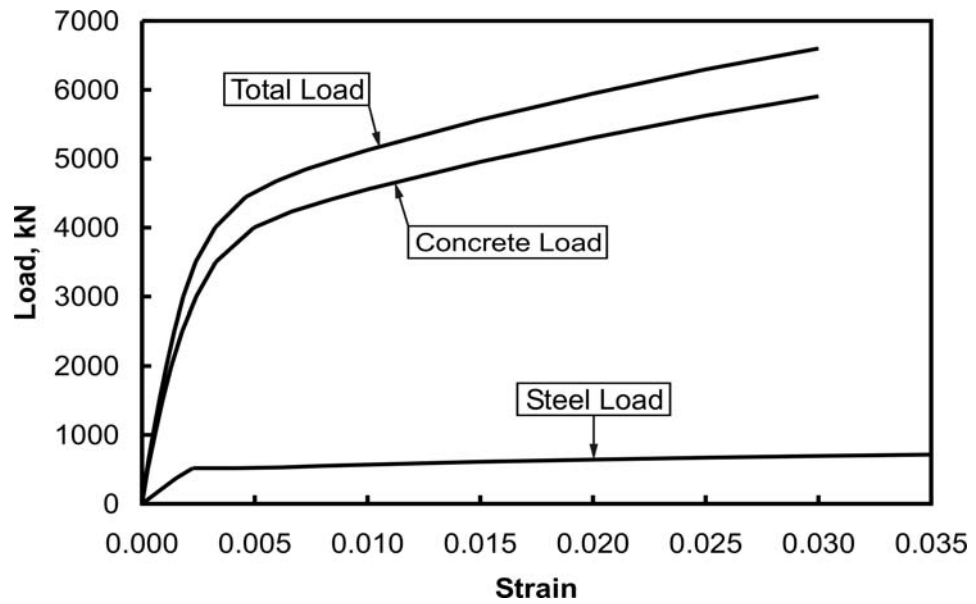


Figure 3-35: Total load, concrete load, and steel load vs. strain curves for C05

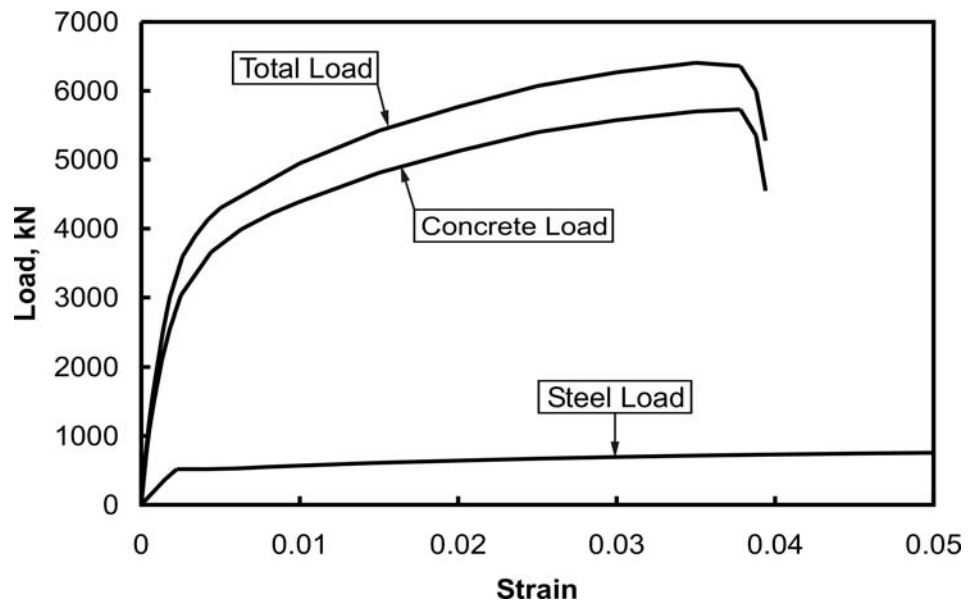


Figure 3-36: Total load, concrete load, and steel load vs. strain curves for C06

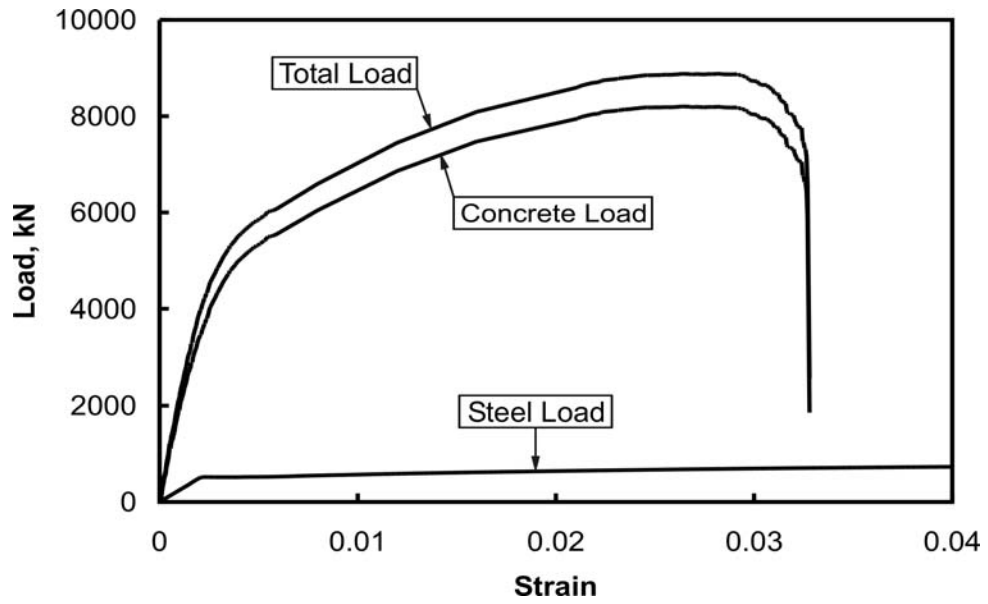


Figure 3-37: Total load, concrete load, and steel load vs. strain curves for C07

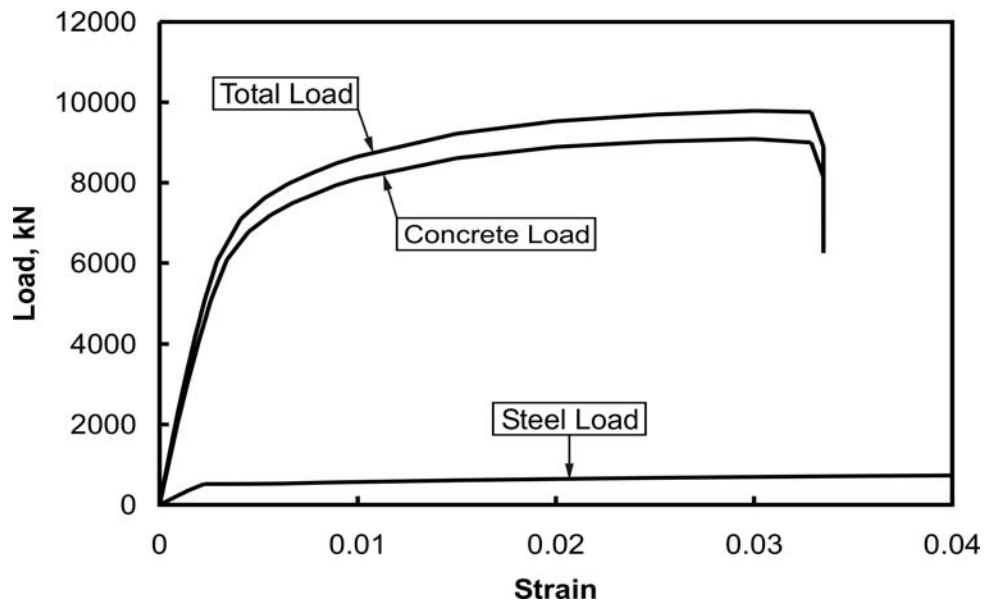


Figure 3-38: Total load, concrete load, and steel load vs. strain curves for C08

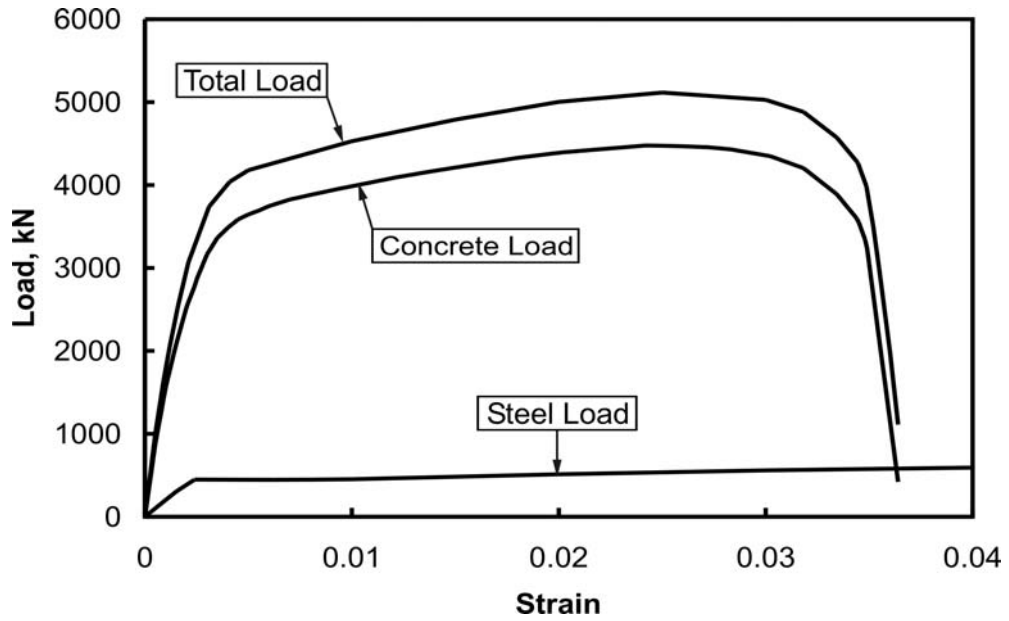


Figure 3-39: Total load, concrete load, and steel load vs. strain curves for C09

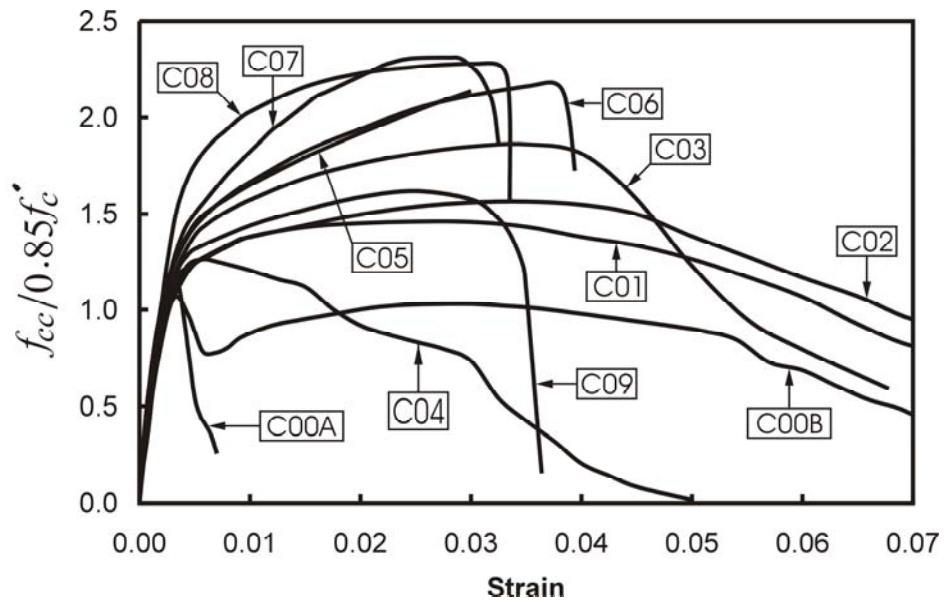


Figure 3-40: Normalized concrete material curves



C00A



C00B



C02



C04



C05



C07

Figure 3-41: Appearance of columns at the end of the tests

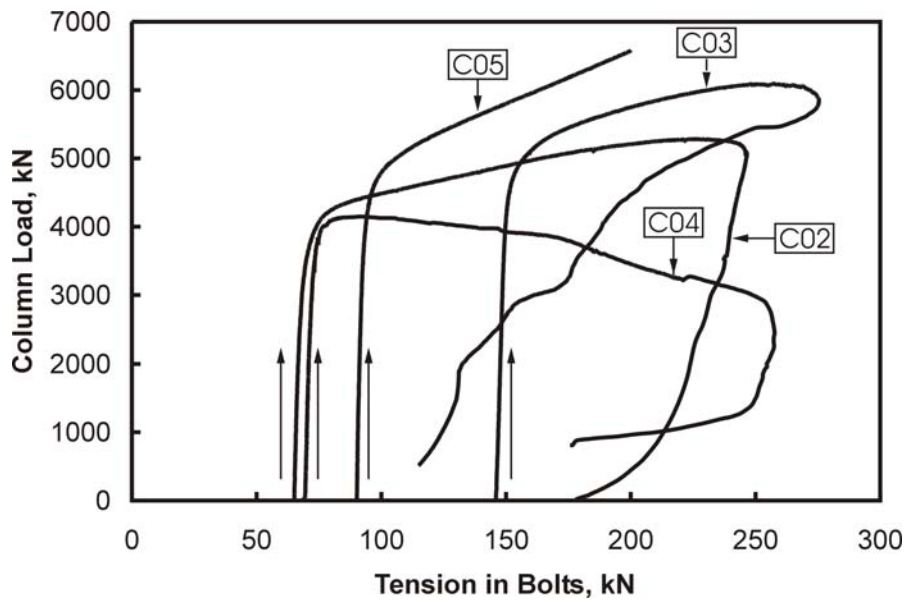


Figure 3-42: Column load vs. tension in the collar bolts

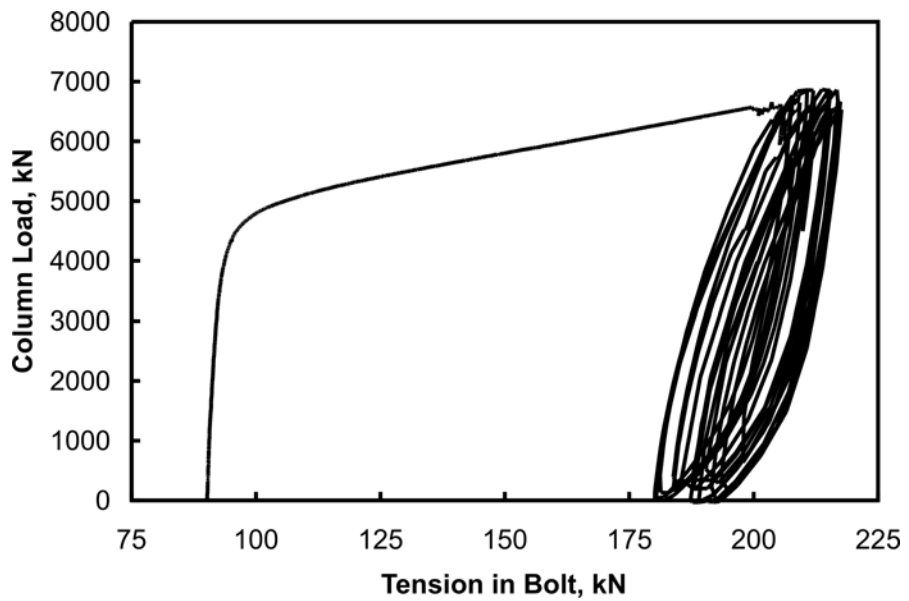


Figure 3-43: Column load vs. tension in the collar bolt for column C05

All dimensions are in millimeters

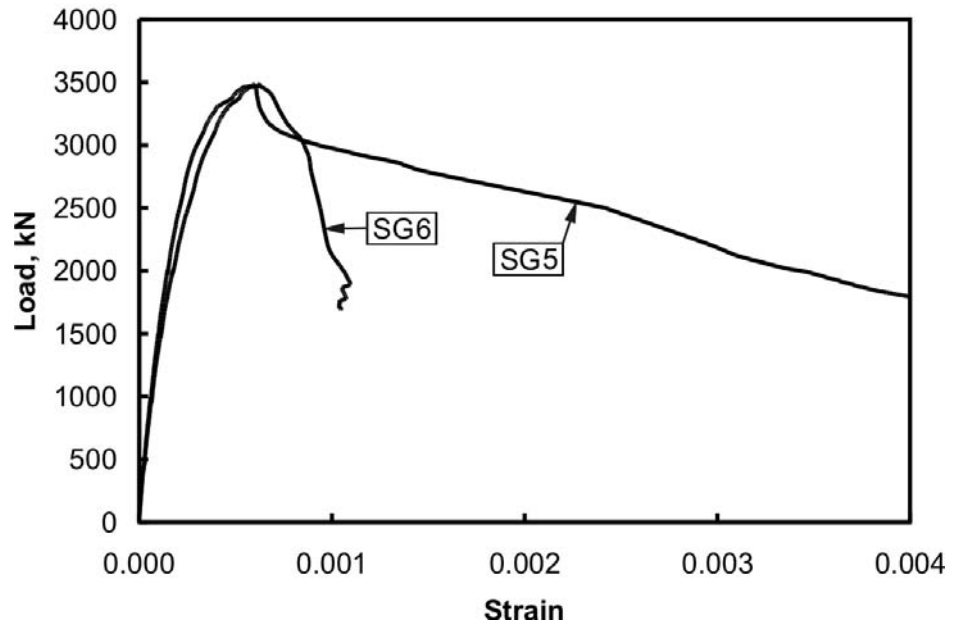
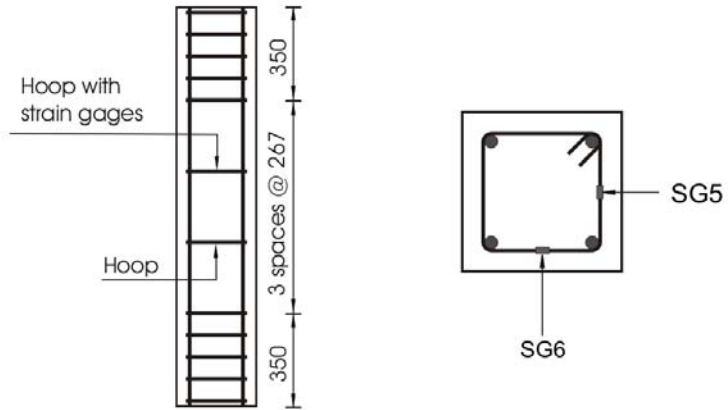


Figure 3-44: Load vs. strain of tie bars for column C00A

All dimensions are in millimeters

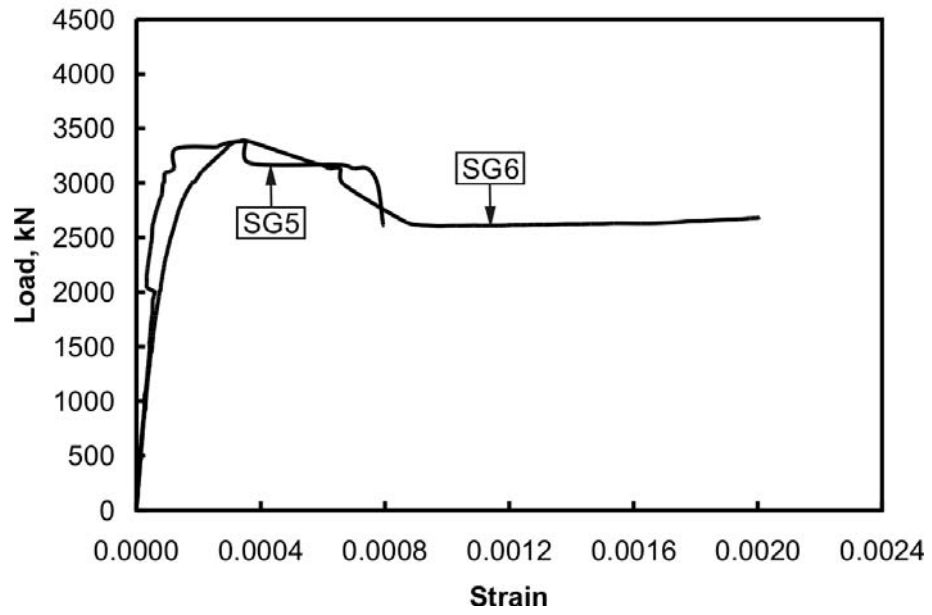
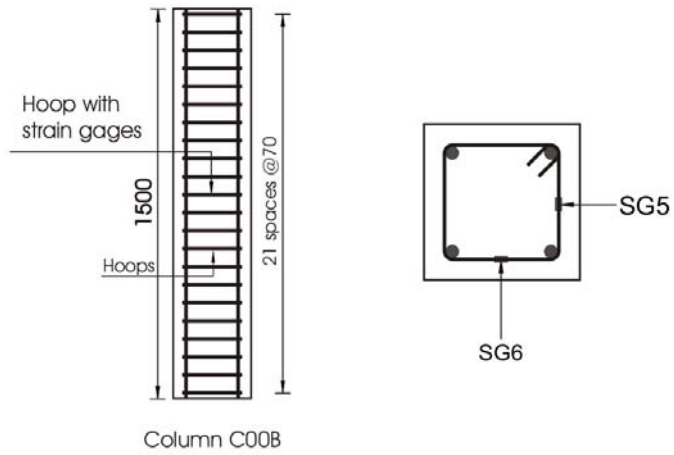


Figure 3-45: Load vs. strain of tie bars for column C00B

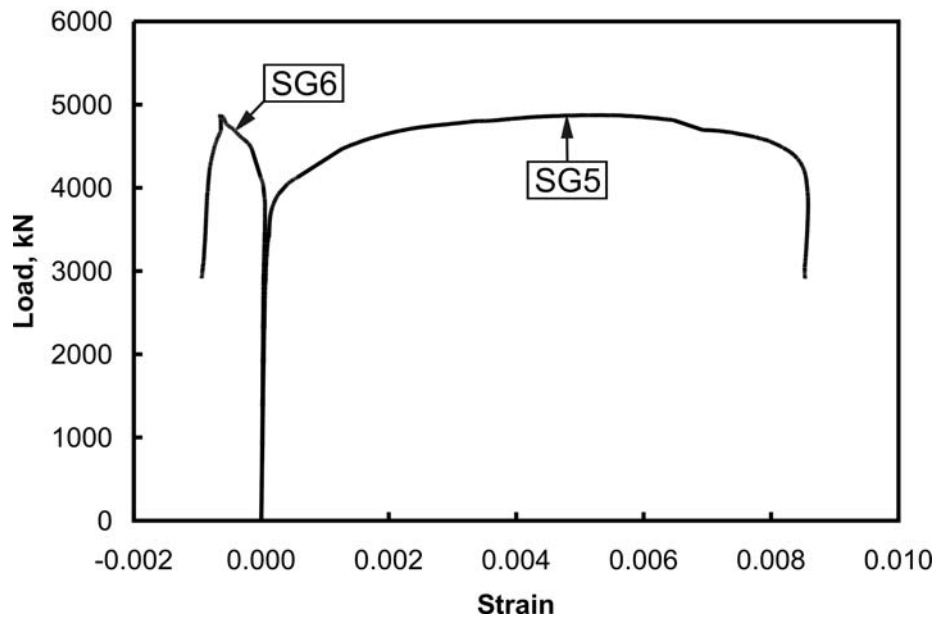
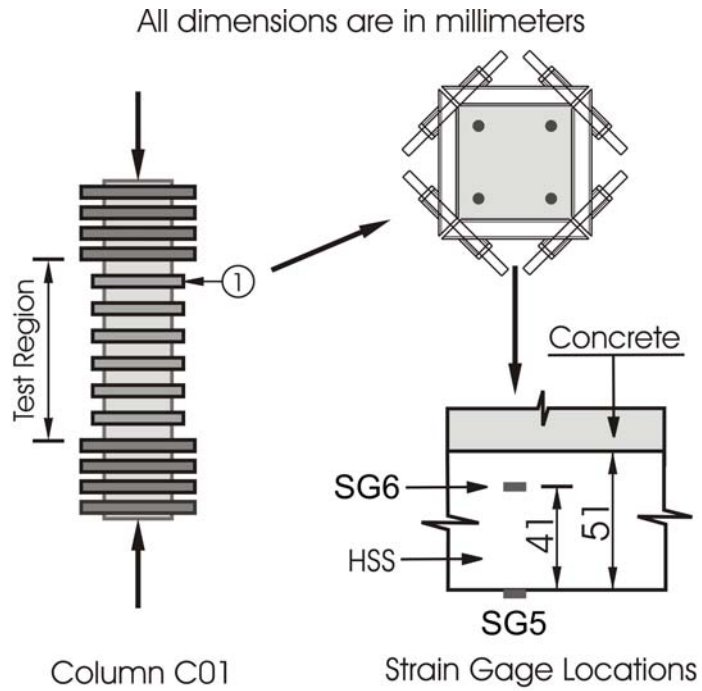


Figure 3-46a: Column load vs. strain of collar (SG5 and SG6) for column C01

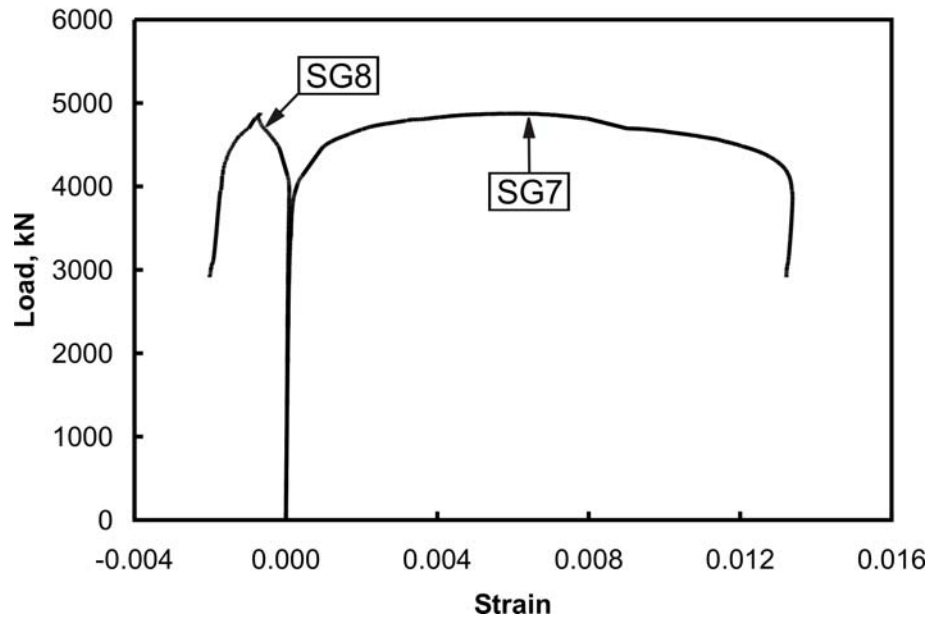
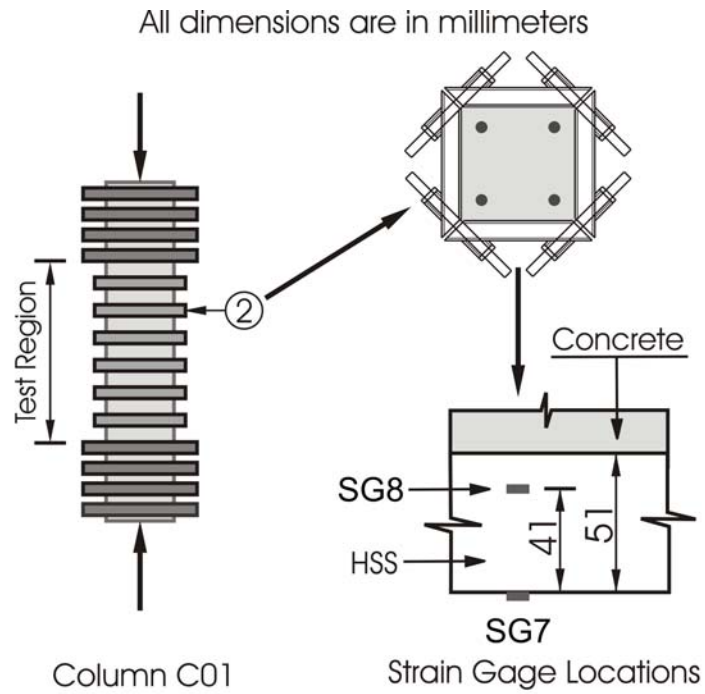


Figure 3-46b: Column load vs. strain of collar (SG7 and SG8) for column C01

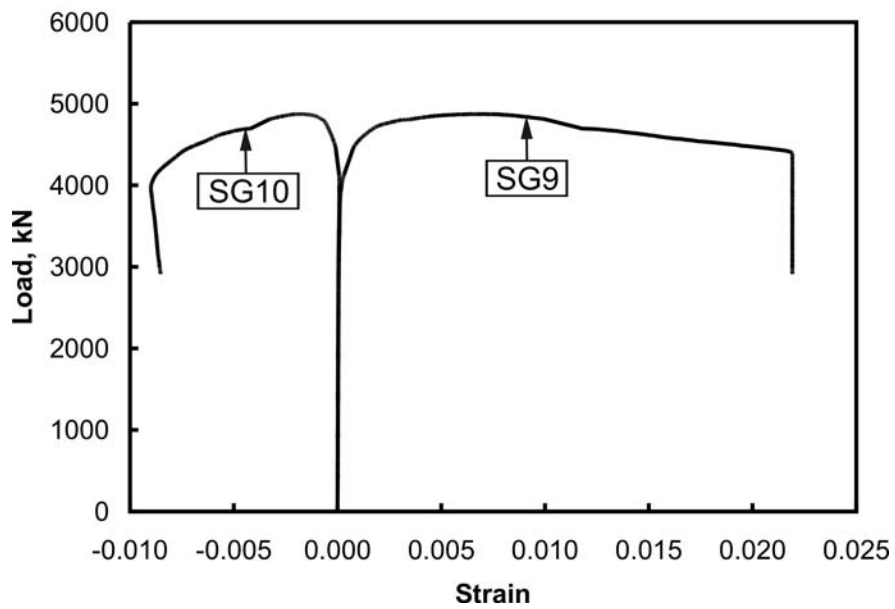
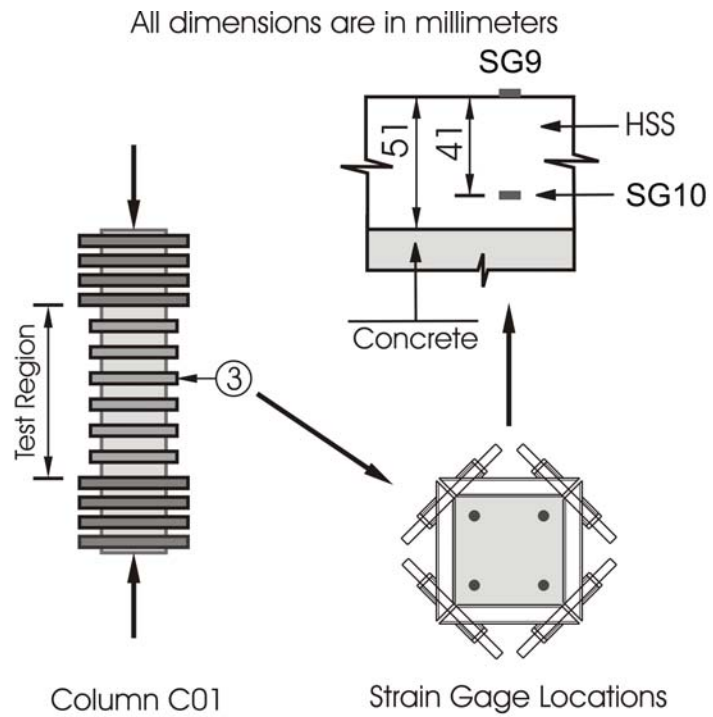


Figure 3.46c: Column load vs. strain of collar (SG9 and SG10) for column C01

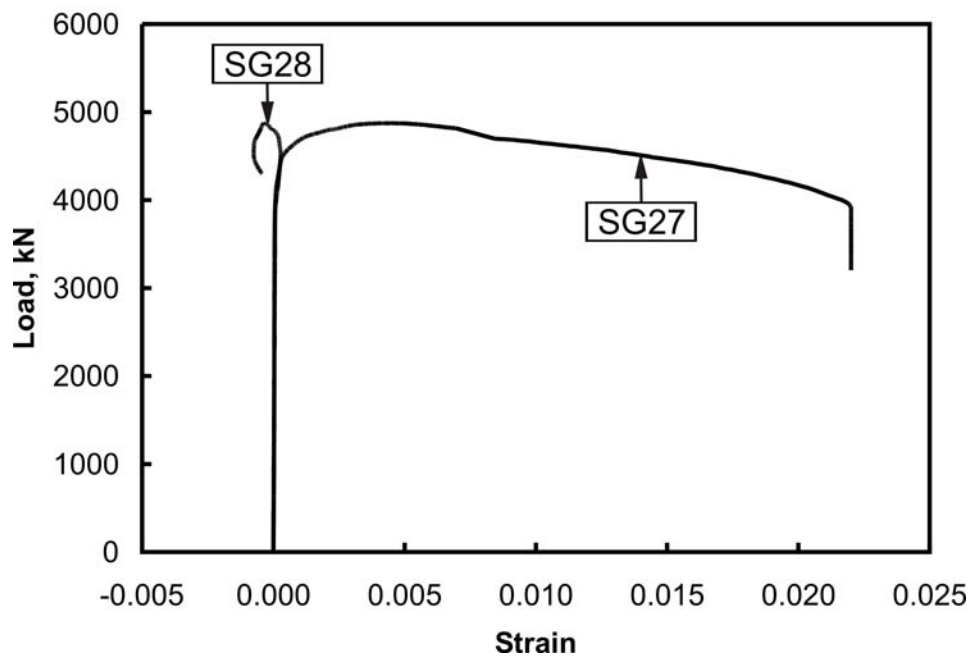
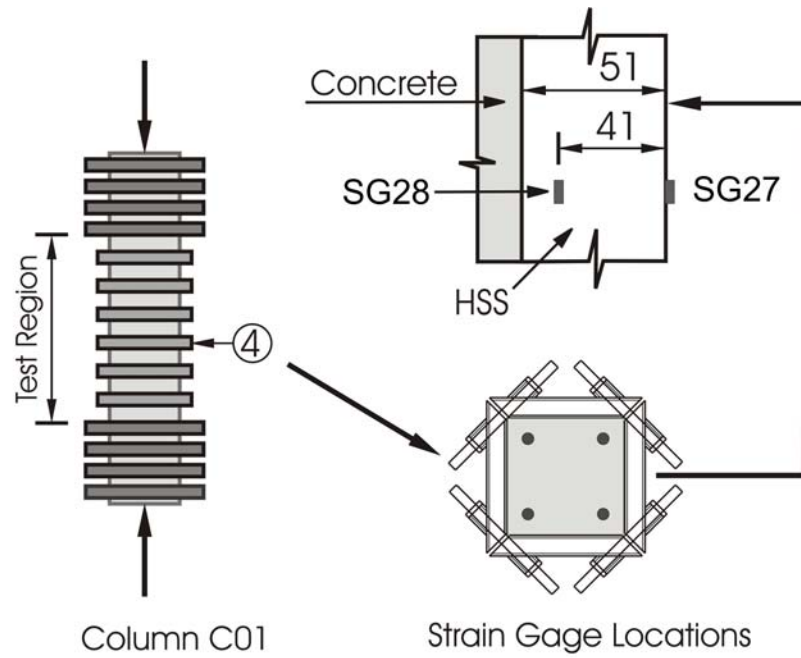


Figure 3-46d: Column load vs. strain of collar (SG27 and SG28) for column C01

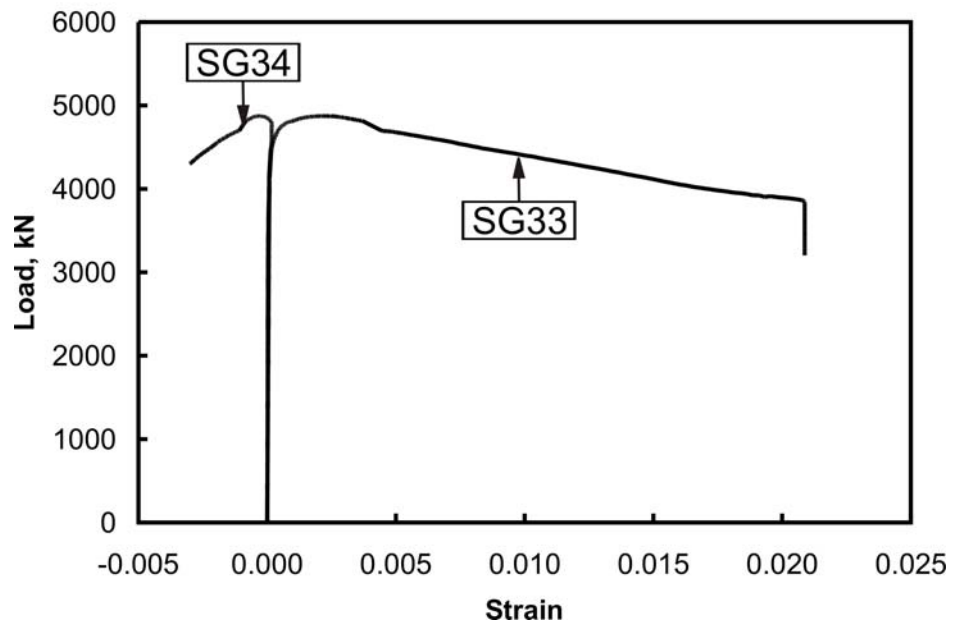
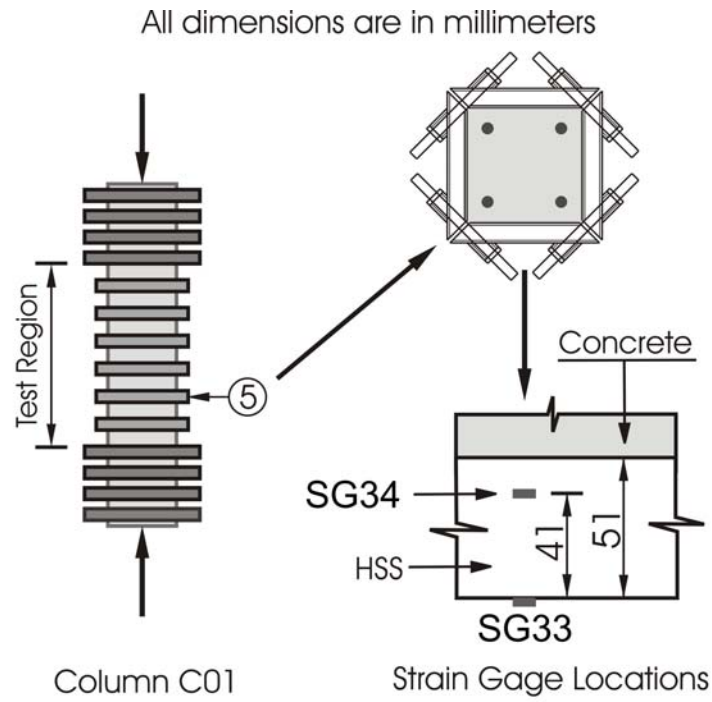


Figure 3-46e: Column load vs. strain of collar (SG33 and SG34) for column C01

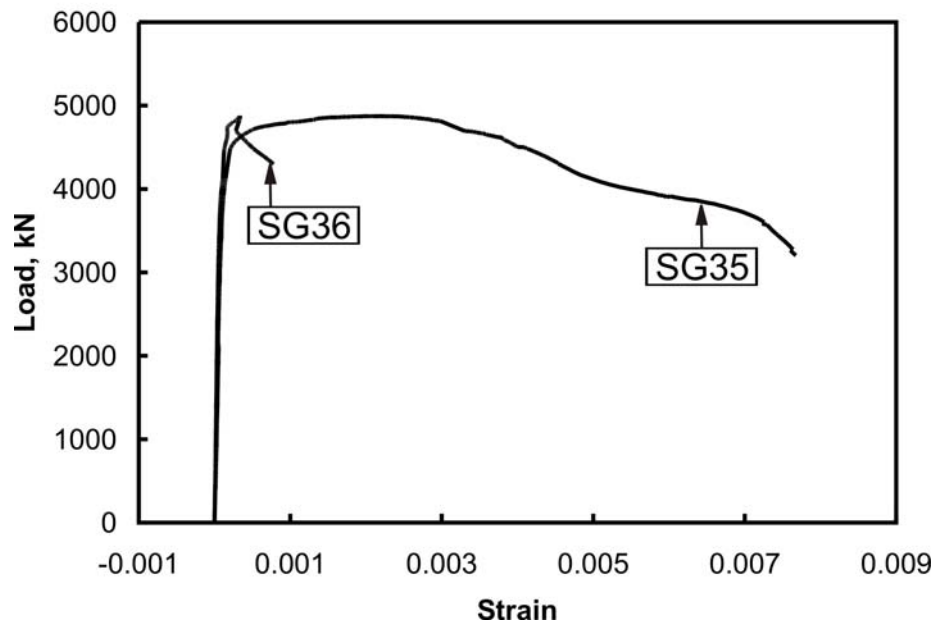
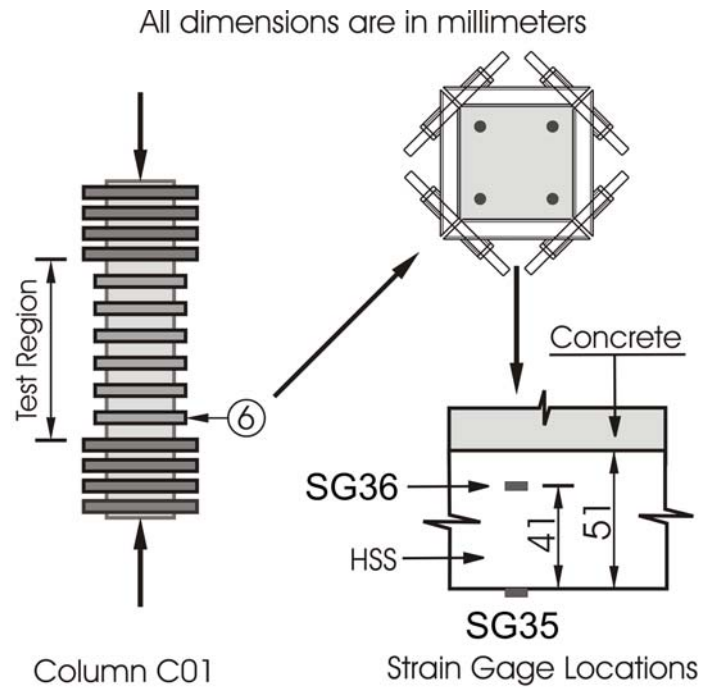


Figure 3-46f: Column load vs. strain of collar (SG35 and SG36) for column C01

All dimensions are in millimeters

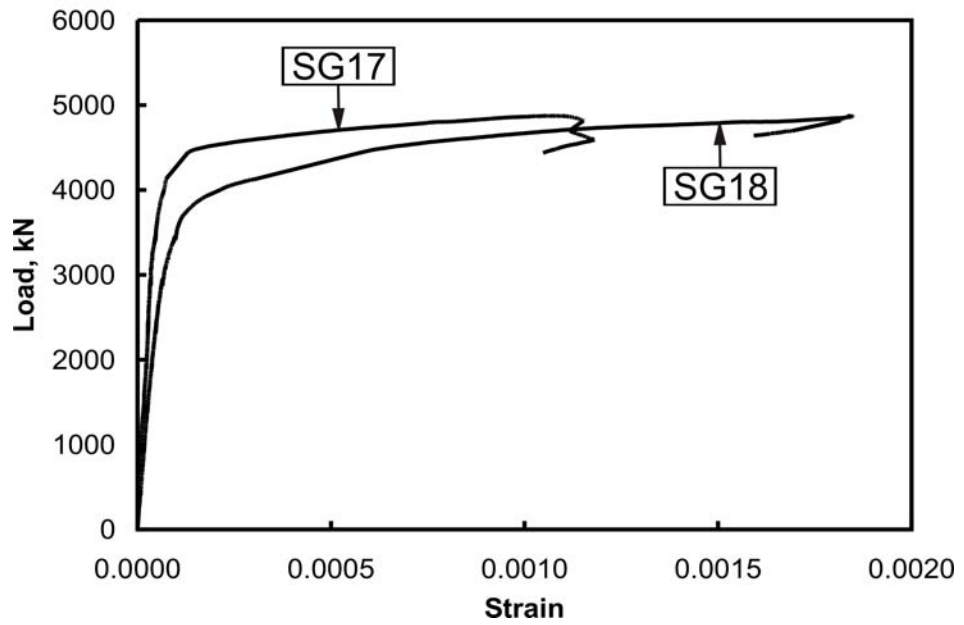
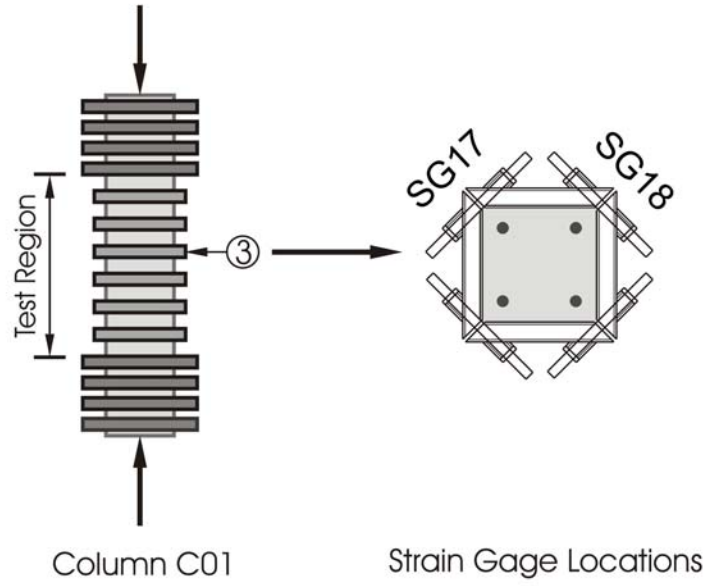


Figure 3-46g: Column load vs. strain of bolts (SG17 and SG18) for column C01

All dimensions are in millimeters

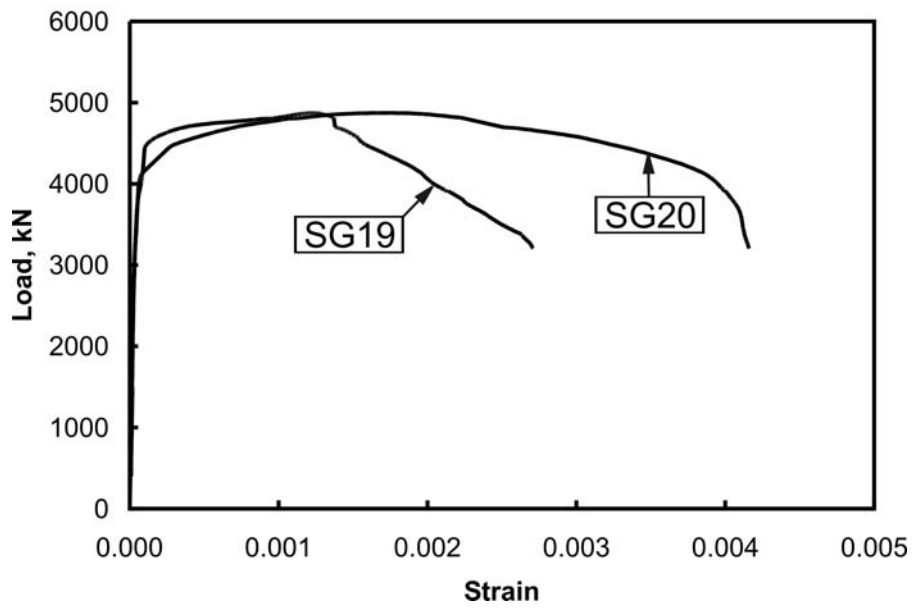
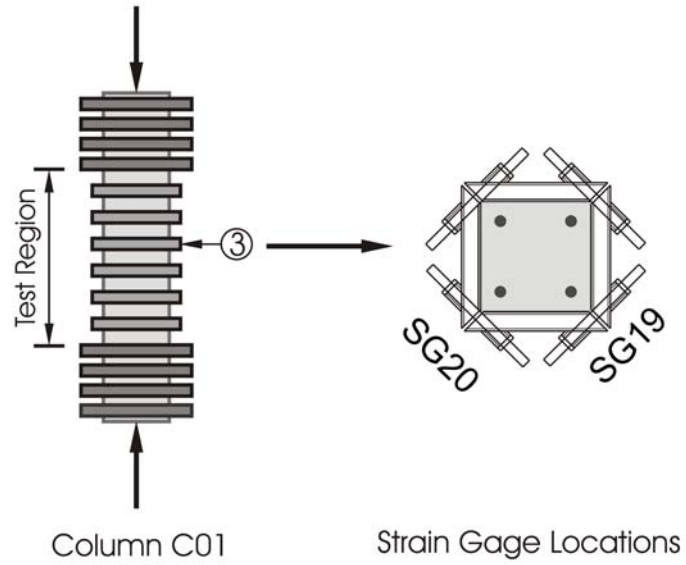


Figure 3-46h: Column load vs. strain of bolts (SG19 and SG20) for column C01

All dimensions are in millimeters

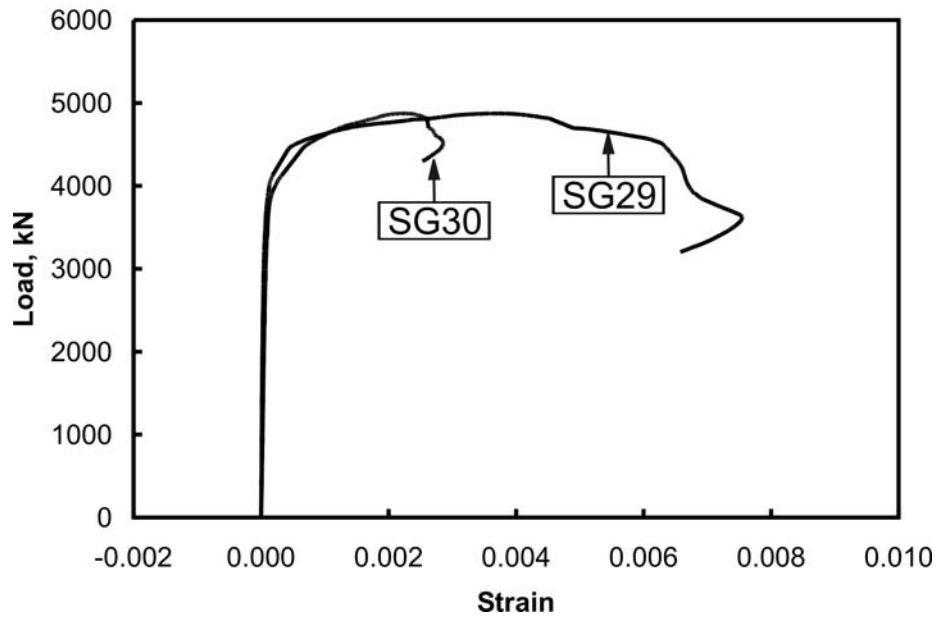
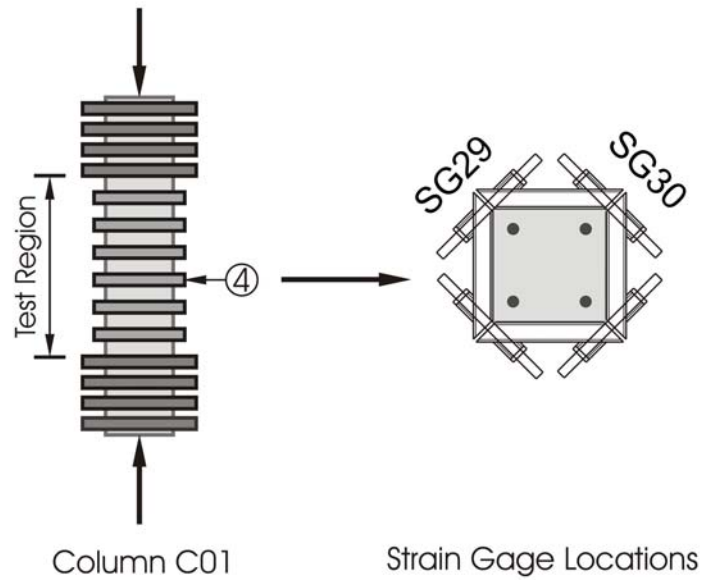


Figure 3-46i: Column load vs. strain of bolts (SG29 and SG30) for column C01

All dimensions are in millimeters

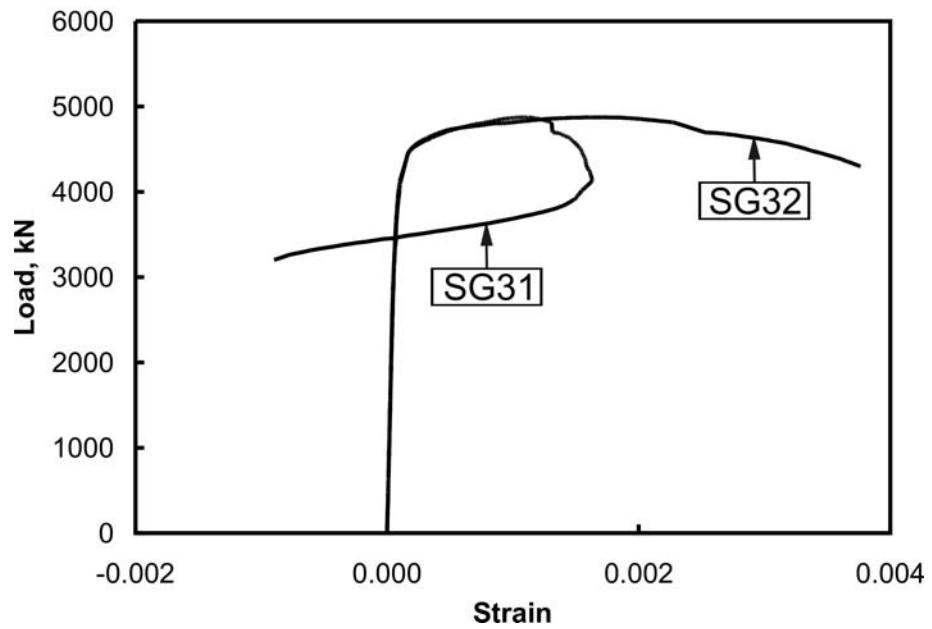
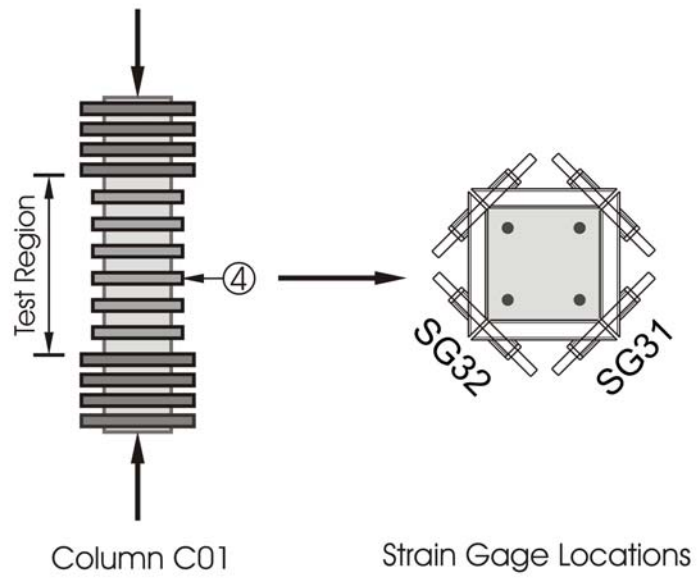


Figure 3-46j: Column load vs. strain of bolts (SG31 and SG32) for column C01

All dimensions are in millimeters

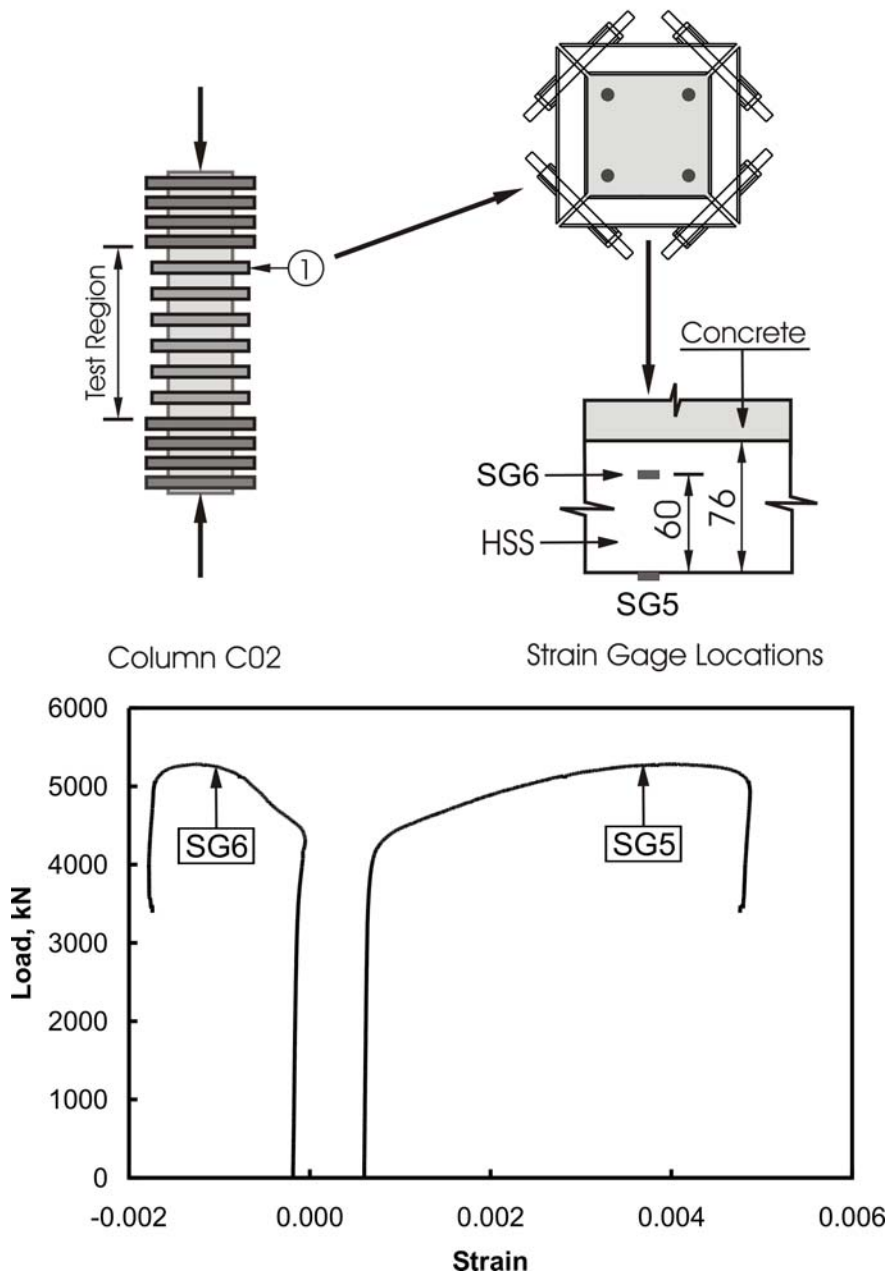


Figure 3-47a: Column load vs. strain of collar (SG5 and SG6) for column C02

All dimensions are in millimeters

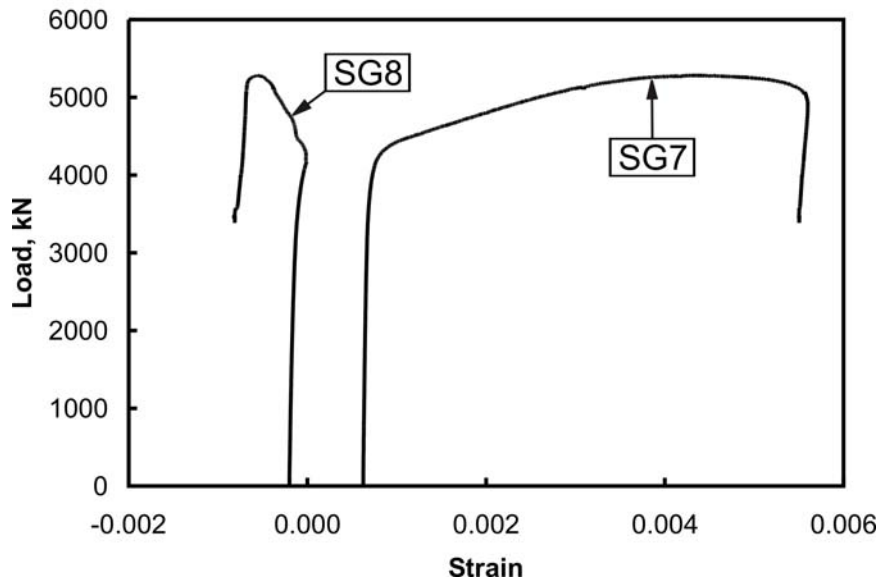
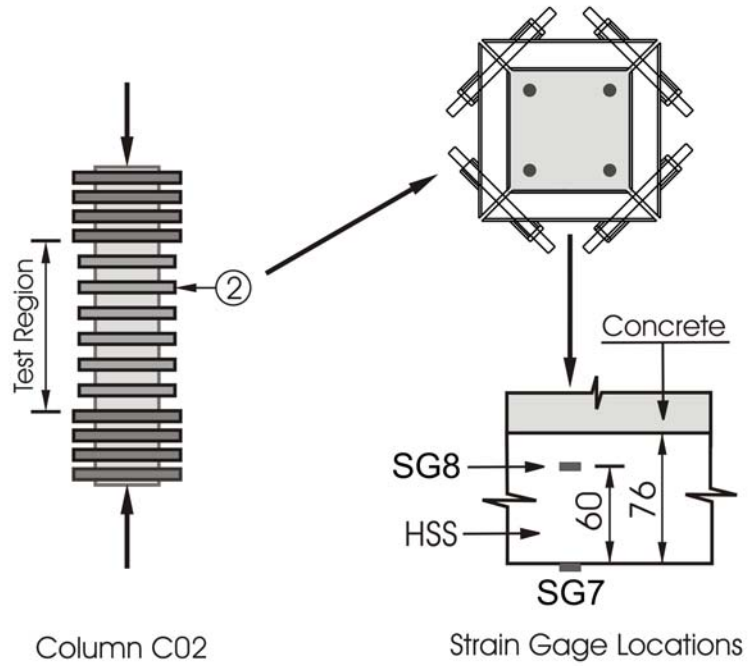


Figure 3-47b: Column load vs. strain of collar (SG7 and SG8) for column C02

All dimensions are in millimeters

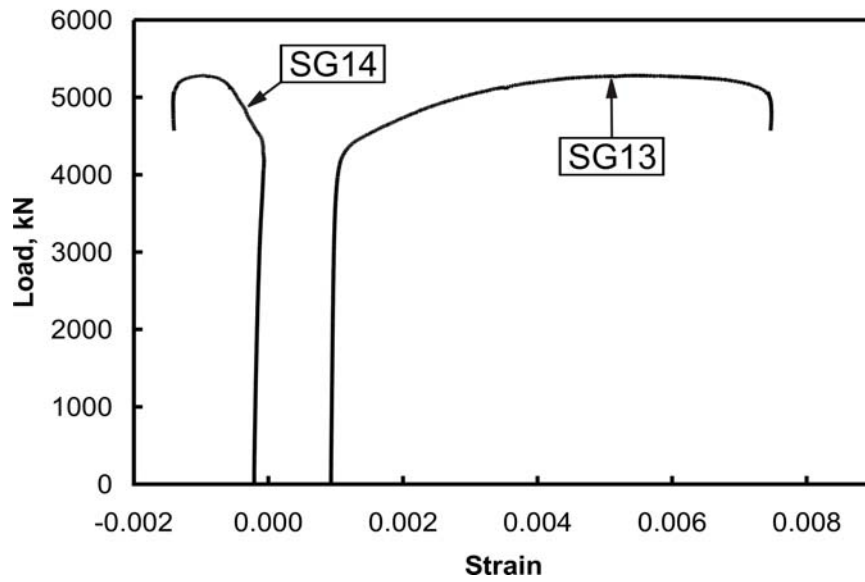
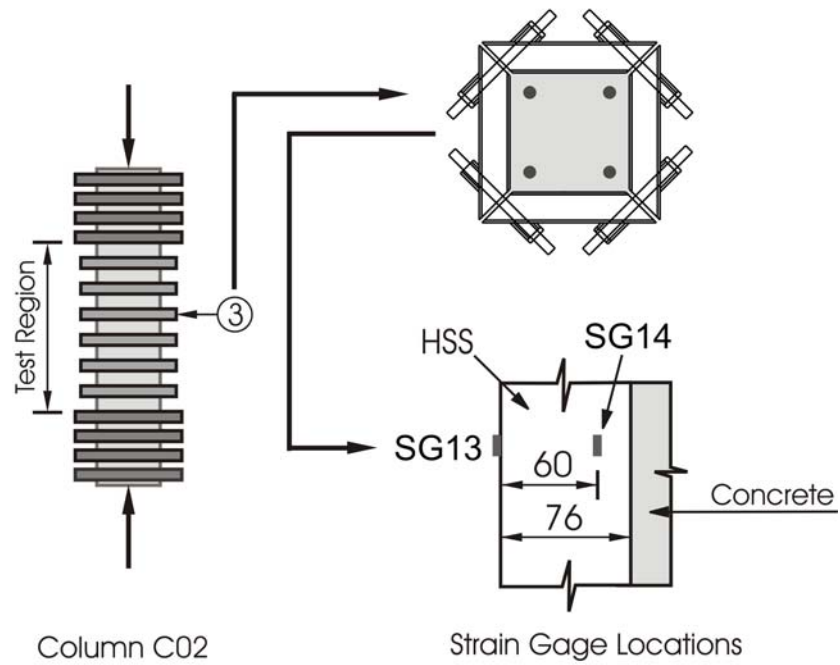


Figure 3-47c: Column load vs. strain of collar (SG13 and SG14) for column C02

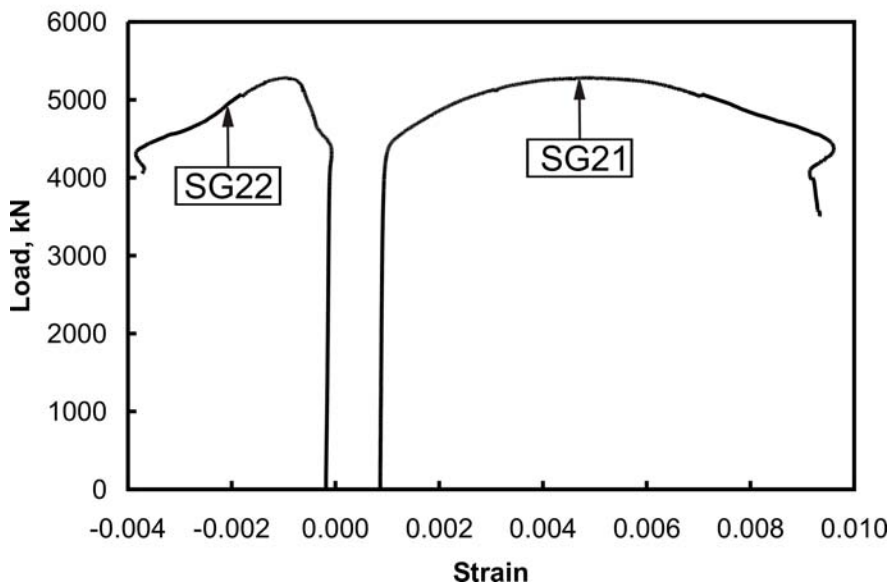
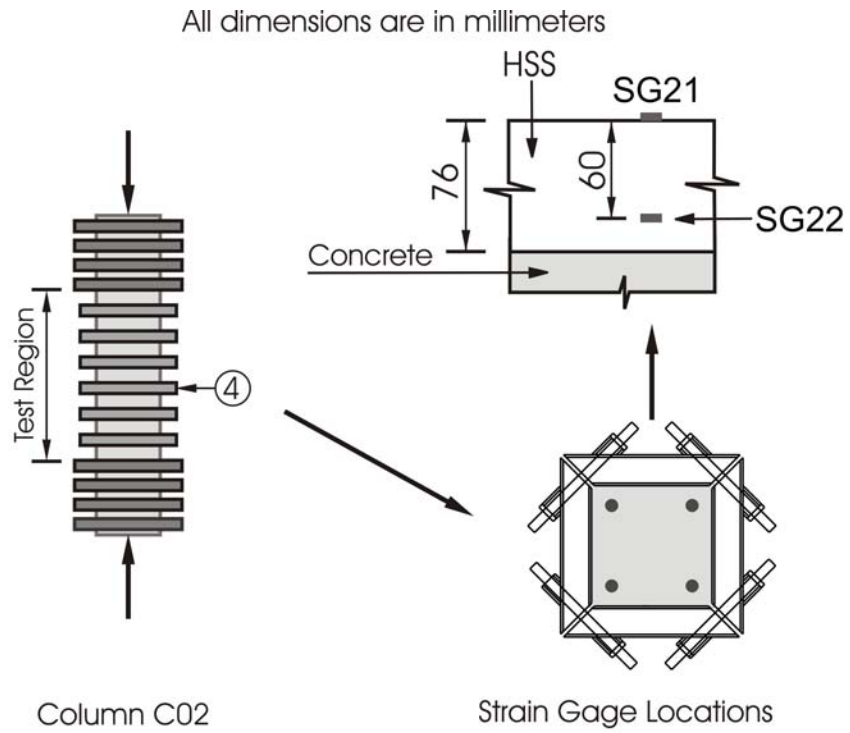


Figure 3-47d: Column load vs. strain of collar (SG21 and SG22) for column C02

All dimensions are in millimeters

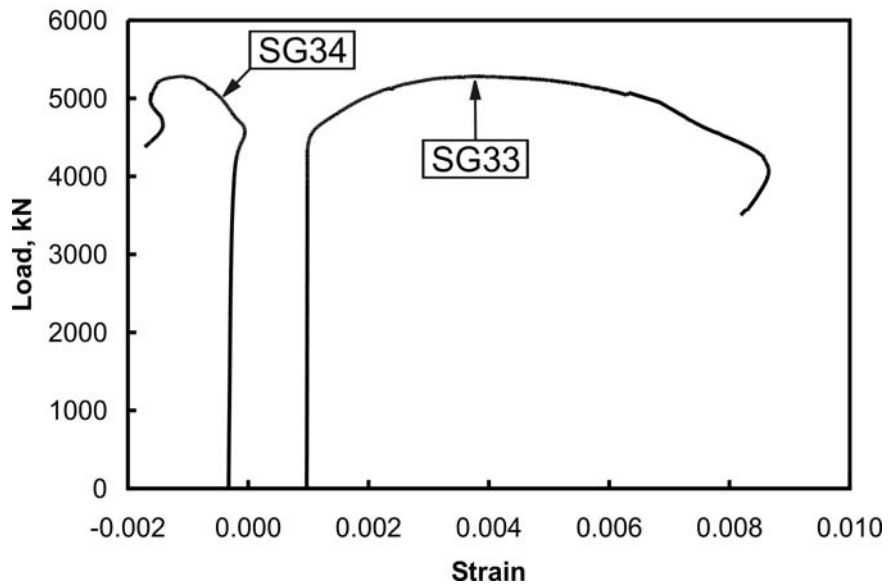
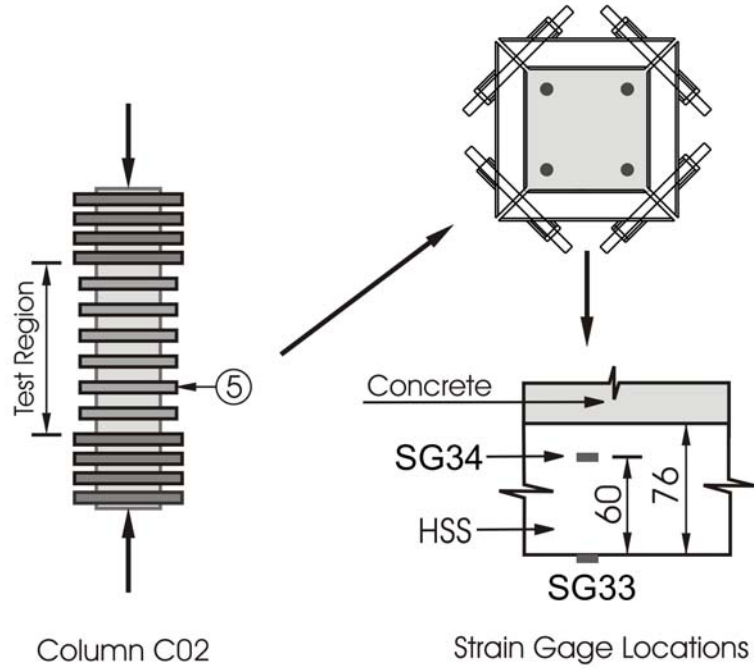


Figure 3-47e: Column load vs. strain of collar (SG33 and SG34) for column C02

All dimensions are in millimeters

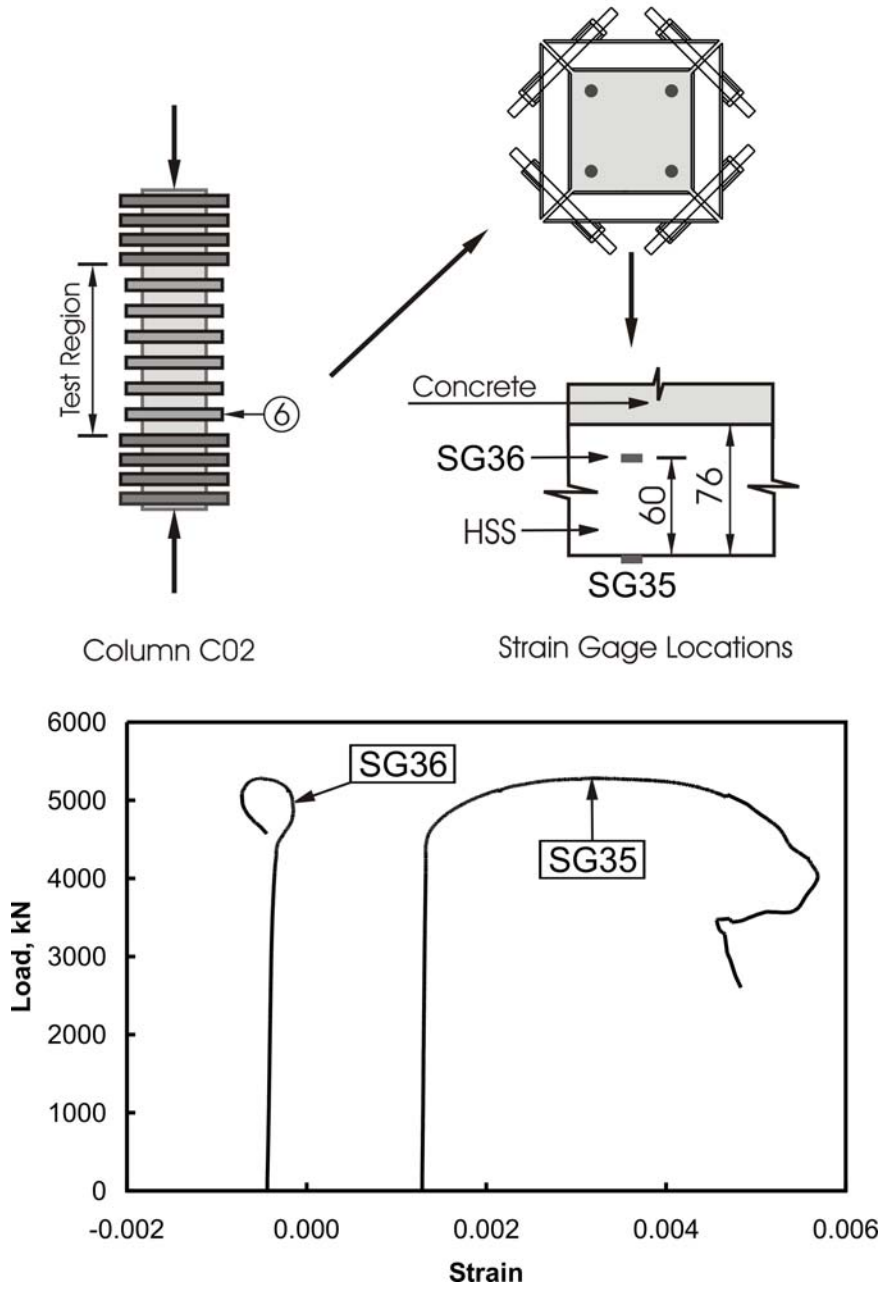


Figure 3-47f: Column load vs. strain of collar (SG35 and SG36) for column C02

All dimensions are in millimeters

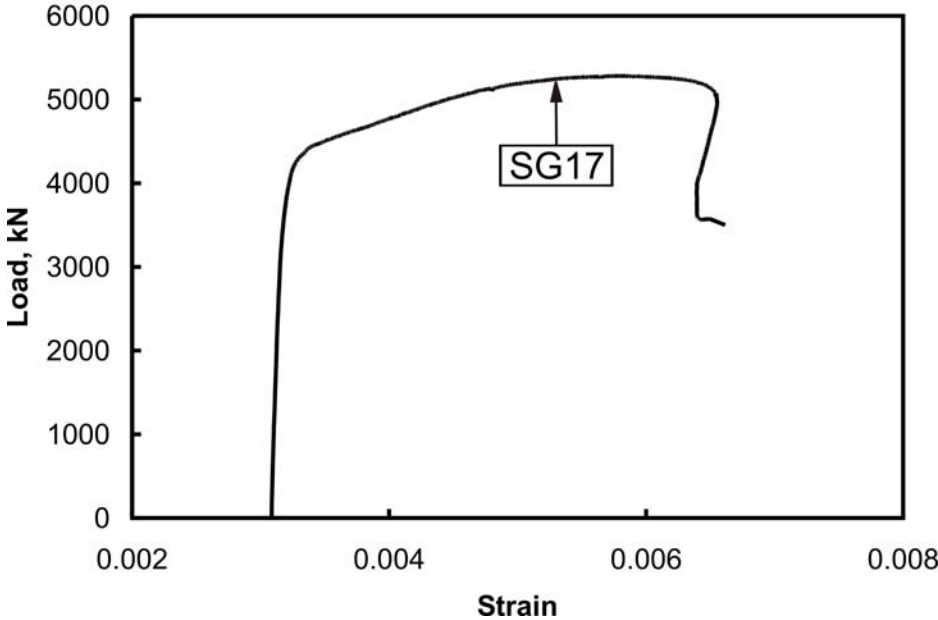
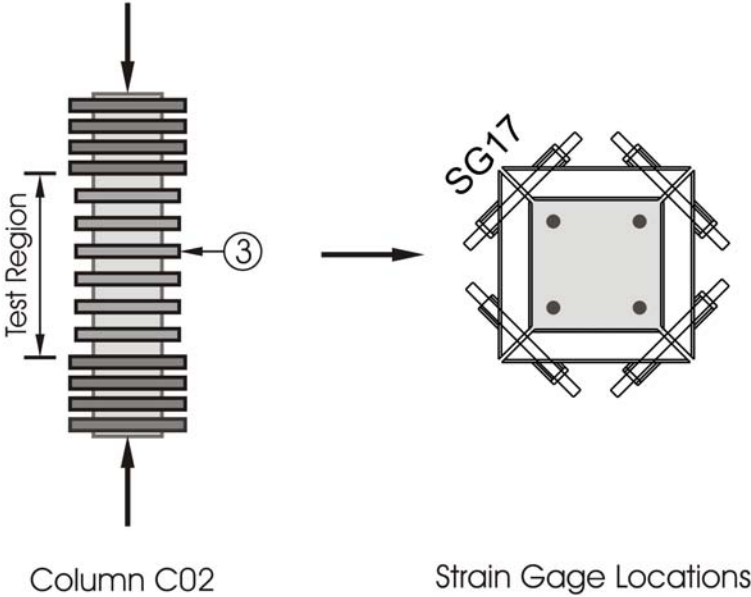


Figure 3-47g: Column load vs. strain of bolt (SG17) for column C02

All dimensions are in millimeters

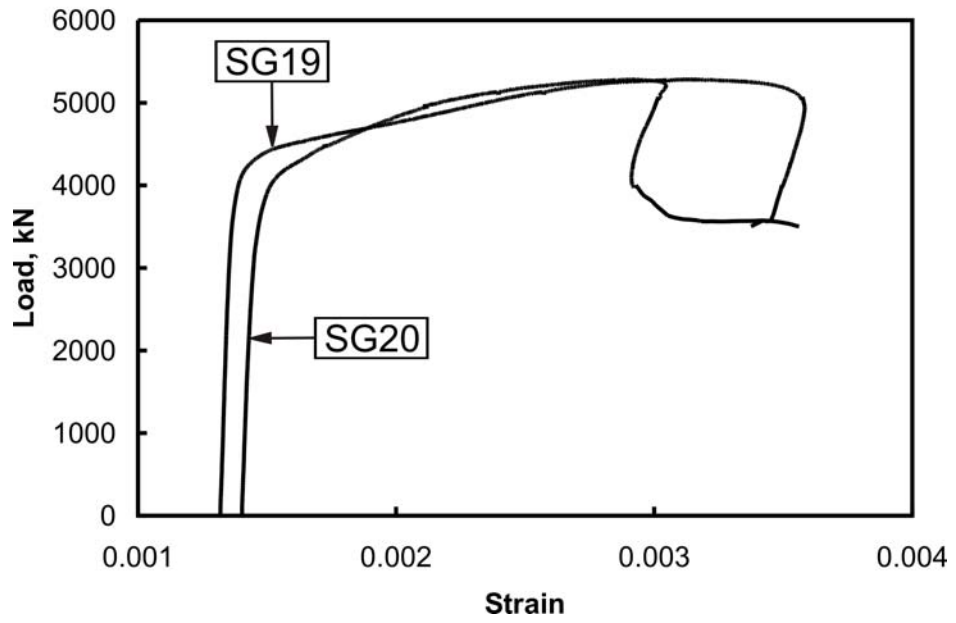
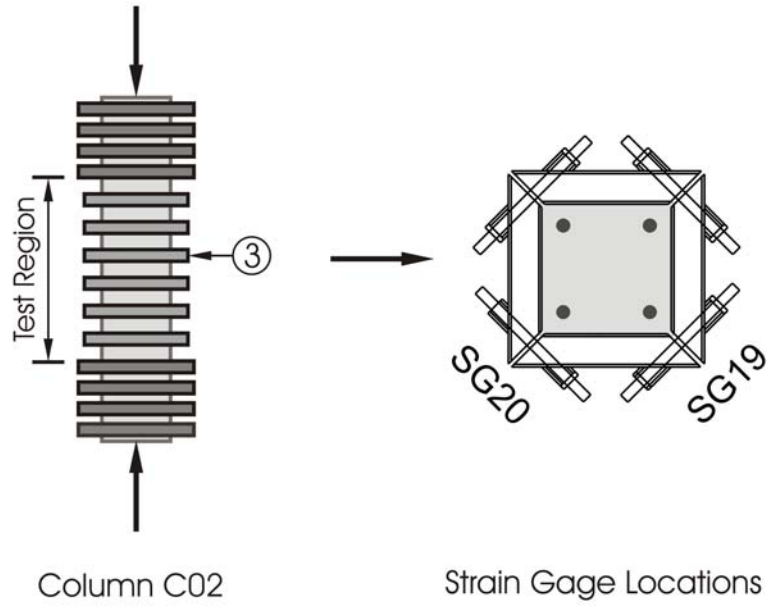


Figure 3-47h: Column load vs. strain of bolts (SG19 and SG20) for column C02

All dimensions are in millimeters

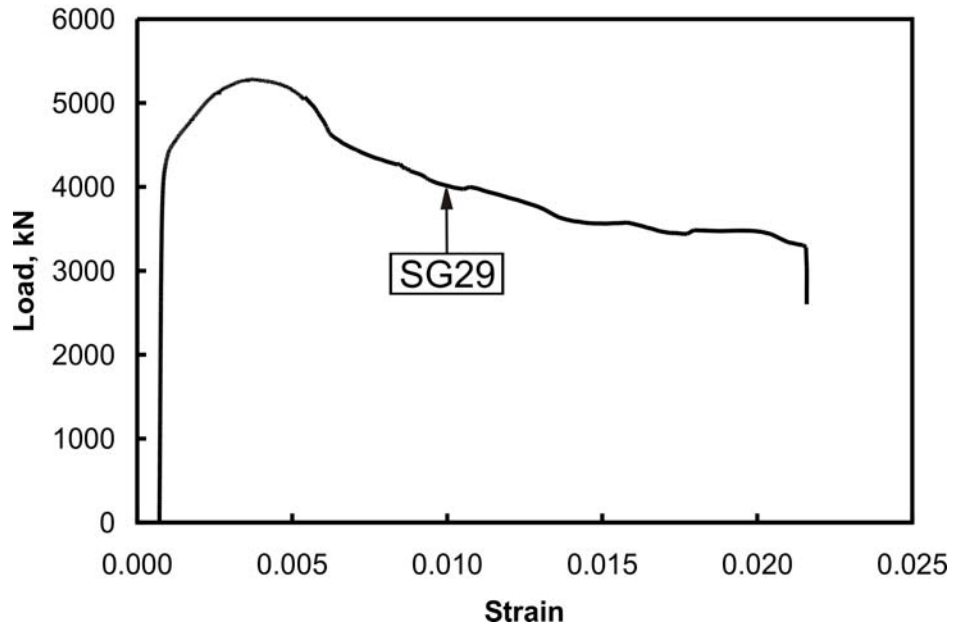
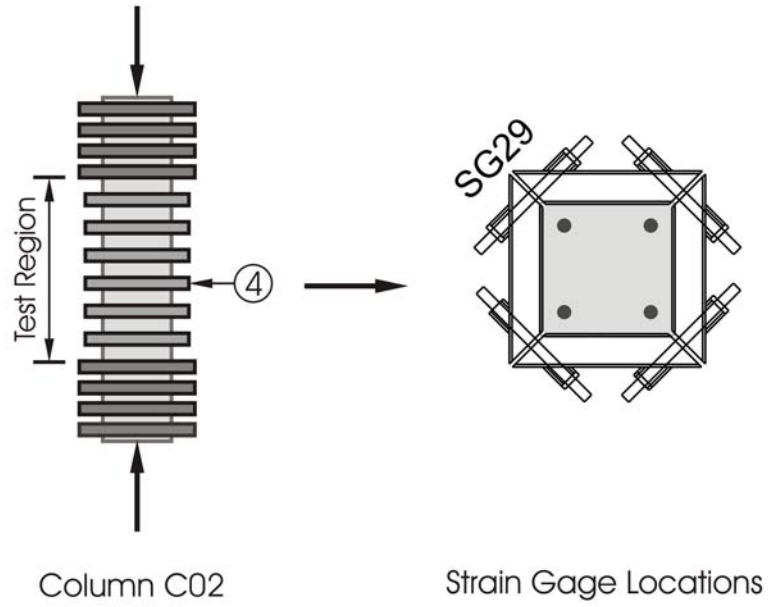


Figure 3-47i: Column load vs. strain of bolts (SG29) for column C02

All dimensions are in millimeters

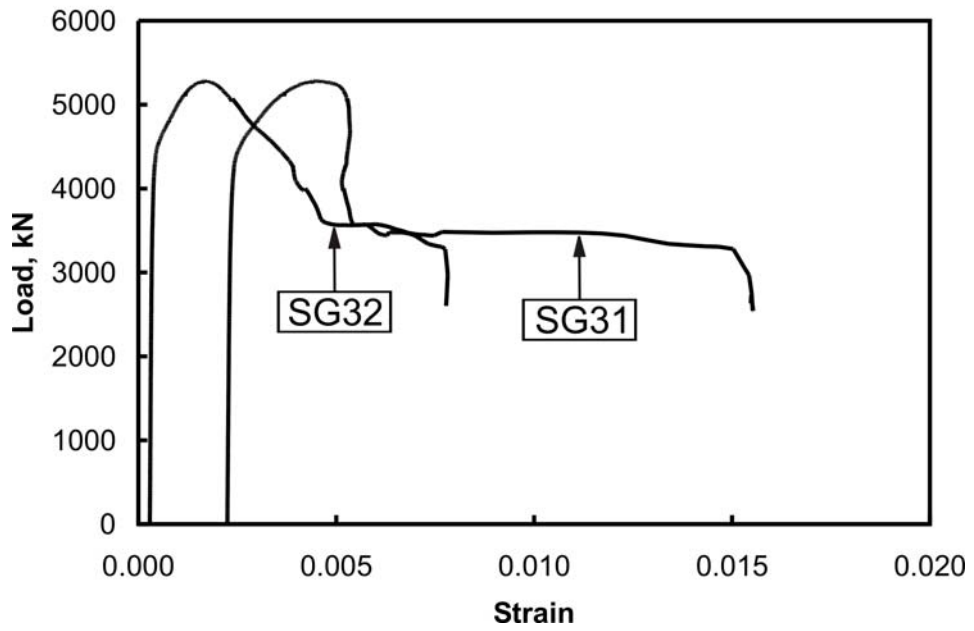
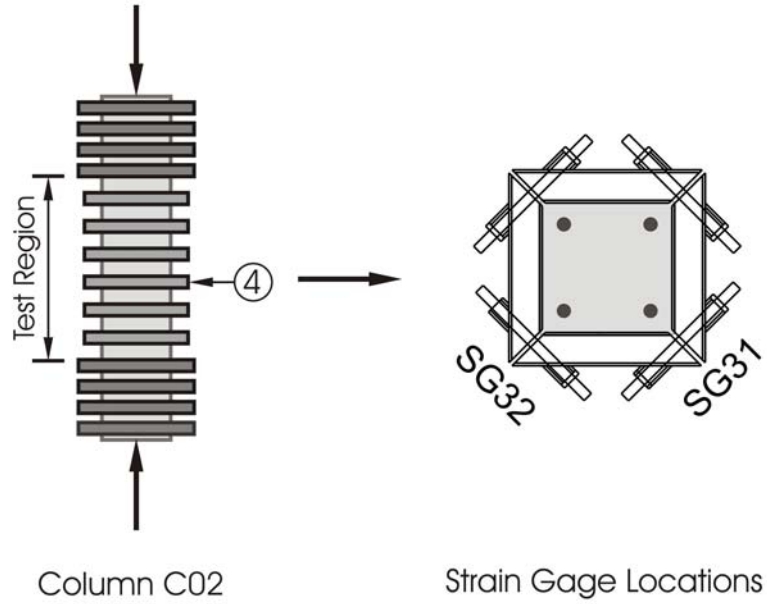


Figure 3-47j: Column load vs. strain of bolts (SG31 and SG32) for column C02

All dimensions are in millimeters

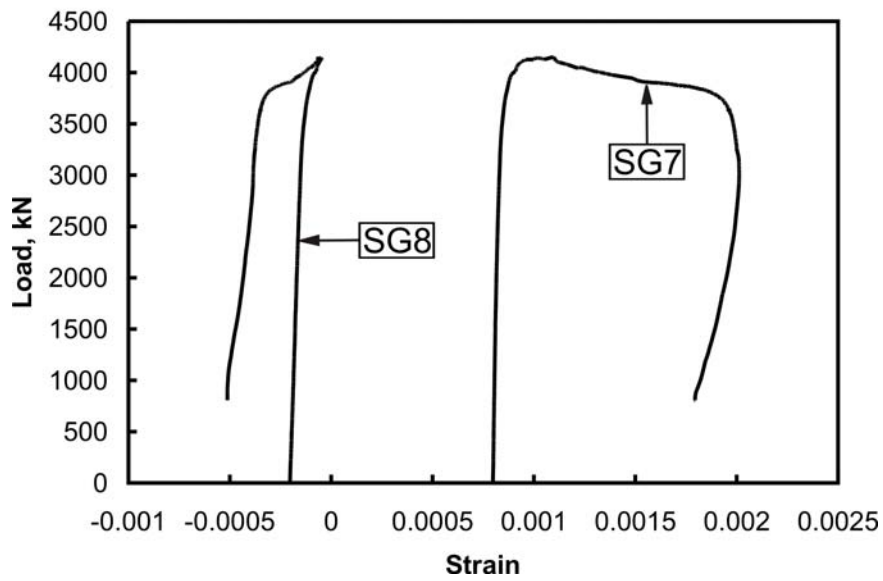
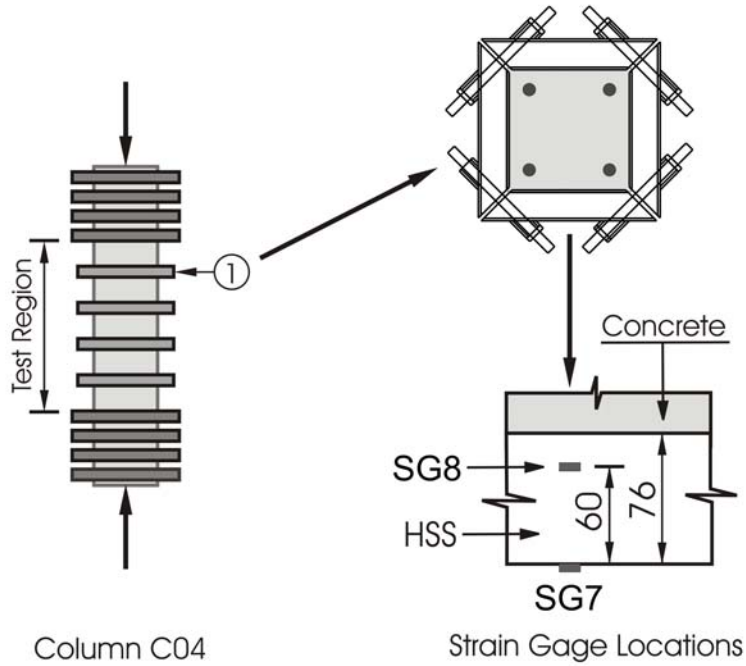


Figure 3-48a: Column load vs. strain of collar (SG7 and SG8) for column C04

All dimensions are in millimeters

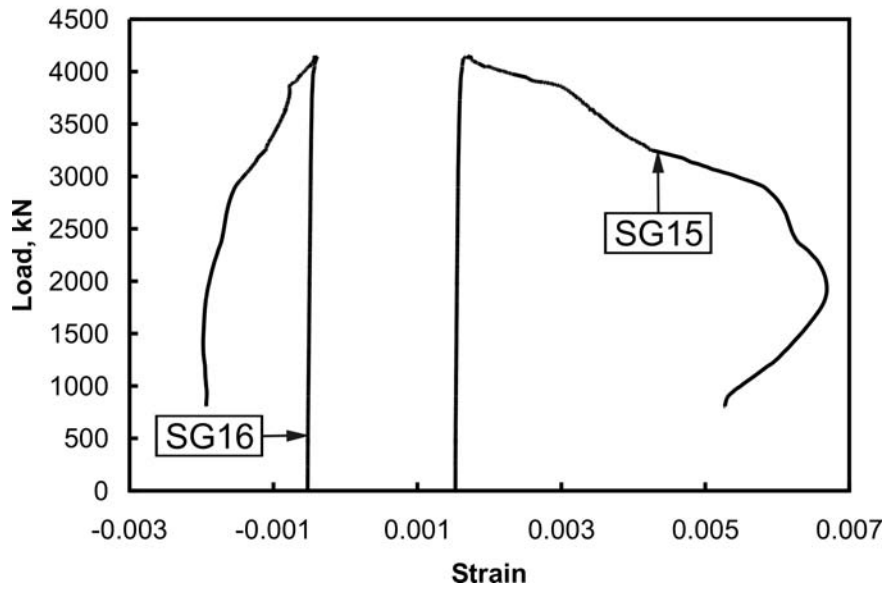
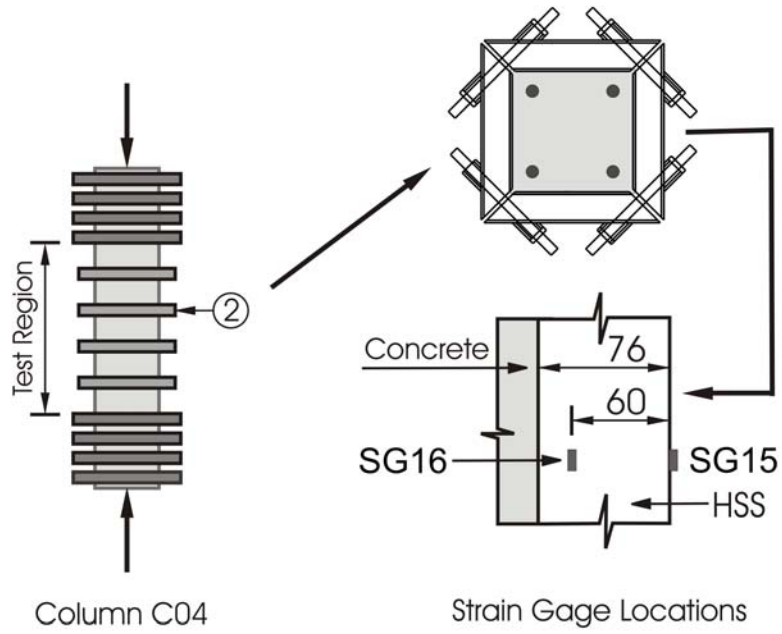


Figure 3-48b: Column load vs. strain of collar (SG15 and SG16) for column C04

All dimensions are in millimeters

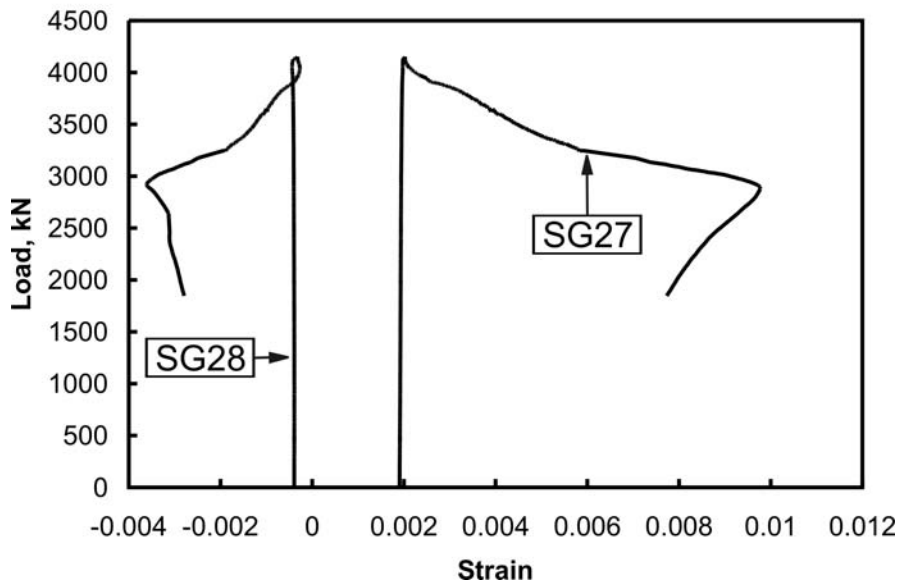
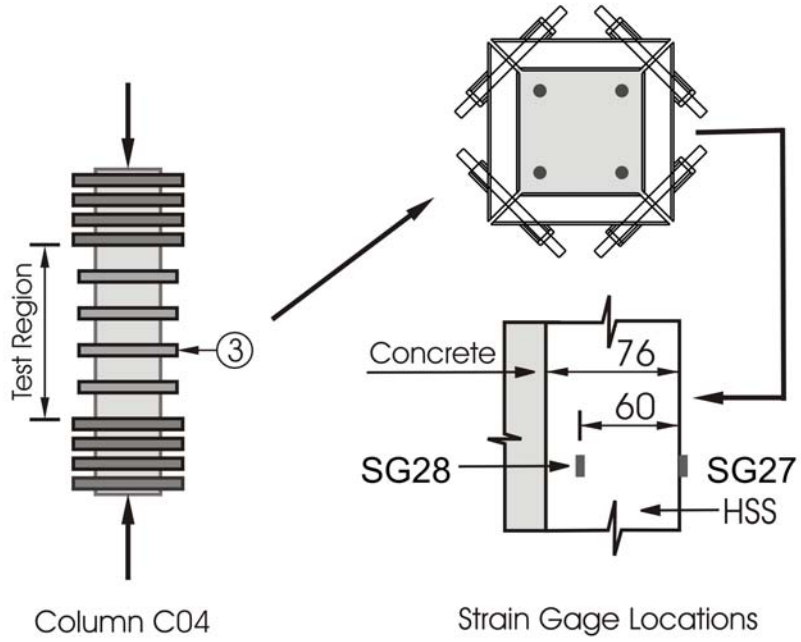


Figure 3-48c: Column load vs. strain of collar (SG27 and SG28) for column C04

All dimensions are in millimeters

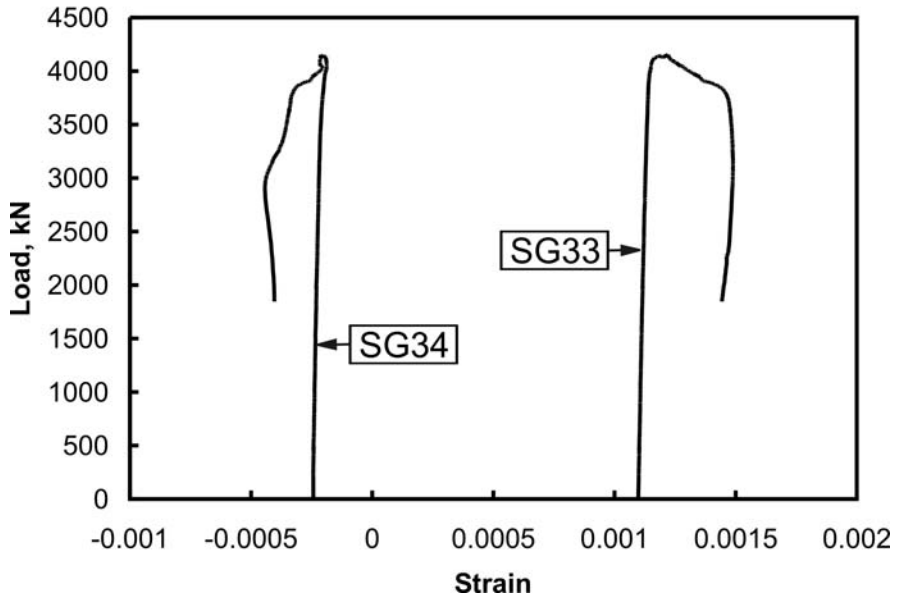
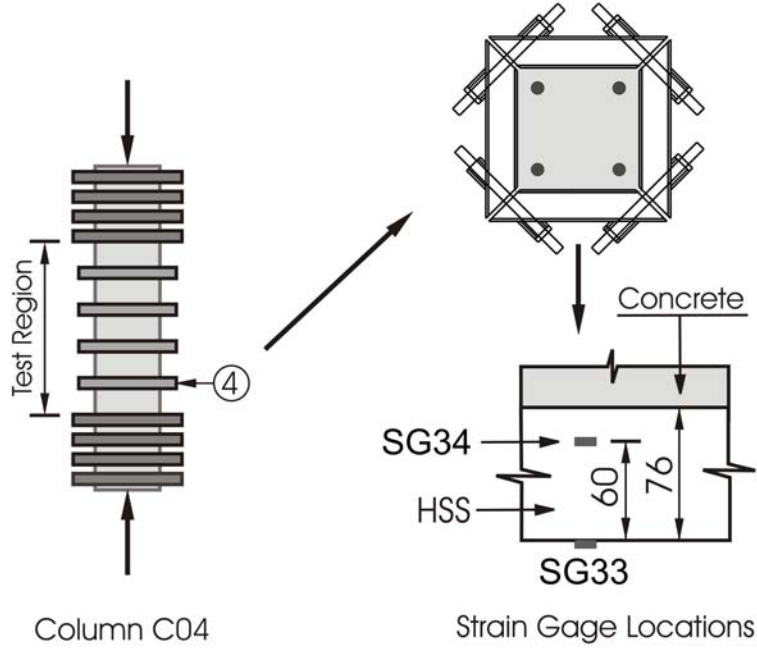


Figure 3-48d: Column load vs. strain of collar (SG33 and SG34) for column C04

All dimensions are in millimeters

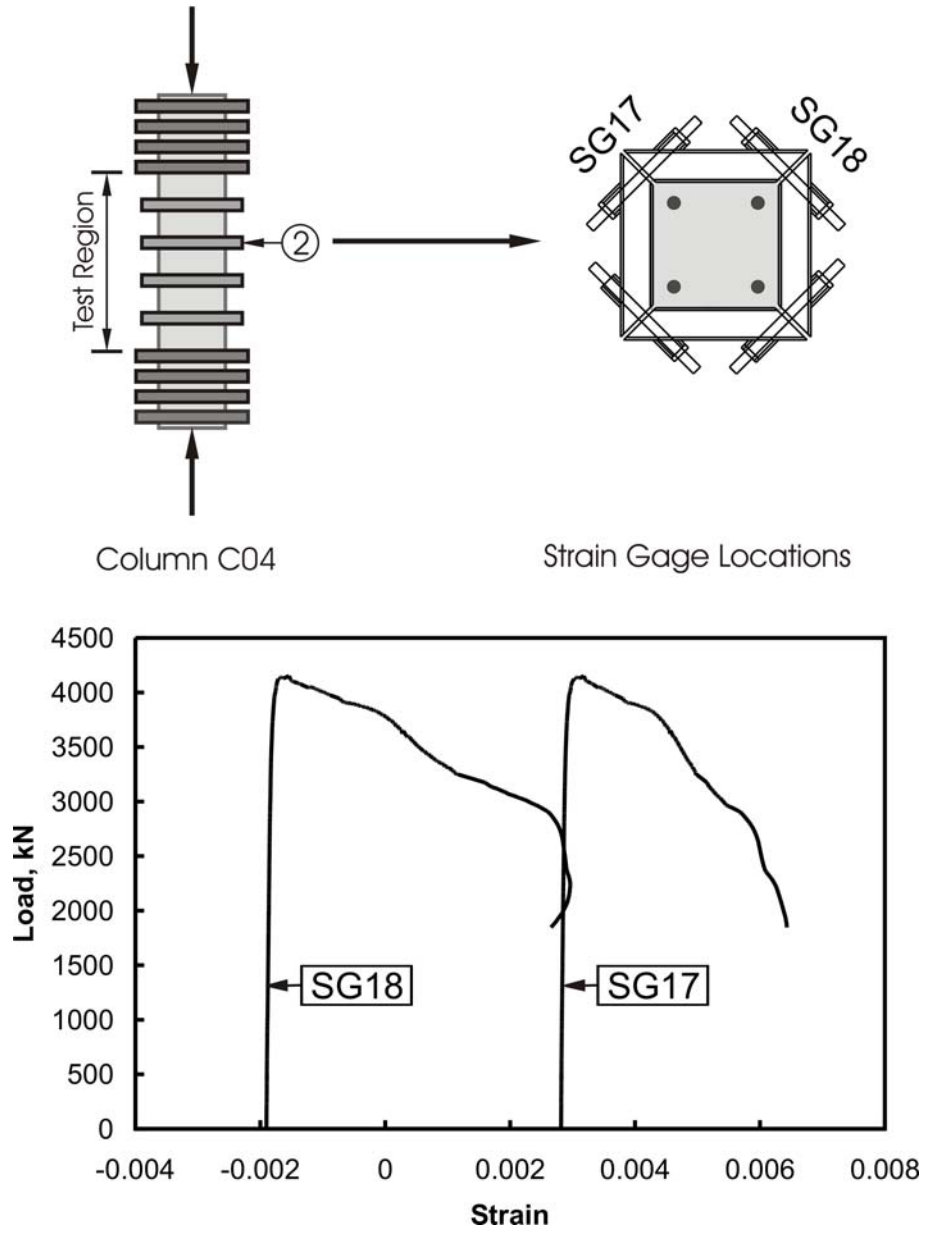


Figure 3-48e: Column load vs. strain of bolts (SG17 and SG18) for column C04

All dimensions are in millimeters

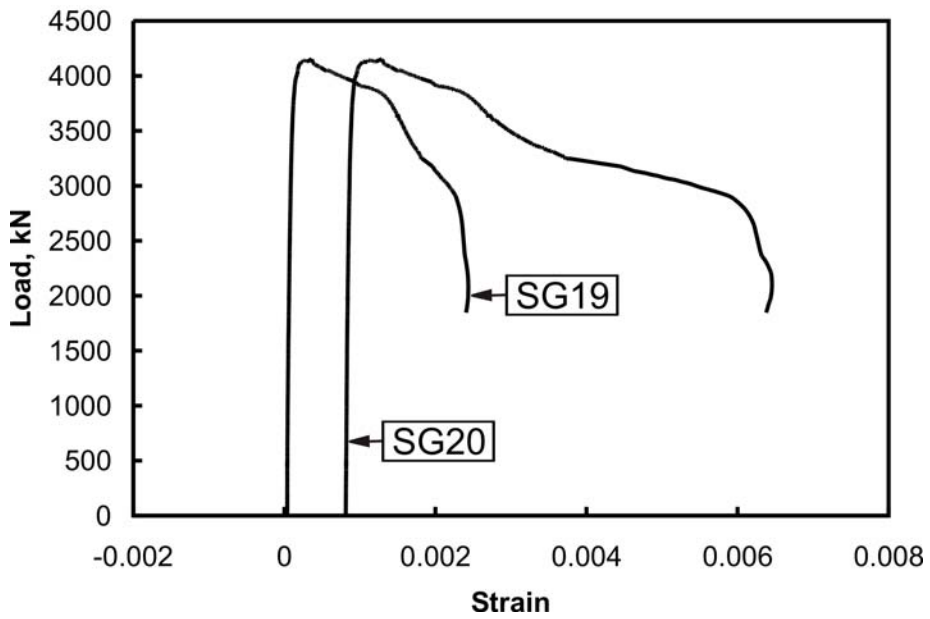
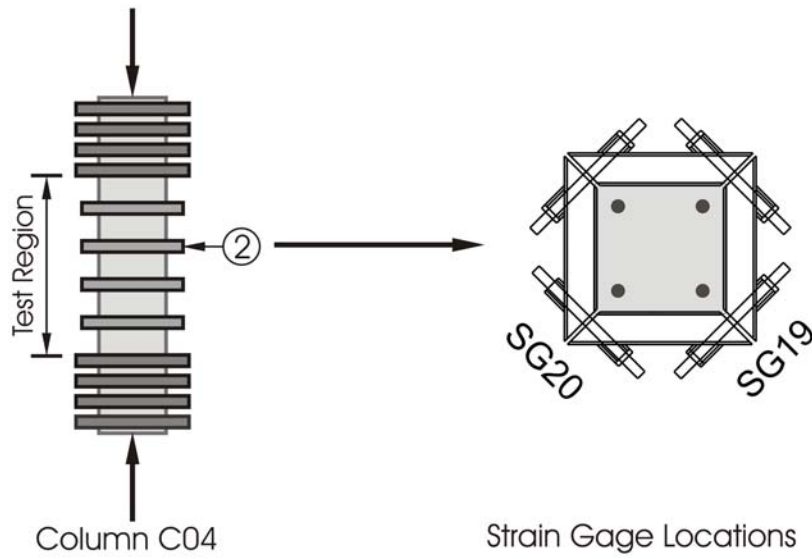


Figure 3-48f: Column load vs. strain of bolts (SG19 and SG20) for column C04

All dimensions are in millimeters

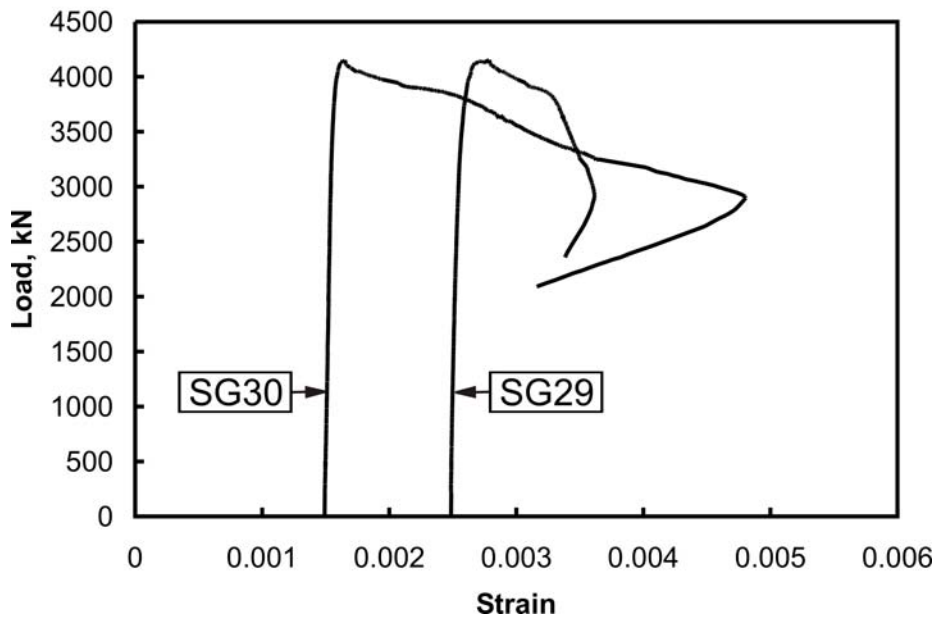
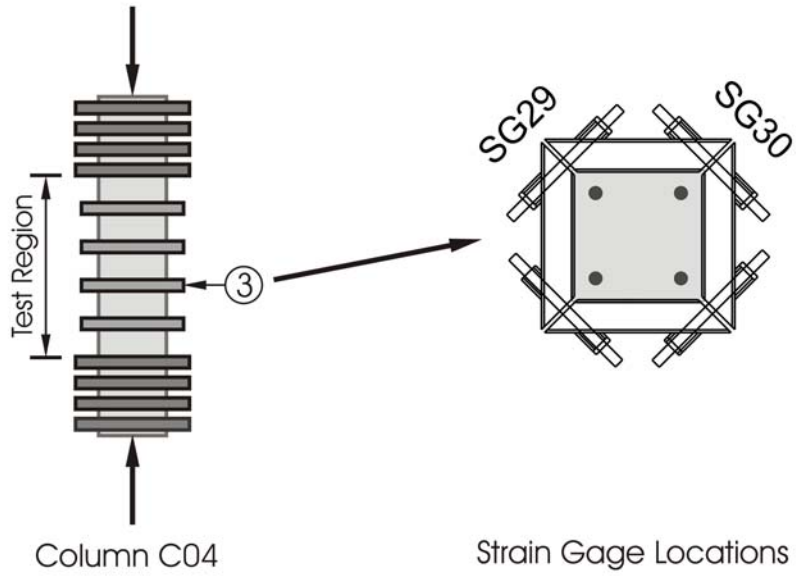


Figure 3-48g: Column load vs. strain of bolts (SG29 and SG30) for column C04

All dimensions are in millimeters

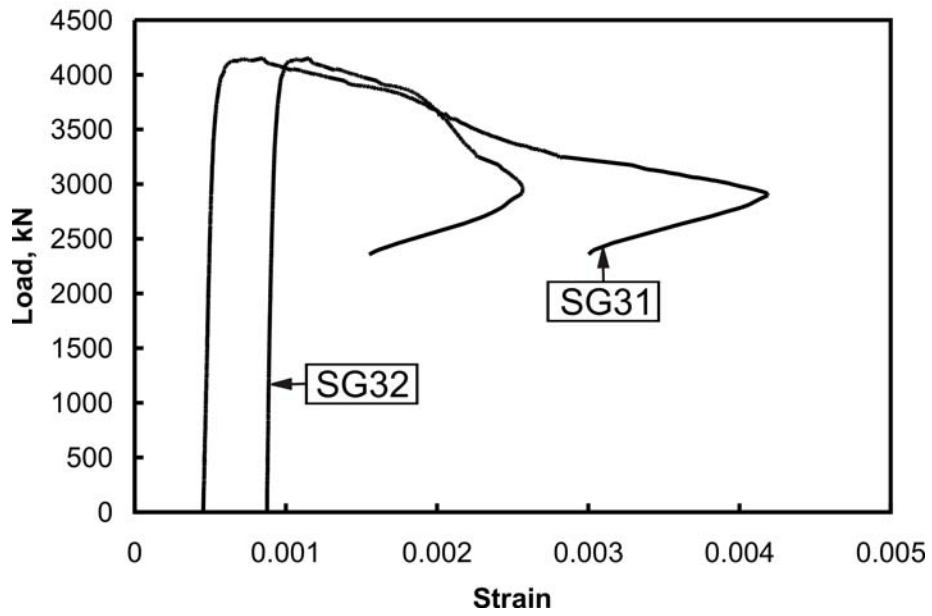
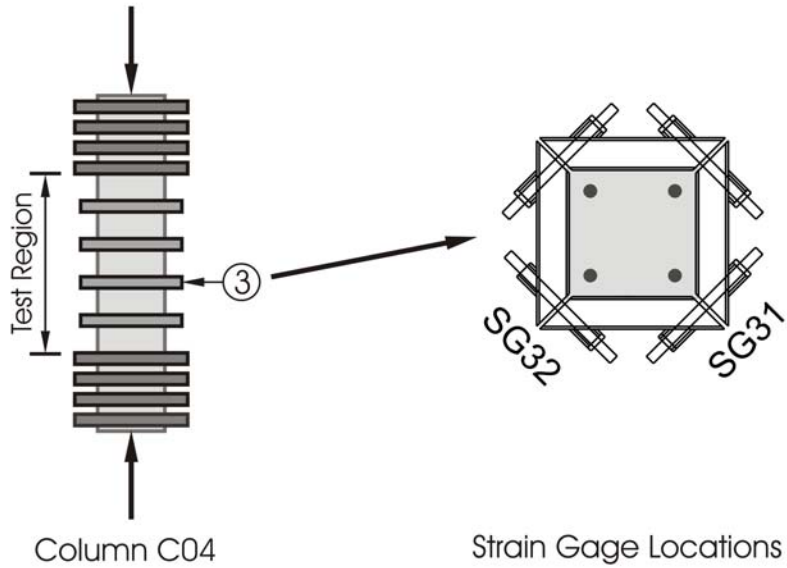


Figure 3-48h: Column load vs. strain of bolts (SG31 and SG32) for column C04

All dimensions are in millimeters

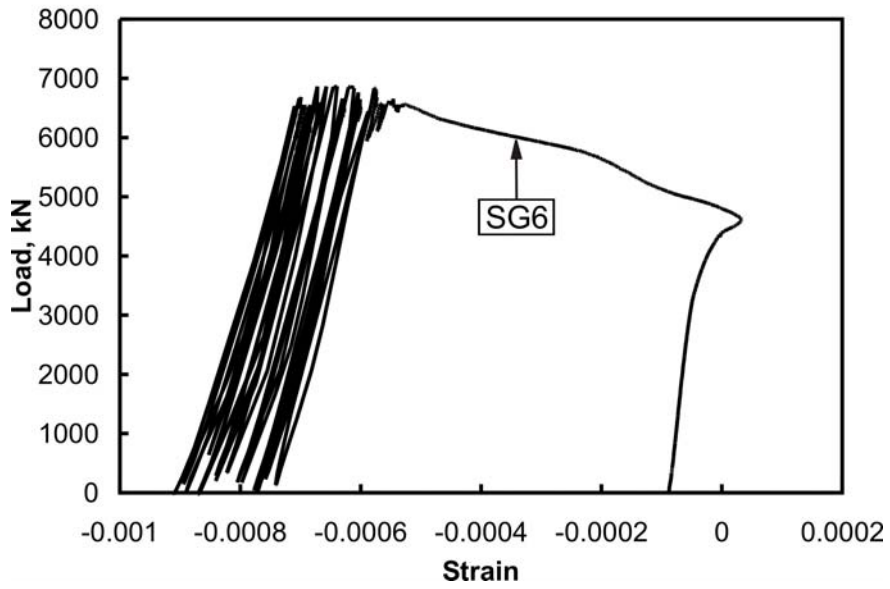
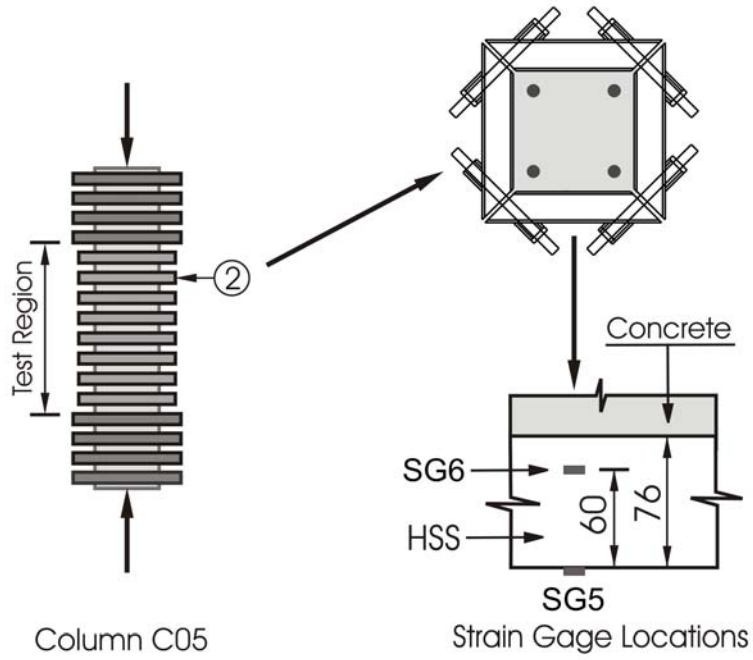


Figure 3-49a: Column load vs. strain of collar (SG6) for column C05

All dimensions are in millimeters

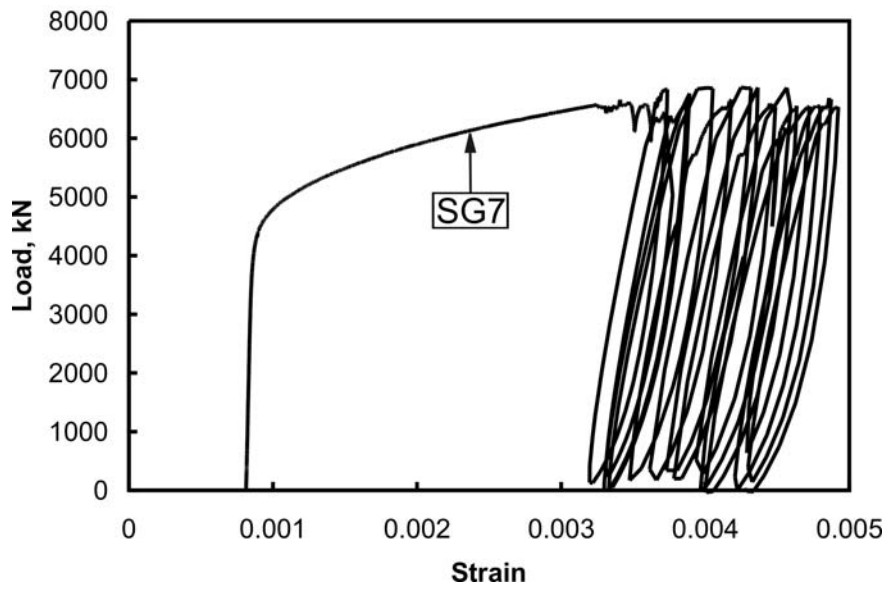
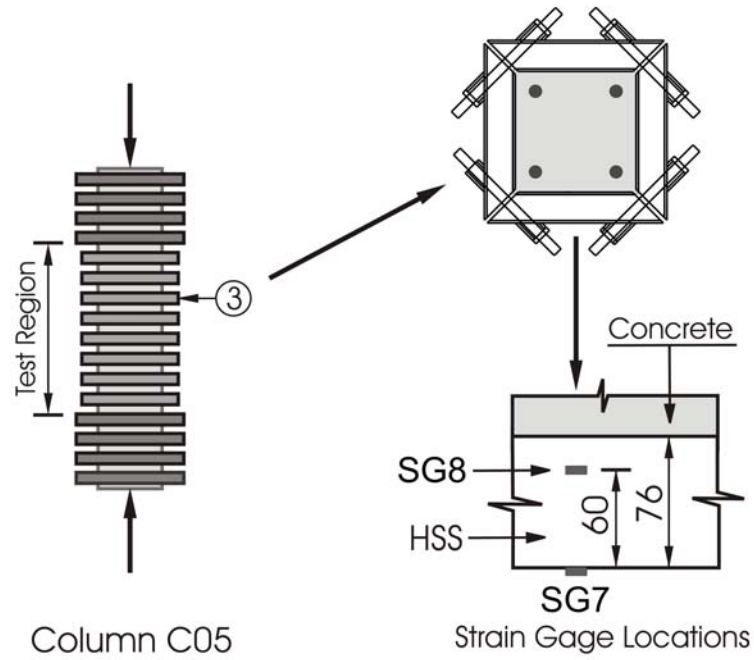


Figure 3-49b: Column load vs. strain of collar (SG7) for column C05

All dimensions are in millimeters

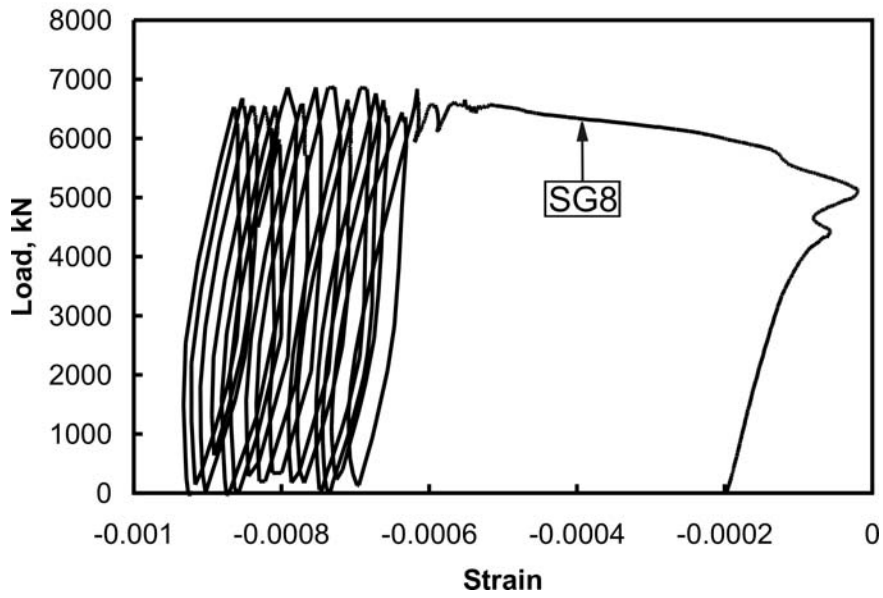
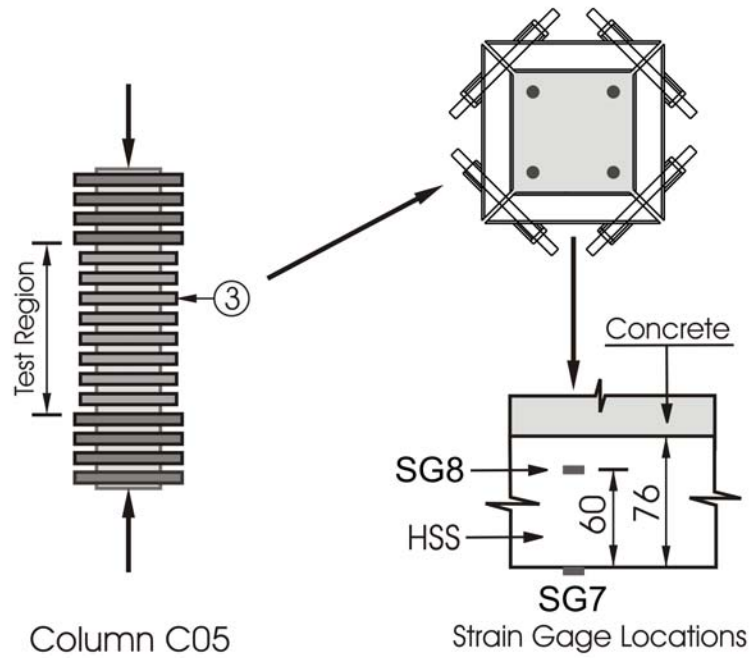


Figure 3-49c: Column load vs. strain of collar (SG8) for column C05

All dimensions are in millimeters

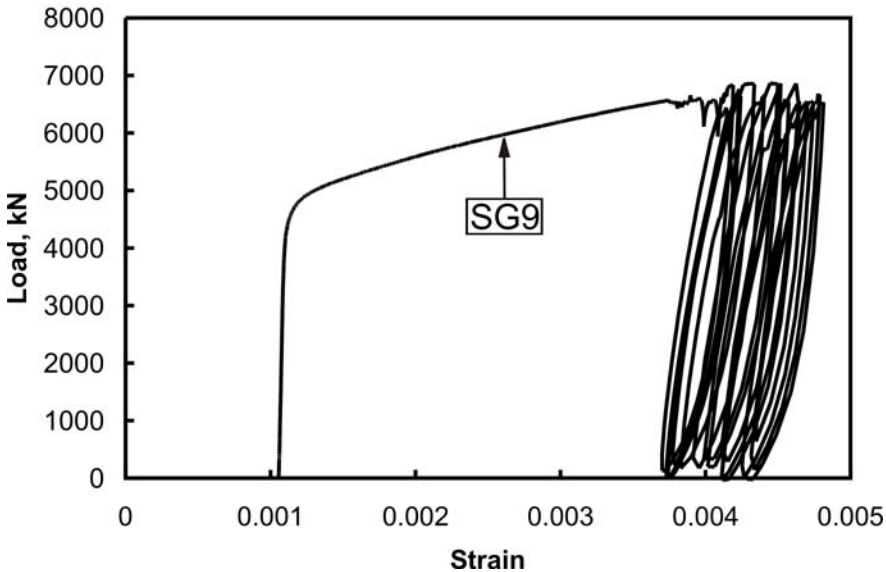
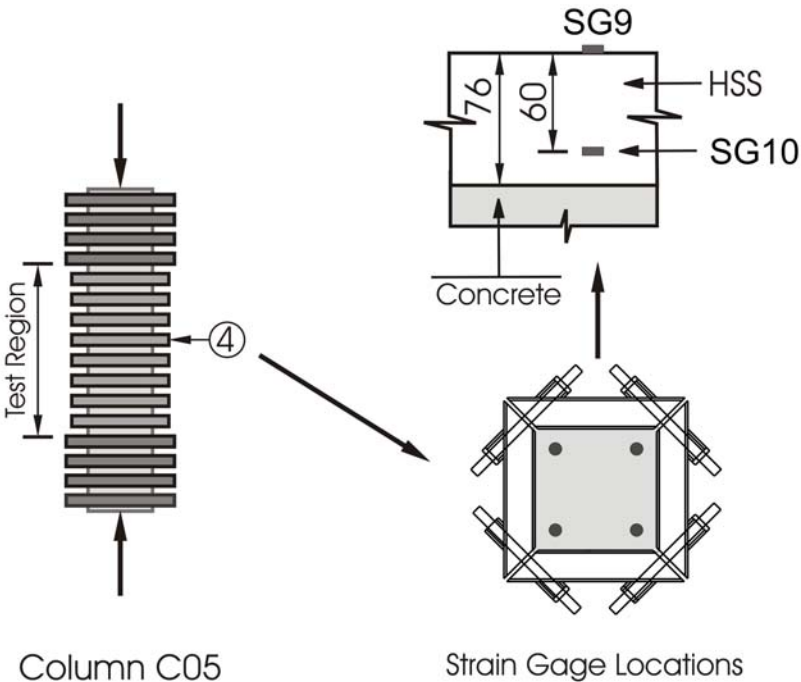


Figure 3-49d: Column load vs. strain of collar (SG9) for column C05

All dimensions are in millimeters

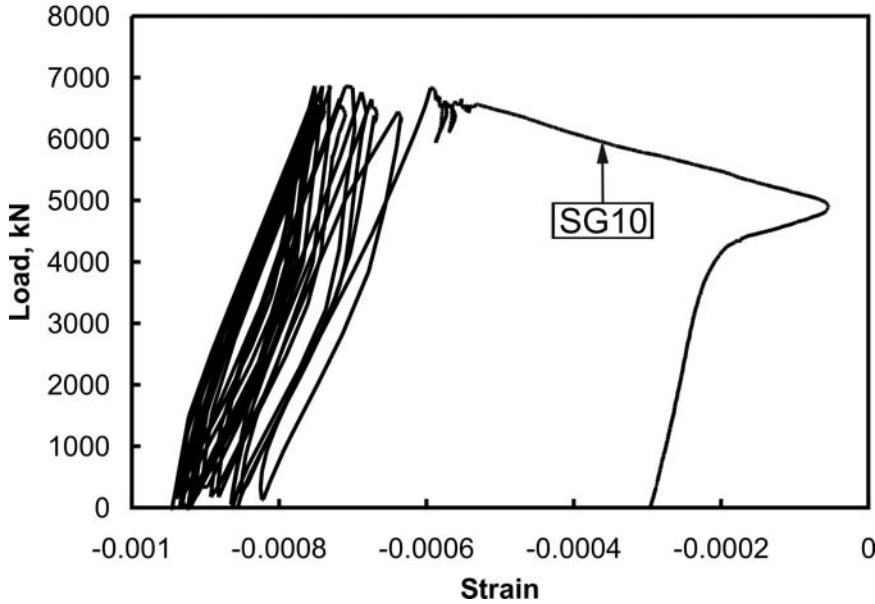
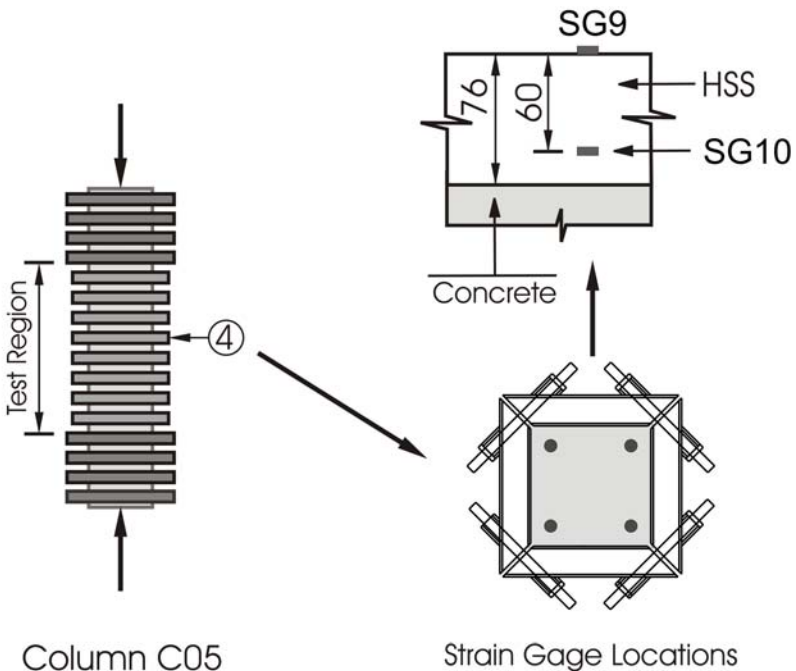


Figure 3-49e: Column load vs. strain of collar (SG10) for column C05

All dimensions are in millimeters

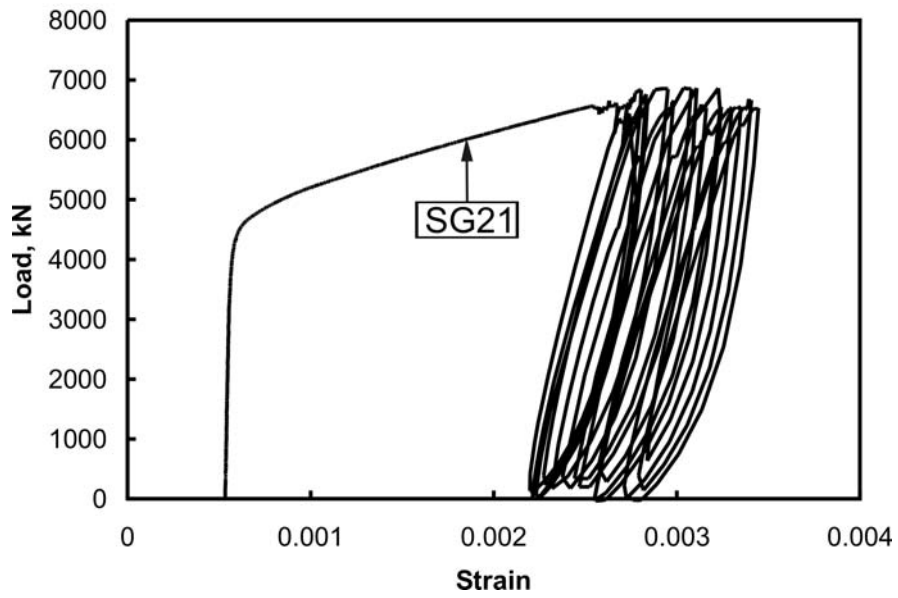
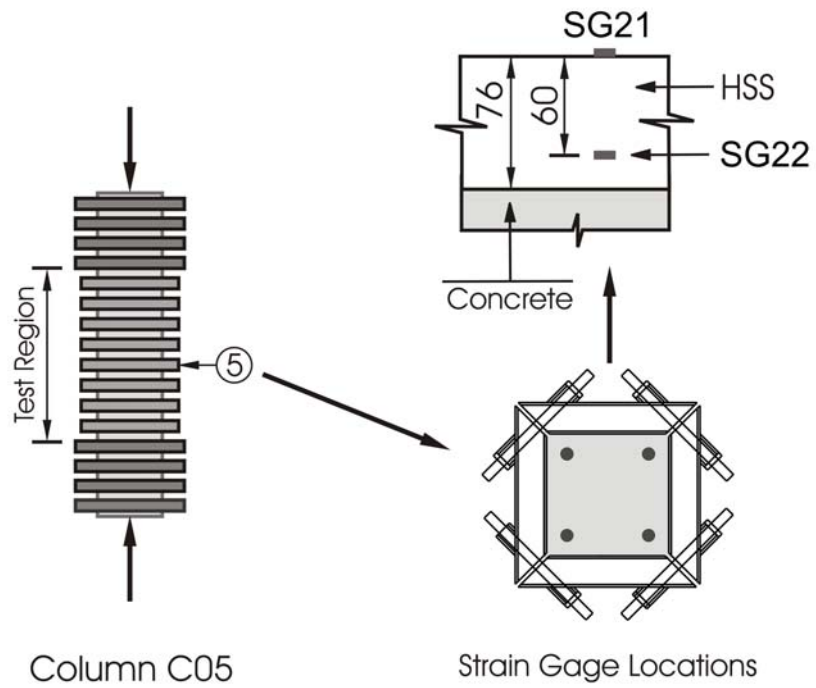


Figure 3-49f: Column load vs. strain of collar (SG21) for column C05

All dimensions are in millimeters

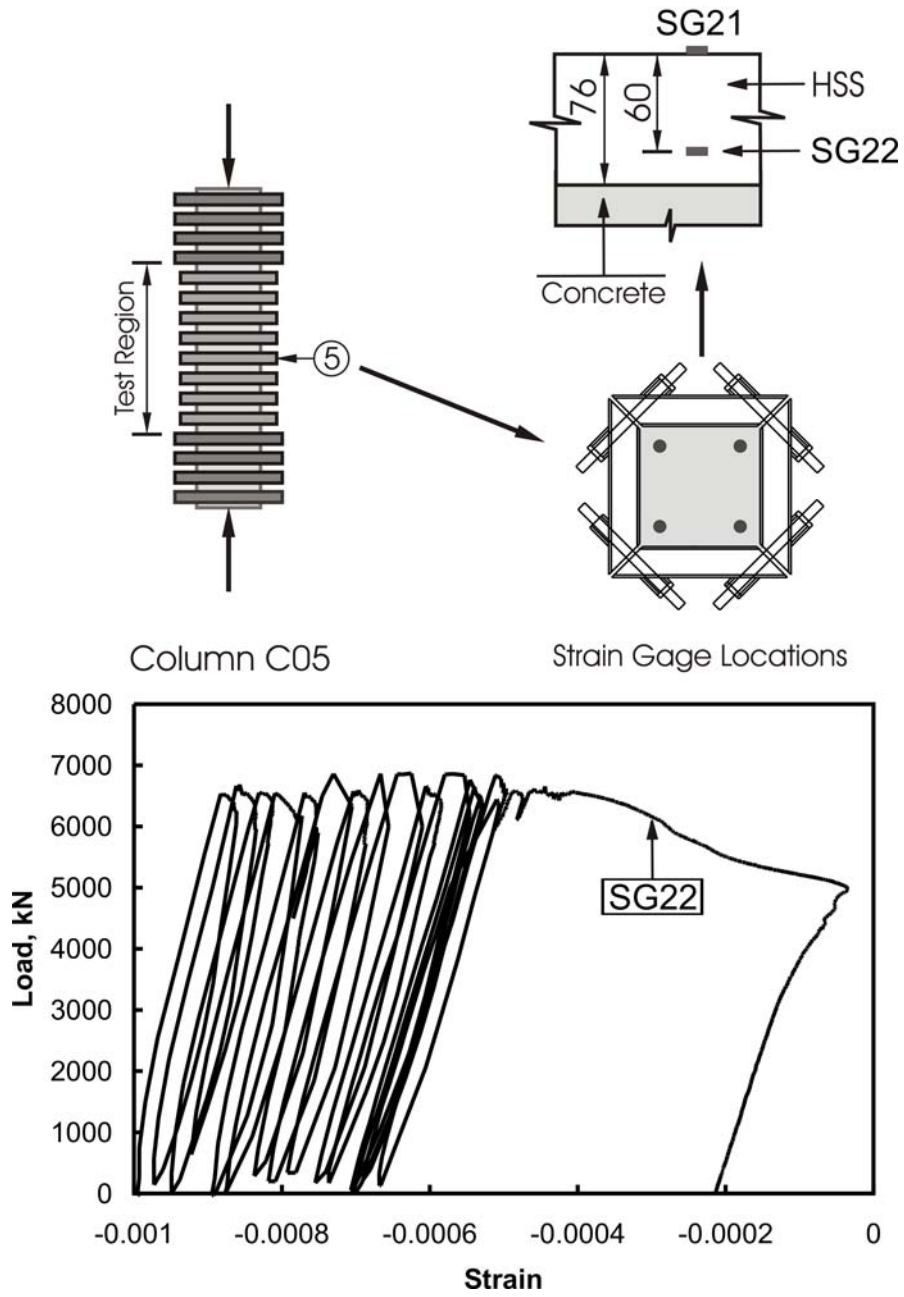


Figure 3-49g: Column load vs. strain of collar (SG22) for column C05

All dimensions are in millimeters

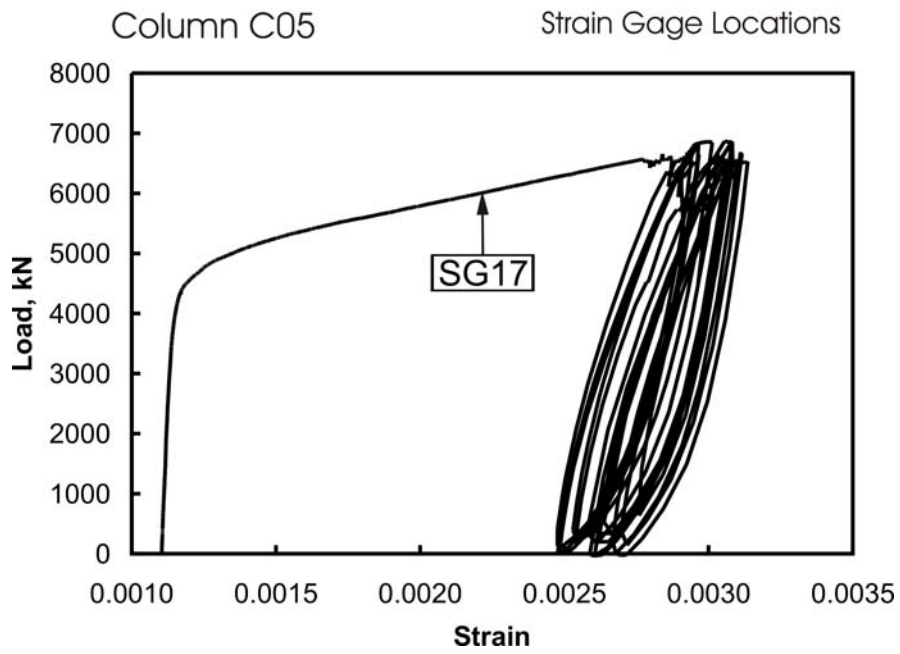
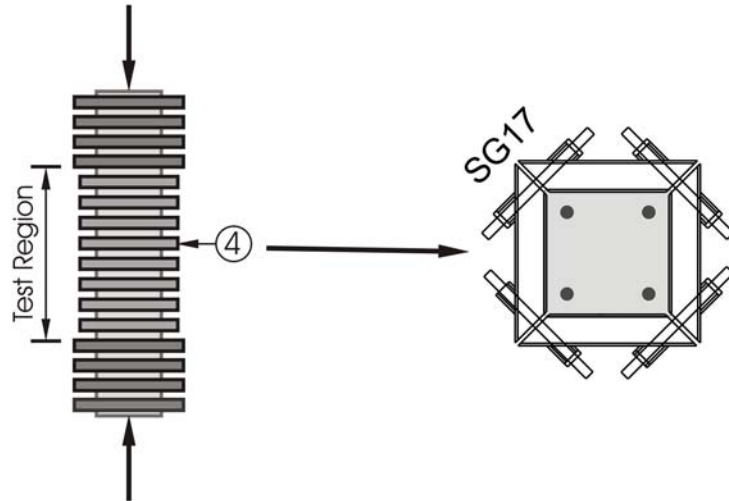


Figure 3-49h: Column load vs. strain of bolt (SG17) for column C05

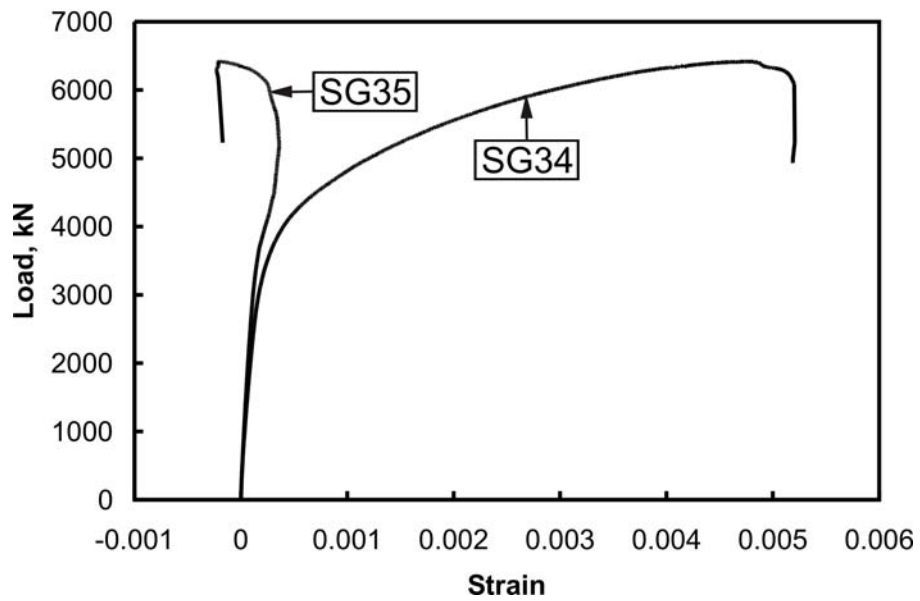
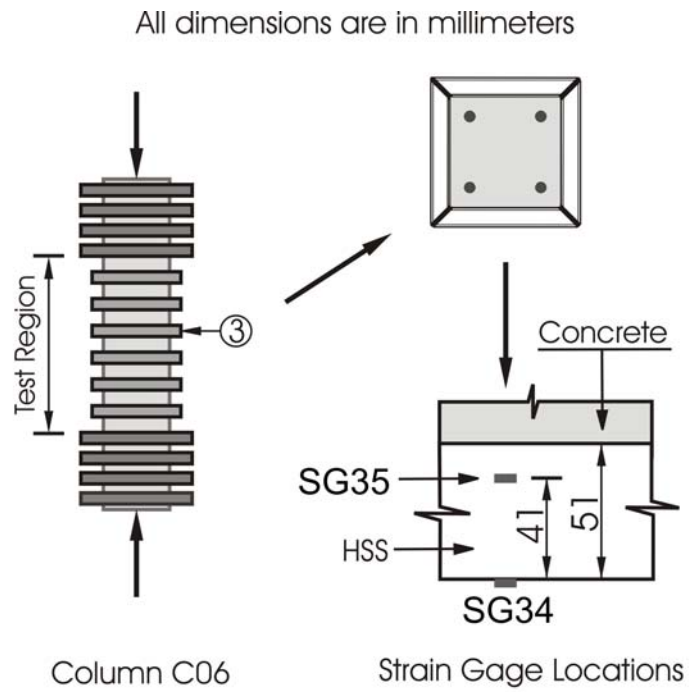


Figure 3-50a: Column load vs. strain of collar (SG34 and SG35) for column C06

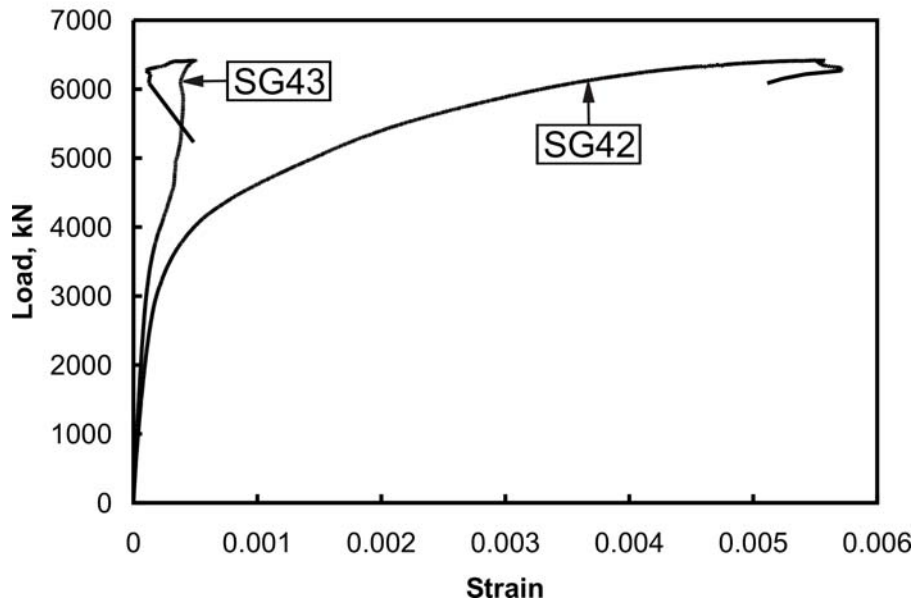
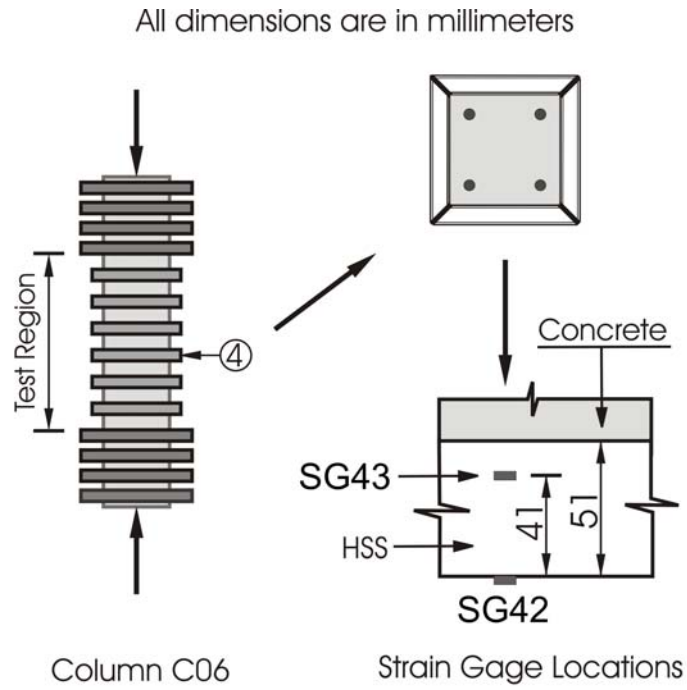


Figure 3-50b: Column load vs. strain of collar (SG42 and SG43) for column C06

All dimensions are in millimeters

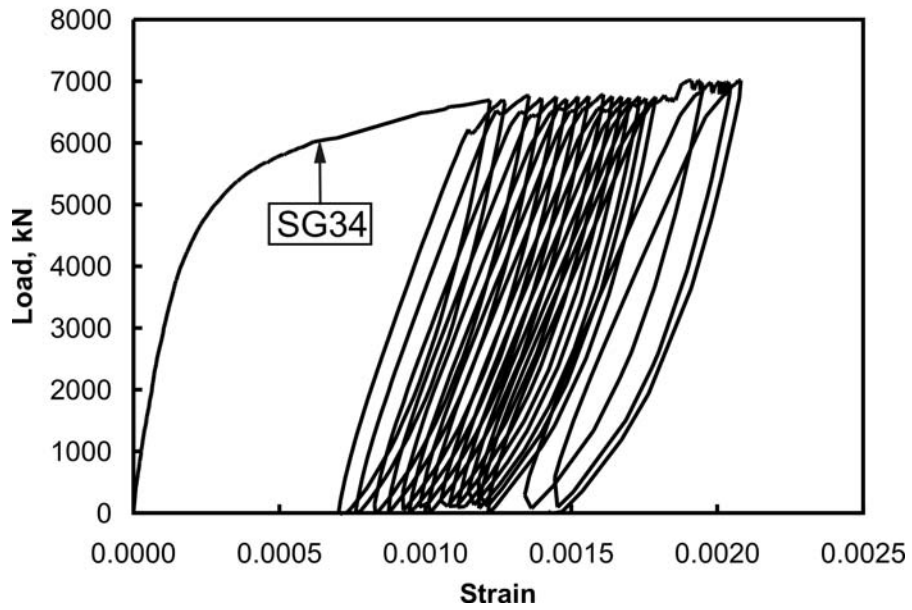
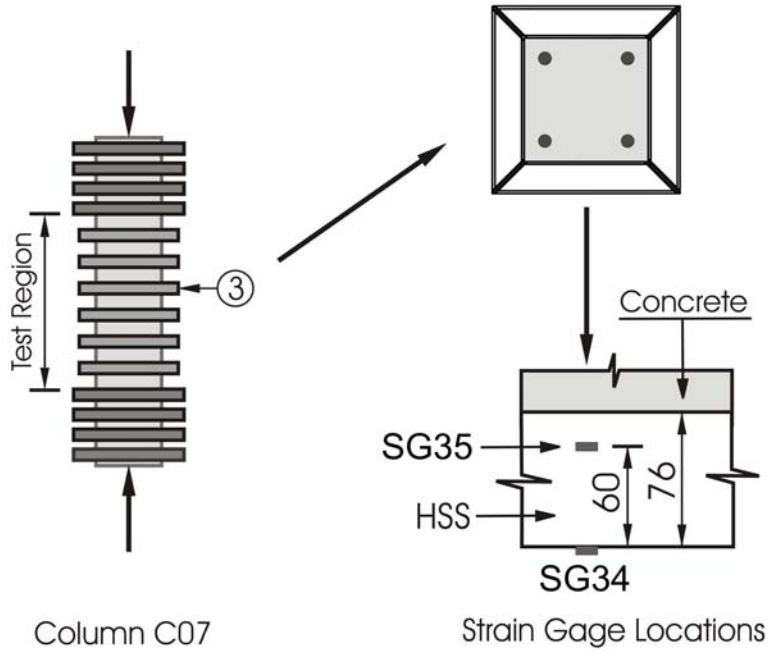


Figure 3-51a: Column load vs. strain of collar (SG34) for column C07 (first loading)

All dimensions are in millimeters

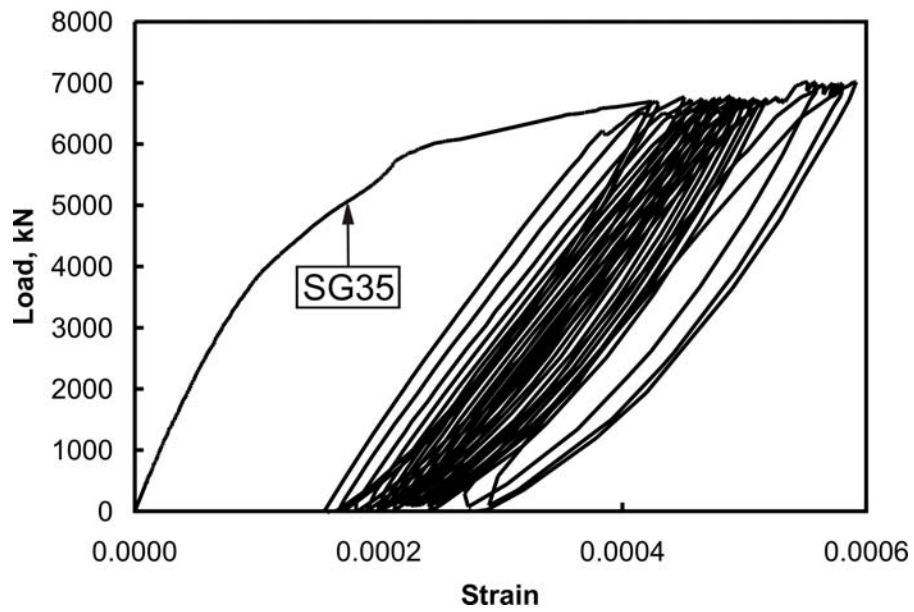
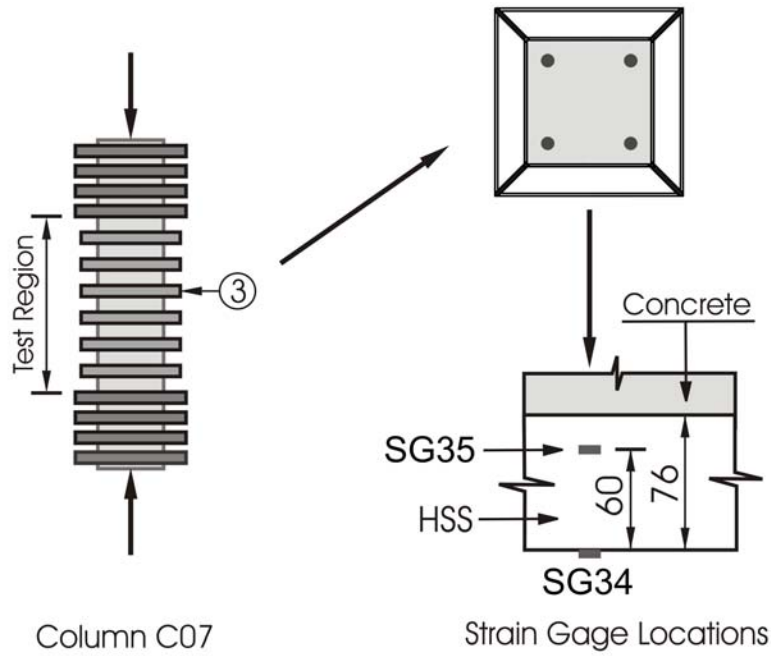


Figure 3-51b: Column load vs. strain of collar (SG35) for column C07 (first loading).

All dimensions are in millimeters

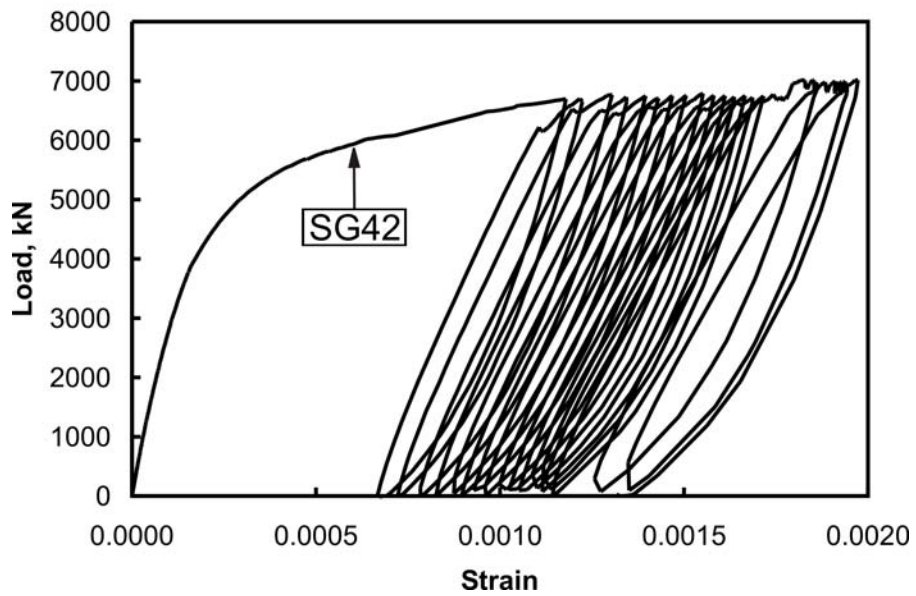
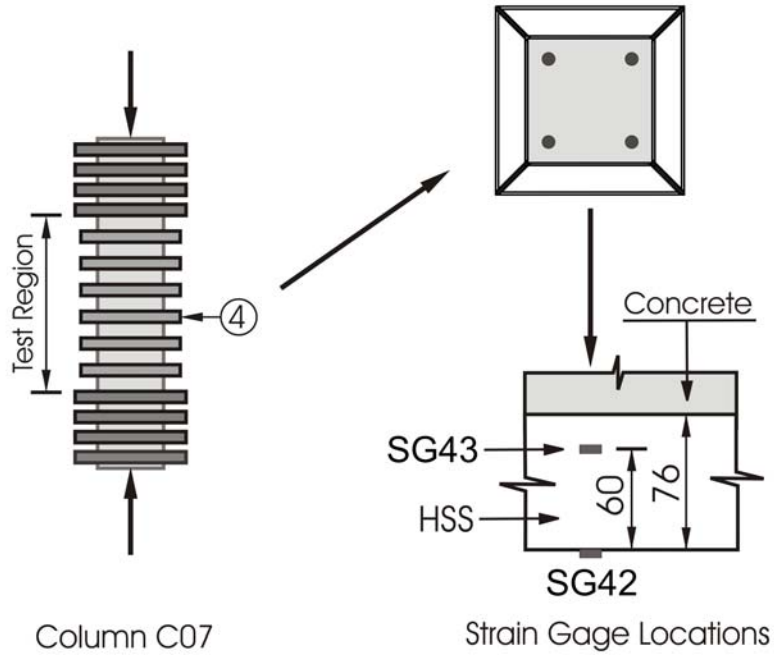


Figure 3-51c: Column load vs. strain of collar (SG42) for column C07 (first loading).

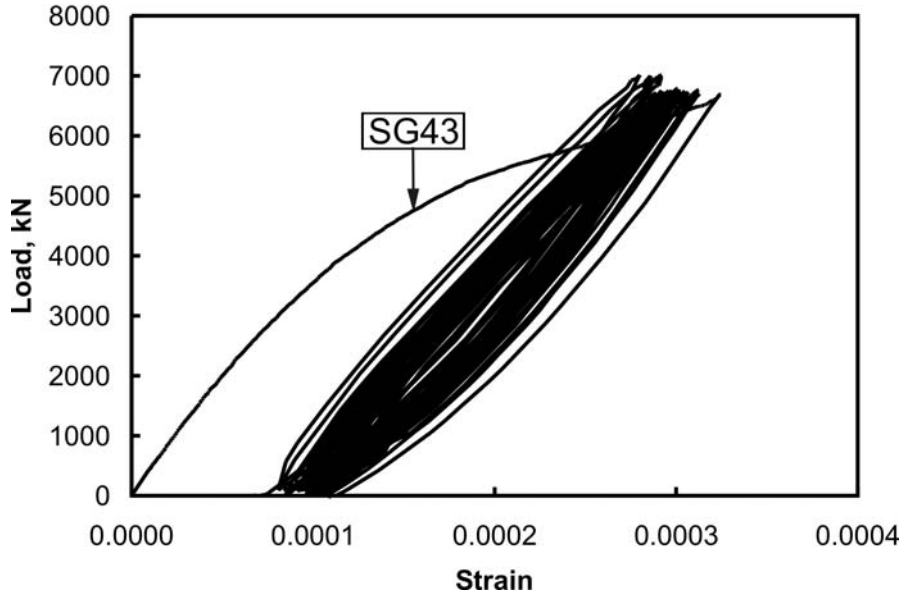
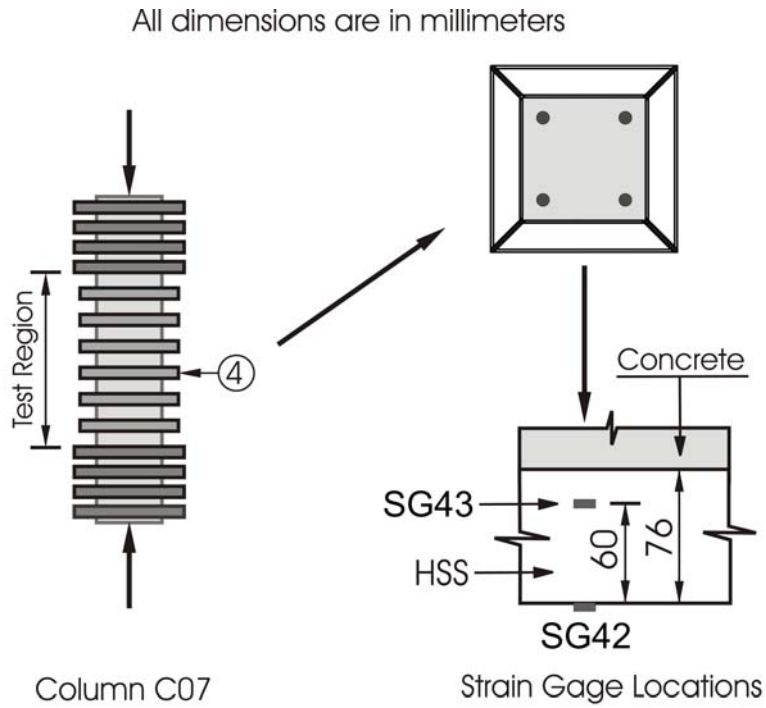


Figure 3-51d: Column load vs. strain of collar (SG43) for column C07 (first loading)

All dimensions are in millimeters

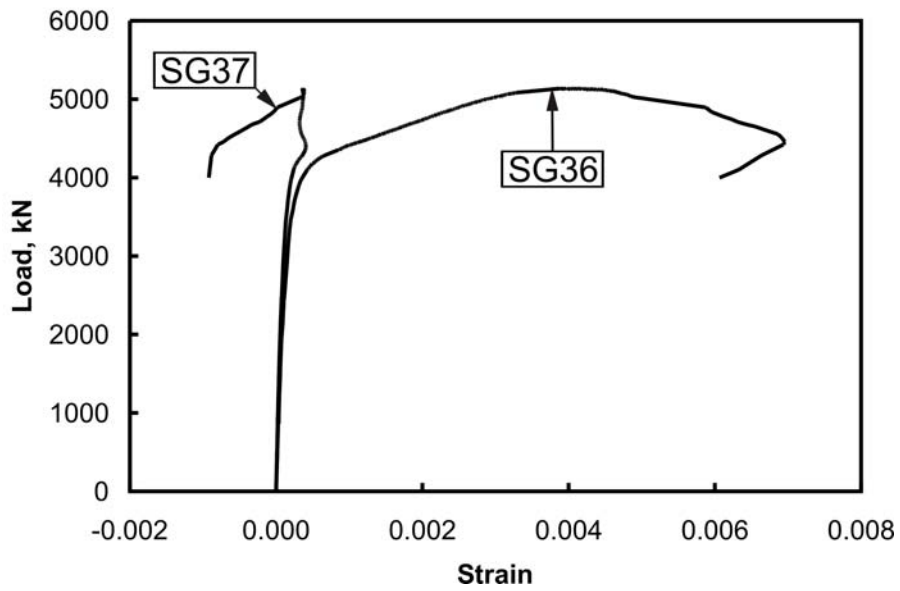
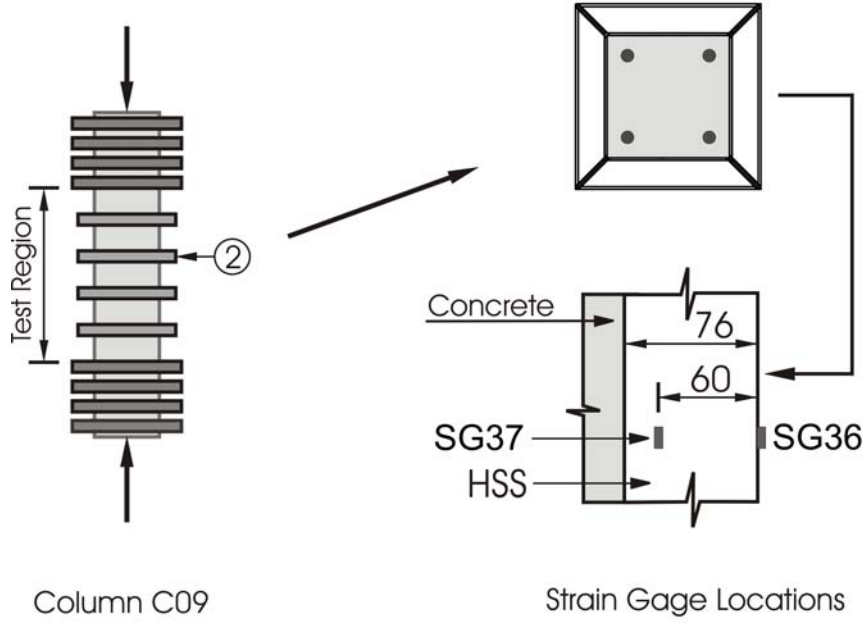


Figure 3-52: Column load vs. strain of collar (SG36 and SG37) for column C09

3.11 References

- Abou-Elfath, H. and Ghobarah, A. 2000. Behaviour of reinforced concrete frames rehabilitated with concentric steel bracing. *Canadian Journal of Civil Engineering*, V. 27, 2000, pp. 433-444.
- Baldelli Jr., J.A. 1983. Steel shear walls for existing buildings. *Engineering Journal*, AISC, pp. 70-77.
- Caner, F.C. and Bažant, Z.P. 2002. Lateral confinement needed to suppress softening of concrete in compression. *Journal of Engineering Mechanics*, ASCE, V. 128, No. 12, December 1, pp. 1304-1313.
- Cusson, D. and Paultre, P. 1994. High-strength concrete columns confined by rectangular ties. *Journal of Structural Engineering*, ASCE, V. 120, No. 3, pp. 783-803.
- Fam, A. and Rizkalla, S.H. 2001. Confinement model for axially loaded concrete confined by circular fiber-reinforced polymer tubes. *ACI Structural Journal*, Vol. 98, No. 4, pp. 451-461.
- Ghobarah, A., Aziz, S.T., and Biddah, A. 1997. Rehabilitation of reinforced concrete frame connections using corrugated steel jacketing. *ACI Structural Journal*, V. 4, No. 3, May-June, pp. 283-291.
- Hussain, M.A. and Driver, R.G. 2001. Finite element study on the strength and the ductility of externally confined rectangular and square concrete columns. *Proc., Canadian Society for Civil Engineering Annual Conference*, Victoria, BC, Canada, May 30-June 2.
- Hussain, M.A. and Driver, R.G. 2005. Experimental investigation of external confinement of reinforced concrete columns by HSS collars. *ACI Structural Journal*, Vol. 102, No. 2, March-April, pp. 242-251.
- Khaloo, A.R. and Bozorgzadeh, A. 2001. Influence of confining hoop flexural stiffness on the behaviour of high-strength light weight concrete columns. *ACI Structural Journal*, V. 98, No. 5, September-October, pp. 657-664.
- Krstulovic-Opara, N. and Thiedeman, P.D. 2000. Active confinement of concrete members with self-stressing composites. *ACI Material Journal*, V. 97, No. 3, May-June, pp. 297-308.
- Neale, K.W. and Demers, M. 1999. Confinement of reinforced concrete columns with fibre-reinforced composite sheets—An experimental study. *Canadian Journal of Civil Engineering*, V. 26, pp. 226-241.
- Mander, J.B., Priestley, M.J.N., and Park, R. 1988. Theoretical stress-strain model for confined concrete. *Journal of Structural Engineering*, ASCE, Vol. 114, No. 8, pp. 1804-1826.
- Priestley, M.J.N, Seible, F., and Chai, Y.H. 1992. Design guidelines for assessment retrofit and repair of bridges for seismic performance. Report No. SSRP-92/01, Dept. of Applied Mechanics and Engineering Sciences, University of California San Diego, August, 266pp.

- Richart, F.E., Brandtzaeg, A., and Brown, R.L. 1928. A Study of the failure of concrete under combined compressive stresses," University of Illinois Engineering Experimental Station, Bulletin No. 185, 104 pp.
- Sakai, K. and Sheikh, S.A. 1989. What do we know about confinement in reinforced concrete columns? (A critical review of previous work and code provisions). ACI Structural Journal, V. 86, No. 2, March-April, pp. 192-207.
- Sheikh, S.A. and Yau, G. 2002. Seismic behaviour of concrete columns confined with steel and fiber-reinforced polymers. ACI Structural Journal, V. 99, No. 1, January-February, pp. 72-80.
- Xiao, Y., and Wu, H. 2003. Retrofit of reinforced concrete columns using partially stiffened steel jackets. Journal of Structural Engineering, ASCE, V. 129, No. 6, May-June, pp. 725-732.

4. PERFORMANCE OF COLLARED COLUMNS UNDER CYCLIC LOADING

4.1 Introduction

With the advancement in earthquake engineering in the past four decades, new codes and standards have been developed that have revealed that many existing reinforced concrete structures are seismically deficient. Some structures have also been deemed seismically deficient due to seismic rezoning of the area. Such structures need to be upgraded to meet the latest codes and standards. The behaviour of structures during an earthquake depends on their strength and stiffness, as well as their ductility. Seismic rehabilitation of structures can be carried out by increasing their strength and stiffness without enhancing their ductility significantly, which is typically achieved by adding new structural walls and/or bracing. These types of rehabilitation schemes may require the structures to deform elastically during strong motions and can impose high demands on the existing foundations, which may, in turn, need to be strengthened. The use of ductility enhancement in the design of new structures, as well as in rehabilitation projects, reduces the seismic design forces considerably. Therefore, attention is given to maximizing ductility in new construction as well as in rehabilitation projects. Such rehabilitation schemes have become increasingly popular in the recent years (Aboutaha *et al.*, 1996; Chai *et al.*, 1990; Ghobarah *et al.*, 1997; and Marsh, 1992). The ductility and energy dissipation at the location of plastic hinges in concrete frames can be enhanced through confinement (Chung *et al.*, 2002; Mander *et al.*, 1988a; Saatcioglu and Razvi, 1992; Sheikh and Uzumeri, 1980). The confinement of concrete is conventionally achieved through closely spaced internal tie reinforcement. However, existing seismically deficient reinforced concrete buildings may possess insufficient ductility due to the lack of internal tie reinforcement at the location of plastic hinges. In these cases, an external means of confinement is required. One such method is proposed in the present research: confinement of concrete columns by steel collars.

The primary objective of this chapter is to evaluate the performance of collared columns under cyclic loading. For this purpose, nine full-scale cantilever columns were tested under cyclic loading. The confinement was provided with collars made from steel hollow structural sections (HSS) with welded corner connections. The effects of parameters such as axial load, collar spacing, collar stiffness, and shear-span on the behaviour of the columns were studied. The tests reported in this chapter were performed at the I.F. Morrison Structural Engineering Laboratory at the University of Alberta.

Using the experimental stress-versus-strain curves of the steel rebars and stress-versus-strain curves of concrete confined externally by steel collars obtained by a model proposed in Chapter 5, moment-versus-curvature relationships were developed. The flexural displacements at the point of application of the horizontal loads were determined with the help of these moment-versus-curvature relationships. For the rotation at the column base due to bond slip at the longitudinal bars, existing models were used. The corresponding displacements at the point of application of horizontal loads were then determined. The flexural displacements and displacements due to base rotation were combined to get the total displacements at the point of application of the horizontal load. The moment versus total displacements are plotted to get the analytical envelope curves, which are compared with the experimental average envelope curves.

4.2 Experimental Program

4.2.1 Test specimens

Nine full-scale column specimens (CL0 to CL8) were designed to simulate typical columns of two to three story reinforced concrete buildings in seismic regions. All the columns were 300x300 mm in cross-section and reinforced with eight longitudinal steel bars of 25 mm diameter, constituting a longitudinal reinforcement ratio of 4.4%. Figure 4-1 shows the details of the internal reinforcement for all the columns and footings. Concrete cover of 60 mm was provided to the centroid of the vertical bars. Column CL0 was a control column and was provided with conventional tie reinforcement in the test region, which satisfied the seismic plastic hinge requirements of ACI 318-02 and CSA Standard A23.3-94 (Equations 3.1 and 3.2). The spacing of the first hoop was set equal to $s/2$ above the footing in this column, where s is the typical hoop spacing of 70 mm. All the remaining columns were provided with external transverse reinforcement by HSS collars in the test regions. In order to study the effect of external confinement separately, no internal tie reinforcement was provided in the test regions of these columns. For the sake of discussion, the collars and the gaps between the collars in the test region are numbered from the bottom upwards. The first collar near the footing is given number 1 and the second collar is given number 2 and so on. Similarly, the gap between the footing and the first collar is given number 1 and the gap between the first and second collars is given number 2 and so on.

The volumetric ratios of transverse confining steel, ρ_t , for all of the test columns are given in Table 4.1. The volume of the confining steel for columns tested under cyclic loading (CL1 to CL8) was calculated by multiplying the cross-sectional area of the HSS by the perimeter of the collar measured at the centroid of the HSS cross-section. Since the collars are placed externally and

prevent most of the spalling, the volume of the concrete was calculated based on the gross area of the column and the centre-to-centre vertical spacing of the collars. Hence, the core of the collared columns was considered equal to the cross-sectional dimensions of the columns. For column CL0, the volume of the tie steel was calculated in a manner analogous to that used for the collars, but the volume of the concrete was based on the core of the column within the reinforcing cage. The core dimensions of column CL0 were 220x220 mm based on the centreline of the ties.

All the columns had 1800x1050x591 mm bases that were anchored to the strong floor of the structural laboratory by four post-tensioned 50 mm diameter high strength steel threaded rods to achieve fixity at the bases of the columns as shown in Figure 4-2. An initial post-tensioning force of about 520 kN was applied to each threaded rod. The column reinforcement cages were erected vertically into the footings before casting the footing concrete and there was no splicing of the vertical bars in the columns, as shown in Figure 4-3. Casting of the columns and the footings was done separately. At the location of the construction joint between the columns and footings, the footing surface was roughened before the hardening of the concrete. The casting of the columns was done vertically in groups of three, as shown in Figure 4-4. A release agent was applied to the plywood forms before closing and then they were sealed with construction sealant to prevent leakage, as shown in Figure 4-5. Six standard 150x300 mm cylinders were cast at the time of casting of the respective column or footing. Two cylinders, tested at 7 days, were used to observe the rate of growth of strength and the remaining four cylinders were used to determine the strength of the concrete at the time of testing of the corresponding column. The curing conditions of the cylinders were identical to those of the respective test specimens so that the cylinder strength would be representative of the strength of the concrete in the specimen. The casting of the footings and the first three columns (CL1 to CL3) was done with commercially prepared ready mix concrete. For each footing a different batch of concrete was used. However, the columns (CL1 to CL3) were cast with concrete from the same batch. However, separate cylinders were cast for each of these columns to find the concrete strength at the time of loading. Therefore, different cylinder strengths are reported for these columns. Columns CL0 and CL4 to CL8 were cast with concrete mixed in the laboratory mixing plant and due to the small capacity of the plant, a separate batch was prepared for each column. A separate batch of concrete was also used for each footing.

Figure 4-6 shows the arrangement for the external confinement of the columns by collars and schematic diagrams for the loading of the columns. Figure 4-7 shows a typical steel HSS collar with welded corner connections. A general view of the first three columns (CL1 to CL3) at different stages of collar installation is given in Figure 4-8(a). Table 4.1 summarizes the details of confinement, axial load, and the dimensions H1, H2 and H3 for all the columns used in this

study. The dimensions H1 (column height), H2 (height to horizontal load point), and H3 (height to vertical load point) have been defined in Figures 4-1 and 4-6. Specimens CL1 to CL8 were provided with external confinement by HSS collars in the test region, the height of which was kept approximately equal to 600 mm based on the premise that the plastic hinge length will not exceed the test region. The clear spacing between the collars, s' , was either 50 or 100 mm. The clear distance between the top of the footing and the bottom of the first collar was equal to $s'/2$. The fabrication of the collars was done in a commercial fabrication shop with full penetration groove welds all around the corners. Inspection of the welds was carried out by sectioning a sample collar and full penetration of the welds was verified. The inner dimensions of the collars were 10 to 12 mm larger than the cross-sectional dimensions of the columns. The collars were threaded over the columns from the top, a procedure clearly not applicable to real structures where collar installation includes assembly around the existing column. The collar was placed on a Styrofoam spacer with a uniform gap all around (Figure 4-8(b)). The gap was then sealed from the bottom with hot glue and epoxy grout was poured into the gap. Although the grout was flowable, a steel strip was vibrated into the gap to eliminate the chance of trapping air bubbles.

4.2.2 Material Properties

There are four materials involved in this study: concrete, steel reinforcing bars, HSS collars, and epoxy grout. The strength of the concrete in the columns and footings was obtained by testing at least four 150x300 mm cylinders as per ASTM C469, one day before the testing of the columns. The average cylinder strengths, standard deviations, and the age of the concrete at the time of testing of the cylinders are given in Table 4.2 for all the columns and footings. Although an error in the ready mix supplied for columns CL1 to CL3 resulted in a very low concrete strength, it was decided to proceed with testing. These columns provide a means of assessing the effect of HSS collars on the behaviour of poor quality concrete. Concrete batches used for subsequent tests were mixed in the laboratory to provide better control. The average stress versus strain curves of the reinforcing steel, the HSS collars, and the epoxy mortar are given in Figure 4-9. Reinforcing bars conformed to CSA Standard G30.18 and were tested as per ASTM A370. The material properties of steel reinforcing bars and steel HSS are reported in Table 4.3. Three tension coupons were tested for each size of rebar, the results of which were then averaged. Master Builders Concessive Liquid LVI epoxy was used to make the epoxy mortar. The epoxy consists of two parts: resin and hardener. The epoxy mortar was obtained by mixing fine sand with the resin and hardener in the ratio of 4:2:1. In order to determine the material properties of the epoxy mortar, three cubes of 51x51x51 mm were made from the same mix as was used for grouting the collars. The testing of the three mortar cubes was done with the bottom end fixed and the top end with a spherical ball joint. A strain rate of 9.45×10^{-5} per second was maintained during the

testing of all three prisms, the results of which were then averaged. The average stress versus strain curve of the epoxy mortar was used to find the modulus of elasticity, peak stress, and the strain at peak stress which were found to be 3.42 GPa, 84.0 MPa and 0.0325, respectively. The HSS conformed to ASTM A500 grade C. Stub-column tests were performed to find the material properties of the HSS. For each size of HSS, one stub-column was tested. The height of the stub columns were 200 and 250 mm for HSS51x51x6.35 mm and HSS 76x51x6.35 mm, respectively. Two LVDTs were used to measure the average strain over the gauge length of 100 mm, in addition to strain gauges, as shown in Figure 4-10. Figure 4-11 shows the deformed configurations of stub-columns of HSS 51 x 51 x 6.35 mm and HSS 76 x 51 x 6.35 mm.

4.2.3 Test Set-up

A schematic diagram of the loading set-up is shown in Figure 4-6. Columns CL0 to CL4 were tested with long shear-spans and columns CL5 to CL8 were tested with short shear-spans. On columns CL1 to CL4, heavy collars were provided in the region between the test region and the bracing channels to prevent failure at that location, as shown in Figure 4-12.

The horizontal load was applied to the columns by two double-acting hydraulic jacks in parallel and coupled to each other by a yoke. The jacks were mounted on a reaction frame. The assembly for horizontal loading is shown in Figure 4-13. Figure 4-14(a) shows the attachment of horizontal loading assembly to the column specimen. Gravity load simulators—similar to those developed by Yarimci *et al.* (1966)—anchored to the strong floor of the laboratory were used to apply the vertical load through a distributing beam at the top of the test column. These devices form a pin-jointed mechanism that keeps the load close to the vertical throughout large in-plane horizontal displacements. The assembly applies gravity load on the test specimen and, in turn, also induces moments due to the $P-\Delta$ effect on the test specimens. A knife-edge assembly was used between the column top and a flat load cell for measuring the vertical applied load (Figure 4-14(b)). The out-of-plane displacement of the columns was prevented by lateral bracing that did not inhibit in-plane movement (Figure 4-12).

4.2.4 Instrumentation

An electronic data acquisition system was used to record the data. Horizontal and vertical loads were measured with load cells. In addition, pressure gages were used to record the hydraulic pressure in the jacks to calculate the loads. Custom load cells, manufactured at the University of Alberta, were fitted to the jack to measure the horizontal loads in tension and compression. A commercial flat load cell of 1360 kN capacity was used to measure the vertical load applied to

the top of the columns. Electrical resistance strain gages were used to measure the strain of the vertical rebars in the test region. A total of 12 strain gages were installed on the vertical bars of a column. Eight strain gages, one on each bar, were installed at a height of 50 mm above the top of the footing and the remaining four strain gages were installed, one on each of the corner bars, at a height of 300 mm from the top of the footing to help characterize the development of the plastic hinge. Cable transducers were used to measure the overall rotation of the test region and were mounted on the top collar in the test region (Figure 4-15(a)). Rotation meters were installed on the collars in the test region to measure the rotation of the collars at different locations in the test region (Figure 4-16). The rotation of the bottom collars were measured using LVDTs (Figure 4-15(b)). Table 4.4 gives the location of devices for measuring rotation of collars along the test region of the column specimens.

4.2.5 Testing Procedure

After checking that all of the instrumentation was functioning properly, the vertical load was applied, followed by the horizontal cyclic loading. For all of the columns, the vertical load was kept constant throughout the tests except for column CL0, in which a load of 1470 kN was applied from cycles 1 to 16 and 720 kN from cycle 17 to the end of the test. When the column reached large displacements, the $P-\Delta$ effect from the high vertical load caused a substantial drop in the lateral force required to reach each subsequent displacement increment. For this reason, the vertical load was reduced to 720 kN and the test was continued. All the remaining columns were tested under 720 kN or zero load as per Table 4.1.

In order to facilitate the discussion, it is to be noted that the columns were originally in the neutral position. After the application of gravity load, if present, the columns were first pushed towards the north (see Figure 4-6) up to the desired level of force or displacement and then back towards their neutral positions. Without stopping at their neutral position, they were pushed towards the south up to the desired level of force or displacement and then back towards the neutral position, completing one full cycle. In general, the cycles were performed one after another without interruption. On the average, the time required to complete a test was about 5 days. Therefore, the test had to be interrupted at the end of each day.

The sequence for horizontal loading shown in Figure 4-17, which has been adapted from Ghee *et al.* (1989), was used for all the columns. Ghee *et al.* (1989) required the horizontal load for the first cycle to be calculated based on 75% of the ideal flexural strength, M_{if} , of the column. The ideal flexural strength, M_{if} , was calculated based on the ACI compression stress block, measured material strengths, and an ultimate compressive strain of concrete of 0.003 (for

unconfined concrete), without considering axial load in calculations. The yield displacement was determined based on the first cycle of loading by extrapolating straight lines from the origin through the peak load displacement points of this cycle to the horizontal load level corresponding to the ideal flexural strength. The term ideal flexural strength, M_{if} , is not commonly used. The present research considers using nominal flexural strength, M_{nuc} , for unconfined concrete sections. The nominal flexural strength, M_{nuc} is the strength of a section without capacity reduction factors and is calculated by taking into consideration the effect of axial load. The yield displacement, Δ_y , determined by this procedure corresponds to a moment that falls between $0.75M_{nuc}$ and M_{nuc} . Hence, according to this procedure the actual moment corresponding to the yield displacement, Δ_y , will always be less than the nominal flexural strength, M_{nuc} . It has been demonstrated in Appendix C using a typical reinforced concrete section that the yielding of tensile reinforcing steel is not guaranteed at Δ_y determined by this procedure.

While applying the above procedure to determine the yield displacements of the columns in the present research, a slight modification was made. Table 4.5 reports the following analytical (using strain compatibility and methods described in Appendix C) and experimental results of the test specimens under consideration (all account for the presence of axial load, if any):

- (1) Moment at the first yield of the tensile steel calculated assuming unconfined concrete in the compression zone, M_{yuc} . The specimens CL0, CL1, CL2, CL3, CL4, CL6, CL7, and CL8 are over-reinforced; the failure is triggered by the crushing of concrete in the compression zone before yielding of the tensile steel occurs. Therefore, the values of M_{yuc} do not exist for these specimens. In specimen CL5, the yielding of the longitudinal steel takes place before the crushing of concrete. (Although column CL1 is nominally identical to CL5 in this regard, the low strength concrete creates the over-reinforced condition.)
- (2) The nominal moment strength of the section calculated assuming unconfined concrete in the compression zone using the method in the ACI code, M_{nuc} .
- (3) Moment at the first yield of the tensile steel calculated assuming confined concrete in the compression zone, M_{ycc} . For column CL0, the confined concrete material curve was obtained using the confinement model proposed by Mander *et al.* (1988b). For the

confined concrete material curves of the collared columns, the confinement model proposed in Chapter 5 was used.

- (4) The nominal moment strengths of the sections assuming confined concrete in the compression zone, M_{ncc} . The values of M_{ncc} reported in this table are the experimental values. These are the peak values obtained from the average envelopes to experimental moment vs. drift (%) hysteresis curves presented later in this chapter. These values can also be calculated analytically. The analytical envelopes to the hysteresis will be presented at the end of this chapter.

It must be determined which of the above-mentioned moments (M_{yuc} , M_{nuc} , M_{ycc} , and M_{ncc}) should be used for the determination of yield displacements for the column specimens. The values of M_{yuc} exist only for column CL5. Therefore, the choice of moment for the determination of yield displacement is limited to M_{nuc} , M_{ycc} , and M_{ncc} . The following are the arguments in selecting one of these moments for the determination of the yield displacement:

M_{nuc} could be used for the yield displacement determination to be consistent with the original procedure. However, the values of M_{nuc} are generally considerably lower than both M_{ycc} and M_{ncc} . Using M_{nuc} means that lower values of the yield displacement will be obtained which will result in higher apparent values of displacement ductility that may not be representative of the actual ductility. Since M_{nuc} is calculated based on the unconfined concrete material curve, and all the columns presented in this chapter are heavily confined columns, the determination of the yield displacement using M_{nuc} does not appear to be realistic.

One can argue that due to the influence of the collars, the maximum moment capacity exhibited by the confined system, M_{ncc} , should be used for yield displacement determination analogous to the determination of the yield displacement of conventional columns using M_{nuc} (Ghee *et al.* 1989). Undoubtedly, the confinement improves the axial deformation capability of the concrete columns as has been reported in literature as well as demonstrated by experimental results of the present research reported in Chapter 3, and it is generally accepted that if the axial behaviour is improved, the cyclic behaviour is also improved. However, the benefits of confinement on the yield displacement are also availed in this option; that is, the yield displacement increases by increasing the level of confinement. Hence, both the maximum

displacement and the yield displacement of the system increase, but their ratio—that is, the displacement ductility of the system—may not increase. Therefore, this tends to be a highly conservative option and it is not recommended that the yield displacement of laterally loaded collared columns be determined by using M_{ncc} . This option gives results similar to the area equalization method (Xu and Niu, 2003) for yield displacement determination. The area equalization method will be presented later in this chapter.

Instead of using one of the two extreme options described above, an intermediate option was selected, *i.e.*, M_{ycc} was used for yield displacement determination in the present research. It is to be noted that the moment versus lateral drift envelope curves becomes non-linear at moments well below M_{ycc} . The moment corresponding to the yield displacement determined by this method (called method 1 in subsequent discussions) is slightly lower than M_{ycc} . Therefore, yielding of the longitudinal bars may not occur at the yield displacement but the displacement determined by this method may represent overall yielding of the section because of the non-linearity of the moment versus lateral drift envelope curves in the proximity of M_{ycc} .

Consistent with the previous discussion, the first five cycles were load controlled, in which a peak moment of 75 percent of M_{ycc} was applied. The applied moment consists of moment due to horizontal loading and due to the $P-\Delta$ effect if axial load is present. The procedure is explained with the help of Figure 4-17. The Figure 4-17(a) shows the first full cycle of a typical moment vs. drift (%) hysteresis. The straight lines starting from the origin and passing through the peak moment vs. drift (%) points of the first cycle are extrapolated to moment M_{ycc} . The corresponding yield drifts in the positive and negative directions, DR_1 and DR_2 , are thereby determined. The average yield drift is taken as the average of DR_1 and DR_2 and is denoted by DR. The yield displacement, Δ_y , is related to yield drift(%), DR, by the equation given in Figure 4-17. The displacement ductility factor, μ , is defined as the ratio of the actual displacement to the yield displacement. Subsequent cycles were displacement controlled and extended to displacement ductilities, μ , equal to 1.5, 2, 4, 6, 8 and so on, with five cycles carried out at each displacement ductility level. The stroke limit of the jack for horizontal loading was about 200 mm in either direction, so when this was reached (specimens with the long shear span) additional cycles were conducted at that displacement. The tests were continued until the horizontal and vertical load carrying capacity of the specimens dropped significantly, up to a maximum of 45 cycles. If the jack stroke limit had been reached in the test, the jack was then

repositioned so that the full stroke was available and the specimen was pushed in one direction to examine the residual strength at large deflections.

In the above-mentioned procedure for determining the yield displacements of the column, the following could be the possible sources of error: (1) difficulty in reversing the load exactly at $0.75M_{ycc}$, especially in flexible systems; and (2) difficulty in determining the exact value of M_{ycc} due to the lack of true material curves of the constituent materials. In the present research, the material curves of the steel were available at the time of testing. However, due to the inefficacy of the existing confinement models for predicting the stress vs. strain curves of concrete confined by steel HSS collars, the correct material curves of concrete confined by the collars were not available. Therefore, the material curves of collar confined concrete for the phase 2 columns were estimated based on the material curves for the phase 1 columns tested under concentric axial loading (Chapter 3). Column CL0 is exempted from this limitation because the confinement was provided with conventional tie reinforcement and the confinement model proposed by Mander *et al.* (1988b) was used. Keeping in view the above two limitations, the yield displacements used to conduct the tests are considered as approximate and are reported under the category of method 1(alternative 1) in Table 4.6. These values are re-evaluated in the next section.

4.3 Test Results

The details of the number of cycles at different displacement ductility levels sustained by the specimens are given in Table 4.7. Any partial cycles at the end of the test during which final failure occurred are not included in the values presented in the table. The strain data of reinforcing bars of the columns is presented in Appendix D.

4.3.1 Test Observations

4.3.1.1 Specimen CL0

The yield displacement used for the test was 30 mm (method 1(alternative 1), Table 4.6). The column sustained a total of 44 complete cycles and failed in 45th cycle. The cycles 26 through 44 (19 cycles) were performed at a displacement ductility level corresponding to the stroke limit of the horizontal jacks.

The testing of column CL0 was started with a gravity load of 1470 kN, which was maintained up to the end of 16th cycle. Due to the large $P-\Delta$ effect, the applied moment exceeded the capacity

of the column in 16th cycle. Therefore, before starting 17th cycle, the gravity load was reduced to 720 kN and the test was continued.

Figure 4-18 shows the appearance of the test region of the column at different stages of the test. Horizontal tension cracks appeared in the first cycle on both the north and south faces of the column that opened and closed during the first five cycles. In the sixth cycle, spalling of the concrete cover was observed in the test region. This figure shows that the most damaged zone in the test region of the column is away from the footing. The level of damage increases with the increase of number of cycles and the extent of damage on the south face is higher than that on the north face. It is also clear from this figure that an upward shift in the location of hinge formation occurs for this column during the regime of cycling. In the 45th cycle, while pushing towards the north, both the horizontal and vertical loads dropped due to sudden shear failure at the most damaged part of the test region (Figures 4-18(h) and 4-18(i)).

It was expected that most of the damage would occur at the point of maximum moment, which is at the interface of the column and footing, but Figure 4-18 shows that the most damaged region of the column is away from the footing. This discrepancy occurs due to the presence of additional restraint (confinement) provided by the footing to the column at the critical section. Similar observations were also made by Sheikh and Houry (1993).

4.3.1.2 Specimen CL1

The testing of this column was carried out without gravity load. The yield displacement used for the test was 23 mm (method 1(alternative 1), Table 4.6). Figure 4-19 shows the appearances of the specimen at different stages of the test. Horizontal hairline cracks appeared in the test region on the north and south faces of the column after the 5th cycle. The number of hairline cracks increased with the increase in the number of cycles and the displacement ductility level at which these cycles were performed. The width of a few cracks increased with the increase of displacement ductility level. Figure 4-19(a) shows the view of a wide-open crack in gap 2 of the test region during the 16th cycle.

In the 17th cycle, when the column was being pushed towards the south, a crack appeared in the footing cover concrete adjacent to the column north face as shown in Figure 4-19(b). A similar crack appeared in the footing cover concrete adjacent to the south face of the column when column was being pushed towards north in the 19th cycle. The appearance of these cracks in the footing cover concrete was due to bond failure and extension of the longitudinal bars of the column in the footing. In the later cycles, these pieces of footing cover concrete spalled off completely.

In the 26th cycle, the crushing of concrete between the footing and the first collar took place both on the north and south faces of the column when the column was pushed towards north and south, respectively.

This specimen was subjected to a total of 45 complete cycles. Cycles 26 through 45 (20 cycles) were performed at the same ductility level corresponding to the stroke limit of the horizontal jacks. The stroke of the jacks was adjusted and then the column was pushed towards the north up to the available stroke limit of the adjusted jacks, but the column could not be failed.

Figure 4-19(c) shows the appearance of the test region of the column at the end of the test. It is clear from this figure that the collars remained in position (*i.e.*, had not slipped) after sustaining 45 cycles and a final push towards the north as described above. Most of the damage occurred in the first and second gap of the test region. Figure 4-19(d) shows the extent of damage in the first and second gap.

4.3.1.3 Specimen CL2

The testing of this column was done with a gravity load of 720 kN. The yield displacement used for this test was 41 mm (method 1(alternative 1), Table 4.6). The column sustained a total of 27 cycles (Table 4.7). Cycle 21 through 27 (seven cycles) were performed at the same ductility level corresponding to the stroke limit of the horizontal jacks.

Figure 4-20 shows the appearances of the column at different stages of the test. The extent of damage can be seen in the first, second, and third gap at the end of 10th and 20th cycles, and at test end. However, the most damage region of the column is in gap 2, where the fractured vertical bars are also visible (Figure 4-20(d)).

The spalling of concrete cover started in the 7th cycle. The spalling increased with the increase in the number of cycles. In the 22nd cycle, the vertical bars of the column became visible due to excessive spalling of the concrete cover. The three vertical bars on the south face of the column fractured in a brittle manner due to low cycle fatigue while pushing the column towards the north; one in each of 26th, 27th, and 28th cycle. The test was stopped after the fracture of the third vertical bar in the 28th cycle. No spalling of cover concrete of the footing adjacent to the column took place (Figure 4-20).

4.3.1.4 Specimen CL3

The testing of this column was carried out with a gravity load of 720 kN. The yield displacement used for testing this column was 38 mm (method 1(alternative 1), Table 4.6). The specimen sustained 45 complete cycles (Table 4.7). Cycles 21 through 45 (25 cycles) were performed at the same ductility level corresponding to the stroke limit of the horizontal jacks. The stroke of the jack was then adjusted and the column was pushed towards the north up to the available stroke limit, but the column could not be failed. The capacity of the column in the final push was significantly lower than the peak capacity. No spalling of concrete occurred in the first ten cycles. Spalling started in the 11th cycle and increased thereafter. However, it remained very limited up to the end of cycle 20. Figure 4-21 shows the appearances of the column at different stages of the test. Spalling occurred on the north and south faces of the column in all the gaps in the test region. However, the spalling of concrete in the first four gaps was relatively high. No slippage of collars is seen at the end of the test. No spalling of cover concrete of footing took place.

4.3.1.5 Specimen CL4

The testing of this column was done with a gravity load of 720 kN. The yield displacement was 28 mm (method 1(alternative 1), Table 4.6). The specimen sustained 45 complete cycles (Table 4.7). Cycles 26 through 45 (20 cycles) were performed at the same ductility level corresponding to the stroke limit of the horizontal jacks. The stroke of the jack was again adjusted and then the column was pushed towards the north up to the available stroke limit of the adjusted jack, but the column could not be failed.

No spalling of concrete occurred in the test region in the first 15 cycles. Spalling started in the 16th cycle and increased with the increase in the number of cycles but it remained very limited at the end of the 20th cycle. Figure 4-22 shows the appearances of the column at different stages of the test. Spalling of concrete is visible in the first five gaps. No slippage of collars is seen at the end of the test.

Cracks in the footing cover concrete adjacent to the column north and south faces appeared after the 20th cycle. With the increase in the number of cycles, the concrete cover was completely removed. Figure 4-22(b) shows the appearance of the specimen at the end of the 30th cycle. The spalled footing concrete can be seen in this figure.

4.3.1.6 Specimen CL5

The testing of this column was done under zero gravity load. The yield displacement was 8 mm (method 1(alternative 1), Table 4.6), which is considerably lower than for the previously discussed specimens due to the smaller shear span. The specimen sustained 37 complete cycles (Table 4.7) and failed due to the fracture of three vertical bars on the south face of the column under low cycle fatigue while pushing the column towards the north: one bar fractured with a bang in 37th cycle while pushing the column towards the north and two bars fractured in the 38th cycle with two consecutive bangs while pushing the column towards the north. Figure 4-23 shows the appearances of the column at the end of the test. This figure shows that most of the damage occurred in the first two gaps. The fractured vertical bars are visible in Figure 4-23(c). No slippage of collars is seen at the end of the test.

Cracks in the footing cover concrete adjacent to the north and south faces of the column appeared in 21st cycle due to extension and the failure of bond of the vertical bars in the footing. In the subsequent cycles, the cover was completely removed. The resulting depression in the footing adjacent to the column face is seen in Figure 4-23(a).

4.3.1.7 Specimen CL6

The testing of this column was done under 720 kN gravity load. The yield displacement was 8.5 mm (method 1(alternative 1), Table 4.6). The specimen sustained 31 complete cycles (Table 4.7) and the column failed due to the fracture of a vertical bar (the middle bar on the north face of the column) due to low cycle fatigue. The test was stopped after the fracture of this bar with a bang while pushing the column towards the south in the 32nd cycle, accompanied by a drop in load.

Figure 4-24 shows the appearances of the column at different stages of the test. Most of the damage occurred in the first gap. After the completion of 15 cycles, the damage was seen in the first gap only. After the completion of the 20th cycle, the level of damage increased in the first gap and some cracks were also seen in the second gap. Figure 4-25 shows the fractured vertical middle bar on the north face of the column at the end of the test. No slippage of collars is seen at the end of the test.

The spalling of footing cover concrete took place from cycle 21 through 25 due to extension and failure of bond of the vertical bars in the footing. The resulting depression in the footing adjacent to the column face is seen in Figures 4-24(d) and 4-25.

4.3.1.8 Specimen CL7

The testing of this column was carried out under 720 kN gravity load. The yield displacement was 11.5 mm (method 1(alternative 1), Table 4.6). The specimen sustained 35 complete cycles (Table 4.7) and the column failed due to the fracture of three vertical bars due to low cycle fatigue. The first vertical bar fractured on the south face while pushing the column towards the north in the 35th cycle and the second fractured on the north face while pushing the column towards the south in the same cycle. The third vertical bar fractured on the north face while pushing the column towards the south in the 36th cycle and then the test was stopped.

Figure 4-26 shows the appearances of the column at different stages of the test. Most of the damage occurred in the first gap. Spalling of the concrete in the test region was not visible after the completion of the first 10 cycles. After the completion of 20 cycles, the damage in the first gap was seen which increased with the increase in the number of cycles. No slippage of collars is seen at the end of the test.

Footing cover concrete adjacent to the north and south faces of the column was completely removed by the end of the 20th cycle due to extension and the failure of bond of the vertical bars in the footings.

4.3.1.9 Specimen CL8

The testing of this column was done under 720 kN gravity load. The yield displacement was 11 mm (method 1(alternative 1), Table 4.6). The specimen sustained 35 complete cycles (Table 4.7) and the column failed in the 36th cycle due to fracture of vertical bars under low cycle fatigue. The middle bar on the south face fractured while pushing the column towards the north in the 36th cycle. While pushing the column towards the south in the same cycle, two more bars fractured on the north face, one after the other and the test was stopped.

Figure 4-27 shows the appearances of the column at different stages of the test. At the completion of the 10th cycle, no spalling of concrete was observed. However, after the completion of the 20th cycle, spalling of concrete was seen in the first gap and some horizontal cracks were seen in the second gap. At the end of the test, damage in the first and second gap increased, with relatively more damage in the first gap (Figure 4-27(d)). No slippage of collars is seen at the end of the test.

After the completion of the 20th cycle, spalling of footing cover concrete was seen adjacent to the north and south faces of the column due to bond failure and extension of column vertical rebars in the footing.

4.3.2 Hysteresis Curves

The results of the tests can be presented in terms of horizontal force versus horizontal displacement at the point of application of the horizontal load. Such hysteresis relationships indirectly reflect the influence of $P-\Delta$ because the horizontal load required to reach a certain displacement is affected by the presence of the vertical load. The results can also be presented in terms of moment at the column base due to both lateral load and axial load (through the $P-\Delta$ effect) vs. percentage drift at the point of application of lateral load. The percentage drift is defined as follows:

$$[4.1] \quad Drift(\%) = \frac{\Delta}{H_2} \times 100$$

where H_2 is the vertical distance to the point of application of the lateral load from the base of the column and Δ is the lateral displacement at that level. The moment-versus-drift(%) relationships are influenced by the $P-\Delta$ effect but it is incorporated directly into the moment values. Therefore, any reduction in moment capacity observed can be attributed solely to a degradation in strength due to cyclic loading. In the present research, the point of application of horizontal load was not same for all the columns (Table 4.1). In addition, the points of application of the vertical loads were not coincident with the point of application of horizontal loads. In columns CL5 to CL8, the distance between the points of application of horizontal and vertical loads was large. In these column specimens, a small horizontal displacement at the point of application of horizontal load caused a large horizontal displacement at the point of application of vertical load, resulting in a large $P-\Delta$ effect. Therefore, presenting the hysteresis behaviour for such columns in terms of horizontal load vs. horizontal displacement at the point of application of horizontal load will not be representative because the $P-\Delta$ effect will be proportionately higher. Therefore, it was decided to present the hysteresis results in terms of moment at the column base vs. percentage drift at the point of application of horizontal load.

Figures 4-28 through 4-36 show the hysteresis curves for specimens CL0 through CL8, respectively. The north push is plotted in the first quadrant and the south push in the third quadrant. The approximate yield displacements used for conducting the tests and given in

Table 4.6 under method 1 (alternative 1) are also shown in Figures 4-28 through 4-36, along with the corresponding displacement ductility levels at which cycles were performed. The starred displacement ductility levels for specimens CL0, CL1, CL2, CL3, and CL4 (Figures 4-28 through 4-32) correspond to the stroke limit of the horizontal jacks. The hysteresis curves for all the columns are flexure-dominated, as will be explained later in this chapter. However, the hysteresis curves for columns with short shear-spans (CL5, CL6, CL7, and CL8) have specific characteristics that are present in those of concrete shear walls (Antoniades *et al.*, 2003) and columns with a significant amount of shear (Ghee *et al.*, 1989; and Saatcioglu and Yalcin, 2003).

Positive envelopes (north push), negative envelopes (south push), and average envelopes (average of positive and negative envelopes) to the hysteresis curves given in Figures 4-28 through 4-36, respectively are given in Appendix E. The maximum drift of an average envelope corresponds to the smaller of the maximum drifts of the positive and negative envelopes.

4.3.3 Revised Yield Displacements

The experiments were performed with approximate yield displacements, as discussed previously. However, other methods of determining yield displacements need to be explored. Two methods for the determination of yield displacements were studied, as specified in Table 4.6. Method 1 (adapted from Ghee *et al.*, 1989) was applied in five alternative ways. Method 2 consists of developing an idealized bilinear (elasto-plastic) moment versus drift curve, that establishes a unique yield displacement, based on the average envelope curve of a specimen such that areas under the two curves up to the drift level corresponding to the peak moment are equal. This method for determining the yield displacements was used by Xu and Niu (2003) in the testing of reinforced concrete braced frames. It was also used by Lam *et al.* (2003) for rectangular columns with low confinement reinforcement tested under lateral cyclic loading and high axial loads. The methods (method 1 and method 2) are explored in the following:

4.3.3.1 Method 1 (alternative 1)

This procedure was used to determine the yield displacements to perform experiments and is considered approximate, as discussed previously.

4.3.3.2 Method 1 (alternative 2)

This alternative is similar to alternative 1 except that the values of M_{ycc} are based on confined concrete material curves obtained from a newly proposed confinement model that takes into

account axial and flexural stiffness of the confining elements (Chapter 5). The procedure was applied to all the columns (Appendix F). These figures also indicate how much the first cycles differ from the values of $0.75M_{ycc}$ determined with the new confinement model. The resulting values of yield displacements are reported in Table 4-6.

4.3.3.3 Method 1 (alternative 3)

In this alternative, the average envelope curves (as opposed to the first cycle) and values of the yield moments, M_{ycc} , determined using the new confinement model are used to determine the yield displacements of the test specimens. By using the envelope curve the point corresponding to a moment of exactly $0.75M_{ycc}$ can be selected for constructing the line that is extended to M_{ycc} to determine the yield displacement. The procedure was applied to all the columns (Appendix F) and the resulting values of yield displacements are reported in Table 4.6.

4.3.3.4 Method 1 (alternative 4)

In this alternative, the average envelope curves and nominal moment capacities, M_{nuc} , calculated based on the unconfined concrete material curves, are used to determine the yield displacements of the test specimens in a manner analogous to alternative 3. The procedure was applied to all the test specimens (Appendix F) and the resulting values of yield displacements are reported in Table 4.6.

4.3.3.5 Method 1 (alternative 5)

In this alternative, the average envelope curves and ultimate moment capacities, M_{ncc} (obtained experimentally), were used to determine the yield displacements of the test specimens. The procedure was applied to all the columns (Appendix F) and the resulting values of yield displacements are reported in Table 4.6.

4.3.3.6 Method 2

The average envelope curves to the moment vs. drift hysteresis are used to determine the yield displacements of the test specimen by establishing a bilinear curve such that the areas under the two curves up to the peak moment are equal. The procedure was applied to all the columns (Appendix F) and the resulting values of yield displacements are reported in Table 4.6. Due to

the unique shape of the curve for column CL0, three cases were considered. In the first case, the procedure is applied to the average envelope curve with respect to the first peak, which results in a yield displacement equal to 22 mm. In the second case, the procedure is applied with respect to the second peak, which results in a yield displacement equal to 29 mm. In the third case, the first peak of the envelope curve is truncated to form a smooth curve and the procedure is then applied with respect to the second (only remaining) peak, which results in a yield displacement equal to 32 mm. The third case might be appropriate for columns with shallow concrete cover.

4.3.4 Revised Hysteresis Curves

Various methods for determining yield displacements of the test specimens have been discussed in the previous section. However, method 1 (alternative 3) seems a more viable option in the present study as described before. Hysteresis curves presented in Figures 4-28 through 4-36 are therefore revised with respect to these yield displacements, and are shown in Figures 4-37 through 4-45. In these figures, the displacement ductility level specified for the first five cycles is in fact the average value (*i.e.*, average of 10 data points) since these cycles were conducted under load control.

4.3.5 Comparison of Envelope Curves

Figures 4-46 through 4-53 show the envelope curves to the moment versus drift hysteresis loops for each of the collared columns (CL1, CL2, CL3, CL4, CL5, CL6, CL7, and CL8, respectively) along with that of the control column (CL0) for comparison.

Before making the comparison of the envelope curves, it is important to describe the failure criterion and the basis on which the tests were ended in the laboratory. The criterion to end the tests was based on the significant reduction in horizontal and vertical load carrying capacity of the specimens. Generally, it was attributed to shear failure (column CL0) or rupture of longitudinal bars (columns CL2, CL5, CL6, CL7, and CL8). However, the upper limit of performing the cycles was 45. The specimens CL1, CL3, and CL4 sustained 45 cycles but could not be failed, even when the jacks were repositioned and the columns were pushed towards the north to a large displacement.

For the analysis of test results and for the comparison of the performance of the test specimens, a failure criterion is required and a 10% reduction in the peak moment capacity of the column (obtained from the average envelope curves) at the column base has been used. The peak moment capacity consists of moment due to horizontal loading and moment due to the $P-\Delta$

effect. Other researchers such as Sheikh and Houry (1993), Bayrak and Sheikh (1997), and Iacobucci *et al.* (2003) used a 10 or 20% reduction in the moment capacity as the failure criterion for the analysis of test results.

Figure 4-46 shows the envelope curve for columns CL0 and CL1. The average, north (positive), and south (negative) envelope curves for column CL1 are shown in Appendix E. The north envelope curve goes up to a higher drift level than the south envelope curve. The average envelope curve also goes up to the extreme drift level of the south envelope curve. The high ductility of this column is clear from the north envelope curve. No failure of this column was observed at the extreme north when pushed with the repositioned jack. Therefore, it was considered reasonable to extrapolate the average envelope curve (Appendix E) up to the extreme drift level of the north envelope. The average envelope curve of column CL4 was also extrapolated using the same procedure as that used for specimen CL1 (Appendix E).

Although column CL3 was pushed towards the north with the repositioned jack, due to the significant reduction in load at the end of 45 cycles, the north envelope curve was not extended up to the end of the final push. Figure 4-31 shows that it does not seem appropriate to extend the north envelope up to the extreme drift of the final push.

The comparison of the envelope curves is done with respect to the following parameters: secant stiffness at 0.25% drift, average peak moments, modulus of toughness, and normalized modulus of toughness, with both moduli calculated up to both the drift level corresponding to the average peak moments and up to that corresponding to 90% of the average peak moment in the descending branch (*i.e.*, the failure condition).

4.3.5.1 Secant Stiffness at 0.25% Drift

The secant stiffnesses of the test specimens are calculated at 0.25% drift and are reported in Table 4.8. The secant stiffness at 0.25% drift was also used by Canbolat *et al.* (2005) to normalize the secant stiffness of high-performance fibre-reinforced cement composite coupling beams at higher drift levels. Generally, the first diagonal cracks appeared at this level of drift in the coupling beams tested under cyclic loading in their experimental program. The reason for the selection of secant stiffness at 0.25% drift for normalization purposes is discussed at the end of this section.

It is assumed that the confinement will not be effective up to this level of drift. Hence, the secant stiffness depends on the strength of unconfined column concrete, f'_{co} ($f'_{co} = 0.85f'_c$),

properties of the steel, and the stresses in the concrete and steel longitudinal bars due to column axial loads. Using the strain compatibility analysis, the stress in the concrete and steel longitudinal bars under the column axial loads are calculated and are reported in Table 4.9. A portion of the total gravity load, P_{ta} , is carried by concrete, P_{ca} , and the remaining is carried by steel longitudinal bars, P_{sa} , which can be calculated from the following equations:

$$[4.2] \quad P_{ca} = \frac{P_{ta}}{1 + \frac{E_s A_{st}}{E_c A_c}}$$

$$[4.3] \quad P_{sa} = \frac{P_{ta}}{1 + \frac{E_c A_c}{E_s A_{st}}}$$

The corresponding stresses in the concrete and steel longitudinal bars can be calculated from the following equations:

$$[4.4] \quad f_{ca} = \frac{P_{ca}}{A_c}$$

$$[4.5] \quad f_{sa} = \frac{P_{sa}}{A_{st}}$$

where:

A_c = Area of concrete in column cross-section, $A_c = A_g - A_{st}$;

A_g = Gross area of column cross-section;

A_{st} = Total area of steel longitudinal bars;

E_s = Modulus of elasticity of steel longitudinal bars (see Table 4.3)

E_c = Secant modulus of elasticity of concrete; in the present study the modulus of elasticity of concrete is calculated as: $E_c = 3700\sqrt{f'_{co}}$;

f'_c = Compressive cylinder strength of concrete based on standard cylinders;

f_{ca}	=	stress in concrete due to axial load;
f'_{co}	=	compressive strength of column concrete, $f'_{co} = 0.85 f'_{co}$;
f_{sa}	=	stress in steel longitudinal bars due to axial load;
P_{ca}	=	Axial load carried by concrete;
P_{sa}	=	Axial load carried by steel longitudinal bars;
P_{ta}	=	Total axial load;

All the columns have same amount of longitudinal steel (8 bars of 25 mm dia.). The moduli of elasticity, E_s , of the steel longitudinal bars for all the columns are essentially identical (Table 4.3). Therefore, the longitudinal steel bars do not contribute to the variations in the secant stiffness of the test specimens at 0.25% drift. The ratios of concrete stress, f_{ca} , due to axial loads to the strength of the column concrete, f'_{co} , are also reported in Table 4.9.

According to Chen (1982), the stress vs. strain curve for unconfined concrete has a linear behaviour up to 30% of its maximum compressive strength. From 30% to 75% or 90% of the unconfined concrete strength, the stress vs. strain curve shows a gradual increase in curvature. Thereafter, it turns more sharply and reaches the peak point of the stress vs. strain curve of the unconfined concrete.

According to Table 4.9, the ratio of concrete stress due to axial load to the strength of the column concrete is highest for column CL0, which is 0.42. Although the curvature of the stress vs. strain curve of the concrete starts increasing beyond 30%, the increase in curvature up to the concrete stress equal to 42% of the concrete strength is assumed to be small. Therefore, the effect of the presence of the axial loads on the secant stiffness at 0.25% drift can be ignored. Hence, the variations in the secant stiffness of the test specimens at 0.25% drift depends on the variations in the modulus of elasticity of the concrete, E_c , due to the variations in the strength of the column concrete, f'_{co} .

It is to be noted that the stiffness of a structural member tends to reduce due to the presence of a compressive axial force. The Euler buckling loads for all the columns are reported in Table 4.9. The loads were calculated based on the secant modulus of elasticity of concrete and gross moment of inertia of the columns assuming a fixed support condition at the bottom and pinned at the point of application of horizontal loads. The unsupported lengths of columns CL0 through

CL4 are 1900 mm and the unsupported length of columns CL5 through CL8 are 750, 760, 755, and 775 mm, respectively. The effective lengths of these columns were obtained by multiplying the unsupported lengths by an effective length factor of 0.699. The axial loads on the columns are much lower than the corresponding Euler buckling loads (Table 4.9). Therefore, the effect of geometric stiffness on the behaviour of the columns is neglected.

The modulus of elasticity of concrete, E_c , for column CL0 is higher than those of columns CL1, CL2, CL3, and CL5 (Table 4.10). Therefore, the secant stiffness at 0.25% drift for column CL0 is higher than those of columns CL1, CL2, CL3, and CL5 (Table 4.9) as expected. This is also apparent from Figures 4-46, 4-47, 4-48, and 4-50.

The modulus of elasticity of concrete, E_c , is almost identical for columns CL0, CL4, and CL6. However, the secant stiffness at 0.25% drift for column CL0 is higher than that of the column CL4 and the secant stiffness of column CL6 is higher than that of column CL0.

The modulus of elasticity of concrete, E_c , for columns CL7 and CL8 are higher than that of the column CL0. The secant stiffness at 0.25% for column CL7 is higher than that of the column CL0, which makes sense. However, the secant stiffness of column CL8 is slightly lower than that of the column CL0.

The following are the possible reasons for these discrepancies:

- (1) There could be differences in the curvature distribution along the test regions of the columns. For the same rotations in the test region, if the curvature is uniformly distributed over a longer length, then the strain level in the concrete will be low as compared to if the curvature is distributed over a smaller length of the test region. The curvature distributions will be shown later in this chapter.
- (2) There could be small differences in column dimensions and the location of longitudinal bars of the columns due to construction errors.
- (3) There are variations in the cylinder strength of concrete. The standard deviations for the cylinder strength of concrete are given in Table 4.2.

Table 4.10 shows the cracking moments of the columns obtained using ACI 318-02. The tensile strengths (modulus of rupture, f_r) of concrete for the columns were calculated based on the strength of concrete in the columns, f'_{co} . For columns CL1 and CL5, the cracking moment can be calculated directly using the code equations because these columns carry no axial load. The

remaining columns (CL0, CL2, CL3, CL4, CL6, CL7, and CL8) have compressive stresses due to axial load (Table 4.9 and Table 4.10). The cracking moments for these columns were obtained by a trial-and-error procedure such that the resultant tensile stress in these columns under the combined effect of axial load and the moment becomes equal to the tensile strength of the concrete (modulus of rupture, f_r). The moment at 0.25% lateral drifts for these columns obtained using the experimental average envelope curves are also reported in this table for comparison. These moments are higher than the corresponding cracking moments. It is to be noted that columns without axial load (CL1 and CL5) have lower values of cracking moments and moments at 0.25% drifts as compared to the columns with axial load.

Theoretically, the stiffness of the concrete columns is higher before cracking. However, it was considered that accurate values of pre-cracked stiffness could not be obtained from the test data due to the low values of the cracking moment as compared to the peak moment, as can be seen from the curves in Figures 4-46 through 4-54. Therefore, in order to represent the initial stiffness of the columns, the secant stiffness at 0.25% drift was determined for all the columns. It is assumed that the moments corresponding to this level of drift are free from the effects of confinement, similar to the cracking moments.

In subsequent sections, peak moments, moduli of toughness up to the peak moments, and moduli of toughness up to failure of the columns are presented, which all include the influence of the level of confinement and the properties of the unconfined concrete. In order to observe the benefits of confinement on the cyclic behaviour of the columns, the influence of the properties of the unconfined concrete need to be eliminated. Therefore, the peak moments are normalized with respect to the moments at 0.25% drift. The moduli of toughness up to peak and up to failure are normalized with respect to the moduli of toughness up to 0.25% drift.

4.3.5.2 Average Peak Moments

The peak moments and the corresponding drifts (%) from the average envelope curves are reported in Table 4.8. Generally, the peak moments of the collared columns are higher than that of the control column (Figure 4-54). The differences in peak moment from column to column are partly due to the inherent strength of the concrete itself and partly due to the differences in the level of confinement. It is assumed that the contribution of the steel to the peak moment is the same in all the columns. It is also assumed that the confinement is not effective up to 0.25% drift. The effect of the inherent strength of the concrete on the peak moments can therefore be taken out by normalizing the peak moments with respect to the moment at 0.25% drift of the corresponding columns. These normalized peak moments are also reported in Table 4.8. The

normalized peak moments of the collared columns are higher than that of the control column (Figure 4-55), indicating the beneficial effects of the collar confinement.

4.3.5.3 Modulus of Toughness

Modulus of toughness is a measure of ductility. The modulus of toughness is equal to the area under the moment vs. drift envelope curves. The moduli of toughness were calculated up to the peak moments and up to 90% of the peak moments in the descending branch of the envelope curves. The values of moduli of toughness obtained from average envelope curves are reported in Table 4.11 and are plotted in Figure 4-56. These values of modulus of toughness include both the effect of strength of concrete and the level of confinement.

4.3.5.4 Normalized Modulus of Toughness

In order to eliminate the effect of strength of concrete from the modulus of toughness, the values of modulus of toughness of a certain specimen are normalized with respect to the modulus of toughness up to 0.25% drift. The normalized moduli of toughness for the test specimens are also reported in Table 4.11 and are depicted in Figure 4-57. Generally, the normalized moduli of toughness for collared columns are higher than that of the control column CL0.

4.3.6 Stiffness Retention

Stiffness degradation of all the nine specimens was evaluated by means of the secant stiffness. Secant stiffnesses of the test specimens were calculated at different levels of drifts with the help of the average envelope curves shown in Appendix E. Other researchers such as Xu and Niu (2003) and Canbolat *et al.* (2005) calculated the secant stiffness with the help of peak values of the cycles at each displacement ductility level.

To account for the variations in the strength of concrete from specimen to specimen, the secant stiffness values were normalized with respect to the secant stiffness values at 0.25% drift for each specimen. Secant stiffnesses at 0.25% drifts were also used for normalization by Canbolat *et al.* (2005) in the evaluation of stiffness degradation of high-performance fibre-reinforced cement composite coupling beams.

The normalized secant stiffness values were plotted with respect to the drifts (%) for all the test specimens. Figures 4-58 through 4-65 show the normalized secant stiffness vs. drift (%) curves

for collared columns along with that of the control column CL0. It is evident from these figures that the level of stiffness retention of the collared columns is higher than that of the control column CL0 (conventional column). This is one distinct advantage of collared columns over conventional columns.

4.3.7 Energy Dissipation Characteristics

The energy dissipation capability of structures is of paramount importance in their performance under cyclic loading. There are various ways to evaluate the energy dissipation capacity of structures. In the present research, the energy dissipation of the test specimens was evaluated by calculating the area enclosed by the moment vs. drift (%) hysteresis loops. The energy dissipation characteristics of the specimens can be evaluated in terms of energy dissipation per cycle, cumulative energy dissipation vs. cycle number, and normalized cumulative energy dissipation vs. cycle number.

4.3.7.1 Energy Dissipation Per Cycle

Figures 4-66 through 4-74 show the bar charts of energy dissipated per cycle for all the nine columns (CL0 to CL8). The energy dissipated in a cycle is the area enclosed by the moment vs. drift hysteresis loop corresponding to that cycle. The numerical values of the energy dissipated per cycle are given in Appendix G. Theoretically, the energy dissipation in the first cycle (primary cycle) out of a total of five cycles at a certain displacement ductility level is more than that of any one of the remaining four cycles (secondary cycles) at that ductility level. These figures show that in some cases, a secondary cycle shows more energy dissipation than does the primary cycle. This is attributed to the small fluctuation in gravity loads and the slight relative difference in amplitude of the cycles at a certain ductility level. In order to demonstrate that the energy dissipated in a primary cycle is more than that of a secondary cycle of the same amplitude, the energy dissipated in the 16th cycle is compared with the energy dissipated in the 17th cycle for all the specimens. The ratios of energy dissipated in cycle 16 to energy dissipated in cycle 17 are about 1.50, 1.23, 1.06, 1.19, 1.28, 1.36, 1.23, 1.23, and 1.09 for columns CL0, CL1, CL2, CL3, CL4, CL5, CL6, CL7, and CL8, respectively. The ratio is higher for column CL0 because of the additional effect due to the large difference in gravity load for cycle 16 and cycle 17 for this specimen. For higher gravity loads, the energy dissipation is higher provided the remaining influencing parameters are kept constant.

Hence, the energy dissipation in a cycle for a column under cyclic loading depends on the displacement amplitude, which is multiple of the yield displacement, and the axial load. The

energy dissipation in a cycle increases with the increase of displacement amplitude and/or axial load. The energy dissipation in the primary cycles is always higher than that of secondary cycles at a particular displacement ductility. In addition, if a large number of cycles are performed at the same displacement ductility, the energy dissipation in a cycle gradually decreases due to degradation in strength and stiffness (Figures 4-69 and 4-70).

4.3.7.2 Cumulative Energy Dissipated vs. Cycle Number

Figures 4-75(a) through 4-82(a) show the cumulative energy dissipated vs. cycle number for all the collared columns along with that of the column CL0. The numerical values of the cumulative energy dissipated per cycle are given in Appendix G.

The relationship between cumulative energy dissipated and cycle number has been used to compare the energy dissipation characteristics of reinforced concrete braced frames (Xu and Niu, 2003). The method has also been used in the literature to characterize the energy dissipation characteristics of columns under cyclic loading. The energy dissipation characteristics of the columns are influenced by various factors such as yield drift, axial load, and the peak moment capacity. The peak moment capacities of the columns include the influence of the properties of the unconfined column concrete and the properties of the steel longitudinal bars of the columns. The influence of these parameters on the energy dissipation characteristics is discussed in the following:

The yield displacements used to conduct the tests are given in Table 4.6 (method 1 (alternative 1)). The heights of the point of application of the horizontal load from the top of the footing, H_2 , are given in Table 4.1. Knowing the yield displacements and the values of H_2 , the yield drifts of the test specimens CL0, CL1, CL2, CL3, CL4, CL5, CL6, CL7, and CL8, expressed in percentage, are calculated to be 1.58, 1.21, 2.16, 2.00, 1.47, 1.07, 1.12, 1.52, and 1.42, respectively.

Figures 4-75(a) shows that the rate of increase of cumulative energy dissipation with respect to cycle number for column CL0 is higher than that of column CL1. This is attributed to the following:

- (1) The yield drift of column CL0 is higher than that of column CL1.
- (2) Column CL0 was tested under heavy axial load, whereas column CL1 was tested without axial load;

- (3) The peak moment capacity, M_{ncc} , of the columns also influence their energy dissipation characteristics. In the present case, the peak moment capacity of column CL0 is lower than that of column CL1. However, its influence on the energy dissipation characteristics of the columns does not appear because of the dominating effect of the other two factors.

Although the cumulative energy dissipated by both columns at the end of the tests is high, it is higher for column CL0. However, column CL1 did not fail after sustaining 45 cycles. Then the stroke of the jack was adjusted and the column was pushed towards north. If the energy dissipated by column CL1 after the 45th cycle is added to the cumulative energy dissipated up to 45th cycle, then the cumulative energy dissipated by column CL1 at the end of the test becomes higher than that of column CL0. The improved energy dissipation characteristics of column CL1 as compared to those of column CL0 are derived from a combination of reduced axial load, which tends to reduce the rate of deterioration, and collar confinement.

Figures 4-76(a) shows the relationships between the cumulative energy dissipated vs. cycle number for columns CL2 and CL0. The rate of increase of cumulative energy dissipation versus cycle number for column CL2 is higher than that of column CL0 because of the higher yield drift and higher nominal moment capacity of column CL2. However, the cumulative energy dissipated by column CL2 is much less than that of column CL0. This poor performance of column CL2 is attributed to the wider spacing of collars in this column.

The rate of increase of cumulative energy dissipation with respect to cycle number for columns CL3 and CL0 are almost the same (Figure 4-77(a)). The cumulative energy dissipation at the end of the test for column CL3 is slightly higher than that of column CL0 (Figure 4-77(a)). It can be concluded that the energy dissipation characteristics of both columns are essentially identical.

Figure 4-78(a) shows the cumulative energy dissipated versus cycle number for columns CL0 and CL4. The cumulative energy dissipated for both columns are comparable at the end of the tests. The test for column CL4 was stopped prematurely. If the energy dissipated by column CL4 after the 45th cycle were to be added, the total energy dissipated by this column would become higher than that of column CL0.

The cumulative energy dissipated at the end of the tests by collared columns with short shear-spans (CL5, CL6, CL7, and CL8) are much lower than that of column CL0

(Figures 4-79(a), 4-80(a), 4-81(a) 4-82(a)). This means that the short shear-span has an adverse effect on the energy dissipation characteristics of the collared columns.

From the above exercise, it can be concluded that the slopes of the energy dissipation curves (cumulative energy dissipation versus cycle number) depend on the magnitude of axial loads, yield drifts, and the nominal moment capacities of the columns. A higher slope of this curve does not guarantee that the cumulative energy dissipation at the end of the test will also be higher. The most important criterion for comparing the energy dissipation characteristics of the columns under cyclic loading is the total energy dissipated by the columns at the end of the tests or at failure. With respect to this criterion, it can be concluded that the energy dissipation characteristics of the collared columns with closely spaced collars are better than, or at least similar, to those of conventional columns (which satisfy the plastic hinge requirements of the codes). However, the energy dissipation capabilities of the collared columns with widely spaced collars were much less than that of conventional column. Similarly collared columns with short shear-spans exhibited poor energy dissipation characteristics as compared to that of the conventional column CL0 that had a long shear span.

4.3.7.3 Normalized Cumulative Energy Dissipated vs. Cycle Number

Similar to the relationship between cumulative energy dissipated and cycle number discussed in the previous section, the relationship between the normalized cumulative energy dissipated and cycle number is also used to characterize the energy dissipation characteristics of the reinforced concrete columns under cyclic loading. This method is less sensitive to differences in the yield displacements.

A procedure for normalizing the cumulative energy dissipation for lateral force vs. lateral displacement curves is given by the following equation (Lukkunaprasit and Sittipunt, 2003):

$$[4.6] \quad E_N = \frac{\left(\sum_{i=1}^n E_i \right)}{H_{max} \Delta_y}$$

where H_{max} is the maximum horizontal load applied. In the present research, the hysteresis curves are presented in terms of base moment vs. lateral drift (%). Therefore, Equation 4.6 is translated to the following for normalizing the cumulative energy dissipated:

$$[4.7] \quad E_N = \frac{\left(\sum_{i=1}^n E_i \right)}{(M_{max} \times yield \ drift)}$$

Figures 4-75(b) through 4-82(b) show the normalized cumulative energy dissipated vs. cycle number for all the collared columns CL1, CL2, CL3, CL4, CL5, CL6, CL7, and CL8 along with that of the control column CL0. When plotted in normalized form, the curve for the control column CL0 is higher than those of all the collared columns. The numerical values of the cumulative energy dissipated per cycle are also given in Appendix-G. The normalized cumulative energy dissipation characteristics of each collared column are compared with that of the control column in the following.

Figure 4-75(b) shows the normalized cumulative energy dissipated versus cycle number for columns CL0 and CL1. The rate of increase of normalized cumulative energy dissipated for both curves is almost the same after the 25th cycle. The normalized cumulative energy dissipated at the end of the test for column CL0 is higher than that of column CL1 at the end of 45th cycle. However, column CL1 did not fail after sustaining 45 cycles and after adjusting the stroke of the horizontal jack, this column was further pushed towards north but still the column could not be failed. If this additional normalized energy is added to normalized cumulative energy dissipated at 45th cycle, the normalized cumulative energy dissipation for column CL1 at the end of the tests will become higher than that of column CL0. This better performance of column CL1 as compared to that of column CL0, with respect to energy dissipation, could be partly due to the absence of axial load in column CL1 and partly due to the benefits of collar confinement.

Figure 4-76(b) shows that the normalized cumulative energy dissipation characteristics of column CL0 are much better than those of column CL2. This is because of the wider spacing of the collars in column CL2.

Figure 4-77(b) shows that the energy dissipation characteristics of column CL0 are better than those of column CL3.

It appears from Figure 4-78(b) that the energy dissipation characteristics of column CL0 are better than those of column CL4. However, column CL4 could not be failed after sustaining 45 cycles. Thereafter, it was pushed towards the north with repositioned jacks. If the normalized cumulative energy dissipated by column CL4 after 45 cycles is added, then the energy dissipated at the end of test becomes higher than that of column CL0. Hence, it appears that the energy

dissipation characteristics of columns with closely spaced collars are indeed better than those of column CL0.

Figures 4-79(b) through 4-82(b) show the relationship between normalized cumulative energy dissipated versus cycle number for columns CL5 through CL8, respectively, along with that of the control column CL0. The normalized cumulative energy dissipated at the end of the test for column CL0 is higher than that of columns CL5 through CL8. It is to be noted that the collared columns CL5 through CL8 were tested with a short shear-span. The short shear-span columns generally exhibit brittle behaviour and dissipate less energy as compared to those with a long shear-span. Hence, the short shear-span collared columns are excluded from the comparison between the conventional column and collared columns with respect to energy dissipation characteristics.

Based on the above, it can be concluded that conventional columns with closely spaced ties and collared columns with the closely spaced collars exhibit comparable energy dissipation characteristics. However, when accounting for the effect of reaching the limit of jack stroke in the tests, a promising potential of collared columns with closely spaced collars is witnessed that such collared columns would dissipate more energy at the end of the tests or at failures as compared to that of conventional columns.

It is noteworthy that the conclusions drawn based on the cumulative energy dissipation characteristics and the normalized cumulative energy dissipation characteristics are the same.

4.3.8 Equivalent Viscous Damping Ratio

Damping helps to reduce the amplitude of vibration of structures when subjected to excitations. Strong earthquake excitations may drive the structures to vibrate in the inelastic range. For these structures, the equivalent damping ratio, β_{eq} , consists of two parts as given by the following equation (ATC-40, 1996):

$$[4.8] \quad \beta_{eq} = \beta_o + \beta_i$$

where β_i is the inherent viscous damping ratio that is always present whether the structure vibrates in the elastic or inelastic range and is usually assigned a constant value of 0.05 and β_o is the hysteretic damping ratio, represented as equivalent viscous damping, that is associated

with a full hysteretic loop area at a certain value of lateral drift. The value of β_0 is calculated as follows (Chopra, 1995):

$$[4.9] \quad \beta_0 = \frac{E_i}{4\pi E_e}$$

where E_i is the energy dissipated in cycle i at a certain value of lateral drift and E_e is the maximum elastic strain energy corresponding to the cycle. Knowing the moment and the drift corresponding to the peaks of the cycle i , the maximum elastic strain energy, E_e , is calculated as follows:

$$[4.10] \quad E_e = \frac{(M_{peak})_i \times (Maximum\ lateral\ drift)_i}{2}$$

For the tests reported herein, the calculations of hysteretic damping ratio, β_0 (Equation 4.9), were based on parameters that were obtained by averaging the results from all the available loops for a particular ductility level. Figures 4-83 through 4-90 show the relationships between the hysteretic damping ratio, β_0 , and the corresponding lateral drifts for the collared columns along with that of the control column CL0 for comparison.

It is clear from these figures that the hysteretic damping ratio increases with the increase of displacement amplitude or the increase of lateral drift. It is also evident that the hysteretic damping ratios for the collared columns are significantly high. However, at a certain level of lateral drift, the hysteresis damping ratio exhibited by control column is generally higher than that of the collared columns. This is attributed to the relatively higher axial load in the first 16 cycles for the control column. As explained previously, the energy dissipation in a cycle at a certain level of displacement ductility depends on the magnitude of axial load, in addition to other parameters; the energy dissipation is higher for higher axial loads.

Although the hysteretic damping ratio has its importance in nonlinear dynamic analyses of structures, nevertheless, it appears to be the best method to determine the energy dissipation characteristics of the specimens for comparison with each other. Due to the presence of maximum strain energy term in the denominator of Equation 4.9, the effect of displacement amplitude and the effect of peak moment of a cycle are automatically normalized.

4.3.9 Curvature Distributions in the Test Regions

Curvature distributions along the test regions of the columns give insight into the nature of the flexural hinging. The curvature distributions can be determined in two ways: (1) using strains of the longitudinal bars of the column; and (2) using rotation of the collars.

The curvature distributions along the test regions can be also be determined using instruments that were placed externally at different heights in the test regions and this method is used in the present research. Since these instruments were attached to the collars, only the results for the collared columns are presented. A summary of the instrumentation used for measuring the rotations on the collared columns is given in Table 4.4.

The average curvature of a segment between the centrelines of any two collars was taken as the difference in rotation (radians) of the collars divided by the length of the segment. Similarly, the average curvatures of all the segments in the test region are determined and then plotted with respect to the distance from the top of the footing to the mid-depth of the respective segments. The average curvature for the north (push) and south (pull) directions are determined separately and then averaged, however no significant difference in the curvature distributions for the directions was found. Curvature distributions along the test regions were determined at different levels of displacement ductility to study the associated variations.

Figures 4-91 through 4-98 show the curvature distributions along the test regions of the collared columns. It can be concluded from the figures that hinging takes place in the lower half of the test region and the maximum curvature takes place below the first collar in columns CL1, CL3, CL4, CL5, CL6, CL7, and CL8. In column CL2, the maximum curvature at large displacement ductilities takes place between the first and second collar (Figure 4-92). The maximum damage and the rupture of the vertical bars of this column took place in this region (Figure 4-20). It is to be noted that the curvature distributions presented are not only due to flexural deformations. The effect of rotations due to anchorage slip at the interface between the column and footing is also present in these diagrams.

The distribution of energy dissipation mechanisms in the test regions of the collared columns (CL1 through CL8) are given in Appendix H.

4.3.10 Other Ductility Parameters

There are several ways to express the ductility and deformability of reinforced concrete sections and members and some of them have been discussed previously in this chapter. In this section, the ductility parameters suggested by Sheikh and Houry (1993) are used to evaluate the performance of sections of the test specimens, These are the curvature ductility factor, μ_ϕ , cumulative ductility ratio, N_ϕ , and energy damage indicator, E_d , defined in the following:

Curvature ductility factor, μ_ϕ :

$$[4.11] \quad \mu_\phi = \frac{\phi_1}{\phi_2}$$

Cumulative ductility ratio, N_ϕ :

$$[4.12] \quad N_\phi = \sum_{i=1}^{i=m} \frac{\phi_i}{\phi_1}$$

Cumulative energy damage indicator, E_d :

$$[4.13] \quad E_d = \frac{1}{M_{max}\phi_1} \sum_{i=1}^{i=m} e_i \frac{L_f}{h} \left(\frac{S_i}{S_1} \right) \left(\frac{\phi_i}{\phi_1} \right)^2$$

The definitions of all terms in these equations are given in Figure 4-99 except L_f and h , which represent, respectively, the length of the most damaged region of the column observed during testing and the depth of the column section.

In the present study, the lengths of the most damaged regions of the test specimens, L_f , were estimated from observations during the tests, curvature distributions along the test regions (Figure 4-91 through 4-98), and the distribution of energy dissipation along the column lengths (Appendix H). These lengths are reported in Table 4.12. The locations of the collars measured from the top of the footing are given in Table 4.4.

In column CL0, the length of a relatively undamaged core region attributed to additional confinement provided by the footing is taken as 300 mm measured from the top of footing. The most damaged region of this column extends from 300 to 550 mm.

In columns CL1, CL5, CL7, and CL8, most of the damage occurs below the 2nd collar. The clear distances from the top of the footings to the bottom of the 2nd collars are taken as the most damaged regions of these columns.

In column CL2, most of the damage occurred between the 1st and 2nd collar, the clear distance of which is taken as the most damaged region of this column.

In columns CL3 and CL4, most of the damage occurred below the 3rd collar. The clear distances from the top of footings to the bottom of the 3rd collars are taken as the most damaged region of these columns.

In column CL6, most of the damage occurred below the 1st collar. The clear distance from the top of the footing to the bottom of the 1st collar is taken as the most damaged region of this column.

In order to calculate the ductility parameters for the sectional performance of the test specimens, moment-versus-curvature hysteresis curves are required. The curvatures could be calculated across the most damaged regions of the columns, using the rotation measurements described previously, and assumed uniform in those regions, and the moments due to horizontal and vertical loading could be calculated at mid-height of those same regions. However, in the present research not all the collars were instrumented for rotation measurements and in column CL0, these measurements were not obtained. To maintain consistency in the location of points (in the test regions) about which moments, M , are calculated, cable transducers located at the top ends of the test regions (Table 4.4) are used to calculate the curvatures, ϕ , over the test regions of the columns. (The moment M at the midpoint of the test region is clearly smaller than the moment at the base of the corresponding column.) The locations of the cable transducers are close, but not exactly the same, for all the specimens. Based on these instruments, the moments-versus-curvature hysteresis curves for columns CL0 through CL8 were developed and are given in Appendix I. The envelopes to these hystereses were determined both for the north and south push, the averages of which are depicted in Figures 4-100 through 4-108. In the cases of columns CL1 (Figure 4-101), CL4 (Figure 4-104), and CL8 (Figure 4-108), the terminate curvatures for the north and south envelopes were significantly different, so the average curvature for these columns can be obtained only up to the smaller of the two terminate curvatures. The remaining part of the average curvature curve for these columns was projected,

keeping in view the trend of the constituent envelope curve with the higher terminate curvature. (It is to be noted that in the case of the envelope curve to the moment at the column base versus drift hysteresis for column CL8, shown in Figure 4-53, this type of projection was not required because the moment corresponding to the terminate point of the curve is well below 90% of its peak moment.)

In the procedure proposed by Sheikh and Khoury (1993), S_1 represents the initial slope of the average curvature curve. In the present research, a slight modification to the procedure was made, where S_1 represents the slope of a secant line that passes through the origin and a point on the average envelope curve having an abscissa equal to 2.5×10^{-6} (rad/mm). This secant line is very close to the initial slope, as is clear from Figures 4-100 through 4-102. The reasons for this modification are:

- (1) The initial slope lines are drawn through judgement and errors may be introduced while applying the procedure from curve to curve; and
- (2) They are highly influenced by the interval of data points in the very first cycle of loading. If the data points of the first cycle are widely spaced, the initial slope lines will, in fact, become a secant line. In addition, the interval of data points can vary from curve to curve and influence the initial slope lines.

The proposed modification overcomes these difficulties to a certain extent. The slopes, S_1 , of the secant lines drawn to the envelope curves are given in Table 4.13. The curvature, φ_1 , corresponds to the point of intersection of the secant line and a horizontal line corresponding to the peak moment of the envelope curve. The curvature, φ_2 , represents the abscissa of the point on the average moment-versus-curvature-envelope curve in the descending branch for which the moment is 90% of the peak moment of the envelope curve (Figures 4-105, 4-106, 4-108). In cases where the moment does not drop to 90% of the peak moment due to any reason, the terminate curvature of the average envelope curve is taken as φ_2 (Figures 4-100, 4-101, 4-102, 4-103, 4-104, and 4-107). The ratio of φ_2 to φ_1 represents the curvature ductility factor, μ_φ . The values of φ_1 , φ_2 , and μ_φ for all the columns are reported in Table 4.13. The starred values of φ_2 , and μ_φ for columns CL0 through CL4 are lower bounds, since the columns did not fail completely.

Figures 4-109 through 4-116 show the relationships between the cumulative ductility ratios, N_ϕ (Equation 4.12), and the cycle numbers for columns CL1 through CL8 along with that of the control column, CL0, for comparison. The curve for the control column is higher than that of the collared columns in all cases. This trend is attributed principally to the relatively lower value of ϕ_1 for column CL0 (Table 4.13).

Figures 4-117 through 4-124 show the relationships between the cumulative energy damage indicator, E_d (Equation 4.13), and the cycle numbers for columns CL1 through CL8 along with that of the control column, CL0, for comparison. The curve for the control column CL0 is much higher than those of the collared columns. The main reason for this trend is considered to be the relatively lower value of ϕ_1 for column CL0 (Table 4.13) and, moreover, that the term $\left(\frac{\phi_i}{\phi_1}\right)$ in the expression for E_d (Equation 4.14) is squared. Although the term $\left(\frac{S_i}{S_1}\right)$ has a reduction effect on the value of E_d for column CL0 because of the relatively higher values of S_1 for this column (Table 4.13), its influence is dominated by the squared values of the term $\left(\frac{\phi_i}{\phi_1}\right)$. The numerical values of the cumulative ductility ratio, N_ϕ , and the cumulative energy damage indicator, E_d , for columns CL0 through CL8 are given in Appendix J.

4.4 Effect of Various Parameters on Column Behaviour

In this section, the effect of several key parameters—axial load, collar spacing, size of collar, and shear-span—on the behaviour of columns confined externally by HSS collars, is studied.

4.4.1 Effect of Axial Load

There are different ways to express the axial load index such as:

$$\frac{P}{0.85f'_cA_g}; \frac{P}{P_0}; \text{ and } \frac{f_{ca}}{f'_{co}}$$

The values of these axial load indices for each of the columns tested are presented in Table 4.14. Column CL0 was subjected to two levels of axial load. Hence, two values for each of the axial load indices are reported for this column. The ratio $\frac{P}{P_0}$ is considered to be the most appropriate way of expressing the axial load index for this purpose because it can be used directly to define the location of the failure point of the column in an axial load versus moment interaction diagram.

Axial load produces three primary effects: (1) it affects the moment capacity of the columns; (2) it produces a $P-\Delta$ effect under lateral displacement (the moment due to $P-\Delta$ is included in the total column moment in the present research); and (3) it increases the compressive strain level in the column resulting in accelerated deterioration taking place under cyclic loading.

In order to study the effect of the variation of axial load on the behaviour of the collared columns, the results of two columns with long shear-spans, CL1 and CL3, and the results of two columns with short shear-spans, CL5 and CL7, are compared. Columns CL1 and CL5 were tested with zero axial load and columns CL3 and CL7 were tested under an axial load of 720 kN. All of these columns were provided with steel collars of HSS 76x51x6.35 mm at a centre-to-centre spacing of 101 mm; therefore, the axial load is the only parameter varied in these comparisons other than the inherent variation in concrete material strength.

4.4.1.1 Comparison of Columns CL1 and CL3

Figures 4-38 and 4-40 show moment-versus-drift hysteresis curves for columns CL1 and CL3, respectively. In testing columns CL1 and CL3, a total of 20 and 25 cycles, respectively, were performed at the stroke limit of the horizontal jacks during which some reduction in strength took place in column CL1 but the reduction in strength in column CL3 was relatively large. By pushing these columns towards the north with adjusted-stroke-jacks at the end of the tests, increases in strength and ductility were witnessed for column CL1 but for column CL3, the large displacement was accompanied by a strength (moment capacity) reduction. This stark difference in behaviour at large displacements is attributed primarily to the difference in axial load.

Figure 4-125 shows the envelope curves to the base moment versus lateral drift hysteresis curves of column CL1 and CL3. It has been demonstrated previously that the initial slope of the curve for column CL3 is not affected significantly by the presence of axial load because the stress on the concrete is very low as compared to the strength of the concrete. Therefore, the difference in the initial slopes of the two curves can be attributed primarily to the difference in the

secant modulus, which is a function of the material strength. Conversely, at ultimate conditions the presence of axial load can have an effect on the performance of the column. Considering the confined concrete material curves, the moments at the first yield of the tensile reinforcing bars, M_{ycc} , were calculated for all the columns and are reported in Table 4.5. The existence of M_{ycc} for a column means that the yielding of tensile steel takes place before the failure of the confined concrete. It means that the column CL3 is under-reinforced. In general, if the axial load of an under-reinforced column is increased, the corresponding moment capacity of the column increases. The fact that the envelope curve for column CL3 is higher than that of column CL1 (Figure 4-125) is attributed primarily to the presence of the axial load. The effect of the difference in the confined concrete strength for these columns (Figure 4-197) on the moment strength of the columns is considered minimal because both of these column sections are essentially under-reinforced.

The normalized peak moments of column CL1 and CL3 are 7.6 and 5.65, respectively (Table 4.8), The normalized moduli of toughness for columns CL1 and CL3 up to peak moment conditions are 468.23 and 376.44, respectively (Table 4.11), and the normalized moduli of toughness up to the end of tests for column CL1 and CL3 are 772.84 and 376.44, respectively (Table 4.11). The lower values of normalized peak moment, normalized modulus of toughness up to peak moment condition, and the normalized modulus of toughness up to the end of the test for column CL3 as compared to that of CL1 are attributed to the following: (1) the full capacity of column CL3 could not be explored due to the exhaustion of the stroke limits of the horizontal jacks; (2) both for column CL1 and CL3 a large number of cycles was performed at the stroke limits (20 and 25, respectively) and due to the presence of axial load, the rate of degradation in strength and stiffness for column CL3 was much higher than that of column CL1. Moreover, it increased with the increase in the number of cycles at the stroke limit of the jacks (refer to Figures 4-38 and 4-40).

Figure 4-126 shows the relationship between normalized secant stiffness and lateral drift (%) for columns CL1 and CL3. This figure depicts that the reduction in normalized secant stiffness with the increase of lateral drift (%) is more rapid for column CL3 than column CL1, although at small drifts the curves are nearly identical. The difference at larger drifts is attributed to the effect of axial load acting on the displaced configuration.

Figure 4-127 shows the relationship between cumulative dissipated energy versus cycle number for columns CL1 and CL3. The curve for column CL3 is higher than that of column CL1 and the rate of increase of energy dissipation with respect to cycle number is higher for column CL3 than column CL1. There are three reasons for this behaviour: (1) the unconfined concrete strength for

column CL3 is higher than that of column CL1; (2) the experimental yield displacement for column CL3 ($\Delta_y = 38$ mm) is higher than that of column CL1 ($\Delta_y = 23$ mm), which results in greater energy dissipated in an equivalent cycle; and (3) the presence of axial load in column CL3 tends to increase its moment capacity, as discussed previously, although the difference in the cumulative energies is considered to be dominated by the other two effects. The deteriorating effect of axial load on ductility is not evident from this figure because both tests were stopped prematurely after pushing the columns towards north with jacks having adjusted strokes after performing 45 complete cycles. Had the stroke limits of the jack not exhausted and the tests not stopped prematurely, the cumulative energy dissipated by column CL1 at the end of the test would likely have been greater than that of column CL3.

To offset the effects of differences in yield displacements, axial load, and unconfined concrete strengths for column CL1 and CL3 on the energy dissipation characteristics, the cumulative energy dissipated is normalized with respect to the maximum moment capacity and the experimental yield drift (*i.e.*, based on the yield displacement used in the test) of the respective column. Figure 4-128 shows the relationship between cumulative normalized dissipated energy versus cycle number for columns CL1 and CL3. The curve for column CL3 is higher up to the end of 27 cycles, then it becomes lower than that of column CL1. This reduction in cumulative normalized energy dissipation towards the end of the test for column CL3 as compared to CL1 can be attributed to the deteriorating effect of axial load. Cumulative normalized energy dissipation is considered to be a better characteristic than cumulative energy dissipation for representing the energy dissipation characteristics of a column.

Figure 4-129 shows the relationship between the hysteretic damping ratio and lateral drift (%) for columns CL1 and CL3. The hysteretic damping ratio of column CL1 is generally slightly higher than that of column CL3. It is anticipated that beyond a lateral drift of 10%, the difference between the two curves will become more pronounced, with column CL3 exhibiting a lower hysteretic damping ratio than CL1. This reduction in hysteretic damping for column CL3 is due to the deteriorating effect of the axial load at large drifts.

The lower-bound values of curvature ductility for columns CL1 and CL3 are 11.92 and 9.78, respectively (Table 4.13). Although these values are both lower bounds, it is believed that they are close to their ductility limits. At the point corresponding to ϕ_2 , the envelope curve for column CL1 (Figure 4-101) is declining to a point near to the failure criterion. Although the envelope curve for column CL3 (Figure 4-103) appears to be well short of the actual peak, the final push with the repositioned jacks showed a rapid decline in capacity. As the values of curvature ductility reported for column CL1 and CL3 are lower-bound, it not possible to make a point on the effect

of axial load on the curvature ductility of the columns. Figure 4-130 shows the relationship between the cumulative ductility ratio, N_ϕ , and cycle numbers for columns CL1 and CL3. The curve for column CL3 is higher than that of column CL1. That is, the trend shown by these curves is opposite to the existing concept that the axial load has a deteriorating effect on the ductility. This is because of the following reasons:

- (1) The experimental yield displacement of column CL3 is 38 mm (alternative 1(method 1), Table 4.6) as compared to the true yield displacement of 32 mm (alternative 3 (method 1, Table 4.6) due to which this column will accumulate higher values of curvatures in the cycles. In the case of column CL1, the experimental yield displacement is 23 mm (alternative 1 (method 1), Table 4.6) as compared to the true yield displacement of 30 mm (alternative 3 (method 1, Table 4.6) due to which this column will accumulate lower values of curvatures in the cycles.
- (2) The value of curvature ϕ_1 is lower for column CL3 as compared to that of CL1 (Table 4.13).

The cumulative energy damage indicator, E_d , is another parameter for representing ductility. Figure 4-131 shows the relationship between the cumulative energy damage indicator and cycle numbers for columns CL1 and CL3. The curve for column CL3 is higher than that of column CL1. This trend is also opposite to the existing concept that the axial load has deteriorating effect on ductility. Some reasons for this discrepancy have already been given in the discussion of the cumulative ductility ratio, N_ϕ . Another reason that contributes to this discrepancy is the larger length of the most damaged region, L_f , for column CL3 as compared to that for column CL1 (Table 4.12).

4.4.1.2 Comparison of Columns CL5 and CL7

The axial load indices $\frac{P}{P_0}$ for columns CL5 and CL7 are zero and 0.15, respectively (Table 4-14). Figures 4-42 and 4-44 show moment-versus-drift hysteresis curves for columns CL5 and CL7, respectively. Figure 4-132 shows the envelope curves to the base moment versus lateral drift hysteresis curves for these columns. The initial slope of the envelope curve for column CL7 is steeper than that of the curve for column CL5. This is due to the difference in the strength of concrete for these columns since the initial slope is not affected by the presence of

axial load. The moment capacity of column CL7 is higher than that of column CL5 due to the following reasons: (1) the strength of concrete for column CL7 is higher than that of CL5; and (2) column CL7 is subjected to an axial load that falls in the range of zero to the balanced load condition in the moment-versus-axial-load interaction diagram for the column, considering the confined concrete material curve. Hence, the presence of axial load enhances the moment capacity of this column.

The normalized moduli of toughness for columns CL5 and CL7 up to peak moment conditions are 107.95 and 122.00, respectively (Table 4.11), and the normalized moduli of toughness up to the end of tests for column CL5 and CL7 are 228.92 and 329.51, respectively (Table 4.11). The normalized moduli of toughness has increased with the increase of axial load. This is consistent with the other ductility parameters given subsequently.

Figure 4-133 shows the relationship between normalized secant stiffness and lateral drift (%) for columns CL5 and CL7. This figure depicts that the reduction in normalized secant stiffness with the increase of lateral drift (%) is more rapid for column CL7 than for column CL5, although at small drifts the curves are nearly identical. The difference at larger drifts is attributed to the effect of axial load acting on the displaced configuration.

Figure 4-134 shows the relationship between cumulative dissipated energy versus cycle number for columns CL5 and CL7. The curve for column CL7 is higher than that of column CL5. There are three reasons for this behaviour: (1) the unconfined concrete strength for column CL7 is higher than that of column CL5; (2) the experimental yield displacement for column CL7 ($\Delta_y = 11.5$ mm) is higher than that of column CL5 ($\Delta_y = 8$ mm), which results in greater energy dissipated in an equivalent cycle; and (3) due to the presence of axial load in column CL7 and the fact that it is under-reinforced, its moment capacity is higher than that of column CL5. The deteriorating effect of axial load on ductility is not evident from this figure.

To offset the effects of differences in yield displacements, axial load, and unconfined concrete strengths for column CL5 and CL7 on the energy dissipation characteristics, the cumulative energy dissipated is normalized with respect to the maximum moment capacity and the experimental yield drift of the respective column. Figure 4-135 shows the relationship between cumulative normalized dissipated energy versus cycle number for columns CL5 and CL7. The two curves match with each other up to the 20th cycle. After that, the curve for column CL5 is slightly higher than that of column CL7. This reduction in cumulative normalized energy dissipation towards the end of the test for column CL7 as compared to CL5 is attributed to the deteriorating effect of the axial load.

Figure 4-136 shows the relationship between the hysteretic damping ratio and lateral drift (%) for columns CL5 and CL7. The hysteretic damping ratio of column CL5 is higher than that of column CL7. The lower hysteretic damping ratio of column CL7 is due to the deteriorating effect of axial load.

The values of curvature ductility, η_ϕ , for columns CL5 and CL7 are 9.14 and 15.59, respectively (Table 4.13). With the increase of axial load, curvature ductility has improved. The axial load improves the moment capacity of the columns. The deteriorating effect of axial load is undermined by the improvement in the moment capacity of the columns by increasing axial load.

Figure 4-137 shows the relationship between cumulative ductility ratio, N_ϕ , and cycle numbers for columns CL5 and CL7. The curve for column CL7 is higher than that of column CL5. That is, the trend shown by these curves is opposite to the hypothesis that the axial load has a deteriorating effect on the ductility. This is because of the following reasons:

- (1) The experimental yield displacement of column CL7 is 11.5 mm (alternative 1 (method 1), Table 4.6), whereas the more accurate yield displacement of this column is 9 mm (alternative 3, (method 1), Table 4.6) due to which this column will accumulate greater curvature at the extremes of the loops. The experimental yield displacement of column CL5 is 8 mm (alternative 1 (method 1), Table 4.6), whereas the true yield displacement of this column is 7.5 mm (alternative 3 (method 1), Table 4.6). Although this column also accumulates greater curvatures at the extremes of the loops, this effect is far less in this column than in column CL7.
- (2) The value of curvature ϕ_1 is lower for column CL7 as compared to that for CL5 (Table 4.13).

Figure 4-138 shows the relationship between the cumulative energy damage indicator and cycle numbers for columns CL5 and CL7. The curve for column CL7 is higher than that of column CL5. This trend is opposite to the hypotheses that the axial load has deteriorating effect on ductility. Reasons for this discrepancy have already been given in the discussion of cumulative ductility ratio, N_ϕ .

4.4.1.3 Discussion on the Effect of Axial Loads

The effect of axial load on the behaviour of the collared columns was studied by comparing the results of columns with long shear-spans and short shear-spans. Based on the results of these column tests, it can be concluded that an increase of axial load causes an increase in the rate of degradation in strength and a decrease in the stiffness retention of the collared columns.

The cumulative energy dissipation with respect to cycle number is a not good measure for assessing the energy dissipation characteristics of the specimens because it is influenced by the difference in concrete strength and differences in yield drifts. The cumulative normalized energy dissipation with respect to cycle number curve is considered to be a better means of assessing this characteristic. The presence of axial load decreased the cumulative normalized dissipated energy at the end of the tests. This observation is valid for both long and short shear-span columns.

The presence of axial load tended to result in a lower hysteretic damping ratios. However, this effect was more pronounced in collared columns with short shear-spans than in those with long shear-spans.

The effect of axial load on the cyclic ductility of the collared columns is not entirely clear from the analyses presented. In the case of columns with long shear-spans, the normalized modulus of toughness and curvature ductility of the column without axial loads was higher than that of the column with axial load, whereas ductility parameters such as cumulative curvature ductility and cumulative energy damage indicators are higher for the column with axial load. In the case of columns with short shear spans, the normalized modulus of toughness, curvature ductility, cumulative ductility ratio, and cumulative energy damage indicator are higher for the column with axial load. Explanations of why these various measures might have exaggerated any beneficial effects of axial load—primarily related to the redefinition of the yield displacement after the tests were complete—have been presented. Nevertheless, it appears that axial load may have some beneficial effects on cyclic ductility, although the increased rate of deterioration in the presence of axial loads is perhaps an overriding consideration. Beneficial effects for the level of axial load used in the present research may have been observed because in columns with axial load, the confinement is mobilized more rapidly resulting in an improvement in the ductility of the columns.

4.4.2 Effect of Collar Spacing

In order to study the effect of collar spacing on the performance of the collared columns under cyclic loading, the results of column CL2 are compared with those of column CL3 (columns with long shear-span), and the results of column CL6 are compared with those of column CL7 (columns with short shear-span). The size of collars in all these columns is the same (*i.e.*, HSS76x51x6.35) but the spacing of collars is higher in columns CL2 and CL6, as compared to the spacing of collars in columns CL3 and CL7 (Table 4.1).

4.4.2.1 Comparison of Columns CL2 and CL3

The axial load indices (ratio of $\frac{P}{P_0}$) for columns CL2 and CL3 are 0.22 and 0.23, respectively (Table 4-14), which are virtually identical. Therefore, the effect of axial load is considered the same.

Figures 4-39 and 4-40 show moment-versus-drift hysteresis curves for columns CL2 and CL3, respectively. The envelopes to these hysteresees are shown in Figure 4-139. The initial parts of these curves are identical because the strength of concrete for these columns is almost the same (the strength of concrete in column CL2 is only marginally higher than that of column CL3 (Table 4.2)). After that, the curve for column CL3 becomes higher. This is because of the higher level of confinement in column CL3 as compared to that of CL2 due to the difference in collar spacing (and the associated value of ρ_l .) The other reason for this behaviour is the more rapid spalling of concrete between the collars for column CL2 as compared to that of column CL3 (Figure 4-20(c) and 4-21(a)).

The normalized peak moments of columns CL2 and CL3 are 5.29 and 5.65, respectively (Table 4.8), the normalized moduli of toughness up to peak moment conditions are 253.66 and 376.44, respectively, and the normalized modulus of toughness up to the end of tests are 315.19 and 376.44, respectively (Table 4.11). The higher values for column CL3 are consistent with the values of ρ_l and the spacing of collars for these columns.

Figure 4-140 shows the relationship between the normalized secant stiffness and lateral drift (%) for columns CL2 and CL3. The curves overlap each other. It means that the stiffness retention of

the collared columns is not affected by the change in the level of confinement due to the change in collar spacing and ρ_t .

Figure 4-141 shows the relationship between cumulative dissipated energy versus cycle number for columns CL2 and CL3. The curve for column CL2 is slightly higher than that of column CL3 because of the difference in the experimental yield displacements of column CL2 ($\Delta_y = 41$ mm) and column CL3 ($\Delta_y = 38$ mm). A similar trend is shown by Figure 4-142, which shows the relationships between cumulative normalized dissipated energy and cycle number. The cumulative energy dissipated and cumulative normalized energy dissipated up to the end of the test for column CL3 is higher than that for column CL2 (Appendix G). This is because of the significantly lower number of cycles sustained by column CL2 as compared to that of column CL3. Hence, with the increase in collar spacing, the energy dissipation capability of the specimens decreases significantly mainly because of the increased rate of deterioration.

Figure 4-143 shows the relationship between the hysteretic damping ratio and lateral drift (%) for columns CL2 and CL3. The hysteretic damping ratio increases with the increase in the lateral drift for both columns. The hysteretic damping ratio of column CL2 is slightly higher than that of column CL3 at a certain drift. This is consistent with the trend shown by the curves in Figures 4-141 and 4-142.

The lower-bound values of curvature ductility, η_ϕ , for columns CL2 and CL3 are 12.96 and 9.78, respectively (Table 4.13). From this information, it appears that the curvature ductility of the collared column increases with the increase in collar spacing, which is not true. As a matter of fact, at the stroke limits of the jacks the damage in the test region of column CL2 is much higher than that of column CL3 due to which more rotation takes place in the test region of column CL2 as compared to that of column CL3 (Appendix H). This results in higher values of ϕ_2 for column CL2 as compared to that of column CL3. Although the slopes, S_1 , for both columns are almost the same, due to the difference in values of M_{ncc} for these columns, the value of ϕ_1 for column CL3 is higher than that of column CL2 (Table 4.13). Had the stroke of the horizontal jacks not been exhausted, the curvature ductility exhibited by column CL3 is expected to have been much higher than that of column CL2.

Figure 4-144 shows the relationship between cumulative ductility ratio, N_ϕ , and cycle numbers for columns CL2 and CL3. The rate of increase in cumulative curvature ductility with the increase

in the number of cycles for column CL2 is much higher than that of column CL3. The reason for this trend has been given in the preceding paragraph. As a matter of fact, it was due to the more rapid accumulation of damage in the test of column CL2 as compared to that of column CL3. The cumulative ductility ratio of column CL3 at the end of the test is much higher than that of column CL2, which means that columns confined with closely spaced collars exhibit more ductility.

Figure 4-145 shows the relationship between cumulative energy damage indicator and cycle numbers for columns CL2 and CL3. The slope of the two curves is the same, which means that the rate of increase in the cumulative energy damage indicator with the increase in the number of cycles is same; however, the curve for column CL2 terminates long before that of column CL3. The cumulative energy damage indicator for column CL3 at the end of the test is much higher than that of column CL2. Based on this parameter, the ductility exhibited by column CL3 is much higher than that of column CL2.

4.4.2.2 Comparison of Columns CL6 and CL7

The axial load indices (ratio of $\frac{P}{P_0}$) for columns CL6 and CL7 is 0.16 and 0.15, respectively (Table 4-14), which are very close to each other. Therefore, the effect of axial load is considered to be the same.

Figures 4-43 and 4-44 show moment-versus-drift hysteresis curves for column CL6 and column CL7, respectively. The envelopes to these hystereses are shown in Figure 4-146. These curves clearly show that the ductility and peak moment capacity exhibited by column CL7 are higher than those of column CL6. This is partly attributed to the higher strength of concrete for column CL7 and partly due to the higher level of confinement for this column CL7. The other reason for this behaviour is the more rapid spalling of concrete between the collars of column CL6 as compared to that of column CL7 (Figure 4-24(c) and 4-26(b)).

The normalized peak moments of columns CL6 and CL7 are 3.15 and 3.49, respectively (Table 4.8), the normalized moduli of toughness up to peak moment conditions are 89.66 and 122.00, respectively, and the normalized modulus of toughness up to the end of tests are 167.93 and 329.5, respectively (Table 4.11). The results are consistent with the level of confinement in these columns.

Figure 4-147 shows the relationship between the normalized secant stiffness and lateral drift (%) for columns CL6 and CL7. The curves are close to each other, which means that stiffness retention of collared columns is not affected significantly by the change in the level of confinement related to spacing and ρ_t .

Figure 4-148 shows the relationship between cumulative dissipated energy versus cycle number for columns CL6 and CL7. The rate of increase in cumulative energy dissipation is higher for column CL7 as compared to column CL6. This is due to the higher strength of concrete, higher level of confinement, and higher experimental yield displacement of column CL7. In addition, the cumulative energy dissipated at the end of the tests for column CL7 is higher than that of column CL6. Similarly, Figure 4-149 shows the relationship between the cumulative normalized energy dissipated for columns CL6 and CL7. The rate of increase of this curve for column CL6 is higher than that of column CL7. However, at the end of the tests, the cumulative normalized energy dissipated for column CL7 is much higher than that of column CL6, which is consistent with the level of confinement in these columns. Hence, with an increase in collar spacing, the energy dissipation capability of the specimens decreases significantly.

Figure 4-140 shows the relationship between hysteretic damping ratio and lateral drift (%) for columns CL6 and CL7. The hysteretic damping ratio increases with the increase in the lateral drift for both columns. However, the rate of increase for column CL6 is higher than that of column CL7. The maximum hysteretic damping ratio exhibited by column CL6 is higher than that of column CL7. Figures 4-143 and 4-150 show the same trend. This behaviour is because of the more rapid damage in columns with widely spaced collars as compared to columns with closely spaced collars.

The values of curvature ductility, η_ϕ , for columns CL6 and CL7 are 14.41 and 15.59, respectively (Table 4.13). Hence, columns with closely spaced collars exhibit higher curvature ductility as compared to columns with widely spaced collars.

Figure 4-151 shows the relationship between the cumulative ductility ratio, N_ϕ , and cycle numbers for columns CL6 and CL7. The two curves overlap each other. However, the cumulative ductility ratio at the end of the test for column CL7 is higher than that of column CL6 as expected, which means that columns confined with closely spaced collars exhibit a higher cumulative ductility ratio.

Figure 4-152 shows the relationship between cumulative energy damage indicator and cycle numbers for columns CL6 and CL7. The rate of increase of the cumulative energy damage indicator with the increase of number of cycles is higher for column CL7. In addition, the cumulative energy damage indicator at the end of the tests is higher for column CL7, which means that column CL7 exhibits more ductility as compared to column CL6.

4.4.2.3 Discussion on the Effect of Collar Spacing

In the regime of both long and short shear-span columns, columns with wider spacing of collars exhibited lower values of normalized peak moments, normalized modulus of toughness up to peak moment condition, and normalized modulus of toughness up to the failure of columns as compared to those of columns with closer spacing.

The rate of deterioration of strength is higher in columns with widely spaced collars as compared to columns with closely spaced collars.

For both long and short shear-span columns, the effect of collar spacing on the stiffness retention of the columns was marginal; columns with closely spaced collars exhibited slightly higher stiffness retention as compared to columns with relatively wider collar spacing.

For both long and short shear-span columns, the cumulative energy dissipated and cumulative normalized energy dissipated at the end of the tests is significantly less for columns with widely spaced collars as compared to columns with closely spaced collars.

In long shear span columns, the hysteretic damping ratio of columns with widely spaced collars is slightly higher than that of columns with closely spaced collars. However, in the regime of columns with short shear spans, the columns with a wider spacing of collars exhibited a significantly higher hysteretic damping ratio at a certain level of lateral drift as compared to that of columns with closely spaced collars.

Both in the regime of long and short shear span columns, columns with widely spaced collars exhibit lower ductility in terms of curvature ductility, cumulative ductility ratio, and cumulative energy damage indicator as compared to columns with widely spaced collars.

4.4.3 Effect of Size of Collar

In order to study the effect of size of collars on the performance of the collared columns under cyclic loading, the results of column CL3 are compared with those of column CL4 (columns with long shear-span), and the results of column CL7 are compared with those of column CL8 (columns with short shear-span).

4.4.3.1 Comparison of Columns CL3 and CL4

The axial load index (ratio of $\frac{P}{P_0}$) for column CL3 and CL4 is 0.23 and 0.16, respectively (Table 4-14), which are quite different from each other. This means that axial load will also have an influence on the behaviour of these columns.

Figures 4-40 and 4-41 show moment-versus-drift hysteresis curves for column CL3 and column CL4, respectively. The envelopes to these hysteresees are shown in Figure 4-153. The strength of concrete for column CL4 is higher than that of column CL3 (Table 4.2), which explains the stiffer behaviour of column CL4 as compared to column CL3 in the initial parts of the envelope curves. Although the strength of concrete for column CL3 is lower than that of column CL4, the peak moment capacity of column CL3 is slightly higher than that of column CL4. This is partly due to the higher level of confinement in column CL3 and partly due to its higher axial load index.

The normalized peak moments of columns CL3 and CL4 are 5.65 and 4.39, respectively (Table 4.8), the normalized moduli of toughness up to peak moment conditions are 376.44 and 244.07, respectively, and the normalized moduli of toughness up to the end of tests are 376.44 (lower-bound) and 463.46 (lower-bound), respectively (Table 4.11). Excluding the lower-bound values from discussion, the remaining results are consistent with the level of confinement in these columns.

Figure 4-154 shows the relationship between the normalized secant stiffness and lateral drift (%) for columns CL3 and CL4. The stiffness retention of column CL3 is higher than that of column CL4. Hence, columns with stiffer collars exhibit more stiffness retention as compared to those with a smaller collar size. In spite of the fact that the axial load index for column CL3 is higher than that of column CL4 and it has been postulated previously that a higher axial load index results in lower stiffness retention (Figures 4-126 and 4-133), column CL3 exhibits higher

stiffness retention. This means that the effect of the difference in axial load indices is dominated by the effect of the difference in the size of the collars.

Figure 4-155 shows the relationship between cumulative dissipated energy and cycle number for columns CL3 and CL4. The rate of increase in cumulative energy dissipation with the increase in cycle number is higher for column CL3 up to 16th cycle. The higher rate for column CL3 is partly due to the difference in the size of collars and partly due to the higher experimental yield displacement of column CL3. After the 16th cycle, the rate of increase of energy dissipation becomes the same for both columns up to the end of 45 cycles. This means that the higher level of confinement was not favourable to energy dissipation. The cumulative energy dissipated is higher for column CL3 as compared to column CL4 at the end of 45 cycles. Figure 4-240 shows the relationship between the cumulative normalized energy dissipated for column CL3 and CL4. Up to the 27th cycle, the curve for column CL3 is higher, after which the curve for column CL4 becomes higher. At 45 cycles, the cumulative normalized energy dissipated by column CL4 is higher than that of column CL3 which means that the performance of column CL4 is better than that of column CL3 with respect to energy dissipation. The strength of concrete in column CL3 is much lower than that in column CL4. The size of collars on column CL3 are bigger than those on column CL4, resulting in higher confining pressure for column CL3. Hence, the maximum ratio of confining pressure to concrete strength for column CL3 is much higher than that of column CL4, resulting in higher tensile stresses on the surface concrete between the collars. The tensile strength of concrete for column CL3 is lower than that of column CL4. Hence, under higher tensile stresses, the spalling of concrete between the collars is more rapid in column CL3 as compared to column CL4. In addition, the axial load index for column CL3 is higher than that of column CL4. The higher axial load index results in a higher deterioration rate for column CL3. All these phenomena contribute to the lower level of energy dissipation for column CL3, although the very low concrete strength makes a direct comparison between these two columns difficult.

Figure 4-157 shows the relationship between hysteretic damping ratio and lateral drift (%) for columns CL3 and CL4. The hysteretic damping ratio increases with the increase in lateral drift for both columns. The curve for column CL3 is slightly higher than that of column CL4. This behaviour is because of the more rapid damage that occurred in column CL3.

The lower-bound values of curvature ductility, η_{ϕ} , for columns CL3 and CL4 are 9.78 and 17.22, respectively (Table 4.13). The curvature ductility exhibited by the column with small size collars is higher than the column confined with large size collars. This is also related to the large difference in concrete strength in the two specimens and is consistent with the previous discussion.

Figure 4-158 shows the relationship between cumulative ductility ratio, N_{ϕ} , and cycle numbers for columns CL3 and CL4. The cumulative curvature ductility for column CL3 is higher initially than that of column CL4. However, at the end of 45 cycles it is the same for both columns. If the cycles would have been continued beyond 45, the cumulative curvature ductility for column CL4 would have been higher than that of the column CL3 as is clear from the slope of the two curves. This is consistent with the observation of curvature ductility, given in the preceding paragraph.

Figure 4-159 shows the relationship between the cumulative energy damage indicator and cycle numbers for columns CL3 and CL4. Initially, the slope of the curve for column CL3 is higher than that of column CL4. After the 26th cycle, the slope of the curve for column CL4 become higher and at the end of 45 cycles, the cumulative energy damage indicator for column CL4 is higher than that of column CL3. Hence, the behaviour of column CL4 is more ductile as compared to the behaviour of column CL3, which is consistent with the observations in the preceding paragraphs.

4.4.3.2 Comparison of Columns CL7 and CL8

The axial load index (ratio of $\frac{P}{P_0}$) for column CL7 and CL8 is 0.15 and 0.16, respectively (Table 4-14), which are close to each other. Hence, the influence of axial load on the performance of these columns would be the same.

Figures 4-44 and 4-45 show moment-versus-drift hysteresis curves for column CL7 and column CL8, respectively. The envelopes to these hystereses are shown in Figure 4-160. The strength of concrete for both columns is almost the same (Table 4.2) but the level of confinement is quite different in these two columns. Based on these envelope curves, the behaviour of column CL7 is almost identical to that of column CL8 in terms of ductility.

The normalized peak moments of column CL7 and CL8 are 3.49 and 3.89, respectively (Table 4.8), the normalized moduli of toughness up to peak moment conditions are 122.00 and 139.65, respectively, and the normalized modulus of toughness up to the end of tests are 329.51 and 380.33, respectively (Table 4.11). These values all imply slightly better performance for the column CL8, which had smaller collars.

Figure 4-161 shows the relationship between normalized secant stiffness and lateral drift (%) for columns CL7 and CL8. The stiffness retention of column CL7 is less than that of column CL8.

Hence, columns with smaller size collars appear to exhibit more stiffness retention as compared to those with larger size collars.

Figure 4-162 shows the relationship between cumulative dissipated energy and cycle number for columns CL7 and CL8. Both columns sustained 35 cycles. The cumulative energy dissipated in column CL7 at the end of 35 cycles is slightly higher than that of column CL8. This is attributed to the higher yield displacement of column CL7. Figure 4-163 show the cumulative normalized energy dissipated versus cycle number for column CL7 and column CL8. The curves overlap each other indicating that the columns possess the same energy dissipation characteristics.

Figure 4-164 shows the relationship between the hysteretic damping ratio and lateral drift (%) for columns CL7 and CL8. The hysteretic damping ratio increases with the increase in lateral drift for both columns. The curves are similar; however, column CL8 exhibits a slightly higher damping ratio.

The curvature ductility, η_ϕ , for columns CL7 and CL8 are 15.59 and 14.78, respectively (Table 4.13). Therefore, the curvature ductility exhibited by the column with larger size collars is slightly higher than that exhibited by the column confined with smaller size collars.

Figure 4-165 shows the relationship between cumulative ductility ratio, N_ϕ , and cycle numbers for columns CL7 and CL8. The cumulative curvature ductility for column CL7 is higher than that of column CL8, which is consistent with the result of examining the curvature ductility at the end of the test alone.

Figure 4-166 shows the relationship between the cumulative energy damage indicator and cycle numbers for columns CL7 and CL8. The cumulative energy damage indicator for column CL7 is slightly higher than that of column CL8, supporting the observation that the behaviour of column CL7 is more ductile as compared to column CL8.

4.4.3.3 Discussion on the Effect of Size of Collars

In case of columns with a long shear-span, the stiffness retention was slightly higher for columns with larger size collars as compared to that for columns with smaller size collars. In the case of columns with a short shear-span, the stiffness retention was slightly higher for the columns with smaller size collars. Although these observations appear to contradict one another, the differences observed were relatively small. It is likely that the stiffness retention characteristics of

the columns were not particularly sensitive to the change in the size of the collars in the range in which this study was conducted.

In the case of columns with a long shear-span, the normalized cumulative energy dissipated at the end of the test for the column with small size collars was higher than that of the column with large size collars because the higher ratio of confining pressure to the strength of concrete in the column confined by large size collars produced high tensile stresses in the concrete between the collars for this column due to which the column might have deteriorated rapidly and, hence, exhibited low energy dissipation characteristics. In the case of columns with a short shear-span, columns with different size of collars exhibited similar energy dissipation characteristics in terms of cumulative normalized energy dissipated versus cycle number. It appears that the energy dissipation characteristics of the columns were not sensitive to the change in the size of the collars in the range in which this study was made.

In the case of columns with a long shear-span, the hysteretic damping ratio was slightly higher for columns with larger size collars as compared to that for columns with smaller size collars. In the case of columns with a short shear-span, the hysteretic damping ratio of columns was slightly higher for columns with smaller size collars. Again, the differences were very small and it is concluded that the hysteretic damping ratio was not sensitive to the change in the size of collars in the range in which this study was made.

In the case of columns with a long shear-span, the columns with larger size collars exhibited a higher modulus of toughness as compared to columns with smaller size collars. However, the columns with larger size collars exhibited lower values of curvature ductility, cumulative ductility ratio, and cumulative normalized energy damage indicator. This discrepancy is attributed to the relatively much higher value of axial load index in the column with larger size collars as compared to that of columns with small size collars. In the case of columns with a short shear span, the columns with larger size collars exhibit higher modulus of toughness, curvature ductility, higher cumulative ductility ratio, and higher energy damage indicator as compared to those of columns with small size collars, although the differences tended to be relatively small. Based on the above, it is concluded that columns with larger size collars exhibit somewhat higher ductility as compared to columns with smaller size collars, although it is not clear that this difference would be significant.

4.4.4 Effect of Shear-Span

In order to study the effect of shear-span on the performance of the collared columns, the results of columns CL1, CL2, CL3, and CL4 are compared with those of columns CL5, CL6, CL7, and CL8, respectively.

4.4.4.1 Comparison of Columns CL1 and CL5

Both of these columns were tested without axial load (Table 4.14). Hence, the influence of axial load is not present in these columns.

Figures 4-38 and 4-42 show moment-versus-drift hysteresis curves for columns CL1 and CL5, respectively. The envelopes to these hysteresees are shown in Figure 4-167. The slope of the initial part of the curve for column CL5 is much higher than that of column CL1 because of the higher strength of the concrete of column CL5. With the increase in lateral drift, the curve for column CL5 descends more rapidly. Hence, the rate of strength deterioration in the column with a short shear-span is much higher than the columns with a long shear span. From these envelope curves, it can also be deduced that columns with short shear spans are less ductile as compared to columns with long shear spans.

The normalized peak moments of columns CL1 and CL5 are 7.60 and 4.00, respectively (Table 4.8), the normalized moduli of toughness up to peak moment conditions are 468.23 and 107.95, respectively, and the normalized moduli of toughness up to the end of tests are 772.84 and 228.95, respectively (Table 4.11). Hence, using these measures the columns with long shear spans are more ductile as compared to columns with short shear spans.

Figure 4-168 shows the relationship between normalized secant stiffness and lateral drift (%) for columns CL1 and CL5. The stiffness retention of column CL1 is higher than that of column CL5. Hence, the column with a short shear-span degraded in stiffness more rapidly than the column with a long shear span.

Figure 4-169 shows the relationship between cumulative dissipated energy and cycle number for columns CL1 and CL5. The two curves overlap each other up to the 27th cycle and then the slope of the curve for column CL1 becomes higher than that of column CL5. The cumulative energy dissipated up to the end of the test for column CL1 is much higher than that for column CL5.

Figure 4-170 shows the relationship between the cumulative normalized energy dissipated for columns CL1 and CL5. After 15 cycles, the rate of increase in cumulative normalized energy dissipation for column CL5 becomes higher than that of column CL1. However, the cumulative normalized energy dissipated at the end of the test for column CL1 is much higher than that of column CL5.

Figure 4-171 shows the relationship between the hysteretic damping ratio and lateral drift (%) for columns CL1 and CL5. The hysteretic damping ratio increases with the increase in lateral drift for both columns. The curve for column CL5 is higher than that of column CL1. The trend of these curves indicates that more rapid damage takes place in column CL5 as compared to that of column CL1.

The curvature ductility, η_ϕ , for columns CL1 and CL5 are 11.92 and 9.14, respectively (Table 4.13). The curvature ductility exhibited by the column with a long shear span is higher than that of the column with a short shear-span. This is consistent with the previous discussion.

Figure 4-172 shows the relationship between cumulative ductility ratio, N_ϕ , and cycle numbers for columns CL1 and CL5. The rate of increase of cumulative curvature ductility with respect to cycle numbers is higher for column CL5 as compared to column CL1. However, the cumulative curvature ductility at the end of the test for both columns is about the same. Had the stroke of the jacks not been exhausted, the cumulative ductility ratio at the end of test for column CL1 would likely have been much higher.

Figure 4-173 shows the relationship between the cumulative energy damage indicator and cycle numbers for columns CL1 and CL5. The rate of increase of the cumulative energy damage indicator with respect to cycle numbers is higher for column CL5 as compared to column CL1. However, the cumulative energy damage indicator at the end of the test for column CL5 is slightly higher than that of column CL1. These observations indicate that the energy damage indicator is relatively insensitive to the change of shear-span of the columns.

4.4.4.2 Comparison of Columns CL2 and CL6

The axial load indices (ratio of $\frac{P}{P_0}$) for columns CL2 and CL6 is are 0.22 and 0.16, respectively (Table 4-14). The axial load indices for these columns are quite different from each other. Hence, the influence of axial load would be present in the performance of these columns.

Figures 4-39 and 4-43 show moment-versus-drift hysteresis curves for columns CL2 and CL6, respectively. The envelopes to these hystereses are shown in Figure 4-174. The slope of the initial part of the curve for column CL6 is much higher than that of column CL2. This is because of the higher strength of concrete of column CL6 as compared to that of column CL2. With the increase in lateral drift, the curve for column CL6 descends more rapidly. Hence, the rate of strength deterioration in the column with a short shear-span is higher than that of the column with a long shear span. From these envelope curves, it can also be deduced that columns with short shear spans are less ductile as compared to columns with long shear spans and are more susceptible to degradation.

The normalized peak moments of columns CL2 and CL6 are 5.29 and 3.15, respectively (Table 4.8), the normalized moduli of toughness up to peak moment conditions are 253.66 and 89.66, respectively, and the normalized modulus of toughness up to the end of tests are 315.19 and 167.93, respectively (Table 4.11). Hence, the column with a long shear span is more ductile than the column with a short shear span in terms of energy absorption.

Figure 4-175 shows the relationship between the normalized secant stiffness and lateral drift (%) for columns CL2 and CL6. The stiffness retention of column CL2 is higher than that of column CL6. Hence, the column with a short shear-span degrades in stiffness more rapidly than the column with a long shear span.

Figure 4-176 shows the relationship between cumulative dissipated energy and cycle number for columns CL2 and CL6. The curve for column CL2 is higher than that of column CL6. This is because of the higher experimental yield drift (%) of column CL2 as compared to that of column CL6 and the higher value of axial load index for column CL2. However, at the end of the tests, the cumulative energy dissipated by both columns is more or less the same. Figure 4-261 shows the relationship between cumulative normalized dissipated energy and cycle number for columns CL2 and CL6. The curve for column CL2 is slightly higher than that of column CL6 up to the 25th cycle. After that it becomes lower than that of column CL6. The cumulative normalized energy dissipated at the end of the test for column CL6 is higher than that for column CL2. Columns with long shear-spans usually exhibit better energy dissipating characteristics, but in the present case, the opposite trend is seen. In the case of column CL2, failure occurs between the first and second collars. In the case of column CL6, the failure happens between the footing and the first collar. The gap between the footing and the first collar is smaller than the gap between the first and second collars in both of these columns. Hence, the longitudinal bars are more prone to lateral bending in the gap between the first and the second collars rather than the gap between

footing and the first collar. The yield drift of column CL2 is much higher than that of column CL6. Under large amplitude cycles, the longitudinal bars of column CL2 ruptured more rapidly as compared to that of column CL6. Therefore, the number of cycles sustained by column CL2 are less than that sustained by column CL6. The discrepancy in the energy dissipation characteristics of these columns is attributed to the different location of damage in the test region of these columns. The unsupported length of bars in the second gap is higher than that of the first gap. Therefore, the bars in the second gap rupture more rapidly as compare to the bars in first gap due to low cycle fatigue. Hence, the total energy dissipated by the column CL6 at the end of the test is higher than that of column CL2.

Figure 4-178 shows the relationship between the hysteretic damping ratio and lateral drift (%) for columns CL2 and CL6. The hysteretic damping ratio increases with the increase in lateral drift for both columns. The curve for column CL6 is higher than that of column CL2. The trends of these curves indicate that more rapid damage takes place in column CL6 as compared to column CL2.

The curvature ductility, η_ϕ , for columns CL2 and CL6 are 12.96 (lower-bound) and 14.41, respectively (Table 4.13). Had the stroke of the jack for column CL2 not been exhausted, the curvature ductility exhibited by column CL2 would have been higher. Therefore, no conclusion can be drawn about curvature ductility based on these results.

Figure 4-179 shows the relationship between the cumulative ductility ratio, N_ϕ , and cycle numbers for columns CL2 and CL6. Near the end of the tests, the rate of increase of cumulative curvature ductility for both columns is the same. The cumulative curvature ductility at the end of the tests is also same. The column with a long shear-span would be expected to exhibit more ductility. However, the axial load index for column CL2 is significantly higher than that for column CL6, which tends to reduce ductility.

Figure 4-180 shows the relationship between the cumulative energy damage indicator and cycle numbers for columns CL2 and CL6. The rate of increase of the cumulative energy damage indicator is higher for column CL2 than for column CL6. In addition, the cumulative energy damage indicator at the end of the test for column CL2 is much higher than that for column CL6. Hence, column CL2 is more ductile as compared to column CL6 according to this measure.

4.4.4.3 Comparison of Columns CL3 and CL7

The axial load indices (ratio of $\frac{P}{P_0}$) for columns CL3 and CL7 are 0.23 and 0.15, respectively (Table 4-14). The axial load indices for these columns are quite different from each other. Hence, the influence of axial load would be present in the performance of these columns.

Figures 4-38 and 4-44 show moment-versus-drift hysteresis curves for columns CL3 and CL7, respectively. The envelopes to these hystereses are shown in Figure 4-181. The slope of the initial part of the curve for column CL7 is much higher than that of column CL3 due to the higher strength of the concrete of column CL7. With the increase in lateral drift, the envelope curve for column CL7 descends, whereas the envelope curve for column CL3 does not. Hence, the rate of strength deterioration in the column with a short shear-span is higher as compared to that in the columns with a long shear span. The normalized peak moments of columns CL3 and CL7 are 5.65 and 3.49, respectively (Table 4.8), the normalized moduli of toughness up to the peak moment conditions are 376.44 and 122.00, respectively, and the normalized modulus of toughness up to the end of tests are 376.44 (lower-bound) and 329.51, respectively (Table 4.11). Hence, the column with a long shear span is more ductile as compared to the column with a short shear-span.

Figure 4-182 shows the relationship between normalized secant stiffness and lateral drift (%) for columns CL3 and CL7. The stiffness retention of column CL3 is higher than that of column CL7. Hence, the column with a short shear-span degrades in stiffness more rapidly than the one with a long shear span.

Figure 4-183 shows the relationship between cumulative dissipated energy and cycle number for columns CL3 and CL7. The curve for column CL7 is initially lower than that of column CL3. After about the 32nd cycle, the curve for column CL7 becomes higher than that of column CL3. The number of cycles sustained by column CL3 are much higher than that of column CL7. Therefore, the cumulative energy dissipated at the end of the tests for column CL3 is higher than that of column CL7. Figure 4-184 shows the relationship between the cumulative normalized energy dissipated for column CL3 and CL7. The curve for column CL7 is higher than that of column CL3. In addition, the cumulative normalized energy dissipated at the end of the tests for both columns is about the same. Had the stroke of the jack not been exhausted, the cumulative normalized energy dissipated by column CL3 would likely have been much higher for column CL7.

Figure 4-185 shows the relationship between the hysteretic damping ratio and lateral drift (%) for columns CL3 and CL7. The hysteretic damping ratio increases with the increase in lateral drift for both columns. The curve for column CL3 terminates at a lower level of lateral drift than that for column CL7. Up to this level of lateral drift, the hysteretic damping ratio exhibited by column CL3 is slightly higher than that of column CL7. However, the hysteretic damping ratio exhibited by column CL7 at the end of the test is higher than that of column CL3.

The curvature ductility, η_ϕ , for columns CL3 and CL7 are 9.78 (lower-bound) and 15.59, respectively (Table 4.13). Since the curvature ductility exhibited by column CL3 is a lower-bound, no conclusion can be drawn on ductility with respect to shear-span.

Figure 4-186 shows the relationship between the cumulative ductility ratio, N_ϕ , and cycle numbers for columns CL3 and CL7. The cumulative curvature ductility at the end of the test for column CL3 is higher than that for column CL7. Hence, column CL3 is more ductile than column CL7 based on this measure.

Figure 4-187 shows the relationship between the cumulative energy damage indicator and cycle numbers for columns CL3 and CL7. The rate of increase of the cumulative energy damage indicator is higher for column CL3 as compared to column CL7. In addition, the cumulative energy damage indicator at the end of the test for column CL3 is higher than that of column CL7, which confirms that columns with a long shear span tend to be more ductile than columns with a short shear-span.

4.4.4.4 Comparison of Columns CL4 and CL8

The axial load indices (ratio of $\frac{P}{P_0}$) for column CL4 and CL8 are same (Table 4-14). Hence, the influence of axial load on the performance of these columns would be the same.

Figures 4-41 and 4-45 show the moment-versus-drift hysteresis curves for columns CL4 and CL8, respectively. The envelopes to these hystereses are shown in Figure 4-188. The slope of the initial part of the curve for column CL8 is slightly higher than that of column CL4, which is consistent with their respective concrete strengths.

The normalized peak moments of columns CL4 and CL8 are 4.39 and 3.89, respectively (Table 4.8), the normalized moduli of toughness up to peak moment conditions are 244.07 and 139.65, respectively, and the normalized moduli of toughness up to the end of tests are 463.46 (lower-bound) and 380.33, respectively (Table 4.11). Hence, the column with a long shear span is more ductile than the columns with a short shear span.

Figure 4-189 shows the relationship between the normalized secant stiffness and lateral drift (%) for columns CL4 and CL8. The stiffness retention of column CL4 is very slightly higher than that of column CL8. Hence, the column with a short shear-span degraded in stiffness marginally more rapidly than the column with a long shear span.

Figure 4-190 shows the relationship between the cumulative dissipated energy and cycle number for columns CL4 and CL8. The cumulative energy dissipated up to the end of the test for column CL4 is much higher than that of column CL8. Figure 4-191 shows the relationship between the cumulative normalized energy dissipated for columns CL4 and CL8. The cumulative normalized energy dissipated at the end of the test for column CL4 is much higher than that for column CL8.

Figure 4-192 shows the relationship between the hysteretic damping ratio and lateral drift (%) for columns CL4 and CL8. The hysteretic damping ratio increases with the increase in lateral drift for both columns. The curve for column CL8 is slightly higher than that of column CL4 in the beginning. At lateral drift of about 9%, the curves converge. The hysteretic damping ratio at the end of the test for column CL8 is much higher than that for column CL4.

The curvature ductility, η_{ϕ} , for columns CL4 and CL8 are 17.22 (lower-bound) and 14.58, respectively (Table 4.13). The curvature ductility exhibited by the column with a long shear span is higher than that of the column with a short shear span, which is consistent with the previous discussion.

Figure 4-193 shows the relationship between the cumulative ductility ratio, N_{ϕ} , and cycle numbers for columns CL4 and CL8. The curves are nearly identical. However, the cumulative curvature ductility at the end of the test for column CL4 is much higher than that of column CL8, which supports the body of evidence indicating that columns with long shear-spans are more ductile.

Figure 4-194 shows the relationship between the cumulative energy damage indicator and cycle numbers for columns CL4 and CL8. The rate of increase of the cumulative energy damage

indicator is higher for column CL4. In addition, the cumulative energy damage indicator at the end of the test for column CL4 is higher than that of column CL8. Again, this confirms that columns with long shear spans are more ductile.

4.4.4.5 Discussion on the Effect of Shear-Span

Based on the results of four collared columns with long shear spans and four with short shear spans, the rate of strength deterioration tends to be higher in columns with short shear-spans. Moreover, the collared columns with long shear-spans exhibited higher stiffness retention. Based on the results of three collared columns with long shear-spans and three with short shear spans, those with long shear-spans exhibit higher energy dissipation characteristics. Generally, the hysteretic damping ratio exhibited by columns with short shear spans was higher than that of columns with long shear spans.

Based on the results of four collared columns with long shear-spans and four with short shear spans, those with long shear-spans exhibit higher values of normalized peak moment, normalized modulus of toughness up to the peak moment condition, and normalized modulus of toughness up to failure of the columns. Hence, those with long shear-spans are more ductile. Other ductility parameters were also evaluated for both long and short shear-span columns such as curvature ductility, cumulative ductility ratio, and cumulative energy damage indicator. Despite some discrepancies in these parameters (discussed previously), it can be concluded that the collared columns with long shear-spans exhibit more ductility as compared to columns with short shear-spans.

4.5 Prediction of Envelope to Hysteresis Curves

In order to predict the envelope curves to the base moment versus lateral drift (%) hysteresis curves of the columns, analytical tools are required to determine the displacement of the columns at the point of application of the horizontal loads. This displacement may consist of elastic flexural displacement, Δ_e , plastic flexural displacement, Δ_p , shear displacement, Δ_{sh} , displacement due to sliding at the base, Δ_{sl} , and displacement resulting from anchorage slip and elongation of the longitudinal bars at the top of the footing, Δ_a .

During the testing of columns, measurements showed that there was no sliding at the base of the columns. Hence, displacement due to sliding, Δ_{sl} , is taken equal to zero.

It is to be noted that the effective shear-span to depth ratio, a/d , where a is the base moment divided by the horizontal force and d is the effective section depth, changes during the experiments due to changes in both the base moment and the horizontal force with the change of lateral drift (%). These changes occur due to the following: (1) change of horizontal force due to changes in the resistance of the column; (2) change in the location of the point of application of the horizontal load due to the presence of a rigid outrigger attached to the column through which the loads were applied (Figure 4-14(a)); (3) the generation of a small vertical component of the jack force due to the slight inclination of the jacks that developed as the drifts increased; and (4) additional moment caused by the P- Δ effect. The original (nominal) shear-span to depth ratios, a/d , based on H_2 , and effective shear-span to depth ratios, a/d , calculated at the location of M_{ncc} , are given in Table 4.15. The a/d ratios at the location of M_{ncc} are higher than the nominal values, except for column CL1. For the two columns that were tested without a vertical applied load—CL1 and CL5—the values are nearly identical, showing that the presence of axial load is highly influential. The a/d ratios remain larger than 3.0 for all the columns; therefore, the effect of shear deformations can be ignored in comparison to the contributions due to flexure. It means all the columns are flexure-dominant.

Hence the total displacement, Δ_{total} , at the point of application of horizontal loads consists of the following:

$$[4.14] \dots \Delta_{total} = \Delta_e + \Delta_p + \Delta_a$$

Not all the components of displacements given in Equation 4.15 necessarily exist at all levels of loading. The displacements Δ_e and Δ_p are flexural displacements, the detail of which is given in the following section.

4.5.1 Flexural Deformations

Each specimen is idealized as a cantilever subjected to a horizontal and a vertical load (Figure 4-195). When the column is in the elastic range, the elastic displacement, Δ_e , at the tip of the cantilever is calculated as follows:

$$[4.15] \quad \Delta_e = \frac{\phi L^2}{3} \text{ for } (\phi \leq \phi_y)$$

where ϕ is the curvature at the column base. When this curvature reaches the yield curvature, ϕ_y , the displacement at the tip of the cantilever is calculated as:

$$[4.16] \quad \Delta_y = \frac{\phi_y L^2}{3}$$

This is the extreme case of elastic displacement. When the curvature at the base of the column exceeds the yield curvature, ϕ_y , the displacement at the tip of the cantilever consists of two parts: yield displacement, Δ_y , and plastic displacement, Δ_p . The yield displacement can be determined from Equation 4.16. In the case of columns CL6, CL7, and CL8, due to the large vertical distance between the points of application of the horizontal and vertical loads (Figure 4-5), some moment due to the $P-\Delta$ effect may be present at the point of application of the horizontal loads. This might have some influence on the elastic displacements, but as the elastic displacements are very small as compared to the plastic displacements, this moment was not taken into consideration and Equations 4.16 and 4.17 were used without change.

For the plastic displacement, plastic rotation at the column base is assumed to be concentrated at the centre of the plastic hinge length, L_p , and the plastic displacement at the tip of the cantilever is expressed as:

$$[4.17] \quad \Delta_p = (\phi_{max} - \phi_y)L_p(L - 0.5L_p)$$

4.5.1.1 Plastic Hinge Length

In order to use Equation 4.18 for the determination of plastic displacement, Δ_p , at the tip of a cantilever, the plastic hinge length, L_p , is required. There exist various empirical equations in the literature for the determination of plastic hinge lengths. In the present research, equations suggested by Corley (1966), Mattock (1967), and Priestley and Park (1987) are used to estimate the plastic hinge lengths of the collared columns. The detail of the equations follows:

Corley's equation:

$$[4.18] \quad L_p = 0.20(L/d)d^{0.5} + 0.5d$$

Mattock's equation:

$$[4.19] \quad L_p = 0.05L + 0.5d$$

Priestley and Park's equation:

$$[4.20] \quad L_p = 0.08L + 6d_b$$

where, L is the distance between the point of contraflexure in the column and the section of maximum moment, d_b is the diameter of the longitudinal bars, and d is the effective depth of the section.

These equations were applied to all the test columns and the results are reported in Table 4.12. Corley's equation gives the smallest equivalent plastic hinge lengths in all cases and Priestley and Park's equation gives the largest. Mattock's equation gives intermediate values of the plastic hinge lengths and seems more suitable for the test specimens in the present research because they show relatively better comparison with the most damaged regions of the columns given in Table 4.12. Hence, the plastic hinge lengths given by Mattock's equation were used to calculate the plastic displacements of the test specimens.

4.5.1.2 Analytical Moment-Versus-Curvature Relationships

In order to use Equations 4.16, 4.17, and 4.18 for the calculation of tip displacements, analytical moment-versus-curvature relationships are required for the sections of all the columns. For the moment-curvature analysis, stress versus strain curves of steel reinforcing bars and concrete material curves are required. The stress versus strain curves of steel reinforcing bars and HSS are given in Figure 4-7 and the corresponding material properties are given in Table 4.3. The material properties of unconfined concrete are given in Table 4.2. The conventional column CL0 consists of a confined concrete core and unconfined concrete cover. The stress versus strain curve for the confined concrete core of this column was determined using a model proposed by Mander *et al.* (1988b) and is shown in Figure 4-196. For determining the confined concrete

material curves of collared columns, a model proposed in Chapter 5 was used and they are given in Figure 4-197.

The moment-versus-curvature relationships were determined for all the column sections using a strain compatibility analysis, with the assumption that plain sections remain plain throughout the tests. For this purpose a FORTRAN computer program, MCR, was written, the listing of which is given in Appendix K along with a typical data file. Figure 4-198 shows the moment-versus-curvature relationship for a typical column (column CL1).

For column CL0, three moment versus curvature relationships were required since the behaviour of the core and cover concrete is different. Therefore, a program for the analysis of this section is required that can deal with at least two different concrete material curves. The program MCR can only deal with one concrete material curve. In addition, this column was subjected to an axial load of 1470 kN in the beginning of the test, which was reduced to 720 kN after completing the 16th cycle. In order to predict the envelope curve of this column with the available computing facility (program MCR), moment-versus-curvature relationships were determined for the following three cases:

- (1) gross column section (300 x 300 mm), using the confined concrete material curve and considering an axial load of 1470 kN. This moment-versus-curvature relationship is useful for predicting the initial part of the envelope curve where the behaviours of core and cover concretes are similar and the benefits of confinement are negligible.
- (2) column core of 235 x 235 mm (measured out-to-out of hoop reinforcement), using the confined concrete material curve for the core concrete and considering an axial load of 1470 kN. This relationship would be appropriate in the second segment of the envelope curve up to and including the 16th cycle.
- (3) column core of 235 x 235 mm (measured out-to-out of hoop reinforcement), using the confined concrete material curve for the core concrete and considering an axial load of 720 kN. This relationship is suitable beyond the 16th cycle.

4.5.2 Rotations at Column Base Due to Anchorage Slip

It was observed in the experiments that relatively wide cracks formed at the interface between the column and the footing. Due to high strains in the tensile reinforcing bars, the bond between the concrete and steel close to the joint deteriorated, resulting in the elongation and slip of the

reinforcing bars that caused additional rotations of the columns at the base. These additional fixed-end rotations are not captured by the flexural analysis presented in the previous section. Various models have been proposed to determine the fixed-end rotations due to anchorage slip. Models proposed by Otani and Sozen (1972) and by Sezen (2000) are used to determine these rotations for the test specimens used in the present research.

Otani and Sozen (1972) proposed the following equation to determine the fixed-end rotation at the base of a column due to anchorage slip:

$$[4.21] \quad \theta_{slip} = \frac{M^2 f_y d_b}{52 E_s \sqrt{f'_c} M_y (d - d')}$$

where,

- d effective depth of the section;
- d' distance from the compression face of concrete to reinforcing bars in compression;
- d_b diameter of steel reinforcing bars;
- f'_c cylinder strength of concrete;
- f_y yield stress of steel reinforcing bars;
- M bending moment at the end of the member;
- M_y yield moment at the end of the member; and
- θ_{slip} additional rotation at column base due to anchorage slip.

Equation 4.20 is based on the following assumptions: it uses the elastic modulus of elasticity of steel, E_s ; and the stress in the reinforcing bars is determined using a linear relationship with the section bending moment. Hence, the model seems more appropriate for the elastic range.

Sezen (2000) proposed two separate equations for the rigid-body rotations due to anchorage slip for the elastic and plastic ranges, respectively:

$$[4.22] \quad \theta_{slip} = \frac{\varepsilon_s f_s d_b}{96 \sqrt{f'_c} (d - c)} \quad \text{for } \varepsilon_s \leq \varepsilon_y$$

$$[4.23] \quad \theta_{slip} = \frac{d_b}{96\sqrt{f'_c}(d-c)} \left[\varepsilon_y f_y + 2(\varepsilon_s + \varepsilon_y)(f_s - f_y) \right] \quad \text{for } \varepsilon_s > \varepsilon_y$$

where,

- c distance from extreme compression fibre to the neutral axis of section;
- d effective depth of section;
- d_b diameter of steel reinforcing bars;
- f'_c cylinder strength of concrete;
- f_s steel stress;
- f_y yield stress of steel;
- ε_s steel strain;
- ε_y yield strain of steel;
- θ_{slip} additional rotation at column base due to anchorage slip.

Knowing the rotation at the base of the columns, the displacements at the point of application of the horizontal load can be determined from the following equation:

$$[4.24] \quad \Delta_a = \theta_{slip} L$$

The models by Otani and Sozen (1972) and Sezen (2000) were both used to determine the rigid-body rotations at the base of the column. However, no considerable difference was found in the overall behaviour of the columns. Therefore, it was decided to present the results using the rigid-body rotations determined by Sezen's model only.

4.5.3 Predicted Envelope Curves

Knowing the moment-versus-curvature relationships, and rigid body rotations at the base due to anchorage slip, the moment versus lateral drift (%) at the point of application of horizontal load, can be determined using Equations 4.14, 4.15, 4.16, 4.17, and 4.24.

Figure 4-199 show the experimental hysteresis curve, the experimental average envelope curve based on north and south envelopes, and the predicted envelope curve for column CL0.

Figure 4-200 shows an enlarged view of the envelope curves given in Figure 4-199 for clarity. The initial slope of the predicted envelope curve (case A) and that of the average experimental envelope curve are more or less the same. In the later stages of the test, the predicted envelope curve (case A) rises much higher than that of the average experimental envelope curve because it is based on the gross concrete section without considering spalling of the cover concrete. The initial slopes of the predicted envelope curves for cases B and C are the same, but they are much lower than that of the predicted envelope curve for case A and the experimental average envelope curve. The predicted envelope curve for case B is slightly higher than that of case C, which is attributed to the difference in the magnitude of axial loads in the two cases. Considering the curve for case A in the initial region, case B in the central region, and case C at higher drifts, according to their respective assumptions, a good simulation of the experimental behaviour is obtained.

Figures 4-201 through 4-204 show the experimental hysteresis curve, average experimental envelope curve, and predicted envelope curve for columns with long shear spans—columns CL1, CL2, CL3, and CL4, respectively. Good agreement exists between the predicted envelope curve and the experimental average envelope curves. Generally, the predicted envelope curves show a slightly higher capacity than the associated experimental average envelope curves in the later stages of the test. This is because the predicted envelope curves are based on the gross column section and therefore they do not consider spalling of the concrete between the collars under cyclic loading. Due to the spalling of the concrete between the collars, the effective column section becomes reduced, resulting in experimental capacities that are less than the predicted capacities.

Figures 4-205 through 4-208 show the experimental hysteresis curve, average experimental envelope curve, and predicted envelope curve for columns with short shear spans—columns CL5, CL6, CL7, and CL8, respectively. Good agreement exists between the predicted envelope curve and the experimental average envelope curves up to about 5% lateral drift. After that, the predicted envelope curves show significantly higher capacity than the associated experimental average envelope curves. This is because with a short shear span, more rapid spalling of concrete takes place as compared to columns with long shear spans, as was observed in the tests, but this reduction of cross section due to spalling is not taken into account in the model. In addition, the effect of cyclic loads on the properties of the concrete and steel reinforcing bars and the effect of lateral bending of longitudinal bars were not included in the model.

4.6 Summary

The seismic behaviour of reinforced concrete structures can be improved through enhancement in strength and ductility at the location of plastic hinges, which can be achieved through external confinement. There are various schemes for providing external confinement to concrete. A new such scheme has been proposed that makes use of collars made from steel hollow structural sections (HSS) for providing confinement to the concrete. The axial behaviour of collared columns was studied in Chapter 3 through an extensive experimental programme. In the present chapter, the behaviour of reinforced concrete columns confined by steel HSS collars has been studied under simulated seismic loading. A total of nine full-scale reinforced concrete columns typical of two to three storey buildings, were tested in the experimental program. One column (CL0) had conventional tie reinforcement in the rest region and it satisfied the seismic plastic hinge requirements of both ACI 318-02 and CSA Standard A23.3-84. All the specimens were 300 x 300 mm in cross-sections and about 2100 mm in height. The variables included in this study were axial load, collar spacing, collar size, and shear span. In addition, envelope curves to the hysteresees of the columns are predicted by using analytical models for flexural deformations and for anchorage slip.

4.7 Conclusions

4.7.1 Conclusions Based on Experimental Results

All the collared columns showed very good behaviour under severe cyclic loading. The desired enhancement in strength and ductility was achieved through confinement of concrete and the presence of the collars made the columns very resistant to degradation under severe cyclic loading. External confinement by HSS collars therefore shows promise of being an effective means of rehabilitating columns in seismically deficient reinforced concrete buildings.

In the collared columns, very little spalling of concrete between the collars was observed at the end of the first 20 cycles, a ductility level equal to 4, which is common in the design of new reinforced concrete structures. In the case of the conventional column (CL0), most of the spalling of the concrete cover occurred at a displacement ductility level of 1.5. Hence, collared columns possess a larger effective core than that of conventionally tied columns and are more resistant to degradation under severe cyclic loading.

Fracture of some vertical bars due to low-cycle fatigue was observed in several collared columns. However, it was more pronounced in columns with a wider collar spacing. No slippage of the collars was observed in any of the collared columns at the end of the tests, a feature which is highly desirable for the success of this rehabilitation scheme.

In the collared columns, most of the spalling was confined to the lower half of the test region, while in the conventional column, spalling took place over a wider range because it did not have collars; the collars restrict the spread of damage.

The normalized peak moment of the control column is less than that of the collared columns used in the present study. The normalized modulus of toughness of the control column is less than that of the collared columns having the same shear span. However, some collared columns with the short shear-span exhibited a lower modulus of toughness than the control column.

All the collared columns exhibited more stiffness retention as compared to the control column. Hence, collared columns are more resistant to degradation under severe cyclic loading than the control column.

The rate of increase of cumulative normalized energy dissipation with respect to cycle number is generally higher for the control column as compared to that of the collared columns. The cumulative normalized energy dissipated at the end of the tests is higher for control column as compared to that of collared columns with a short shear-span. A direct comparison between the control column and collared columns with a long shear-span cannot be made with respect to cumulative normalized energy dissipated at the end of the tests because the tests of most of the collared columns with a long shear span were stopped prematurely due to the limitation in jack stroke. Had the tests not stopped prematurely, the cumulative normalized energy dissipated at the end of the tests of collared columns with long shear span would likely have been higher than that of the control column.

The hysteretic damping ratios of all the columns were plotted with respect to lateral drift of the columns. The hysteretic damping ratio increases with the increase of lateral drift for all the columns. The hysteretic damping ratio of the control column is generally higher than that of collared columns. Very rarely, the hysteretic damping ratio of collared columns became higher than that of the control column.

The curvature ductility of the control column was higher than that of the collared columns. The cumulative ductility ratio and cumulative energy damage indicator at the end of test are

significantly higher for the control column than the collared columns. The collared columns exhibited less ductility using these measures because the damage is concentrated within a smaller length of the test region as compared to the length of damaged region in the control column.

In addition, the following conclusions are drawn with respect to the effect of various parameters on the behaviour of the collared columns.

4.7.1.1 Effect of Axial Load

Based on the results of these columns with short and long shear-spans, it can be concluded that an increase of axial load on the columns causes an increase in the rate of degradation in strength and a decrease in the stiffness retention of the collared columns. Moreover, the presence of axial load caused a reduction in the cumulative normalized dissipated energy at the end of the tests.

All the columns exhibited an increase in the hysteretic damping ratio with the increase of lateral drift. With the increase in axial load the hysteretic damping ratio of collared columns decreased at the lateral drift under consideration. However, this effect was more pronounced in collared columns with short shear-spans as compared to columns with long shear spans.

The application of axial loads in the range of $0.15P_0$ to $0.23P_0$ generally caused improvement in the ductility of the collared columns. It is assumed that in columns with this range of axial loads, the axial load improves the ductility by mobilizing confinement more rapidly as compared to columns without axial load. Furthermore, the presence of axial compression is known to improve shear behaviour, which is particularly important for the columns with the short shear span. It is considered that the beneficial effect of this range of axial load on ductility is greater than its contribution to deterioration.

4.7.1.2 Effect of Collar Spacing

In the regime of both long and short shear-span columns, columns with a wider spacing of collars exhibited lower values of the normalized peak moment, normalized modulus of toughness up to the peak moment, and normalized modulus of toughness up to the failure of the columns as compared to those of columns with a closer collar spacing.

The rate of deterioration of strength is higher in columns with widely spaced collars as compared to columns with closely spaced collars. However, in the regime of both long and short shear-span columns, the effect of collar spacing on the stiffness retention of the columns was marginal; columns with closely spaced collars exhibited slightly higher stiffness retention.

For both long and short shear-span columns, the cumulative energy dissipated and the cumulative normalized energy dissipated at the end of the tests was significantly less for columns with widely spaced collars as compared to columns with closely spaced collars.

For long shear span columns with widely spaced collars, the hysteretic damping ratio was slightly higher than that of columns with closely spaced collars. However, in columns with a short shear span, the columns with a wider spacing of collars exhibited a significantly higher hysteretic damping ratio at a certain level of lateral drift.

In both long and short shear span columns, columns with widely spaced collars exhibit less ductility in terms of curvature ductility, cumulative ductility ratio, and cumulative energy damage indicator as compared to columns with widely spaced collars.

4.7.1.3 Effect of Collar Size

In the case of columns with a long shear span, the stiffness retention was slightly higher for columns with large size collars as compared to that of columns with small size collars. In the case of columns with a short shear span, the stiffness retention was slightly higher for columns with small size collars. In both cases, the differences were small and it is concluded the energy dissipation characteristics of the columns were not sensitive to the change in the size of the collars in the range in which this study was made.

In the case of columns with a long shear-span, the normalized cumulative energy dissipated at the end of the test for column with small size collars was higher than that of column with large size collars. In the case of columns with a short shear-span, columns with different sizes of collars exhibited similar energy dissipation characteristics in terms of cumulative normalized energy dissipated versus cycle number. This implies that the energy dissipation characteristics of the columns were not sensitive to the change in the size of the collars in the range in which this study was made.

In the case of columns with long shear spans, the hysteretic damping ratio of the columns was slightly higher for columns with large size collars as compared to that of columns with small size

collars. In the case of columns with short shear spans, this ratio was slightly higher for columns with small size collars. The hysteretic damping ratio was not particularly sensitive to the change in the size of collars in the range in which this study was conducted.

In the case of columns with long shear spans, the column with large size collars exhibited a higher modulus of toughness as compared to the column with small size collars. However, it exhibited lower values of curvature ductility, cumulative ductility ratio, and cumulative normalized energy damage indicator. This discrepancy is attributed to a relatively higher value of axial load index in the column with the large size collars as compared to that in the column with the small size collars. In the case of columns with short shear spans, the column with the large size collars exhibited a higher modulus of toughness, curvature ductility, cumulative ductility ratio, and energy damage indicator. Based on the above, it can be concluded that columns with large size collars tend to exhibit higher ductility as compared to columns with small size collars.

4.7.1.4 Effect of Shear-Span

The rate of strength deterioration is higher in collared columns with a short shear-span as compared to that in columns with a long shear-span. Moreover, collared columns with long shear-spans exhibit higher stiffness retention.

The collared columns with long shear-spans exhibited higher energy dissipation characteristics as compared to those of columns with short shear-spans. Generally, the hysteretic damping ratio exhibited by the columns with short shear-spans was higher than that of columns with long shear spans.

Based on parameters such as the normalized modulus of toughness, curvature ductility, cumulative ductility ratio, and cumulative energy damage indicator, the collared columns with long shear-spans are more ductile as compared to collared columns with short shear-spans.

4.7.2 Conclusions Based on Analytical Results

The envelope to the hysteresis curves of the control column, collared columns with long shear spans, and collared columns with short shear spans were predicted analytically. In general, the predicted envelope curves showed very good agreement with those of the average experimental envelope curves. For the control column, this agreement was obtained through three different models that simulated the behaviour in three different ranges of the test. In the case of collared columns with short shear spans, the predicted envelope curves showed very good agreement

with the experimental envelope curves up to a lateral drift of about 5%. After this level of lateral drift, the predicted envelope curves over-estimate the capacity of the columns because in columns with short shear-spans, more rapid spalling of concrete takes place as compared to columns with long shear spans. Rapid spalling of concrete between the collars results in a reduction in the column cross-section that also reduces the experimental capacity of the columns rapidly. This reduction of cross-section due to spalling is not taken into account in the model. In addition, the effect of cyclic loads on the properties of the concrete and steel reinforcing bars and the effect of lateral bending of longitudinal bars were not included in the model.

Table 4.1: Detail of test specimens

Specimen	Confinement Steel				Axial Load (kN)	Location of Horizontal and Vertical Loads		
	Size of confining steel (mm)	s (mm)	s' (mm)	ρ_t (%)		H ₁ (mm)	H ₂ (mm)	H ₃ (mm)
CL0	Ties: $\phi 15$	70	55	5.19	1470/720	2075	1900	2200
CL1	HSS76x51x6.35	101	50	21.80	0	2075	1900	—
CL2	HSS76x51x6.35	151	100	14.58	720	2075	1900	2200
CL3	HSS76x51x6.35	101	50	21.80	720	2075	1900	2200
CL4	HSS51x51x6.35	101	50	15.42	720	2075	1900	2200
CL5	HSS76x51x6.35	101	50	21.80	0	2075	750	—
CL6	HSS76x51x6.35	151	100	14.58	720	2125	760	2250
CL7	HSS76x51x6.35	101	50	21.80	720	2125	755	2245
CL8	HSS51x51x6.35	101	50	15.42	720	2125	775	2250

Table 4.2: Cylinder strengths of concrete

Specimen	Cylinder strength of footing concrete, f'_c			Cylinder strength of column concrete, f'_c		
	Average value (MPa)	Standard deviation (MPa)	Age of concrete (days)	Average value (MPa)	Standard deviation (MPa)	Age of concrete (days)
CL0	31.1	1.52	108	32.7	0.51	63
CL1	40.0	1.73	139	12.3	2.69	104
CL2	32.2	0.56	154	15.9	1.01	131
CL3	33.1	1.31	203	15.4	1.36	187
CL4	38.6	1.46	116	32.7	0.77	82
CL5	46.2	2.34	154	26.3	1.19	131
CL6	43.3	1.18	60	32.6	1.54	33
CL7	44.4	0.88	66	35.4	1.54	50
CL8	45.9	0.85	80	35.3	1.41	71

Table 4.3: Properties of steel rebars and steel HSS

Steel Type	Size (mm)	f_y (MPa)	E_s (MPa)	f_p (MPa)	ϵ_p	ϵ_{sh}	H' (MPa)
Rebars	$\phi 15$	517	206 800	802	0.1070	-	-
	$\phi 25$ (CL0 TO CL4)	510	199 930	710	0.0600	0.0110	8529
	$\phi 25$ (CL5 TO CL8)	515	199 795	687	0.1370	0.0170	5377
HSS	HSS 51x51x6.35	464	202 140	601	0.1004	-	-
	HSS 76x51x6.35	512	206 660	660	0.0415	-	-

Table 4.4: Length of test regions and types of instrumentation

Specimens	Test region lengths (mm)	Location of collars from footing and instrumentation in the test regions						
		Type of Instrument	Collar 1	Collar 2	Collar 3	Collar 4	Collar 5	Collar 6
CL1	590	Type	LVDTs	—	RTM	—	—	CTD
		Distance (mm)	55	154	256	357	452	565
CL2*	558	Type	LVDTs	RTM	—	CTD	—	—
		Distance (mm)	76	240	389	533	—	—
CL3	630	Type	LVDTs	—	RTM	—	—	CTD
		Distance (mm)	64	176	294	394	505	605
CL4	615	Type	LVDTs	—	RTM	—	—	CTD
		Distance (mm)	66	175	285	385	490	597
CL5	590	Type	LVDTs	—	RTM	—	—	CTD
		Distance (mm)	50	150	260	360	460	565
CL6*	586	Type	LVDTs	RTM	RTM	CTD	—	—
		Distance (mm)	97	254	405	556	—	—
CL7	581	Type	LVDTs	RTM	RTM	RTM	RTM	CTD
		Distance (mm)	51	152	253	354	455	556
CL8	599	Type	LVDTs	RTM	RTM	RTM	RTM	CTD
		Distance (mm)	65	170	270	375	477	574

*In specimen CL2 and CL6, there were only four collars in the test region.

Note: The counting of collars is done from bottom upwards. The first collar near the footing is given number 1.

LVDTs: Linear variable differential transformers

RTM: Rotation meter

CTD: Cable transducers

Table 4.5: Analytical and experimental moment capacities of columns

Specimes	M_{yuc} (kN.m)	M_{nuc} (kN.m)	M_{ycc} (kN.m)	M_{ncc} (kN.m)
CL0	no yielding of steel	180.31	246.76	216.50
CL1	no yielding of steel	142.56	151.11	235.47
CL2	no yielding of steel	132.43	194.29	276.92
CL3	no yielding of steel	130.41	198.19	300.96
CL4	no yielding of steel	187.75	212.50	296.84
CL5	135.45	164.34	163.78	207.42
CL6	no yielding of steel	187.45	217.83	282.93
CL7	no yielding of steel	193.34	221.73	296.90
CL8	no yielding of steel	193.16	220.89	296.48

Note: The columns CL1 and CL5 were tested without axial load

Table 4.6: Summary of yield displacements determined by different methods

Specimens	Yield displacement, Δ_y (mm)					
	Method 1					Method 2
	Alt. 1*	Alt. 2	Alt. 3	Alt. 4	Alt. 5	
CL0	30	30	30	16	24	22; 29; and 32
CL1	23	29	30	28	58	70
CL2	41	34	31	17	59	71
CL3	38	37	32	16	67	81
CL4	28	28	28	23	49	57
CL5	8	8	7.5	7.5	10.5	12.5
CL6	8.5	8	7	5.5	11	11.5
CL7	11.5	10	9	7	15	17
CL8	11	10	9	7.5	16	17.5

*Approximate yield displacements used to perform experiments

Table 4.7: Detail of number of complete cycles at different ductility levels and total number of cycles sustained by the specimens

Specimens	Number of complete cycles sustained								
	$M = 0.75M_{ycc}$	Displacement Ductility, μ							Total
		1.5	2	4	6	8	10	12	
CL0	5	5	5	5	5	19*	-	-	44
CL1	5	5	5	5	5	20*	-	-	45
CL2	5	5	5	5	7*	-	-	-	27
CL3	5	5	5	5	25*	-	-	-	45
CL4	5	5	5	5	5	20*	-	-	45
CL5	5	5	5	5	5	5	5	2	37
CL6	5	5	5	5	5	5	1	-	31
CL7	5	5	5	5	5	5	5	-	35
CL8	5	5	5	5	5	5	5	-	35

Note: The starred number of cycles were performed at the stroke limit of the horizontal jacks instead of the ductility levels specified.

Table 4.8: Values of moments and drifts from envelope curves at 0.25% drift, at peak moment, and at failure.

Specimens	At 0.25% drift			At peak moment			At failure	
	Drift (%)	Moment (kN.m)	Secant stiffness at 0.25% drift (kN.m)	Drift (%)	Moment (kN.m)	Normalized peak moments w.r.t. moment at 0.25% drifts	Drift (%)	Moment (kN.m)
CL0	0.25	77.70	31 080	8.00	216.50	2.79	10.62*	208.30
CL1	0.25	30.98	12 392	10.10	235.47	7.60	15.60*	225.00
CL2	0.25	52.37	20 948	8.80	276.92	5.29	10.49*	275.04
CL3	0.25	53.31	21 324	10.45	300.96	5.65	10.45*	300.96
CL4	0.25	67.66	27 064	8.91	296.84	4.39	16.02*	255.00
CL5	0.25	51.83	20 732	4.53	207.42	4.00	8.84	186.73
CL6	0.25	89.85	35 940	4.66	282.93	3.15	8.25	254.65
CL7	0.25	85.16	34 064	6.31	296.90	3.49	15.58	267.30
CL8	0.25	76.23	30 492	5.67	296.48	3.89	13.68	266.85

Note: The starred values are lower bound

Table 4.9: Stress in concrete and steel longitudinal bars before the application of horizontal loads

Specimen	Total axial load (kN)	f'_{co} (MPa)	E_c (MPa)	Steel load, P_{sa} (kN)	Concrete load, P_{ca} (kN)	Steel stress, f_{sa} (MPa)	Concrete stress, f_{ca} (MPa)	Ratio (f_{ca} / f'_{co})	Euler Buckling Load P_{cr} (kN)
CL0	1470	27.8	19 507	474.5	995.5	118.64	11.58	0.42	73 676
CL0	720	27.8	19 507	232.4	487.6	58.11	5.67	0.20	73 676
CL1	0	10.5	11 964	0	0	0	0	0	45 186
CL2	720	13.5	13 602	292.4	427.6	73.09	4.97	0.37	51 375
CL3	720	13.1	13 387	295.1	424.9	73.78	4.94	0.38	50 561
CL4	720	27.8	19 507	232.4	487.6	58.11	5.67	0.20	73 676
CL5	0	22.4	17 494	0	0	0	0	0	424 050
CL6	720	27.7	19 477	232.6	487.4	58.14	5.67	0.20	459 773
CL7	720	30.1	20 296	226.1	493.9	56.53	5.74	0.19	485 478
CL8	720	30.0	20 267	226.3	493.7	56.59	5.74	0.19	460 093

Table 4.10: Cracking moments of the columns

Specimen	Axial load (kN)	Axial stress on concrete f_{ca} (MPa)	f'_{co} (MPa)	f_r (MPa)	M_{cr} (kN.m)	Moment at 0.25% drift (kN.m)
CL0	1470	11.58	27.80	3.28	66.88	77.70
CL1	0	0	10.46	2.01	9.06	30.98
CL2	720	4.97	13.52	2.29	32.65	52.37
CL3	720	4.94	13.09	2.25	32.36	53.31
CL4	720	5.67	27.80	3.28	40.28	67.66
CL5	0	0	22.36	2.94	13.25	51.83
CL6	720	5.67	27.71	3.28	40.29	89.85
CL7	720	5.74	30.09	3.42	41.23	85.16
CL8	720	5.74	30.01	3.41	41.21	76.23

Note: The cracking moments and the moments at 0.25% drift for columns CL1 and CL5 are relatively less because of the absence of axial stress.

Table 4.11: Moduli of toughness and normalized moduli of toughness for the test specimens

Specimen	Modulus of toughness (kN.m)		Normalized modulus of toughness	
	Up to peak moment	Up to end of test	Up to peak moment	Up to end of end
CL0	15.67	21.90*	132.79	185.55*
CL1	19.45	32.10*	468.23	772.84*
CL2	19.20	23.86*	253.66	315.19*
CL3	29.90	29.90*	376.44	376.44*
CL4	22.04	41.85*	244.07	463.46*
CL5	7.69	16.30	107.95	228.92
CL6	11.09	20.77	89.66	167.93
CL7	15.40	41.59	122.00	329.51
CL8	13.43	36.59	139.65	380.33

Note: The starred values are lower bound

Table 4.12: Equivalent plastic hinge lengths and most damaged region of the test specimens

Specimens	Plastic hinge lengths (mm)			Most damaged region L_f (mm)
	Corley (1966)	Mattock (1967)	Priestley and Park (1987)	
CL0	144.5	215.0	302.0	250
CL1	144.5	215.0	302.0	129
CL2	144.5	215.0	302.0	113
CL3	144.5	215.0	302.0	269
CL4	144.5	215.0	302.0	260
CL5	129.7	157.5	210.0	125
CL6	129.8	158.0	210.8	72
CL7	129.7	157.8	210.4	127
CL8	130.0	158.8	212.0	145

Note: It appears that the spacing of collars has an influence on the length of the most damaged region of the columns

Table 4.13: Curvature ductility factors for columns CL0 to CL8

Specimens	S_1 $\times 10^6$ kN.m/(1/mm)	φ_1 $\times 10^{-6}$ (rad/mm)	φ_2 $\times 10^{-6}$ (rad/mm)	μ_φ
CL0	22.46	9.13	180.25*	19.74*
CL1	8.96	22.23	264.91*	11.92*
CL2	17.74	14.82	192.00*	12.96*
CL3	16.63	16.79	164.20*	9.78*
CL4	16.61	16.49	284.00*	17.22*
CL5	8.61	15.02	137.20	9.14
CL6	16.03	13.38	192.80	14.41
CL7	18.75	12.69	197.96	15.59
CL8	16.82	13.96	206.32	14.78

Note: The starred values are lower bound.

Table 4.14: Axial load indices for columns CL0 through CL8

Specimen	Axial Load P kN	Cylinder Strength f'_c MPa	Axial load indices		
			$\frac{P}{0.85f'_cA_g}$	$\frac{P}{P_0}$	$\frac{f_{ca}}{f'_{co}}$
CL0	1470	32.7	0.59	0.33	0.42
CL0	720	32.7	0.29	0.16	0.20
CL1	0	12.3	0	0	0
CL2	720	15.9	0.59	0.22	0.37
CL3	720	15.4	0.61	0.23	0.38
CL4	720	32.7	0.29	0.16	0.20
CL5	0	26.3	0	0	0
CL6	720	32.6	0.29	0.16	0.20
CL7	720	35.4	0.27	0.15	0.19
CL8	720	35.3	0.27	0.16	0.19

Note: $P_0 = 0.85f'_c(A_g - A_{st}) + f_y A_{st}$, and $f'_{co} = 0.85f'_c$

Table 4.15: Ratio of shear-span a to effective depth d

Specimen	Nominal		Effective a/d ratio at M_{ncc}			
	H_2 (mm)	Ratio a/d	M_{ncc} (kN.m)	F_h (kN)	$a = \frac{M_{ncc}}{F_h}$ (mm)	Ratio a/d
CL0	1900	7.92	216.5	43.11	5022	20.93
CL1	1900	7.92	235.47	124.32	1894	7.89
CL2	1900	7.92	276.92	69.39	3991	16.63
CL3	1900	7.92	300.96	75.27	3998	16.66
CL4	1900	7.92	296.84	82.37	3604	15.02
CL5	750	3.13	207.42	272.76	760	3.17
CL6	760	3.17	282.93	266.92	1060	4.42
CL7	755	3.15	296.90	282.74	1050	4.38
CL8	775	3.23	296.48	281.06	1055	4.40

Note:

a : shear-span;

d : effective depth of the column section equal to 240 mm for all columns;

M_{ncc} : nominal moment capacity of the column corresponding to the peak of moment versus drift (%) average envelope curve; and

F_h : average horizontal force at drift (%) at which M_{ncc} occurs

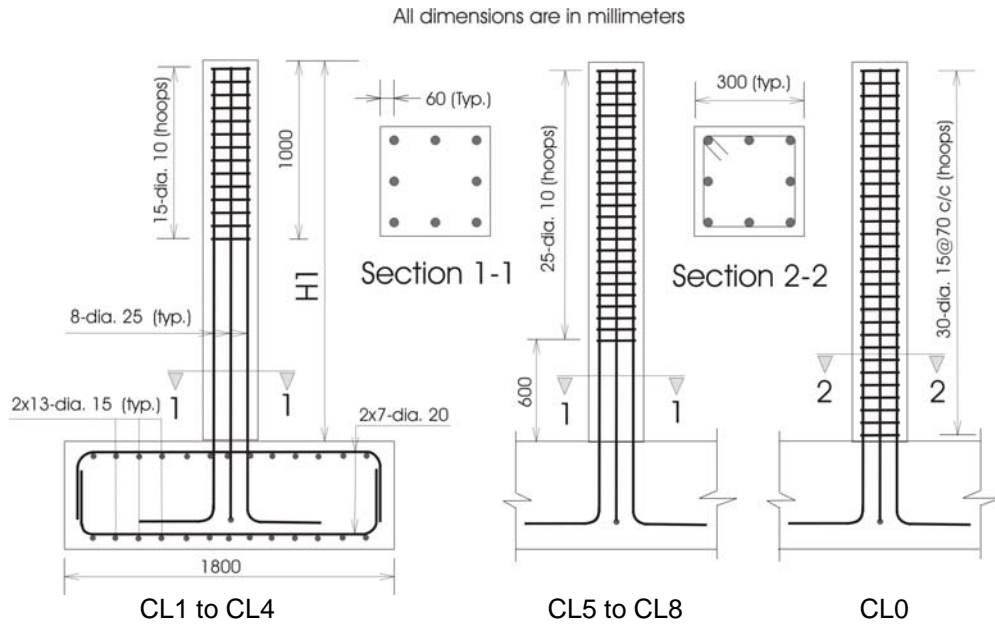


Figure 4-1: Reinforcement details of columns CL0 to CL8

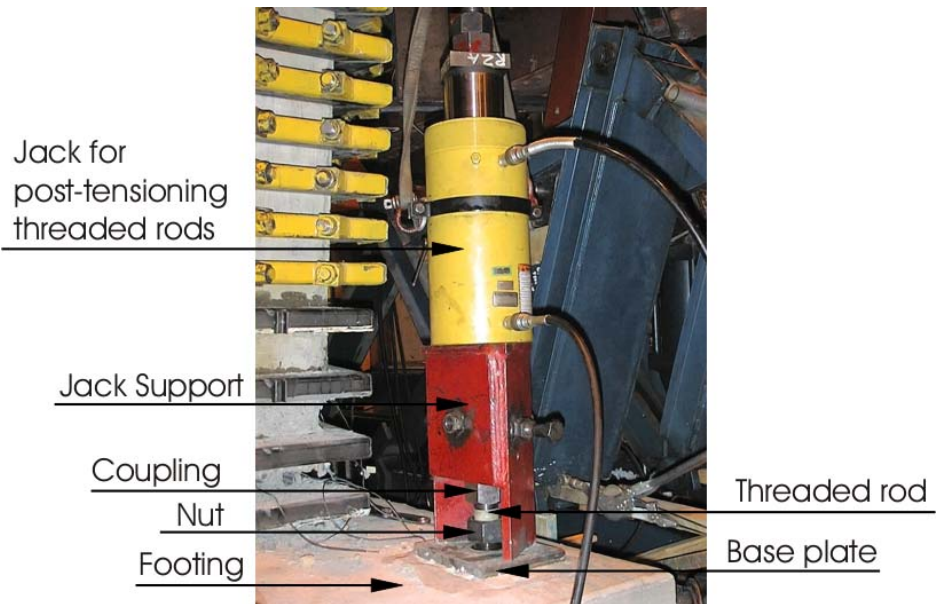


Figure 4-2: Photograph showing the detail of set-up for prestressing and release of prestressing in the threaded rods



Figure 4-3: Photograph showing the reinforcement of a typical collared column with no splicing in the longitudinal bars of the column

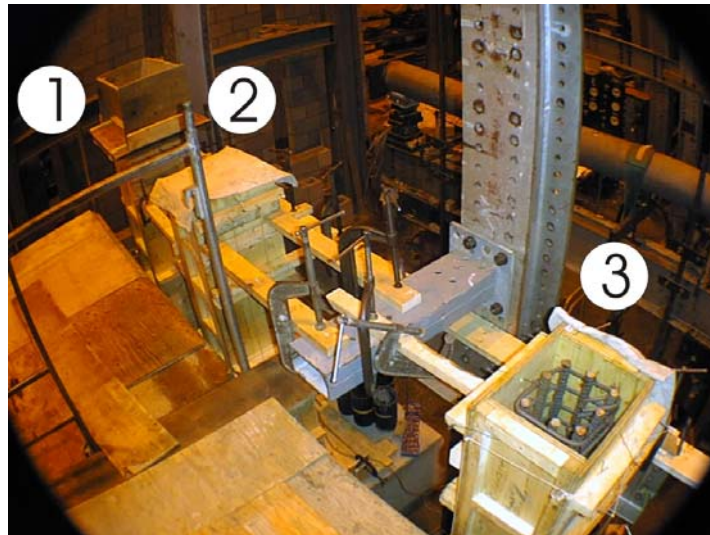


Figure 4-4: Photograph showing three columns ready for pouring



Figure 4-5: Construction sealant applied at potential location of leakages

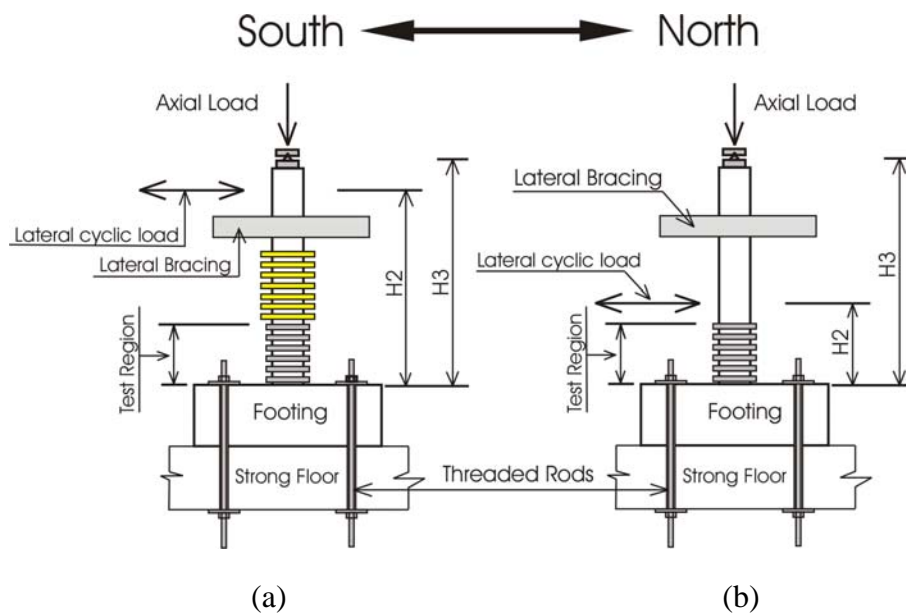


Figure 4-6: Loading scheme: (a) with long shear span; (b) with short shear span. Test region lengths are given in Table 4.4.

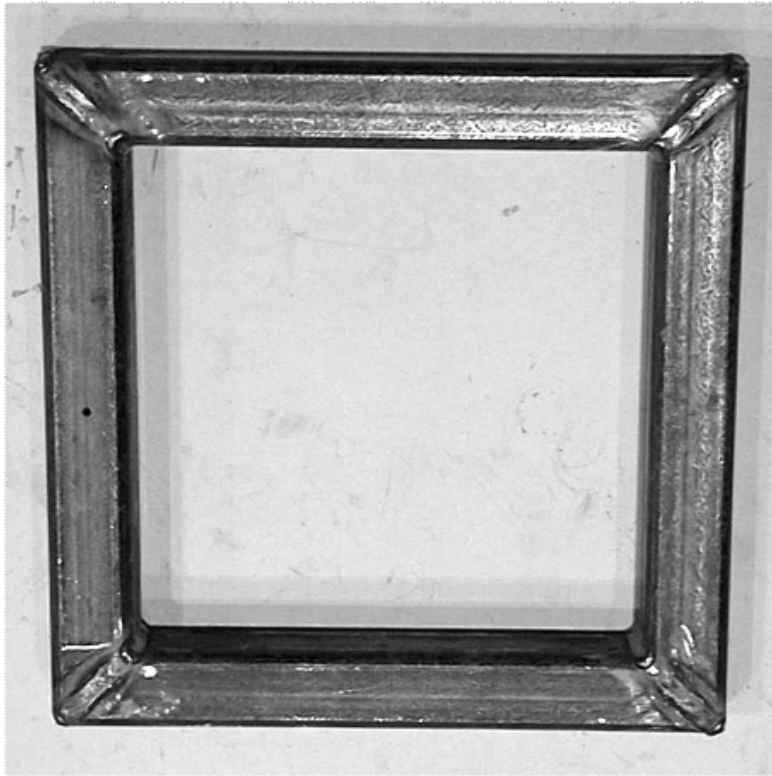
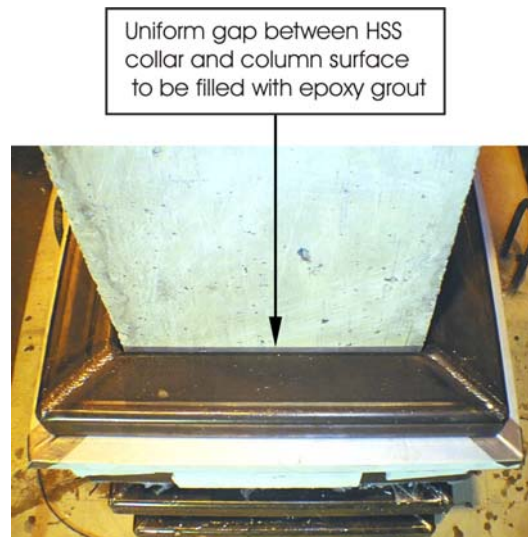


Figure 4-7: A typical HSS collar with welded corner connections



(a) A general view of collar installation



(b) Uniform gap between the collar and column before pouring epoxy grout

Figure 4-8: Installation of HSS collars on the concrete columns

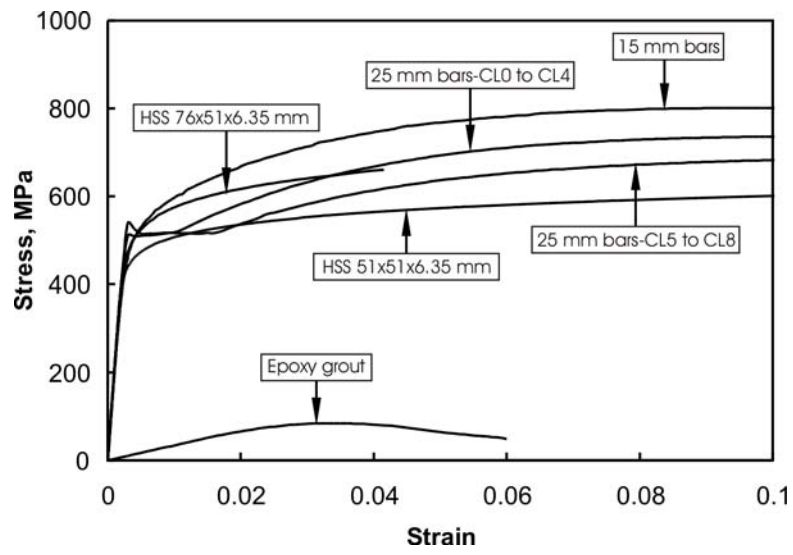


Figure 4-9: Stress vs. strain curves for rebar, HSS, and epoxy grout



Figure 4-10: A typical stub column in the loading set-up



(a) HSS51x51x6.35



(b) HSS76x51x6.35

Figure 4-11: Deformed configuration of stub-columns

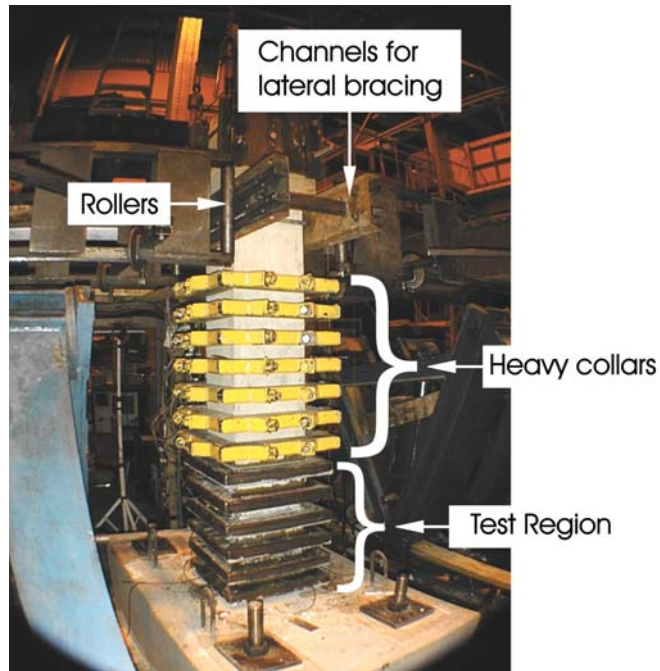


Figure 4-12: Photograph of a typical column in test set-up

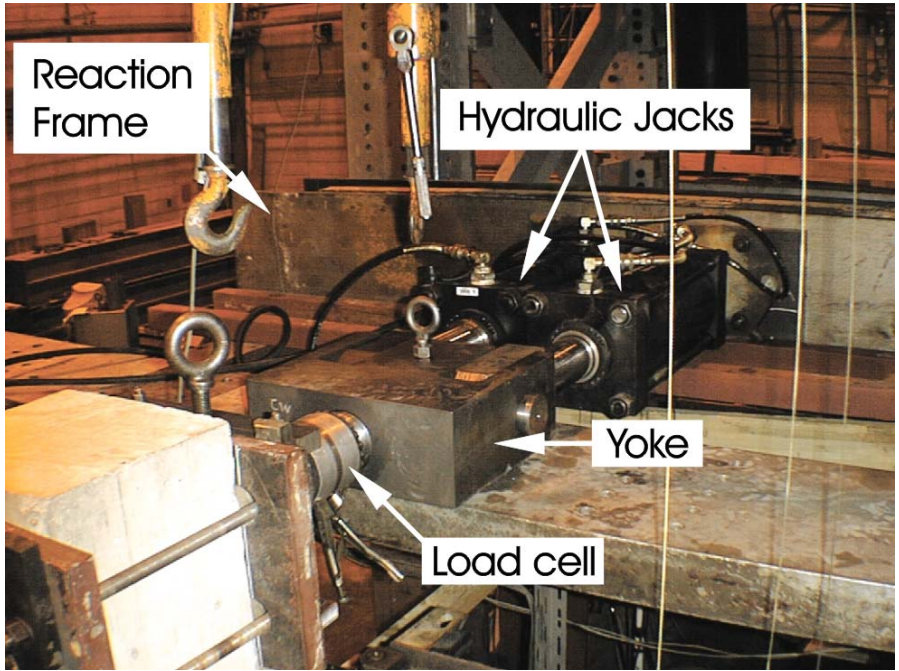


Figure 4-13: Photograph showing the assembly for horizontal loading



Figure 4-14(a): Photograph showing the attachment of horizontal loading assembly to the column specimen



Figure 4-14(b): Photograph showing the knife edge support and flat load cell for measuring vertical loads



(a) Cable Transducers



(b) LVDTs

Figure 4-15: Photograph showing cable transducers and LVDTs for measuring the rotation of collars



Figure 4-16: Photograph showing rotation meter for measuring the rotation of collars

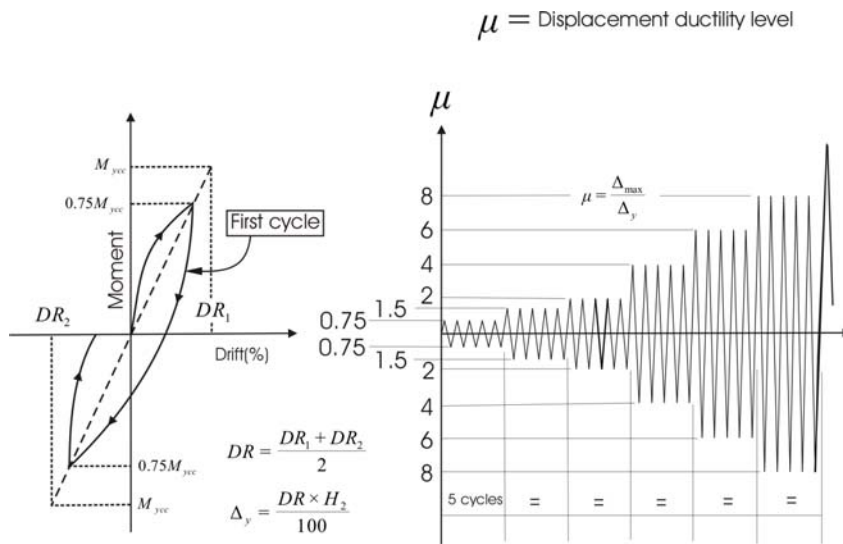
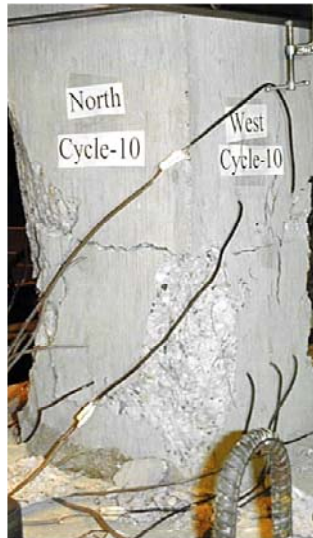


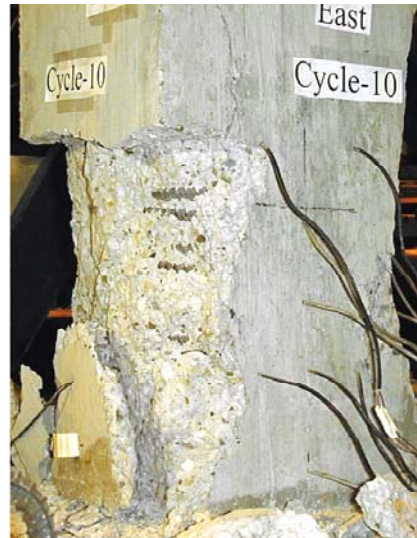
Figure 4-17: Sequence of imposed horizontal displacements (adapted from Ghee *et al.* (1989))



(a) before loading

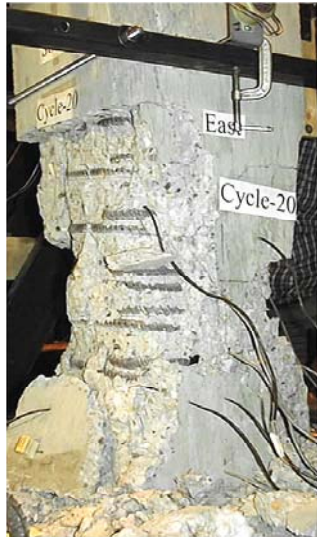


(b) North and West faces at the end of cycle 10

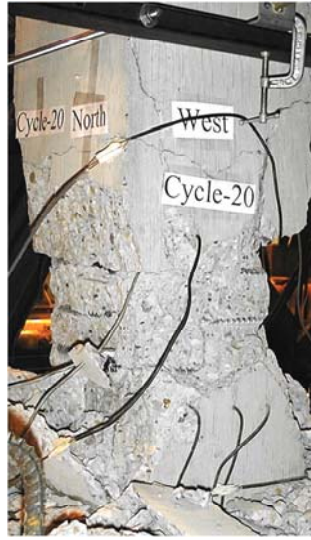


(c) South and East faces at the end of cycle 10

Figure 4-18: Appearance of test region of specimen CL0 at different stages of test



(d) South and East faces at the end of cycle 20



(e) North and West faces at the end of cycle 20



(f) North and West faces at the end of cycle 30



(g) South and East faces at the end of cycle 30



(h) East face at the end of test



(i) West face at the end of test

Figure 4-18: Appearance of test region of column CL0 at different stages of test (continued)



(a) a view of crack in gap 2



(b) a view of crack in footing cover concrete
on north side of the column

Figure 4-19: Appearances of specimen CL1 at different stages of the test



(c) a view of the test region at test end



(d) a view of damage in gaps 1 and 2 at test end

Figure 4-19: Appearances of test region of specimen CL1 at different stages of the test (continued)



(a) before loading



(b) after 10th cycle



(c) after 20th cycle



(d) after test

Figure 4-20: Appearances of test region of specimen CL2 at different stages of test



(a) after cycle 20



(b) after cycle 30



(c) after cycle 40



(d) at test end

Figure 4-21: Appearances of test region of specimen CL3 at different stages of test



(a) after cycle 20



(b) after cycle 30



(c) after cycle 40



(d) after test

Figure 4-22: Appearances of test region of specimen CL4 at different stages of test



(a) South face



(b) East face



(c) a close-up of lower portion (ruptured bars visible)

Figure 4-23: Appearances of test region of specimen CL5 at the end of the test



(a) after 10th cycle



(b) after 20th cycle



(c) after 30th cycle



(d) after test (ruptured bars visible)

Figure 4-24: Appearances of test region of specimen CL6 at different stages of test



Figure 4-25: A close-up of ruptured longitudinal bars of specimen CL6 at the end of test



(a) after 10th cycle



(b) after 30th cycle



(c) East face at test end



(d) West face at test end

Figure 4-26: Appearances of test region of specimen CL7 at different stages of test



(a) after 10th cycle



(b) after 20th cycle



(c) after 30th cycle



(d) after test

Figure 4-27: Appearances of test region of specimen CL8 at different stages of test

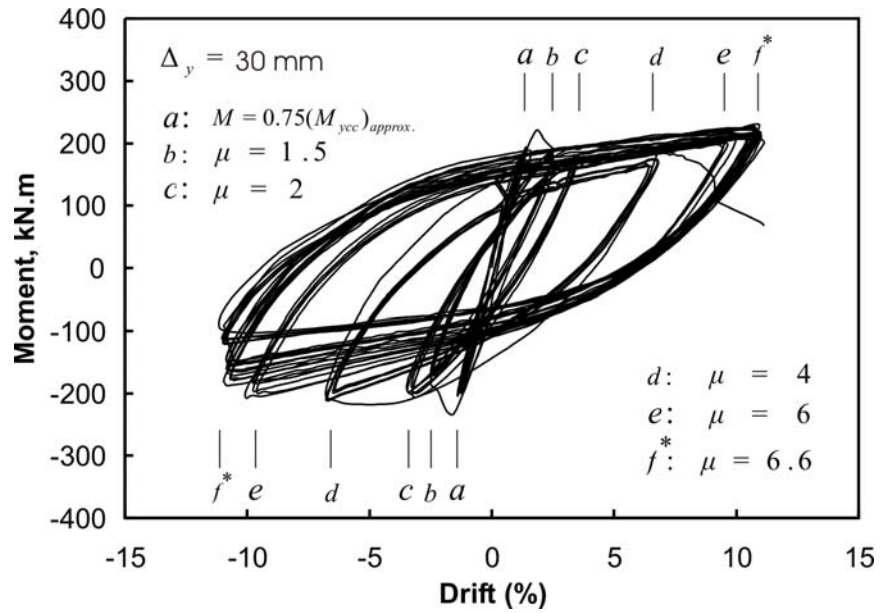


Figure 4-28: Moment at column base vs. lateral drift hysteresis for specimen CL0

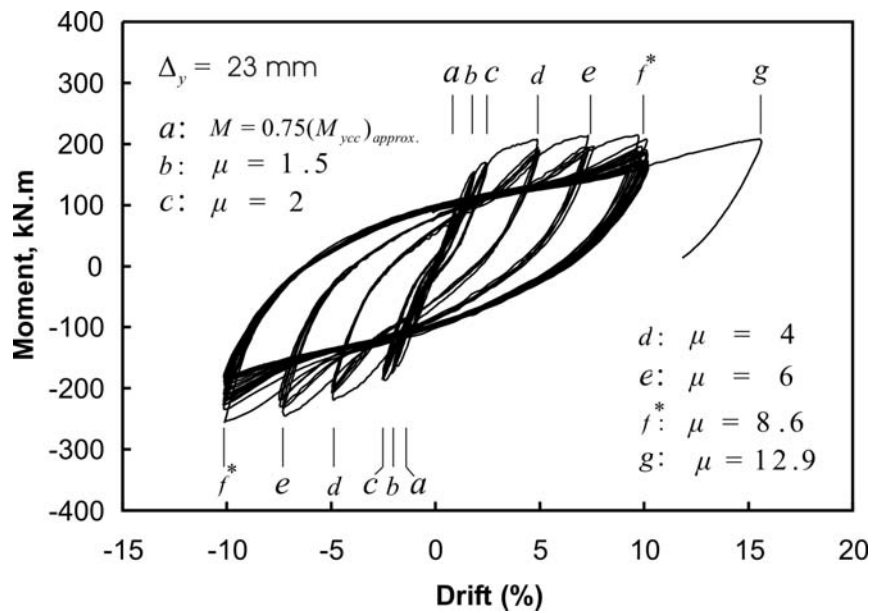


Figure 4-29: Moment at column base vs. lateral drift hysteresis for specimen CL1

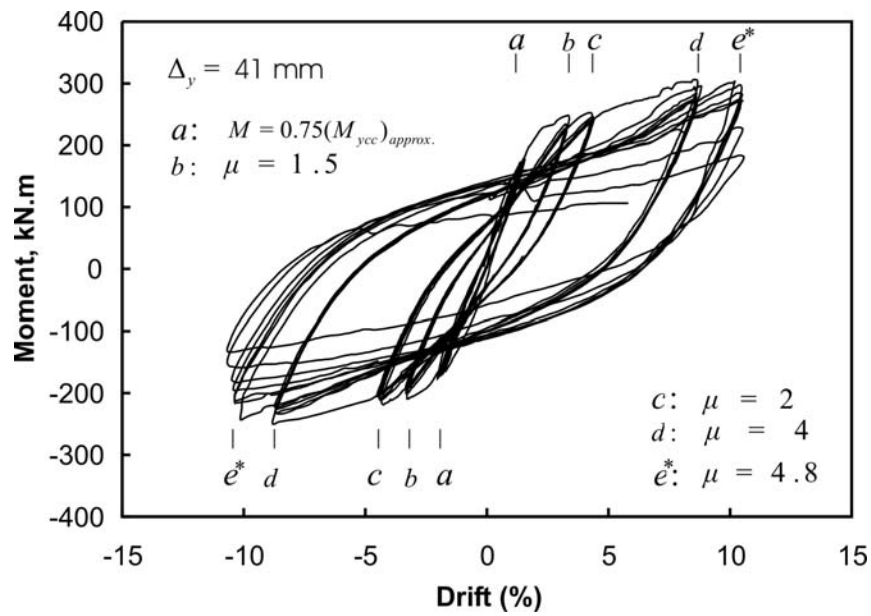


Figure 4-30: Moment at column base vs. lateral drift hysteresis for specimen CL2

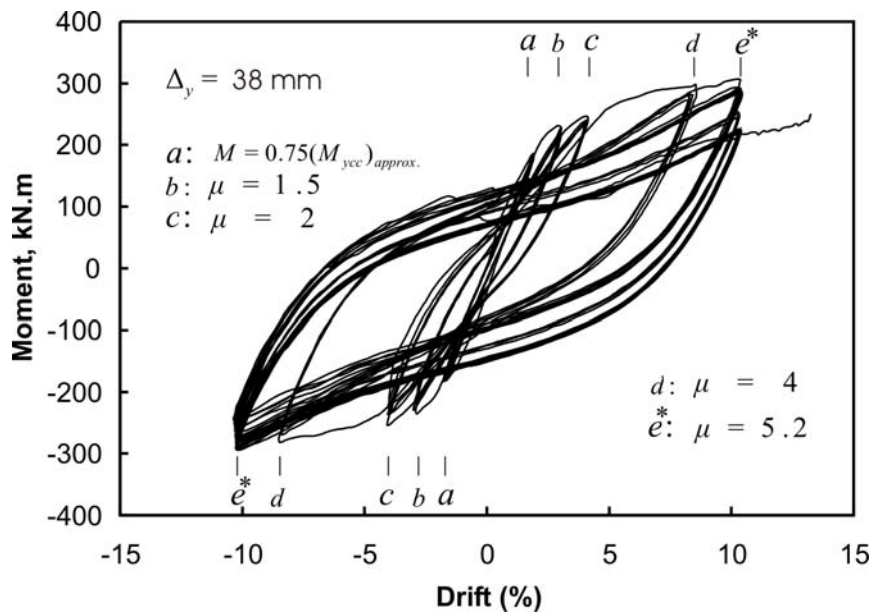


Figure 4-31: Moment at column base vs. lateral drift hysteresis for column CL3

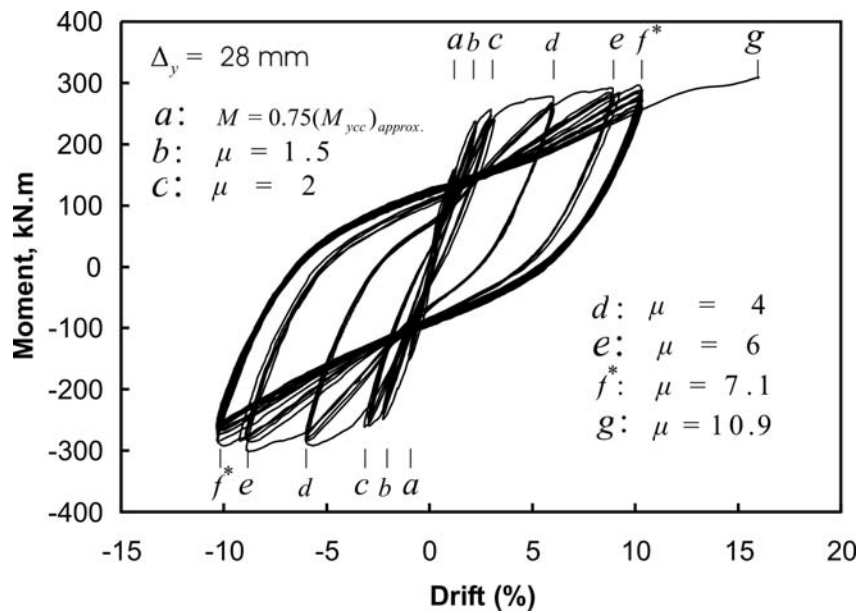


Figure 4-32: Moment at column base vs. lateral drift hysteresis for specimen CL4

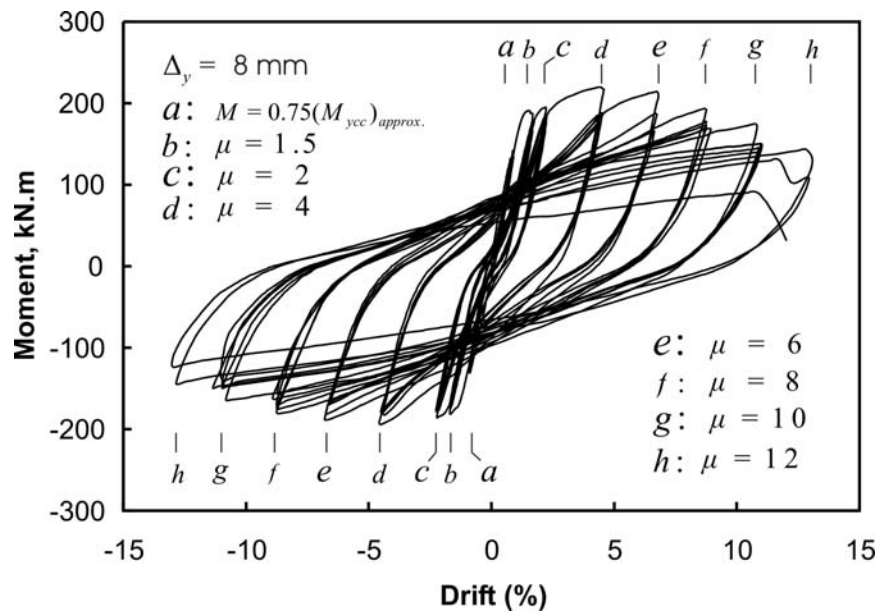


Figure 4-33: Moment at column base vs. lateral drift hysteresis for specimen CL5

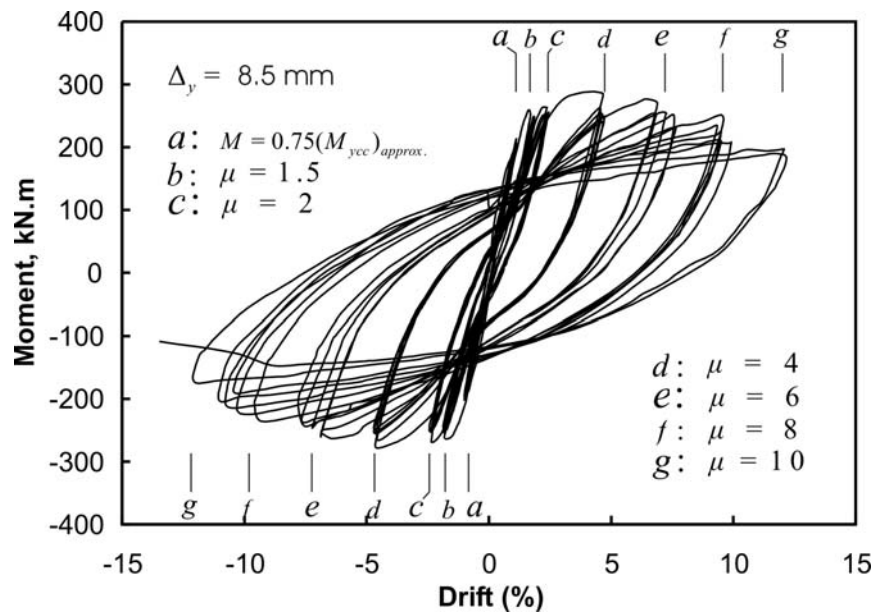


Figure 4-34: Moment at column base vs. lateral drift hysteresis for specimen CL6

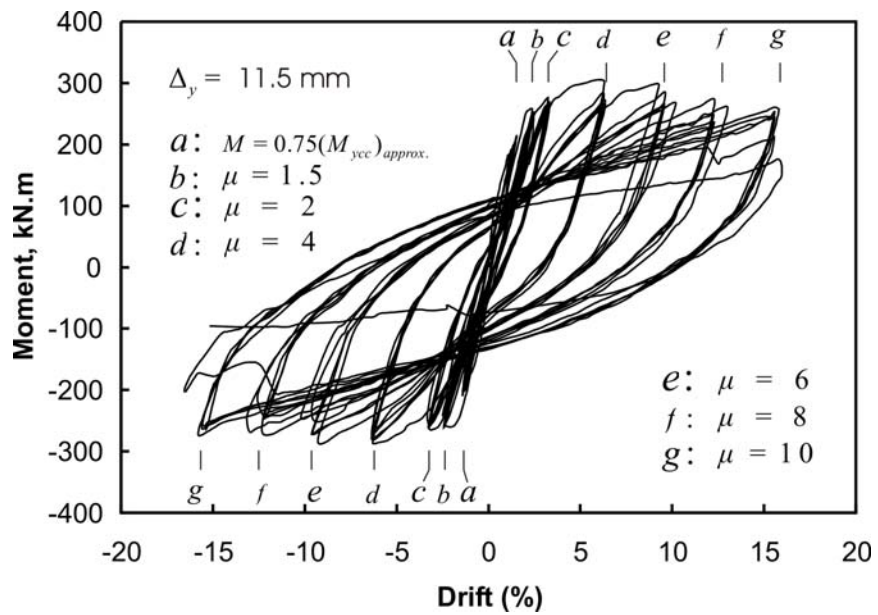


Figure 4-35: Moment at column base vs. lateral drift hysteresis for specimen CL7

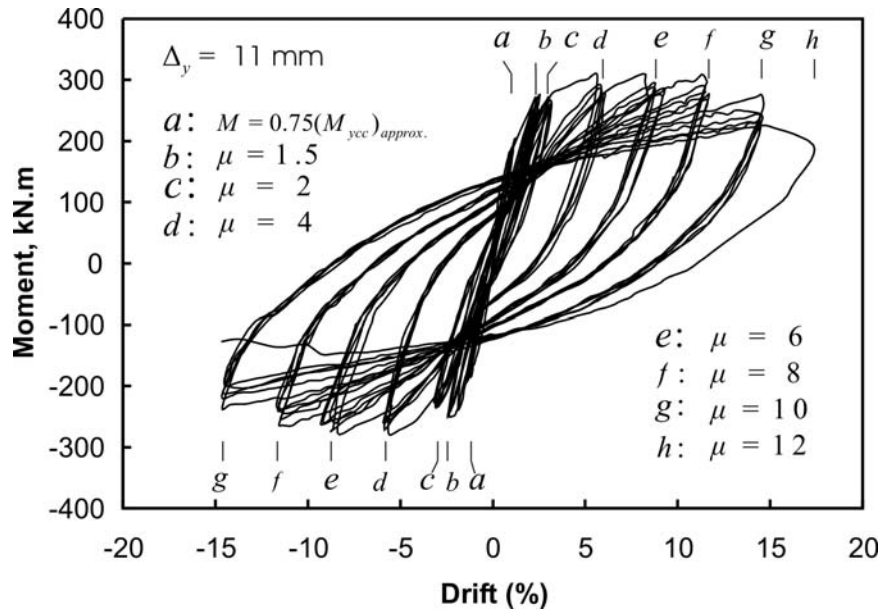


Figure 4-36: Moment at column base vs. lateral drift hysteresis for column CL8

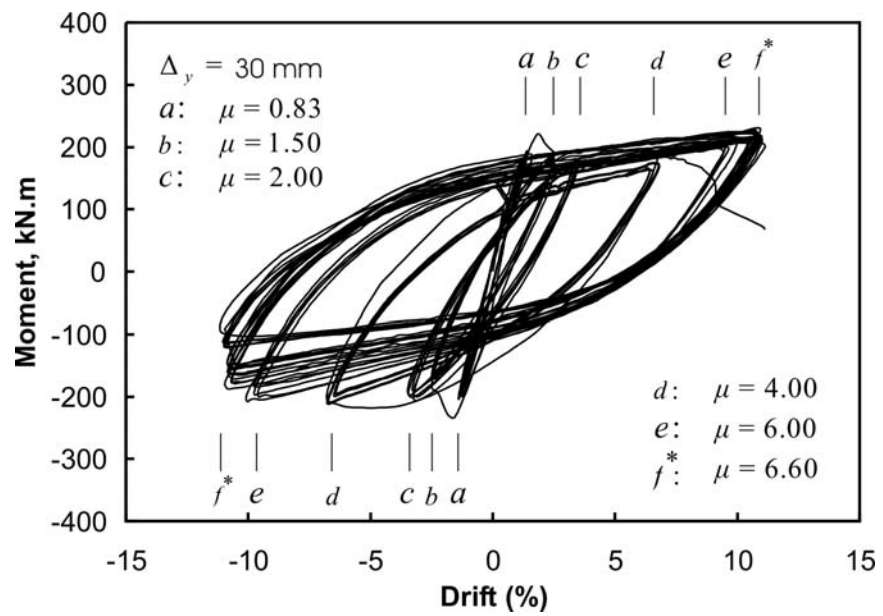


Figure 4-37: Revised moment vs. drift hysteresis for column CL0

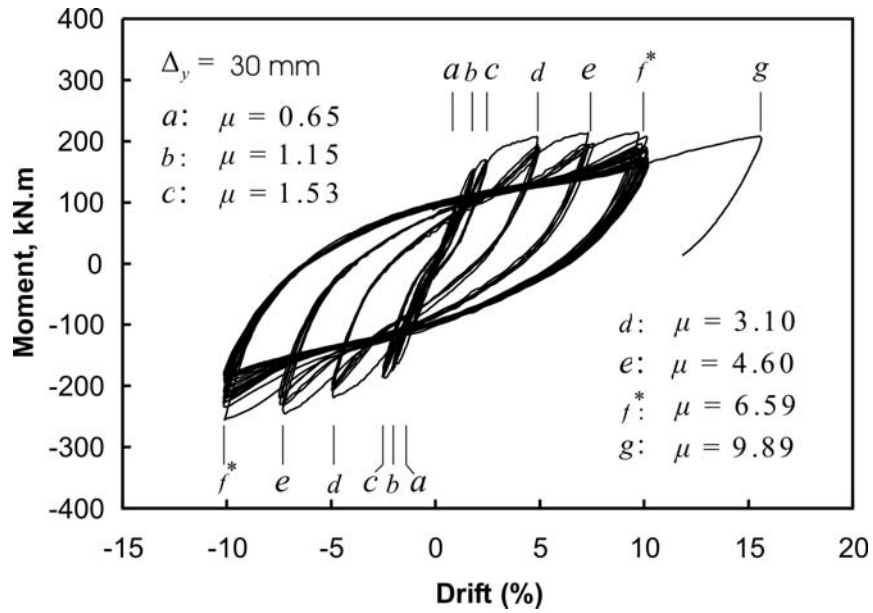


Figure 4-38: Revised moment vs. drift hysteresis for column CL1

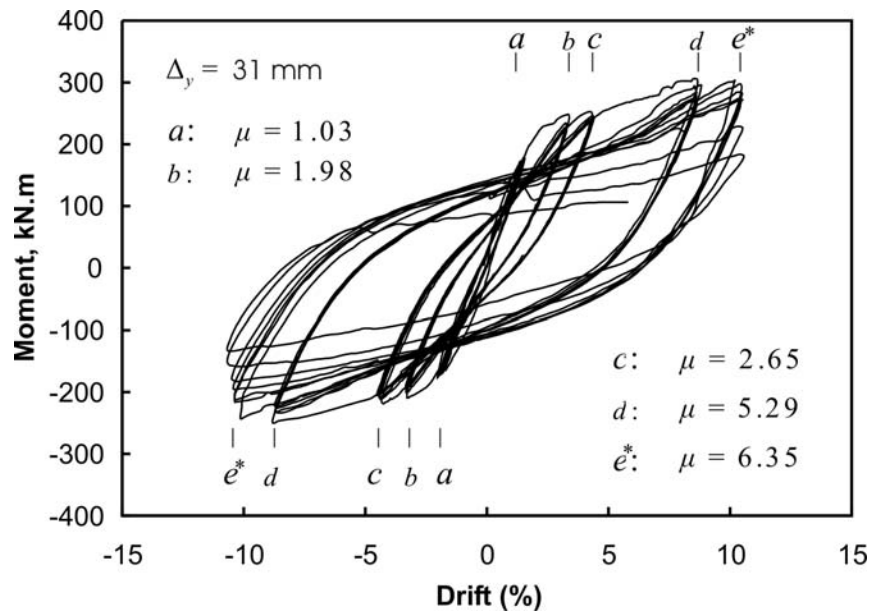


Figure 4-39: Revised moment vs. drift hysteresis for column CL2

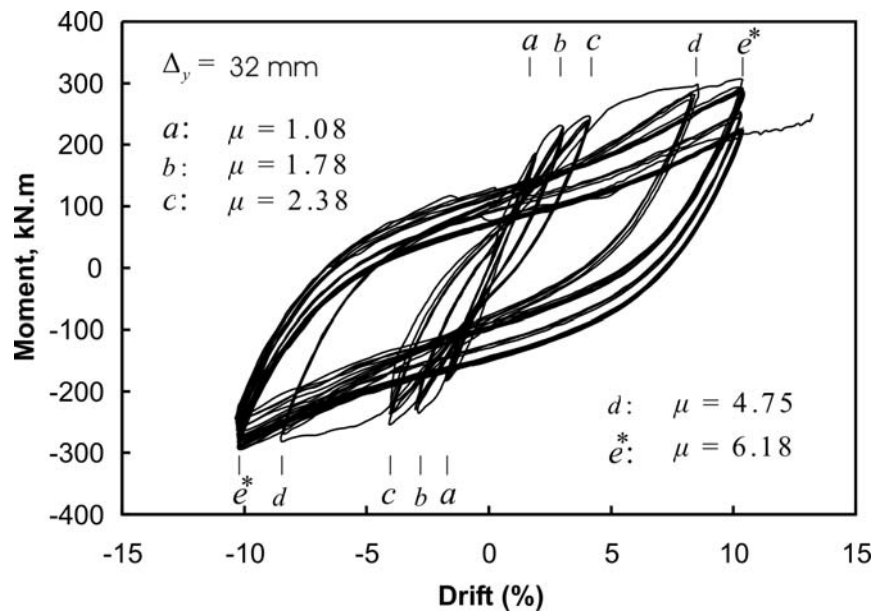


Figure 4-40: Revised moment vs. drift hysteresis for column CL3

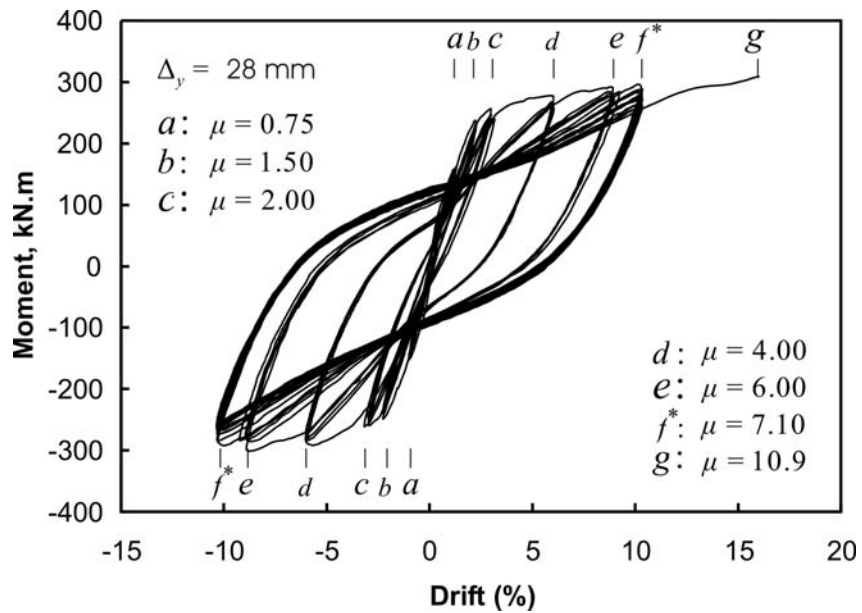


Figure 4-41: Revised moment vs. drift hysteresis for column CL4

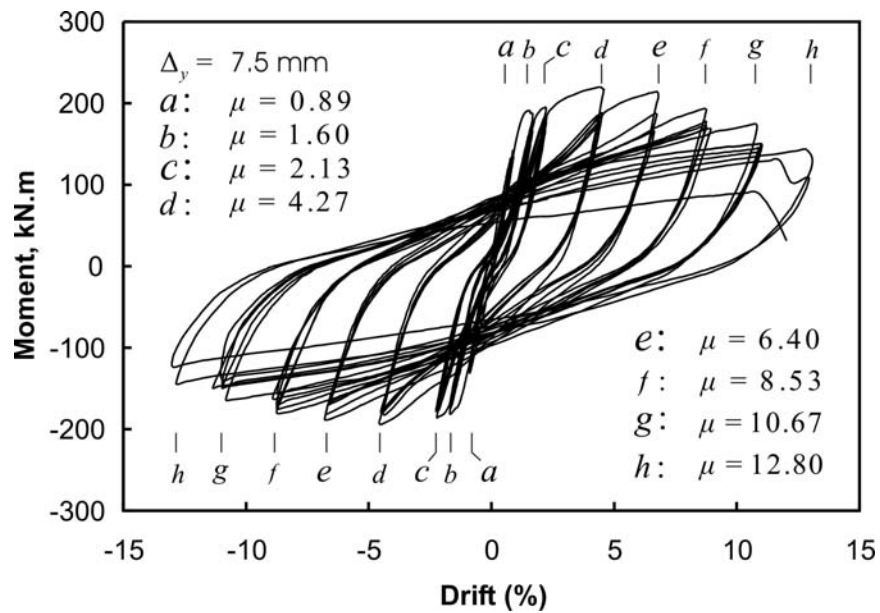


Figure 4-42: Revised moment vs. drift hysteresis for column CL5

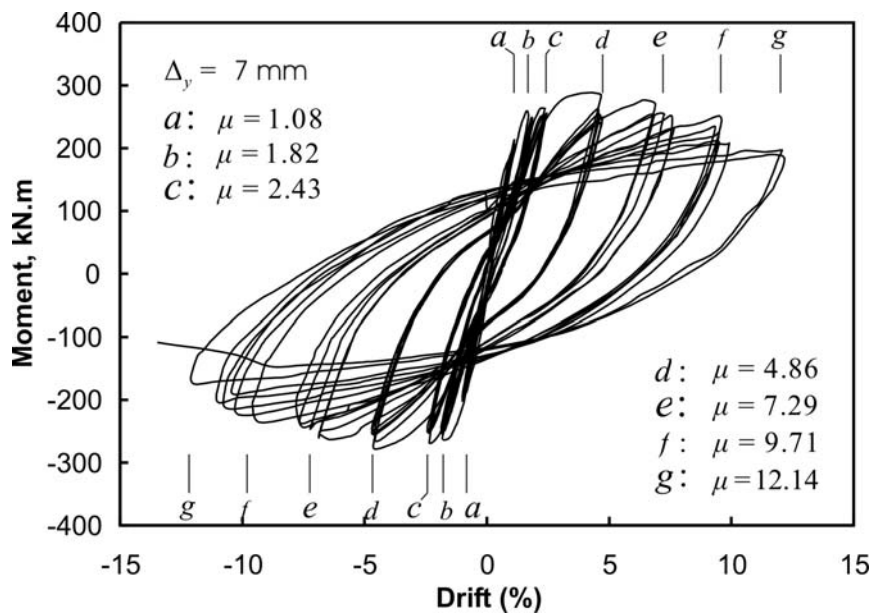


Figure 4-43: Revised moment vs. drift hysteresis for column CL6

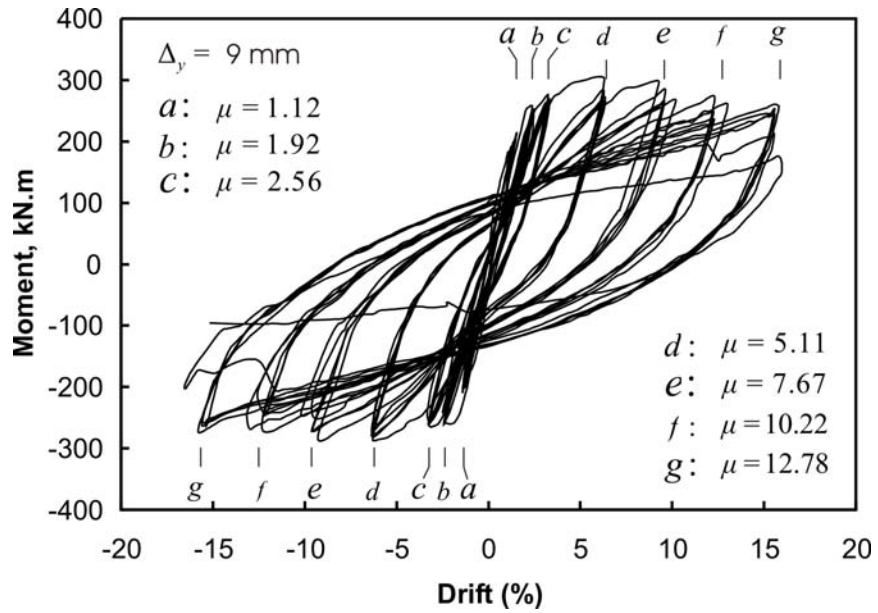


Figure 4-44: Revised moment vs. drift hysteresis for column CL7

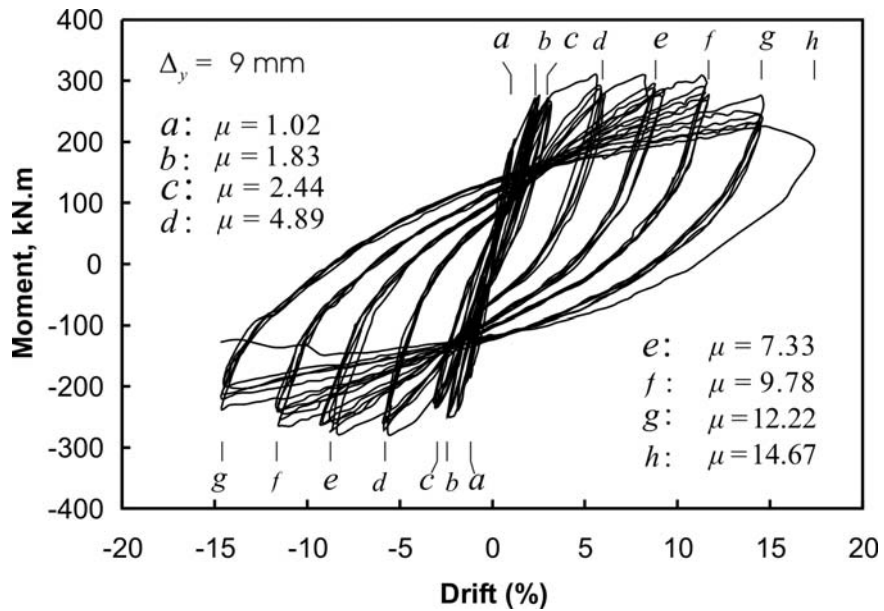


Figure 4-45: Revised moment vs. drift hysteresis for column CL8

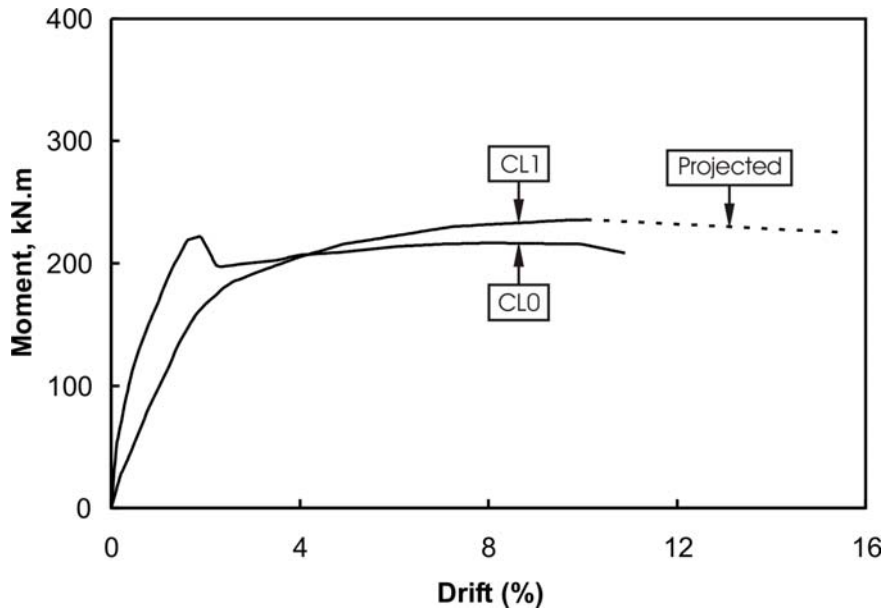


Figure 4-46: Envelope curves for specimen CL0 and CL1 (assumed projected part for CL1)

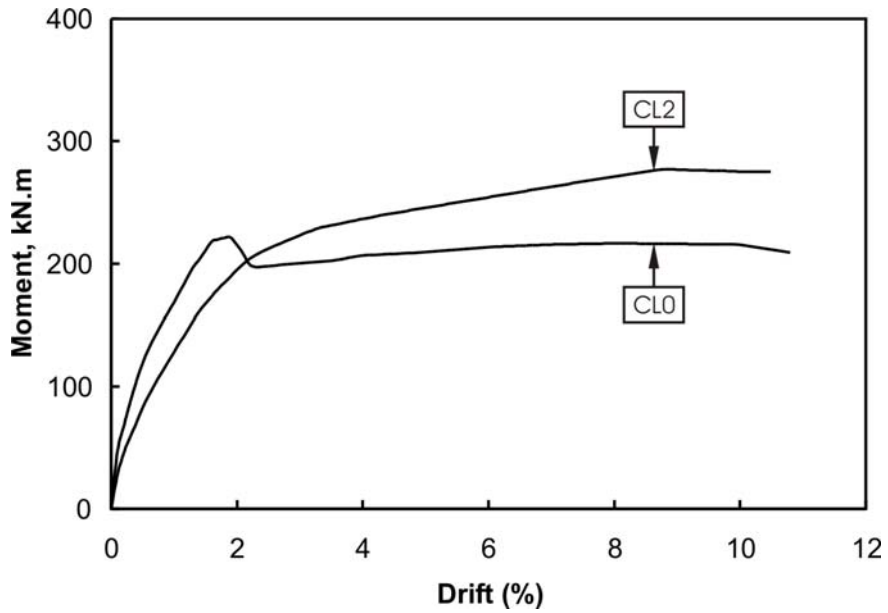


Figure 4-47: Envelope curves for specimen CL0 and CL2

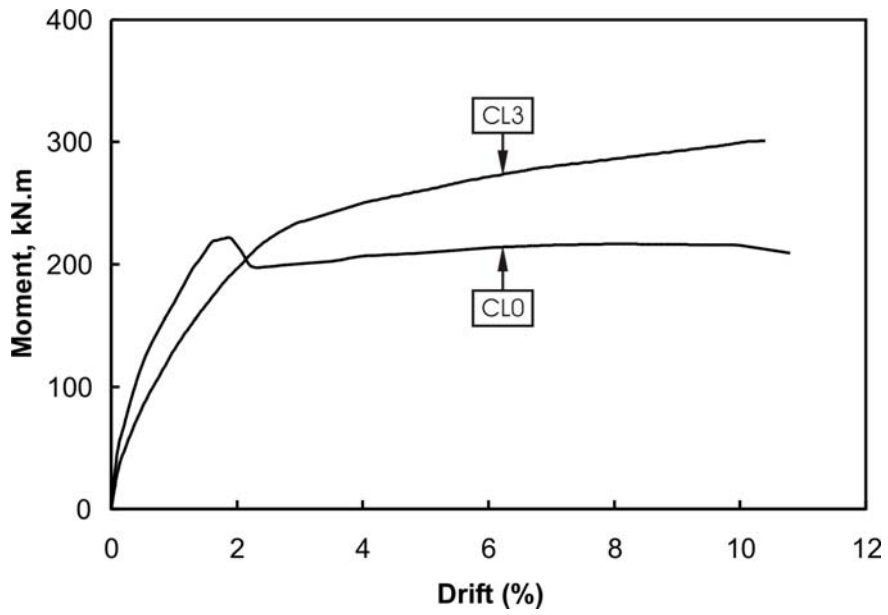


Figure 4-48: Envelope curves for specimen CL0 and CL3

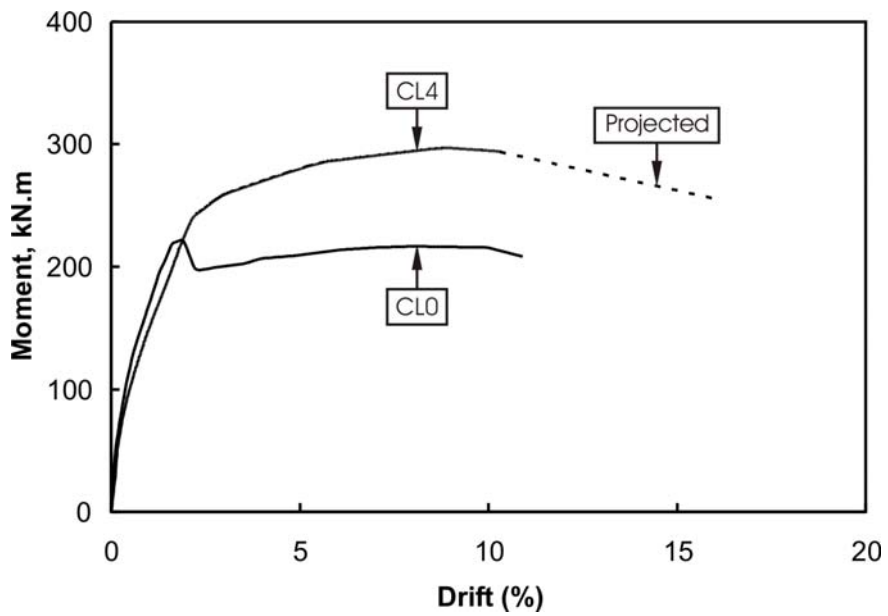


Figure 4-49: Envelope curves for specimen CL0 and CL4 (assumed dashed part in CL4)

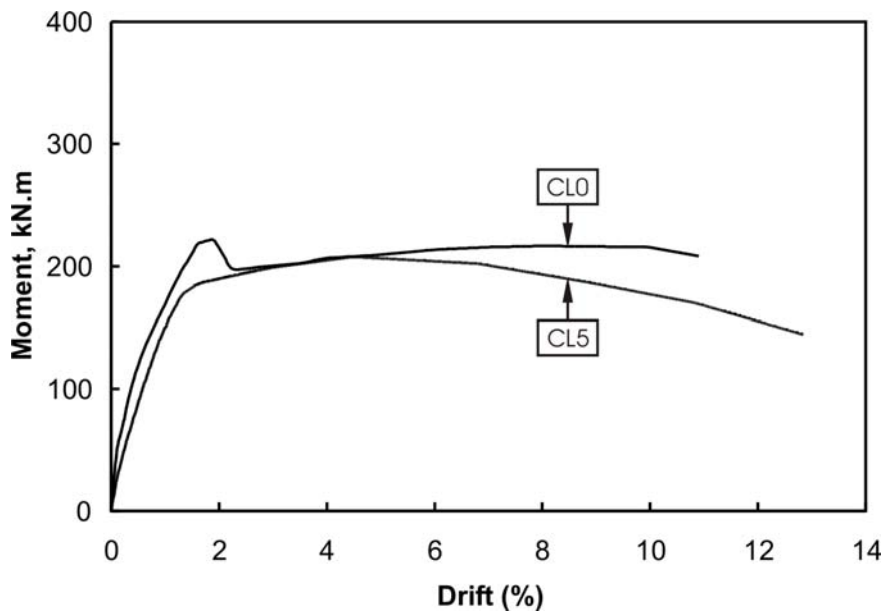


Figure 4-50: Envelope curves for specimen CL0 and CL5

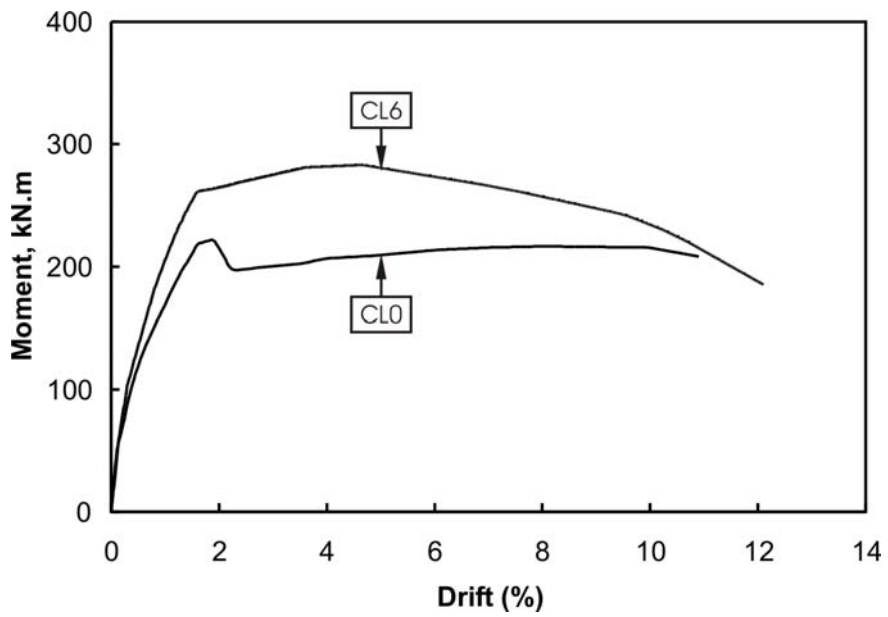


Figure 4-51: Envelope curves for specimen CL0 and CL6

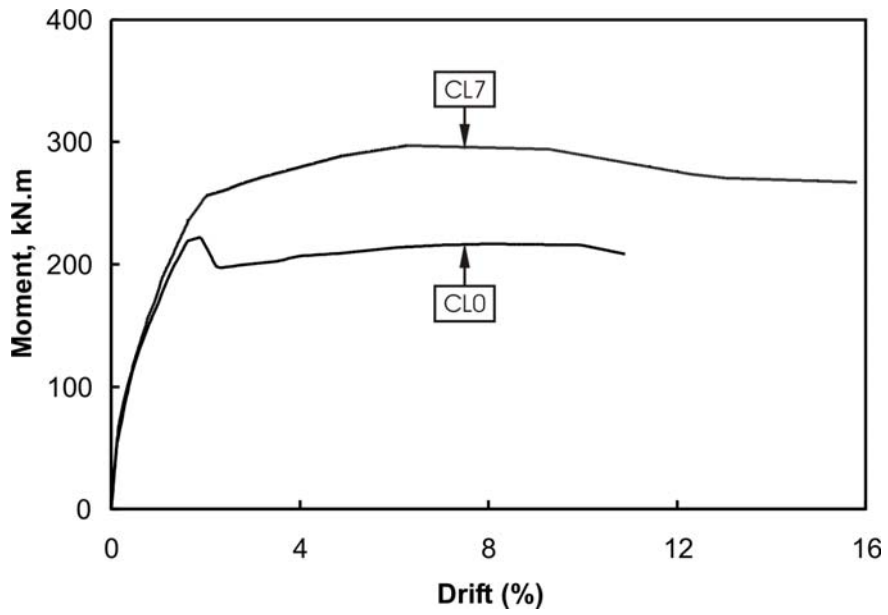


Figure 4-52: Envelope curves for specimen CL0 and CL7

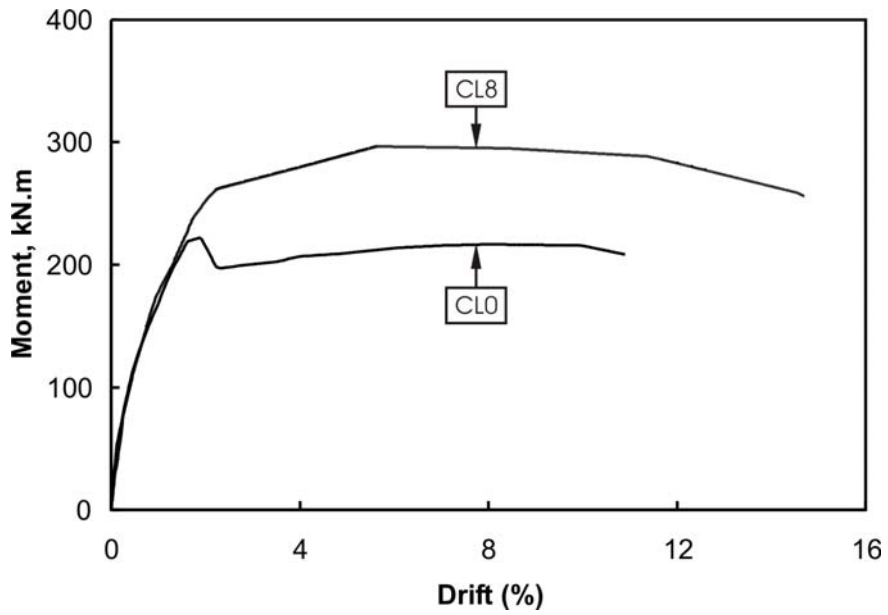


Figure 4-53: Envelope curves for specimen CL0 and CL8

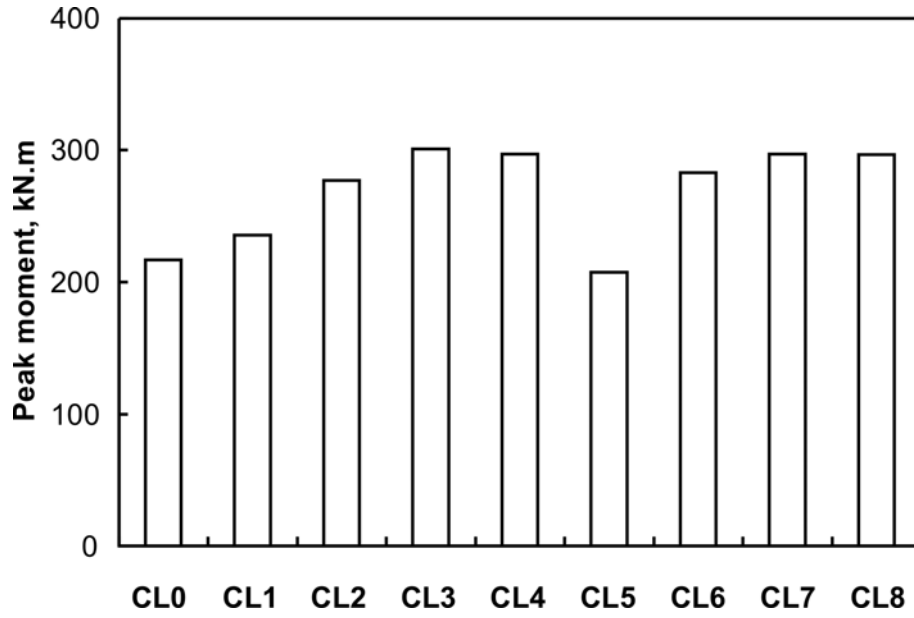


Figure 4-54: Peak moments of the columns from the average envelope curves.

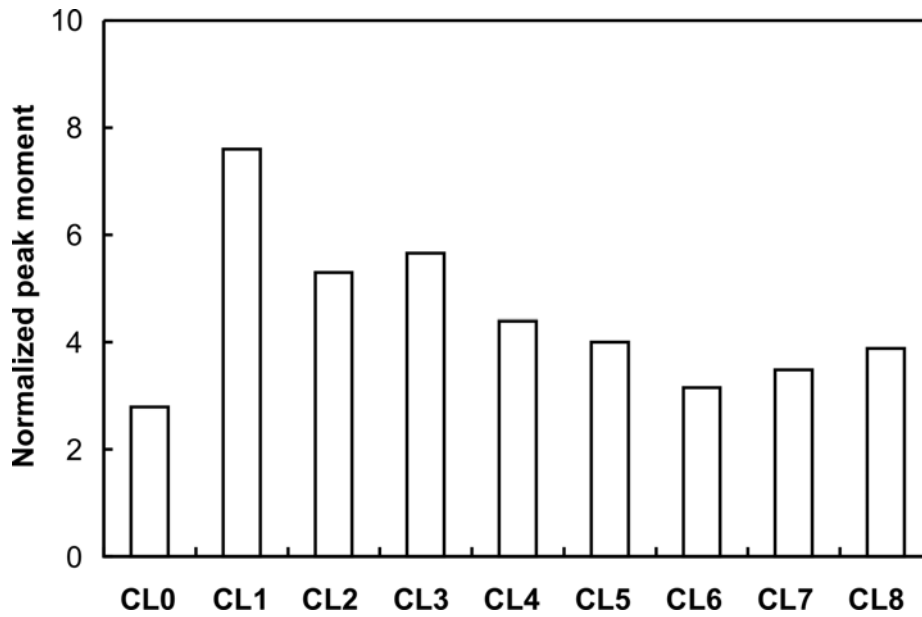


Figure 4-55: Normalized peak moments of the columns from the average envelope curves.

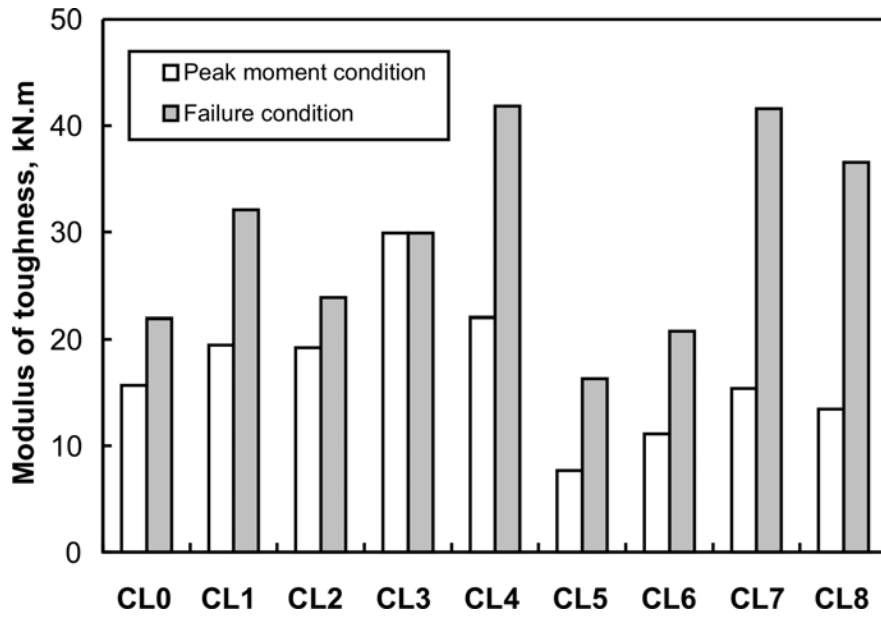


Figure 4-56: Modulus of toughness for all the specimens

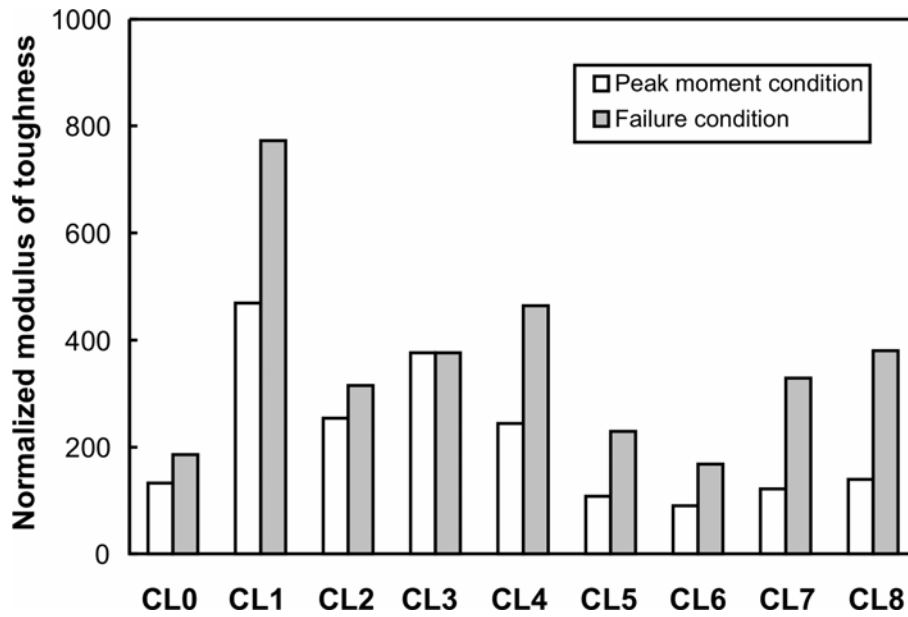


Figure 4-57: Normalized modulus of toughness for all the specimens

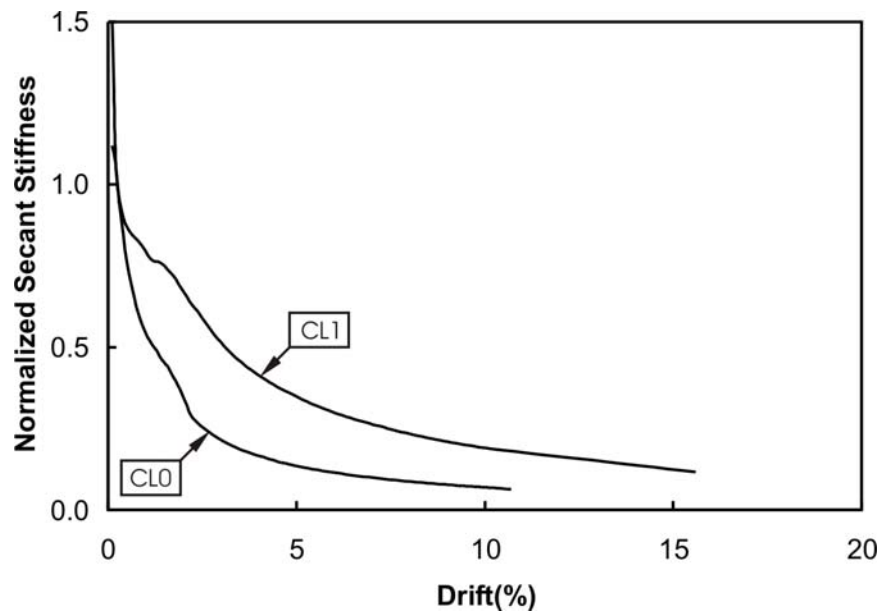


Figure 4-58: Normalized secant stiffness vs. drift (%) for specimens CL1 and CL0

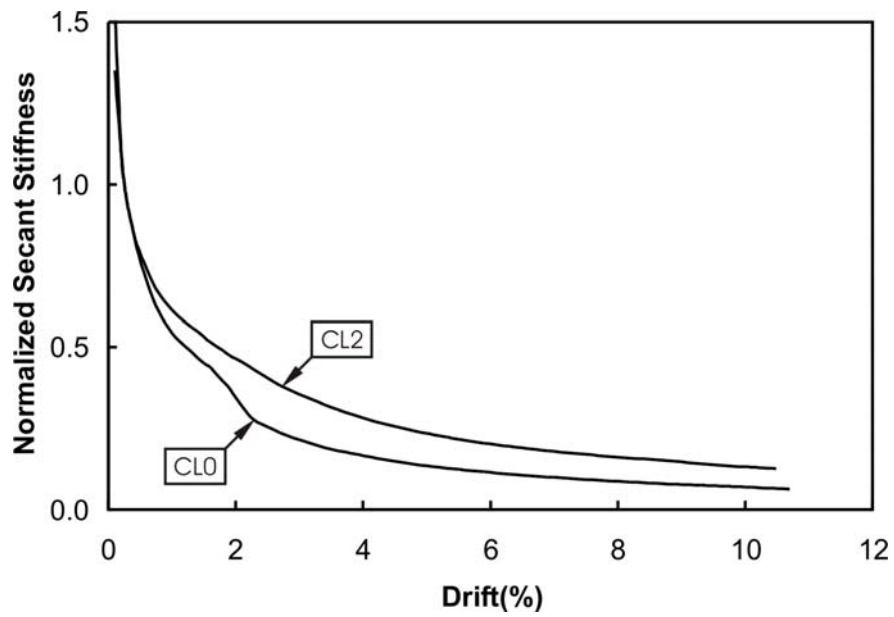


Figure 4-59: Normalized secant stiffness vs. lateral drift (%) for specimens CL2 and CL0

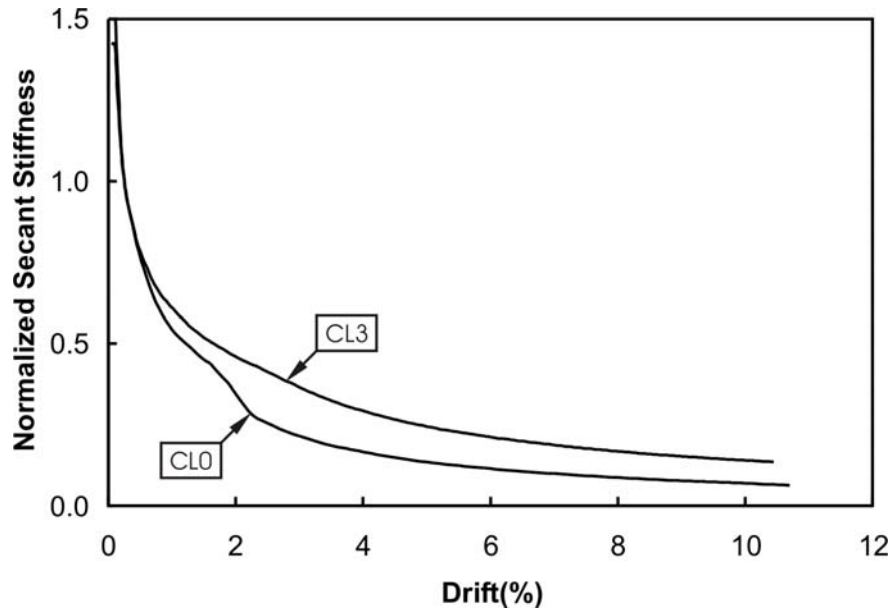


Figure 4-60: Normalized secant stiffness vs. lateral drift (%) for specimens CL3 and CL0

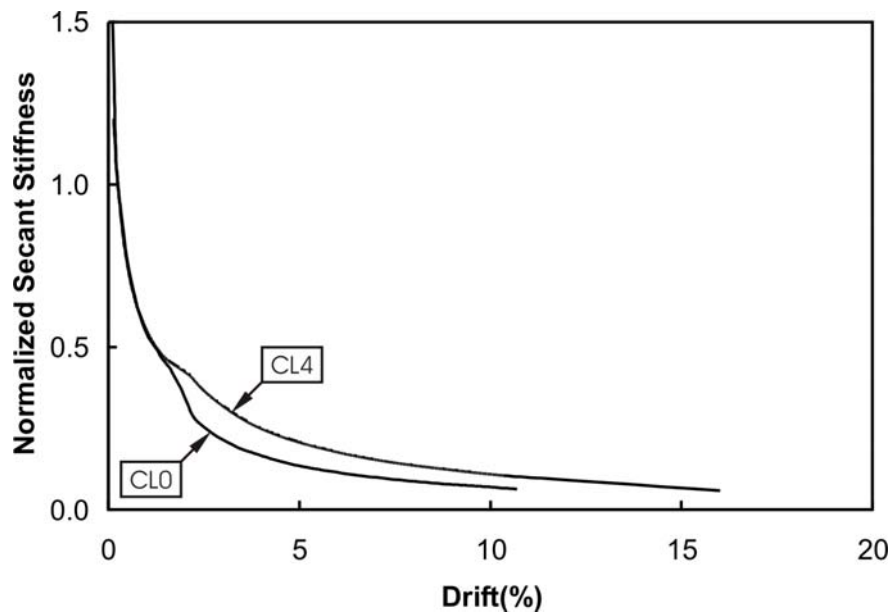


Figure 4-61: Normalized secant stiffness vs. lateral drift (%) for specimens CL4 and CL0

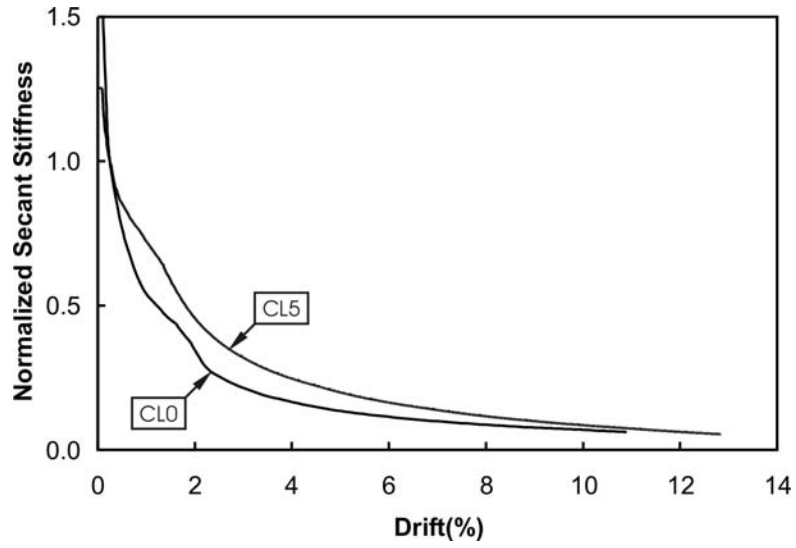


Figure 4-62: Normalized secant stiffness vs. lateral drift (%) for specimens CL5 and CL0

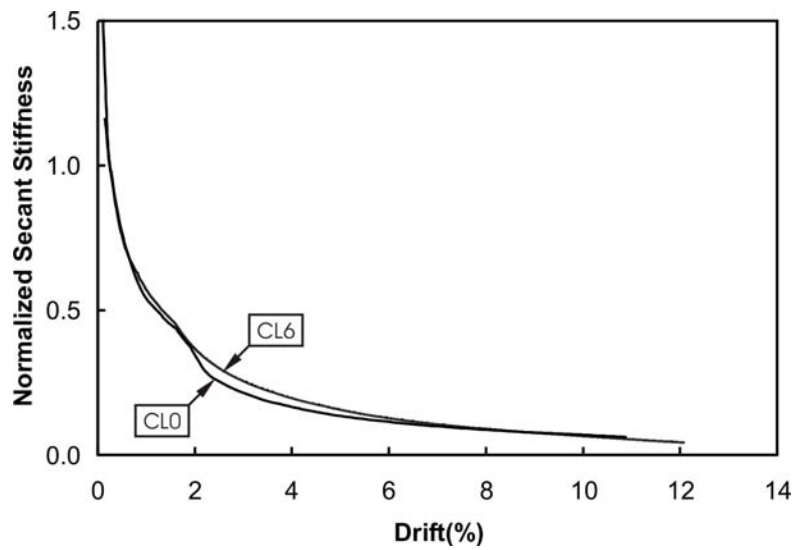


Figure 4-63: Normalized secant stiffness vs. lateral drift (%) for specimens CL6 and CL0

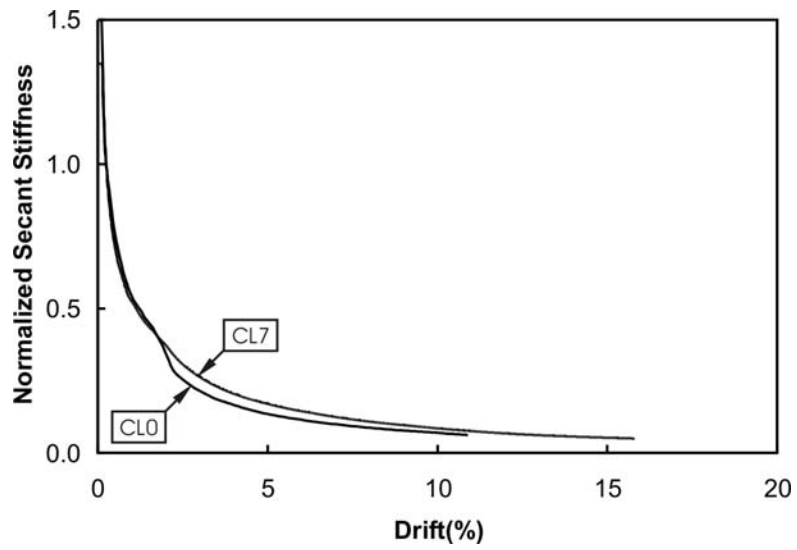


Figure 4-64: Normalized secant stiffness vs. lateral drift (%) for specimens CL7 and CL0

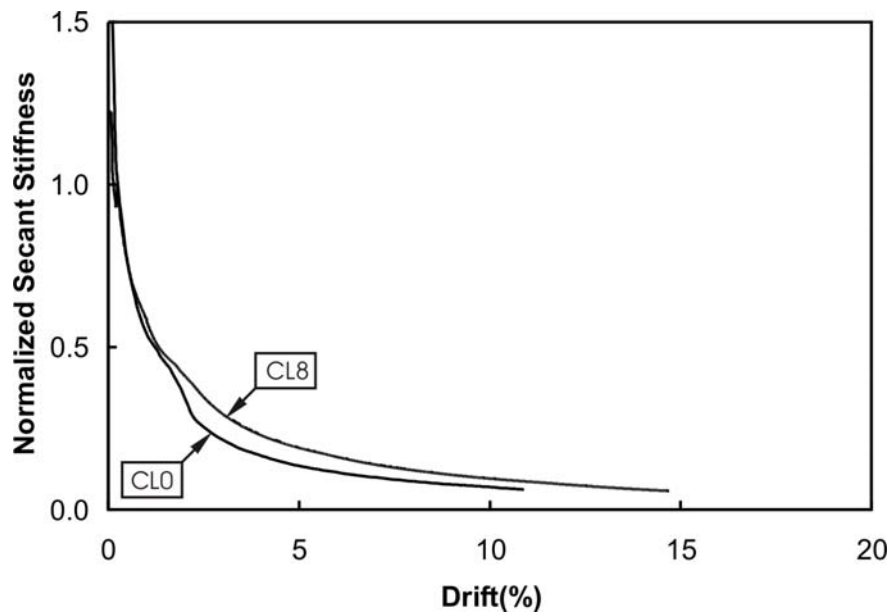


Figure 4-65: Normalized secant stiffness vs. lateral drift (%) for specimens CL8 and CL0

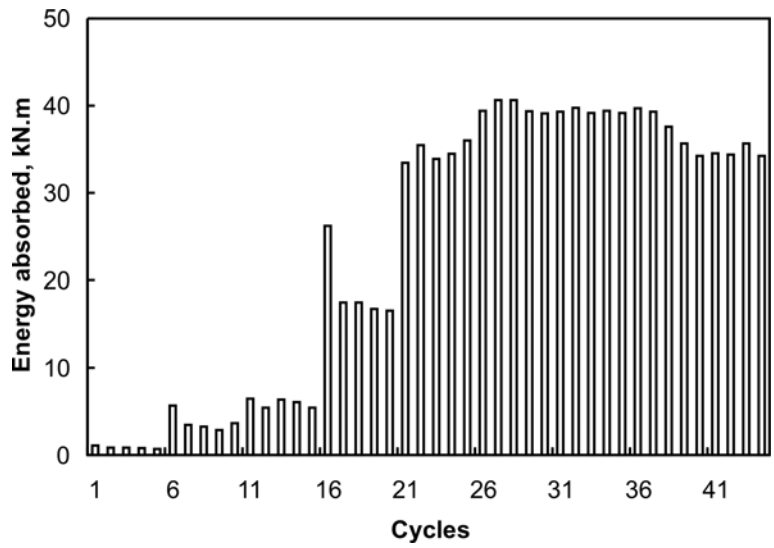


Figure 4-66: Energy absorbed by specimen CL0 per cycle based on overall system.

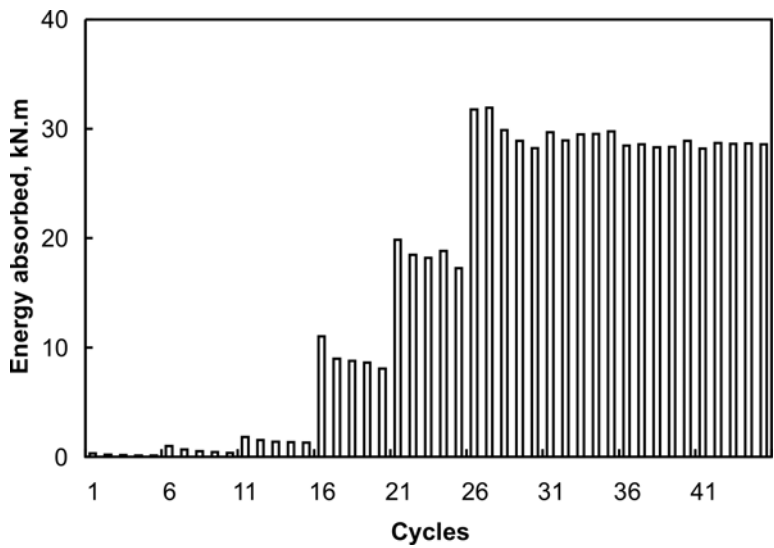


Figure 4-67: Energy absorbed by specimen CL1 per cycle based on overall system.

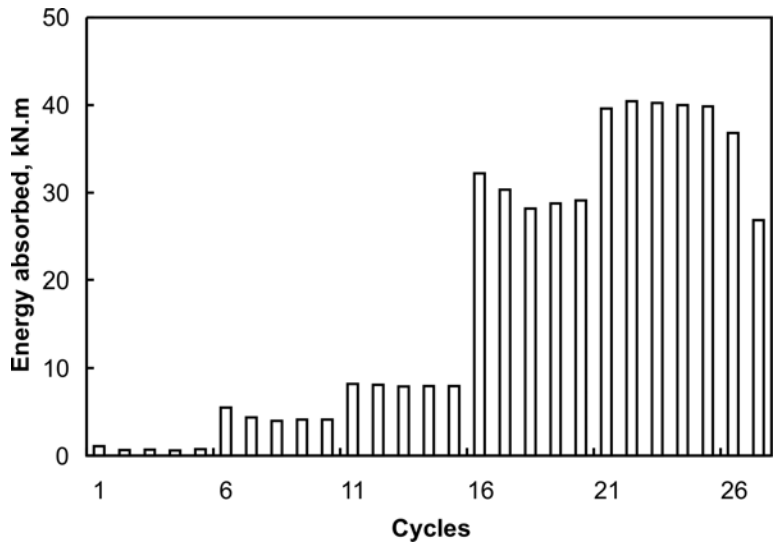


Figure 4-68: Energy absorbed by specimen CL2 per cycles based on overall system.

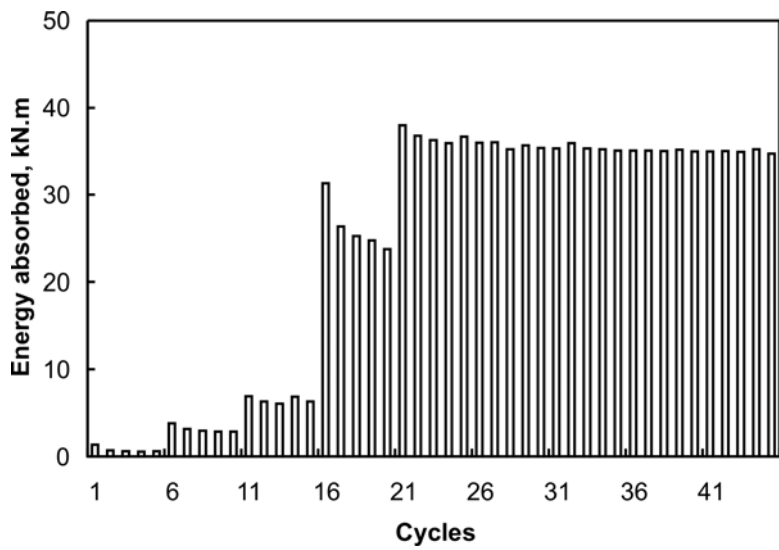


Figure 4-69: Energy absorbed by specimen CL3 per cycles based on overall system.

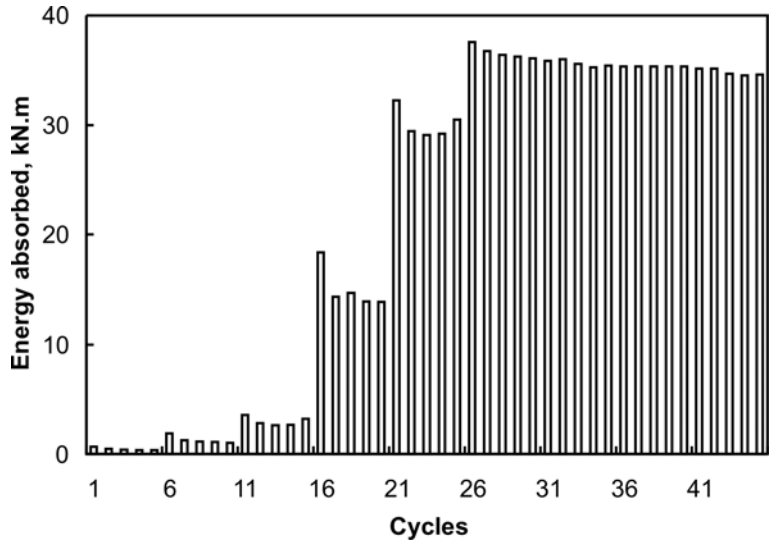


Figure 4-70: Energy absorbed by specimen CL4 per cycles based on overall system.

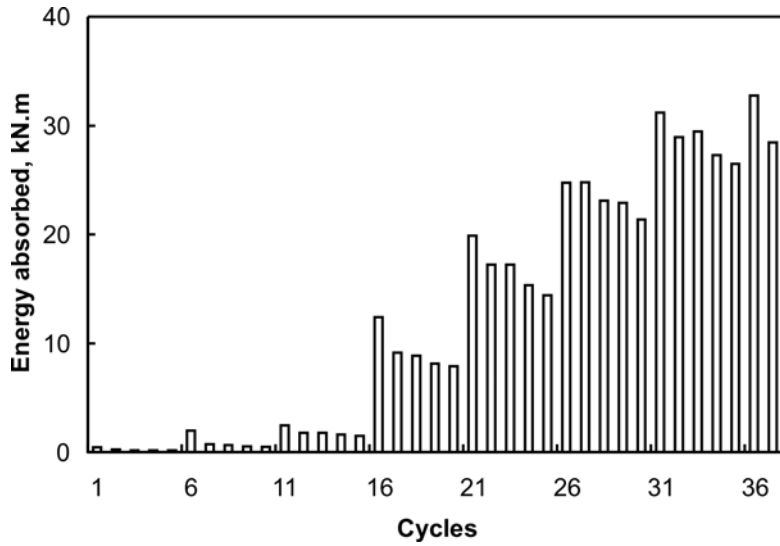


Figure 4-71: Energy absorbed by specimen CL5 per cycles based on overall system.

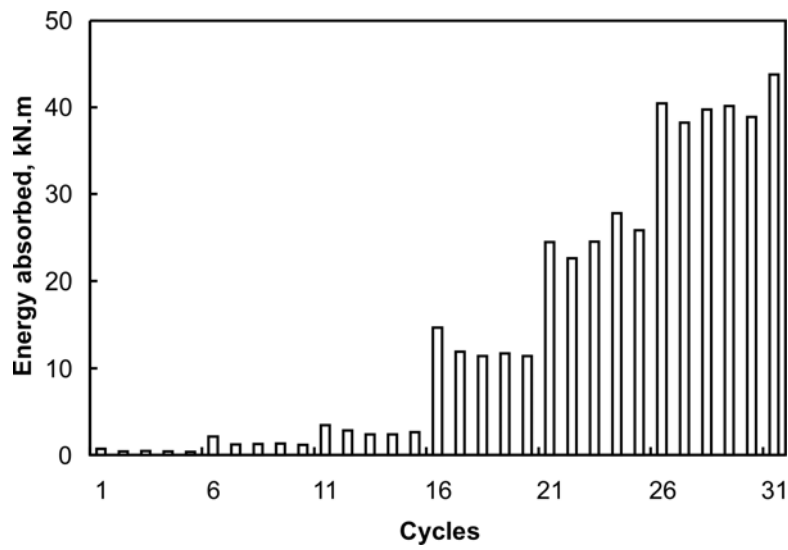


Figure 4-72: Energy absorbed by specimen CL6 per cycles based on overall system.

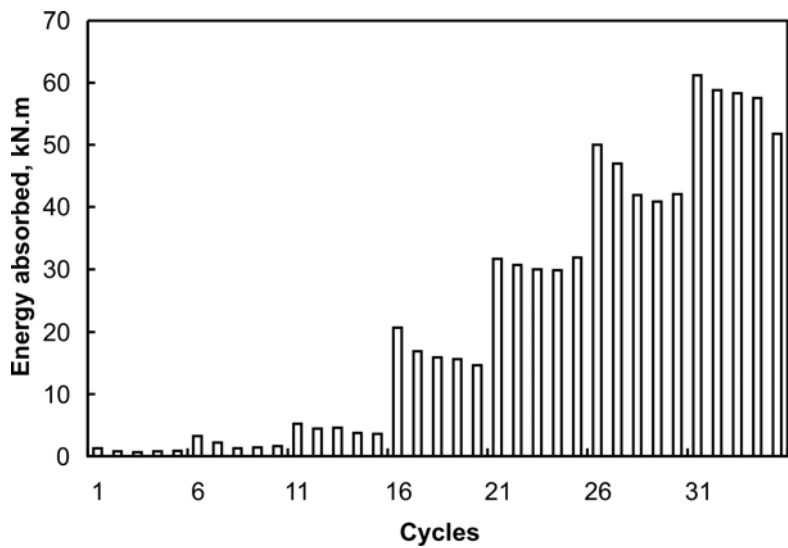


Figure 4-73: Energy absorbed by specimen CL7 per cycles based on overall system.

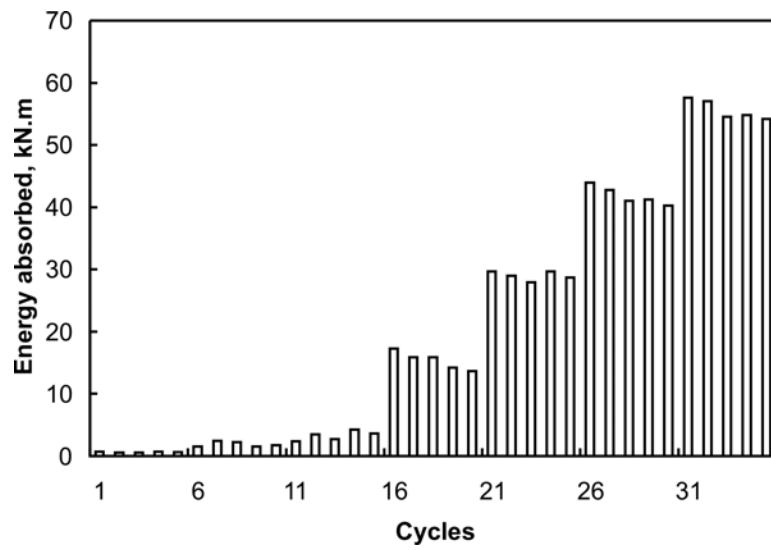


Figure 4-74: Energy absorbed by specimen CL8 per cycles based on overall system.

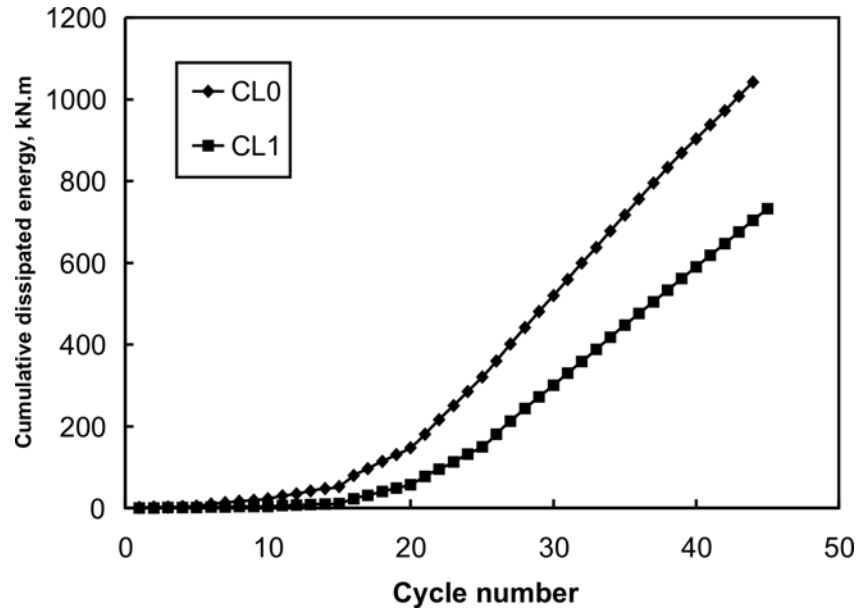


Figure 4-75(a): Cumulative dissipated energy vs. cycle number for specimens CL1 and CL0 based on overall system

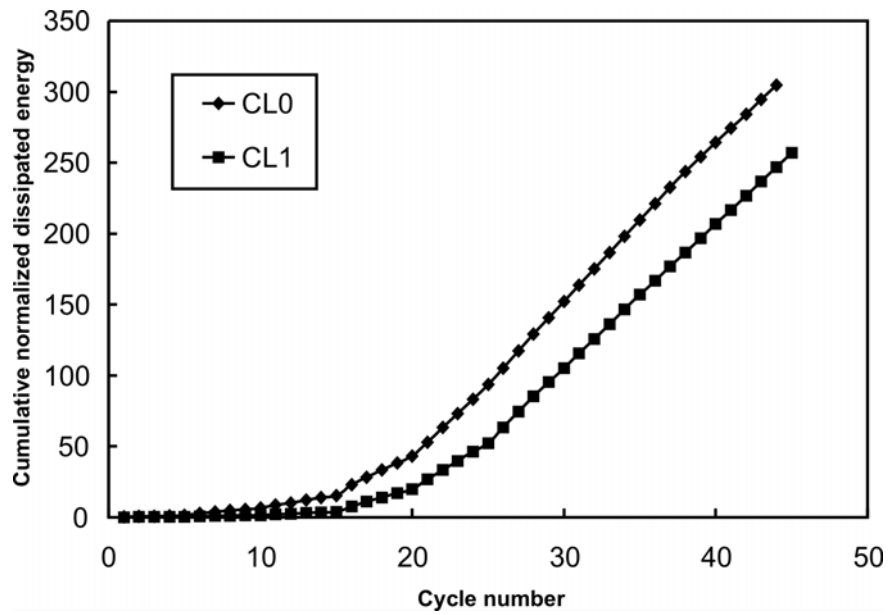


Figure 4-75(b): Cumulative normalized dissipated energy vs. cycle number for specimens CL1 and CL0 based on overall system

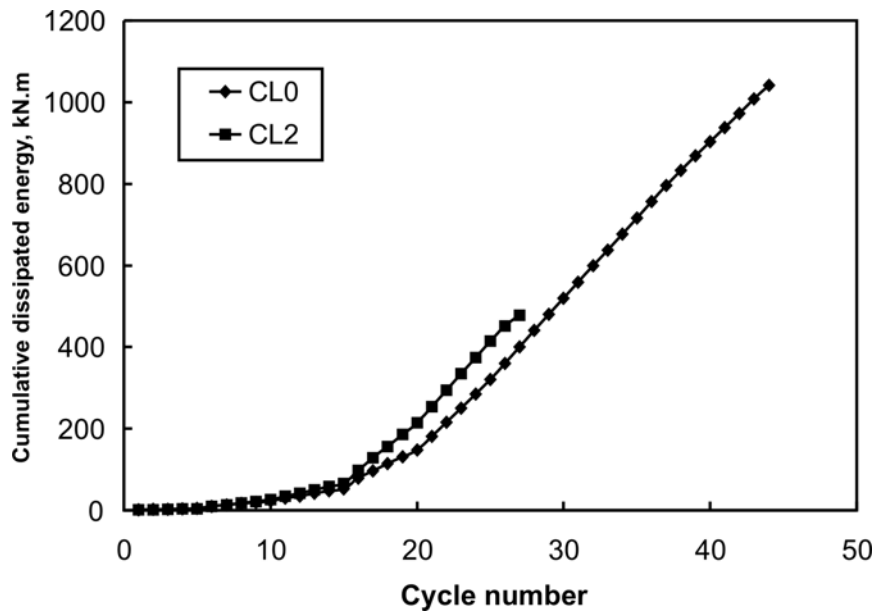


Figure 4-76(a): Cumulative dissipated energy vs. cycle number for specimens CL2 and CL0 based on overall system

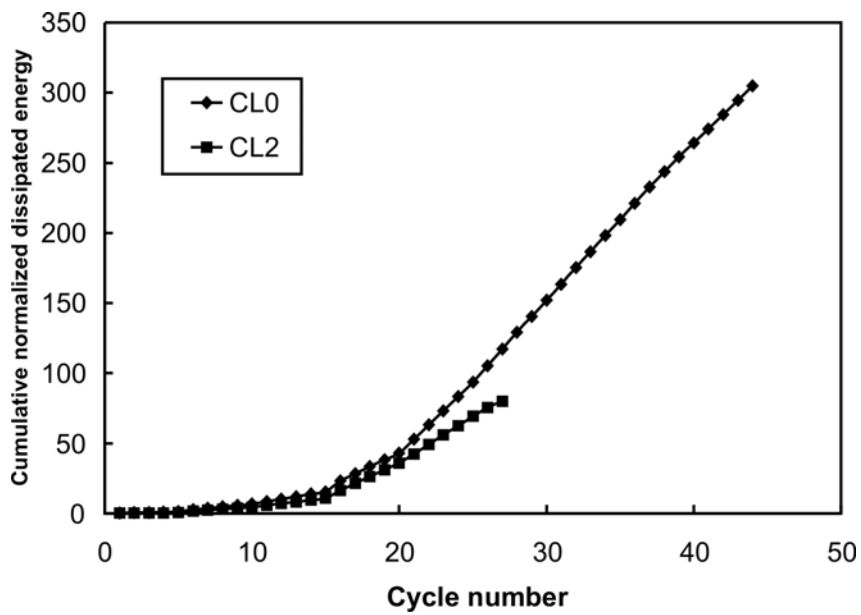


Figure 4-76(b): Cumulative normalized dissipated energy vs. cycle number for specimens CL2 and CL0 based on overall system

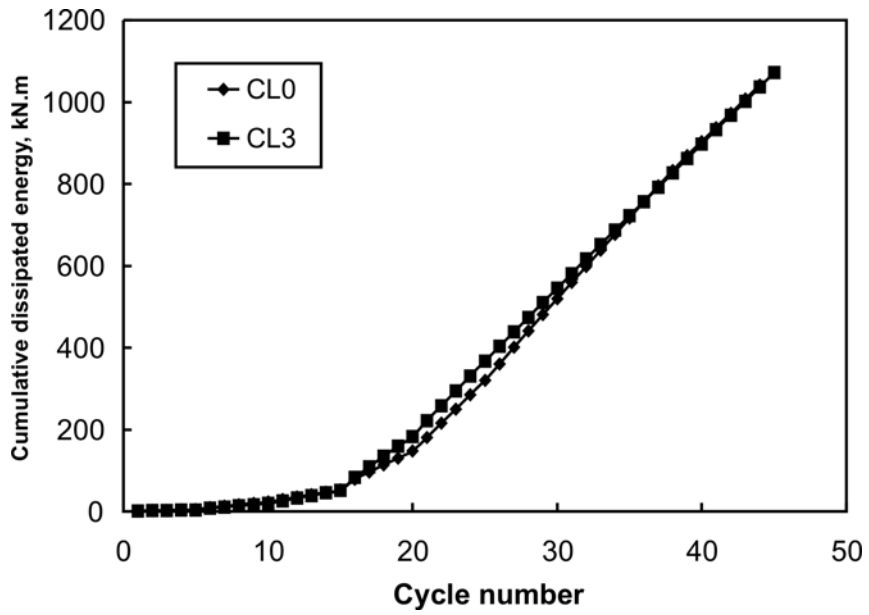


Figure 4-77(a): Cumulative dissipated energy vs. cycle numbers for specimens CL3 and CL0 based on overall system

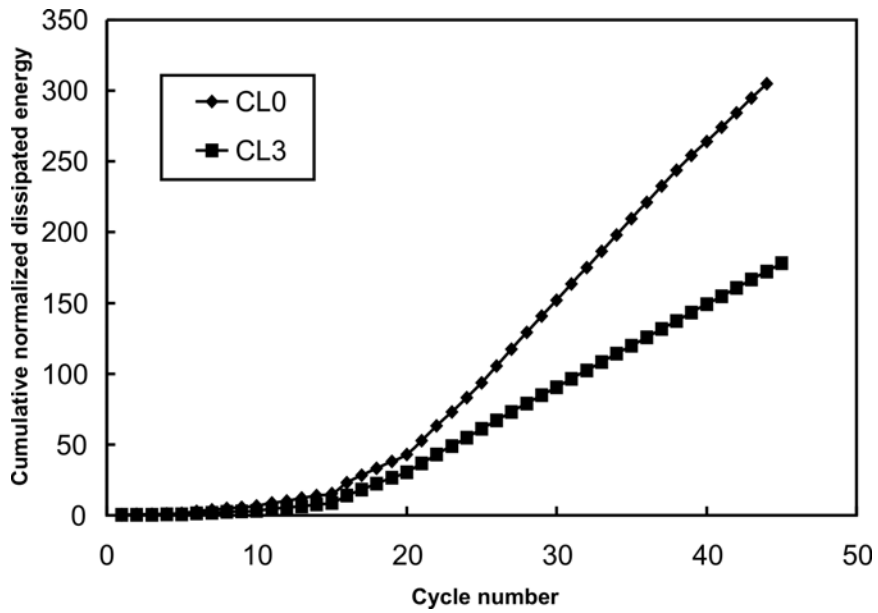


Figure 4-77(b): Cumulative normalized dissipated energy vs. cycle number for specimens CL3 and CL0 based on overall system

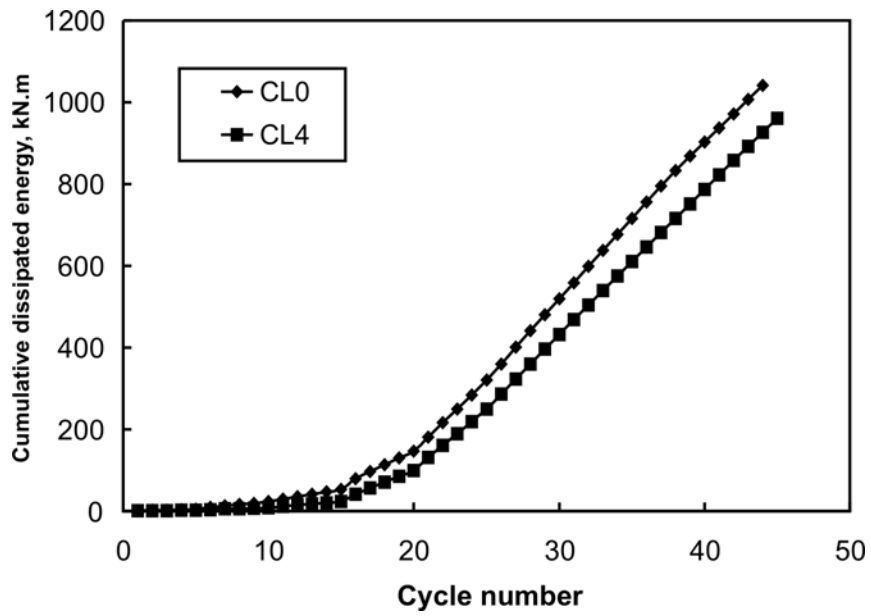


Figure 4-78(a): Cumulative dissipated energy vs. cycle number for specimens CL4 and CL0 based on overall system

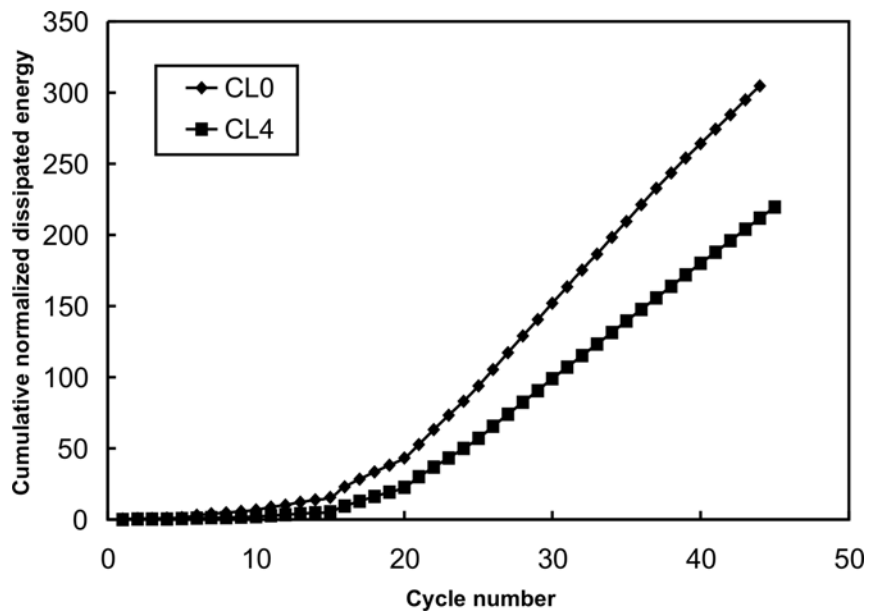


Figure 4-78(b): Cumulative normalized dissipated energy vs. cycle number for specimens CL4 and CL0 based on overall system

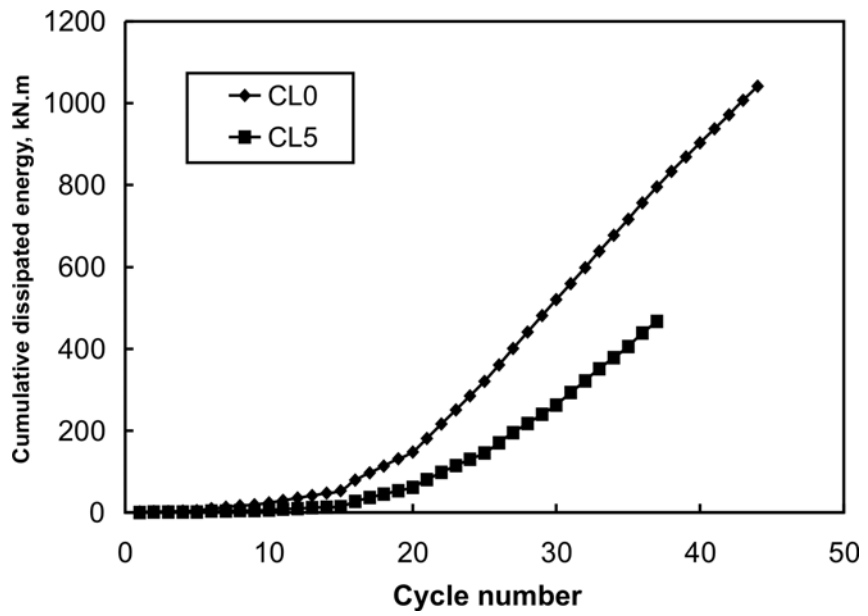


Figure 4-79(a): Cumulative dissipated energy vs. cycle number for specimens CL5 and CL0 based on overall system

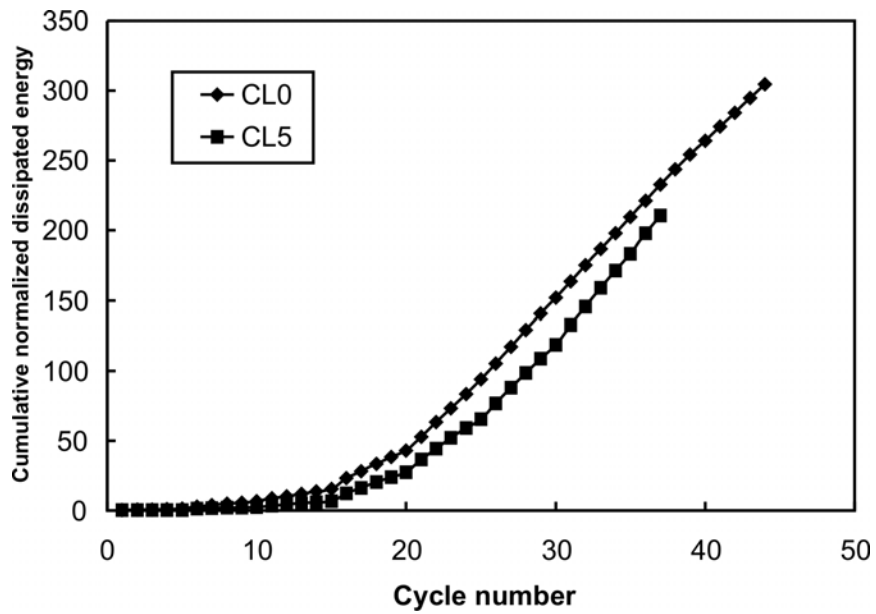


Figure 4-79(b): Cumulative normalized dissipated energy vs. cycle number for specimens CL5 and CL0 based on overall system

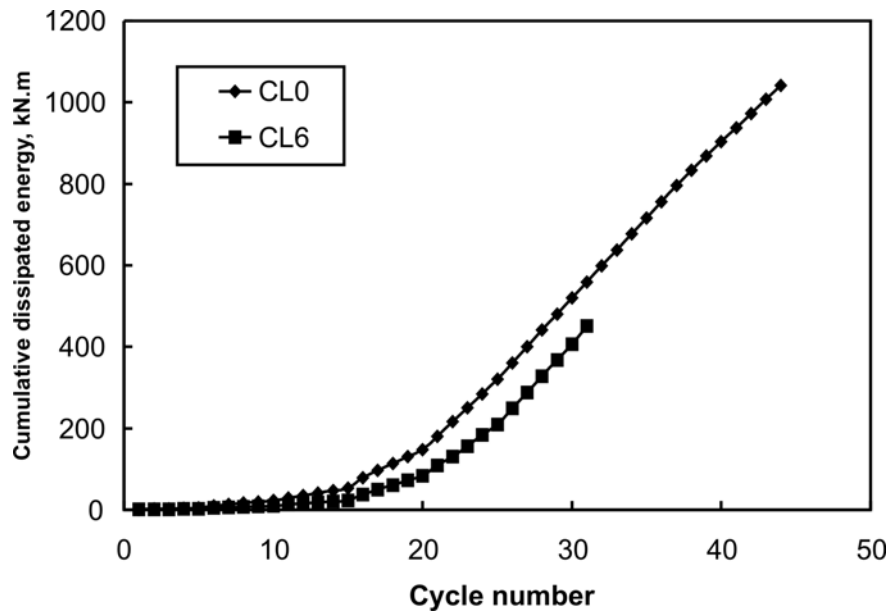


Figure 4-80(a): Cumulative dissipated energy vs. cycle number for specimens CL6 and CL0 based on overall system

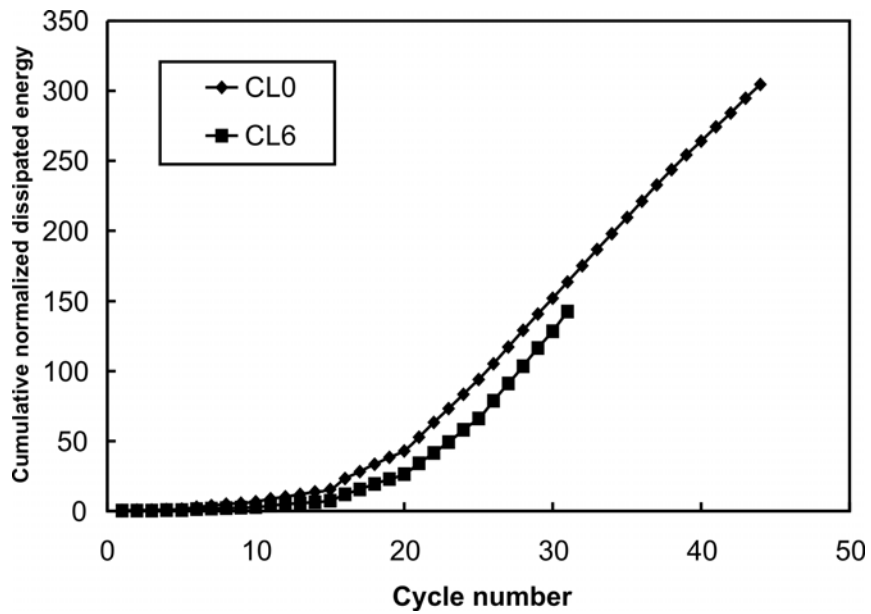


Figure 4-80(b): Cumulative normalized dissipated energy vs. cycle number for specimens CL6 and CL0 based on overall system

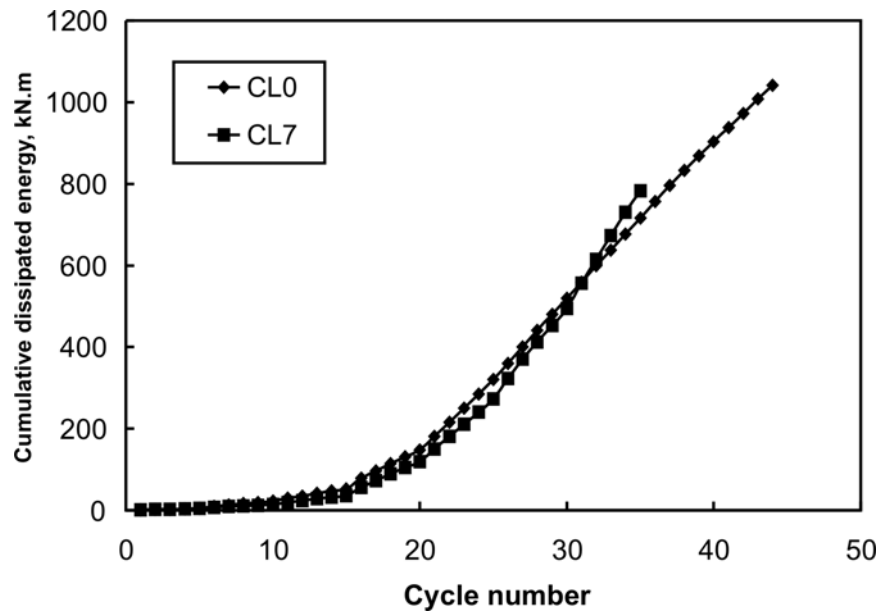


Figure 4-81(a): Cumulative dissipated energy vs. cycle number for specimens CL7 and CL0 based on overall system

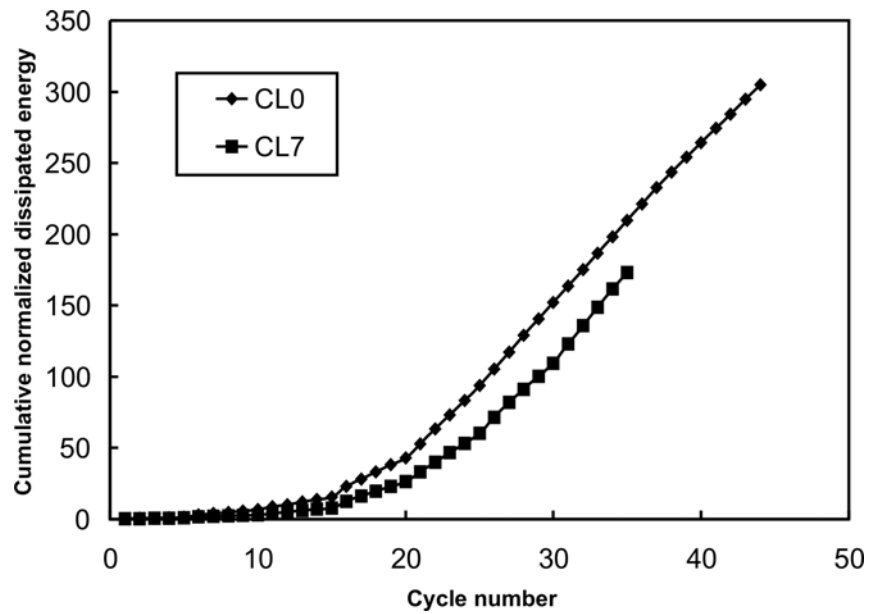


Figure 4-81(b): Cumulative normalized dissipated energy vs. cycle number for specimens CL7 and CL0 based on overall system

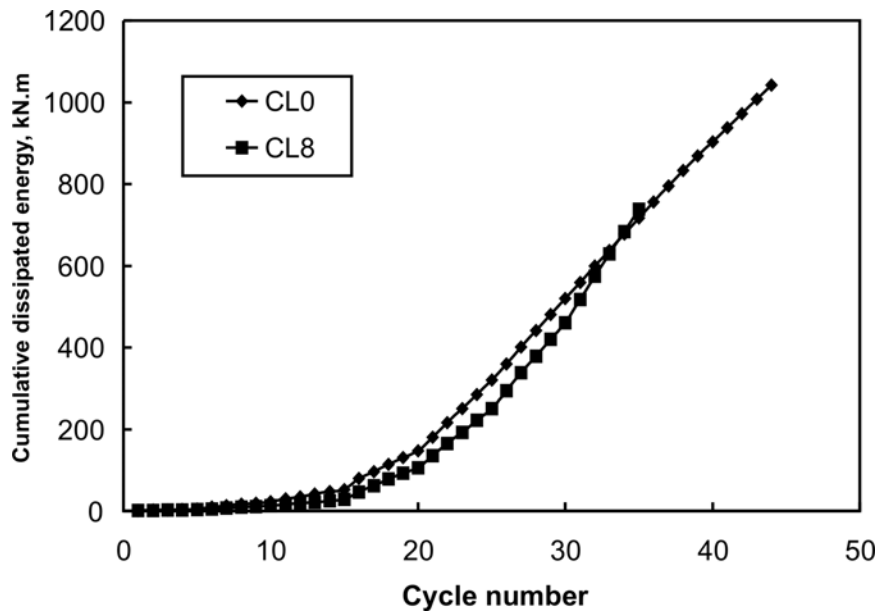


Figure 4-82(a): Cumulative dissipated energy vs. cycle number for specimens CL8 and CL0 based on overall system

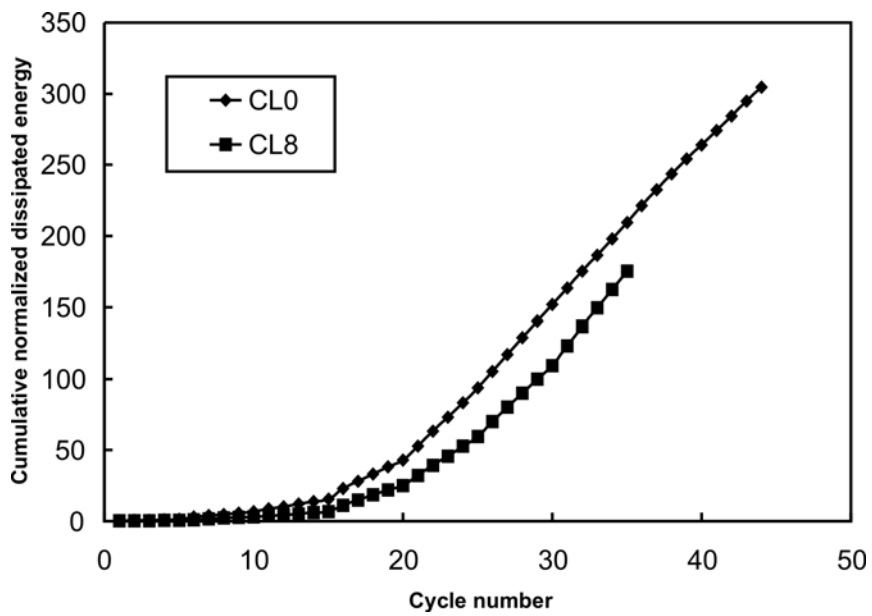


Figure 4-82(b): Cumulative normalized dissipated energy vs. cycle number for specimens CL8 and CL0 based on overall system

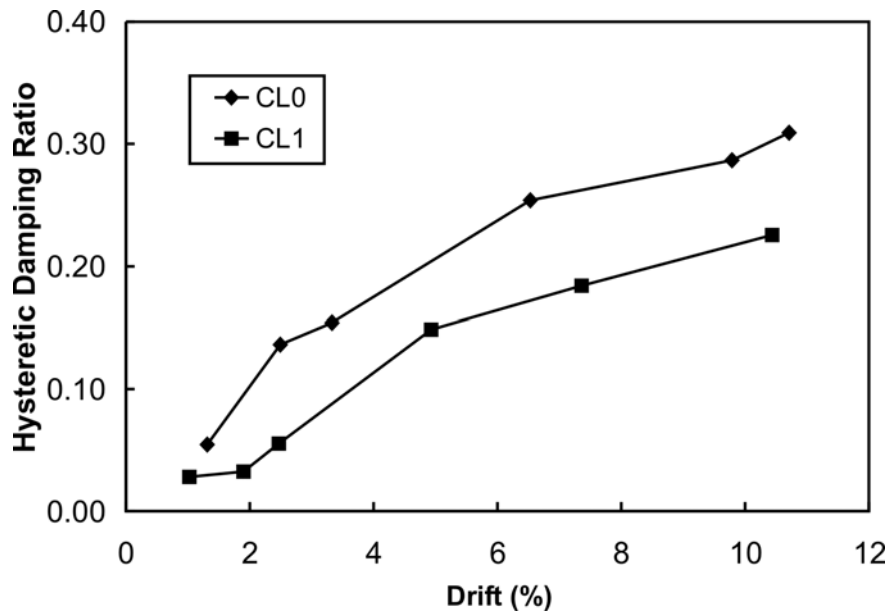


Figure 4-83: Hysteretic damping ratio vs. drift for specimens CL1 and CL0

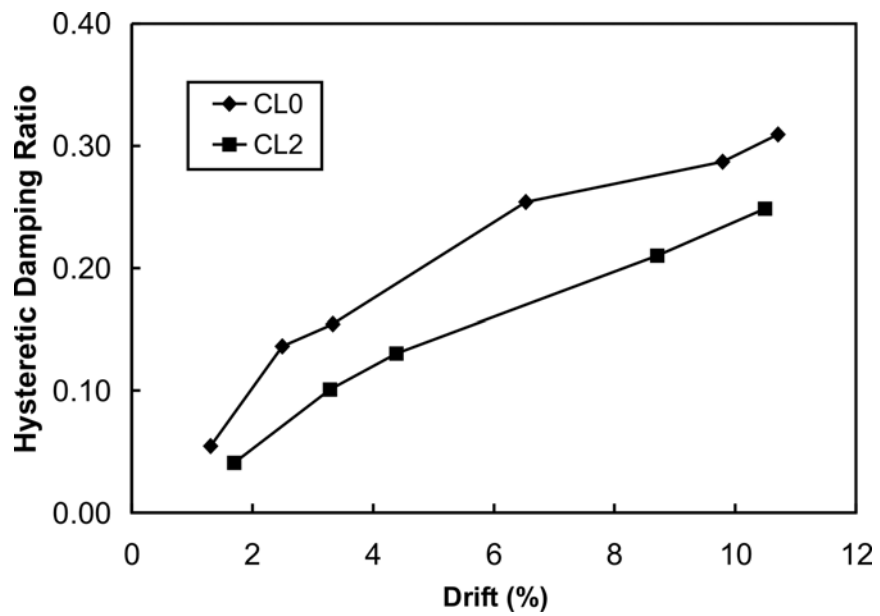


Figure 4-84: Hysteretic damping ratio vs. drift for specimens CL2 and CL0

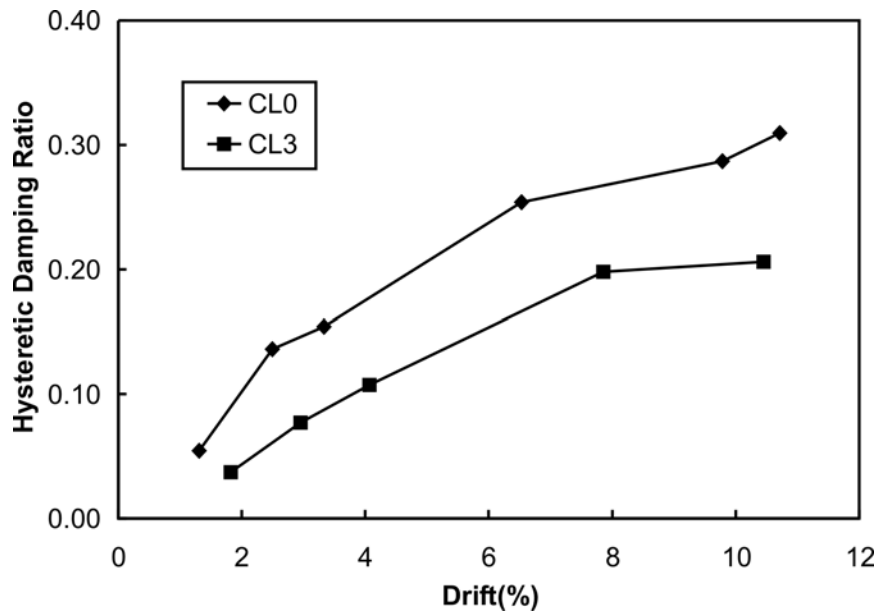


Figure 4-85: Hysteretic damping ratio vs. drift for specimens CL3 and CL0

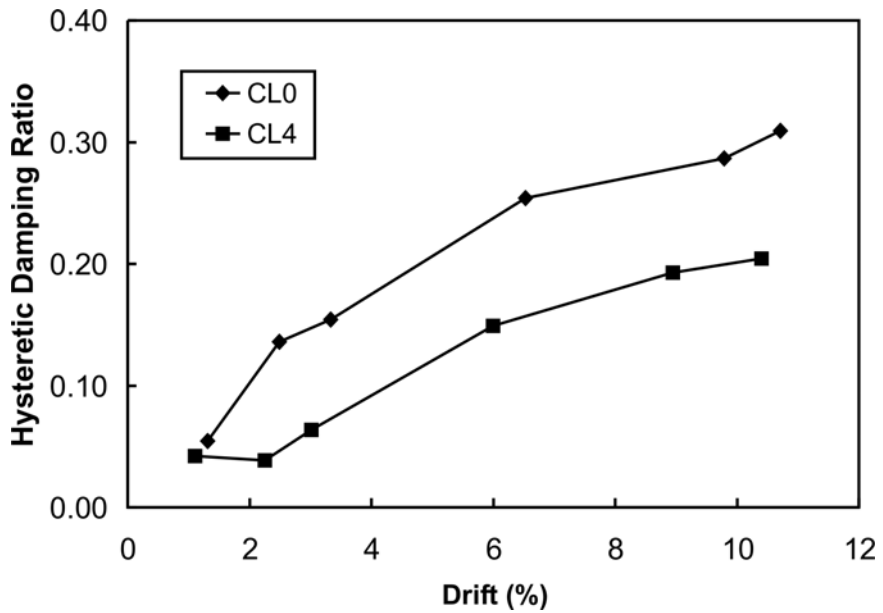


Figure 4-86: Hysteretic damping ratio vs. drift for specimens CL4 and CL0

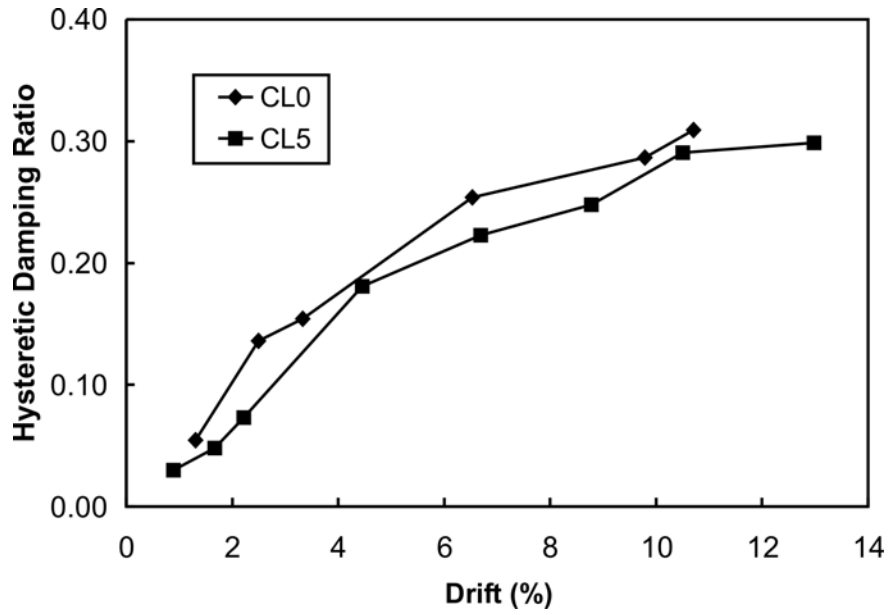


Figure 4-87: Hysteretic damping ratio vs. drift for specimens CL5 and CL0

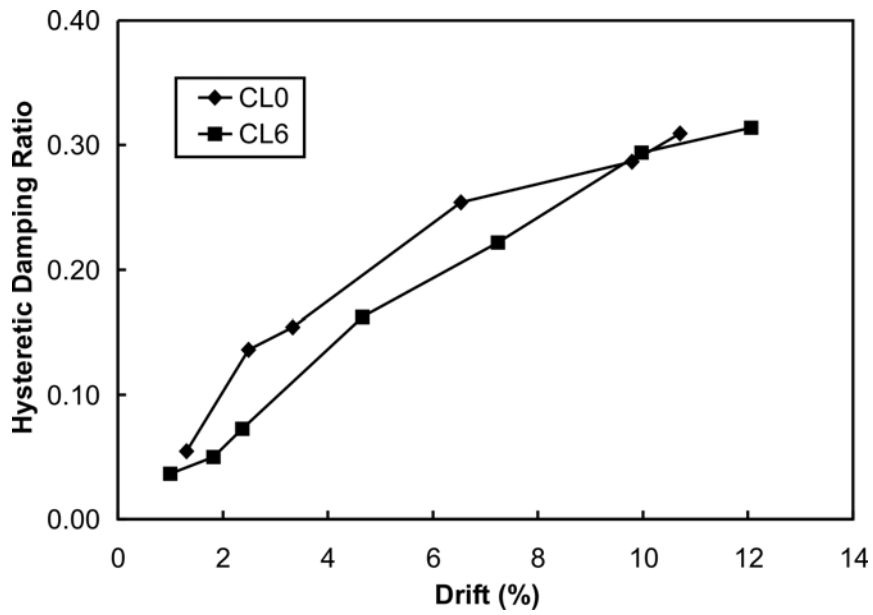


Figure 4-88: Hysteretic damping ratio vs. drift for specimens CL6 and CL0

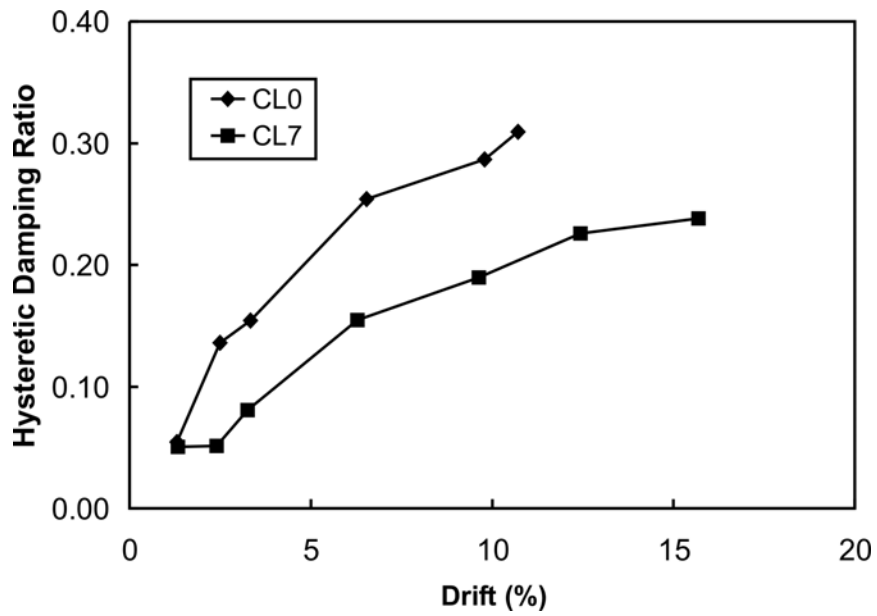


Figure 4-89: Hysteretic damping ratio vs. drift for specimens CL7 and CL0

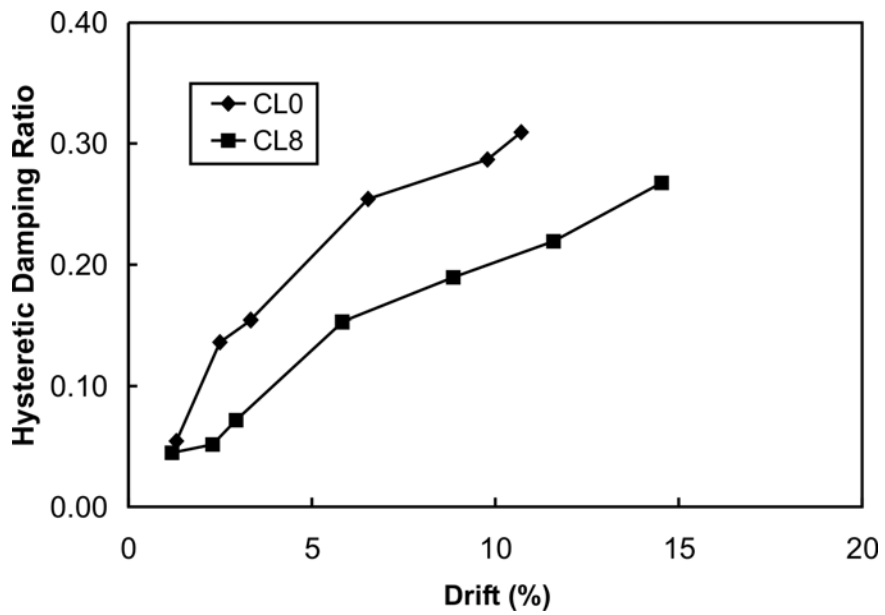


Figure 4-90: Hysteretic damping ratio vs. drift for specimens CL8 and CL0

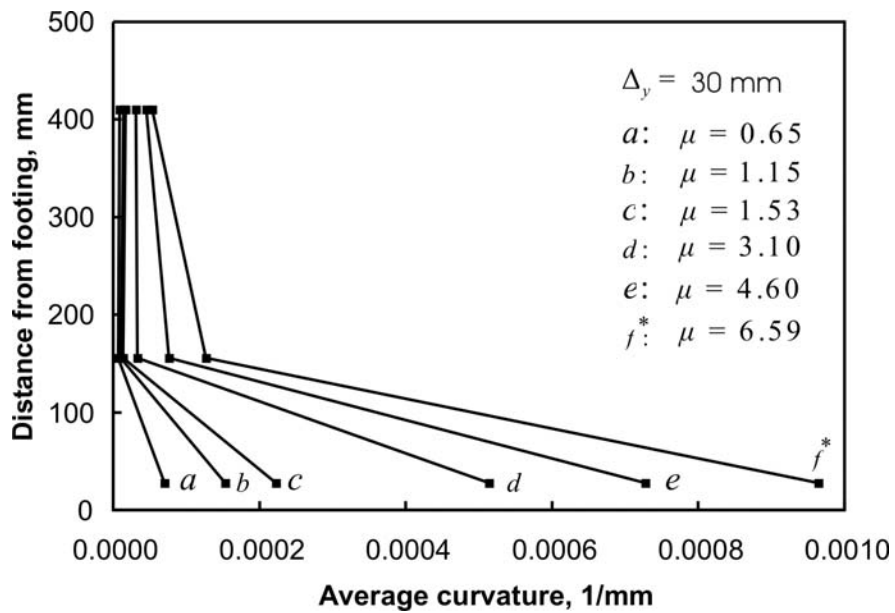


Figure 4-91: Curvature distribution in the test region of column CL1 at different levels of displacement ductility

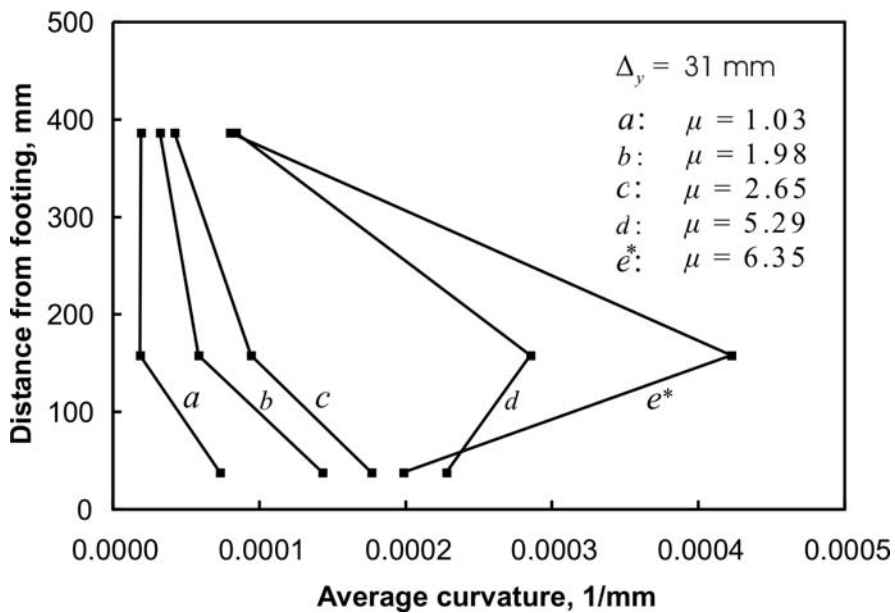


Figure 4-92: Curvature distribution in the test region of column CL2 at different levels of displacement ductility

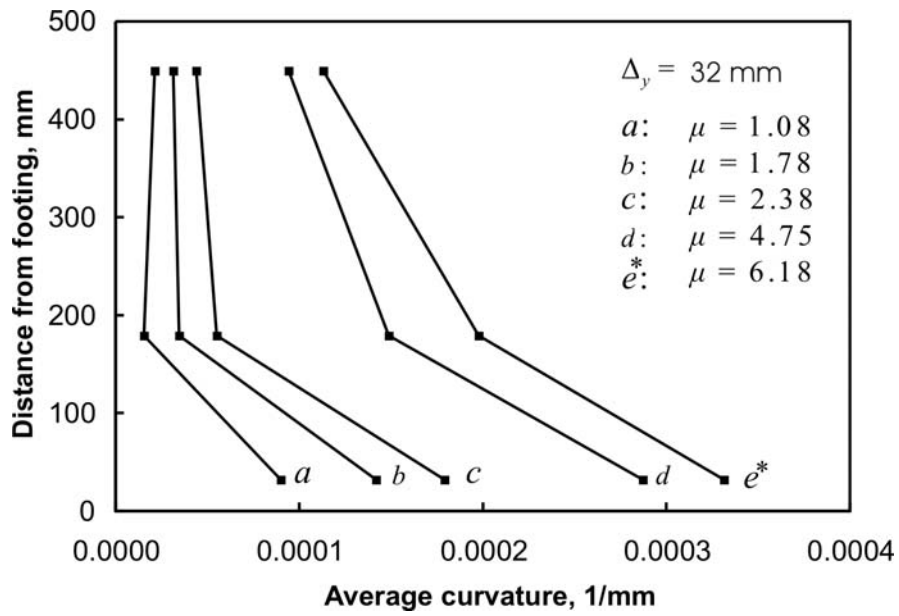


Figure 4-93: Curvature distribution in the test region of column CL3 at different levels of displacement ductility

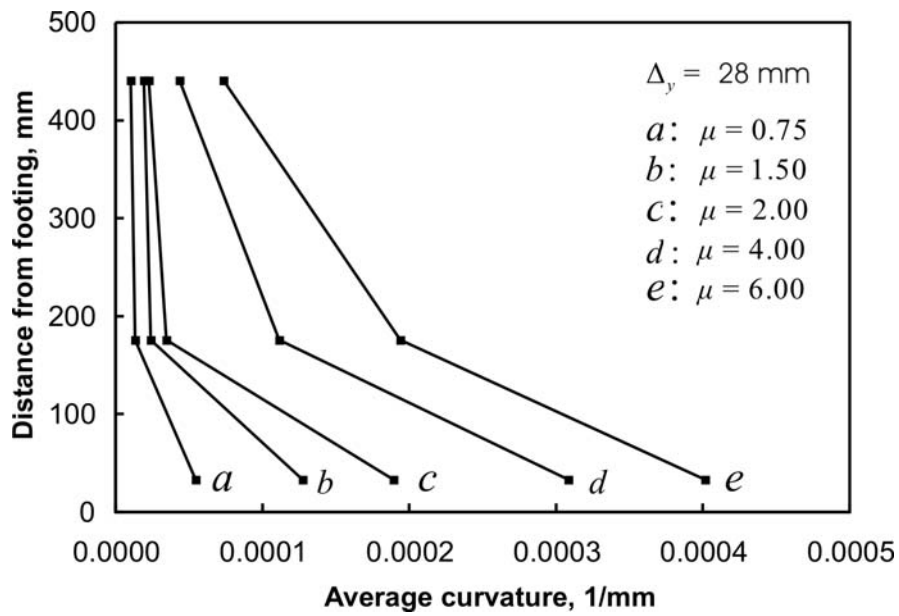


Figure 4-94: Curvature distribution in the test region of column CL4 at different levels of displacement ductility

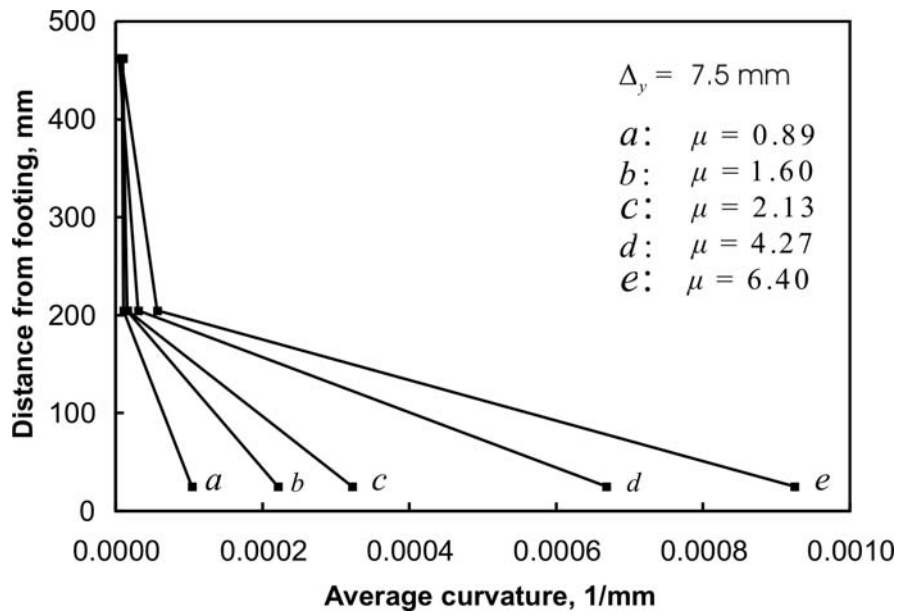


Figure 4-95: Curvature distribution in the test region of column CL5 at different levels of displacement ductility

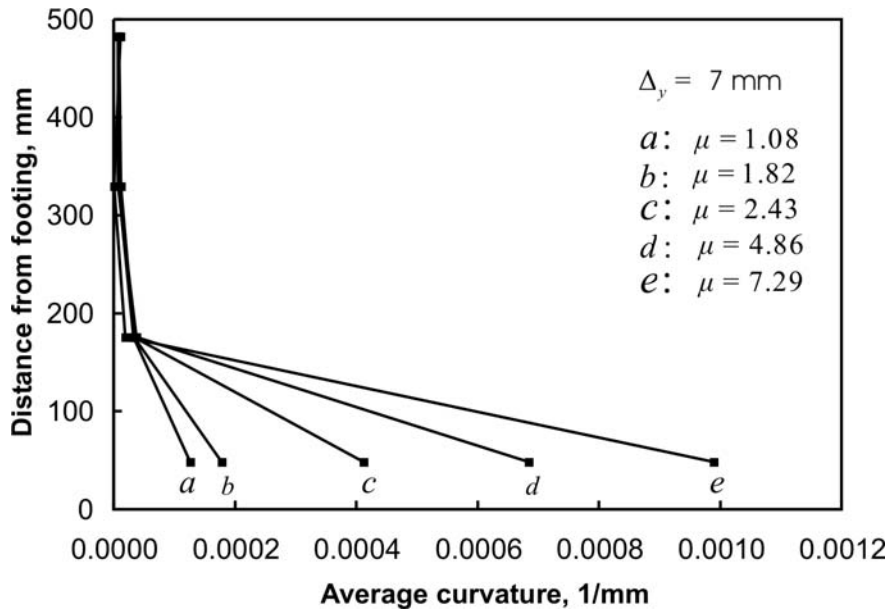


Figure 4-96: Curvature distribution in the test region of column CL6 at different levels of displacement ductility

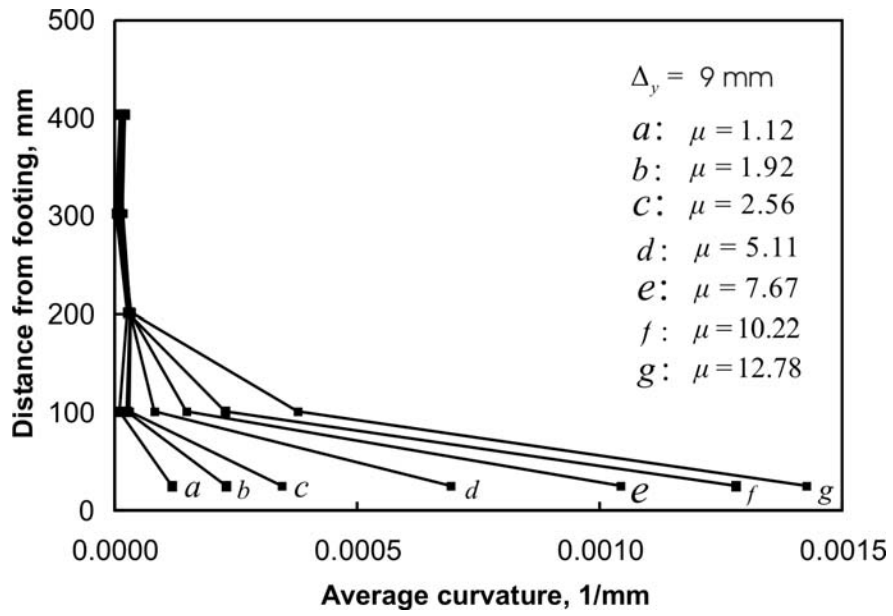


Figure 4-97: Curvature distribution in the test region of column CL7 at different levels of displacement ductility

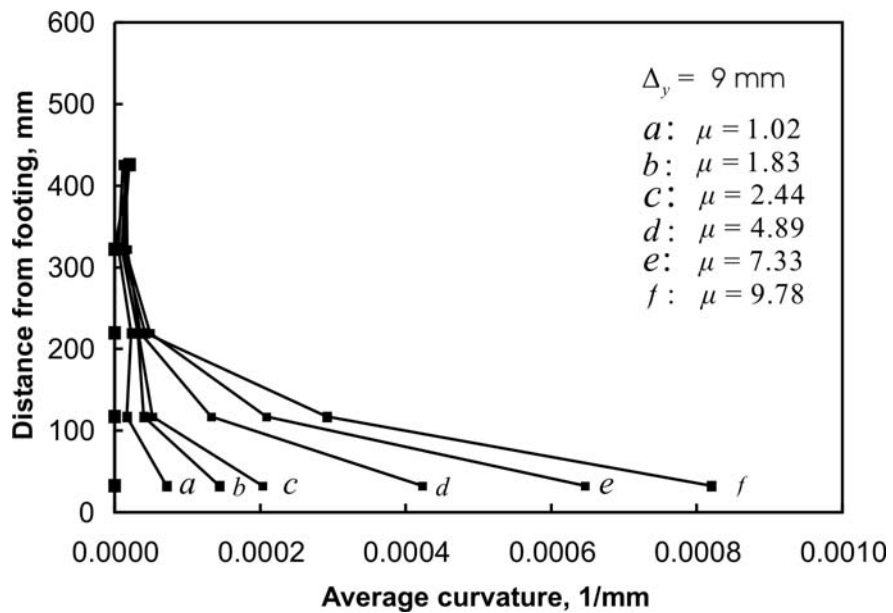


Figure 4-98: Curvature distribution in the test region of column CL8 at different levels of displacement ductility

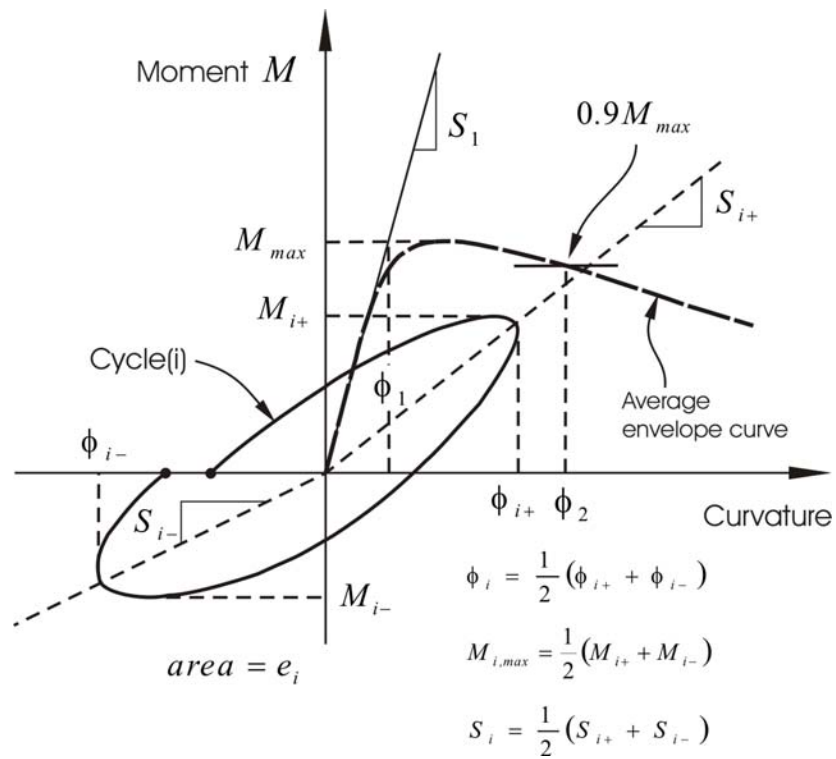


Figure 4-99: Definitions of various terms in ductility parameters (adapted from Sheikh and Khoury (1993))

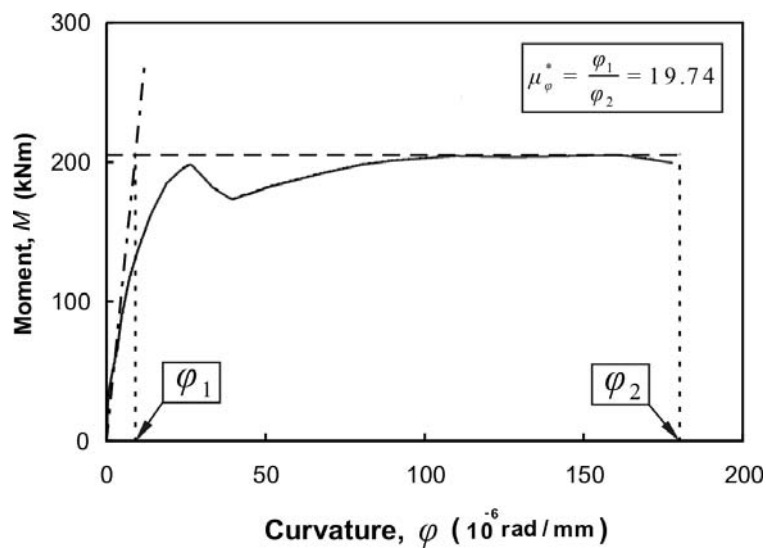


Figure 4-100: Curvature ductility, μ_{ϕ} , for column CL0

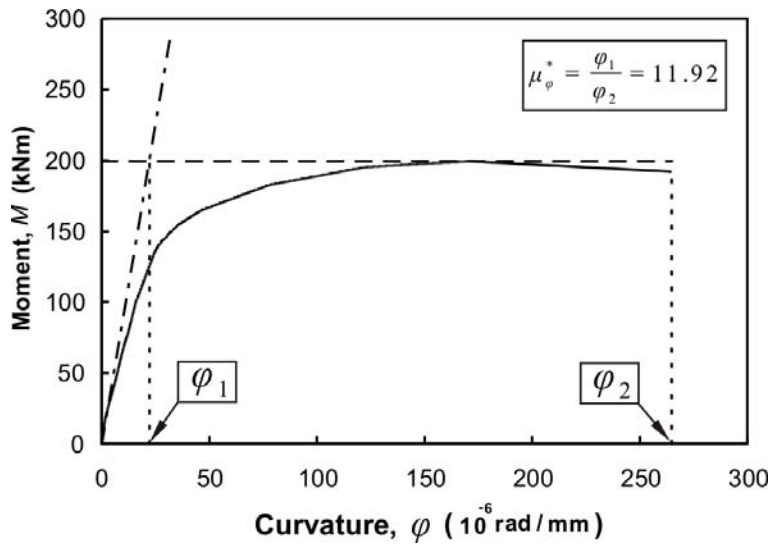


Figure 4-101: Curvature ductility, μ_{φ} , for column CL1

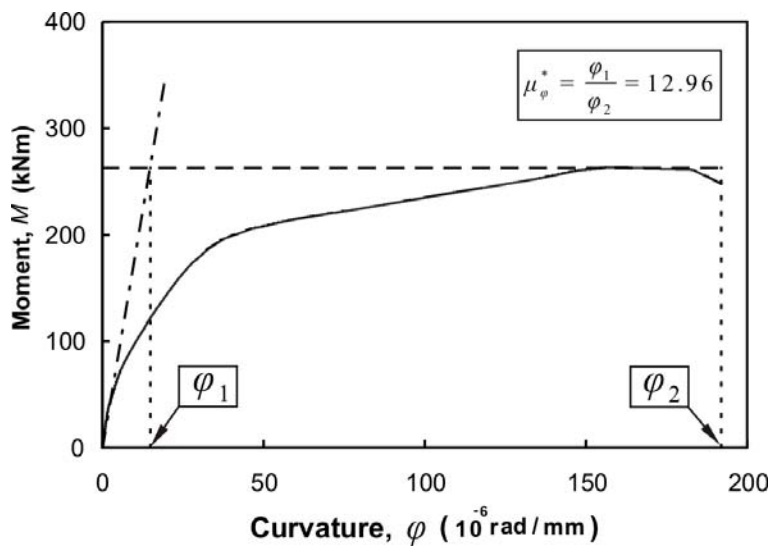


Figure 4-102: Curvature ductility, μ_{φ} , for column CL2

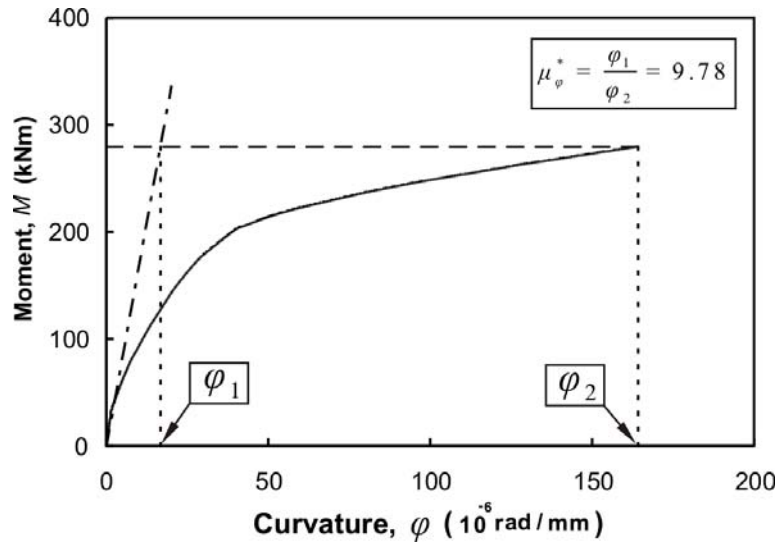


Figure 4-103: Curvature ductility, μ_{ϕ} , for column CL3

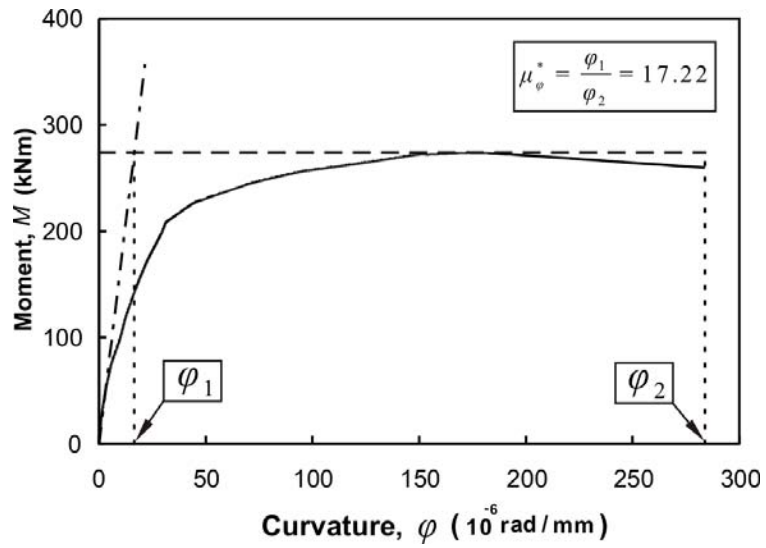


Figure 4-104: Curvature ductility, μ_{ϕ} , for column CL4

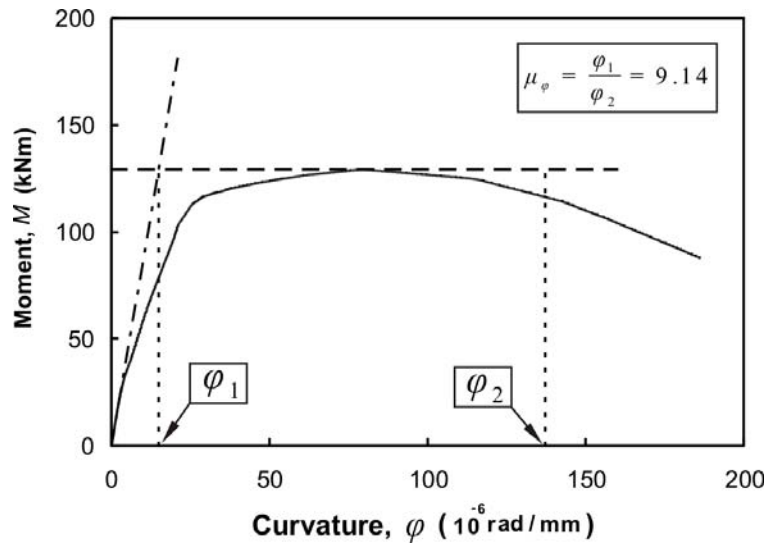


Figure 4-105: Curvature ductility, μ_ϕ , for column CL5

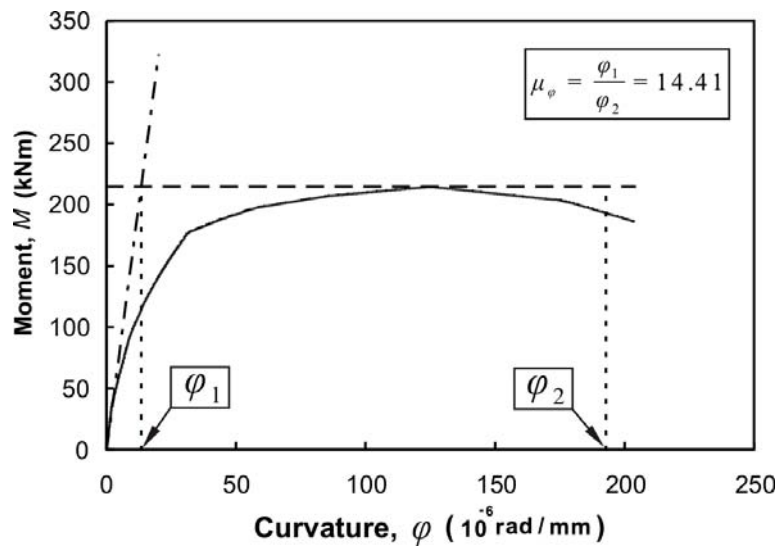


Figure 4-106: Curvature ductility, μ_ϕ , for column CL6

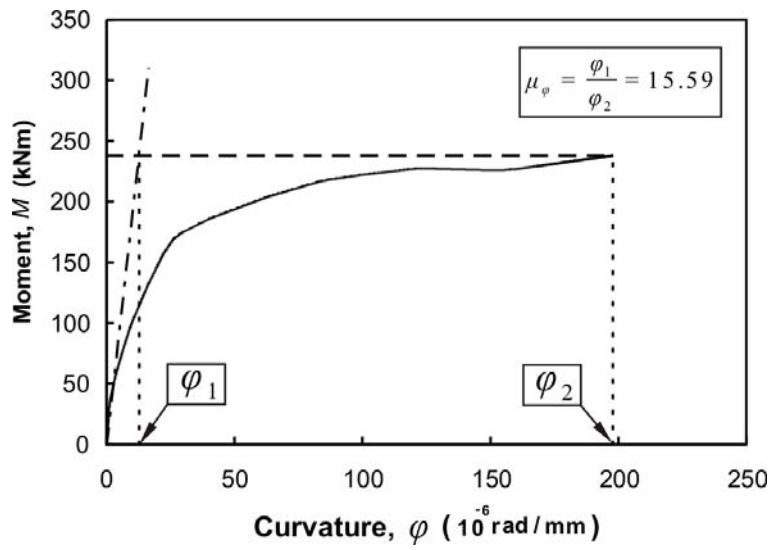


Figure 4-107: Curvature ductility, μ_φ , for column CL7

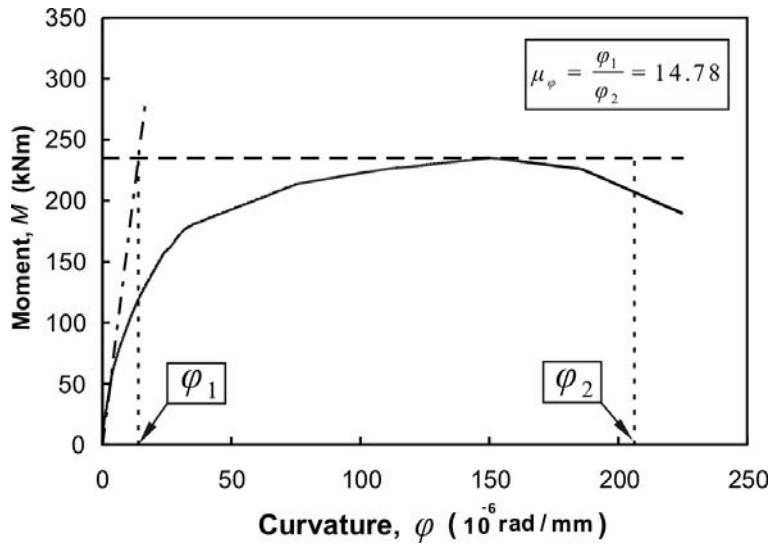


Figure 4-108: Curvature ductility, μ_φ , for column CL8

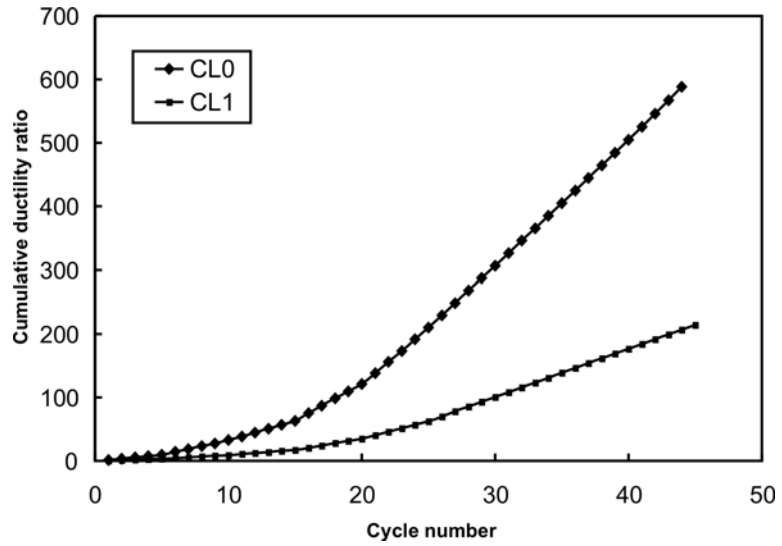


Figure 4-109: Cumulative ductility ratio for column CL0 and CL1

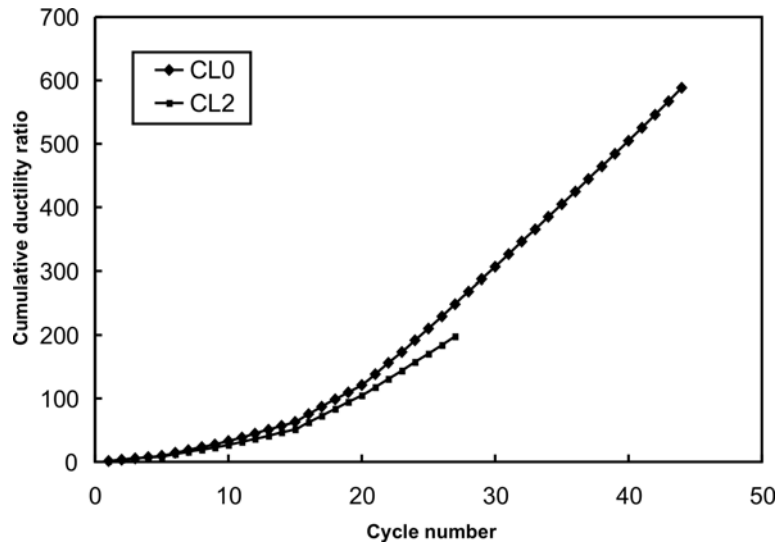


Figure 4-110: Cumulative ductility ratio for column CL0 and CL2

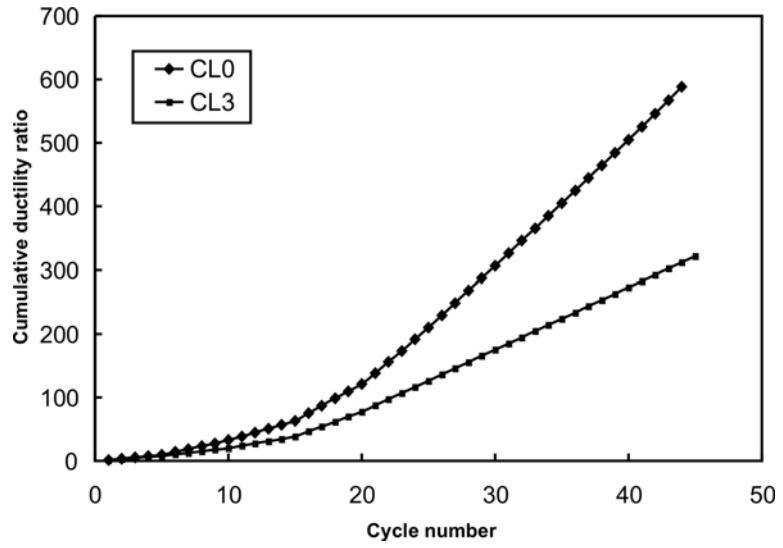


Figure 4-111: Cumulative ductility ratio for column CL0 and CL3

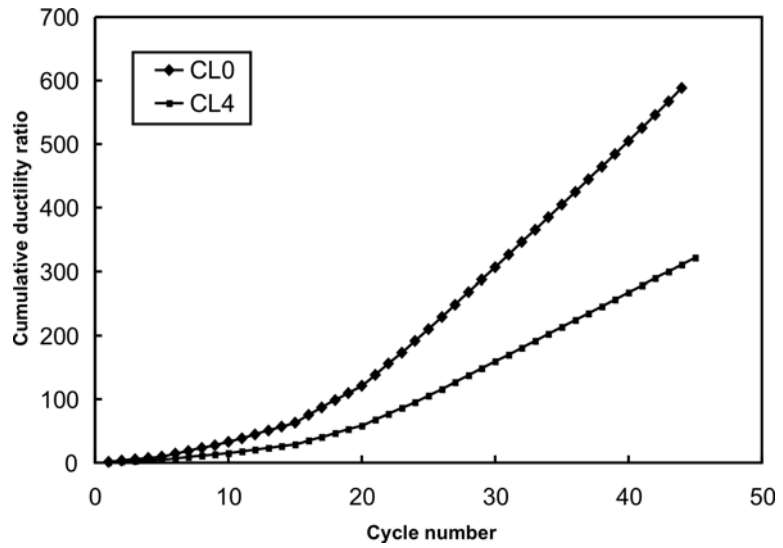


Figure 4-112: Cumulative ductility ratio for column CL0 and CL4

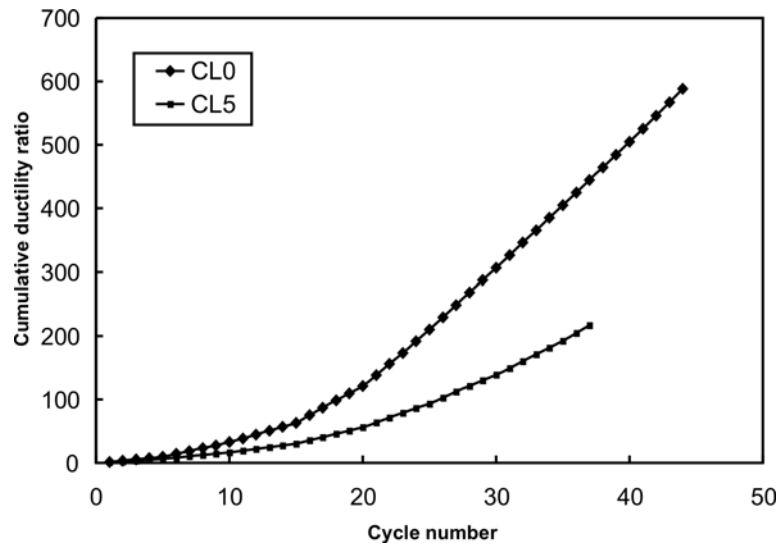


Figure 4-113: Cumulative ductility ratio for column CL0 and CL5

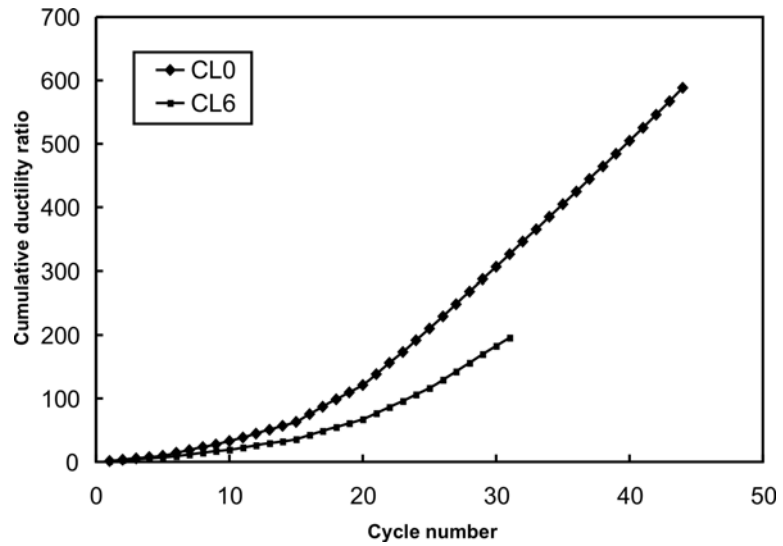


Figure 4-114: Cumulative ductility ratio for column CL0 and CL6

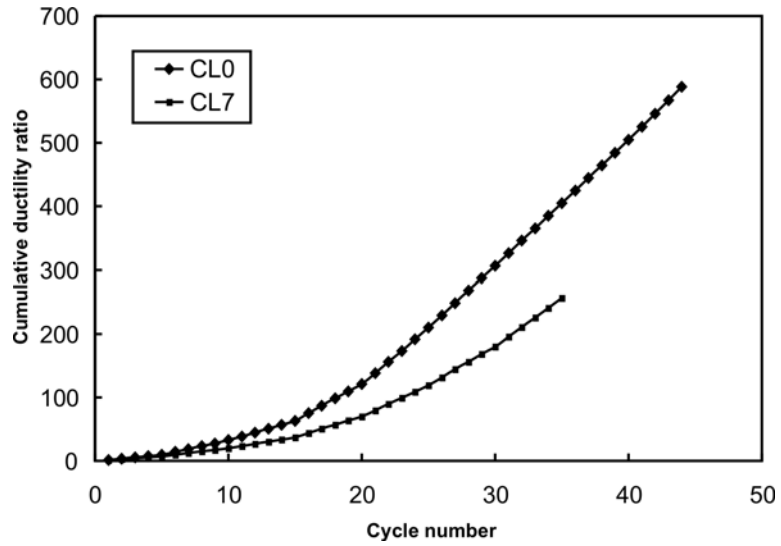


Figure 4-115: Cumulative ductility ratio for column CL0 and CL7

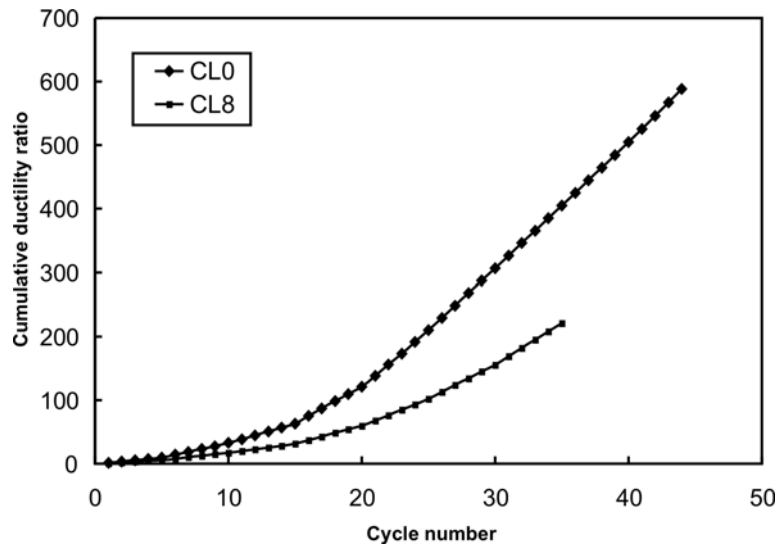


Figure 4-116: Cumulative ductility ratio for column CL0 and CL8

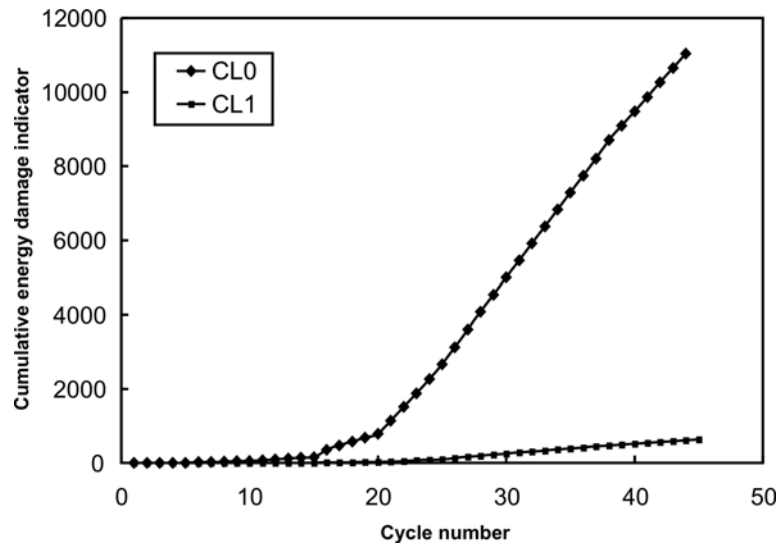


Figure 4-117: Cumulative energy damage indicator for columns CL0 and CL1

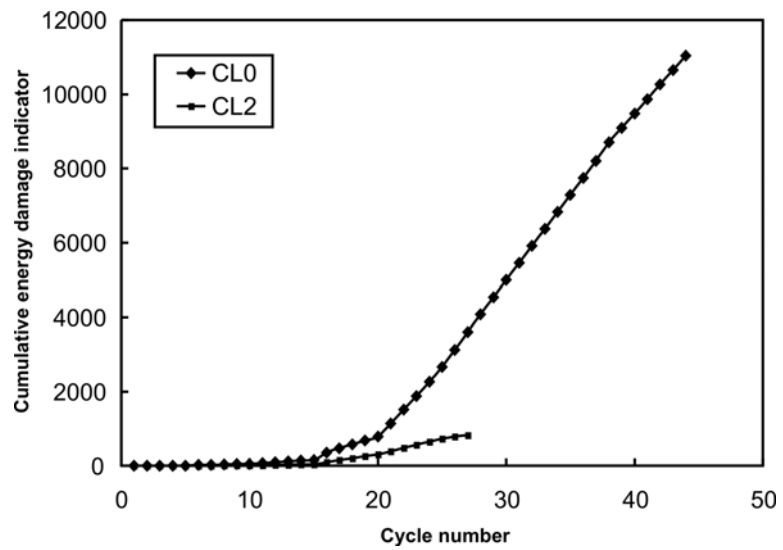


Figure 4-118: Cumulative energy damage indicator for columns CL0 and CL2

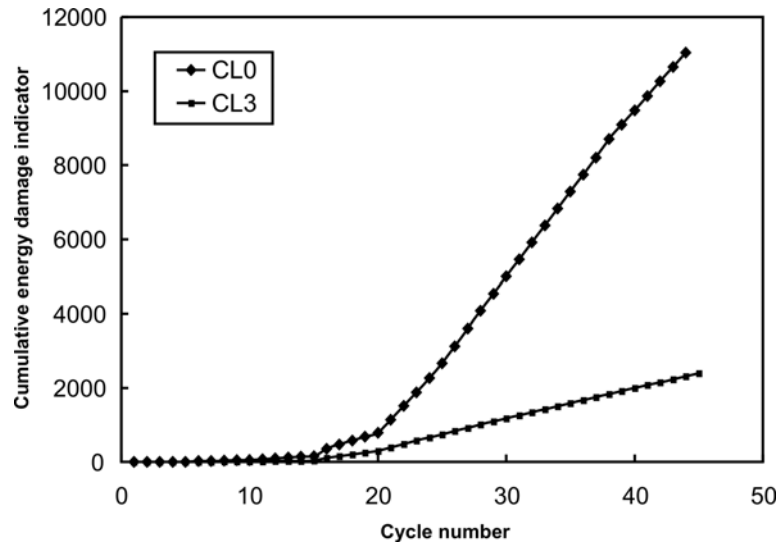


Figure 4-119: Cumulative energy damage indicator for columns CL0 and CL3

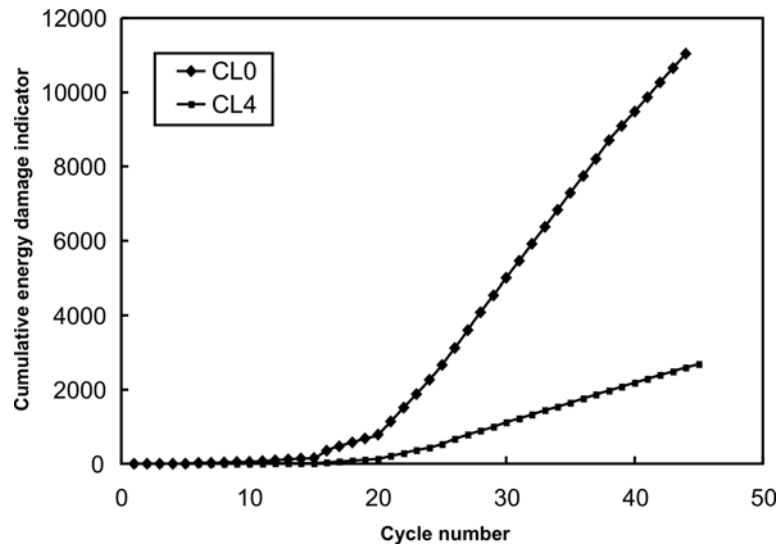


Figure 4-120: Cumulative energy damage indicator for columns CL0 and CL4

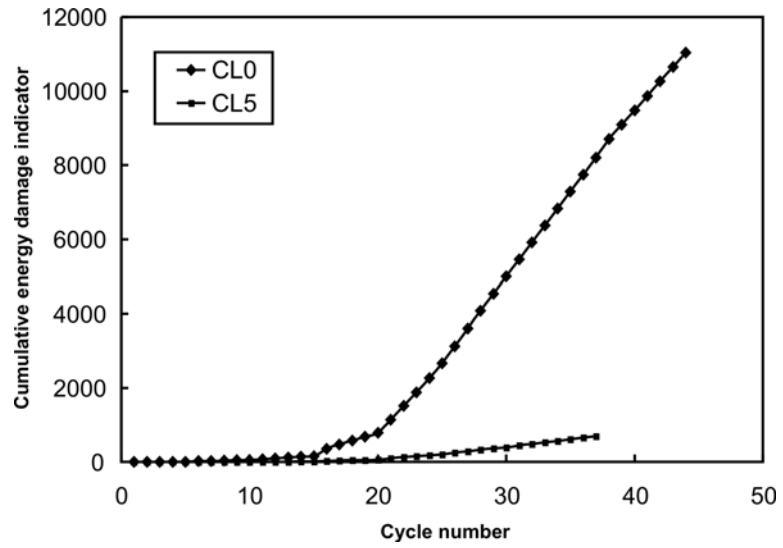


Figure 4-121: Cumulative energy damage indicator for columns CL0 and CL5

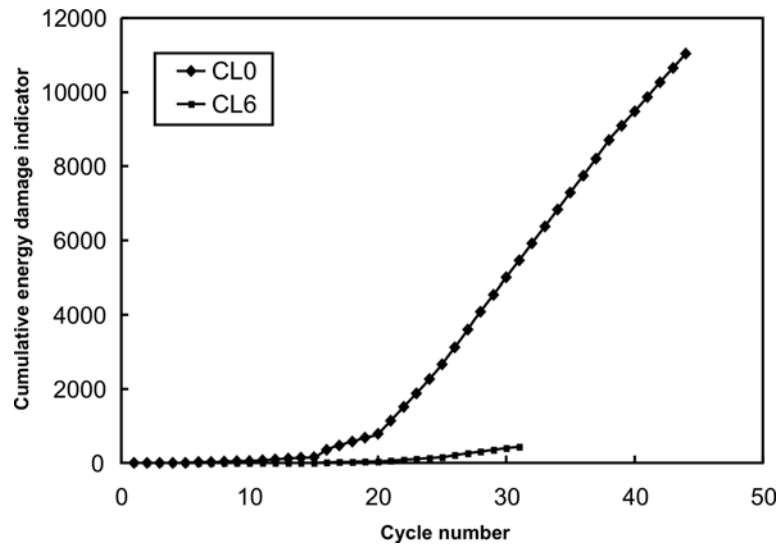


Figure 4-122: Cumulative energy damage indicator for columns CL0 and CL6

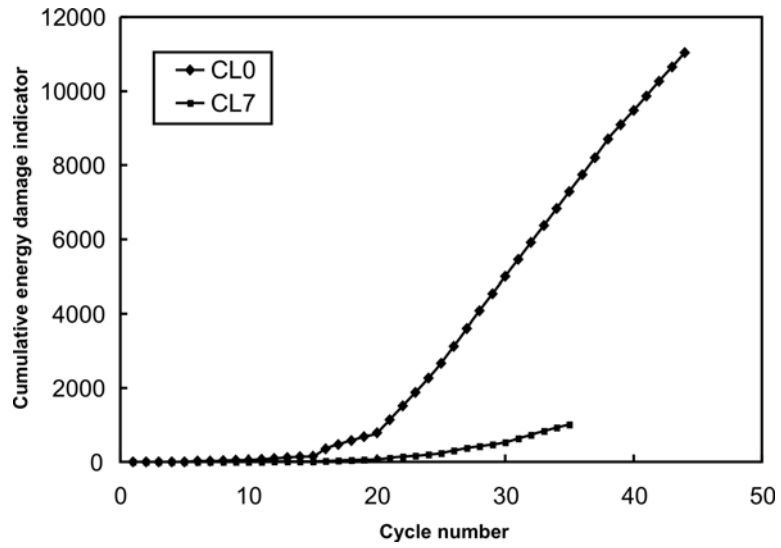


Figure 4-123: Cumulative energy damage indicator for columns CL0 and CL7

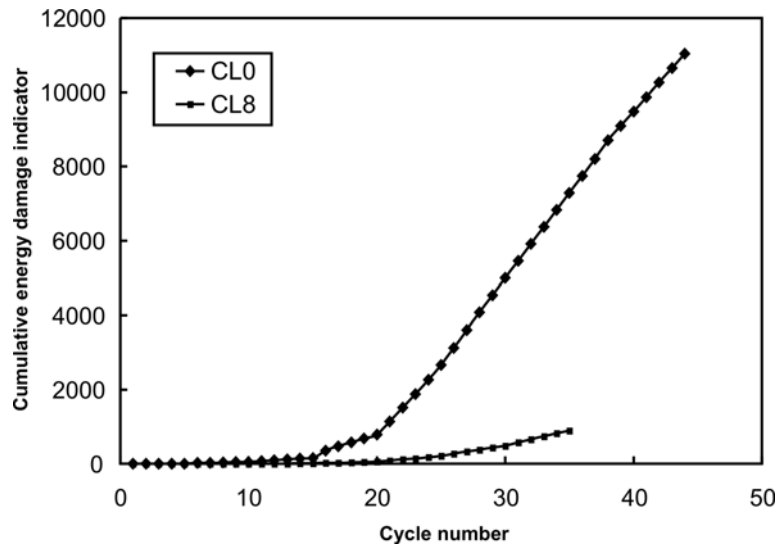


Figure 4-124: Cumulative energy damage indicator for columns CL0 and CL8

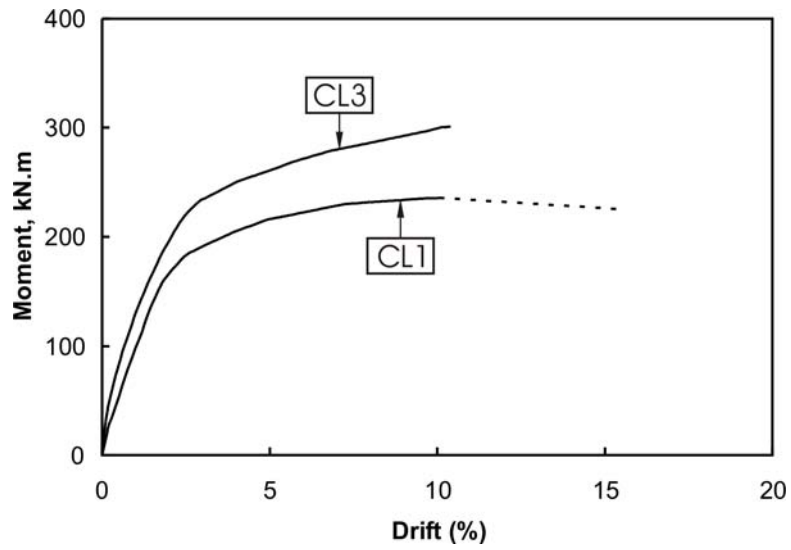


Figure 4-125: Moment at column base versus lateral drift (%) envelope curves for columns CL1 and CL3

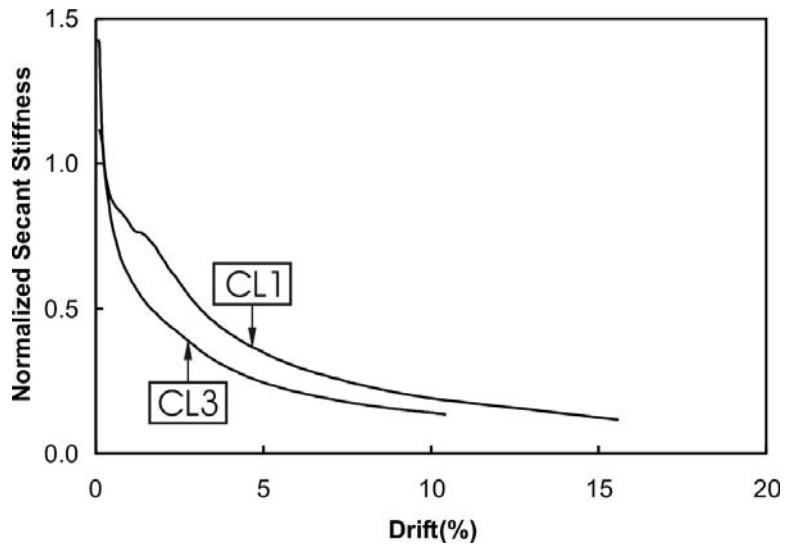


Figure 4-126: Relationship between normalized secant stiffness and lateral drift (%) for columns CL1 and CL3

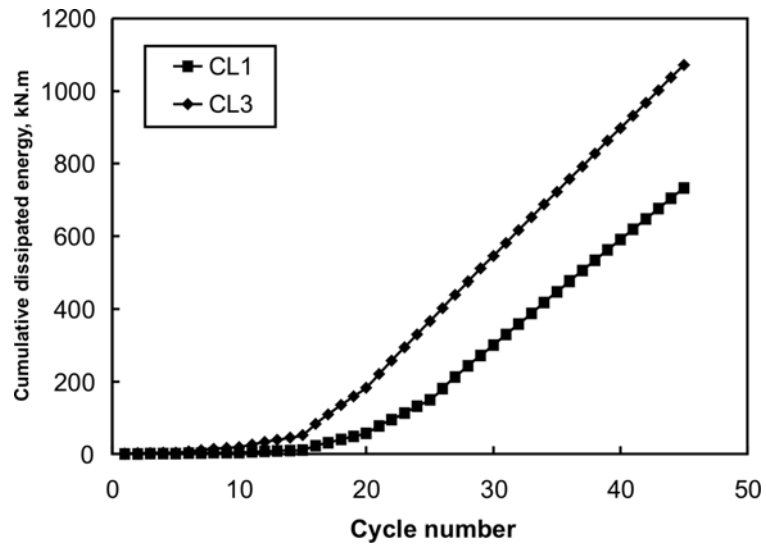


Figure 4-127: Cumulative energy dissipated based on overall system versus cycle number for columns CL1 and CL3

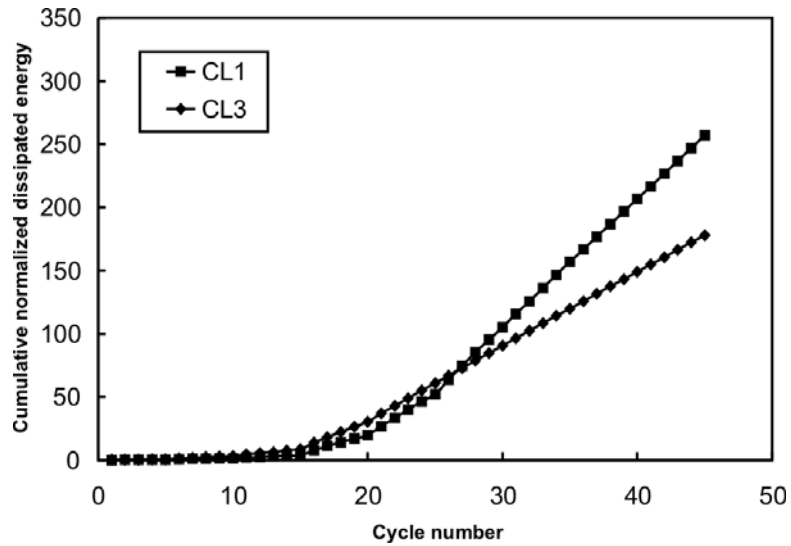


Figure 4-128: Cumulative normalized dissipated energy based on overall system versus cycle number for columns CL1 and CL3

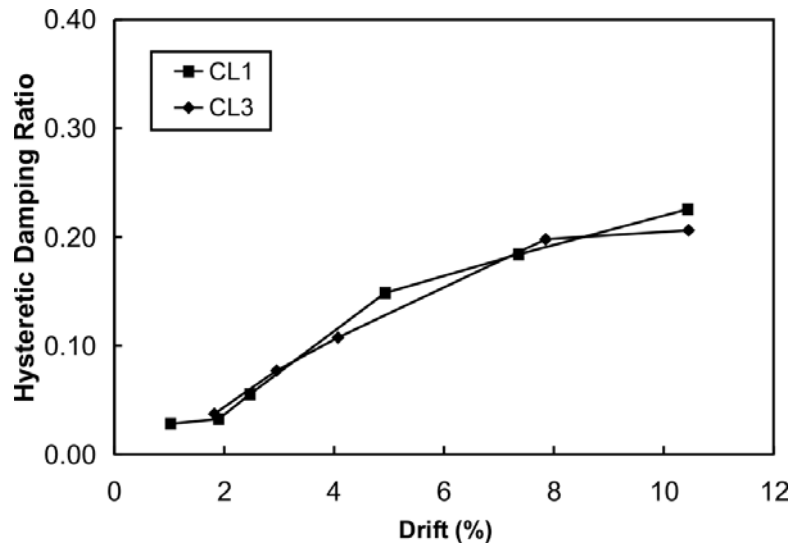


Figure 4-129: Hysteretic damping versus lateral drift (%) for columns CL1 and CL3

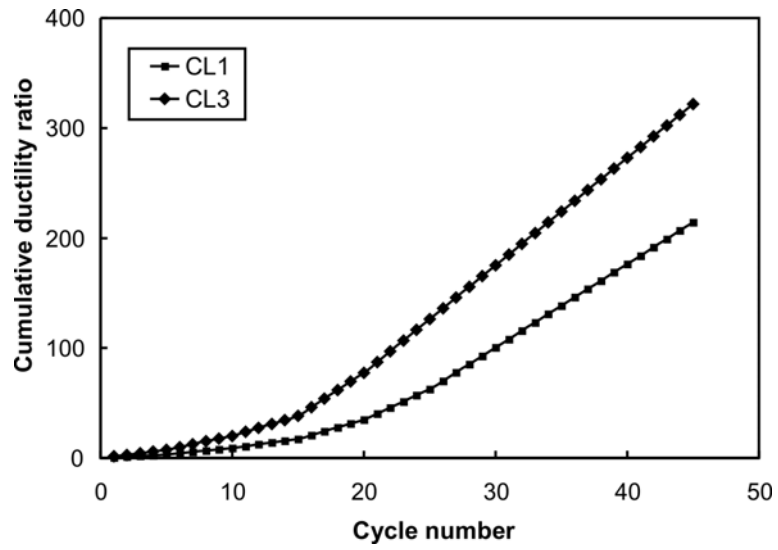


Figure 4-130: Cumulative ductility ratio versus cycle number for columns CL1 and CL3

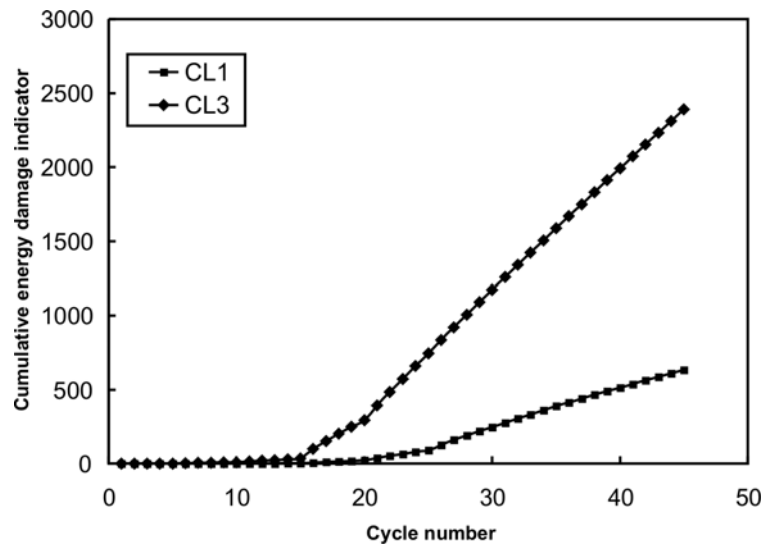


Figure 4-131: Cumulative energy damage indicator versus cycle number for columns CL1 and CL3

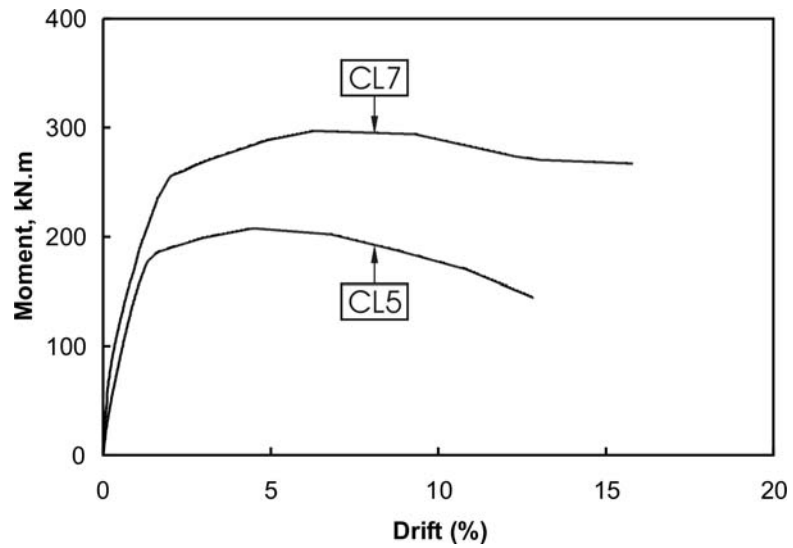


Figure 4-132: Moment at column base versus lateral drift (%) envelope curves for columns CL5 and CL7

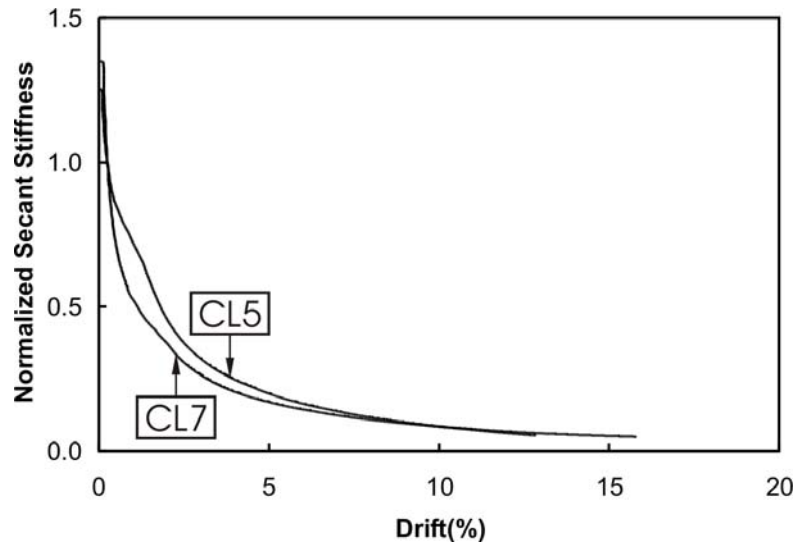


Figure 4-133: Relationship between normalized secant stiffness and lateral drift (%) for columns CL5 and CL7

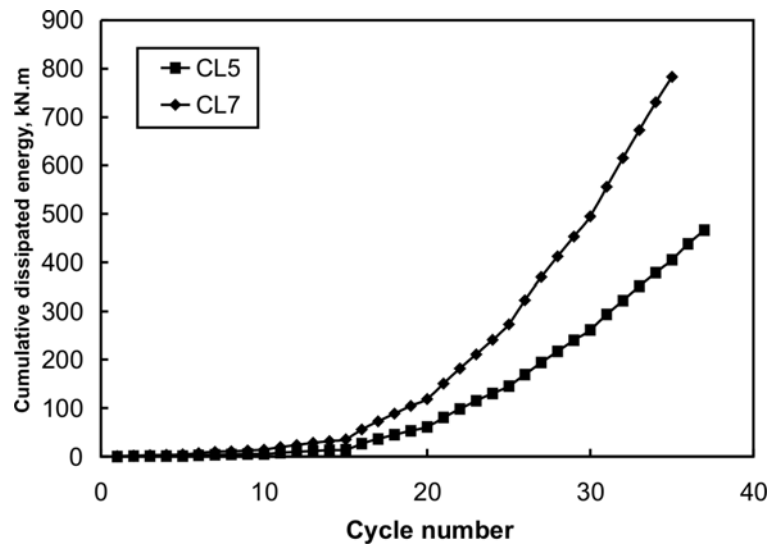


Figure 4-134: Cumulative energy dissipated versus cycle number for columns CL5 and CL7

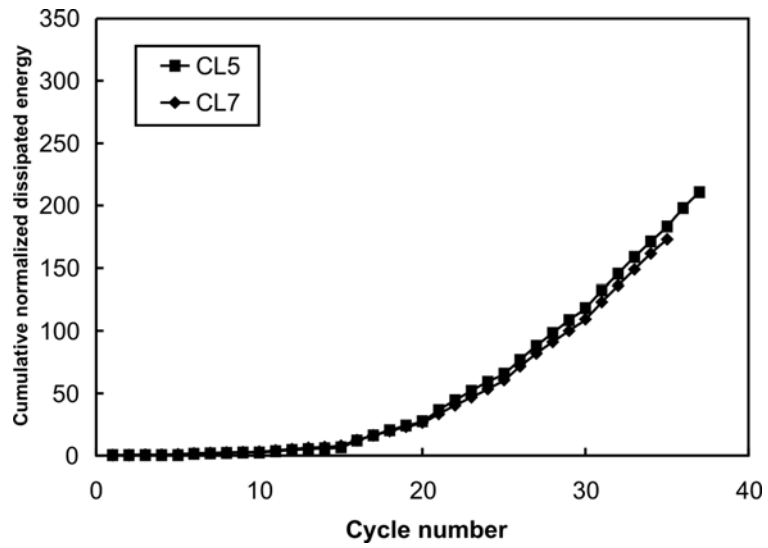


Figure 4-135: Cumulative normalized dissipated energy versus cycle number for columns CL5 and CL7

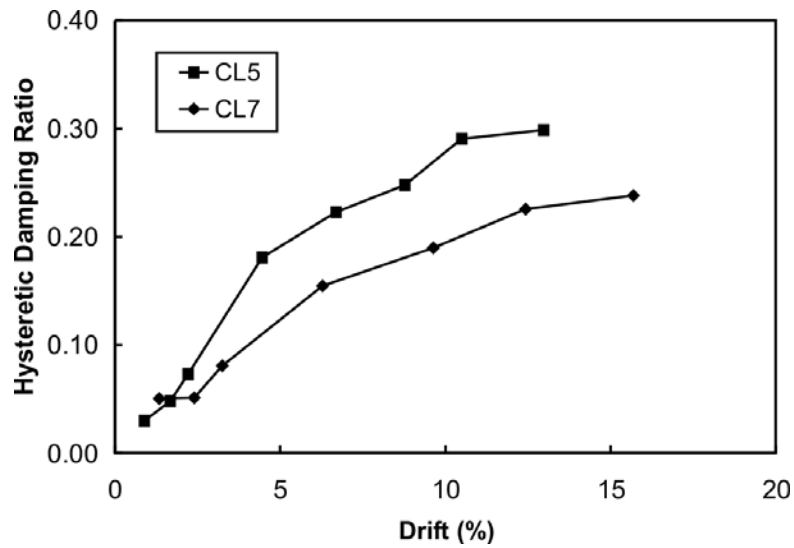


Figure 4-136: Hysteretic damping ratio versus lateral drift (%) for columns CL5 and CL7

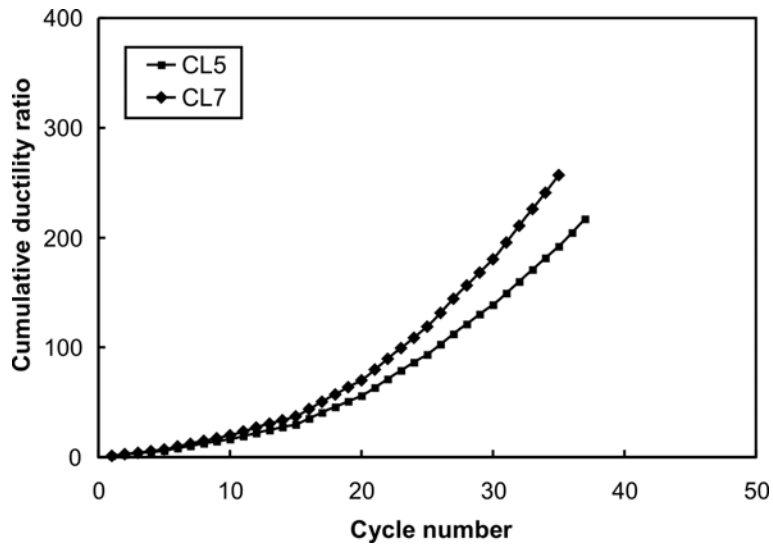


Figure 4-137: Cumulative ductility ratio versus cycle number for columns CL5 and CL7

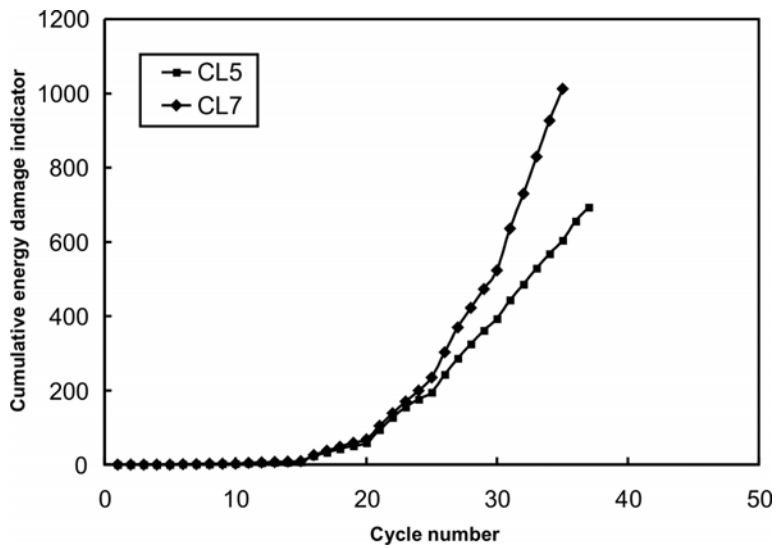


Figure 4-138: Cumulative energy damage indicator versus cycle number for columns CL5 and CL7

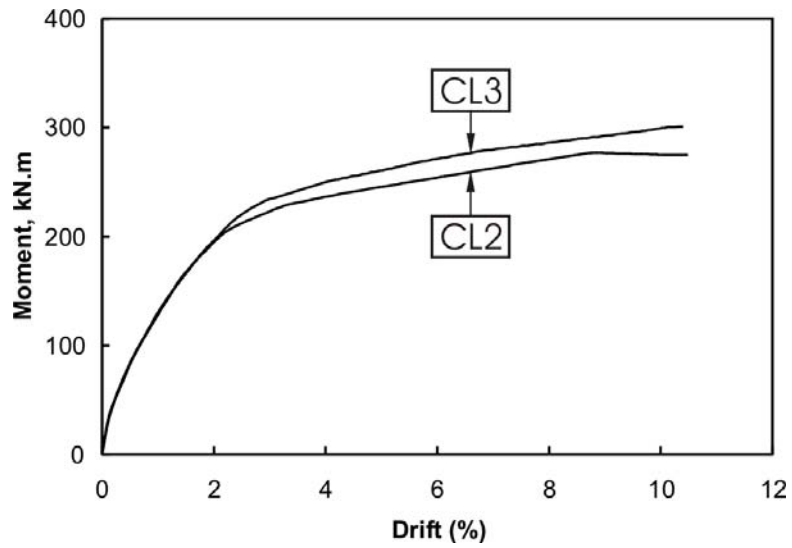


Figure 4-139: Moment at column base versus lateral drift (%) envelope curves for columns CL2 and CL3

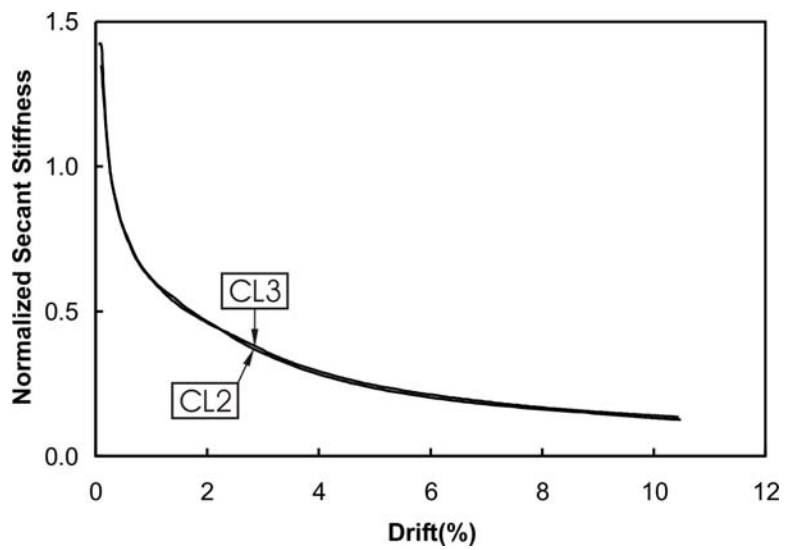


Figure 4-140: Relationship between normalized secant stiffness and lateral drift (%) for columns CL2 and CL3

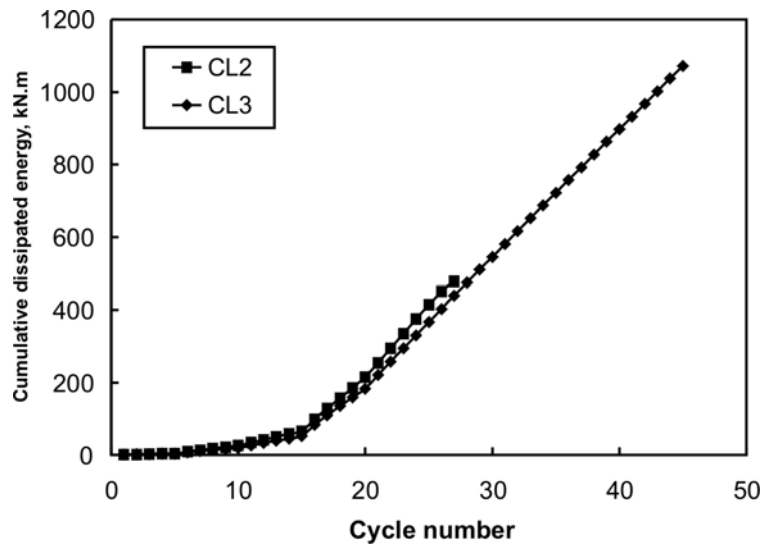


Figure 4-141: Cumulative energy dissipated versus cycle number for columns CL2 and CL3

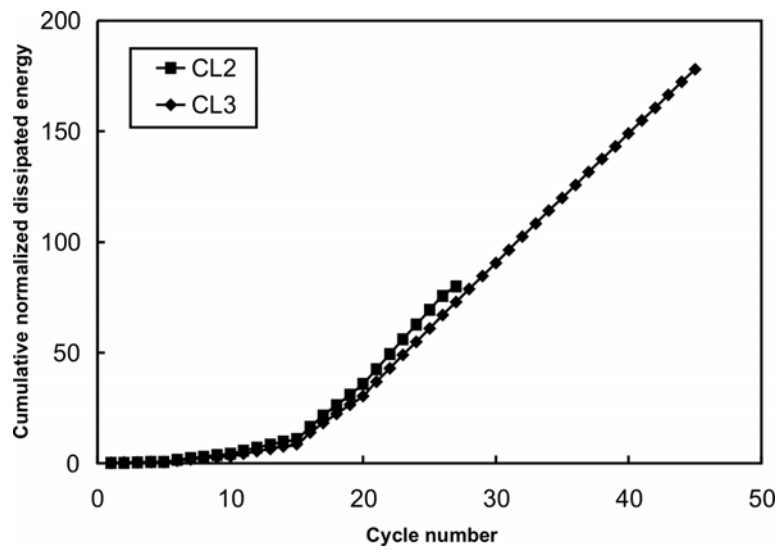


Figure 4-142: Cumulative normalized dissipated energy versus cycle number for columns CL2 and CL3

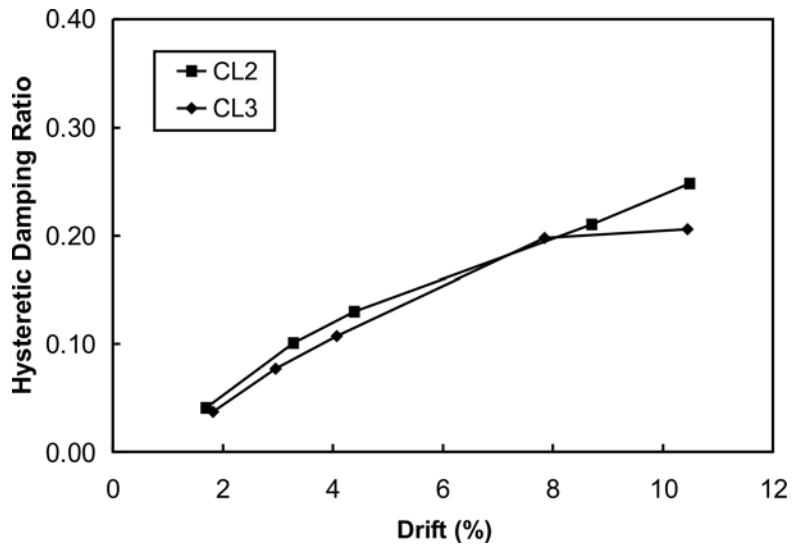


Figure 4-143: Hysteretic damping ratio versus lateral drift (%) for columns CL2 and CL3

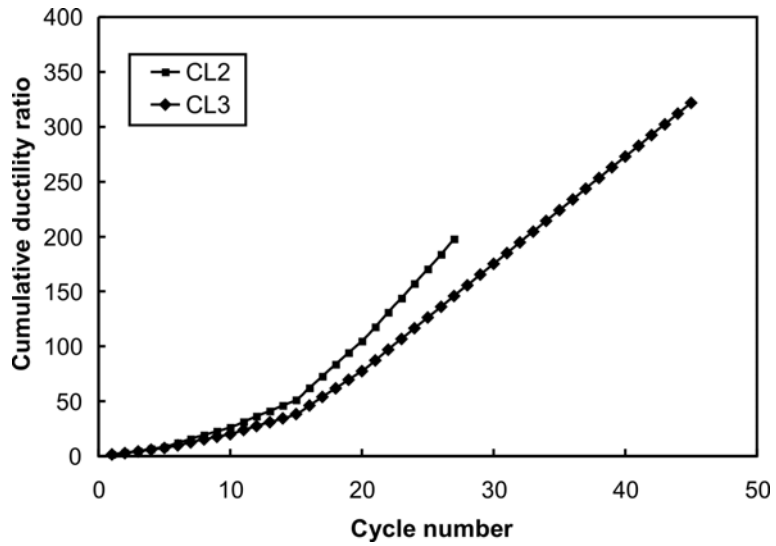


Figure 4-144: Cumulative ductility ratio versus cycle numbers for columns CL2 and CL3

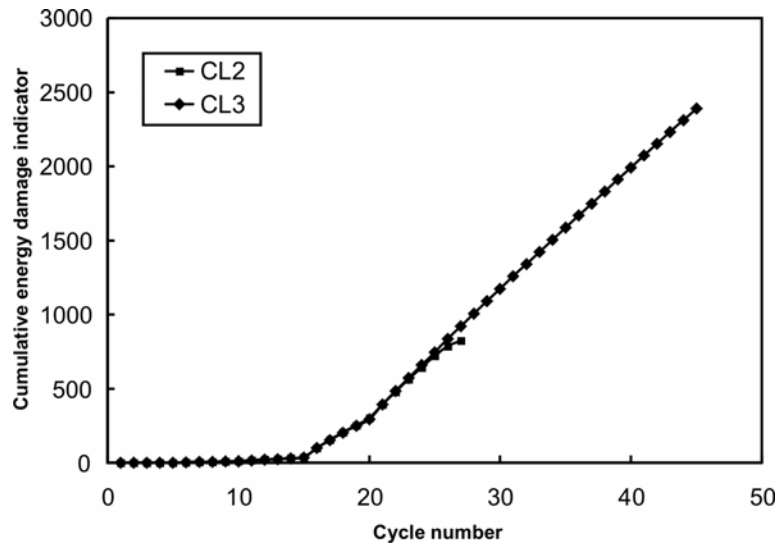


Figure 4-145: Cumulative energy damage indicator versus cycle number for columns CL2 and CL3

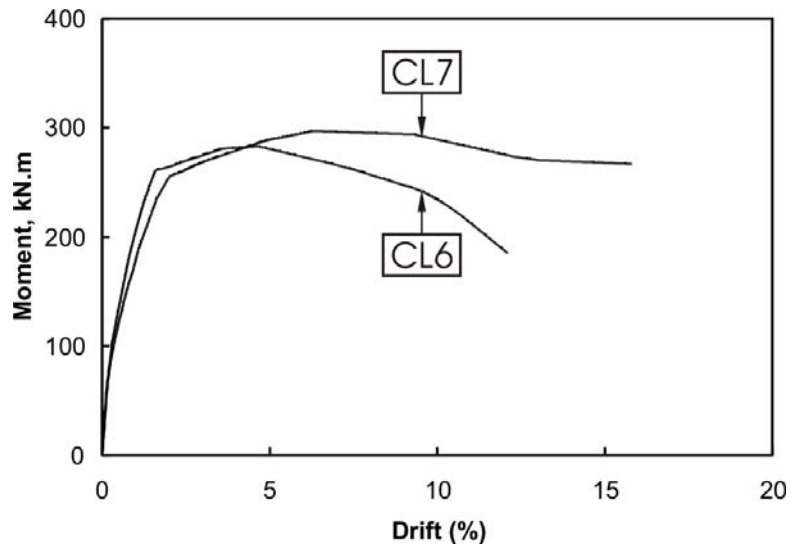


Figure 4-146: Moment at column base versus lateral drift (%) envelope curves for columns CL6 and CL7

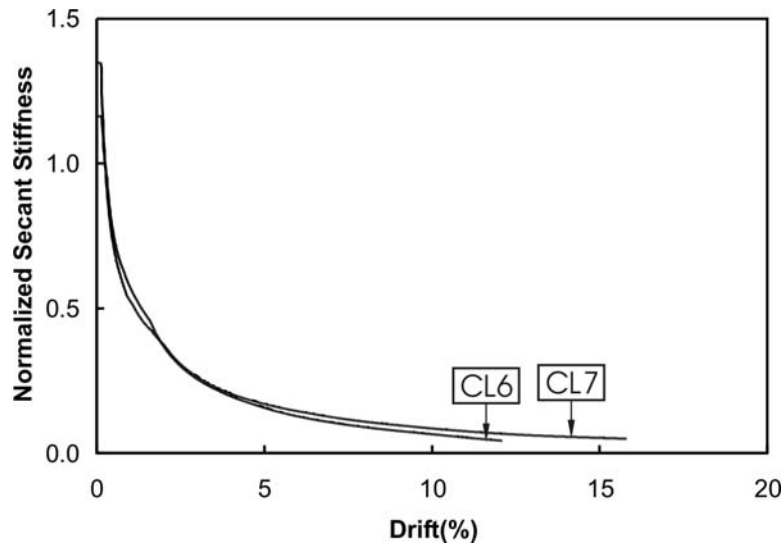


Figure 4-147: Relationship between normalized secant stiffness and lateral drift (%) for columns CL6 and CL7

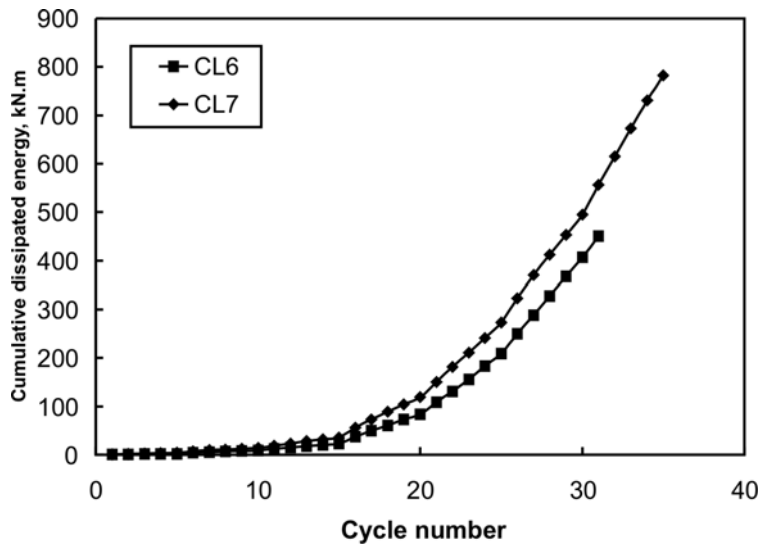


Figure 4-148: Cumulative energy dissipated versus cycle number for columns CL6 and CL7

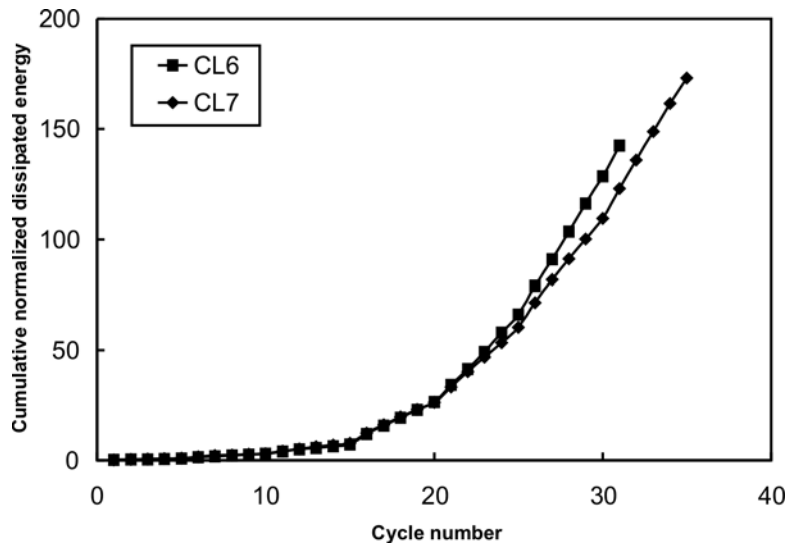


Figure 4-149: Cumulative normalized dissipated energy versus cycle number for columns CL6 and CL7

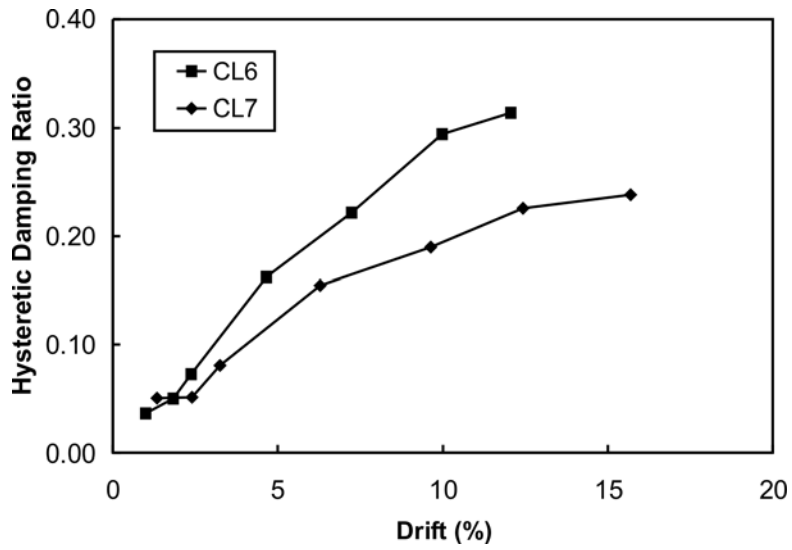


Figure 4-150: Hysteretic damping ratio versus lateral drift (%) for columns CL6 and CL7

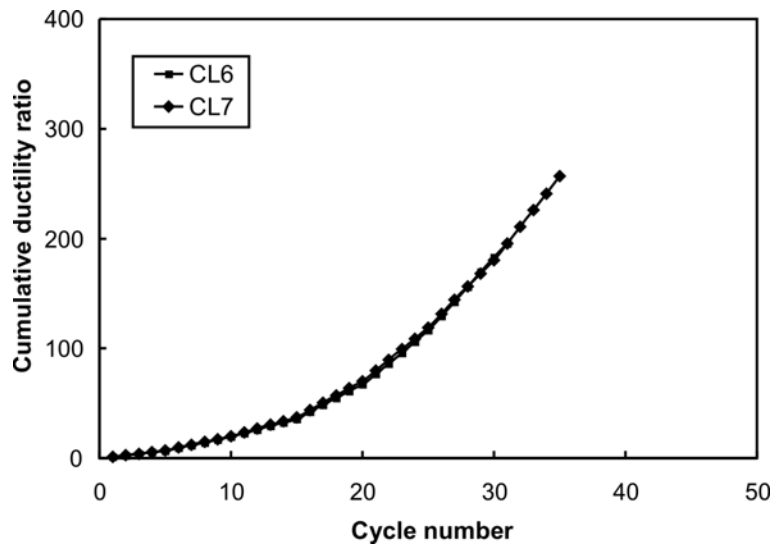


Figure 4-151: Cumulative ductility ratio versus cycle numbers for columns CL6 and CL7

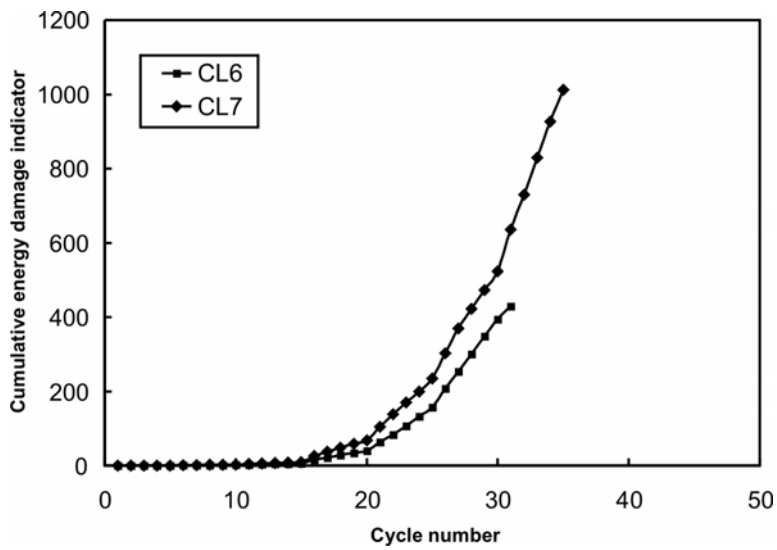


Figure 4-152: Cumulative energy damage indicator versus cycle number for columns CL6 and CL7

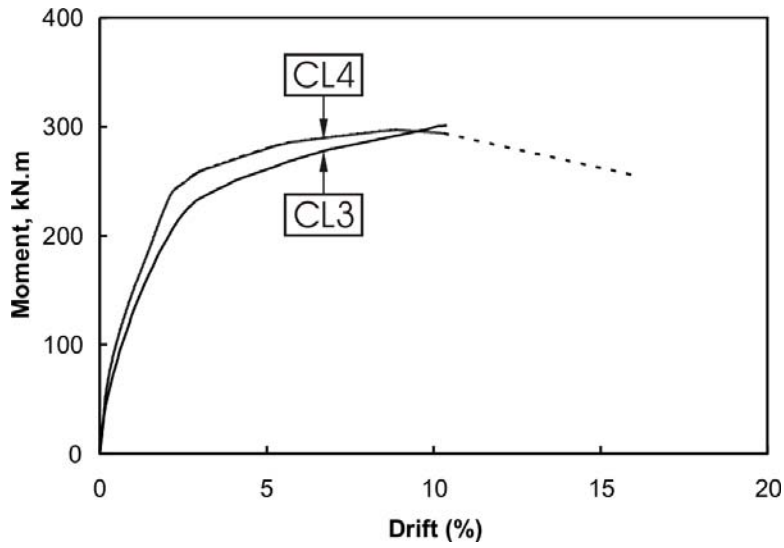


Figure 4-153: Moment at column base versus lateral drift (%) envelope curves for columns CL3 and CL4

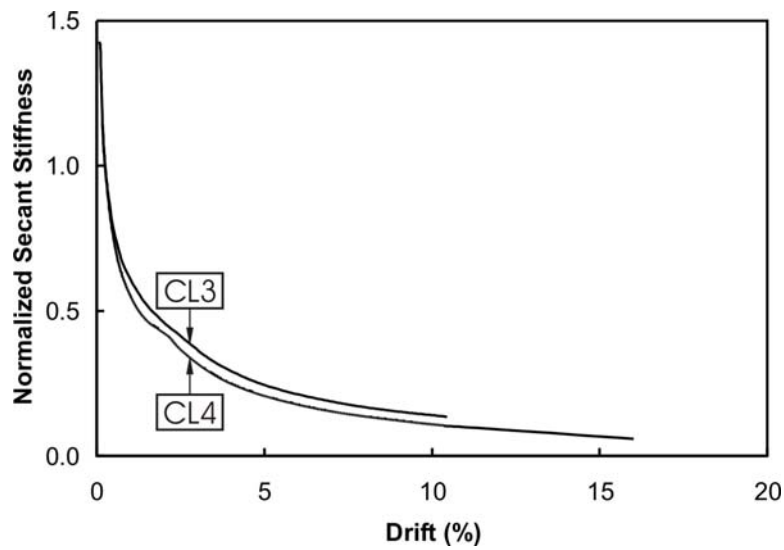


Figure 4-154: Relationship between normalized secant stiffness and lateral drift (%) for columns CL3 and CL4

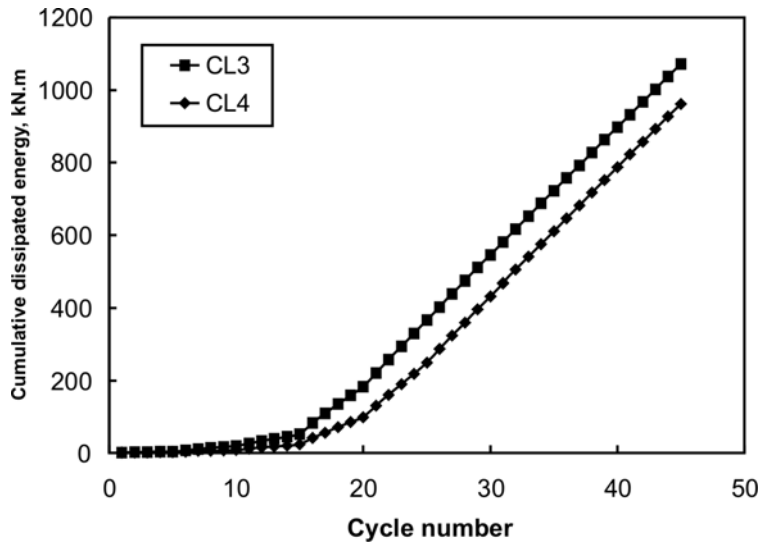


Figure 4-155: Cumulative energy dissipated versus cycle number for columns CL3 and CL4

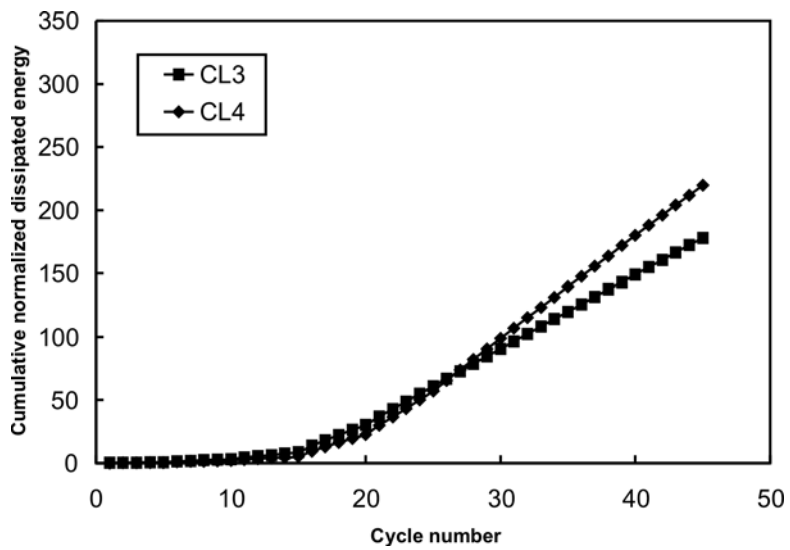


Figure 4-156: Cumulative normalized dissipated energy versus cycle number for columns CL3 and CL4

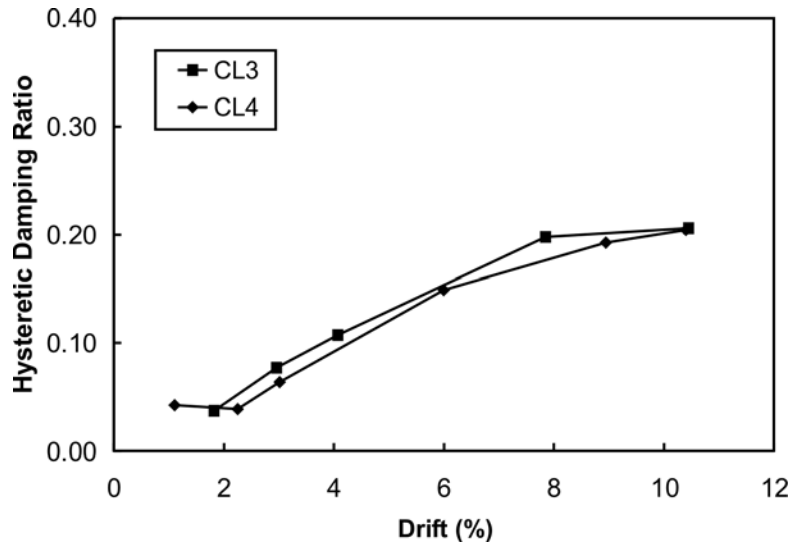


Figure 4-157: Hysteretic damping ratio versus lateral drift (%) for columns CL3 and CL4

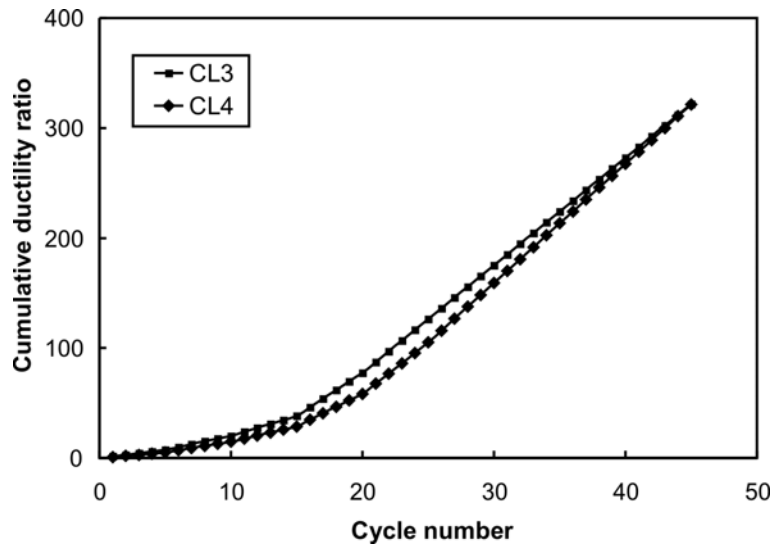


Figure 4-158: Cumulative ductility ratio versus cycle numbers for columns CL3 and CL4

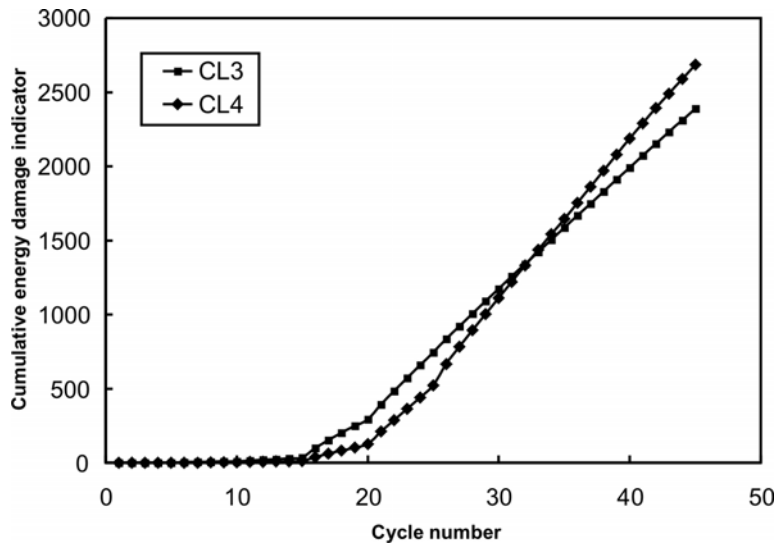


Figure 4-159: Cumulative energy damage indicator versus cycle number for columns CL3 and CL4

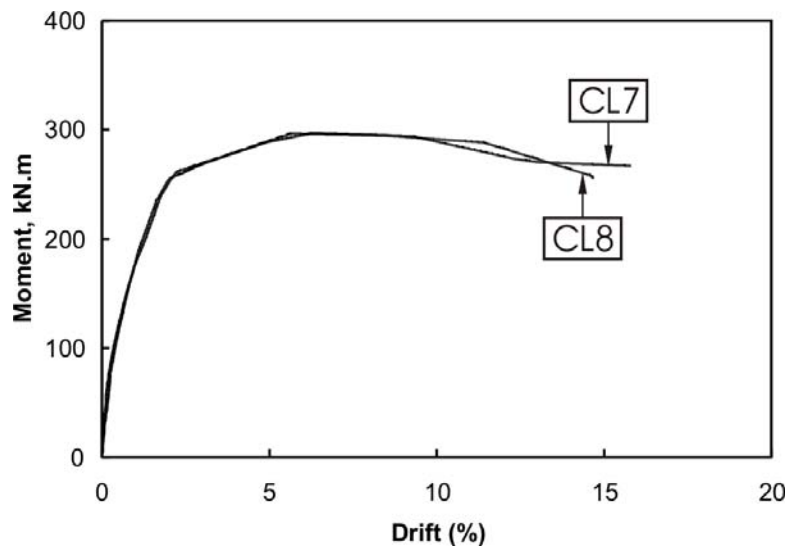


Figure 4-160: Moment at column base versus lateral drift (%) envelope curves for columns CL7 and CL8

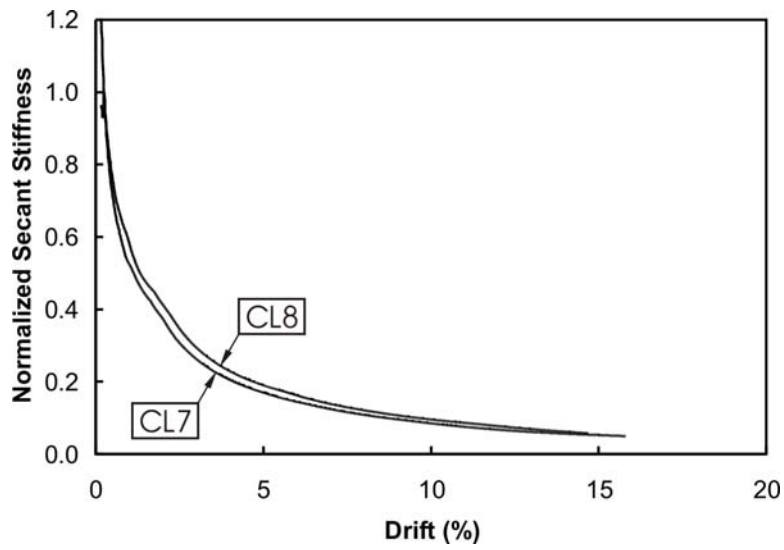


Figure 4-161: Relationship between normalized secant stiffness and lateral drift (%) for columns CL7 and CL8

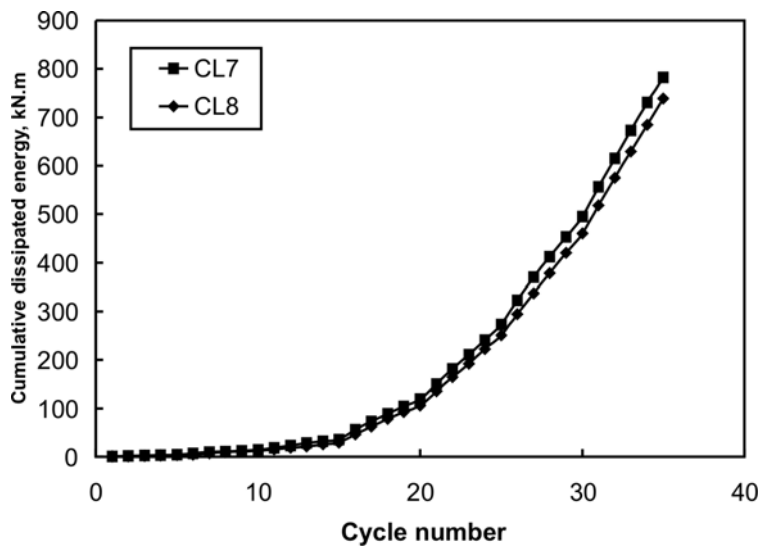


Figure 4-162: Cumulative energy dissipated versus cycle number for columns CL7 and CL8

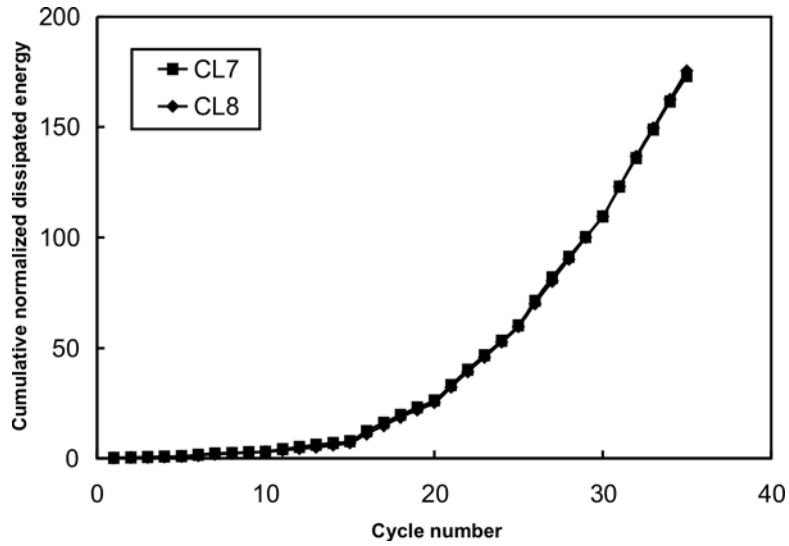


Figure 4-163: Cumulative normalized dissipated energy versus cycle number for columns CL7 and CL8

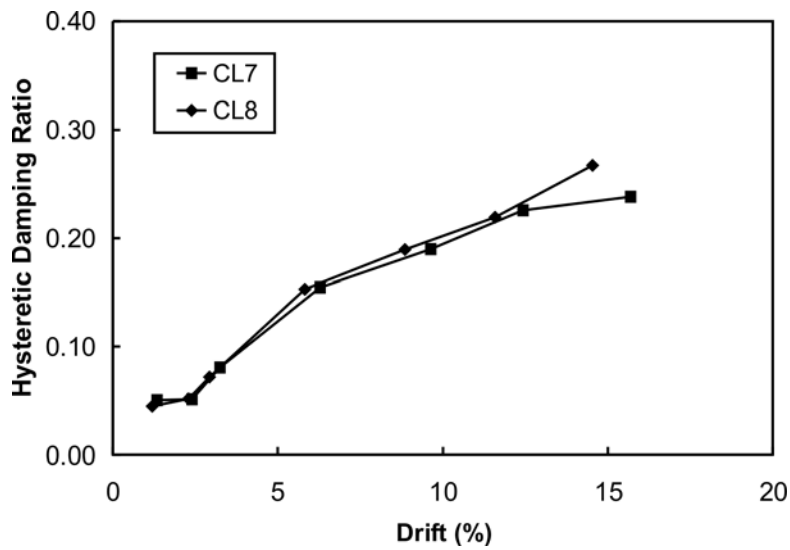


Figure 4-164: Hysteretic damping ratio versus lateral drift (%) for columns CL7 and CL8

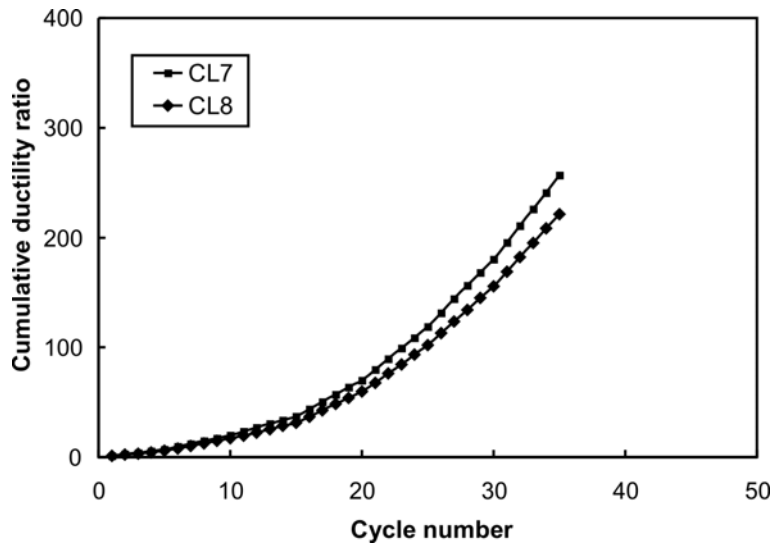


Figure 4-165: Cumulative ductility ratio versus cycle numbers for columns CL7 and CL8

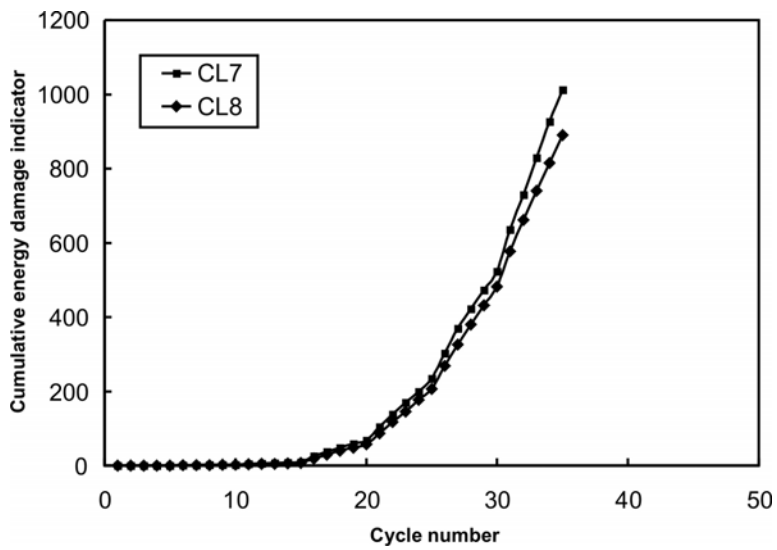


Figure 4-166: Cumulative energy damage indicator versus cycle number for columns CL7 and CL8

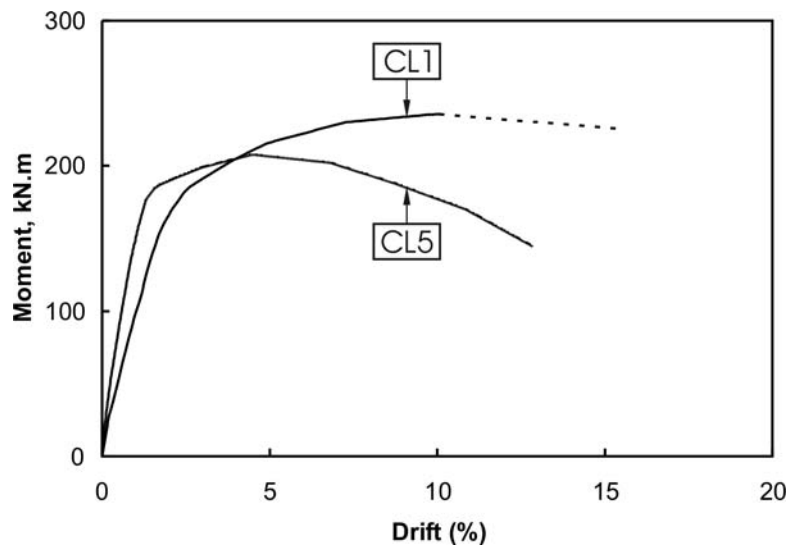


Figure 4-167: Moment at column base versus lateral drift (%) envelope curves for columns CL1 and CL5

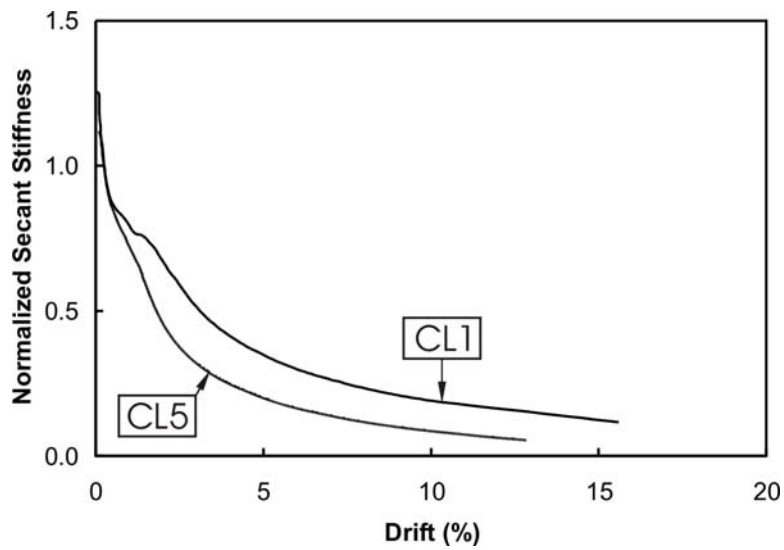


Figure 4-168: Relationship between normalized secant stiffness and lateral drift (%) for columns CL1 and CL5

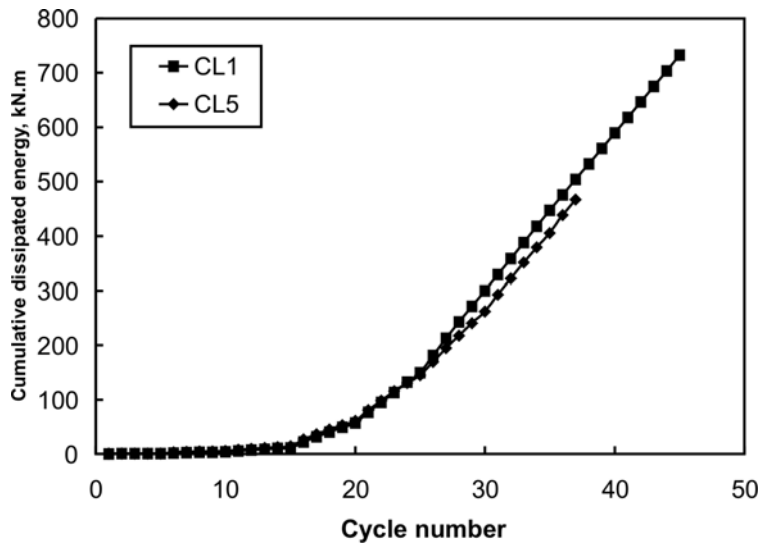


Figure 4-169: Cumulative energy dissipated versus cycle number for columns CL1 and CL5

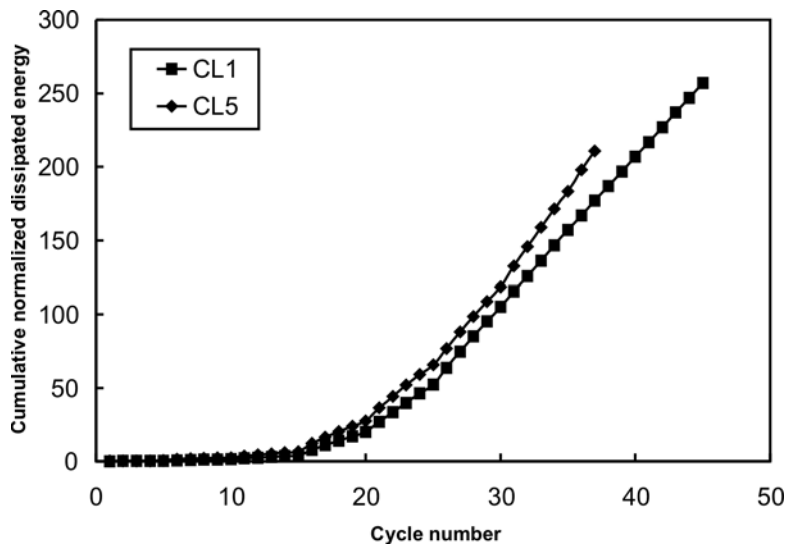


Figure 4-170: Cumulative normalized dissipated energy versus cycle number for columns CL1 and CL5

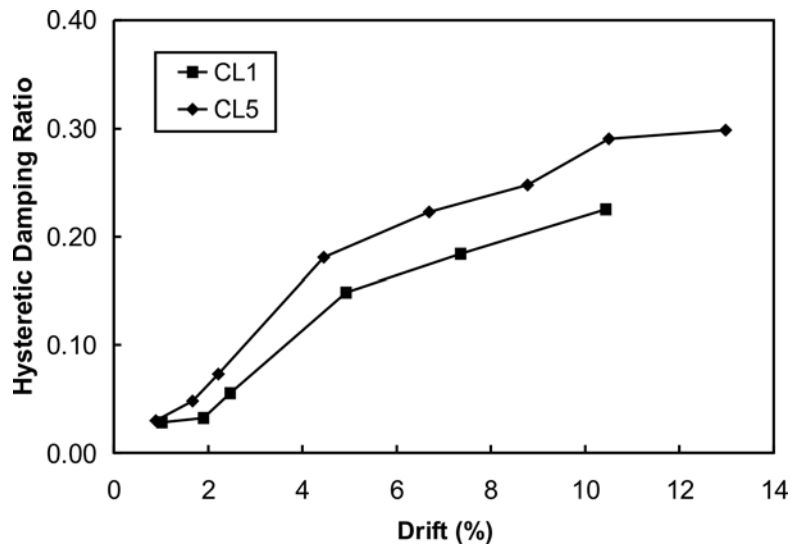


Figure 4-171: Hysteretic damping ratio versus lateral drift (%) for columns CL1 and CL5

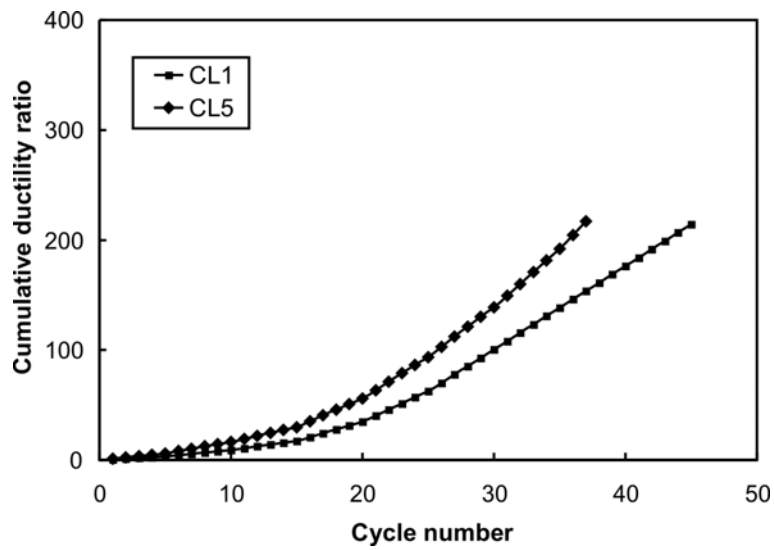


Figure 4-172: Cumulative ductility ratio versus cycle numbers for columns CL1 and CL5

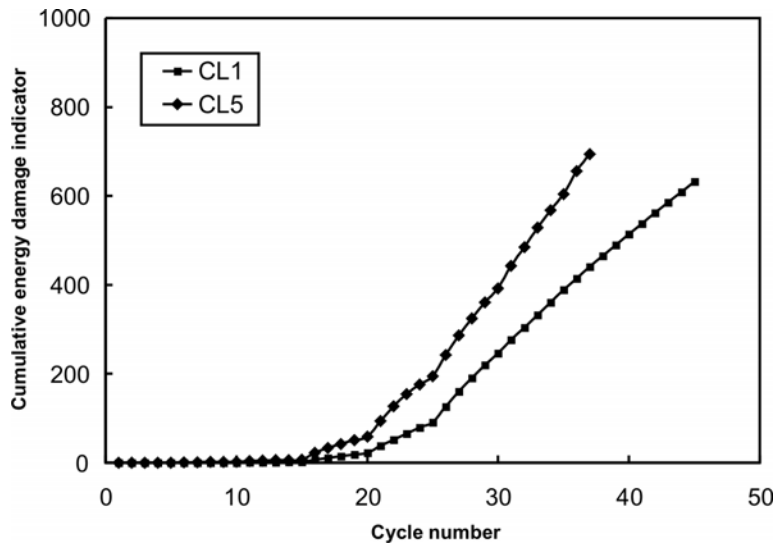


Figure 4-173: Cumulative energy damage indicator versus cycle number for columns CL1 and CL5

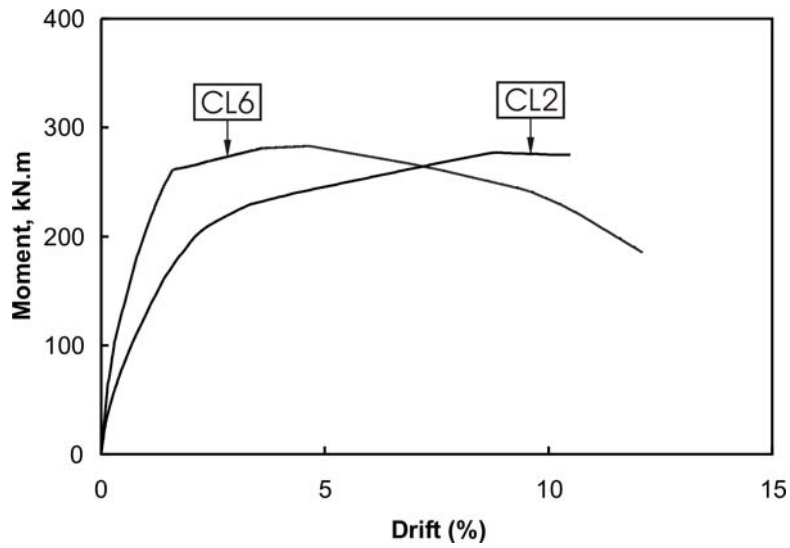


Figure 4-174: Moment at column base versus lateral drift (%) envelope curves for columns CL2 and CL6

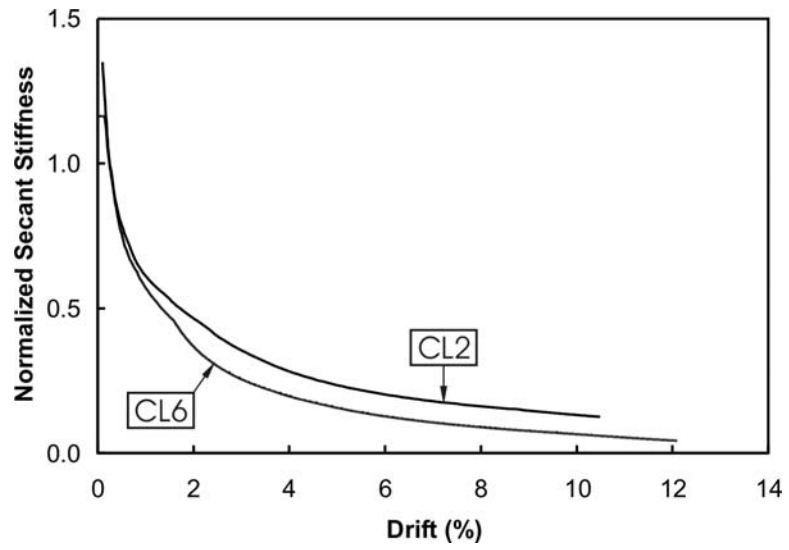


Figure 4-175: Relationship between normalized secant stiffness and lateral drift (%) for columns CL2 and CL6

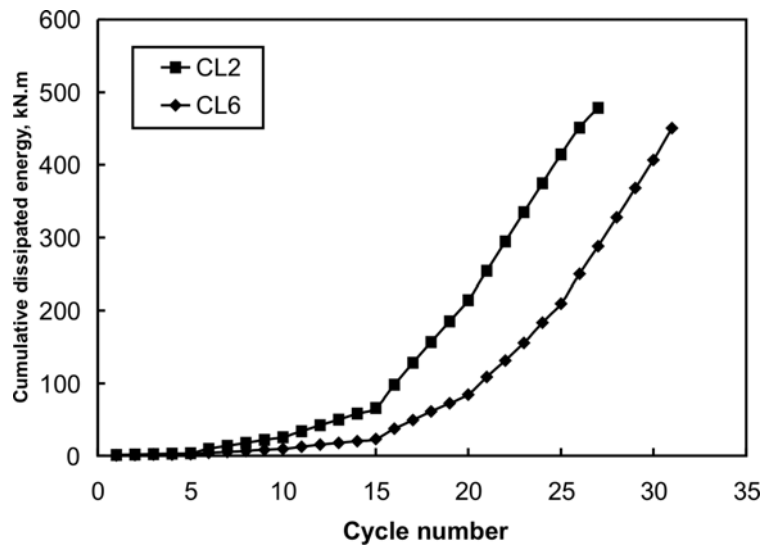


Figure 4-176: Cumulative energy dissipated versus cycle number for columns CL2 and CL6

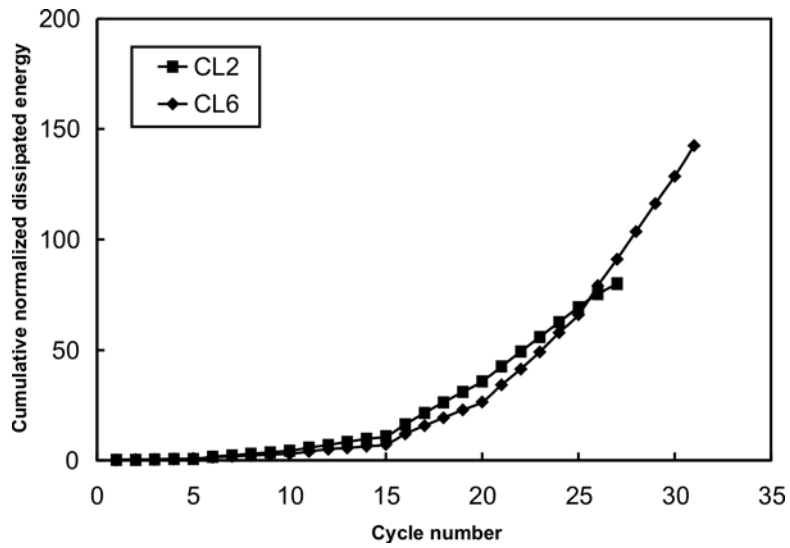


Figure 4-177: Cumulative normalized dissipated energy versus cycle number for columns CL2 and CL6

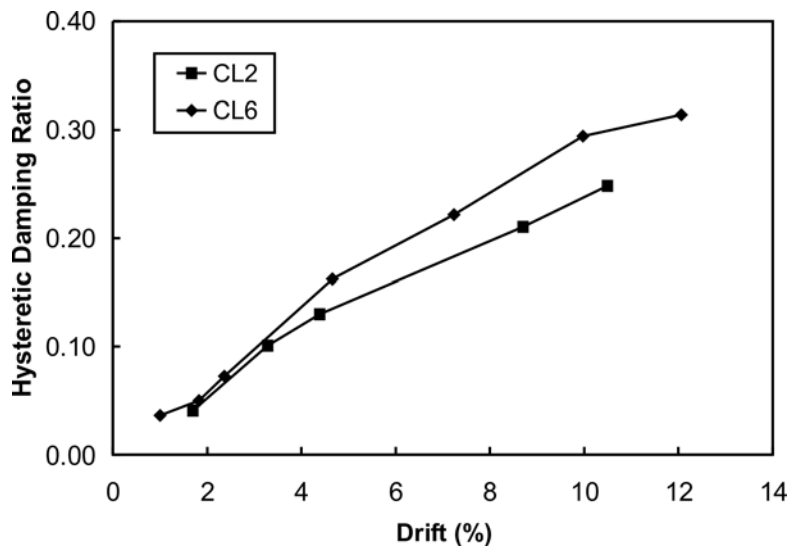


Figure 4-178: Hysteretic damping ratio versus lateral drift (%) for columns CL2 and CL6

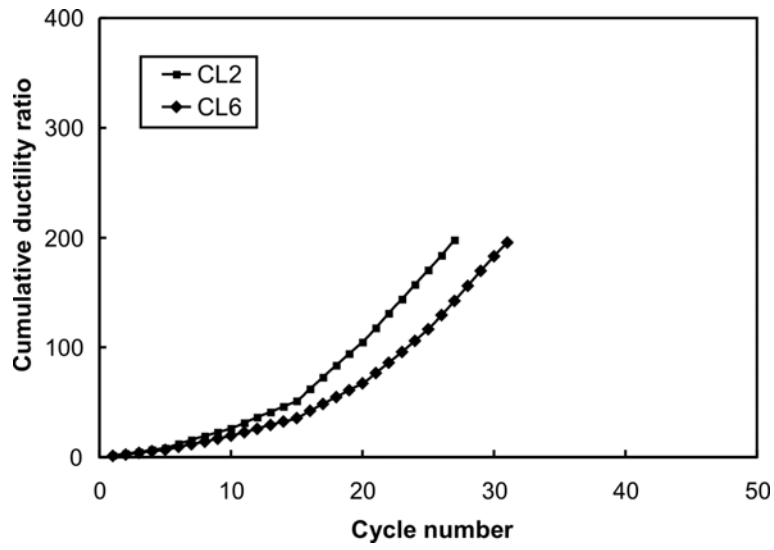


Figure 4-179: Cumulative ductility ratio versus cycle numbers for columns CL2 and CL6

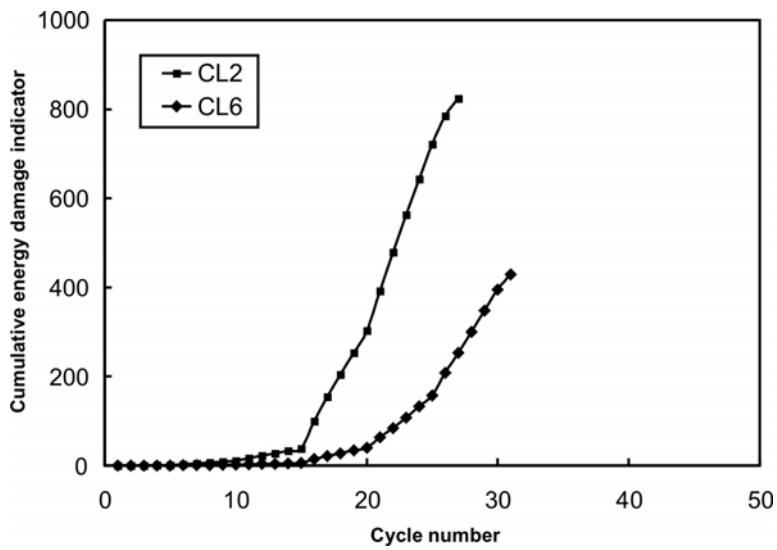


Figure 4-180: Cumulative energy damage indicator versus cycle number for columns CL2 and CL6

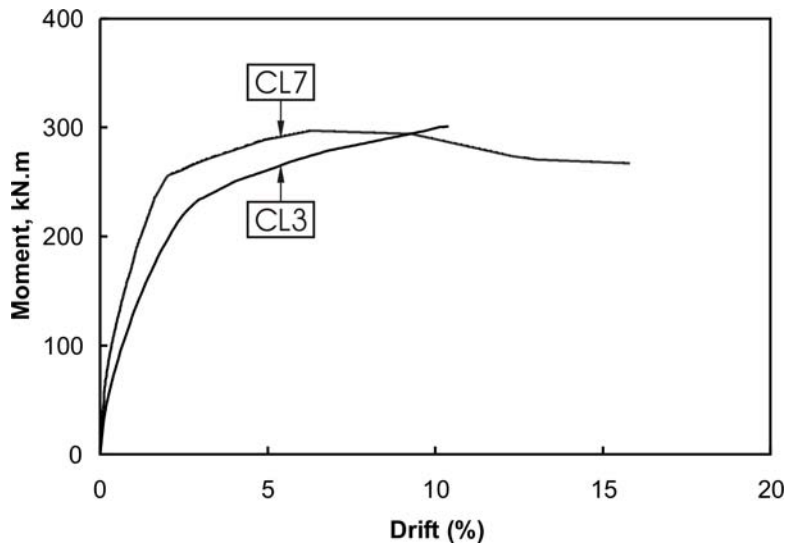


Figure 4-181: Moment at column base versus lateral drift (%) envelope curves for columns CL3 and CL7

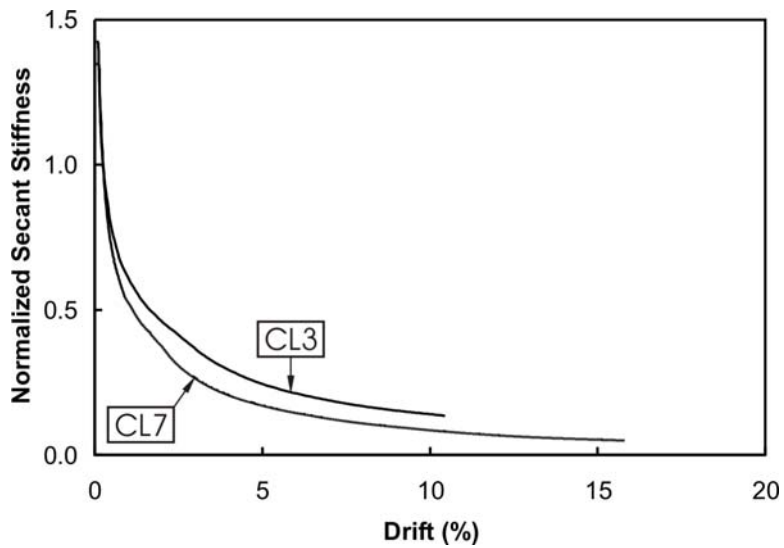


Figure 4-182: Relationship between normalized secant stiffness and lateral drift (%) for columns CL3 and CL7

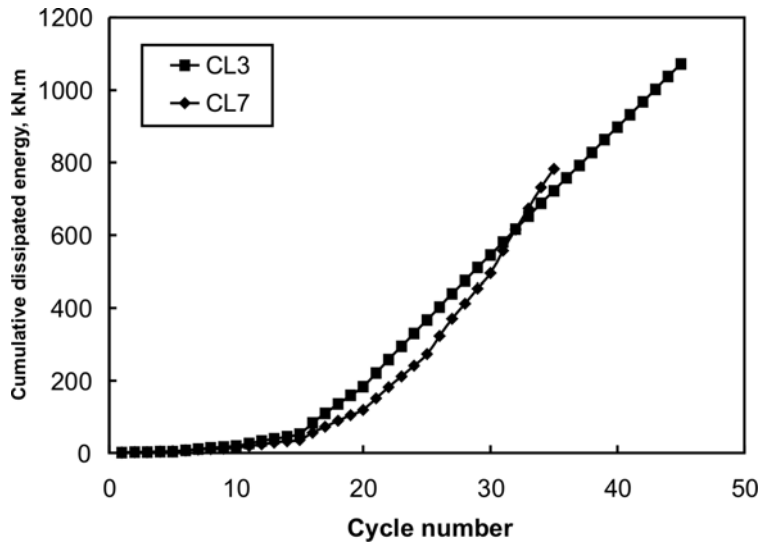


Figure 4-183: Cumulative energy dissipated versus cycle number for columns CL3 and CL7

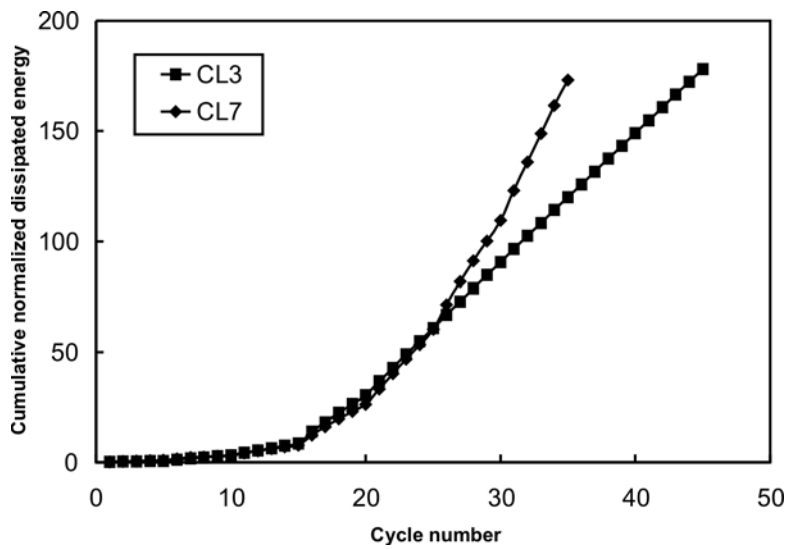


Figure 4-184: Cumulative normalized dissipated energy versus cycle number for columns CL3 and CL7

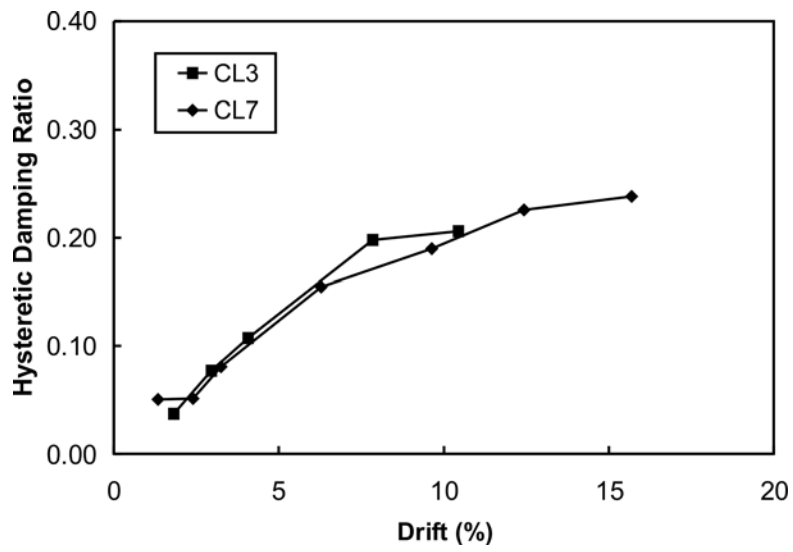


Figure 4-185: Hysteretic damping ratio versus lateral drift (%) for columns CL3 and CL7

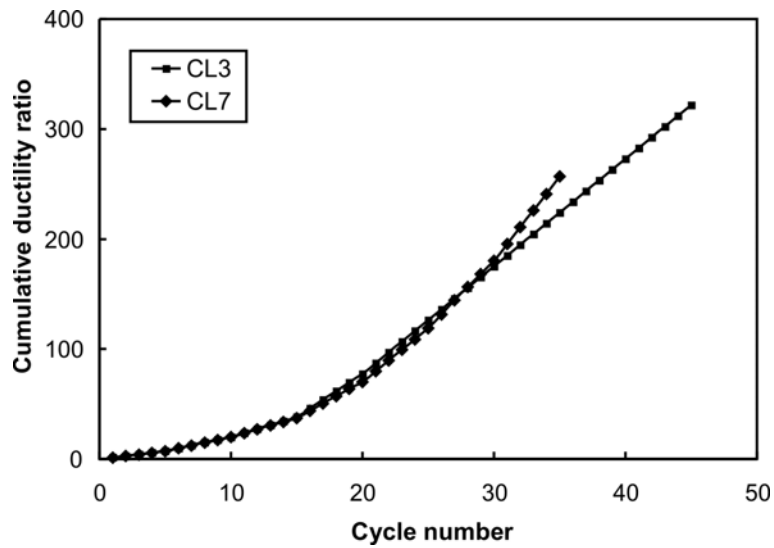


Figure 4-186: Cumulative ductility ratio versus cycle numbers for columns CL3 and CL7

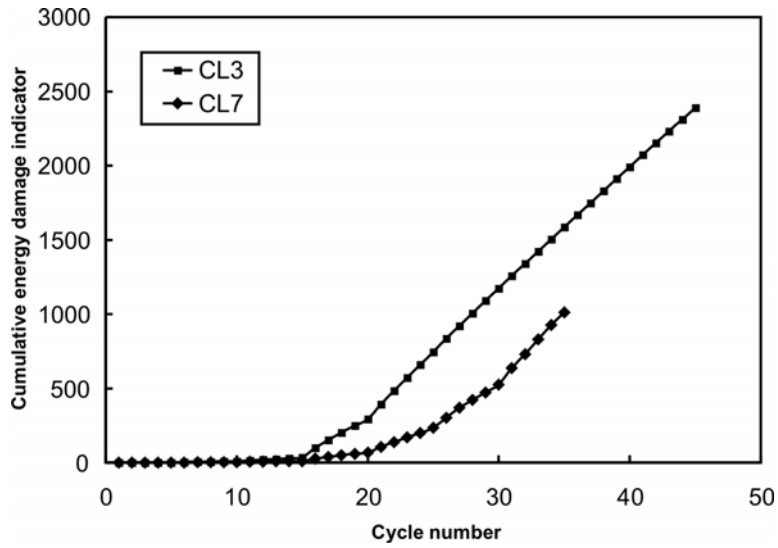


Figure 4-187: Cumulative energy damage indicator versus cycle number for columns CL3 and CL7

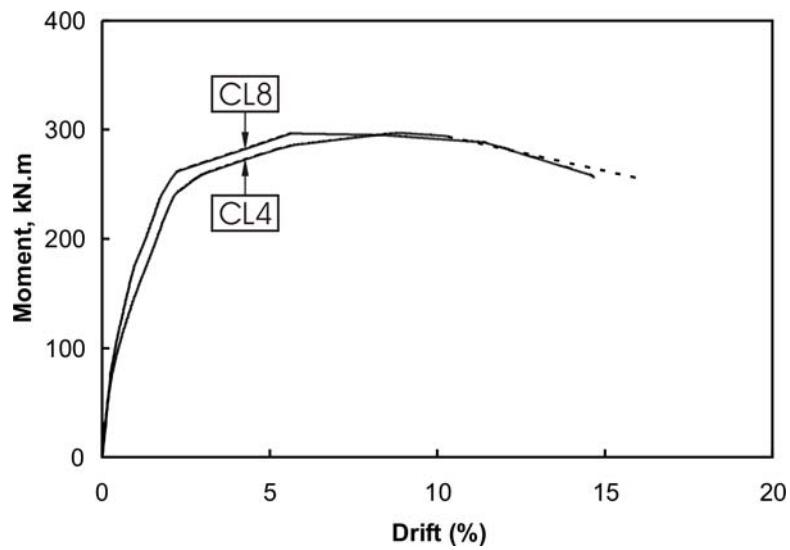


Figure 4-188: Moment at column base versus lateral drift (%) envelope curves for columns CL4 and CL8

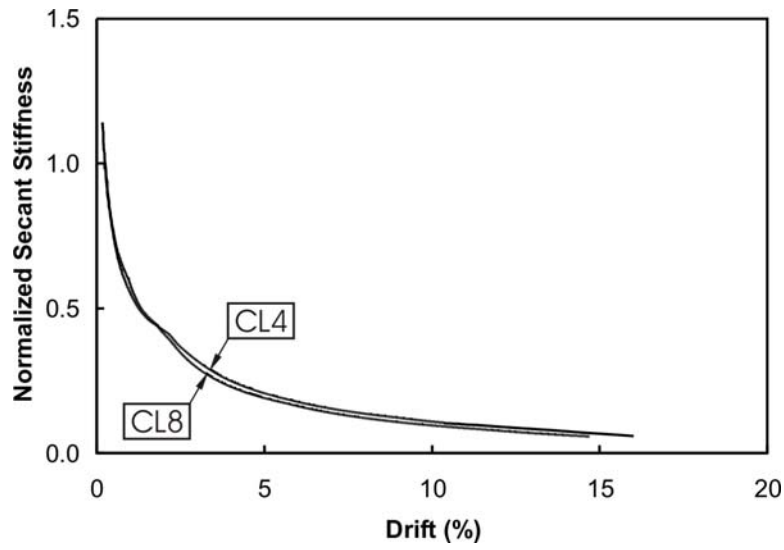


Figure 4-189: Relationship between normalized secant stiffness and lateral drift (%) for columns CL4 and CL8

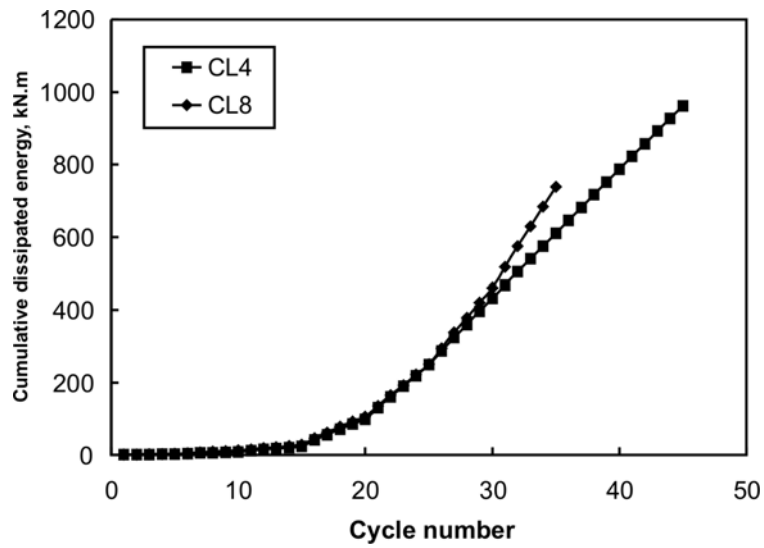


Figure 4-190: Cumulative energy dissipated versus cycle number for columns CL4 and CL8

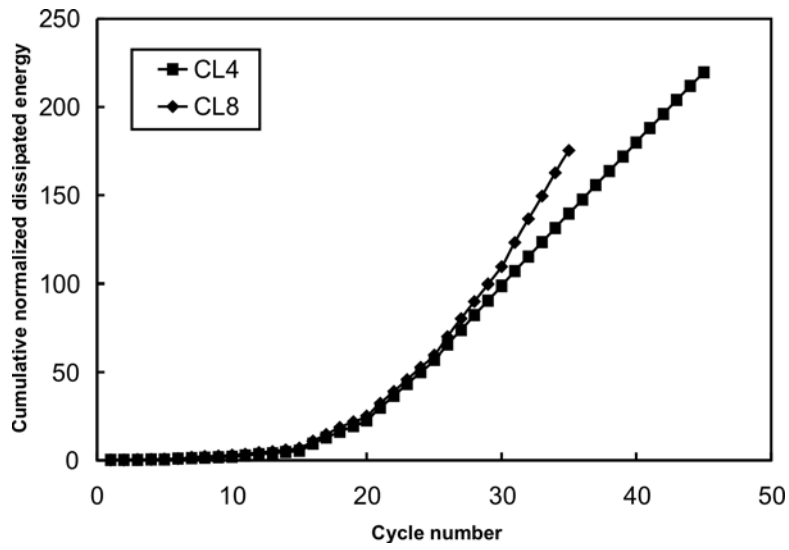


Figure 4-191: Cumulative normalized dissipated energy versus cycle number for columns CL4 and CL8

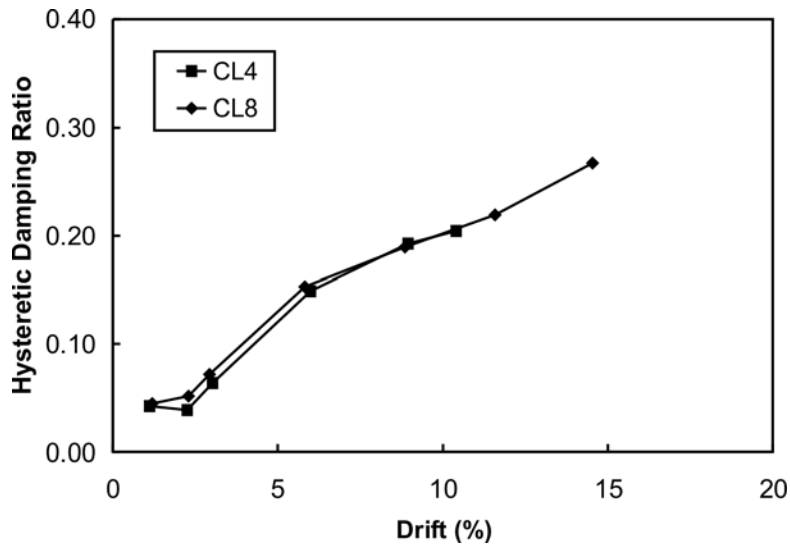


Figure 4-192: Hysteretic damping ratio versus lateral drift (%) for columns CL4 and CL8

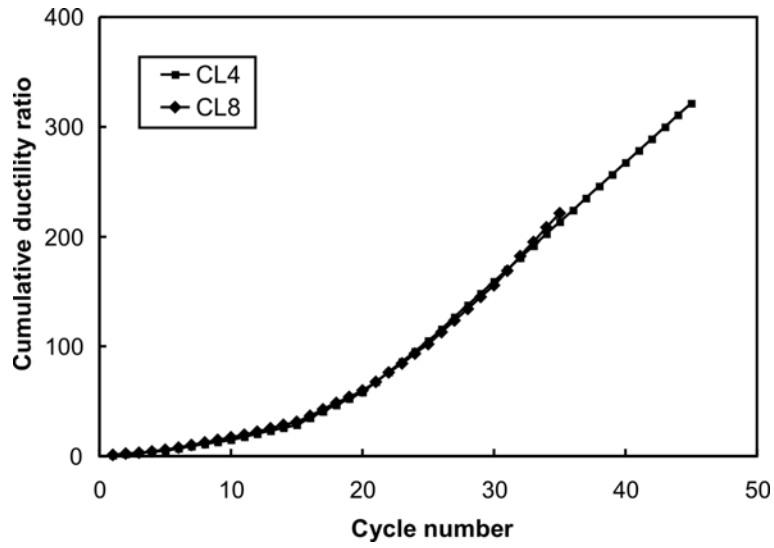


Figure 4-193: Cumulative ductility ratio versus cycle numbers for columns CL4 and CL8

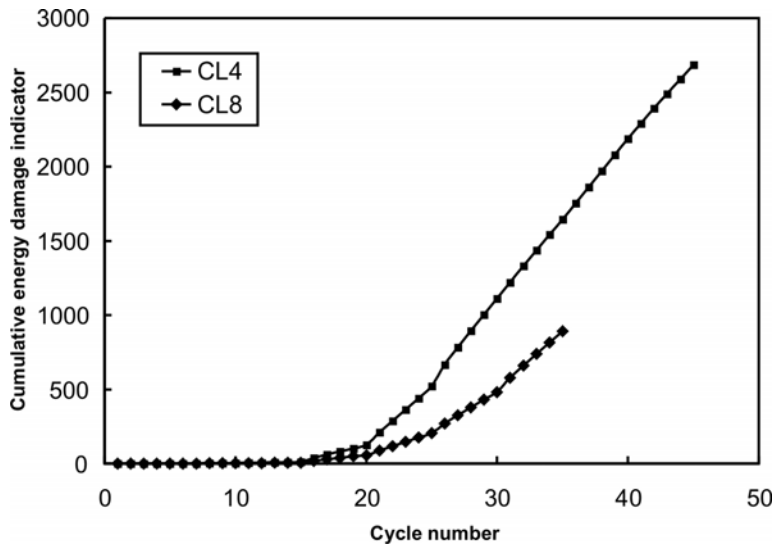


Figure 4-194: Cumulative energy damage indicator versus cycle number for columns CL4 and CL8

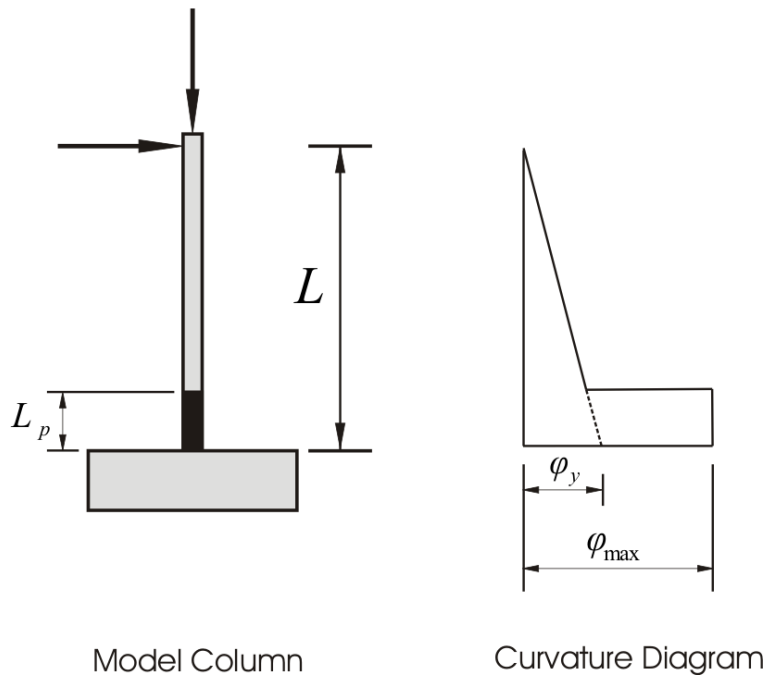


Figure 4-195: A model column along with a typical curvature distribution diagram

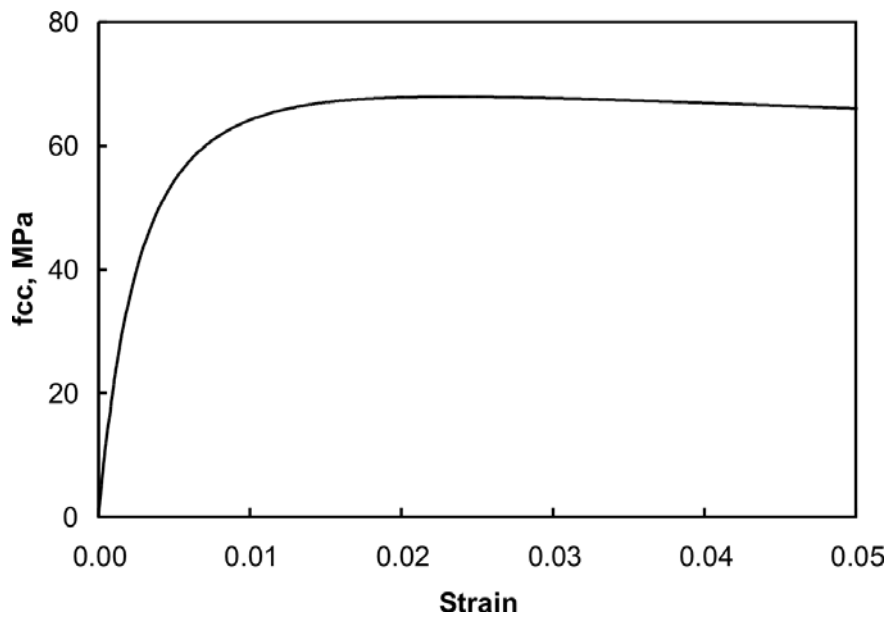


Figure 4-196: Confined concrete material curve for column CL0 obtained using model proposed by Mander *et al.* (1988b)

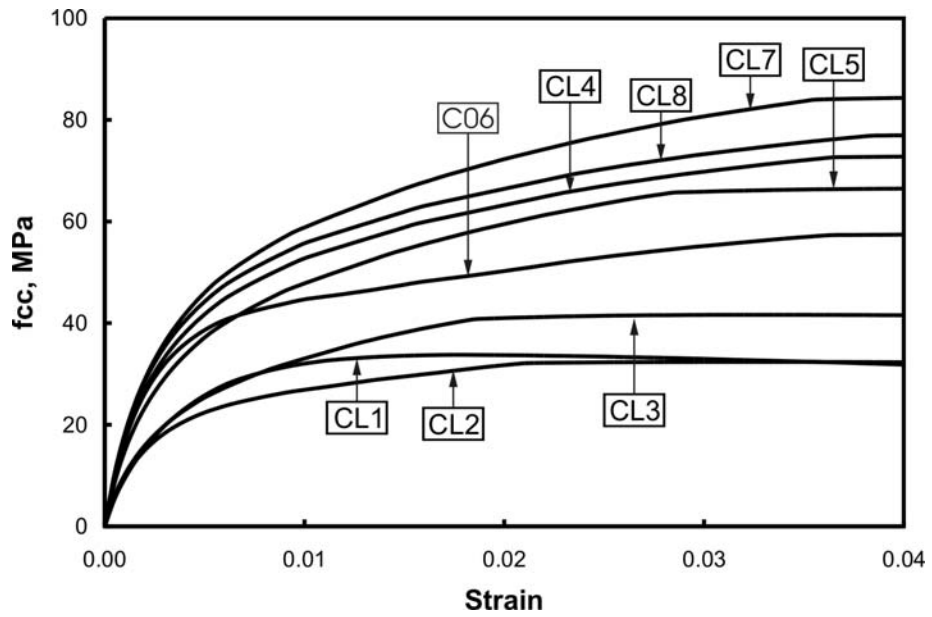


Figure 4-197: Confined concrete material curves for collared columns (CL1 to CL8)

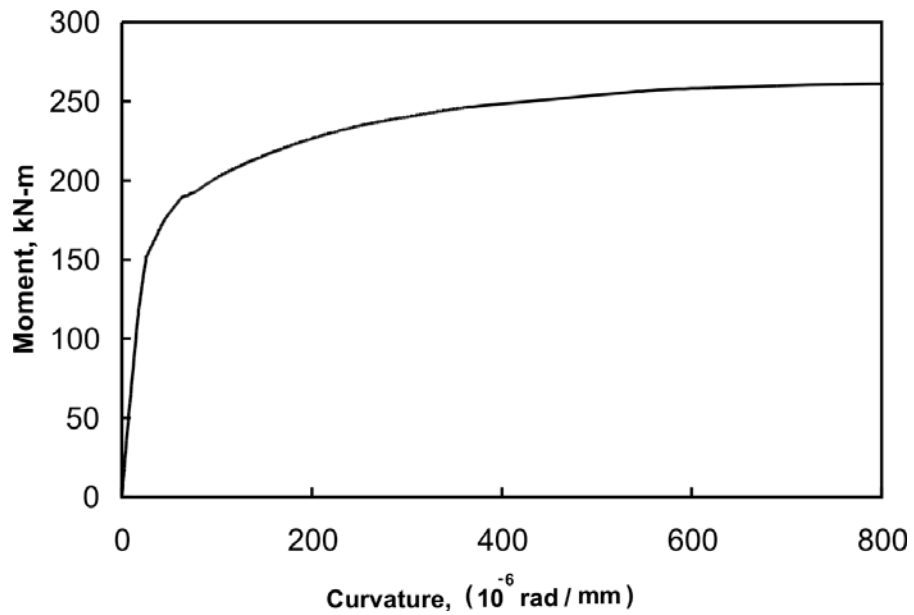


Figure 4-198: Analytical moment versus curvature relationship for column CL1

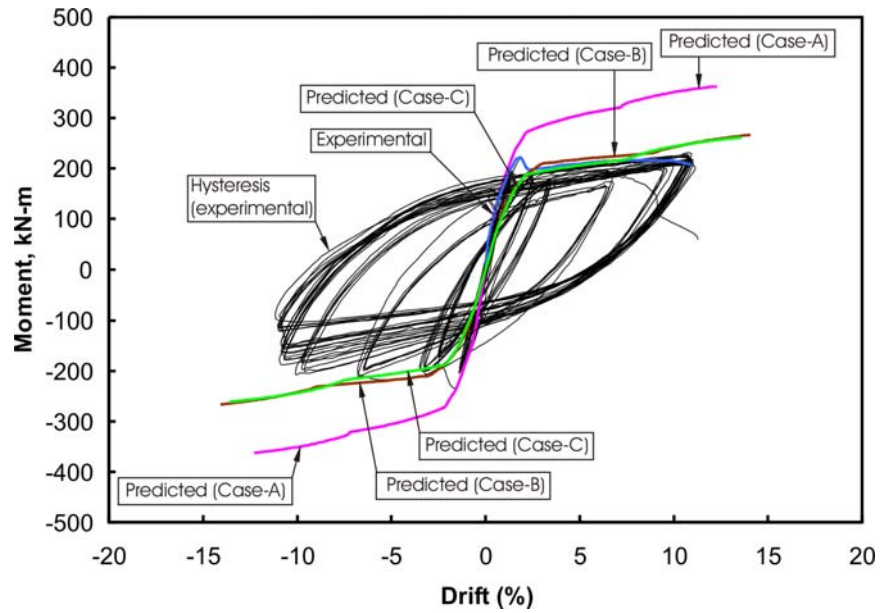


Figure 4-199: Predicted and experimental average envelope curve for column CL0

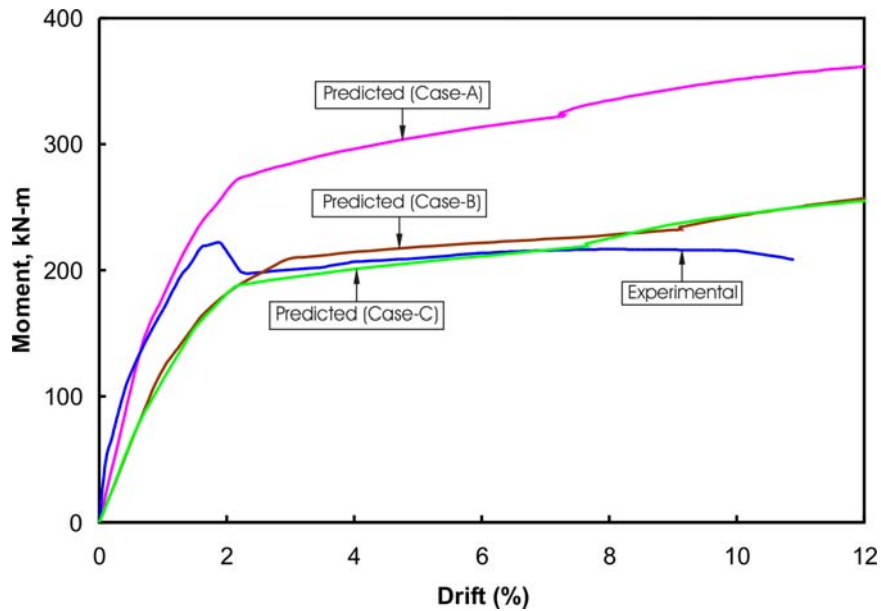


Figure 4-200: Predicted and experimental average envelope curve for column CL0

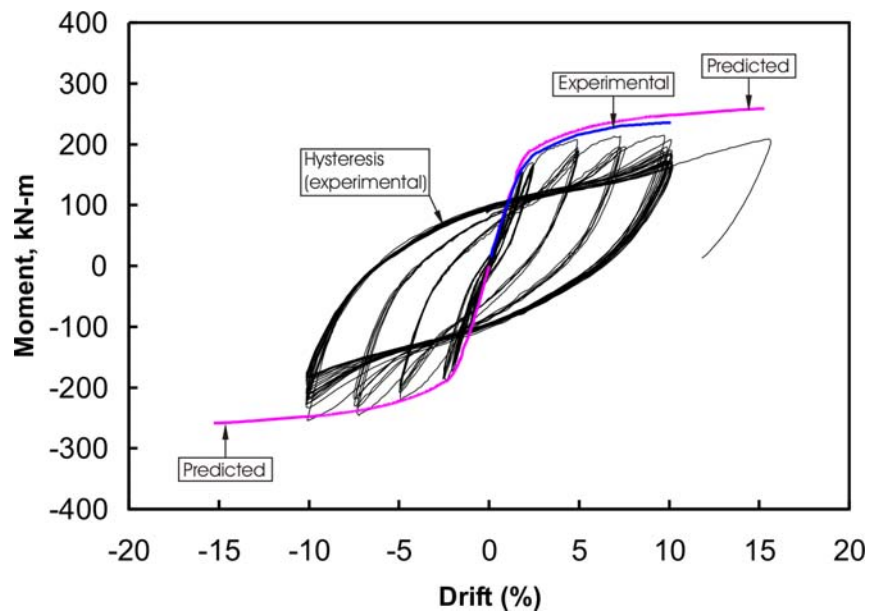


Figure 4-201: Predicted and experimental average envelope curve for column CL1

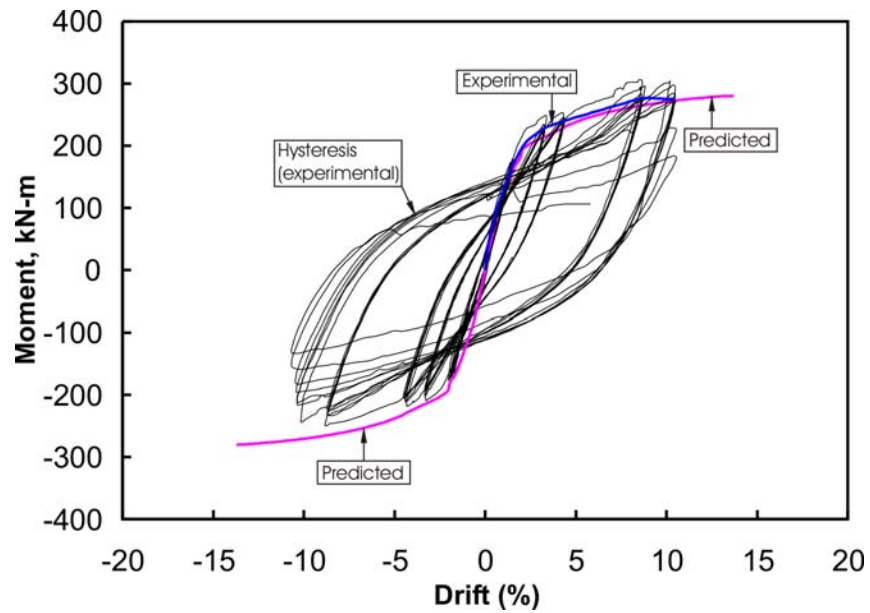


Figure 4-202: Predicted and experimental average envelope curve for column CL2

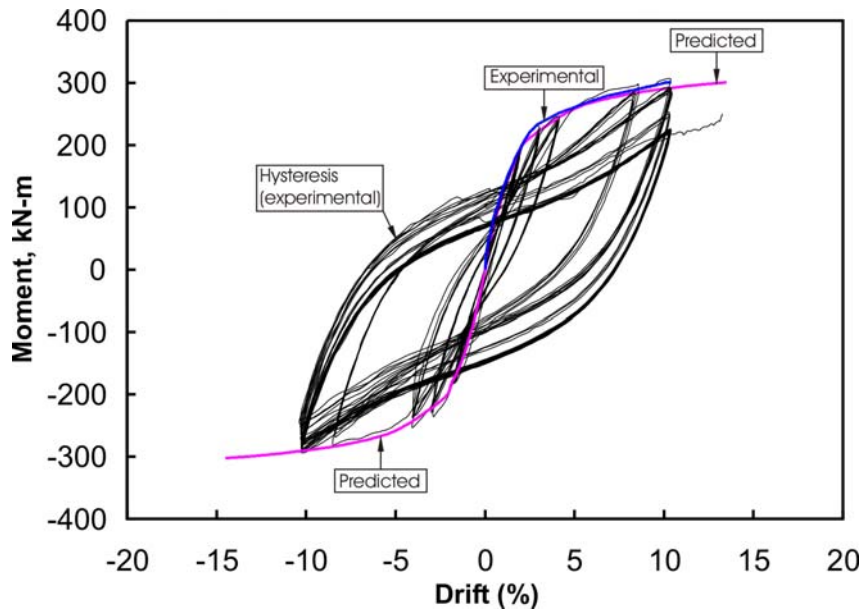


Figure 4-203: Predicted and experimental average envelope curve for column CL3

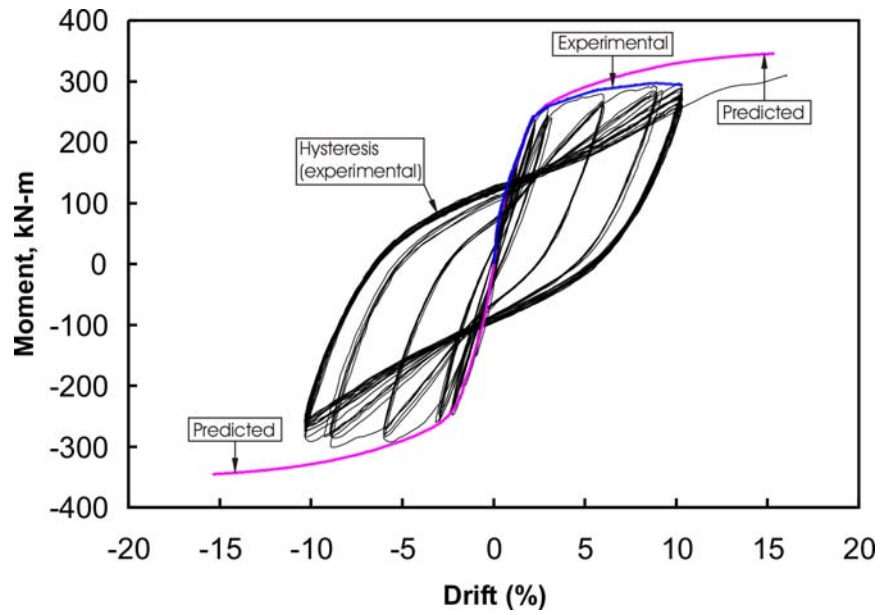


Figure 4-204: Predicted and experimental average envelope curve for column CL4

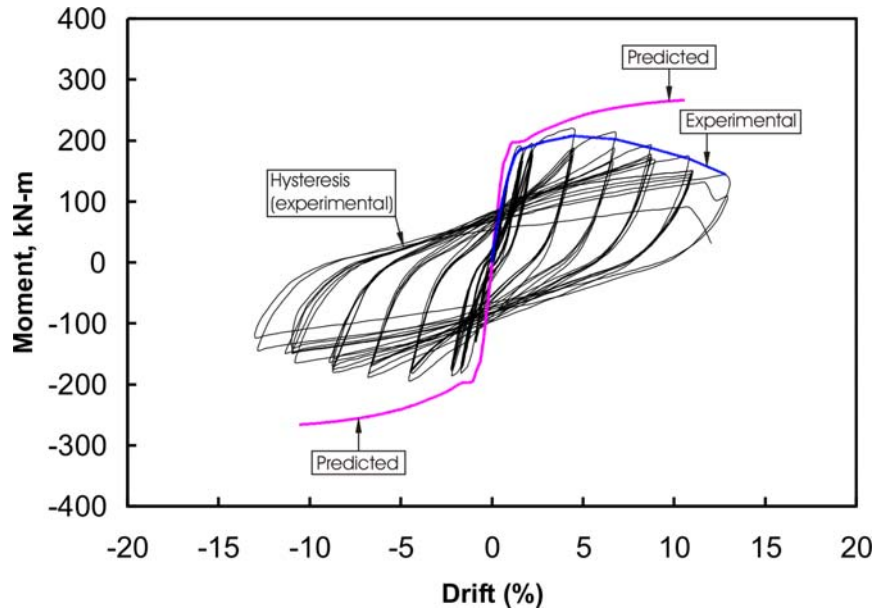


Figure 4-205: Predicted and experimental average envelope curve for column CL5

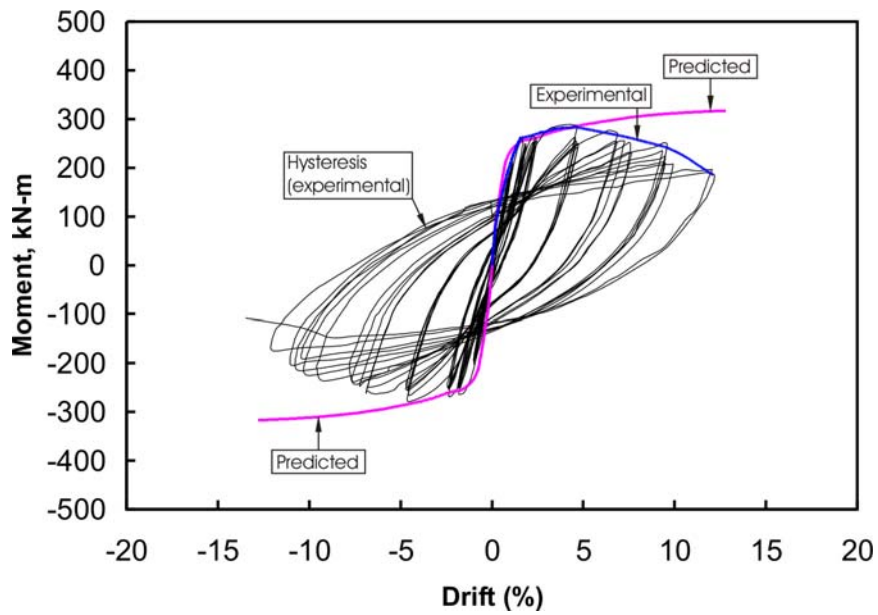


Figure 4-206: Predicted and experimental average envelope curve for column CL6

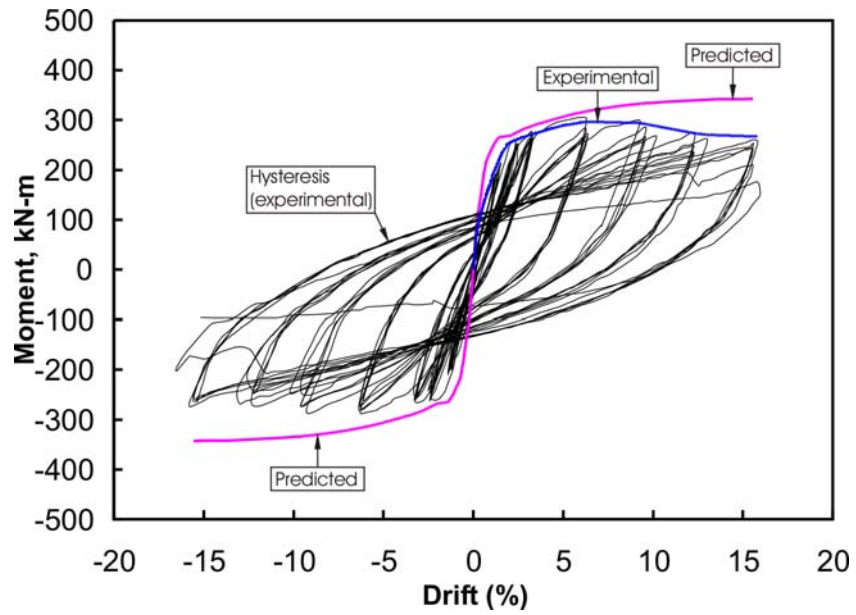


Figure 4-207: Predicted and experimental average envelope curve for column CL7

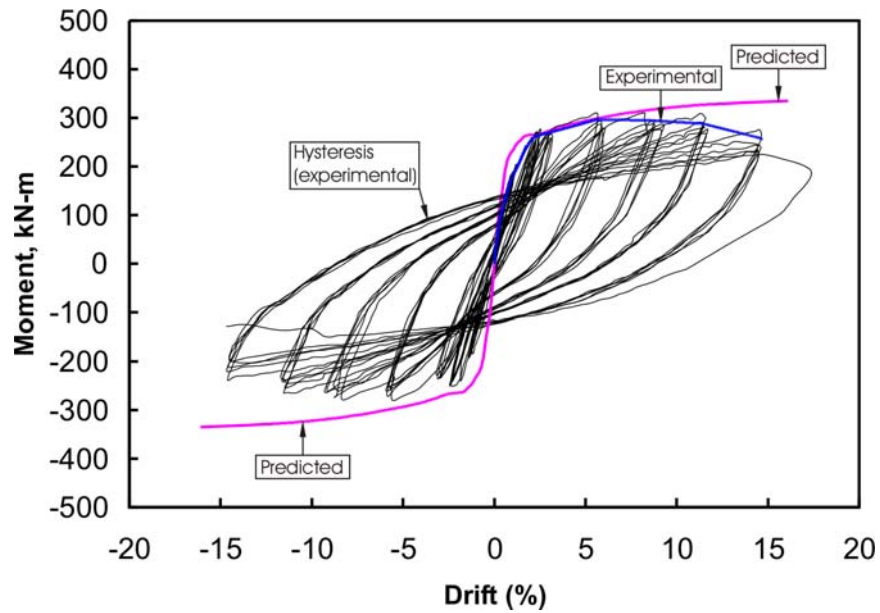


Figure 4-208: Predicted and experimental average envelope curve for column CL8

4.8 References

- Aboutaha, R.S, Engelhardt, M.D., Jirsa, J.O., and Kreger, M.E. 1996. Retrofit of concrete columns with inadequate lap splices by the use of rectangular steel jackets. *Earthquake Spectra*, Vol. 12, No. 4, November, pp. 693-714.
- Applied Technology Council, 1996. Seismic evaluation and retrofit of concrete buildings. seismic, safety commission, State of California, Report No. SSC 96-01(ATC-40), Vol. 1 and 2, November.
- Antoniades, K.K., Salonikios, T.N., and Kappos, A.J., 2003. Cyclic tests on seismically damaged reinforced concrete walls strengthened using fiber-reinforced polymer reinforcement. *ACI Structural Journal*, Vol. 100, No. 4, pp. 510-518.
- Bayrak, O. and Sheikh, S.A. 1997. High-strength concrete columns under simulated earthquake loading. *ACI Structural Journal*, Vol. 94, No. 6, pp. 708-722.
- Canbolat, B.A., Parra-Montesinos, G.J., and Wight, J.K. 2005. Experimental study on the seismic behavior of high-performance fiber-reinforced cement composite coupling beams. *ACI Structural Journal*, January-February, pp. 159-166.
- Chai, Y.H., Priestley, M.J.N., Seible, F. 1990. Retrofit of bridge columns for enhanced seismic performance. *Proceedings of U.S.-Japan Workshop on Seismic Retrofit of Bridges*, Tsukuba, Japan, December, pp. 321-339.
- Chen, W.F. 1982. *Plasticity in reinforced concrete*. McGraw-Hill, New York.
- Chopra, A.K. 1995. *Dynamics of structures-Theory and applications to earthquake engineering*. Englewood Cliffs, New Jersey:Prentice-Hall, Inc.
- Chung, H., Yang, K., Lee, Y. and Eun, H. 2002. Strength and ductility of laterally confined columns: *Canadian Journal of Civil Engineering*, Vol. 29, pp. 820-830.
- Corley, W.G. 1966. Rotational capacity of reinforced concrete beams. *ASCE, Proceedings*, V. 92, ST5, October, pp. 121-146.
- Ghee, A.B., Priestley, M.J.N. and Paulay T. 1989. Seismic shear strength of circular reinforced concrete columns. *ACI Structural Journal*, January-February, pp. 45-59.

- Ghobarah, A., Aziz, T.A., and Biddah, A. 1997. Rehabilitation of reinforced concrete frame connections using corrugated steel jacketing. *ACI Structural Journal*, Vol. 94, No. 3, pp. 283-293, May-June.
- Iacobucci, R.D., Sheikh, S.A., and Bayrak, O. 2003. Retrofit of square concrete columns with carbon fiber-reinforced polymer for seismic resistance. *ACI Structural Journal*, Vol. 100, No. 6, pp. 785-794.
- Lam, S.S.E., Wu, B., Wong, Y.L., Wang, Z.Y., Liu, Z.Q., and Li, C.S. 2003. Drift capacity of rectangular reinforced concrete columns with low lateral confinement and high-axial load. *Journal of Structural Engineering*, Vol. 129, No. 6, pp. 733-742.
- Lukkunaprasit, P. and Sittipunt, C. 2003. Ductility enhancement of moderately confined concrete tied columns with hook-clips. *ACI Structural Journal*, Vol. 100, No. 4, July-August, pp. 422-427.
- Mander, J.B., Priestley, M.J.N., Park, R. 1988a. Observed stress-strain behaviour of confined concrete: *Journal of Structural Engineering*, Vol. 114, No. 8, pp. 1827-1849.
- Mander, J.B., Priestley, M.J.N., and Park, R. 1988b. Theoretical stress-strain model for confined concrete. *Journal of Structural Engineering*, Vol. 114, No. 8, pp. 1804-1826.
- Marsh, L. 1992. Seismic retrofit for R/C column bar splices. *Proceedings of the 1992 Structures Congress, ASCE, San Antonio, Texas, April 13-15.*
- Mattock, A.H. 1967. Discussion of "Rotational capacity of reinforced concrete beams." *Journal of Structural Division, ASCE*, Vol. 93, No. ST2, pp. 519-522.
- Otani, S., and Sozen, M.A. 1972. Behavior of multistory reinforced concrete frames during earthquakes. *Structural Research Series No. 392, University of Illinois, Urbana, 551pp.*
- Priestley, M.J.N., and Park, R. 1987. Strength and ductility of concrete bridge columns under seismic loading. *ACI Structural Journal*, V. 84, No. 1, January-February, 1987, pp. 69-76.
- Saatcioglu, M. and Razvi, S.R. 1992. Strength and ductility of confined concrete: *Journal of Structural Engineering, ASCE*, Vol. 118, No. 6, pp.1590-1607.
- Saatcioglu, M. and Yalcin, C. 2003. External prestressing concrete columns for improved seismic shear resistance. *ASCE, Journal of Structural Engineering*, Vol. 129, No. 8, August, pp. 1057-1070.
- Sezen, H. 2000. Seismic behavior and modeling of reinforced concrete building columns. Phd. Dissertation, University of California, Berkeley.

- Sheikh, S.A and Khoury, S.S. 1993. Confined concrete columns with stubs. ACI Structural Journal, Vol. 90, No. 4, pp. 414-431.
- Sheikh, S.A and Uzumeri, S.M. 1980. Strength and ductility of tied concrete columns: Journal of the Structural Division, ASCE, Vol. 106, No. ST5, pp. 1079-1102.
- Xu, S. and Niu, D. 2003. Seismic behaviour of reinforced concrete braced frame. ACI Structural Journal, Vol. 100, No. 1, January-February, pp. 120-125.
- Yarimci, E., Yura, J.A., and Lu, L.-W. 1966. Techniques for testing structures permitted to sway. Fritz Engineering Laboratory Report No. 273.40, Lehigh University, Bethlehem, PA.